ACCELERATING TREATMENT OF RADIOACTIVE WASTE BY EVAPORATIVE FRACTIONAL CRYSTALLIZATION

A Thesis
Presented to
The Academic Faculty

by

Laurent Nassif

In Partial Fulfillment
of the Requirements for the Degree
Doctor of Philosophy in the
School of Chemical and Biomolecular Engineering

Georgia Institute of Technology
May 2009

ACCELERATING TREATMENT OF RADIOACTIVE WASTE BY EVAPORATIVE FRACTIONAL CRYSTALLIZATION

Approved by:

Dr. Ronald W. Rousseau, Chair and Advisor
School of Chemical and Biomolecular Engineering
Georgia Institute of Technology

Dr. Amyn S. Teja
School of Chemical and Biomolecular Engineering
Georgia Institute of Technology

Dr. Charles Liotta
School of Chemistry
Georgia Institute of Technology

Dr James Frederick
Institute of Paper Sciences and Technology
Georgia Institute of Technology

Dr. Matthew Realff
School of Chemical and Biomolecular Engineering
Georgia Institute of Technology

Dr Sankar Nair
School of Chemical and Biomolecular Engineering
Georgia Institute of Technology

Date Approved: December 17th 2008

To Viola Karam Nassif

PREFACE

There is currently 53 million gallon of mixed and highly radioactive wastes waiting for treatment at Hanford site, in Washington State. These wastes are stored in 177 underground shielded tanks reparsed into 18 tank farms. Wastes have accumulated at Hanford site as a result of more than fifty years of nuclear materials production. Waste is a term referring to liquids and solids that are radioactive and/or hazardous (DOE/EM-0319; 1997). Isotopes responsible for the radioactivity of the waste stored at Hanford are mainly uranium fission products that remained unspecified. A methodology was hence developed in order to select the most important radionuclides presents in the Hanford waste along with their concentrations (Cowley W.L et al.; 1998). This methodology allowed the identification of Cesium (Lewis R.E et al.; 1965), Technetium (Vance E.R et al.; 1998) and Strontium (Fullam H.T et al.; 1976) as radioactive species present into Hanford waste. Among these radioactive isotopes, 137Cesium has been identified as major isotope remaining in the low and medium curie wastes that needed to be removed before immobilization. Furthermore, the bulk of the waste is composed of non-radioactive inorganic chemicals issued from the fuel reprocessing operations. Speciation studies showed the importance of the presence of several sodium double salts and of certain heavy elements. (Herting D. et al.; 2003)

Since limited thermodynamic information were available for these sodium double salts at the conditions present in the Hanford tanks, there were a need of simulation tools

in order to predict their thermodynamic behavior. The Environmental Simulation Program (developed by OLI system inc.) was chosen in order to simulate the salt cake dissolution, tank retrieval and pipelines transfer operations. Simulations of phase equilibrium of 9 saltcakes in the high ionic strength inorganic system conditions of the Hanford waste tanks were performed, but the validity of these simulations can only be assessed experimentally (Toghiani R.K. et al.: 2002). The performance of crystallization experiments on several simulated waste compositions, the determination of the nucleation curve, and the confrontation to simulated thermodynamic equilibrium is one of the main objectives of this thesis.

The treatment of both Low Level Liquid Waste (LLLW) and High Level Liquid Waste (HLLW) accumulated at Hanford site was intended to be performed by a single structure called Waste Treatment Plant (WTP). The Hanford Waste Vitrification Plant (HWVP) is intended to immobilize the liquid waste in borosilicate glass cast into stainless steal canisters. The filled canisters will be stored in the HWVP until final disposal in a federal geologic repository (Carreon R. et al.; 2002), (Rabiger K. et al.; 1995), (Colombo P. et al.; 2003). To demonstrate the feasibility of Vitrification and the durability of the high-level waste glass, a high level waste sample from tank AZ-101 was processed to glass, analyzed with respect to chemical composition, radionuclide content and waste loading capacity (Hrma P., Crum J.V, Bates D.J; 2005). The vitrified borosilicate glass was then tested to demonstrate its compliance with regulatory requirements (Hrma P., Crum J.V, Bredt P.R; 2005). These results were compared with the non radioactive simulant glass results and models were used in order to identify the impact of spinels-a sulfate based crystal- formation on glass composition and leachability

(Wilson B.K et al.; 2002), (Mika M. et al.; 2001). Results and model demonstrated the importance of reducing the molar concentration of sulfate in the waste to be vitrified (Manara D et al.; 2006).

The US department of Energy awarded a 14 billions US $ contract for the construction of the Waste Treatment Plant and the cleaning of the Hanford site by the due date of 2030 (Smith R.A. et al.; 1990). However since the WTP construction contract was awarded in 2000, the WTP building estimated cost has increased more than 150 %, from 4.3 to 11 $billion. In addition the completion date for the building of the WTP has been postponed of 6 years or more (Aloise G. et al.: 2006). Safety issues were also raised as an effect of extended storage time at Hanford site (DOEM/EM-0266; 1996), (DOEM/EM-0232 and DOEM/EM-0290; 1995-1996), (DOE; 1996). Many of Hanford's older single wall tanks have leaked and some one millions gallons of waste are believed to have leaked from the older single-shell tanks in the last fifty years due to waste and tanks aging (DOE/EM-0319; 1997). The double shell tanks, some of these having been built in the early 80's, were expected to last for 50 years but the extension in the project completion time increased the risks of liquid waste or flammable gases leaking due to the aging of the waste (Bryan S. et al.; 2003).

Based on these new information, the US. Department of Energy has determined that the preferred alternative to remediate the Hanford tank waste would be to submit it to pretreatment (Herting D.L et al.; 2005), (Nassif L.; 2007), (Nassif L. et al.; 2008). This process would separate the waste into Low Activity Waste (LAW) and High Level Waste (HLW) that would both be vitrified into borosilicate glasses (Carreon R. et al; 2002). The LAW would be immobilized through Bulk vitrification for on-site disposal on

contrary to the HLW that would be immobilized as glass through the WTP for ultimate disposal in the national repository. During bulk vitrification the simulant is mixed with soil and small amounts of chemical additives before being melted at 1300 degrees. The melter used for the vitrification represents also the container for the immobilized waste and can be stored in situ (Tyree G. et al.), (Kaldor R.A et al.; 1985), (Huang F. et al.; 1994). This vitrification method, by supplementing the WTP, would greatly decrease the final repository and overall project costs while accelerating the treatment of Hanford waste (Thompson L.E et al.; 2003). In addition, the reduction of the volume of liquid waste to be sent to the WTP would greatly reduce the overall cost of the project and the disposal cost of the vitrified glass (Herting D. L. et al.; 1997).

Several methods have been proposed and studied for use in removing cesium from Hanford wastes. Such methods include ion exchange, solvent extraction, tetraphenylborate precipitation, nanofiltration-complexation and evaporative fractional crystallization. Ideally, the selected technology will remove at least 99% of the cesium from the waste and add no additional waste streams to the process (Carreon R. et al.; 2002). The proposed ion exchange process uses a SuperLig® 644 resin material containing a poly (hydroxyarlyne) ligand, which is highly selective for the cesium cation. Research has proven that by operating two ion exchange columns in series, cesium removal yields can range from 99.4-99.98%. This process is very attractive since the resin can be reused by eluting the column with nitric acid (removing the cesium) and regenerating the resin with sodium hydroxide. The downside to this technology is that it introduces an acid and base stream to the process, which could increase the total waste volume (Hassan N.M et al.; 2002).

A second possible method for removing cesium from Hanford wastes is an extraction process using magnetic microparticles. These particles are composed of magnetite (Fe_3O_4), crystalline silicotitanate (CST), and polyacrolein, and are known by the trade name MagAcryl^{TM}-CST. During the process cesium binds to the CST in the micropores and after an appropriate contact time a high gradient magnetic separator is used to separate the particles from the liquid stream. This method has proven to remove between 90-98% of the cesium in a single stage. The major drawback to this method is that magnetite is susceptible to dissolution under extreme conditions, and since the magnetic separation step relies on magnetite, dissolution would ruin this process (Kaminski M. D. et al.: 2002).

Tetraphenylborate (TPB) precipitation is another alternative for cesium removal from Hanford wastes. To begin this process, aqueous NaTPB is mixed with the cesium containing waste. Ion exchange occurs between sodium and cesium and insoluble CsTPB is precipitated from the solution. This cesium precipitate is then separated, dissolved in a propylene carbonate stream, and sent to a three phase extraction. The extraction step involves an upper layer of tripropylamine, a middle layer of aqueous $NaNO_3$, and a lower layer of cesium-containing propylene carbonate. During the extraction process, ion exchange occurs again between cesium and sodium, with aqueous $CsNO_3$ being the final product of interest. TPB precipitation has proven to have a cesium removal yield of at least 99.8%, but there are several drawbacks to this method. These drawbacks include the additional process streams necessary for the separation process and the potential decomposition of TPB into benzene and other flammable organics (Ponder S.M. et al.; 2001).

The fourth alternative method discussed here is nanofiltration-complexation. This process utilizes a cesium-selective ligand to form a cesium-ligand complex in the waste stream, which is then sent to a nanofiltration step. The ligand chosen for testing was tetrahydroxylated bis-crown-6 calix[4]arene. This process is attractive since it does not add additional wastes to the process, but studies have shown that a single stage of complexation-nanofiltration only removes 90% of the cesium in the feed stream (Chitry F. et al.; 2001).

The pretreatment method selected and investigated in this thesis is fractional crystallization (Hamilton D.W et al.; 2006), (Felder R.M and Rousseau R.W; 2000). "A process was already demonstrated in the laboratory for separating clean, virtually non radioactive sodium nitrate from Hanford tank waste." Flowsheet modeling has shown that the process could reduce the volume of vitrified low activity waste (LAW) by 80% to 90%, reducing disposal costs by an estimated $240 million, and would eliminate the need for building a $2.2 billion large scale Vitrification plant planned for privatization Phase II (Herting D.L. et al.; 1997). Evaporative crystallization method use experimental solubility data obtained for three main sodium salts present in the simulant solutions. The effects of the other species present in simulated waste solutions were found negligible (Reynolds D.A et al.; 1985). A general procedure for the evaporative fractional crystallization of simulated Hanford Waste Solutions was established (Rousseau R.W et al.; 2006). It concerns notably the crystal formation of burkeite and sodium salts. This method would decrease the volume of radioactive waste but also the sodium to sulfate molar ratio that prevent the formation of stable glass matrices during vitrification (Geniesse D. J. et al.; 2004). The application and improvement of this

method, in the case of single shell tank wastes, is one aim of this thesis (Nassif L; 2007). The crystal identification of the solid phases issued from research on Hanford simulated wastes are performed through Polarized Light Microscopy (PLM). (Herting D.L et al.; 1992). The precise inventory and importance of the data collected on inorganic species likely to crystallize made of this technique the preferred method for crystal characterization.

The other major aspect of the study presented in this thesis is the preparation of the waste pretreatment technology to pilot scale application. Larger scale operations are to be performed with a continuous crystallizer (Randolph and Larson; 1988). Due to the difficulty and cost of obtaining kinetics results at larger scale, the investigation of the operating condition effect on specific kinetics will be performed with semi-batch equipment.

Several methods may be used to derive the crystallization kinetics from a given feed solution. The literature reports the use of (1) Focused Beam Reflective Measurement (FBRM), (2) in-Process Video Microscopy (PVM), (3) sampling and microscopy, (4) validation of modeling based kinetics with population distribution. These methods were typically applied to single species system for pharmaceutical compounds batch and semi batch crystallization. In some instances the in situ non-sample methods (FBRM and PVM) were combined (Kougolos E. et al.; 2005). The multi species systems typically used sampling and microscopy based method or an indirect method such as the validation of kinetics model with a resulting population distribution. The latest technique uses the quadrature method of moments (QMOM) or method of classes (MOC) to derive the kinetics

(http://www.emse.fr/pratsolis/list/animp2002barresi.pdf, November 2008). In essence, the system of study (single or multi species, single or multiple shapes) and the type of process (continuous, batch, semi batch) determine which of these techniques should be applied.

FBRM is a method typically used for single species system with a known morphology (Al Nasser W.N et al.; 2007), (Trifkovic M. et al.; 2008). FBRM consists in (1) focusing a laser beam into a sample cell located in a specific position in the well mixed region of a crystallizer and (2) recording the chord length of crystals that crosses the laser beam. This method present the advantage of recording "in situ" the evolution of the chord length inside the vessel and being able to detect and quantify nucleation when it occurs. This type of inline method was used previously in a semi batch or batch context. The issues with this method are that (1) the chord length distribution may need to be converted to a crystal size distribution, which is typically done by developing a conversion matrix unavailable commercially (Barthe S. et al.; 2006), (2) this method is not appropriate for multiple species kinetics presenting varying shapes, (3) the small size crystals, the agglomerates, and round shape crystals are difficult to detect.

PVM is another in situ method that identifies the crystal size, shape, agglomeration and presence of several species in a crystallizer without performing sampling (O Grady D. et al; 2005). The method consists in inserting a camera inside the crystallizer and sending the images to real time image analysis software that translate them into a crystal count and size. The actual application of PVM is the validation of nuclei and morphology detections when the system already uses a FBRM probe. The main drawbacks of this method are: (1) taking 3D images may lead to altered crystal

sizes due to depth effect, (2) taking 3 D images may lead to improper count due to excessive overlap of crystals in the image, and (3) the slurry density becomes rapidly too high to obtain accurate imaging analysis. Current effort went into understanding these drawbacks to improve analytical software to obtain more accurate estimate. (Larsen P.A et al.; 2006)

Single and multi species system for which a population or mass density distribution can be obtained usually uses an indirect method estimating kinetics from the quadrature methods of moments (Oncul A. A. et al; 2006) or the method of classes (Puel F et al.; 2003). These techniques provide good models and simulations but do not provide experimental measurements of crystal nucleation and growth rate.

The method selected and investigated in this thesis is the combined used of sampling and image analysis using microscopy. This method was selected because: (1) the system we are working with presents multiple crystalline species with multiple shapes, (2) there is no need of in situ analysis and no possibility to use FBRM, (3) some agglomeration may occur in the crystallizer leading toward image analysis method, and (4) we want to monitor the kinetics experimentally to develop a model and confront it to resulting crystal size and mass density distributions. This method was already used with a single species system crystallized under batch conditions (Krumme A. et al; 2003), [Salmeron Sanchez M. et al.; 2007) to determine length evolution, crystal counts, morphologic change, and detect nucleation.

The specific kinetics obtained experimentally with the semi-batch crystallization apparatus will be used as parameter of a model for steady state continuous operations. The model will be developed assuming a steady state Mixed Suspension Mixed Product

Removal process for which the mass and population balances equation were already defined (Puel F. et al.; 2003), (Garside J. et al.; 2002), (Mc Cabe W.L. et al.; 2005), (Ohman G. et al.; 1997). The suggested model will define the total population density as a summation of the population density of the main species crystallizing with simulated waste feed solutions. The modeling of the steady state continuous crystallizer should provide: (1) the plot of the population density with respect to the crystal size, and (2) the cumulative and differential distributions of crystal count, size and mass with respect to the particle size by using classical techniques of crystal population balance modeling (Seader J.D et al.; 2006), (Ohman G. et al.; 1997). Furthermore, a simple parameter study may be performed with the steady state continuous crystallizer model, displaying the sensitivity of the population density function to process variables such as temperature, evaporation and residence time.

ACKNOWLEDGEMENTS

I would like to especially thank my parents, Atef and Christiane, my brother Christian, and Anriada, without whose continuous support, love and faith in me I would not be here. I wish to express my deepest gratitude to my thesis advisor, Dr Ronald. W. Rousseau, for his knowledge, guidance and help and my main coworker and friend, George "Pj" Dumont, with whom I am sharing the work and results presented in this thesis. I wish to include to this research work the name of my two other coworkers, Cosmas Bayuadri and Hatem Alsyouri with whom we shared long hours to complete the experimental part of this project.

I wish to acknowledge the financial support for the research project provided by the U.S. Department of Energy's Office of Environmental Management (EM-21 – Office of Cleanup Technology) through CH2M HILL and COGEMA, Inc. The interaction with Eric Nelson has been beneficial in keeping the activities moving forward and focused on the project objectives. His style in reminding us of deadlines is commendable and effective.

Guidance from Dr. Daniel L. Herting of the CH2M HILL provided very helpful insights to many of the issues concerning fractional crystallization from the Hanford solutions. In addition, his knowledge and willingness to help our team learn to use polarized light microscopy in studying crystals produced in this work were invaluable.

Don Geniesse of COGEMA, Inc. provided knowledgeable and timely guidance with his simulations of fractional crystallization. He did not mind answering even the most mundane questions regarding the systems with which we worked, and he was especially helpful in responding to "what if" questions regarding process modifications.

The work benefited considerably from discussions with Tim Nordahl, President of Swenson Inc. He provided perspectives and suggestions regarding the most important data for taking the results of our work to a scaled-up process.

The experimental apparatus and procedures developed in this thesis benefited considerably from the input of John Smith and Dave Bechtold from CH2M HILL, whose practical point of view and experience in the field becomes a great asset for the project.

We express appreciation to Jeff Dillener of Galbraith laboratories and Victor De Jesus of GTRI at Georgia Tech for his diligence in working with us to provide analytical results that were as useful as possible. We also would like to thank Mike Buchanan at the IPST Center at Georgia Tech and Victor for his assistance with chemical analyses.

I would like to particularly thank past and present members of this research group that provided valuable inputs, encouragement and friendship: Karsten Bartling, Krystle Chavez, Ana Fernandez, Chee-wei Jenifer Luk, Jose Mendez del Rio and Young-soo Kim.

I give my sincere thanks to all my friends, professors, and staff I met at Georgia Tech and in Toulouse, France. I wish to especially thank Pr Patrick Garnier, Mr. Joel Bertrand, Pr. Xavier Joulia and Pr. Joel Albet from the INP Toulouse and LGC Toulouse.

Finally and most importantly, I dedicate this thesis to the loving memory of my grandmother, Viola Nassif, whose sincere love and faith inspired me to be the person I am and the one I aim to become.

TABLE OF CONTENTS

LIST OF TABLES

LIST OF FIGURES

LIST OF ABBREVIATIONS

Abbreviations and Acronyms

ACS	American Chemical Society
ASTM	American Society of Testing Materials
CD	Compact Disk
CSD	Crystal Size Distribution
CST	Crystalline Silicotitanate
DST	Double Shell Tank
DAQ	Data Acquisition
DF	Decontamination Factor
DOE	Department Of Energy
ECN	Engineering Change Notice
GTRI	Georgia Tech Research Institute
HLLW	High Level Liquid Waste
HLW	High Level Waste
HWTP	Hanford Waste Treatment Plant
LAW	Low Activity Waste
LLLW	Low Level Liquid Waste
MC	Method of Classes
MW	Molecular Weight
NNPP	Naval Nuclear Propulsion Program
OD	Outside Diameter
PLM	Polarized Light Microscopy
PTFE	Poly Tetrafluoroethylene
QA	Quality Assurance
QMOM	Quadrature Method Of Moments
SST	Single-Shell Tank
TPB	Tetraphenylborate
WTP	Waste Treatment and Immobilization Plant
XRD	X Ray Diffraction

Units

ft	foot
g	gram
°C	degrees centrigrade
wt%	weight percent
mol	mole
M	molar
L	Liter
mL	milliliter
ppm	parts per million
Ci	curies
mm	millimeter
mA	milliampere
Ω	ohms
pH	potential of Hydrogen – measure of acidity or alkalinity
in	inch
µm	micrometer
h	hour
min	minute

SUMMARY

The purpose of the work described in this thesis was to explore the use of fractional crystallization as a technology that can be used to separate medium-curie waste from the Hanford Site tank farms into a high-curie waste stream, which can be sent to a Waste Treatment and Immobilization Plant (WTP), and a low-curie waste stream, which can be sent to Bulk Vitrification. The successful semi-batch crystallization of sodium salts from two single shell tank simulant solutions (SST Early Feed, SST Late Feed) demonstrated that the recovered crystalline product met the purity requirement for exclusion of cesium, sodium recovery in the crystalline product and the requirement on the sulfate-to-sodium molar ratio in the stream to be diverted to the WTP. The experimental apparatus, procedures and results obtained in this thesis on scaled-down experiments of SST Early and Late Feed simulated solutions were adapted and reproduced under hot-cell with actual wastes by our partners at Hanford. To prepare the application of the pretreatment process to pilot scale process, several varation to the feed solutions were investigated including the presence of carboxylates and amines organics compounds and solids particles. Results of the study showed that 4 organics species presented complications to the process (NTA, HEDTA, EDTA and sodium citrate) while the other species (Formate, acetate, glycolate and IDA) and solids particles did not in the conditions of the stored wastes.

In this thesis, the kinetics of the crystalline species formed at the condition of the early feed certification run (66 °C and 25 g/h evaporation) were determined along with the effect of the operating temperature and evaporation rate on these kinetics. On one hand, the study of evaporation rate values ranging from 25g/h to 75g/h showed that an increase in evaporation rate increased the specific nucleation while decreasing the specific growth rate. On the other hand, experiments on operating temperature ranging from 35 °C to 75 °C displayed that the nucleation rate of all species increased with temperature at the exception of sodium carbonate monohydrate and burkeite crystals, and that the growth rate of all species increased with temperature at the exception of sodium nitrate. Furthermore, sulfate based crystals such as trisodium fluoride sulfate were only roduced at 45 °C and 75 °C.

To simulate the application of the technology to a continuous crystallizer, a simple steady state MSMPR population balance model was developed expressing the total population density function as the sum of the specific population density functions. The specific semi-batch crystallization kinetics were implemented in this model to provide the population density function profile and cumulative mass density from the continuous pretreatment of early feed solutions at a residence time of 12 hours. Variations of operating temperature, evaporation rate and residence time were also simulated.

KEY WORDS

Crystallization, Evaporative Fractional Crystallization, Nuclear Waste Pretreatment, Cesium Removal, Hanford, SST Early and Late feed, Multi-solute, Multi-salts, Simulant Testing, MSMPR, Nucleation and Growth Rates.

CHAPTER 1: INTRODUCTION

1.1 HANFORD WASTE REMEDIATION PROJECT

Fifty-three million gallons of mixed and highly radioactive wastes currently await treatment at the Hanford site in the State of Washington. The wastes were disposed at Hanford as a legacy of the US Defense activities during the cold war area, and are reparsed in 177 double-shell (DST) and single-shell (SST) tanks. The remediation of low-, medium-, and high-level liquid waste accumulated at the Hanford site was originally intended to be performed by a single structure called Waste Treatment Plant (WTP). Considering the increased risk to the environment resulting from prolonged storage of the wastes and the high overall cost of the project, a pretreatment operation on the low- and medium-curie wastes is under consideration. The pretreatment operation is to accelerate waste treatment and to reduce the volume of nuclear waste to be sent to the Waste Treatment Plant. The pretreatment process is expected to separate the waste into a solid low-activity and a liquid high-activity fraction that may be handled separately (Figure 1).

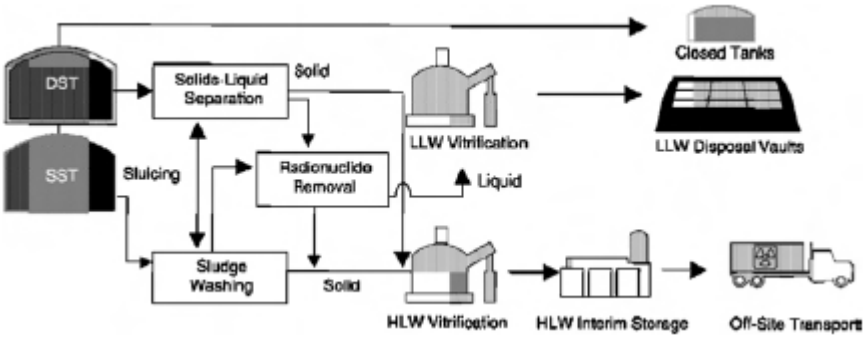

Figure 1. Process diagram for the waste treatment and accelerating project at Hanford site

Evaporative fractional crystallization is considered the most promising technology to perform the waste separation and radionuclide removal. It consists of crystallizing sodium salts from a feed solution by achievement of supersaturation through solvent removal (evaporation), and then separating the resulting slurry from the mother liquor and other soluble species. This technology is intended to ensure that problematic waste components, such as sulfates, are diverted preferentially to a bulk vitrification facility, while radionuclide species, primarily ^{137}Cs and ^{99}Tc, are sent to the WTP. Two categories of waste solution will be investigated. The SST waste obtained from early removal from the Hanford storage tank are reffered as Early Feed while the waste from the lat removal will be defined as Late Feed.

The following study assesses the objectives fixed by the Pretreatment Testing and Demonstration Program. The overall objective of the Program is to demonstrate that fractional crystallization is an effective way to condition feed streams for the CH2M HILL Low Activity Waste (LAW) supplemental treatment system. Minimum separation goals were provided (in order of priority) in the Statement of Work for ^{137}Cs activity (<0.05 Ci/L or 2.89E-03 g/L in a 5 molar (M) sodium solution, based on 20% ^{137}Cs to total cesium) in the recovered stream going to the pretreatment facility, sodium removal (50%), and sulfate-to-sodium M ratio (<0.01) in the stream going to the Waste Treatment and Immobilization Plant. The preliminary thermodynamic models applied by COGEMA, Inc. for each of the simulant feeds indicated that these goals can theoretically be met by fractional crystallization. The models further indicated that it was possible to approach the desired removal levels (<0.0012 Ci/L or 6.93E-05 g/L, 90%, and ≤ 0.0022, respectively). These are to be achieved by crystallization of sodium salts, especially those containing nitrate, carbonate and sulfate ions, while leaving the highly soluble cesium in solution. The evaporative crystallization method and requirements are presented in Figure 2.

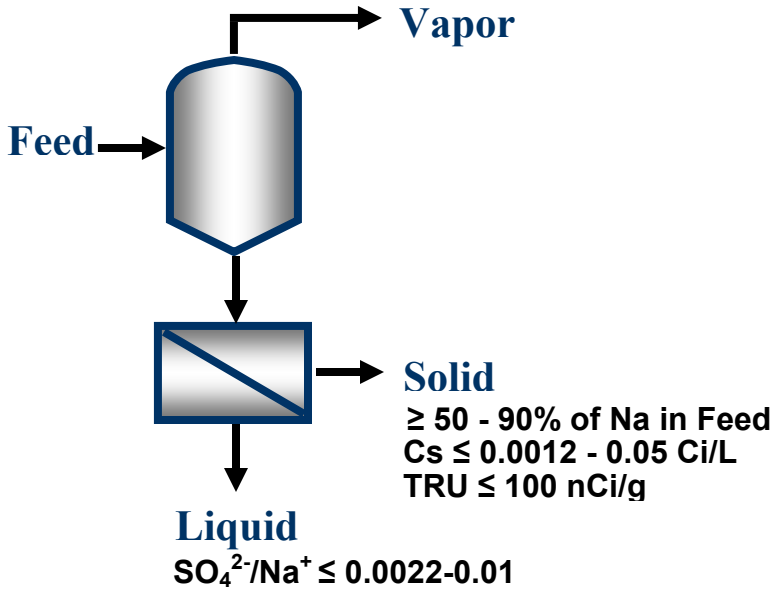

Figure 2. Schematic of evaporative fractional crystallization technology applied to Hanford waste treatment and corresponding requirements

1.2 FRACTIONAL CRYSTALLIZATION

When a solution has a single species that can be crystallized by cooling, evaporation, addition of a non-solvent or some other means of concentrating the solution, such an operation may be thought of as simple crystallization. However, when a solution contains multiple solutes, solutes may be expected to come out of solution (crystallize) when each has reached its solubility limit. For example, suppose a solution contains three solutes (A, B, and C) that all saturate the solution as solvent is evaporated from a solution, and the solution also contains additional solutes whose concentrations increase as evaporation occurs, but do not reach saturation. Figure 3 illustrates the hypothetical distribution of products if the solution is progressively saturated with A, then B, and finally C in the course of evaporating solvent from the solution. The unique behavior of each solute is readily apparent: similar to the behavior of burkeite, the production of A is limited after one of its constituent reaches a concentration at which it begins to crystallizeas

a pure component. The mass of crystalline B accumulates rapidly immediately after it saturates the solution, but its production decreases slowly thereafter. The mass of crystalline C builds slowly after saturation and then rapidly as the end of the operation is approached. Clearly, the point at which the slurry is sent to a solid-liquid separator will influence the composition of the final product and, concomitantly, the characteristics of the separation.

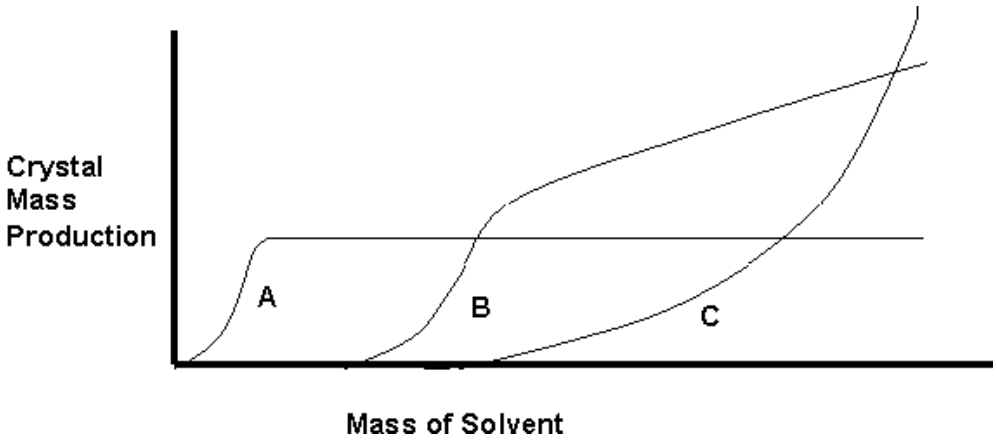

Figure 3. Hypothetical product distribution from fractional crystallization: solution becomes saturated with solutes at different times in the evaporation

Now consider a different situation, one in which the solutes achieve saturation at roughly the same time in process. Assuming that all nucleate and grow as such conditions are achieved, the product generation is expected to look more like that in Figure 4. In this situation, separation of species from one another by simple fractional crystallization is not possible; instead, this instance of fractional crystallization only facilitates separation of a physical mixture of the crystalline solutes from the residual mother liquor.

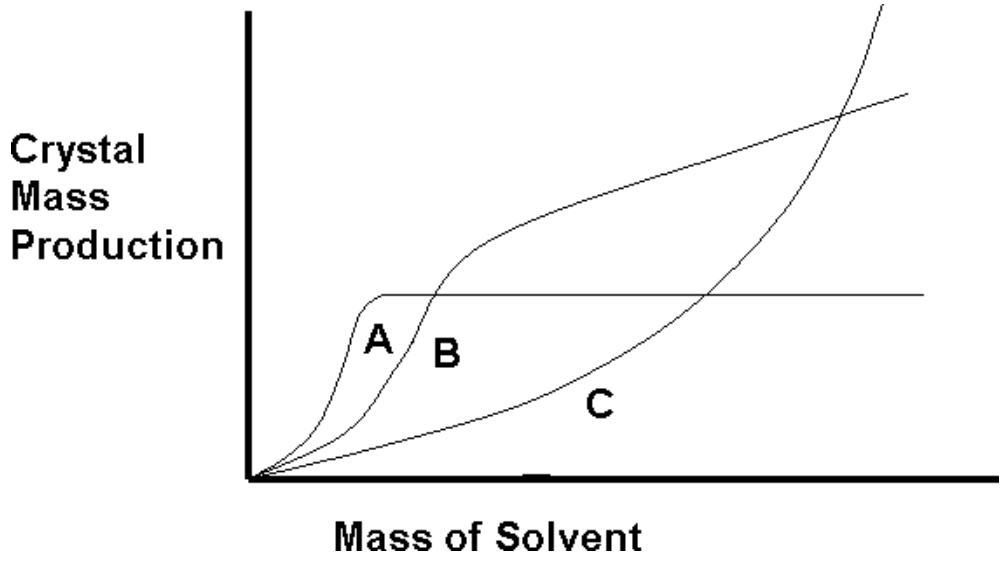

Figure 4. Hypothetical product distribution from fractional crystallization: solution becomes saturated with solutes at roughly the same times in the evaporation

In the simulation files provided by CH2M HILL, the feed contained sodium carbonate, sodium sulfate, sodium nitrate, sodium hydroxide and aluminum hydroxide in proportions similar to Single-Shell Tank (SST) Early Feed Solution. The total solute concentration was adjusted so that the solution would reach saturation at 60 °C after 200 grams (g) of water had been evaporated. Note that in Figure 5, burkeite saturates the solution after approximately 200 g of water have been evaporated. At that point in the process, the only solid that forms is burkeite and the mass of crystals of this species continues to grow, without other crystalline material being formed, until approximately 380 g of water have been evaporated. At that point, sodium nitrate begins to come out of solution and the mass of these crystals increases rapidly. At about the same time, sodium carbonate monohydrate saturates the solution and crystals of this species begin to form.

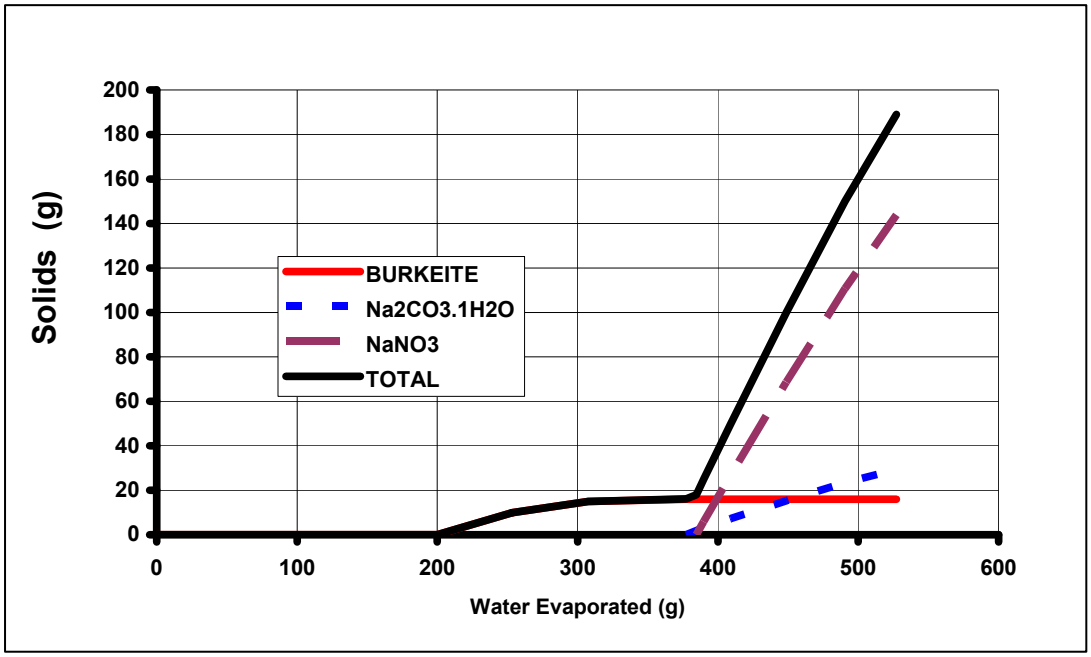

Figure 5. Mass of crystals produced in simulated evaporation of solutions containing sodium carbonate, sodium sulfate, and sodium nitrate at 60 °C (LAB3.XLS)

The behavior described is expected to be characteristic of all simulant solutions: SST Early Feed Solution and SST Late Feed Solution. Since the objective of the operation is to remove a significant fraction (more than 50%) of the sodium salts from the feed solution, irrespective of the counter ion, this behavior presents no apparent problem.

1.3 SEPARATION OF CRYSTALS FROM MOTHER LIQUOR

As described in the preceding section, the formation of crystals removes sodium salts and other species from solution. For this to be an effective separation process, the crystals must then be separated from the residual mother liquor by solid-liquid segregation. It is possible to do this by filtration, centrifugation, or other commonly used techniques. However, the nature of the crystals, in particular their morphology and size distribution, determine how easily they can be segregated from the mother liquor. In general, a narrow crystal size distribution leads to easier

separation than one that is broad; bulky crystals as opposed to flakes or needles also mean an easier separation.

For single-solute simple crystallization, the size distribution is determined by the nucleation and growth kinetics of the crystalline species. In fractional crystallization of the type characterized by the behavior in Figure 4, the nucleation and growth kinetics of each species leads to a determination of the final crystal size distribution.

As will be described in later sections of this thesis, considerable effort went into developing a means to segregate the complex crystalline solids from the mother liquor on a laboratory scale. Similar effort led to the development of a means to wash the mother liquor from the interstices of filter cakes produced in the experimental program. A secondary part of this work led to development of washing procedures that allowed sieve analyses to determine product crystal size distributions without significant distortion by crystal agglomeration.

1.4 CERTIFICATION RUNS AND CHEMICAL ANALYSIS

The culmination of studies leading to process protocols for each of the feed solutions (SST Early Feed and SST Late Feed) was performance of runs that were designed to test those protocols against the process specifications cited earlier. The masses of each stream were determined carefully, and appropriate samples were sent to Galbraith Laboratories (Galbraith) or Georgia Tech Research Institute (GTRI) for analysis. The results, which were obtained using Quality Assurance (QA) certified techniques, form the basis of demonstrating the applicability of the fractional crystallization pretreatment technology.

1.5 COMPARING ANALYTICAL RESULTS TO PROCESS OBJECTIVES

As stated above, the objectives of the technology described in the present thesis involve the cesium content of the recovered crystals, the recovery of sodium in the solid product, and the separation of sulfate ions from the liquid destined for feed to the Waste Treatment and Immobilization Plant. Minimum and desired targets for these criteria are as follows:

- Obtain a crystalline product that upon dissolution in water to a 5 M sodium concentration has a Cs content low enough to produce a specific activity of less than 0.05 Ci/L, and preferably less than 0.0012 Ci/L.
- Recover at least 50% of the sodium from the feed solutions as crystalline product, and preferably at least 90%.
- Produce a filtrate that has a molar ratio of sulfate to sodium less than 0.01, and preferably less than 0.0022.

The analytical results obtained from Galbraith and GTRI provide compositions of samples in wt % for major components and parts per million (ppm), which is mass of a species per million mass units of the sample. There are at least two ways to use such information to compare the outcome of a fractional crystallization run with Objective 1.

One method uses the compositions of the streams and estimates of the fraction of the total cesium in the streams of interest that is present as ^{137}Cs. To illustrate the methodology, assume that a sample of the final product crystals has been analyzed and found to contain 25 wt% sodium (Na) and 0.2 ppm cesium (Cs). The basis of calculation for determining if the product meets Objective 1 is to estimate the activity of a solution of this material containing 5 mole Na/L. As specified in the SOW, it may be assumed that there is 1 g ^{137}Cs/5 g Cs in typical

streams at Hanford. It may also be assumed that the activity of ^{137}Cs is 86.58 Ci per g of ^{137}Cs. This means, then, that the specific activity associated with the product is

$$5\frac{\text{mol Na}}{\text{L}}\times\frac{23\text{ g Na}}{\text{mol Na}}\times\frac{100\text{ g}}{25\text{ g Na}}\times\frac{0.2\text{ g Cs}}{1{,}000{,}000\text{ g}}\times\frac{86.58\text{ Ci}}{\text{g }^{137}\text{Cs}}\times\frac{1\text{ g }^{137}\text{Cs}}{5\text{ g Cs}}=0.0016\frac{\text{Ci}}{\text{L}} \quad (1)$$

This value can be compared to the criterion in Objective 1.

A second method for estimating the approach to Objective 1 is in terms of a decontamination factor (DF), defined as the activity of ^{137}Cs in real waste or the total cesium concentration in a simulant feed at 5 M sodium concentration divided by the corresponding activity or concentration in the salt recovered from the fractional crystallization process, also at a 5 M sodium concentration. The decontamination factors corresponding to Objective 1 are as given in Table 1.

Table 1. Required decontamination factors to meet objective on 137Cs activity

Feed Solution to Fractional Crystallization	^{137}Cs activity (Ci/L)		Decontamination Factor (*DF*)	
	Minimum	Desired	Minimum	Desired
SST Early Feed	0.05	0.0012	1.15	48
SST Late Feed	0.05	0.0012	—[1]	14

The decontamination factors can be estimated from the following relationship:

$$DF=\frac{\left[\text{activity of }^{137}\text{Cs (at 5 M Na)}\right]_{\text{feed}}}{\left[\text{activity of }^{137}\text{Cs (at 5 M Na)}\right]_{\text{waste}}}=\frac{\left[\frac{\text{ppm Cs}}{\text{wt \% Na}}\right]_{\text{feed}}}{\left[\frac{\text{ppm Cs}}{\text{wt \% Na}}\right]_{\text{waste}}} \quad (2)$$

where the compositions in the term on the farthest right are given by the analyses of crystals produced in the operation. For example, suppose the feed to a process contains 10 wt% sodium and 0.20 ppm Cs, and crystals produced contain 28 wt% sodium and 0.04 ppm Cs. Such results correspond to a DF of 14, which has been calculated as follows:

[1] Activity of feed is below minimum required; therefore minimum DF does not apply.

$$DF = \frac{\left[\frac{0.20 \text{ ppm Cs}}{10 \text{ wt\% Na}}\right]_{\text{feed}}}{\left[\frac{0.04 \text{ ppm Cs}}{28 \text{ wt\% Na}}\right]_{\text{waste}}} = 14 \quad (3)$$

1.6 VARIABILITY IN FEED COMPOSITION AND HOT CELL APPLICATION

The program is divided into three phases: Phase I and Phase II, which essentially differ only in the composition of the feed material, and Phase III, which involves the application of the technology to pilot scale. Phase I uses a non-radioactive simulant for the solutions being treated, while Phase II includes the use of both simulant solutions and actual tank waste samples for testing in a radioactive hot cell (Hammitt A.P et al.; 1979). The crystallization technology must first be developed at laboratory scale on simulated solutions previous to being implemented with actual waste to hot-cell environment and pilot scale.

Under the hot-cell conditions, due to the risks of contamination of operators and equipment by the radioactive waste, every unit operations is to be performed with automated arms (Figure 6). The successful preparation to hot-cell waste processing hence necessitates modifying the typical crystallization and post-crystallization processes to comply with these restrictions. These restrictions imply that: (1) efficient mass balance closures around each unit of the process must be achieved; (2) crystallization equipment must be easy to build in a restricted space, and (3) operating conditions (evaporation rate, evaporation profile, temperature, and processing time) must be optimized and easy to control. Furthermore, the experiments performed by Hanford's operators under hot-cell with apparatii and procedures identical to the

ones developed in this thesis, displayed identical results – i.e identical yields, population distribution, and requirements values-.

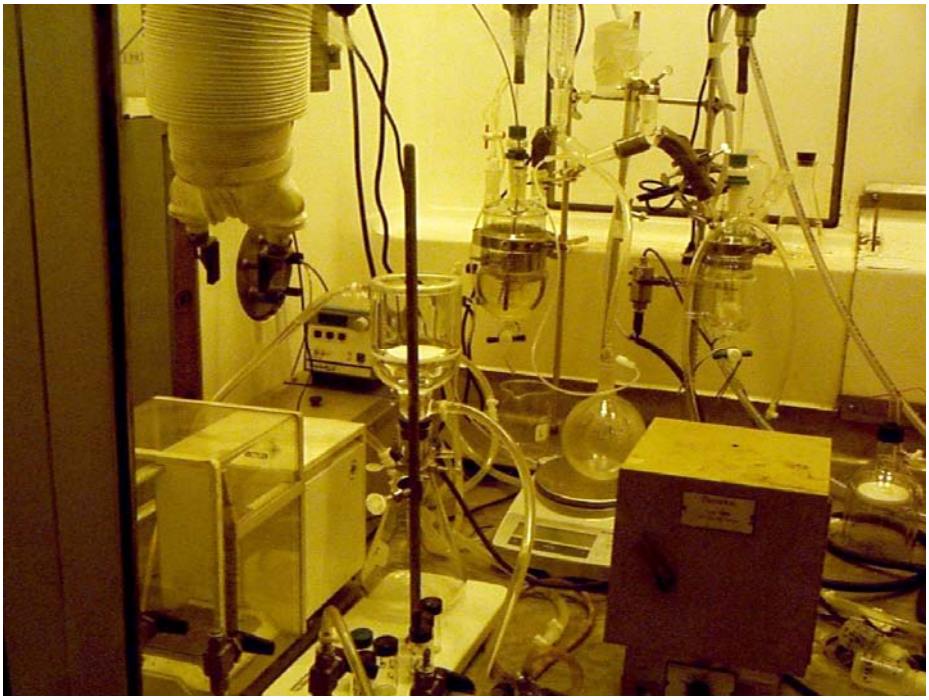

Figure 6. Reproduced crystallization process under hot-cell at Hanford site
(Courtesy of John Smith and Dave Bechtold, CH2M HILL)

Furthermore, the actual composition of the low- and medium-curie waste stored in the Hanford storage tank presents great variability from one tank to another. Variation in waste composition comes from (1) the early and late removal from the storage tank, and (2) the presence of organics compounds and solids particles in the early feed type waste. The impact of these variations must be studied in order to apply the evaporative crystallization technology to pilot scale.

1.7 OPERATING CONDITIONS VARIATION

The simulated waste solutions are composed of several sodium salts (among which sodium nitrate, carbonate, sulfate, oxalate, hydroxide and aluminate), trace of radionuclide species (cesium and technetium) and other insoluble species. The detailed composition of the

simulant solutions issued from the early and late removal of the single-shell tanks are presented in Table 2.

Table 2. SST early and late feed simulated solutions compositions

Chemical	MW	Species Molarities	
		Early Feed	Late Feed
$NaAlO_2 \cdot 2H_2O$	118.0	0.26	0.04
NaOH	40.0	0.62	0.01
Na_2CO_3	106.0	0.61	0.24
$Na_2C_2O_4$	134.0	0.01	0.01
KNO_3	101.1	0.02	0.01
$NaNO_3$	85.0	3.26	1.59
$NaNO_2$	69.0	0.51	0.07
Na_2SO_4	142.0	0.13	0.17
$Na_3PO_4 \cdot 12H_2O \cdot 0.25NaOH$	390.1	0.05	0.05
NaCl	58.4	0.07	0.01
NaF	42.0	0.01	0.1
$Na_2Cr_2O_7 \cdot 2H_2O$	298.0	0.02	0.009
$CsNO_3$	194.9	0.005 g/L	0.00035 g/L

Assuming that the insoluble species do not participate to the crystallization, several species are likely to form upon solvent evaporation depending on the operating variables (operating temperature, evaporation rate, evaporation profile, and operating time). Figure 7 displays Polarized Light Microscopy (PLM) images of the crystalline species that formed with simulated waste solution using different set of crystallization conditions.

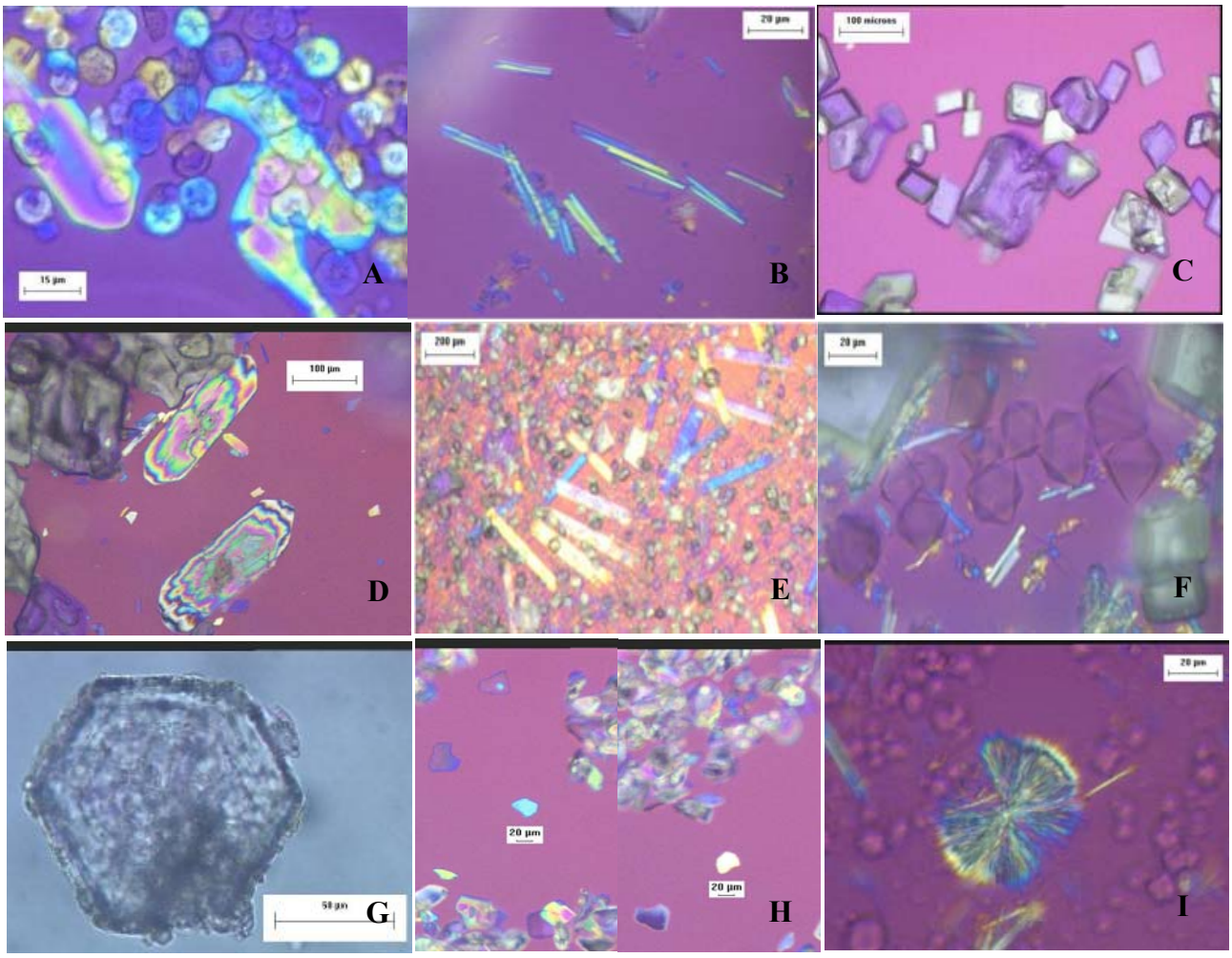

Figure 7. Crystalline species formed by SST early and late feed simulant feed solution crystallization at various operating conditions
(Panel A, burkeite crystal, Panel B, sodium oxalate, Panel C, sodium nitrate and sodium nitrite, Panel D, sodium carbonate monohydrate, Panel E, sodium phosphate, Panel F, sodium fluoride sulfate, Panel G, trisodium fluoride phosphate, Panel H, sodium sulfate, Panel I, sodium aluminate)

Phase II and Phase III evaporative fractional crystallization operation require thorough knowledge on the effect of operating conditions on population distribution, crystal size distribution, crystal yield, and crystallization kinetics. These elements are keys to the selection

of the process conditions and the development of accurate empirical models. An example of the effect of these parameters on the mass density distribution is presented in Figure 8.

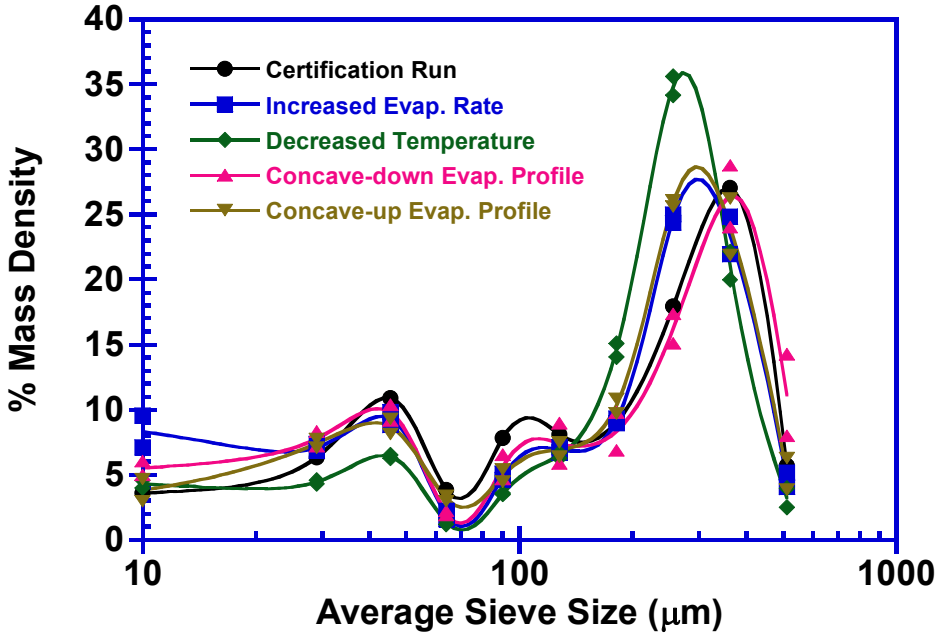

Figure 8. Measured dependence of mass density on operating conditions

1.8 CRYSTALLIZATION KINETICS

Phase I and II work involve the application of evaporative crystallization following a semi-batch approach. The nucleation points (operating time at which nucleation occurs), specific nucleation and growth rates may be obtained for batch processes under the base-case study conditions (early feed solution at 66 °C and 25 g/h evaporation rate) and varying operating conditions. By performing sampling at regular time steps and applying PLM analysis to the recovered samples, one can obtain the evolution of the crystal number and size with operating time. The specific crystallization kinetics may be computed from these profiles and used in developing a population balance based model for a continuous crystallizer.

1.9 OBJECTIVES

The following objectives are to be accomplished in the context of evaluating the feasibility of evaporative fractional crystallization pretreatment of Hanford radioactive waste:

(1) *Establish a laboratory system and formulate operating procedures that allow physical simulation of a large-scale fractional crystallization process that has been proposed for pretreatment of Hanford waste. Test the capability of the system by determining the approach to criteria whose achievement is deemed essential for a successful process.*

The nature of the medium-curie waste removed from the storage tanks at the Hanford site presents great variability from one tank to another. Such variability includes different compositions of the key sodium salts, the presence of organic constituents and solids, and differences in the effluent over the period of time a tank is being emptied. For the purposes of this study, primary emphasis was given to early-feed and late-feed compositions: i.e. solutions withdrawn early and late during the tank-emptying period. Two perturbations from these were examined: one that considered the effects of organic constituents and a second considering the impact of solids.

Using fractional crystallization for pretreatment is deemed feasible provided the following three targets are achieved: (1) recovering between 50 and 90% of the sodium in the solid stream diverted to the bulk vitrification, (2) removing the cesium with a decontamination factor higher than 14, and (3) obtaining a sulfate-to-sodium molar ratio in the liquid stream diverted to a waste treatment plant ranging between 0.01 and 0.0022. In the base-case study, the solution simulating late-feed being removed from the storage tanks has lower concentrations of sodium nitrate, carbonate, sulfate, aluminate, hydroxide, oxalate, and in cesium nitrate than the

early-feed solution. There are eight critical organic compounds (4 amines and 4 carboxylic acids) that have been identified as potentially having significant impacts on evaporative fractional crystallization. Moreover, the medium-curie tank waste also may include insoluble solid particles that could affect fractional crystallization. The effects of the organic compounds and the solids are to be assessed by (1) identifying the components or combination of components problematic for the process, (2) quantifying the impact on crystallization by comparing the crystal size distribution characteristics (coefficient of variation, number of modes, and fines concentrations.), and (3) quantifying the effect on solid-liquid separation by determining the corresponding separation time.

(2) *Determine the crystallization kinetics for the key sodium salts at the specific operating conditions of the simulated waste pretreatment; evaluate the effects of temperature and evaporation rate on the kinetics and develop appropriate models to describe those effects.*

The crystallization kinetics (nucleation and growth rates) of sodium salts from the simulant solutions play an essential role in determining the outcome of the Hanford waste pretreatment. Such kinetics control the population distribution, are influenced by variables such as temperature and supersaturation, set the total evaporation time based on thermodynamic simulation of the crystal yields, and have great impact on solid-liquid separations. In this study we plan to (1) determine experimentally the nucleation and growth rates of solutes crystallizing from the early-feed solution at 66 °C and an evaporation rate of 25 g/h and (2) quantify with an appropriate model the impact of temperature and evaporation rate on the specific crystal yields and kinetics.

Early work has shown that the interplay between nucleation and growth rates of the solutes present in the early feed solution produced a trimodal population distribution composed

primarily of sodium nitrate, sodium carbonate monohydrate, and burkeite crystals. For these species the specific kinetics and successive nucleation points are to be determined experimentally. Furthermore, the impact of the operating conditions on crystallization may be quantified by performing two series of experiments at variable evaporation rates and operating temperatures. The evolutions of the specific growth and nucleation rates with respect to the temperature and supersaturation may be used to derive two empirical equations modeling the crystallization kinetics of key solutes from simulated waste solutions. Further analysis of the empirical nucleation model will allow quantifying the final crystal yields of each crystalline species and monitor their evolution with respect to operating conditions. Similarly, the specific growth rate model may be used to compute the final population distribution evolution with respect to temperature and supersaturation. Finally, the actual crystal size distribution characteristics (spread, mode sizes and fines masses), direct result from the experimental crystallization kinetics, will be determined for the main case study and each set of operating variables.

(3) *Formulate a population balance model incorporating the kinetics from Objective 2 that can be used to assess the performance of a continuous evaporative crystallizer.*

The large-scale pretreatment of Hanford Waste is intended to be performed in a continuous operation. Therefore, there is a need to provide a framework within which the results from the experimental component of the present research—all of which were obtained using batch operations— can be used to explore the characteristics of products from a continuous crystallizer. A simple model will be developed describing the steady state crystallization of three major solutes (sodium nitrate, sodium carbonate and sodium sulfate) in a perfectly mixed crystallizer assuming that no crystal breakages or agglomeration occurred upon evaporation.

In the base case study, these solutes, whose feed concentrations correspond to the early feed composition, will undergo crystallization at 66 °C and 25 g/h evaporation rate. The nucleation and growth rates of each crystalline species were included in the overall population balance as a first approximation. Furthermore, making the realistic assumption of low and constant supersaturation, the total crystal population density function will be computed using each of the specific population density functions.

CHAPTER 2: APPARATUS AND PROCEDURES

The experimental apparatus and procedures used in performing the certification runs (the essential runs described in the Statement of Work) evolved as experience was gained in working with the different solutions comprising SST early feed and SST late feed. The evolution resulted from knowledge learned about feed-specific characteristics and interrelationships between solute crystallization and crystallizer configuration. The original system configuration is shown schematically in Figure 9. Although the same basic configuration was used in all runs, several modifications were made to address problems associated with accumulation of crystal encrustations on the walls and baffles of the crystallizer. The key modification was to add the capability of periodic addition of feed solution so that the active volume in the crystallizer was constant. Figure 10 is a photograph of the modified apparatus with a feed vessel positioned above the crystallizer. Note also that the reflux condenser has been removed from the system as it was considered unnecessary when the system was operated in the constant-volume mode.

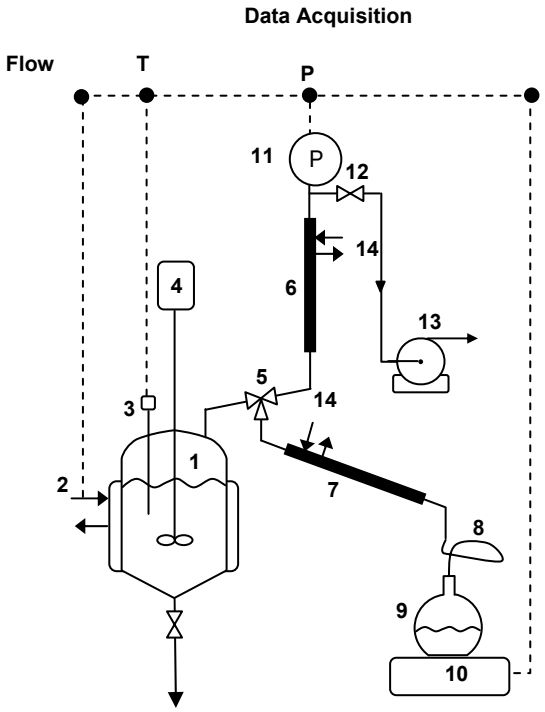

Figure 9. Schematic flowsheet of system used in all crystallization runs
(1) Crystallizer, (2) Heating Fluid, (3) Thermocouple, (4) Motor to Drive Stirrer, (5) 3-Way Valve, , (6) Reflux condenser, (7) Product Condenser, (8) Flexible Tube Adapter, (9) Condensate Collection Flask, (10) Digital Balance, (11) Pressure Sensor, (12) On-Off Valve Plus Metering Valve, (13) Vacuum Pump, (14) Cooling Water.

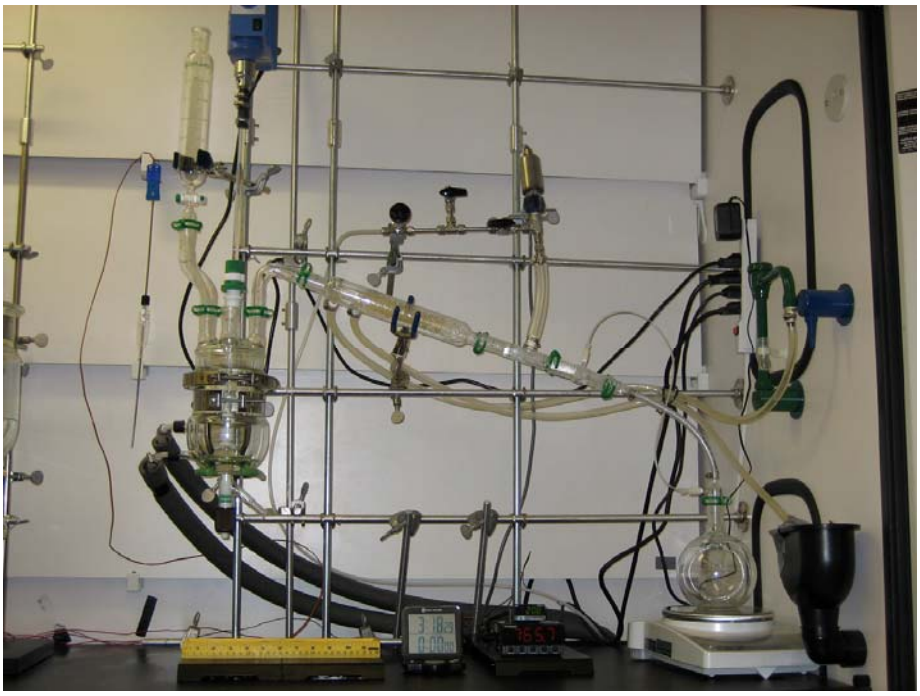

Figure 10. Evaporative crystallization system with 300-mL crystallizer installed at Georgia Tech laboratory

2.1 EQUIPMENT

The following items of equipment are described: crystallizers, filtration and crystal-washing apparatus, data-logging software and hardware, and analytical equipment (sieves and ro-tap, polarized light microscope, balances).

2.1.1 CRYSTALLIZERS

The vessels used as crystallizers were of 1-L, 600-mL, 300-mL and 100-mL nominal sizes, and the 1-L vessel is shown in Figure 11. The reason different sizes were used was to facilitate multiple-stage batch and semi-batch operations in which the volume of feed available for successive stages was reduced because of the vapor generated in preceding stages. For example, this would mean that if the batch feed was 1 L and 400 mL of condensate were generated in the first stage of operation, the available feed for the second stage would be approximately 600 mL, and so forth for subsequent stages.

The internals of the crystallizers included four equally spaced baffles that were contoured so that they rested on the curved portion of the vessel. The baffle cages for the three crystallizers are shown in Figure 12. They were manufactured in-house and designed so that they did not interfere with the impeller and accommodated other crystallizer internals. The four metal baffles fit snugly against the crystallizer wall.

Figure 11. 1-L vessel used as a crystallizer in preliminary experiments

Figure 12. Baffles used in the three crystallizers

From Left to Right in Each Photograph: 1-L, 600-mL, and 300-mL Baffle Cages.

The heads for the crystallizers had four openings: one was used for the agitator, one for vapor withdrawal, one for insertion of a thermocouple, and one for addition of feed or seed crystals. The feed vessel shown sitting atop the crystallizer in Figure 10 was used to add feed solution during the course of a run. The vessel has a valve that allows regulation of the flow of feed solution into a short length of glass tubing leaving the vessel. A length of tygon tubing is

connected to the glass tubing, and the end of the tygon tubing is adjusted so that the feed falls onto the active surface near the agitator in the crystallizer; in other words, the apparatus is designed so that the feed can be rapidly and thoroughly distributed upon entering the crystallizer.

The temperature of the crystallizer contents was measured by the thermocouple and readings were recorded on a computer. Heat was added to the system by a heating fluid that was pumped through the jacket of the crystallizer. The rate of evaporation was manipulated by adjusting the temperature of the heating fluid.

As vapor was generated in the crystallizer, it passed into a heat exchanger where it was condensed. The heat exchanger had cooling water flowing through a jacket. The condensate flowed from the heat exchanger through a flexible tube to a collection vessel resting on a balance. The condensate collection receiver was equipped with a pressure equalization Teflon tube to prevent accumulation of the condensate on top of the receiver. Readings from the balance were transmitted to and stored on a computer. A vacuum pump reduced the pressure in the system to the desired value.

The agitators used in the crystallizers varied according to the size of the vessel. For the 1-L and 600-mL vessels, two impellers were used. They are shown in Figure 13. A third smaller impeller of the same type as that shown on the left of Figure 13 was used in the 300-mL and 100-mL vessel when crystallizations from SST solutions were performed. The mixing intensity was controlled by an adjustable speed motor connected by a rubber tube to the glass shaft turning the impellers. It was important to have good mixing to keep the crystals, especially the larger ones, from settling to the bottom of the vessel; on the other hand, excessive intensity splashed liquid on the upper walls of the crystallizer, which contributed to scaling problems and subjected crystals in the system to possible attrition (breakage).

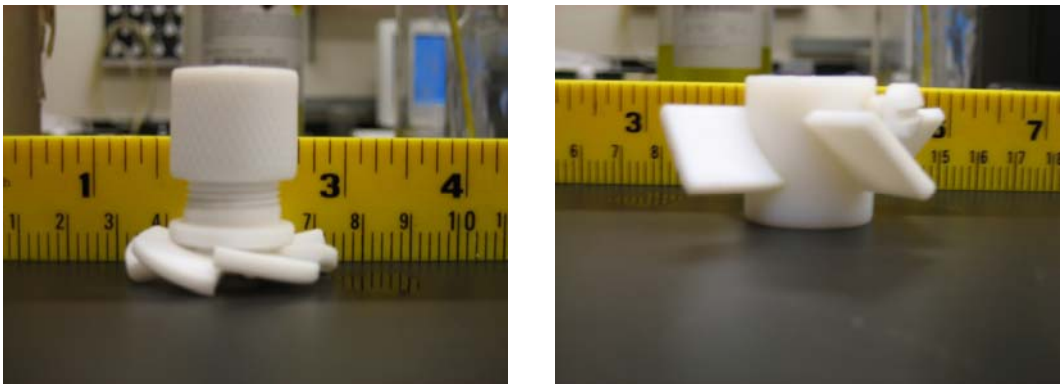

Figure 13. Impellers used in the stirred-tank crystallizers

(Both impellers were used in the 1-L and 600-mL crystallizers, with the one on the right positioned approximately a few mm from the surface of the slurry, while the one on the left was close to the bottom of the vessel. The impeller on the left was used alone in the 300-mL and 100-mL crystallizers.)

2.1.2 FILTRATION AND CRYSTAL WASHING

Two types of devices were used to perform filtration and washing on the crystals recovered from the SST solutions crystallizations. The first apparatus used to filter crystals from the slurry and to wash mother liquor from the filter cake is shown in Figure 14. It was designed by the research team at Georgia Tech; the design criteria included (1) a slurry volume of 800 mL, (2) the dimensions of the crystallizer and medium-frit filter previously purchased, and (3) the manufacturing limitations of the provider (Chemglass). The final drawings of the apparatus were sent to Chemglass for a quote and design confirmation, and the details of the apparatus manufactured by Chemglass are provided in appendix A.

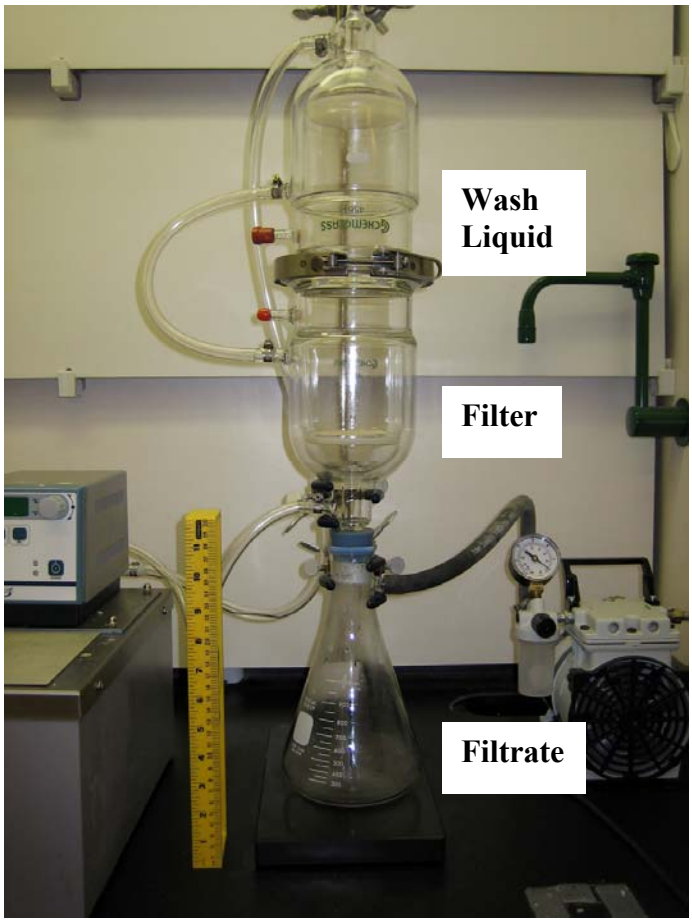

Figure 14. Apparatus used for filtration and washing

The filter has a glass frit onto which the process slurry was poured. It also could be possible to transfer the slurry directly from the crystallization vessel to the filter by drawing it through flexible tubing and into an opening just below the clamping ring. A vacuum was drawn on the filtrate receptacle, and the frit captured the crystals and separated them from the filtrate, which flowed through the frit and into the receptacle. At the conclusion of the filtration step, wash liquid (usually an aqueous solution saturated with the major solutes) was added to the upper vessel and then was drawn from the feed vessel through a perforated plate that dispersed the liquid over the filter cake. The filter and wash-liquid receptacles were jacketed and a fluid at a temperature corresponding to that of the crystallizer flowed through the jacket. The objective

was to maintain the temperature of the process slurry at a near-constant value. The vacuum pump in the picture pulled a vacuum in the filtrate receptacle.

This apparatus allowed filtration and washing to be performed under isothermal conditions since both top and bottom parts possessed a double jacket. It also provided good distribution of the washing liquid by forcing it to flow through a plate perforated with holes having a diameter of 1 mm. The distribution of the wash liquid provided superior washing efficiency. The system can be operated at atmospheric conditions or under vacuum.

The second apparatus used to perform the filtration and washing of the slurry corresponded to a regular double jacket medium frit filter, purchased from Chemglass. This device was used on the final experiments (experiments described in this thesis) due to its ease of implementation and operation under hot cell conditions. This very simple device had the advantages to allow performing filtration and washing under isothermal conditions and allow mixing of the filter cake during the two operations. The crystal washing was performed by pouring the wash solution onto the filter cake, mixing and pulling the vacuum through the medium frit filter. This method will be referred to the slurrying method in the following sections.

2.1.3 DATA LOGGING SOFTWARE AND HARDWARE

The data-acquisition system monitored temperature and pressure inside the crystallizer, along with the mass of condensate collected on the balance. Temperature was measured with a hastalloy thermocouple (T-type C-276 purchased from Chemglass) while pressure was monitored with an Omega transducer. These sensing devices were connected to meters for direct display of readings; analog temperature controller/display (CNi3253, Omega) and process meter controller (DP25B-E, Omega) for pressure reading. These meters were connected to a data

acquisition (DAQ) board (PMD-1208FS, Measurement Computing) for continuous recording of data. This board accepted voltage signals for data storage and connected to the computer through a USB port. The pressure transducer and temperature meter gave current outputs (4-20 mA), so 250 Ω resistors (249XBK-ND, Digi-Key) were used to convert the current signals to voltage signals compatible with the DAQ board. The digital balance used to measure the condensate mass (PB1502-S Mettler Toledo obtained from VWR) was connected to the computer through a RS-232 port. Due to the fact that multiple RS-232 ports were needed, a computer board was installed that provided four RS-232 connections (PCI-COM232/4-9, Measurement Computing). Readings from the DAQ board and the RS-232 ports were collected in a LabView program and the voltage signals from the DAQ board were calibrated to the corresponding temperature and pressure values. A simplified layout of the DAQ connections is shown in Figure 15.

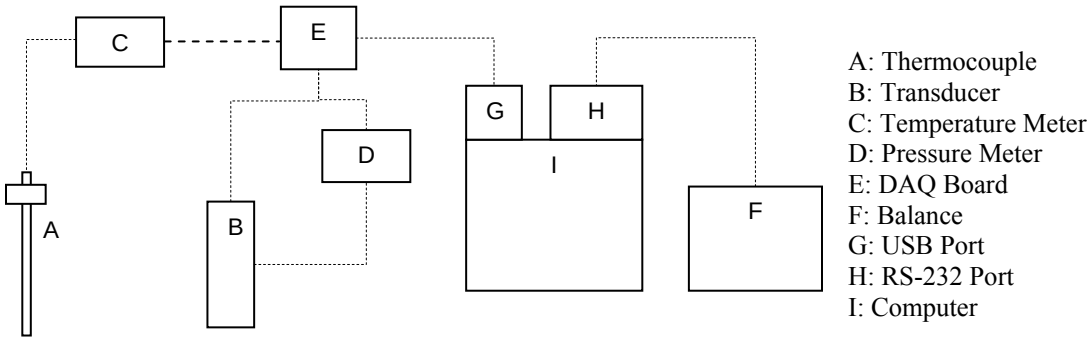

Figure 15. Data acquisition system setup

2.1.4 ANALYTICAL EQUIPMENT

Sieves and Rotap

Crystal size distribution (CSD) analysis was conducted by sieving on a Ro-Tap test sieve shaker (RX-29, serial 24210, Tyler) utilizing US standard sieve nests obtained from Dual Manufacturing Co. The sieving apparatus is shown in Figure 16. The shaker features a

combination circular motion along with a vertical vibration induced by an upper hammer tapping that allows good size segregation of crystals as they attempt to pass through the sieving apertures. The shaker can accommodate test sieves of 3-in., 6-in., or 8-in. diameter and can be adjusted to fit various numbers of sieves depending on their depth. In the present work, 3-in. diameter x 1-in. depth test sieves were used and the shaker was adjusted to accommodate a stack of 11 sieves, including the pan. Shaking time can be adjusted by turning a thumb screw until the desired value appears in a digital window. The shaker is placed on a stand inside a Ro-Tap sound enclosure cabinet to reduce the noise level.

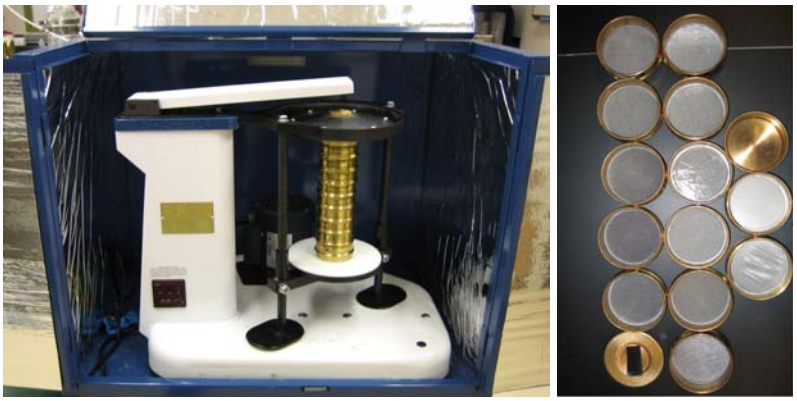

Figure 16. Ro-tap test sieve shaker placed inside a sound enclosure cabinet (left) and test sieving nests top view (right).

The test sieves are US standard sieves with brass frames and stainless-steel mesh. Table 3 shows the sieves available for the current analyses; they ranged in nominal aperture from 10 to 1180 μm. They were selected so that the ratio of aperture sizes on consecutive sieves is almost $\sqrt{2}$. Sieve tests were typically performed using the 38 to 850 μm nests, unless the operation involved particularly large or small crystals. In these cases the 10-, 20-, or 1180-μm sieves were used to provide a more accurate distribution. The sieves can hold about 27 g of sample mass, but only 15 to 20 g were used.

Table 3. Sieves used for CSD analysis

No.	ASTM Sieve No.	Nominal Sieve Opening (μm)
1	16	1180
2	20	850
3	30	600
4	40	425
5	50	300
6	70	212
7	100	150
8	140	106
9	200	75
10	270	53
11	400	38
12	635	20
13	850	10

All Sieves From Dual Manufacturing Co.

Polarized Light microscope (plm)

PLM images were obtained on a Meiji Techno trinocular polarizing microscope (Model ML9300), which is illustrated in Figure 17. Images are either observed in the eyepiece and/or acquired on a computer. The source of light in the microscope is provided by a Koehler-type illuminator with intensity controlled by a knob (6). The substage polarizer (5) is fully rotatable, sending polarized light within angles between 0–360 degrees up to the specimen. When the polarizer is swung-out, the light is un-polarized. The analyzer (16) is a slide-in plate mounted in an in-tube slider positioned after the specimen which moves the analyzer in and out of the optical path. When the analyzer is "in" and the polarizer (5) is swung in and set at 0 degrees, the elements are crossed and the field of view is said to be extinguished. In this condition the field of view is dark, except for an optically active specimen in the field path, which rotates the polarization angle and becomes visible against the dark background.

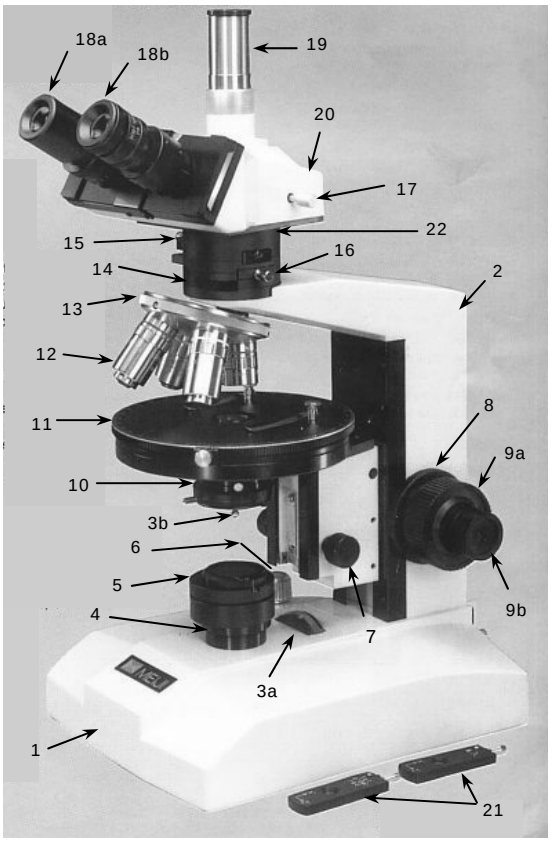

1 Microscope base
2 Microscope limb
3 Iris control (a) field (b) aperture
4 Koehler type illuminator
5 Polarizer, rotatable swing-out
6 Light intensity control knob
7 Substage focus control
8 Tension control knob
9 Focus (a) coarse (b) fine
10 Substage condenser (N.A. 1.25)
11 Rotating stage
12 Objective lenses (4, 10, 40, 60X)
13 Objective revolving nosepiece
14 Compensator slot
15 Bertrand lens aperture
16 Analyzer slider
17 Beam splitter lever
18 10X eyepiece (a) wide field (b) focusing cross-line
19 Photo tube
20 Rotatable 360°/60° inclination
21 Compensator plates (red and ¼ wave-length)
22 Switch-over beam splitter

Parts not shown in Figure
Camera attached to photo tube
Computer for image processing
Wrenches for objective centering

Figure 17. Polarized Light Microscope used in this project

Other elements of the microscope serve to improve the image quality. The iris diaphragm (3) and the condenser (10), a lens between the illuminator and specimen, are used to control the angle of the illumination cone that passes through optical train and improve the contrast. The circular stage (11) rotates through a full 360 degrees, with angular measurement ability, to facilitate orientation studies in polarized light. The objectives (12) are mounted in a rotatable ball bearing nosepiece (13) allowing easy swing of the required objective in the optical path. Objectives with 4X, 10X, 40X and 60X magnifying powers were utilized in this study. A 100X objective is also available but was not used. If the 100X objective is to be used, immersion oil must be applied to the specimen slide so when the objective is swung in, as the slide and the

100X objective are in good and bubble-free contact. The beam splitter (22) is used to switch the image between the binocular eyepiece (18) and the digital camera photo tube (19).

The focusing knob (9) allows course and fine adjustment of the distance between the specimen and objective for sharper images. The compensator (or retardation) plate (21) is a crystal that is selectively placed between the sample and analyzer to introduce a known optical path length difference to the re-combined light ray components and shift the colors of the generated images. The plates are sliding in a slot (14) cut in the tube just above the objective nosepiece (13). The microscope visual images can be observed through the eyepieces (18) or more conveniently snapped on a computer using a camera attached to the phototube (19). A photo camera (Sony DKC-5000, serial 10322) was used to generate digital images on a computer employing Image-Pro Plus (version 4.5.1.22, serial 41N40000-13717, Media Cybernetics Inc.) for image processing and manipulation.

A preparatory step to PLM operation is the preparation of good specimen slides with uncrowded fields (few crystals with empty spaces). Crystals are best viewed mounted in their mother liquor or in some solvent which will not dissolve the crystals, e.g., paraffin oil. Mounting them in air causes a large change in refractive index at the air-crystal interface and reduces the image resolution. Samples from crystallization experiments are normally taken from the slurry (or flash) solution at the end of the run using a plastic pipette. A small drop of the slurry is placed at the center of a 3”×1” plain slide (Part 2947, Corning) and preheated to the slurry temperature (40-60ºC). Then the drop is covered with a 22 mm circular glass cover (Part 12-546-1, Fisher Scientific) to spread the sample drop over the cover area. To test dry crystals, a small drop of paraffin oil (HR3-411, Hampton Research) is placed on the slide and a small number of the dry crystals are spread over the oil before they are covered with the circular glass.

The circular cover should rest evenly on the slide without any air spaces or crystal stacking. Such flaws can be fixed by gentle tapping on the cover with a spatula or by mild movement of the glasses.

The microscope may require some initial adjustments before its use; the major ones are illumination setup and objective centering. They would lead to good focusing, overlapping, and centering of the specimen image in the field of view, either in the eyepiece or computer preview screen. Illumination setup normally should be performed on each objective upon the use of microscope. A detailed procedure for optical setup and illumination adjustment is provided in appendix B. Objective centering is required less frequently if the microscope is properly treated. However, it should be tested from time to time to ensure good centering of the image. Centering can be simply tested by observing a crystal sample in the eyepiece with cross-line (18b). If the focused image of the crystal strays from the center of the cross-line upon stage (11) rotation, then the objective is slightly off the optical axis. The objective (12) can be centered using two hexagon keys supplied with the microscope accessories according to the procedure summarized in appendix B. The centering test must be performed for all the objectives attached to the nosepiece (13).

It should be noted that initial adjustments of the microscope while observing the crystal specimen through the binocular eyepiece (18) will also adjust the image in the computer display if the digital camera is well aligned with the optical path. The computer display is more convenient although the field of view is somewhat more limited than the binocular eyepiece especially at high magnifications. Size scales can be added to the recorded images for crystal size analysis. However, this requires a size calibration for each magnification objective using a 2.5 mm stage micrometer slide graduated with precise grids of 25, 100, 500, and 1000 μm. This

can be done by snapping an image of the scaled grids of the micrometer slide with each objective and use a grid of known length in the image to calibrate the length estimated by the Image-Pro Plus software. Details of the calibration procedure are provided in appendix B.

For PLM characterization of the crystallization runs, a sample is taken from the slurry solution and mounted on a preheated slide as described before. The slide is preheated to the temperature of slurry to minimize formation of additional crystals on the slide by cooling; therefore, the slides should be tested immediately after preparation.

To characterize:

- Turn on the illuminator and pass some light by switching the intensity control knob (6);
- Turn on the digital camera button and start the Image-Plus Pro imaging software menu on the computer desktop;
- From the main menu select the Video/Digital icon on the tool bar or from *Acquire* → *Video/Digital* commands to activate the Preview Page for video capturing and image setup.;
- Start the live preview by pressing "Start Preview." The preview will look white if the analyzer (16) is out. Make sure the substage polarizer (5) is swung in and set at 0 degrees then slide the analyzer plate (16) in. The live preview gets black because the polarizer and analyzer are crossed which prevents any light from passing through;
- Place the crystal slide on the rotatable stage (11) with the sample centered in the field of light and rotate the smallest objective, 4X, into position for focus. Crystal bodies should appear on the live preview;

- Modify the light intensity using the control knob (6) then focus down on the crystal slides with coarse and fine focus (9) until details can be seen. Most of the crystals in this study had a grey color with poor contrast so the red compensator (21) was used most of the time. The compensator turns the background into pink and improves the crystal coloring;
- Scan the whole crystal slide and study various crystals available in the sample. Crystal types can be identified from the shape and color of the crystals. Also rotate the stage about the axis of crystals and observe the change in colors and the extinction positions. These observations can be used to distinguish crystals which have similar shapes, e.g., sodium nitrate vs. sodium nitrite, sodium oxalate vs. sodium phosphate, etc.;
- Switch to higher power objectives by revolving the nosepiece (11) to enlarge crystal view and get more details. Switching between objectives requires re-adjustment of the lighting intensity and focusing;
- Desired PLM images can be recorded by pressing "Snap" from the Preview Page window. The recorded image will appear separately behind the live preview screen; and,
- Add a scale to the recorded image by pressing the Spatial Calibration icon (the vernier icon on the top right) on the tool bar or by selecting *Measure* → *Calibration* → *Spatial* sequence from the command Menu. A new small calibration window will open. From that window select the objective power from the drop menu list (4X, 10X, 40X, or 60X) then press "Mark" to write the desired scale, e.g. 100μ for the 10X images. The scale bar will appear on the image.

Move it to the desired location on the image then right click to fix it there. The image is finally renamed and saved in the desired location. These steps are repeated for every recorded image from the slide.

Crystal identification is carried out by comparing the crystal images obtained from our crystallization runs with typical PLM image of crystals found in Hanford waste tanks. The typical images were provided on a CD (Herting et al.; 2002).

Balances

Three different digital balances were used. Condensate mass was determined on a Mettler Toledo digital balance (PB1502-S, obtained from VWR) attached through DAQ board to a computer for continuous recording of the mass. Another Mettler Toledo digital balance (PG2002-S) was utilized for assorted measurements of beakers, chemicals, sieves, and experimental accessories. When extremely small masses were involved, a sensitive balance (Ohaus Analytical Plus, AP2500, serial M99315) was used; e.g., this balance was used for weighing small quantities of cesium nitrate in the preparation of simulant solutions.

2.1.5 CHEMICALS

Chemicals used in this project were sodium hydroxide pellets (NaOH, ACS grade), potassium nitrate (KNO_3, ACS grade), sodium nitrate ground ($NaNO_3$, ACS grade), sodium sulfate anhydrous (Na_2SO_4, ACS grade), sodium chloride (NaCl, ACS grade), sodium carbonate anhydrous (Na_2CO_3, ACS grade), sodium oxalate ($Na_2C_2O_4$, ACS grade), and sodium dichromate dihydrate ($Na_2Cr_2O_7 \cdot 2H_2O$, ACS grade) all from EMD Chemicals Inc., and sodium aluminate anhydrous ($NaAlO_2$, technical grade), sodium nitrite ($NaNO_2$, 97 + % ACS reagent), sodium phosphate dodecahydrate ($Na_3PO_4 \cdot 12H_2O$, 98 + % ACS reagent), sodium fluoride

(NaF, 99 + % ACS reagent), sodium acetate trihydrate ($NaC_2H_3O_2 \cdot 3H_2O$, ACS reagent) and cesium nitrate ($CsNO_3$, 99.99%) from Sigma-Aldrich. A polydimethylsiloxane heating fluid for the heater/circulator (Dow Corning 200, 5) was purchased from Ashland, Georgia.

2.2 CRYSTALLIZATION EXPERIMENTAL PROCEDURES

2.2.1 GENERAL OPERATIONS

There were two types of crystallization runs performed in the study: batch and semi-batch. Most of the early runs in Phase I were batch and, thus, involved adding a feed charge to the crystallizer prior to the start of the run and removal of product slurry after the requisite amount of vapor had been generated. Variables in such runs include the rate at which vapor is generated, operating temperature (pressure), and whether or not seed crystals are added.

Prior to the start of either a batch or a semi-batch run, water was boiled in the crystallizer to saturate dead spaces in the system with water. A known mass of deionized water was charged to the crystallizer and boiled for at least 20 minutes. This procedure saturated dead spaces in the glassware with around 15 g of water (determined from a mass balance around the system). A batch or semi-batch crystallization could then be done with the apparatus, and closure of mass balances around the system was enhanced.

Several difficulties were encountered with batch operation that led to use of the alternative semi-batch procedure for the certification runs. The primary and overriding difficulty was the quantity of vapor that must be produced to obtain the desired yield of solute. This led to production of a slurry of much reduced volume in a crystallizer of fixed dimensions. For example, the agitator in the largest crystallizer was designed to provide good mixing when the active volume was around 1000 mL; after nearly 60% of the charge had been vaporized, the

remaining fraction may very well fall at or below the impeller used to mix the slurry. In either case, the contents of the crystallizer were poorly mixed. Furthermore, as the level in the crystallizer fell, the exposed, wet walls of the crystallizer had a tendency for scale to form on them. This resulted in what was called accumulation in the system. An additional problem with using pure batch operation was that the amount of material recovered from the first stage of a two-stage process was too small to provide good operation in the second stage.

In the semi-batch procedure, an initial charge of the feed material was added to the crystallizer, and the conditions throughout the system were brought to their desired state: the pressure in the system was set, flow of cooling water through the jacket of the condenser started, mixing in the crystallizer begun, and all monitoring instrumentation started. At this point the flow of the heating fluid was started, and the temperature of the material in the crystallizer began to rise to a value that corresponded to the system pressure. When vapor began to form and produce condensate that entered the receptacle on the balance, the temperature of the heating fluid was adjusted to set the rate at which vapor was generated.

As vapor was generated, the feed solution was added manually from the vessel atop the crystallizer so as to maintain the level in crystallizer. This was done carefully so that the vacuum in the system was not broken. Vapor generation continued until crystals were observed in the crystallizer. At this point the evaporation was stopped and additional feed, which was unsaturated, was added to dissolve all of the crystals in the system. From this point on, the rate of evaporation was much slower than had been the case in the earlier phases of the run. Figure 18 shows data from an early run in which this procedure was developed.

The approach was chosen so as to minimize run time by rapidly evaporating water while the solution was undersaturated, but then to eliminate all crystals that had been formed under

such conditions; this was followed by slowly evaporating solvent to minimize nucleation in relationship to crystal growth.

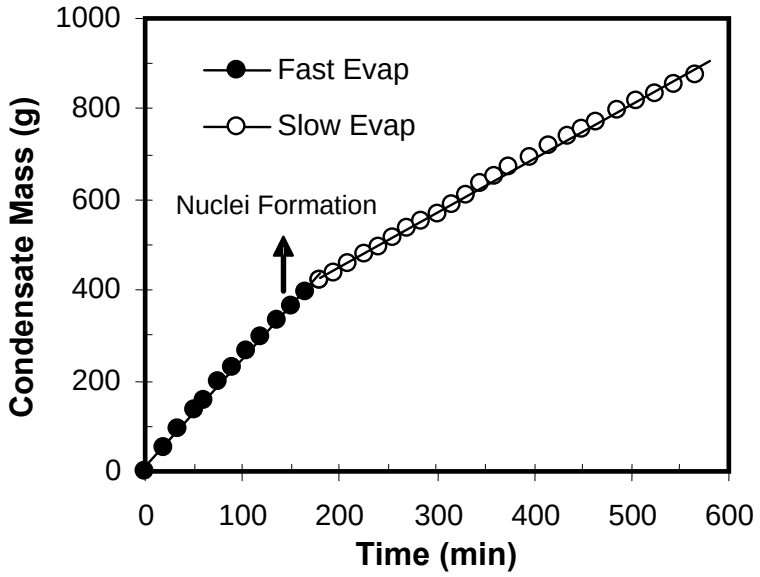

Figure 18. Plot of mass of condensate generated from an early semi-batch run in which rapid evaporation to saturation was followed by dissolution of crystals and subsequent slow evolution of vapor

The vacuum in the system had to be adjusted during a run to control the temperature of slurry in the crystallizer. This was necessary because there was an increase in the concentrations of non-crystallizing species as solvent was evaporated. The concomitant decrease in vapor pressure required an increase in temperature or decrease in pressure to continue evaporation. The regulating valve on the vacuum pump was closed slightly to increase the vacuum drawn in the equipment. Unfortunately, this tended to increase violent boiling of the solution in the vessel, which often led to splashing of the slurry on the upper walls of the crystallizer. Gradual closing of the valve somewhat mitigated this problem.

When the desired amount of condensate had been collected (as determined by a condensate-to-feed ratio set by a corresponding simulation), the monitoring Labview software was stopped and the final slurry was collected for subsequent treatment and characterization.

2.2.2 WASHING AND FILTRATION

The slurry was drained from the bottom opening of the crystallizer into a beaker, which had been heated to the temperature of the slurry, and transferred to the jacketed filter. In order to maintain a constant temperature, heating fluid at the crystallization temperature was pumped through the jacketed portion of the apparatus. As the slurry was transferred to the filter, a vacuum pump pulled a vacuum in the filtration flask in which the filtrate was collected. During filtration, the top half of the apparatus was disconnected from the filter, leaving the funnel open to the air.

The rate of slurry addition to the filter depended on the difficulty of filtration; this is generally a function of the size of the crystals, as fine crystals, especially when part of a broad distribution, have a tendency to plug the filter and slow the rate of filtration. When extreme problems of this kind were encountered the difficulty was mitigated by using three jacketed filters mounted in parallel so as to process the slurry as rapidly as possible. It was important to keep access to the slurry during the filtration step in order to mix it with a Teflon spatula. Such mixing sped filtration by alleviating filter plugging.

After the filtration step, the filtration flask was changed, the mass of unwashed solids determined, and the wet crystals returned to the filter. The top half of the apparatus was placed in position and sealed. At this time the upper valve was put in the closed position and the washing solution loaded into the funnel. The vacuum pump was turned on to decrease the

pressure inside the vessel and then the upper valve was opened to distribute the solution through the perforated plate.

2.2.3 ACCUMULATION REMOVAL

Accumulation of crystalline material on the walls of the crystallizer above the baffle cage was considered another major product from a run. Although attempts were made to minimize the amount of this material, it was almost always found after a run had been completed. Of course, it had to be collected at the end of a run and its mass determined for closure of mass balances.

In order to collect the accumulation, the condenser and agitator (with its motor) were removed from the apparatus and the vessel lid was removed. The solids that remained on the walls and baffles were collected carefully using a spatula; they were then weighed and stored in a sealed bottle for further analysis. Solids that could not be recovered contributed to non-closure of mass balances.

2.2.4 PREPARATION OF WASH SOLUTIONS

All stages of the certification runs included a washing step that used an aqueous solution of sodium nitrate and sodium carbonate. Sodium hydroxide was also included in the wash solution so that alkaline conditions were maintained. In all cases, the wash solution was prepared in a beaker of known mass and the salts were added in measured quantities. Water was added slowly to the salt mixture and the beaker was placed on a hot plate stirrer, which turned a magnetic stir bar that had been placed in the beaker, and the solution was brought to the desired temperature. Once the solution reached the appropriate temperature, additional water was added

until all crystals had dissolved. Before using the wash solution, the full beaker was weighed to determine the amount of water added to the solution.

2.2.5 STAGE TWO PREPARATION

In a two-stage crystallization run, the filtrate from the first stage was the feed to Stage 2. A known amount of water was added to the filtrate to dissolve any crystals that had formed as the filtrate cooled. This also was necessary to preserve the integrity of samples of the filtrate; i.e., without dilution, the filtrate quickly became a two-phase mixture that would have been difficult to analyze. In any case, the diluted filtrate was used as feed for the second stage, and the ratio of pure filtrate to dilution water was used in mass balance calculations. All other procedures for operating the second stage were identical to those followed for the first stage.

2.2.6 MASS BALANCE AND LOSS ESTIMATE

Continual improvement in procedures led to mass balance closures to within 3% for each stage of the certification runs. The tare weights of all beakers and flasks were determined before use and after they were filled with the designated process stream (slurry, accumulation, etc.). The beakers were also weighed after they have been emptied to determine the amount of residual mass remaining in the beaker. Other possible losses of mass came from (1) the crystallization vessel, (2) the filtration apparatus, and (3) the washing apparatus. In order to account for accumulations in each apparatus, they were each washed with a known amount of water, and the collected water was weighed to determine the amount that remained in the apparatus. In order to account for wash water that remained on the inner wall of the vessel or filters, a dry laboratory paper of measured mass was used to collect this water. To close the mass balance further, all the

accessories (Teflon and metal spatulas) used during the experiments were washed with a known amount of water. The addition of a trap before the vacuum pump reduced water loss through the pump during a run and collected water could be included in the overall mass balance.

The overall mass balance data are presented in tables similar to that shown in Table 4. These tables give the mass and species composition of each element and provide data in three columns: (1) *Input*, corresponding to the feed and wash solution, (2) *Output*, including the condensate water ("cond"), the washed solids (final crystals obtained after the washing step), the filtrate (liquid obtained at the end of the filtration step), the spent wash (liquid obtained at the end of the washing step) and the accumulation (solids remaining on the wall of the crystallizer at the end of the evaporation), and (3) *Loss,* which corresponds to the difference between the total input mass and the total output mass. Percentage loss is given as two values in the bottom two rows. The first corresponds to the overall closure percentage when no observable mass losses are accounted for. The second is the closure value deduced after all known losses are accounted for (following the procedures explained above). The mass balance data are also represented by a flow diagram summarizing the mass and flow patterns of all streams in addition to various processes and stages used in the experiment. Figure 19 gives an example of such a flow diagram. In both overall mass balance closure table and flow diagrams, the wash was performed using a solution saturated in the main sodium salts (typically sodium nitrate, carbonate, sulfate, fluoride, phosphate and hydroxide). The prepared solution was filtered to ensure saturation and the mass of the solution was measured before and after use.

Table 4. Example of a mass balance table (SST early feed run prior to certification run)

	Input (g)		Output (g)					Loss (g)
Species	**Feed**	**Wash**	**Cond**	**Washed Solids**	**Filtrate**	**Spent Wash**	**Accum. Solids**	
	6479.97							
H_2O		330.58	4482.99					
Na_2CO_3		56.36						
$NaNO_3$		233.2						
Solution				469.25	1205.2	639.91	4.16	
Total	6479.97	620.14	4482.99	469.25	1205.2	639.91	4.16	298.6
Combined	7100.11		6801.51					298.6
						Loss (%)		4.21%
						Corrected loss (%)		3.5 %

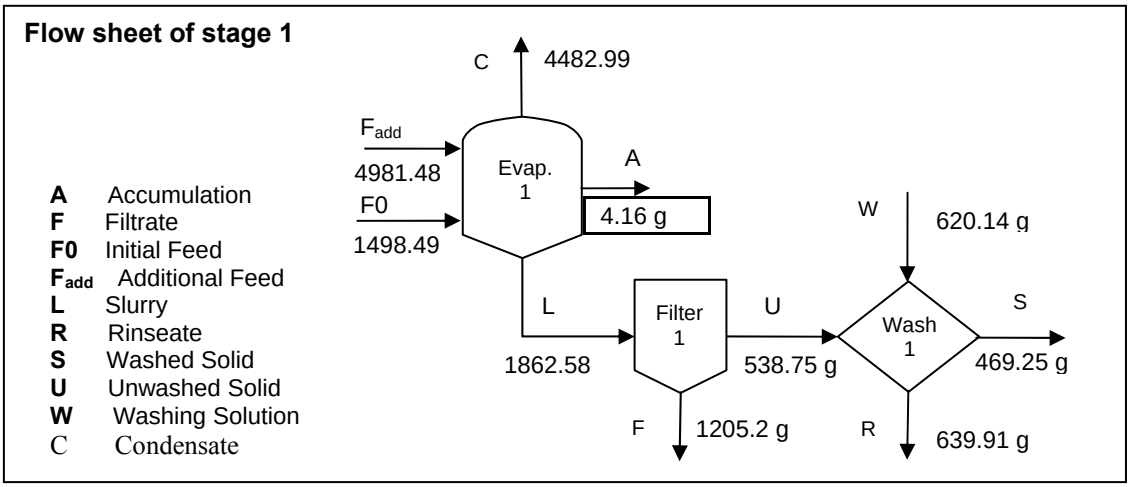

Amounts shown in grams.

Figure 19. Example of flow diagram

2.2.7 CHEMICAL ANALYSIS

Chemical analysis was required in order to perform species mass balances and determine whether or not specifications given in the SOW had been met. For each stage in the certification runs the following samples were taken: feed solution, filtrate, spent wash, unwashed crystals,

accumulation, and final crystals. These samples can be seen graphically in a two-stage schematic shown below in Figure 20. In order to ensure homogeneity in the samples and eliminate sampling uncertainties with two-phase mixtures, dilution water was added to the spent wash, filtrate, unwashed crystals, and accumulation. The amount of water added to each pure sample was recorded so mass balance calculations could be performed accurately. The only samples sent for analysis in solid form were the final crystals obtained from the certification runs.

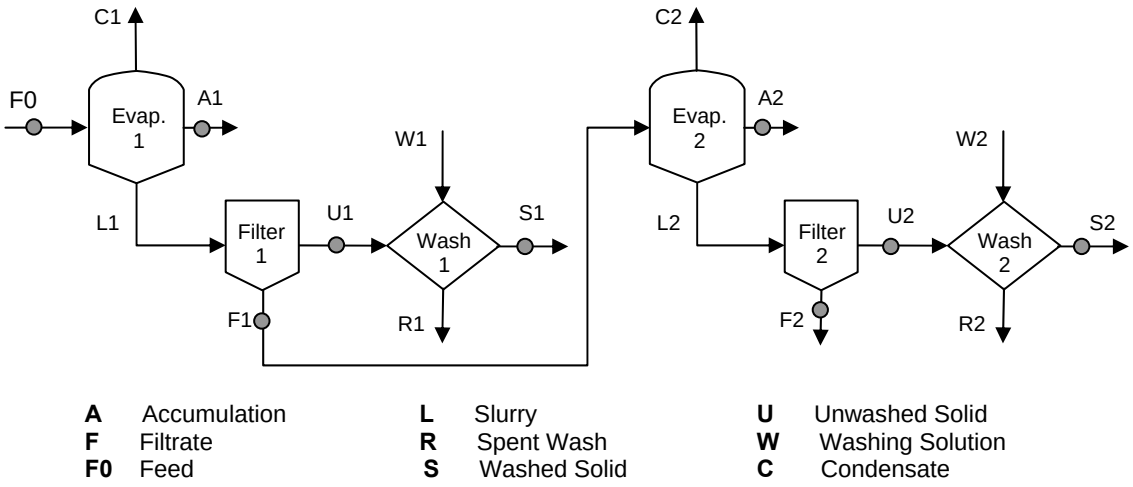

(Sample points marked with gray circles)

Figure 20. Schematic of the two-stage certification runs

2.2.8 SIEVING PROCEDURE

Crystal agglomeration was the major problem affecting CSD analyses throughout the test runs. Microscopic observation of samples taken directly from the crystallizer proved that agglomeration plaguing CSD analysis was not a result of events within the crystallizer, but rather an artifact associated with filtration and drying of product crystals. It was caused by residual traces of mother liquor on crystal surfaces after filtration and/or washing that led to crystallization of solute from the mother liquor as the solvent was evaporated; as this material crystallized it bound adjacent crystals into agglomerates. To reduce this phenomenon, two extra

steps were introduced to the procedures followed prior to sieving. First, the final washed crystals were flushed with a hydrophilic solvent (acetone) to wash any residual mother liquor from the crystals and reduce the extent of agglomeration. Then after drying, the crystals were subjected to a manual, gentle separation process to disrupt any remaining agglomerates. The overall sieving procedure summarized below was applied to all certification runs.

All of the product crystals that had been washed with saturated solution were placed in the washing/filtration apparatus and washed with an approximately equivalent mass of acetone. The acetone was introduced from the top part of the washing apparatus and was evenly distributed over the crystal sample upon being drawn into the filtering flask. The crystals were then collected, spread wide on a pan and left overnight to allow evaporation of residual solvent.

Washing with acetone did not totally eliminate agglomeration, but significantly reduced it; some crystal agglomerates still appeared in the dried crystals. These agglomerates would contribute significantly to the sieve fraction larger than 500 μm and negligibly to the fraction less than 200 μm. It was found that these agglomerates could be disrupted with gentle manipulation using a spatula. Microscopic observation confirmed that such manipulation did not break the constituent crystals, but it did improve the true representation of single crystals that is required for representative CSD data.

The selection of sieve sizes to use in an analysis depended on the size of crystals generated in a run. Guidance was obtained from the simulation files (e.g., sodium nitrate is often over 100 μm while burkeite is about 20 μm) and from visual observations of crystals grown during the experiment. All sieve analyses were performed with the 38 to 850 μm test sieves. If fine crystals (< 38 μm) were significant in the crystal sample (by having large mass collected in

the bottom pan), they were further separated by using 10- and 20-μm sieves in place of the two largest aperture sieves.

Each sieve analysis was performed with 10 sieves in a nest, in addition to the bottom pan and the cover. The sieves were rinsed with hot water and dried in an oven prior to use. The empty weight of individual sieves was recorded and they were stacked in a nest, from top to bottom in order of decreasing openings. A 15 to 20 g sample of the crystals to be analyzed was then added to the top-most sieve and covered. The sieve stack was assembled and loaded in the Ro-Tap. The timer was adjusted to 30 min and the machine was started.

When the operation was completed, the stack was removed and each sieve was weighed; the tare weights of the sieves were subtracted from the final weights to determine the mass of crystals recovered on each sieve. By definition, the crystals collected in each nest ranged in size from the aperture of the sieve opening to that of the sieve above the one being analyzed; for example, crystals collected in the 38-μm sieve were between 38 and 53 μm (the upper nest according to Table 2) in size. These data were then used to evaluate the crystal size distribution, which could be expressed as histograms, density functions, or cumulative distributions. Samples were collected from several of the sieves and held in vials for further analysis by polarized light microscopy. Such analyses facilitated determination of the crystal composition in each size range and detection of crystal breakage or agglomeration. A simplified sieve test procedure is present in appendix C.

2.2.9 PRELIMINARY RUNS

To become familiar with the experimental apparatus and prepare for certification runs, numerous runs were performed on simple salt solutions. A total of 90 runs (including the certification runs) were done in the laboratory. The simple salt solutions began with sodium

nitrate and evolved to a more complicated mixture of sodium nitrate, sodium carbonate, and sodium sulfate and also included attempts at seeding (see Appendix D). Initial runs were purely batch crystallizations where the heating bath was maintained at a constant temperature and pure water was used for crystal washing. During these runs experience was gained with the crystallization equipment, which led to the final apparatus design and crystallization procedure. The procedure involved running semi-batch crystallizations at constant volume, varying the heating rate to promote crystal growth, and washing with a saturated solution to maximize the mass of final crystals. A listing of all crystallization runs is given in Appendix E.

2.2.10 RESULTS VALIDATION BY X-RAY DIFFRACTION

The distribution of the chemical species within the different size ranges can be obtained by comparing the PLM images and x ray diffractograms of the sieved crystals. X ray diffraction measurements were performed with XRD equipment from the Xpert Pro family. The diffracted optics was performed with a X celerator detector, an anti-scatter of 5 mm and a soller of 0.04 rad. No collimator or filter was used for the diffracted optics. The incident beam optics used a divergence slit of 1/8, an anti-scatter of ¼, nickel filter, a soller of 0.04 rad, and a mask of 5mm. no mirror was used for the incident beam optics. The XRD analyses were performed with the Xpert Highscore software 2.0 from Panalytical, Inc. The software possesses a built in library of the common species diffractograms and crystallography properties. The software allows the qualitative and semi quantitative analysis of the diffractograms from powder diffraction samples.

An illustration of validation through XRD is provided by the diffractograms in Figure 21. The diffractograms in Figure 21 were obtained from the powder XRD measurements and analysis of sieved crystals obtained from a preliminary run performed on early feed solutions.

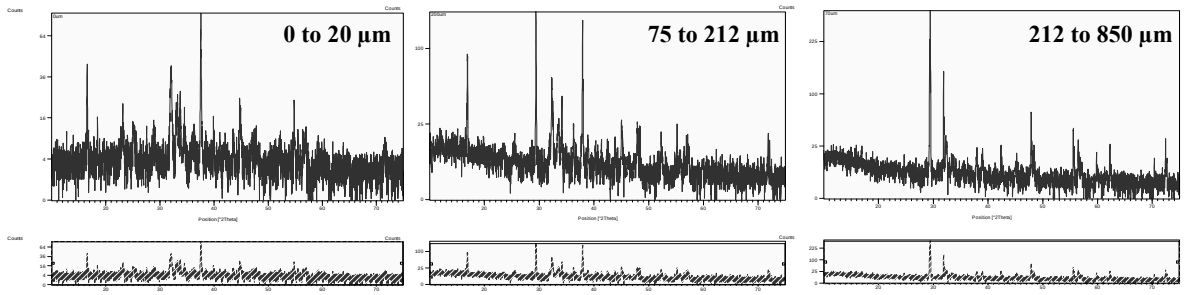

Figure 21. Series of diffractograms from preliminary early feed crystallization experiment

The PLM analyses on sieved crystals from the first stage showed that:

- The 500 µm size range was exclusively composed of single sodium nitrate crystals with sodium nitrate agglomerates observed in the 600 to 850µm size range.
- The crystals in the 53 to 75 µm size range included mainly sodium carbonate monohydrate and sodium nitrate crystals with sodium carbonate monohydrate was observed in sieves up to 200 µm.
- The 0 to 53µm size was composed of sodium nitrate, sodium carbonate monohydrate and trace amounts of sodium sulfate, sodium oxalate, sodium nitrite and burkeite.

The series of diffractograms obtained from the sieved crystals from Stage 1 showed that three main changes in peaks position. The diffractograms for the crystals ranging between 212 and 850 µm had one specific series of peaks which corresponds to a unique species identified as sodium nitrate. The diffractograms for the crystals ranging from 75 and 212 µm displayed an additional series of peaks. The two species identified were sodium carbonate monohydrate and sodium nitrate. Finally, from 0 to 75 µm more than two series of peaks were present. Sodium nitrate, sodium carbonate, sodium sulfate, sodium nitrite, sodium oxalate and burkeite were identified. Furthermore, the intensity of the peaks corresponding to sodium nitrate increased in

the series of diffractograms from the pan to 850 μm size. The concentration of sodium carbonate monohydrate also increased from 0 to 106 μm and decreased from 106 to 212 μm based on the peaks intensity.

2.3 MODIFICATIONS FOR HOT-CELL IMPLEMENTATION

2.3.1 CRYSTALLIZATION APPARATUS

The constancy and control of the operating temperature is a key issue for the scale down crystallization to be performed in the hot cell environment. The experimental apparatus was modified to achieve a higher vacuum (lower pressure) so that the system temperature could be maintained as the dissolved solids content increased. A vacuum pump with an ultimate pressure of 1.5×10^{-2} torr (compared to 9 torr that could be achieved by the previous pump used for Phase I experiments) was installed in the system.

With the help of a tesla coil, it was determined that there were a few small leaks around the necks of both Stage 1 and Stage 2 crystallizers. The leaks were sealed by a glass shop as described below in more detail. In addition, the vacuum was also increased by reducing the resistance to gas flow between the crystallizer and the pump. This was done by replacing the ¼ in. OD- (0.035–in. wall) stainless steel tubing with 3/8–in. tygon vacuum tubing and by eliminating two unnecessary control valves. With these changes, shown in Figure 22B and Figure 22C, the system achieved a pressure of 7 torr.

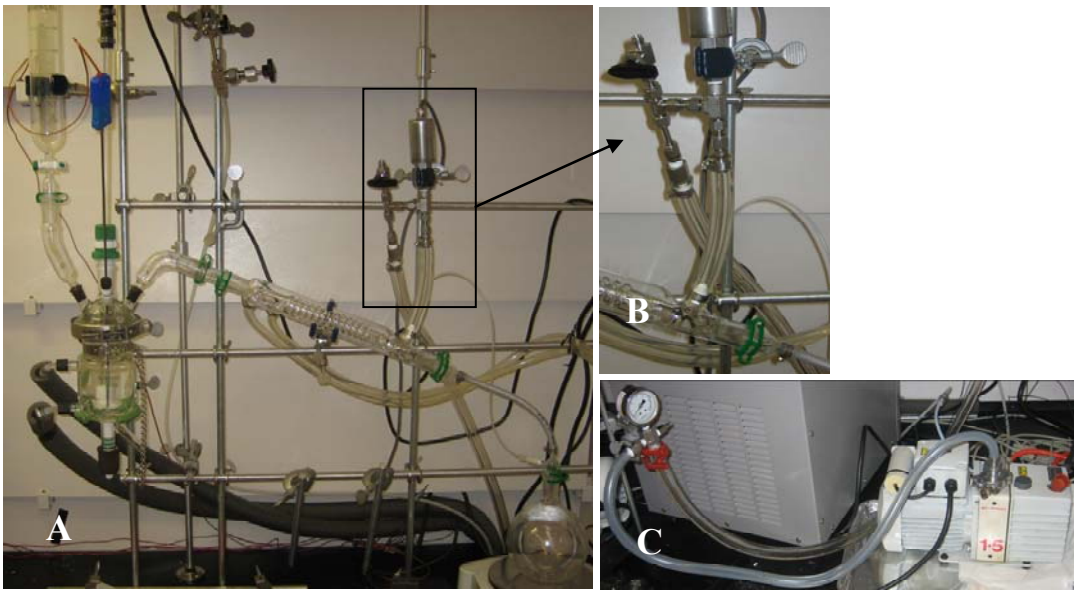

Figure 22. New equipment setup
(Panel A, main view, Panel B, zoom on pressure sensor, Panel C, new vacuum system)

The glass connections of the 300-mL vessel lid were treated with ground glass and sealed with wax as presented in Figure 23. The wax (Apiezon® W) is resistant to a temperature of 150 ˚C and is not likely to add any impurities to the slurry during the runs. The tesla coil was used to demonstrate that the treatment of the vessel lid eliminated the leaks described above. In addition, having one continuous piece of glass makes assembly of the apparatus much easier. This should be especially helpful for the case of hot cell experiments.

Figure 23. 300-mL vessel lid

Similar modifications were performed on the 100-mL vessel lid, as shown in Figure 24. In addition to sealing the connections, the enlarging adapter was eliminated to simplify the equipment and reduce its length.

Figure 24. 100-mL vessel lid

Another modification was the improvement of the condenser, which was flattened on downstream side to avoid collection of water in a dead space. In addition, the condenser length was considerably reduced by adding the vacuum outlet and the pressure equalization opening to

the condenser. This eliminates the connecting adapters that were previously used for these purposes. The new condenser, shown in Figure 25, will improve water collection, reduce the size of the apparatus, and simplify assembly.

Figure 25. New condenser

2.3.2 CRYSTALLIZATION PROCEDURE

Heating Medium

Due to restrictions at the Hanford laboratories, silicone oil could not be used as a heating medium. For this reason, water was used to replace silicone oil. The use of water induced the formation of gas bubbles in the double jacket that revealed to be only temporary and disappeared after the first experiment. These bubbles would not directly affect the crystallization run, but would be likely to reduce the heat transfer efficiency. The use of water also induced a limitation on the evaporation rate since the evaporation is controlled by the temperature difference between the heating medium and the slurry temperature. To perform crystallization under very high evaporation rate, the temperature of the heating fluid might be increased to a temperature close to the water boiling point making necessary the regular control of the water level inside the heating bath.

Accumulation handling

A simpler way to handle the accumulation generated during the process was developed. After draining the slurry, the accumulated crystals were redissolved by adding a known amount of water to the crystallizer. This allowed estimation of the mass of accumulation, and it also

eliminated the need to disassemble the apparatus for cleaning. This simple method should be particularly useful for hot-cell experiments.

2.3.3 CONTROL SYSTEMS

In order to help automate the crystallization process for future hot cell experiments, two control systems were proposed.

The first controlled the heating bath temperature using the scheme in Figure 26. The heating bath would be controlled through LabView by specifying a temperature difference between the slurry and the heating fluid. For example, during the initial phase of each stage, this difference could be set to 15 ^{o}C for rapid evaporation, and then lowered to 5 ^{o}C for the portion of the run during which there is slow evaporation. In Figure 26, the temperature difference is set to 5 ^{o}C, and if the temperature difference drops below that value the program will increase the heating bath temperature. This program has been added to the laboratory control scheme and was used in the majority of the SST solutions experiments.

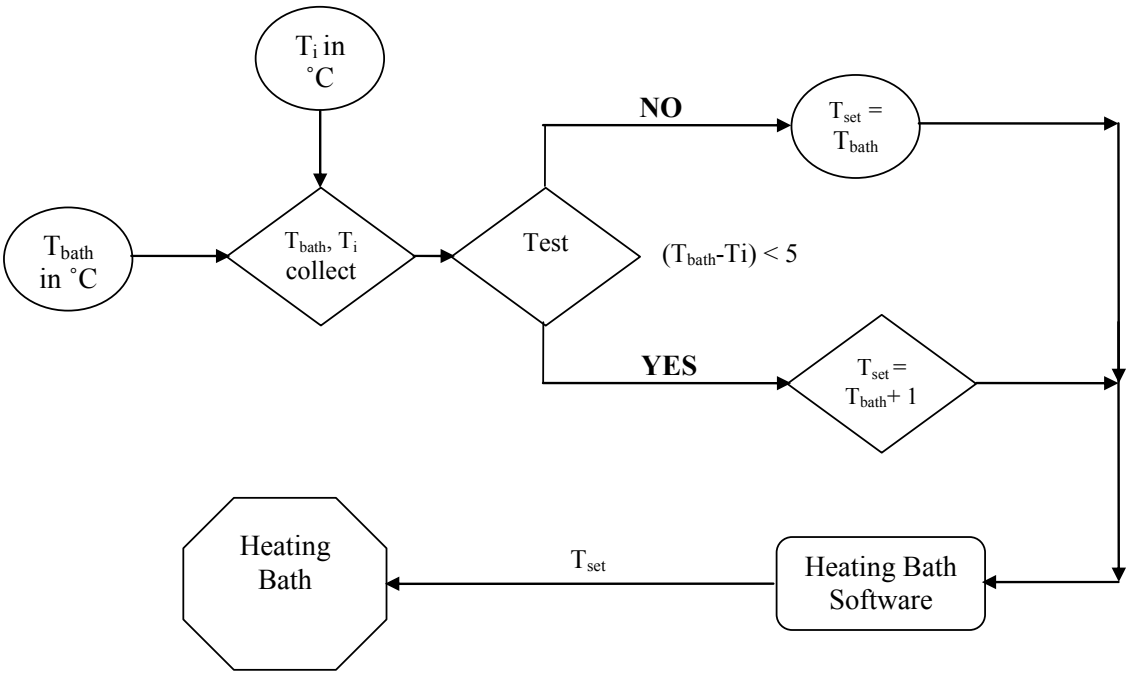

Figure 26. Heating bath control diagram

The second process improvement involves control of the system pressure. Reducing the pressure too rapidly causes intense boiling and subsequent accumulation of crystal mass on the walls of the crystallizer. Digital regulators, such as the one manufactured by J-KEM Scientific, Inc, can be automatically controlled through LabView software, and are advertised to regulate the pressure within +/- 0.1 torr. This device would increase the sensitivity of the manually operated valve used to reduce the pressure inside the crystallizer. The proposed control system is outlined in Figure 27.

In this control system the pressure will be varied based on the slurry temperature. If the temperature of the slurry begins to rise above the target value (40 ^{o}C in the above example), a new pressure set point will be created and the regulating valve will close slightly to reduce the pressure and, thereby, maintain a constant temperature. Maintaining the pressure in this manner should reduce the amount of accumulation that forms on the walls of the vessel.

Implementing the control schemes described above should eliminate most of the manual tweaking of controls during the crystallization process. This may facilitate operations in controlled hot-cell environments.

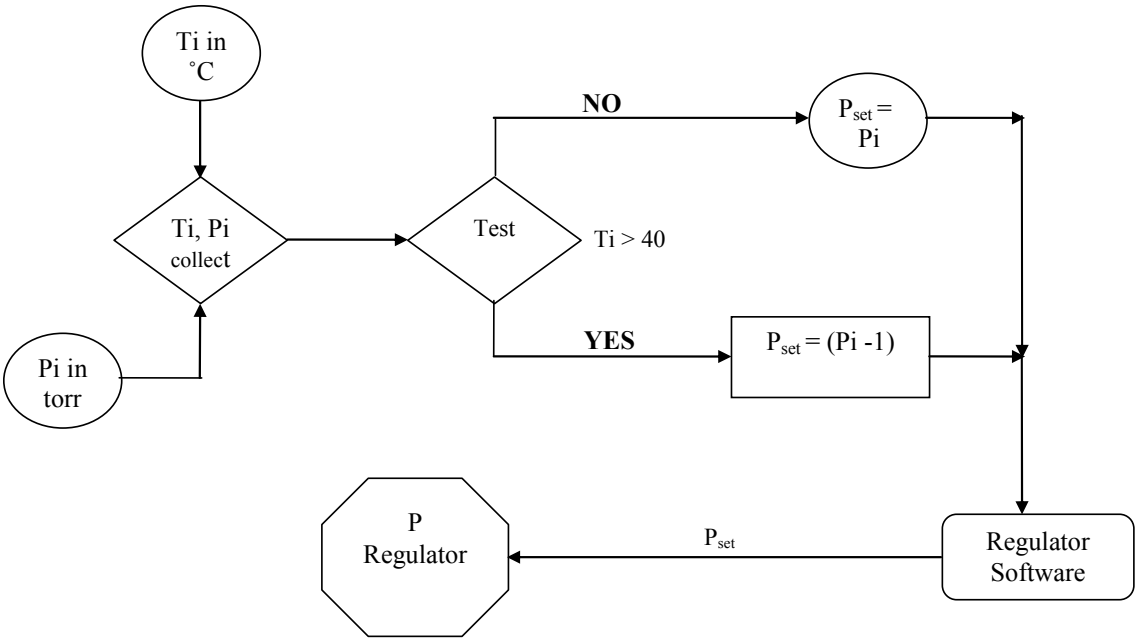

Figure 27. Pressure control diagram

2.4 KINETICS AND MODELING EXPERIMENTAL PROCEDURES

The literature reports the use of image analysis methods to (1) determine and quantify morphology changes for a single species (polymorphic transformation) (Faria N. et al.; 2003) (Pons M. et al.; 1999) (Puel F. et al.; 1997), (2) determine number of crystal evolution with time (crystal count) (Krumme A. et al.; 2003), (3) determine crystal length evolution with time (Polannen K at al.; 2006), (4) determine shape evolution with time (facets elongation) (Wang et al; 2007), (5) metastable width and solubility curve (Barrett P. et al.; 2002), (6) derive/validate modeling of crystallization kinetics parameters.

In this study we propose to use image analysis to determine the crystal count, the crystal length evolution, metastable zone width and nucleation points of a multi species system presenting different morphologies. This thesis presents three originalities compared to study typically using image analysis: (1) all the criteria mentioned above will be estimated and used to

derive correlations of the specific kinetics that may be compared to resulting crystal size and mass density distributions , (2) the system of study is composed of multi species with different shapes and kinetics, (3) the method to be used is PLM microscopy image analysis which present less drawbacks than regular PMV (depth issues, overlap of crystals, slurry density) but is not considered an in situ measurements method.

2.4.1 SAMPLING METHODOLOGY

Sample Location in Crystallizer

Samples of the slurry were taken at regular time intervals from a specific location in the well mixed region of the vessel. The main issues associated with sampling are: (1) obtaining a homogenous sample representing the content of the crystallizer, (2) performing sampling at the same location, (3) taking enough sample to perform analysis without affecting the experiment. The stirring rate and the use of a baffle cage in the crystallizer improved mixing and homogeneity of the slurry in the vessel. In order to ensure that the sampling region was appropriate in assessing the three objectives stated above, a study was performed on samples taken at several locations from the surface to the bottom of the crystallizer. Figure 28 panel A displays the positions for which the sampling of the slurry was performed and analyzed through PLM analyses. In Figure 28 panel A sampling analysis was performed every inches from the liquid surface to the bottom of the vessel, on a slurry produced from the evaporative crystallization of early feed solution at 66 °C and an evaporation rate of 25 g/h. The study was performed at C: F of 0.32 to ensure that: (1) the sample population was composed of several species at high number and varying sizes and (2) the slurry density was low enough to perform accurately PLM analysis on sample micrographs. Figure 29 displays the series of selected PLM images extracted from samples at 0, 1, 2, 3, 3.2, 4, 5 and 6 inches from the liquid surface.

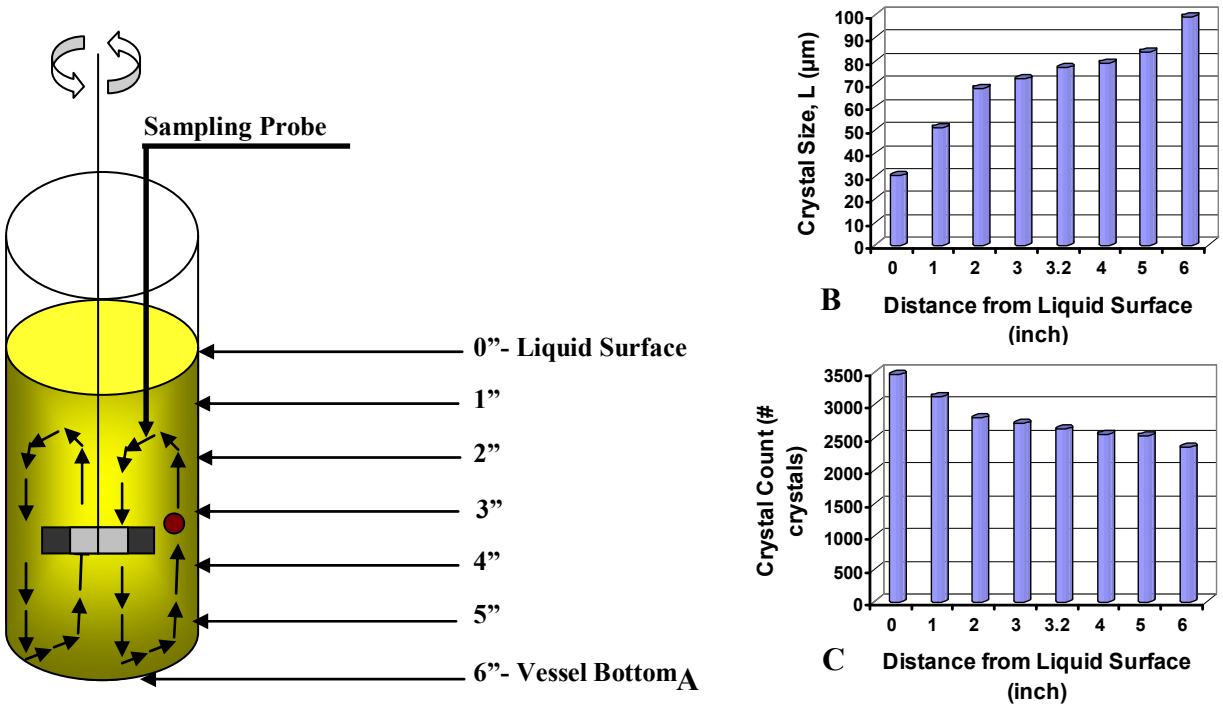

Figure 28. Selecting sampling location in crystallizer and corresponding crystal count and sodium carbonate monohydrate average size
(Panel A, Vessel schematic where sampling was performed, Panel B, Average sodium carbonate monohydrate size with respect to sampling location, Panel C, Crystal count with respect to sampling position). The red point on Panel A represents the selected location for sampling.

PLM analysis performed on sample micrographs displayed in Figure 29 shows that: (1) the liquid surface presents a larger number of crystals mainly as burkeites with smaller size sodium carbonate monohydrate, (2) the sample located 1" below the liquid surface presents larger size crystals with lesser number of crystals than the sample at the surface, (3) samples from 2" to 5" presents very similar compositions with broader distribution of sodium carbonate monohydrate and still large number of burkeite crystals, (4) the bottom of the vessel presents larger size sodium carbonate crystals with lesser amounts of burkeite. In essence, (1) the first inch from the surface presents smaller crystals and higher number which is due to the easier suspension of lighter crystals, (2) some large sodium carbonate monohydrate crystals settled at the bottom of the crystallizer due to their higher mass, and (3) no real crystal classification can be observed between 1" to 4" in the crystallizer. The position of the impeller in the last third of

the crystallizer allowed avoiding intensive crystal settling during the run. One can quantify these observations by measuring the average crystal size and total crystal count for each sample micrograph. The evolution of the sodium carbonate monohydrate average crystal size is presented in Figure 28B. The distribution showed that the average size varied of only 10µm between 1" to 5" while it varied of close to 30µm within the first inch from the surface and close to 15µm in the bottom of the vessel. This validates that the sample should be taken between 1" and 5" from the liquid surface, that larger crystals were recovered in the bottom and that smaller at the surface. The total crystal count for each sample image is presented in Figure 28C. The total number of crystals between 1" to 5" from the liquid surface remained nearly constant (200 crystals variation) while it varied of 800 crystals within the first inch and 200 crystals from 5" to the bottom of the crystallizer. The selected sampling region that presented a homogenous population representative of the contents of the crystallizer was chosen at 2.8 inches from the bottom of the crystallizer in the well-mixed region of the vessel located right above the impeller. This choice ensures to have a homogenous sample representative of the content of the crystallizer even at high slurry density.

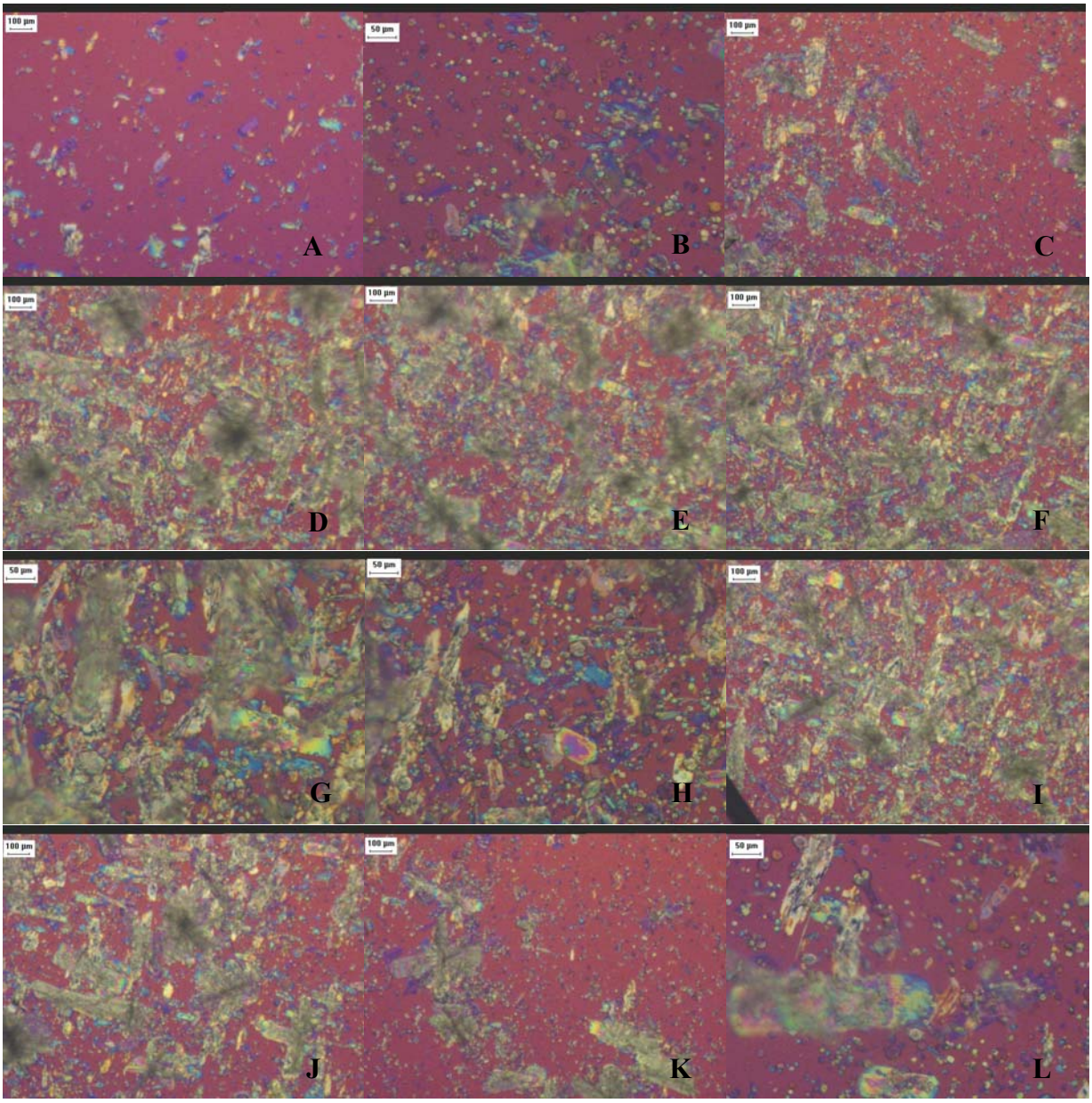

Figure 29. Series of PLM images of sample taken at different locations in the vessel for a population obtained with the evaporation of early feed solution at 66 °C at an evaporation rate of 25 g/h per hour and at 32 % water mass evaporated

(Panels A and B represent sodium carbonate monohydrate and burkeite crystals from the liquid surface, Panels C, D and E the samples taken from 1", 2" and 3" from the surface, Panels F, G and H, micrographs of sodium carbonate monohydrate and burkeites taken at the selected sampling location of 3.2 ", Panels I and J at 4" and 5" from liquid surface, Panel K and L samples from the bottom of the crystallizer)

Sampling Methodology and Equipment

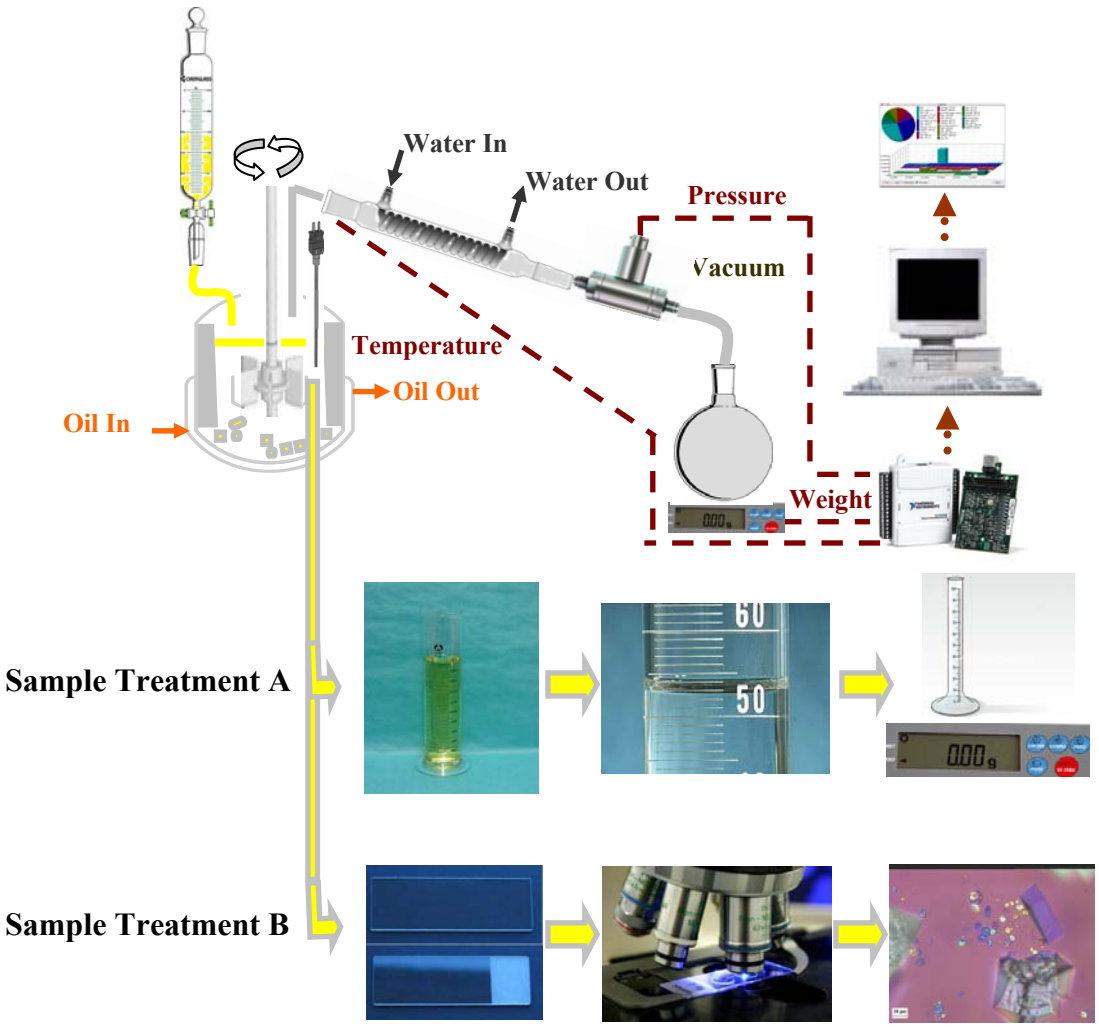

Figure 30. Schematic of the equipment and methodology used for slurry sampling applied to SST feed evaporative crystallization

The apparatus and methodologies used to perform sampling of the slurry are presented in Figure 30. As displayed by Figure 30, two treatments were performed on the slurry sample taken from the crystallizer. Treatment A was used to monitor the evolution of the slurry density with respect to the operating time, and treatment B was used to monitor the evolution of the crystal count and crystal average size evolution with the operating time.

A specific fraction of the slurry sample described in Figure 30 (0.05 mL) was evenly spread on microscope slides for PLM analysis following sample treatment B. The slides used for PLM

analysis were preheated to the slurry temperature to avoid crystallization upon cooling. Figure 31 displays an example of crystal size measurement and crystal count using two different focal planes. Figure 31 shows that this analysis method of the slurry sample photomicrographs allowed to (1) eliminate the uncertainty on the crystal size due to depth effect, and (2) observe several focus planes for a single sample in case of higher slurry density

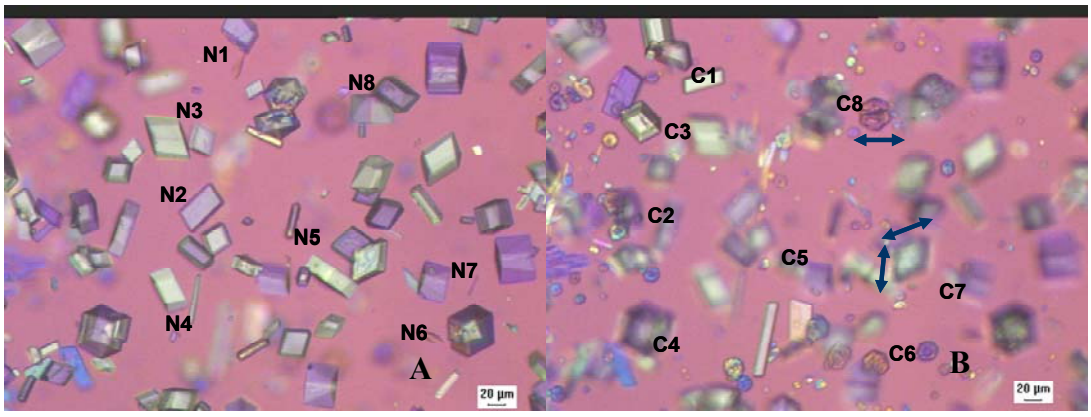

Figure 31. Examples of crystal counting with PLM analysis using two focal planes for the same slurry sample (Panel A, first focus plane with counting of sodium nitrate crystals, Panel B, second focus plane with total crystal count and crystal size measurement)

Specific Nucleation Measurement

The PLM images were used to count the number of crystals for each crystalline species. The crystal count per image was (1) converted to a crystal count per sample by using the known geometric characteristic of the cover slide, and (2) adjusted with the sample volume to a total crystal count per volume. An example of calculation is provided with the information from Table 5. In Table 5 the area of the view was measured with the software available with the PLM microscope and the sample area corresponds to the area of the cover slide. Since the depth of the sample and the view are identical, the crystal count per volume could be computed using equation 4:

$$NT_{\text{burkeite}} = Count \times \frac{SampleArea \times Depth}{ViewArea \times Depth} \times \frac{1}{SampleVolume} \equiv \left[\frac{\text{Crystals\#}}{\text{mL}}\right] \quad (4)$$

Table 5. Example of burkeite number measurements for a specific slurry sample

Sample #	Operating Time (min)	Total Burkeite (crystal #)	View Area (μm2)	Sample Area (μm2)	Sample Volume (mL)	Burkeite Count per volume (crystal#/mL)
12	715	318	291808.42	324000000	0.05	7.061×10^{6}

Based on the information of Table 5 the total count of burkeite per volume is computed by

$$NT_{\text{Burkeite}} = \frac{318}{0.05} \times \frac{324000000}{291808.42} = 7.061\times10^{6}\,\frac{\text{burkeite}}{\text{mL}} \tag{5}$$

This methodology was performed for each species, and the results were tabulated as displayed by Table 6, which provides the values associated with sodium nitrate and burkeite under the conditions of the certification run (66 °C and 25 g/h evaporation rate).

Table 6. Evolution of total burkeite and sodium nitrate number with operating time using experimental data of Certification Run 38b slurry samples

Operating Time (min)	**Sodium Nitrate Number (crystals/ mL)**	**Operating Time (min)**	**Burkeite Number (crystals/ mL)**
289	0	390	0
780	2.220×10^{4}	640	3.330×10^{5}
840	3.330×10^{5}	750	7.061×10^{6}
960	5.151×10^{6}	840	8.927×10^{6}
1020	6.863×10^{6}	960	9.300×10^{6}

Specific Growth Measurement

Since the growth rates of different crystalline species are to be determined, the characteristics dimensions of each need to be defined. There are given in Figure 32, along with identification of the largest two dimensions of each crystal.

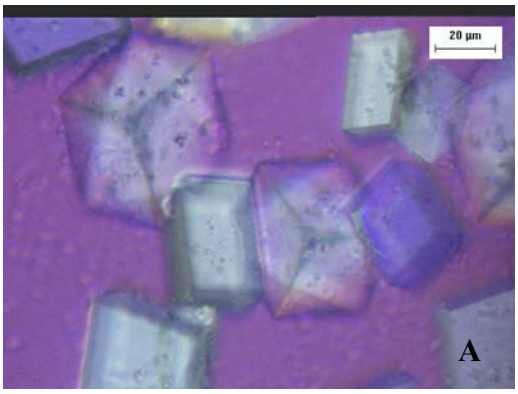
20 µm
A

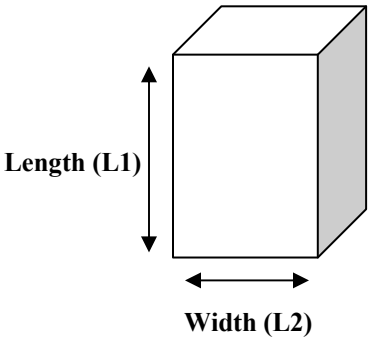
Length (L1)
Width (L2)

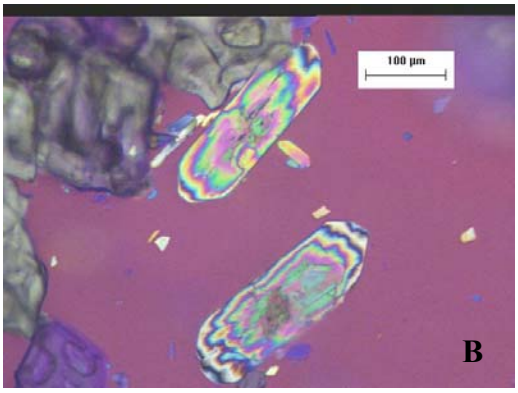
100 µm
B

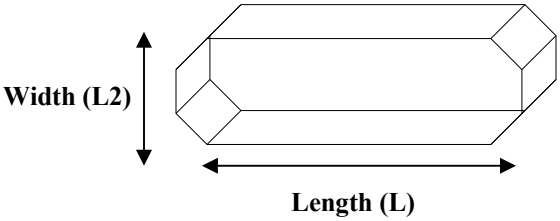
Width (L2)
Length (L)

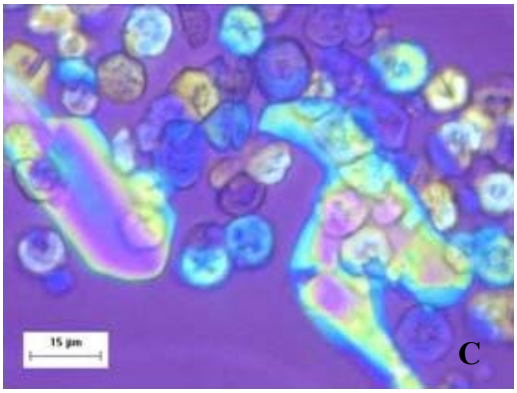
15 µm
C

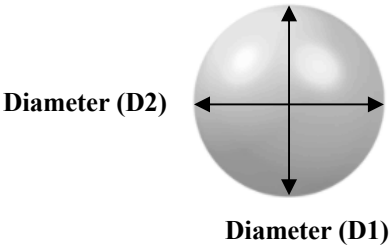
Diameter (D2)
Diameter (D1)

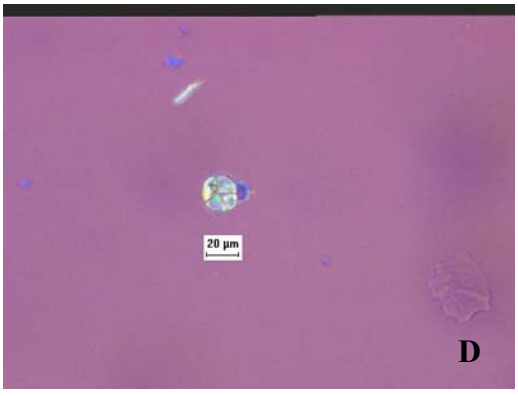
20 µm
D

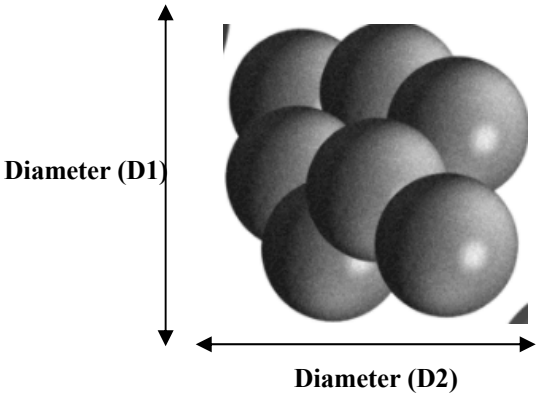
Diameter (D1)
Diameter (D2)

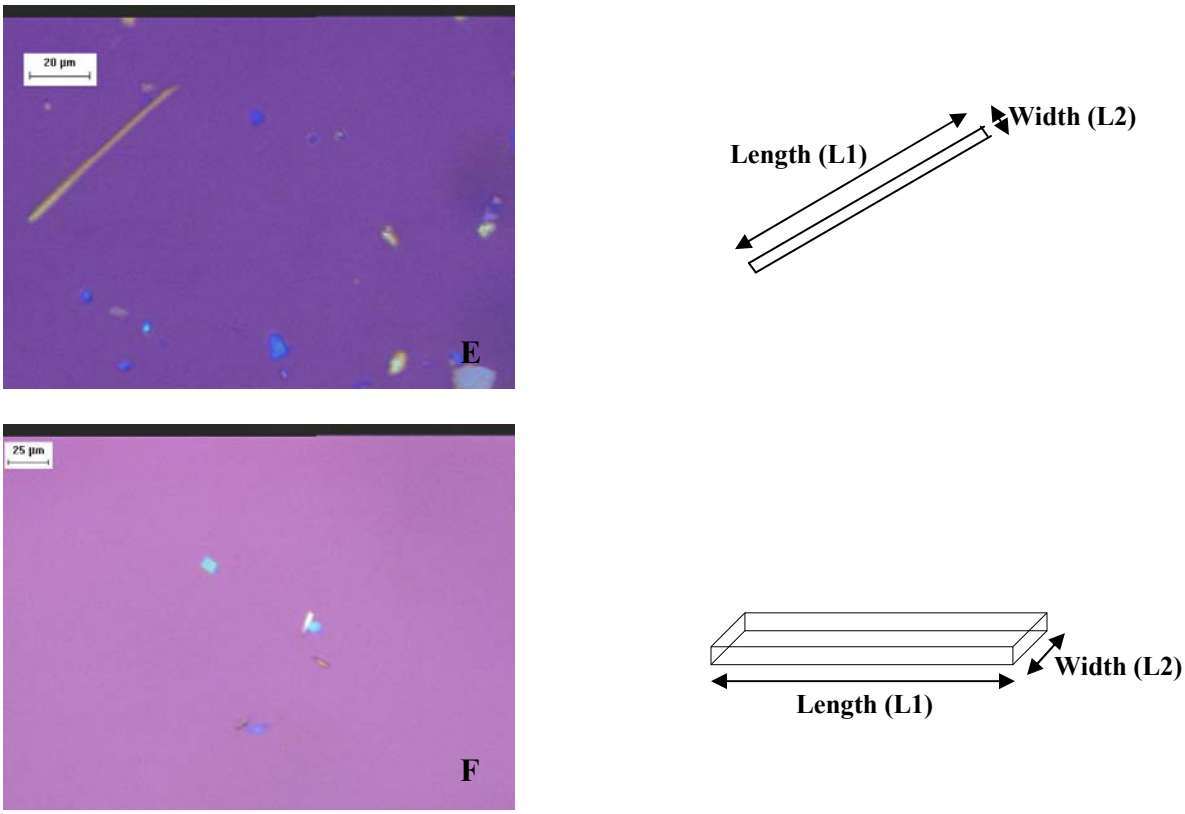

Figure 32. Measurement of the largest two dimensions of each type of crystalline species produced during the multi-species evaporative crystallization of SST feed solutions
(Panel A, Sodium nitrate, Panel B, Sodium carbonate monohydrate, Panel C, Single burkeite, Panel D, Burkeite agglomerate, Panel E, Sodium oxalate, Panel F, Sodium sulfate)

When monitoring the crystal size evolution with the operating time to compute a specific growth rate, the recent crystal nucleation may decrease the apparent average size of a crystal population. To isolate the effect of crystal growth from crystal nucleation, we assumed that: (1) crystal growth was independent from size meaning that large and small crystals present identical growth rates, and (2) used the initial growth rate to determine the maximum size of crystals that were just nucleated to monitor the size evolution of the crystals above the maximum size. An example of the average diameter of burkeite and the length and width of sodium carbonate crystals under the conditions of the early feed Certification Run 38b is displayed in Table 7.

Table 7. Evolution of burkeite, sodium carbonate monohydrate and sodium nitrate crystal size with the operating time during the early feed Certification Run 38b

Operating Time (min)	Burkeite Average Diameter (µm)	Sodium Carbonate Monohydrate Average Length (µm)	Operating Time (min)	Sodium Nitrate Average Length (µm)
390	0.0	0	780	0
620	7.1	16.2	840	0
640	14.6	33.1	960	43.9
715	19.6	95.2	985	100
840	21.2	127.5	1020	145

Slurry Density Measurement

As shown in Figure 33, a fraction of the sample was spread on a microscope slide while the remaining of the sample was collected in a graduated cylinder following pretreatment A. The mass and the volume of the sample were measured by placing the cylinder on a balance. The sample mass was included as a recovered slurry loss and used to perform correction on mass balance closure. The mass and volume of the sample were used to determine the evolution of the slurry density with respect to the operating time. This evolution was used as an additional validation of the nucleation points. An example of these measurements is displayed in Figure 33. The sample points displayed in Figure 33 correspond to an experiment performed with an early feed solution at a temperature of 55 °C and 25 grams per hour evaporation rate.

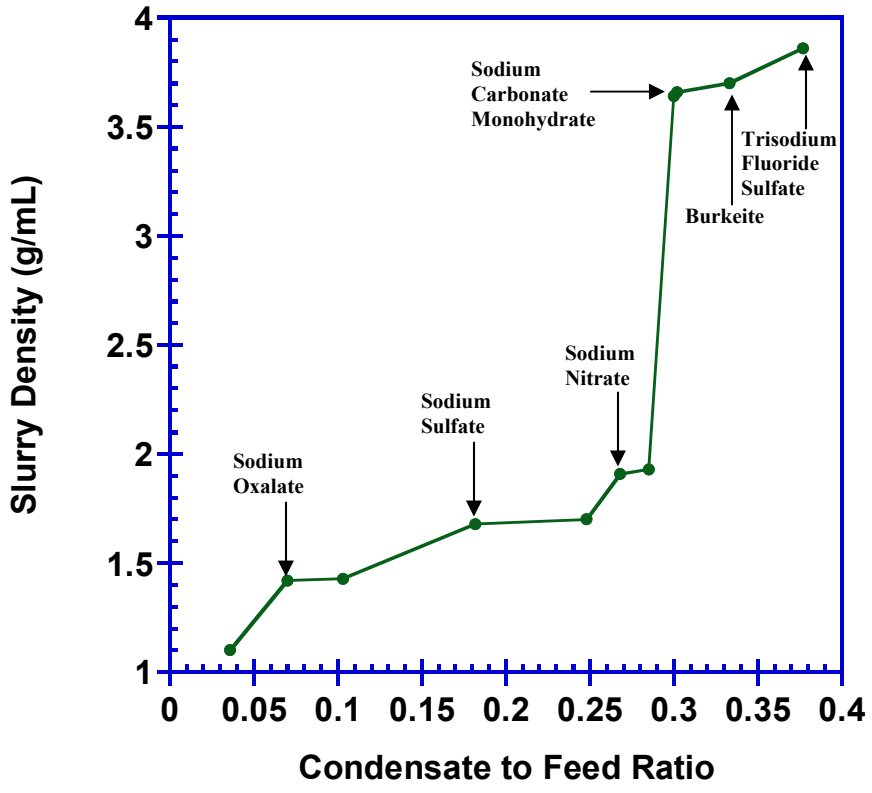

Figure 33. Evolution of slurry density with the operating time

The detection point of each crystalline species was inserted in Figure 33. In this study we called "nucleation point" the point (operating time or condensate to feed ratio) at which the crystalline species was first detected. Nucleation technically occurred before the first crystals can be detected, however based on the slurry density evolution and the initial growth rate value, it can be inferred that detection point and nucleation point are very similar.

2.4.2 NUCLEATION AND GROWTH RATE CALCULATIONS

Average Specific Nucleation Rate Calculation

The experimental results of the species nucleation such as these displayed in Table 6, were used to define the evolution of the crystal number with the operating time as displayed in Figure 34.

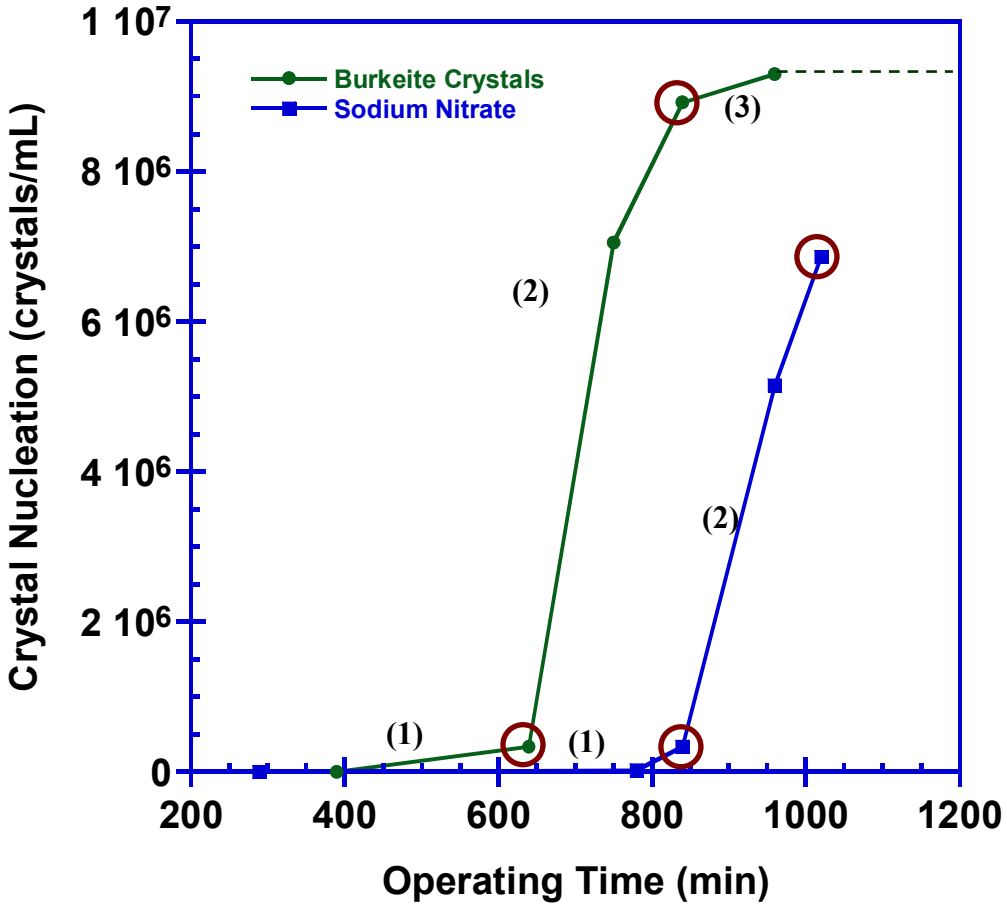

Figure 34. Illustration of the calculation of the average nucleation rate

Two main types of profiles were obtained from these experimental results displayed in Table 6. Sodium nitrates display an exponential or power law profile with a slow nucleation followed by a large and constant nucleation section. The average nucleation rate for sodium nitrate corresponds to the second section which is constant. The slope of the profile (line in between the red circles) was computed by:

$$N^{o}\text{Nitrate} = \frac{(6863405 - 333095)}{(1020 - 840)} = 36279.5 \frac{\text{crystals}}{\text{mL} \cdot \text{min}} \tag{6}$$

The second type of profile is illustrated by burkeite in Figure 34. One can identify three sections: (1) a slow initial nucleation rate, (2) a constant profile following a power law or

exponential, (3) a slowing in the nucleation rate expressed by a curve and a plateau. The last section of the profile is due to the depletion of sulfate in the solution and is an effect of the semi-batch operation. The average nucleation rate was hence calculated in the constant section of the profile before the depletion meaning before the large curvature change leading to a plateau (line marked by the red circles). The average nucleation rate for burkeite is hence computed by:

$$N^{o}\text{Burkeite} = \frac{(8926953 - 333095)}{(840 - 640)} = 42969.28 \frac{\text{crystals}}{\text{mL} \cdot \text{min}} \tag{7}$$

Average Specific Growth Rate Calculation

A similar computational method than the one applied to determine the specific average nucleation rate was applied to determine the average growth rate based on the crystal size evolution profiles. The experimental results of the species average crystal size such as these displayed in Table 7, were used to define the evolution of the crystal average size with the operating time as displayed in Figure 35. Two main types of profiles were obtained from these experimental results displayed in Table 7. Sodium nitrates display an exponential or power law profile with a slow growth followed by a large and constant growth section. The average growth rate for sodium nitrate corresponds to the second section which is constant. The slope of the profile (line in between the red circles) was computed by:

$$G_{\text{Nitrate}} = \frac{(145.0 - 43.9)}{(1020 - 960)} = 1.684 \frac{\mu\text{m}}{\text{min}} \tag{8}$$

The second type of profile is illustrated by burkeite in Figure 35. One can identify two sections: (1) a constant section following the beginning of a power law or exponential profile, (2) a slowing in the growth rate expressed by a curve and a plateau. The last section of the profile is due to the depletion of sulfate in the solution and is an effect of the semi-batch operation. The average growth rate was hence calculated in the constant section of the profile before the

depletion meaning before the large curvature change leading to a plateau (line marked by the red circles). The average growth rate for burkeite is hence computed by:

$$G_{\text{Burkeite}} = \frac{(19.6 - 0)}{(640 - 600)} = 0.171 \frac{\mu\text{m}}{\text{min}} \tag{9}$$

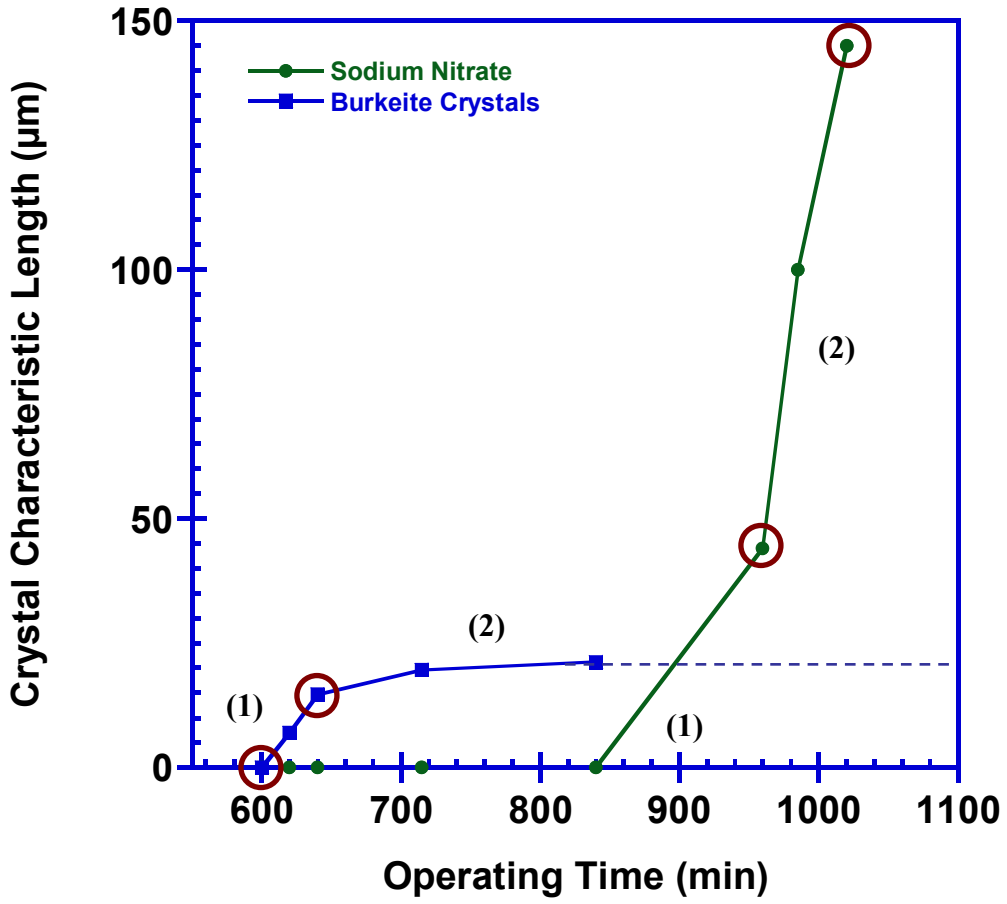

Figure 35. Illustration of the calculation of the average growth rate

Estimate of Error Bars on Crystal Count and Average Size

The early feed certification run was reproduced and the kinetics of the reproduced run at identical sample time were determined using the methodology described in the previous sections. The values of the total number of crystals per unit volume for each species was compared between the certification and reproduced experiment. Table 8 represents the comparison of the

total burkeite count for each sampling time between the certification and reproduced run. In Table 8 the percent variation column represent the absolute value of the percent discrepancy of the burkeite total count in the reproduced run compared to the certification run and was calculated as follow:

$$\%Variation = 100 \times \left| \frac{(n_{\text{T,certification}} - n_{\text{T,reproduced}})}{n_{\text{T,certification}}} \right| \quad (10)$$

An example of the application of equation 10 is displayed in equation 11:

$$\%Variation = 100 \times \left| \frac{(7.24 \times 10^6 - 7.06 \times 10^6)}{7.24 \times 10^6} \right| = 2.5\% \quad (11)$$

Table 8. Comparison of burkeite total crystal counts for the certification and reproduced run and display of percent variation between these values

Operating Time (min)	Reproduced Run	Certification Run	Variation (%)
	Burkeite Number (crystals/ mL)	Burkeite Number (crystals/ mL)	
390	0	0	0
640	3.55×10^5	3.33×10^5	6.7
750	7.24×10^6	7.06×10^6	2.5
840	9.13×10^6	8.93×10^6	2.2
960	9.46×10^6	9.30×10^6	1.7

The average percent error associated with the burkeite total crystal count was 3.3 %. This value will be applied as the value of the error bars associated with burkeite total crystals count. Figure 36 displays the evolution of the burkeite total crystal count with respect to the operating time for the early feed certification run that was performed at 66 °C and 25 g/h, and the associated error bars.

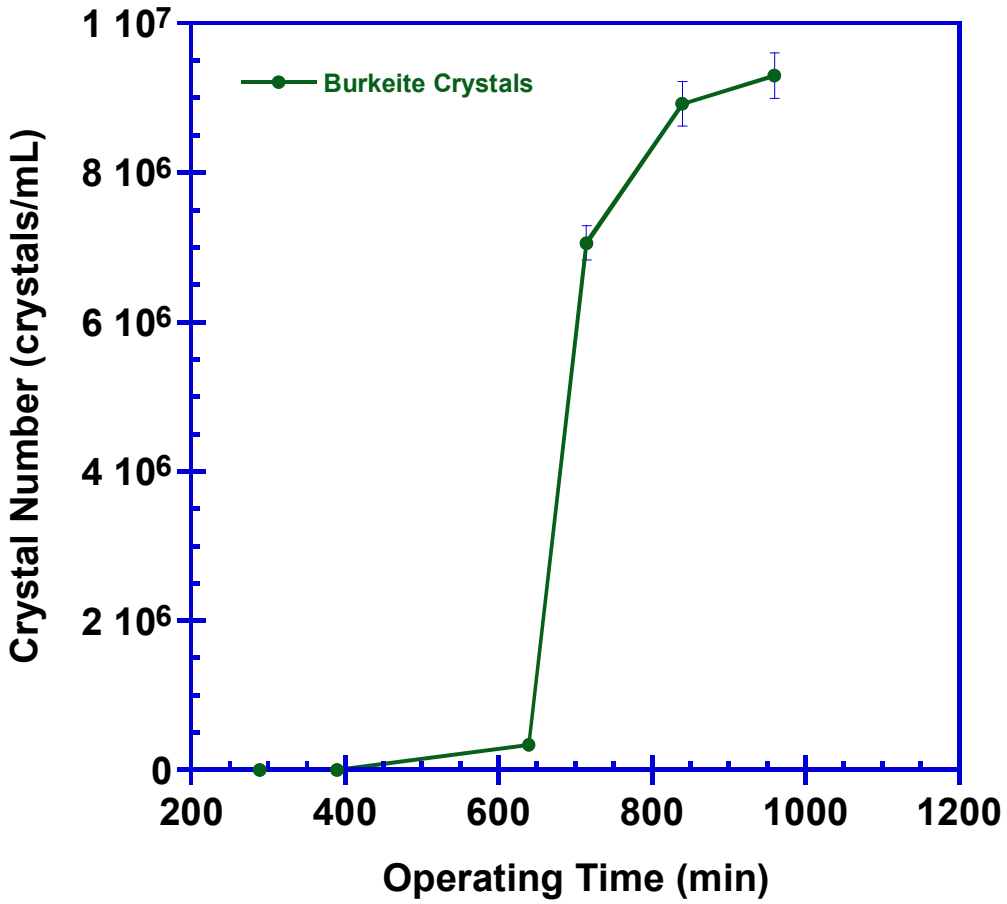

Figure 36. Evolution of the burkeite total crystal count with respect to the operating time for the early feed certification run and the associated error bars

The values of the average crystal size for each species was compared between the certification and reproduced experiment. Table 9 represents the comparison of the average burkeite diameter for each sampling time between the certification and reproduced run. In Table 9 the percent variation column represent the absolute value of the percent discrepancy of the burkeite average diameter in the reproduced run compared to the certification run and was calculated as follow:

$$\%Variation = 100 \times \left| \frac{(\overline{L}_{\text{certification}} - \overline{L}_{\text{reproduced}})}{\overline{L}_{\text{certification}}} \right| \quad (12)$$

An example of the application of equation 12 is displayed in equation 13:

$$\%Variation = 100 \times \left| \frac{(19.9 - 19.6)}{19.9} \right| = 1.5\% \quad (13)$$

Table 9. Comparison of average burkeite diameter for certification and reproduced runs: percent variation shown

Operating Time (min)	Reproduced Run	Certification Run	Variation (%)
	Burkeite Average Diameter (µm)	Burkeite Average Diameter (µm)	
390	0.0	0.0	0
620	7.3	7.1	2.7
640	14.8	14.6	1.3
715	19.9	19.6	1.5
840	21.5	21.2	1.4

The average percent error associated with the burkeite average crystal size was 1.75 %. This value will be applied as the value of the error bars associated with burkeite total crystals count. Figure 37 displays the evolution of the burkeite average size with respect to the operating time for the early feed certification run that was performed at 66 °C and 25 g/h, and the associated error bars. Table 10 displays the errors associated with the specific total crystal count and average size evolution with the operating time. The values of the variations were calculated from the average discrepancy between the early feed certification and reproduced runs sample values at 66 °C an 25g/h.

Table 10. Errors associated with the specific total crystal count and average size evolution with the operating time

Crystalline Species	Average Variation on Crystal Average Size (%)	Average Variation on Crystal Total Count (%)
Sodium Nitrate	2.7	5.1
Sodium Carbonate Monohydrate	5.6	2.3
Burkeite	1.75	3.3
Sodium Sulfate	4.2	3.5
Sodium Oxalate	6	9.3

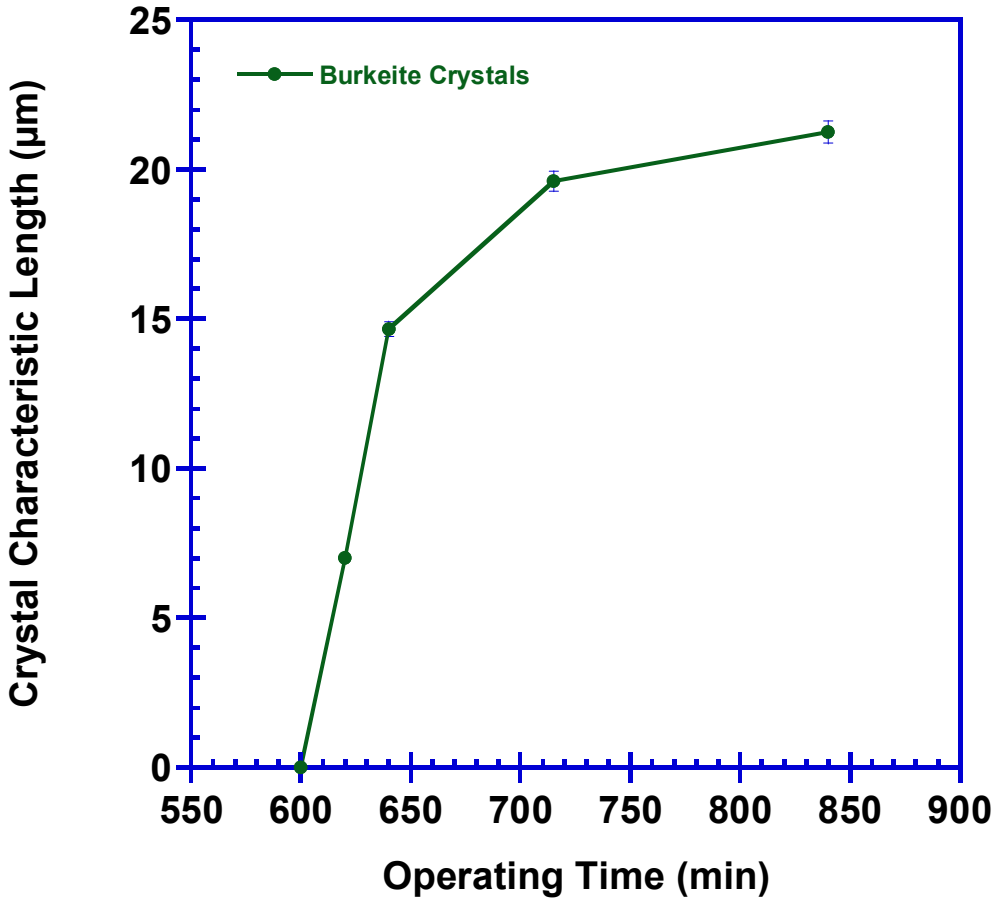

Figure 37. Evolution of the burkeite average diameter with respect to the operating time for the early feed certification run and the associated error bars

Estimate of Error Bars on Average Nucleation and Growth Rates

The average nucleation and growth rates of the early feed certification and reproduced run were computed using the method described in the previous sections. The percent variation between the specific kinetics were computed and used as an estimate of the values associated to the error bars used in this thesis. Table 11 displays the percent vaiations associated with each species that crystallize during the early feed evaporative crystallization performed at 66 °C and 25 g/h evaporation rate. These values will be used in the thesis for every early feed crystallization experiment average growth and nucleation rates.

Table 11. Error associated with the specific average nucleation and growth rate for early feed crystallization

Crystalline Species	Reproduced Run	Certification Run	Variation (%)
	Average Nucleation Rate (crystals/ mL·min)	Average Nucleation Rate (crystals/ mL·min)	
Sodium Nitrate	3.627×10^4	3.610×10^4	0.4
Sodium Carbonate Monohydrate	3.245×10^3	3.263×10^3	0.5
Total Burkeite	4.296×10^4	4.385×10^4	2.0
Single Burkeite	3.686×10^4	3.752×10^4	1.8
Burkeite Agglomerate	6.106×10^3	6.328×10^3	3.6
Sodium Sulfate	2.724×10^3	2.756×10^3	1.1
Sodium Oxalate	79	95	19.9
Crystalline Species	**Reproduced Run**	**Certification Run**	**Variation (%)**
	Average Growth Rate (µm/min)	**Average Growth Rate (µm/min)**	
Sodium Nitrate	1.684	1.687	0.2
Sodium Carbonate Monohydrate	0.159	0.148	6.7
Single Burkeite	0.171	0.173	1.5
Burkeite Agglomerate	0.039	0.039	0.2
Sodium Sulfate	0.294	0.296	0.6
Sodium Oxalate	0.193	0.212	9.6

2.4.3 NUCLEATION POINT

Definition of Nucleation Point

In this thesis, the nucleation points of each crystalline species will be defined as the condensate-to-feed ratio (or corresponding operating time) at which the first crystals were detected. Sizes of crystals at nucleation point depend on the time intervals between two samples

and the precision of the PLM microscope. Average crystal size at nucleation is typically 5 µm. The accuracy of the nucleation point estimate may be calculated using the initial growth rate of each crystalline species. For instance, for burkeite crystals produced at 66 °C and 25 g/h evaporation rate with an early feed solution, the first crystals were detected with sizes < 5 µm at an operating time of 640 min. The initial growth rate of burkeite at these conditions was close to 0.5 µm/min, and the actual nucleation point was hence closer to 640 min- 10 min = 630 min. Note that a difference of 10 minutes corresponds to a difference in condensate-to-feed ratio in the order of 1 to $2x10^{-3}$. The error between detection and nucleation point hence depends on the initial kinetics of each of the species but remains very low.

Sodium Nitrate First and Second Nucleation

All species produced from early feed evaporative crystallization present a unique nucleation point, however sodium nitrate under certain operating conditions may display a first nucleation point followed by an important spike in nucleation. For instance, at 66 °C and 25 g/h evaporation rate (Experiment 1), sodium nitrate came out of solution after 466 min with only small amount of sodium nitrate crystals produced. For 250 minutes the low total number of sodium nitrate crystals remained constant and the existing sodium nitrates were grown. At an operating time of 905 min the total number of sodium nitrate crystals increased of $5x10^6$ crystals per mL. In the thesis, the nucleation point and spike in nucleation observed for sodium nitrate were labeled "1^{st} Nucleation" and "2^{nd} Nucleation". This distinction is important for the calculation of the average nucleation and growth rate of sodium nitrate. Furthermore, this phenomenon is dependant on the operating conditions as evaporative crystallization of early feed at 66 °C and maximum evaporation rate of 75 g/h (Experiment 2) led to one spike in sodium nitrate total count at nucleation point after 160 minutes of operating time. Figure 38 displays the

resulting total crystal counts for early feed experiments presenting one and two sodium nitrate spikes in nucleation.

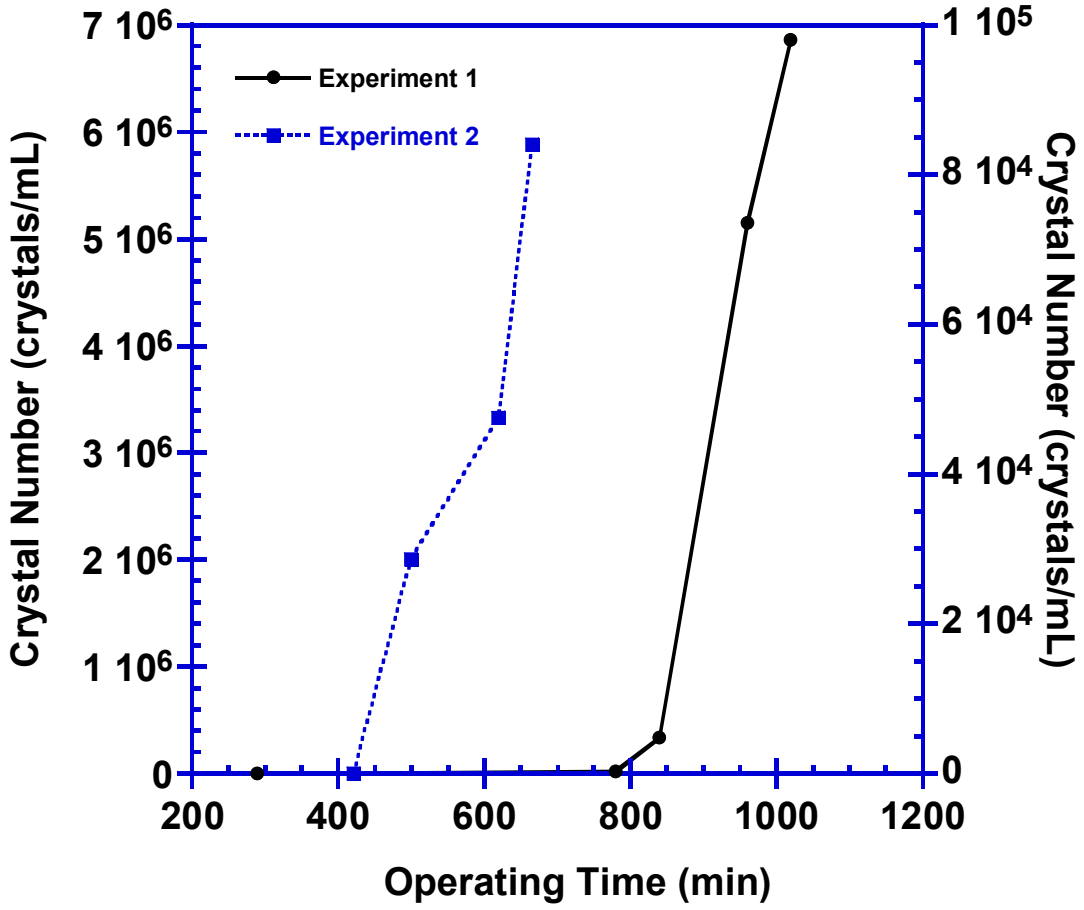

Figure 38. Comparison of total crystal count for two experiments presenting one and two spikes in sodium nitrate nucleation

2.4.4 INFLUENCE OF SULFATE CO-CRYSTALS FORMATION ON KINETICS

The production of co-crystalline species such as burkeite may affect the kinetics of the other species and is responsible for the observed depletion in burkeite, sodium sulfate or trisodium fluoride sulfate for early feeds crystallization at different operating conditions. For instance, performing evaporative crystallization on sodium sulfate single salt feed at the condition of the early feed pretreatment would lead to an increase in sulfate concentration due to

solvent removal. After reaching sodium sulfate saturation, crystals may be observed while the evaporation continues and the solution remains at saturation. In the case of the early feed evaporative crystallization, in addition to sodium sulfate crystals two sulfate co-crystals were formed: burkeite ($Na6SO_42CO_3$) and trisodium fluoride sulfate ($Na3FSO_4$). If the saturation of burkeite crystals is lower than the saturation of sodium sulfate it is likely that the sodium sulfate kinetics (nucleation and growth rate) will be affected and that sodium sulfate total number and average size will decrease. A similar reasoning can be applied to trisodium fluoride sulfate species when it is produced and sodium carbonate monohydrate when burkeite is crystallized. In the base case of Certification Run 38b, sodium sulfate is the first species to reach saturation followed by sodium carbonate monohydrate, burkeite slightly after and trisodium fluoride sulfate in the second stage. It is hence expected that with increasing operating time the burkeite average nucleation and growth rates will remain constant due to earlier saturation of sodium carbonate monohydrate and sodium sulfate. The apparent depletion in a crystalline species is dependant on the operating conditions as operating temperature and evaporation rates may affect the nucleation points of each species.

CHAPTER 3: PRETREATMENT OF HANFORD WASTE

The Hanford wastes are to be extracted from the storage tank at Hanford site previous to further processing and immobilization through vitrification. Figure 39 displays the main steps involved in the removal of the waste from the storage tank and the classification of the liquid wastes after extraction. This operation is accomplished by (1) pumping out the supernatant and (2) injecting water to dissolve the remaining salt slurry cake and sludge. The recovered liquid wastes present a higher concentration in the main solutes -mainly sodium salts and radionuclides, cesium and technetium- at the early stage of the removal than at the later stage, defining the two major waste categories displayed by Figure 39.

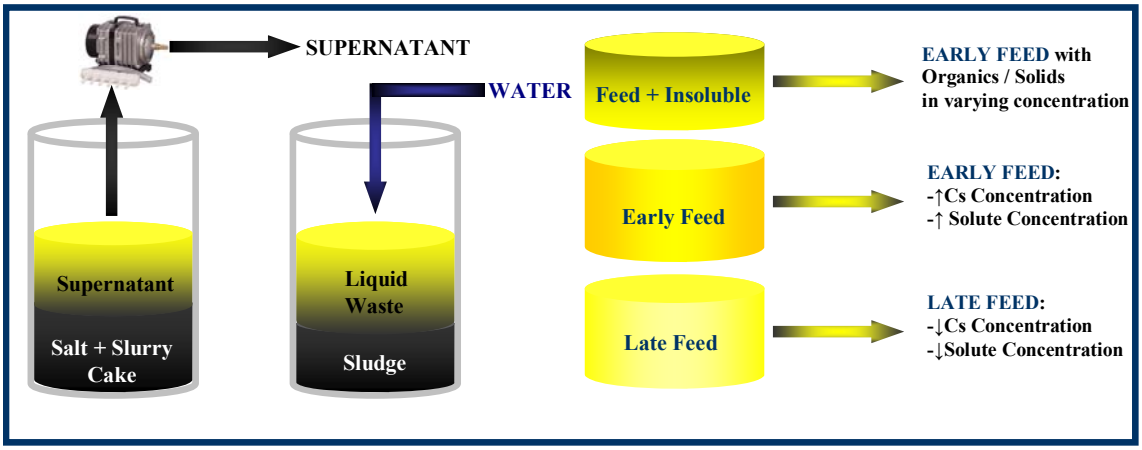

Figure 39. Extraction of radioactive low- and medium-curie waste from Hanford storage tanks

Furthermore, the medium-curie waste removed from the Hanford storage site presents great variability from one tank to another. Such variability includes different concentrations of the key sodium salts, the presence of organic constituents and solid particles, and variability in

the effluent composition over the period of time a tank is being emptied. For the purposes of this study, primary emphasis was given to early-feed and late-feed compositions: i.e. solutions withdrawn early and late during the tank-emptying period. Two perturbations from these were examined: one that considered the effects of organic constituents and a second considering the impact of solids. In this chapter, the certification runs were two runs performed with early and late feed solutions that were designed to test protocols against the process specifications cited in Chapter 1. Appropriate samples from the certification runs were sent to Georgia Tech Research Institute (GTRI) for analysis and the results of these analyses were used to demonstrate the applicability of the fractional crystallization pretreatment technology. The early and late feed certification runs were performed using feed solutions that had been prepared according to procedures provided by CH2M HILL[2]. The procedures led to formulation of a feed solution having the composition given in Table 12.

Table 12. Composition of SST simulated waste feed solution (early and late feed solutions)

Chemical	MW	Species Molarities	
		Early Feed	Late Feed
$NaAlO_2 \cdot 2H_2O$	118.0	0.26	0.04
NaOH	40.0	0.62	0.01
Na_2CO_3	106.0	0.61	0.24
$Na_2C_2O_4$	134.0	0.01	0.01
KNO_3	101.1	0.02	0.01
$NaNO_3$	85.0	3.26	1.59
$NaNO_2$	69.0	0.51	0.07
Na_2SO_4	142.0	0.13	0.17
$Na_3PO_4 \cdot 12H_2O \cdot 0.25NaOH$	390.1	0.05	0.05
NaCl	58.4	0.07	0.01
NaF	42.0	0.01	0.1
$Na_2Cr_2O_7 \cdot 2H_2O$	298.0	0.02	0.009
$CsNO_3$	194.9	0.005 g/L	0.00035 g/L

[2] Communication by Don Geniesse to Dan Herting and E. A. Nelson, March 14, 2006.

3.1 CRYSTALLIZATION OF SOLUTION REPRESENTING THE EARLY REMOVAL FROM THE WASTE TANK

3.1.1 OPERATING CONDITIONS

The simulated waste solution was submitted to a two-stage crystallization process conducted using the 300-mL and the 100-mL crystallizers for Stage 1 and Stage 2, respectively. The procedures followed in performing the crystallizations were outlined in Chapter 2. Figure 40 displays the condensate mass evaporated as a function of the operating time for Stage 1 and 2 of the certification run, showing that each stage was operated at constant evaporation rate. The evaporation rate was controlled by varying the temperature difference between the heating medium and the slurry. This was done by adjusting the temperature of the heating fluid and the pressure in the vessel. In the Stage 1 of the certification run, vapor was generated at a rate of 26 g/h by setting the temperature of the heating fluid to 77 °C and adjusting the pressure in the crystallizer during the run, so that the slurry temperature stabilized at 66 °C. Evaporation proceeded at these conditions for over 30.5 h, at which time the target condensate-to-feed mass ratio was achieved (see Appendix D). The ending condensate-to-feed ratio for the first stage was 0.481, close to the target ratio of 0.474 given by the batch simulation from COGEMA, Inc. (EARLY_FEED_FINAL_LABORATORY_FLOWSHEET.xls).

The filtrate from the first stage was diluted and used as feed for the second stage. The target condensate-to-feed ratio from the above-cited simulation was adjusted to 0.627 in order to account for the dilution water added. Because the volume of the second-stage crystallizer was 100 mL and the run was performed with feed addition, all the diluted filtrate was required for its operation. The evaporation rate for Stage 2 followed a constant evaporation rate of 39 g/h with a

slurry temperature at 40 ºC, as shown in Figure 40. Evaporation proceeded at these conditions for over 12.9 h, at which time the target condensate-to-feed mass ratio of 0.626 was achieved.

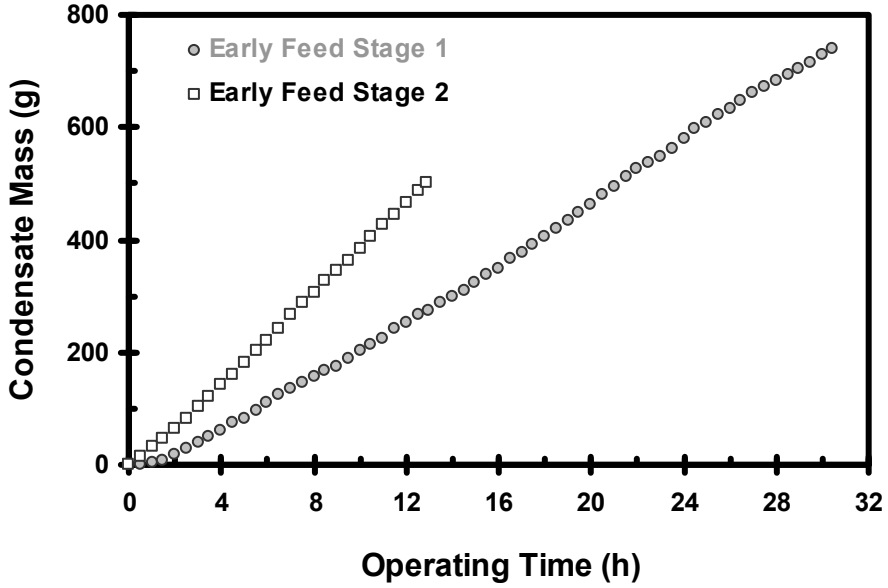

Figure 40. Mass of condensate generated as a function of operating time for early feed Certification Run 38 b: run was operated at 25 g/h evaporation rate

Figure 41 displays the temperature and pressure profiles for early feed certification run 38b. Throughout the first stage the temperature was controlled to within +/- 1 ^{o}C of the target value of 66 ^{o}C. Assessing Stage 2, except for an excursion at around 7 h, the temperature was controlled to within +/- 1 ^{o}C of the target value of 40 ^{o}C. For the two crystallization stages, the pressure profile reflects the step-wise changes in vacuum associated with manual adjustments of the regulating valve.

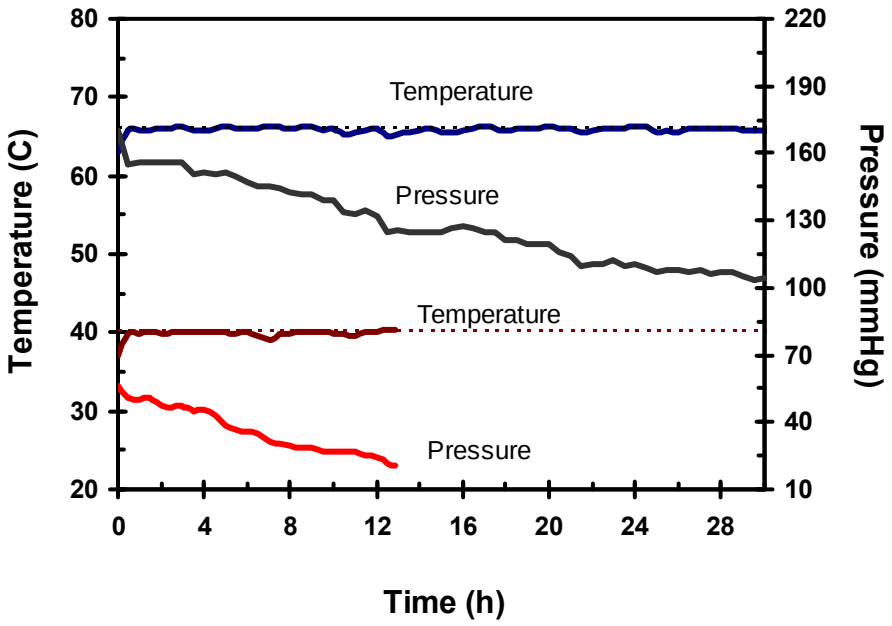

Figure 41. Temperature and pressure profiles for early feed Certification Run 38b.
(The blue and grey lines represent the first stage temperature and pressure profiles and the red and dark red lines the second stage temperature and pressure profiles. The dotted lines represent the target operating temperatures of 66 and 40 °C for the first and second stage respectively)

3.1.2 BALANCES ON TOTAL MASS

Mass balances closures were performed as described in Chapter 2. The objectives were to (1) determine the fate of species entering the process, and (2) identify potential problems with the operating procedures. Figure 42 is a schematic diagram illustrating the results of the overall mass balance around Stage 1. Included in the figure are definitions of quantities used in closing mass balances around each of the unit operations. The figure shows the masses of vapor generated and either recovered in the condensate receiver or the cold trap protecting the vacuum pump, crystals that accumulated on the walls of the vessel, material that adhered to the vessel and was lost in the transfer process, and the recovered slurry. The slurry recovered from the evaporative crystallization was filtered. The filtrate stream corresponds to the mass of filtrate collected inside the vacuum flask, and the funnel loss corresponds to the loss recovered after the

combined filtration and crystal washing operations. The loss was determined by washing the filtration funnel with a known amount of water and using a dry paper of known mass to collect the water accumulated on the wall of the apparatus. The unwashed crystals correspond to the solids recovered at the end of the filtration and their mass was estimated by performing mass balance closure around the filtration unit. The unwashed crystals were washed with a solution saturated in the main species (sodium nitrate, sodium carbonate monohydrate, sodium sulfate, sodium hydroxide and sodium fluoride) as described in Chapter 2. The final crystals were the solid phases obtained at the end of the process and the spent wash was the filtrate of the crystal washing operation. Figure 43 is the schematic diagram of the second crystallization stage. The process unit functioned as described for Stage 1, and the methods of closing total mass balances were identical.

Since the unwashed solids mass was not measured, a mass balance around the combined filtration-washing step was performed. The results of the mass balance closures around each unit operation are displayed in Table 13. The difference between input and output for each of the first stage units was as follows: evaporation, 0.13%; filtration and washing, 0.47%. Assessing the second stage, the closure around the filtration unit was 0.36% while the closure around the combined solid-liquid separations was 1.8%. Most of the mass loss in both crystallization stages was generated during filtration.

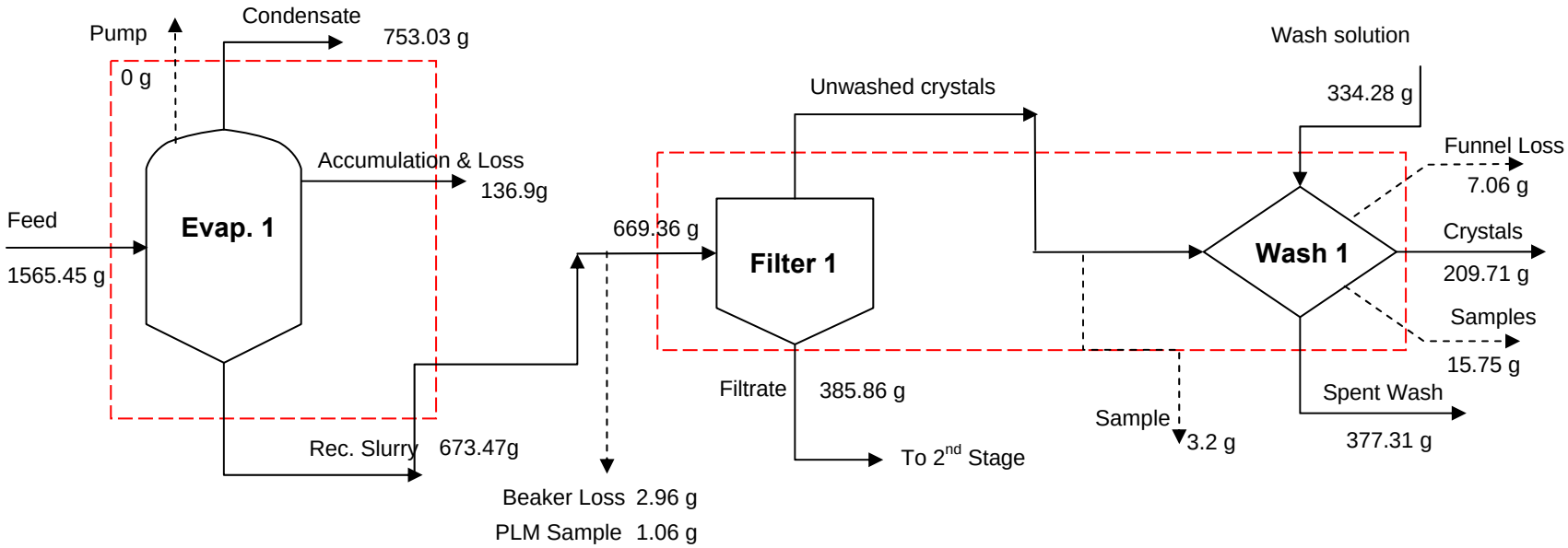

Pump	Mass of the condensate collected in the cold trap protecting the vacuum pump.
Rec. Slurry	Mass of slurry recovered from the crystallizer.
Accumulation & Loss	Mass recovered by washing the vessel with a known amount of water.
Funnel Loss	Mass recovered by washing the funnel with a known amount of water and then drying with paper of a known weight. Performed after the filtration and washing operations.
Beaker Loss	Mass of slurry lost in the beaker necessary for the transfer from the vessel to the filter.
Sample	Mass collected from the unwashed crystals or washed crystals.
PLM Sample	Mass taken from the slurry for PLM imaging.

Solid arrows are process streams and dotted arrows represent quantified losses. Closure on a total mass balance was performed for each dashed box around a process unit.

Figure 42. Overall mass balance on Stage 1 of Run 38b (SST early feed solution): run was performed at 66 °C and 25 g/h evaporation rate

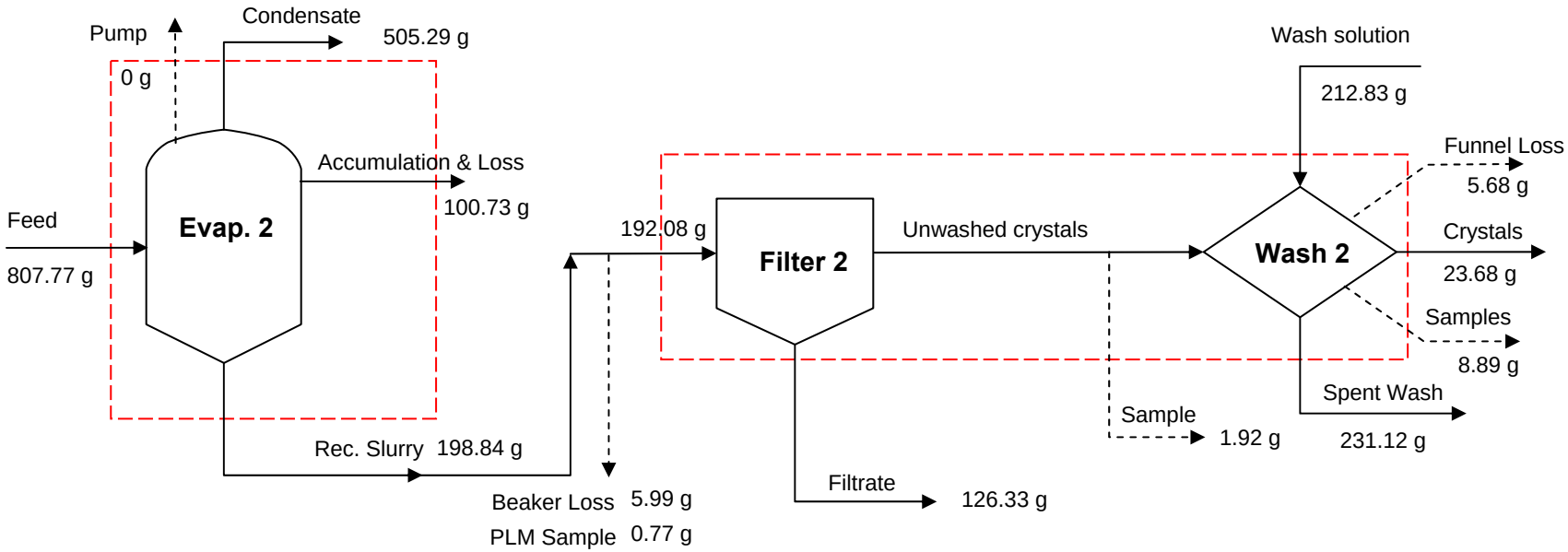

Pump	Mass of the condensate collected in the cold trap protecting the vacuum pump.
Rec. Slurry	Mass of slurry recovered from the crystallizer.
Accumulation & Loss	Mass recovered by washing the vessel with a known amount of water.
Funnel Loss	Mass recovered by washing the funnel with a known amount of water and then drying with paper of a known weight. Performed after the filtration and washing operations.
Beaker Loss	Mass of slurry lost in the beaker necessary for the transfer from the vessel to the filter.
Sample	Mass collected from the unwashed crystals or washed crystals.
PLM Sample	Mass taken from the slurry for PLM imaging.

Solid arrows are the process streams and the dotted arrows represent the quantified losses. Closure on a total mass balance was performed for each dashed box around a process unit.

Figure 43. Overall mass balance on Stage 2 of Run 38b (SST Early Feed Solution): run was performed at 40 °C and 39 g/h evaporation rate.

Table 13. Mass balances around process units of early feed certification run (SST early feed Run 38b)

Unit	Input (g)	Output (g)	Difference (g)	% Closure of Mass Balance
Evaporator 1	1565.45	1563.4	2.05	0.13
Filtration & Washing 1	1003.64	998.89	4.75	0.47
Evaporator 2	807.77	804.86	2.91	0.36
Filtration & Washing 2	404.91	397.62	7.29	1.80

3.1.3 CHARACTERIZATION OF CRYSTAL PRODUCT

Polarized Light Microscopy:

Samples of crystals removed from the slurry produced in each stage were examined using polarized light microscopy (PLM). Figure 44 and Figure 45 display the PLM photmicrographs obtained from the first and second stage respectively. From Figure 44, five different crystalline species can be identified: burkeite, sodium oxalate, sodium sulfate, sodium carbonate monohydrate, and sodium nitrate. Panels B, C anf F display the presence of burkeite, panels C and E the presence of sodium carbonate monohydrate and panels A through H the presence of sodium nitrate and sodium sulfate. In addition to burkeite crystals, sodium carbonate and sodium nitrate were found in large amounts, along with trace amounts of sodium sulfate and sodium oxalate crystals. Figure 44 panels E to H are PLM images showing sodium nitrate crystals over a size range from 100 to 500 μm, while sodium carbonate monohydrate crystals had a maximum size of around 200 μm. The single burkeite crystals had a size of about 20 μm and a size range between 30 to 50 μm when presenting different sections. Trace amounts of sodium sulfate were also identified.

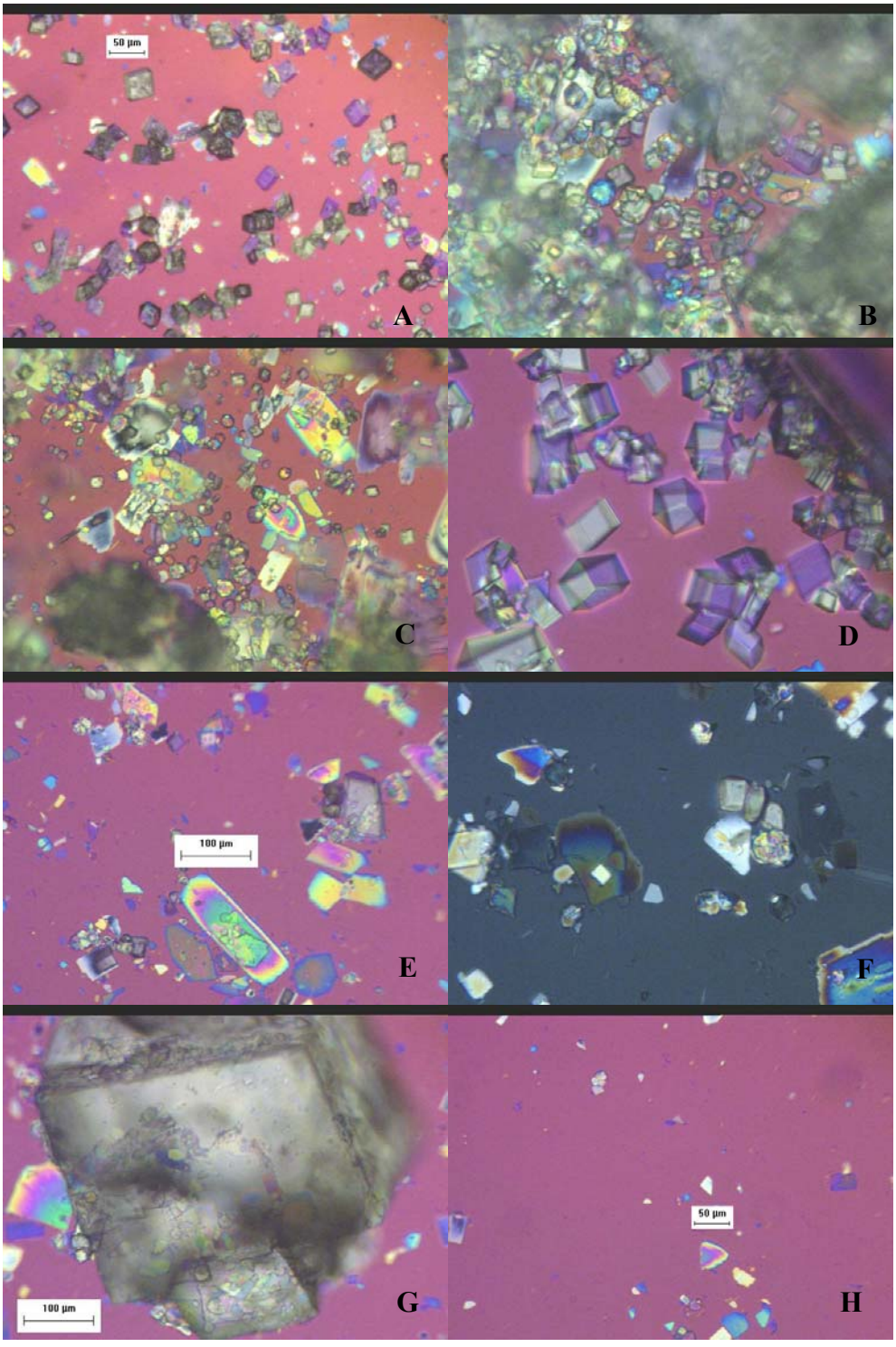

Figure 44. PLM images of the crystals obtained from the first stage slurry (images A to D) and unwashed crystals (imges E to H) of Certification Run 38b
(Panel A, sodum nitrate and sodium sulfate, Panel B, burkeite crystals, Panel C, sodium carbonate monohydrate, Panel D, sodium nitrate crystal, Panel E, large sodium carbonate monohydrate, Panel F, multi section burkeite, Panel G, large sodium nitrate, Panel H, average size sodium sulfate and small sodium carbonate monohydrate).

Figure 45 displays PLM images taken from the slurry of the second stage of certification run 38b. Panels A and B show the exclusive presence of sodium nitrate in the slurry of Stage 2. The sodium nitrate crystals have different geometries and a large spread in their size range (from 10 μm to several hundreds of micrometers).

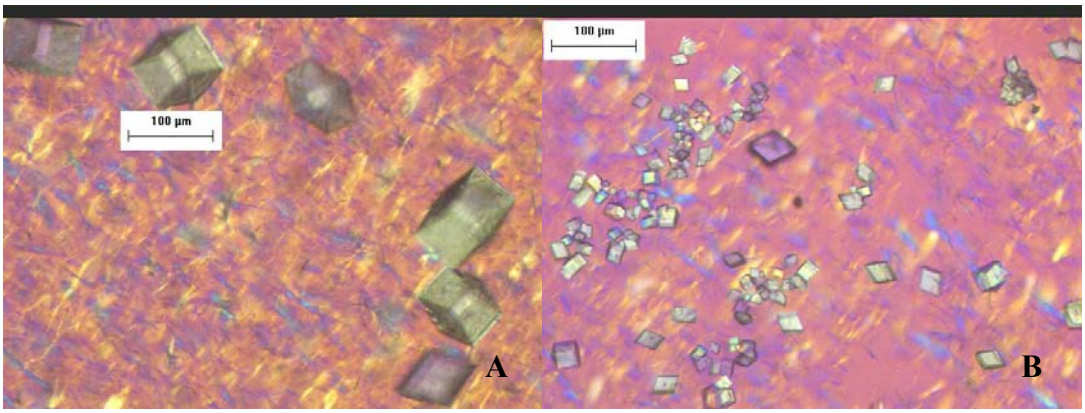

Figure 45. PLM images of the crystals obtained from the second stage slurry of Certification Run 38b

Figure 46 displays the simulation graph for the early feed crystallization at 66 °C which corresponds to the condition of the certification run. A similar graph was described in Chapter 2. The simulations (EARLY_FEED_FINAL_LABORATORY_FLOWSHEET.xls) predicted formation of all of the crystals at the conditions of the run at the exception of sodium sulfate. Further details on the nucleation points will be provided in Chapter 4.

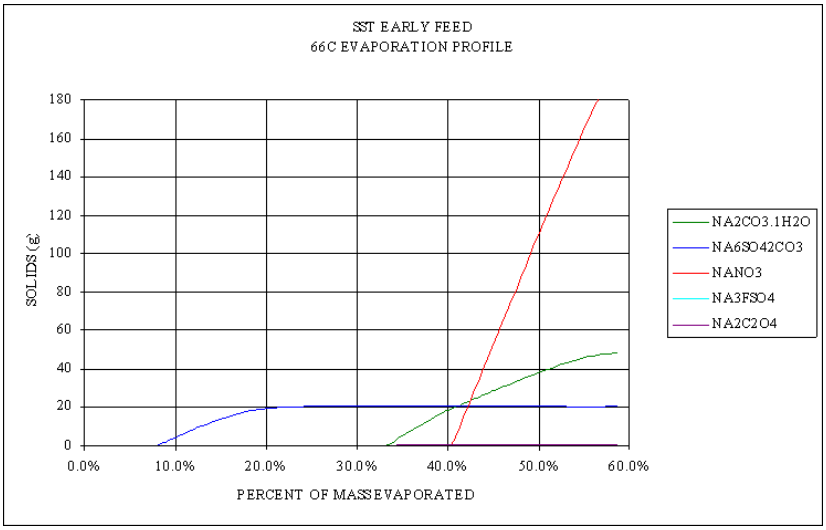

Figure 46 Thermodynamic yield simulations for early feed semi-batch crystallization at 66 °C

Figure 46 assumes that the system is equilibrated at 66 °C; i.e., it is assumed that the solution is at saturation throughout the evaporative process.

Sieve Analyses:

A fraction of the crystals obtained at the end of Stage 1 was washed with acetone as outlined in Section 2 and allowed to air dry. The crystals were then subjected to sieving as described in Chapter 2. Figure 47 shows the resulting histograms and cumulative distributions for the first and second stage of the early feed certification run 38b.

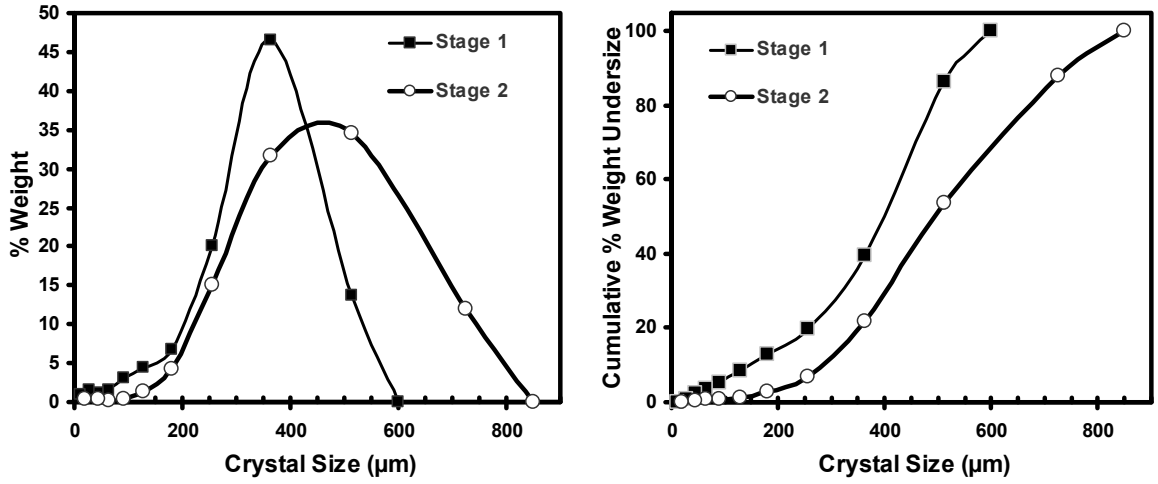

Figure 47. Histograms and cumulative distributions for the early feed Certification Run 38b

These samples displayed a mode size around 350 µm. In addition, the cumulative distribution show that only 5% of the crystal mass is below 75 µm. This mass was expected to correspond mostly to burkeite, since these crystals were observed in PLM images and were typically grown to small sizes. The distribution was relatively narrow and gave a coefficient of variation of 34.7%, where the coefficient of variation was defined by:

$$CV = \frac{100(d_{84\%} - d_{16\%})}{2d_{50\%}} \tag{14}$$

Appendix G presents the details on the coefficient of variation calculation for the first stage of Run 38b. Assessing the sieve results obtained on Stage 2 crystals, the CSD displayed a mode size around 500 μm. In addition, the cumulative distribution showed that less than 5% of the crystal mass was below 100 μm. This result was consistent with the PLM images in Figure 45 and the crystals were expected to be only sodium nitrate. The distribution was relatively narrow and gave a coefficient of variation of 36.6 %. Figure 47 highlights the fact that a small mass of fines and large crystals were produced.

Species Distribution:

Fractional crystallization typically generates a product that contains several solid phases. The distribution among various size fractions of the product depends upon the interplay between the solid-liquid equilibrium, nucleation and growth kinetics of each species. After sieving, samples from several sieves were analyzed to determine how the crystalline species were distributed according to size. The PLM images of crystals from Stage 1 of run 38b are shown in Figure 48 and Figure 49.

Several species can be identified in the product from Stage 1. Those found on the sieve with the smallest opening were characteristic of the oblong shape of sodium carbonate (Figure 48A and Figure 48B), the round shape of burkeite crystals (Figure 48A), and small rod (or prismatic) shape of sodium oxalate. Note that the crystals were not broken not was there significant agglomeration. Sodium carbonate monohydrate (Figure 48C and Figure 48D) and burkeite crystals (Figure 48C) were the only crystals observed in the vicinity of the first mode (30 μm). The irregularity, considered as a second mode, observed in the 50-150 μm size range appeared to be mainly composed of sodium carbonate crystals associated to burkeite agglomerates around the 50 μm size (Figure 48E), and sodium nitrate crystals around the 150 μm

size (Figure 48F). Only trace amounts of sodium carbonate were observed in samples from the 150-212μm sieve, and no sodium oxalate crystals were observed from the 20-38 μm sieve. Crystals in the vicinity of the second mode (350 μm) appeared to be only sodium nitrate. Again they do not involve agglomerates or broken crystals. The sodium nitrate crystals are all independent (no agglomerates), allowing us to validate the sieving procedure and the CSD (Figure 48G). The largest sieve had mainly agglomerated particles. Figure 49 confirmed the presence of three different shapes or forms of burkeite crystals, which may result from three different growth mechanisms: (1) single round crystals of 20 μm, (2) heterogeneous crystals resulting from the growth of burkeite around one or more sodium nitrate or sodium carbonate crystals, and (3) subdivided burkeite crystals resulting from single crystal growth, agglomeration, and association. Another important remark is the high proportion of heterogeneous burkeite crystals in the crystalline population.

Crystals in the vicinity of the mode from the second stage (500 μm) showed nicely formed sodium nitrate crystals. There were no agglomerates or broken crystals in the observations.

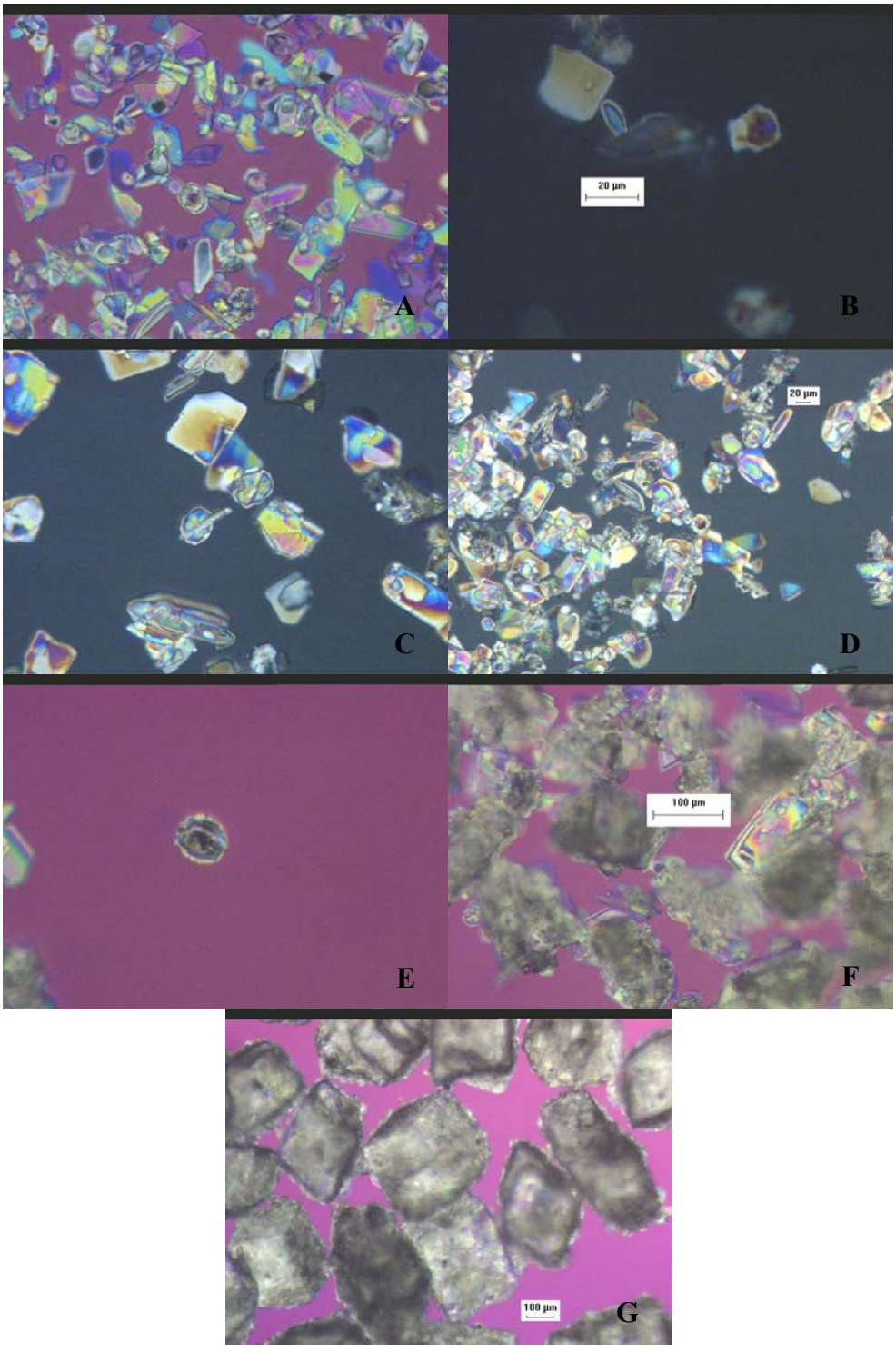

Figure 48. PLM images of sieved crystals from Stage 1 of early feed Certification Run 38b
(Panel A and B, sodium carbonate monohydrate, Panel C, burkeite and sodium oxalate, Panel D and E, sodium carbonate and burkeite in the 30 to 50µm size range, Panel F, large sodium carbonate monohydrate, Panel G, large single sodium nitrates)

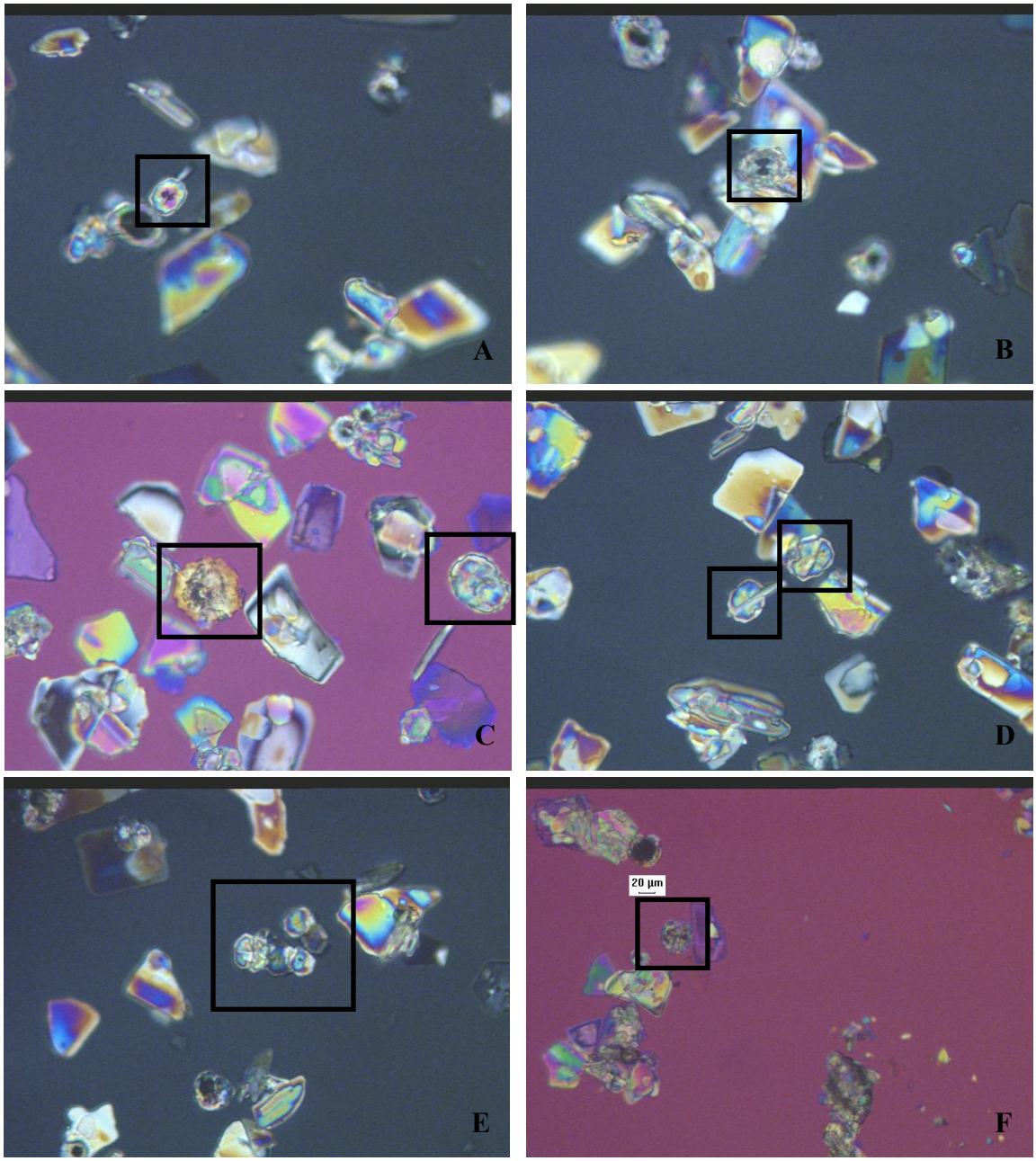

Figure 49. PLM images of sieved burkeite crystals from Stage 1 of early feed Certification Run 38b
(Panels A and B, heterogeneous burkeite crystals presenting more likely nuclei of sodium nitrate and carbonate monohydrate as inclusion., Panel C, two different morphologies of burkeite crystals, Panels D and E, single homogenous burkeite crystals and "flower like" habit of burkeite agglomerate, Panel F, random shape agglomerate of burkeite crystals)

3.1.4 CHEMICAL ANALYSIS AND SPECIES MASS BALANCES

Certification Run Requirements:

As stated in Chapter 1 and Chapter 2, the objectives of the technology described in the present thesis involve the cesium content of the recovered crystals, the recovery of sodium in the solid product, and the separation of sulfate ions from the liquid destined for feed to the Waste Treatment and Immobilization Plant. Minimum and desired targets for these criteria were as follows: (1) Obtain a crystalline product that upon dissolution in water to a 5 M sodium concentration has a Cs content low enough to produce a specific activity of less than 0.05 Ci/L, and preferably less than 0.0012 Ci/L; (2) Recover at least 50% of the sodium from the feed solutions as crystalline product, and preferably at least 90%; (3) Produce a filtrate that has a molar ratio of sulfate to sodium less than 0.01, and preferably less than 0.0022.

In this chapter, the methodology used to assess the completion of these requirements was the following: (1) determine the accounting of the total mass entering and leaving the two-stage process, (2) perform sampling and prepare samples following the protocols defined in Chapter 2 and appendix H, (3) send the samples to GTRI for chemical analysis, (4) determine species mass balances for the two-stage process based on chemical analysis results with the methodology described in Chapter 2, (5) validate the three technology requirements by applying calculations defined in Chapter 1 and 2 on cesium decontamination, sodium recovery and sulfate to sodium molar ratio.

Balance on Total Mass:

Figure 50 illustrates the accounting associated with the total mass entering and leaving Stage 1 and Stage 2 of the SST early feed solution certification run. The streams label used in this figure were defined in Chapter 2. Table 14 shows the mass balances closures around each

crystallization stage of the early feed certification run. The values of the mass associated which each of the streams involved in the process were taken from Figure 50. Chapter 2 defines the methodology used to compute the overall mass balance for each crystallization stage and the adjusted mass balance closure calculated based on the recovered mass. The results of the balances on total mass showed that 36.92 g were lost in Stage 1, but that 28.47 g could be accounted for using the methods described in Chapter 2. This meant that the unaccounted for loss was 8.45 g; another way of saying this is that the balance on total mass was closed to within 0.4%. Addressing Stage 2: there was a loss of 33.45 g, of which 10.9g were unaccounted for; in other words the total mass balance closed to within 1.0%.

Samples of each stream were obtained and sent to GTRI Laboratories for chemical analyses (appendix I). The samples were of the feed solution, filtrate, spent wash, wash solution, unwashed crystals, washed crystals after each wash, and accumulation. All samples were sent for analysis in liquid form in order to give a homogeneous sample. Results obtained from GTRI were tabulated in a spreadsheet and the mass of each ionic species was calculated at each sample point in the process.

Table 14 gives inputs, outputs, and closures of mass balances around the process for each species tested by GTRI. The mass balance closures for each of the species were in the order of magnitude that can be expected from the chemical analysis of diluted samples. For the species present in larger concentrations in the original feed solutions and diluted samples (sodium, aluminum and chromium), closures were all within 10 percent. For the species present in lesser concentration (cesium, sulfate and phosphate) the closures were in the order of 29%. Details of the stage-wise and stream repartition of the species mass balances are given in

Table **15** and Table 16.

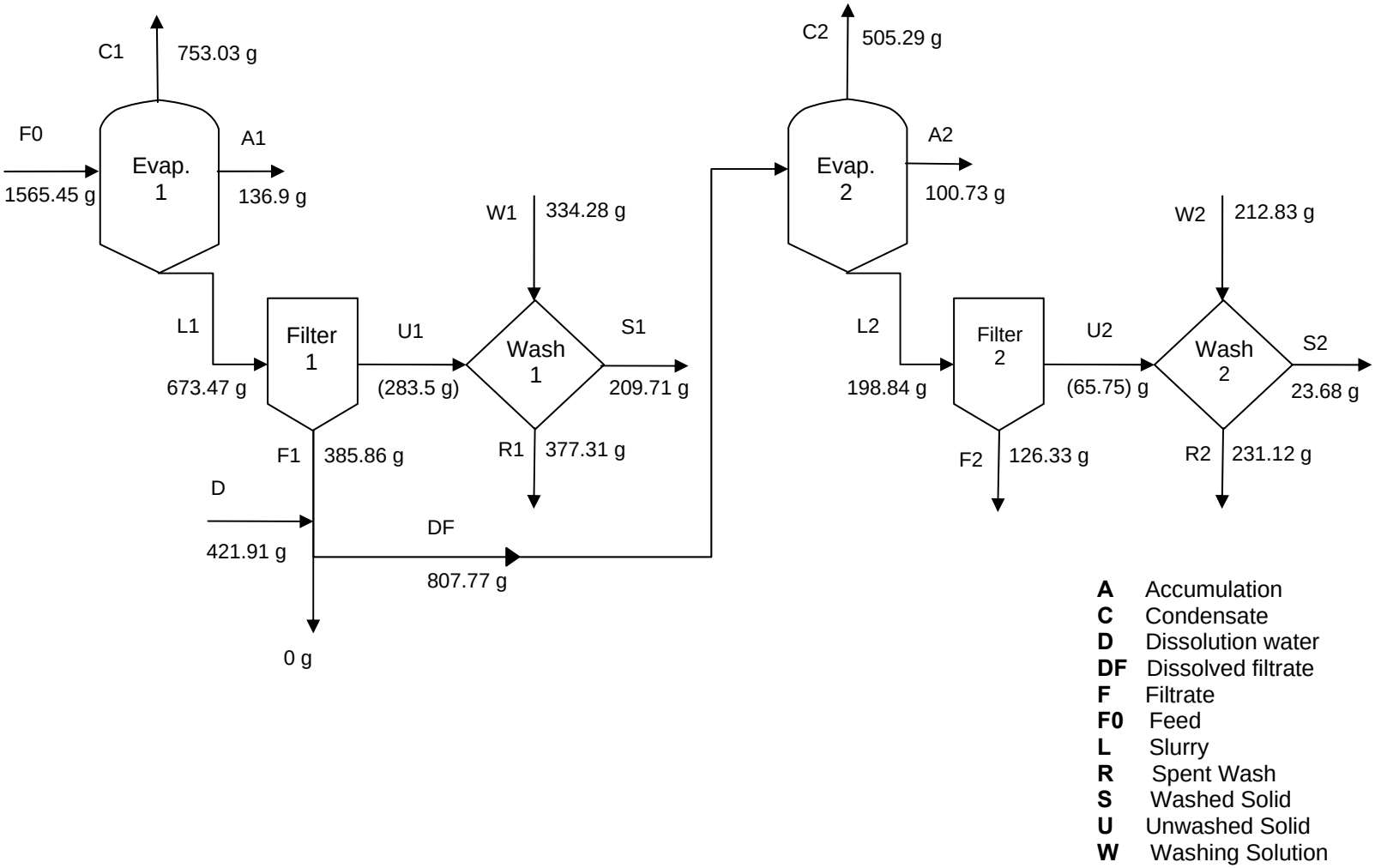

Figure 50. Balances on total mass for each process unit in early feed Certification Run 38b

Table 14. Balances on total mass and mass balance closures for each crystallization stages in early feed Certification Run 38b

Stage 1	Input (g)		Output (g)					Loss (g)
Species	Feed	Wash	Cond	Washed Solids	Filtrate	Spent Wash	Accum.	
Early Feed	1565.45							
H_2O			753.03					
Na_2CO_3								
$NaNO_3$								
Solids or Solution		334.28		209.71	385.86	377.31	136.9	
Total	1565.45	334.28	753.03	209.71	385.86	377.31	136.9	36.92
Combined	1899.73		1862.81					36.92
						% Loss		1.9%
						Accounted loss (g)		28.47
						% Corrected Loss		0.4%

Stage 2	Input (g)		Output (g)					Loss (g)
Species	Feed	Wash	Cond	Washed Solids	Filtrate	Spent Wash	Accum	
Filtrate stage 1	352.62							
H_2O	455.15		505.29					
Na_2CO_3								
$NaNO_3$								
Solids or Solution		212.83		23.68	126.33	231.12	100.73	
Total	807.77	212.83	505.29	23.68	126.33	231.12	100.73	33.45
Combined	1020.6		987.15					33.45
						% Loss		3.2%
						Accounted loss (g)		23.25
						%Corrected Loss		1.0%

Table 15. Species mass balances closures for the early feed Certification Run 38b

Species	Input (g)	Output (g)	Closure (%)
Al	11.9	10.8	9.4
Cr	2.35	2.28	3.0
Cs	4.93E-03	3.49E-03	29.3
SO_4	18.6	13.1	29.9
P	2.50	1.85	26.0
Na	343.7	308.3	10.3

Table 16. Species mass balances foreach streams of the early feed Certification Run 38b Stage 1

Stage 1	Input (g)		Output (g)					Closure
Species	Feed	Wash	Condensate	Filtrate	Spent Wash	Crystals	Accumulation	%
Al	11.9	0	0	9.72	1.86	4.82E-02	1.12	-7.2
Cr	2.35	0	0	1.94	0.39	1.52E-02	0.26	-11.4
Cs	4.93E-03	0	0	2.95E-03	1.40 E-03	1.76E-05	3.98E-04	21.5
SO_4^{2-}	18.6	0	0	1.10	0.71	6.44	4.51	29.6
P^-	2.50	0	0	1.59	0.38	1.42E-02	0.23	11.3
Na	234.8	65.6	0	84.0	78.1	76.9	41.7	6.6

Table 17. Species mass balances foreach streams of the early feed Certification Run 38b Stage 2

Stage 2	Input (g)			Output (g)					Closure
Species	Filtrate 1	Dilution	Wash	Condensate	Filtrate	Spent Wash	Crystals	Accumulation	%
Al	8.89	0	0	0	4.66	1.22	4.69E-02	1.15	20.3
Cr	1.78	0	0	0	0.95	0.26	9.55E-03	0.25	17.3
Cs	2.70E-03	0	0	0	1.51E-03	4.52E-04	1.55E-05	3.68E-04	13.0
SO_4^{2-}	1.01	0	0	0	0.60	0.19	2.00E-02	0.14	5.8
P^-	1.45	0	0	0	0.55	0.21	1.54E-02	0.35	23.1
Na	76.7	0	39.5	0	27.5	46.7	9.76	18.0	12.2

Note that the masses of the final crystals and the crystals from the solids sample were combined during the treatment of the results from the chemical analysis used to obtain the results

in Table 16 and Table 17. In essence this means that the cesium value displayed in these tables can be directly used for the calculation of the decontamination factor as shown in Chapter 1. Table 16 displays that (1) two thirds of the sulfate originally present in the feed solution was recovered in the solid form (final crystals and accumulation) which is in agreement with the formation of burkeite and sodium sulfate crystals, (2) a large fraction on the sodium was recovered in the solid phases even if the filtrate retained 84 g of sodium, (3) a very large fraction of the cesium was collected in the liquid streams leaving very small concentration of cesium in the solid phases. Assessing the results displayed by Table 17, improvements were made mainly for the cesium recovery in the liquid streams while the sodium recovery was improved and the sulfate recovery in the solid phase was relatively low due to the low formation of sulfate based (sodium sulfate, burkeite or trisodium fluoride sulfate) crystals.

3.1.5 COMPARISON TO MINIMUM AND DESIRED TARGETS

Table 18 compares the results of the early feed certification run 38b three process requirements. The values displayed are based on the chemical analysis performed by GTRI.

Table 18. Comparison of required and desired outcomes to experimental results obtained for the three process requirements specified for the early feed Certification Run 38b

SST Early Feed	Stage	Required	Actual	Desired
Cs Decont. Factor	1	1.15	210	48
	2	1.15	66	48
	Total	1.15	162	48
Sodium Recovery	Total	50%	63.4%	90%
Sulfate-to-Sodium	1	0.01	0.0032	0.0022
	2	0.01	0.0052	0.0022
	Total	0.01	0.0037	0.0022

The sodium recovery was 63.4%, which exceeds the minimum target of 50% but was lower than the desred recovery of 90%. The cesium activity was calculated directly from the chemical analyses performed by GTRI on the washed crystals obtained from Stages 1 and 2. The estimated decontamination factor associated with blending the two products of washed crystals from Stages 1 and 2 was 162. This value is above both the minimum and desired value of 48. Finally, the sulfate-to-sodium molar ratio in the filtrate streams from Stages 1 and 2 were calculated using the relative amounts of the two ions in the filtrate streams and showed a sulfate-to-sodium ratio of 0.0037, which exceeds the minimum requirement of 0.01 mole sulfate ion per mole sodium ion but is slightly above the desired value of 0.0027 mole sulfate ion per mole sodium ion.

3.1.6 REPRODUCIBILITY STUDY

A two-stage crystallization run was performed with early feed simulated waste solution at the same conditions of certification Run 38b. The outcomes of this "reproduced run" were compared to the results obtained for Run 38b. Table 19 provides a comparison of the operating conditions used for the certification and the reproduced Early Feed run. This table showed that the main operating conditions were exactly identical for both runs, with a temperature of 66 °C and an evaporation rate close to 26 g/h.

Table 19. Comparison of operating conditions of certified and reproduced early feed run

Operating Condition	Certification Run	Reproduced Run
Evaporation Rate	26.0 g/h	26.1 g/h
Operating Temperature	66 °C ± 1 °C	66 °C ± 1 °C
Condensate-to-feed Ratio	0.481	0.477
Evaporation Profile	Linear	Linear

The comparison of the resulting crystal size distributions of the two runs was used as a validation of the process reproducibility. The outcome of the sieving analysis, displayed in Figure 51 shows similar tri-modal distributions for both runs. The coefficient of variation for the reproduced run was slightly smaller than for the certification run with values of 30 and 34 % respectively. The XRD and PLM analyses of sieved crystals validated similar species distribution with respect to sizes for both runs.

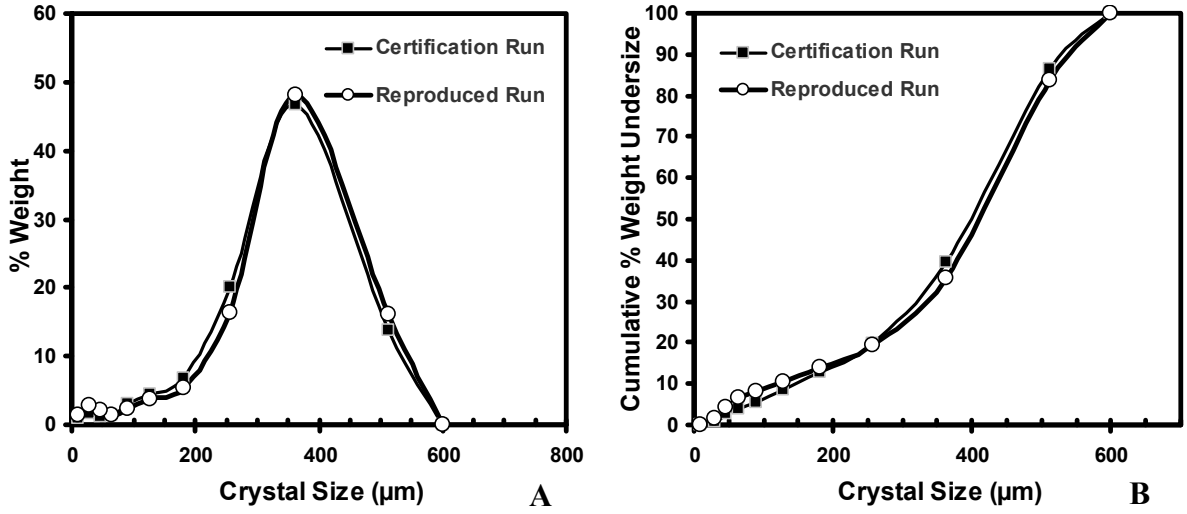

Figure 51. Histograms (Panel A) and cumulative distribution (Panel B) comparison for the early feed certification and reproduced runs

Table 20 presents a summary of the species nucleation points obtained for two early feed runs performed at 66 °C and 26 g/h. The nucleation points are very similar for both runs and are in agreement with similar crystal distributions and kinetics as shown in Chapter 2.

Table 20. Nucleation points of the main species produced during two early feed evaporative crystallizations at 66 °C and 26 g/h

Operating Condition	Certification Run	Reproduced Run
Nucleation Point Nitrate	0.363	0.357
Nucleation Point Carbonate	0.298	0.300
Nucleation Point Burkeite	0.299	0.306

3.2 CRYSTALLIZATION OF SOLUTION REPRESENTING THE LATE REMOVAL FROM THE WASTE TANK

3.2.1 OPERATING CONDITIONS

The late feed solution simulates the waste recovered from the late removal from the waste storage tank. A longer evaporation phase is necessary because a larger amount of water was added to dissolve the salt cake compared to the early feed. This deference in evaporation time is translated by an increase in the final condenstate-to-feed ratio. In order to simplify the process the simulated waste solution was submitted to single-stage crystallization process conducted using the 100 mL crystallizer. This decision of using only one crystallization stage was based on (1) preliminary late feed runs result that displayed that the performance of the second stage did not greatly improve the three technology requirements on sodium recovery, cesium decontamination and sulfate-to-sodium molar ratio (Nassif L.; 2007), (2) the composition of the late feed solution which is lower in sodium, cesium and sulfate and for which a single stage at extended evaporation time might be performed as efficiently as a two-stage process, and (3) the ease of implementing a single stage process under hot-cell environment. The procedures followed in performing the crystallization were outlined in Chapter 2. Figure 52 displays the condensate mass evaporated as a function of the operating time for the late feed certification run 40, showing that the crystallization was operated at constant evaporation rate.

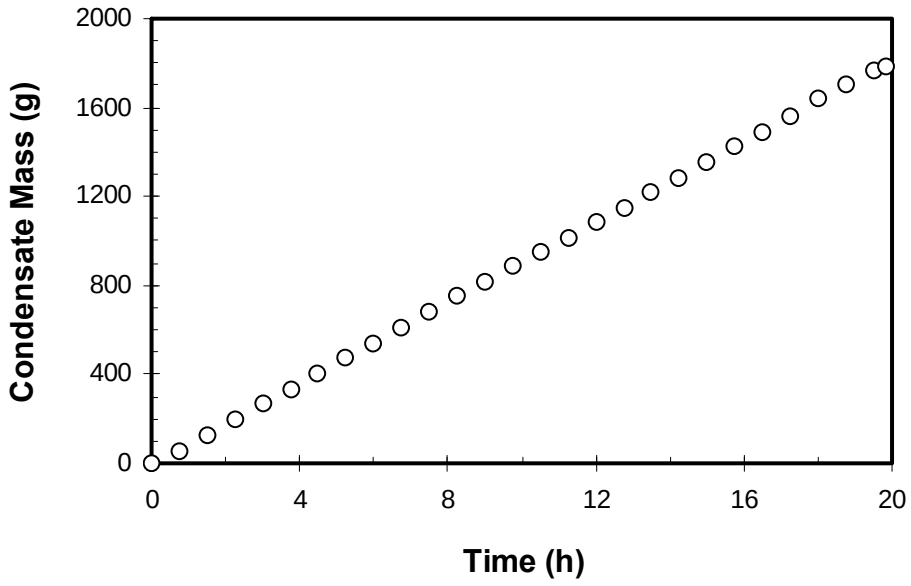

Figure 52. Mass of condensate generated as a function of operating time for late feed Certification Run 40: run was operated at 91 g/h evaporation rate

The evaporation rate was controlled by varying the temperature difference between the heating medium and the slurry. Vapor was generated for 19.8 hours at a rate of 91 g/h. by setting the temperature of the heating fluid to 90 °C and adjusting the pressure in the crystallizer during the run, so that the slurry temperature stabilized at 60 °C. The target and actual condensate-to-feed ratios were 0.882 and 0.881, respectively. Figure 53 displays the simulation graph for the elate feed crystallization at 60 °C which corresponds to the condition of the certification run 40. A similar graph was described in Chapter 2. The simulations (LATE_FEED_FINAL_LABORATORY_FLOWSHEET.xls) were used to determine the condensate-to-feed ratio applied to the late feed certification run 40. The simulations predicted formation of sodium nitrate, sodium carbonate monohydrate, burkeite, sodium oxalate and trisodium fluoride sulfate.

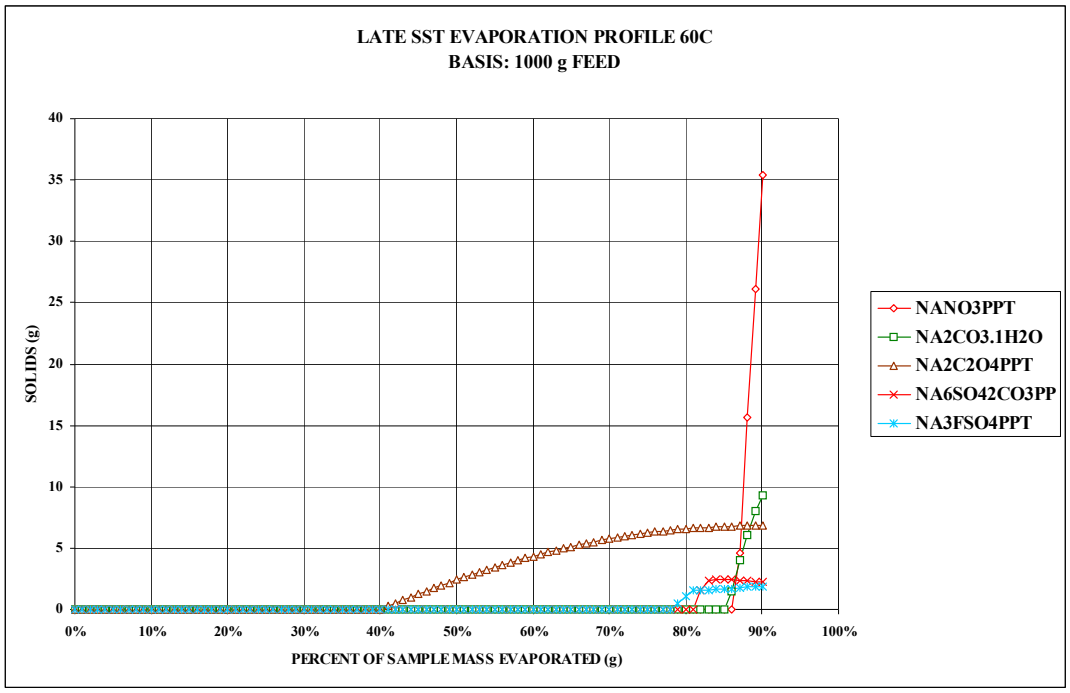

Figure 53. Thermodynamic yield simulations for late feed semi-batch crystallization at 60 °C

Figure 54 displays the temperature and pressure profiles for late feed run 40. Throughout the run the temperature was controlled to within ± 1 °C of the target value of 60 °C. The pressure profile displays the step-wise changes in vacuum level, which correspond to adjustments of the regulating valve.

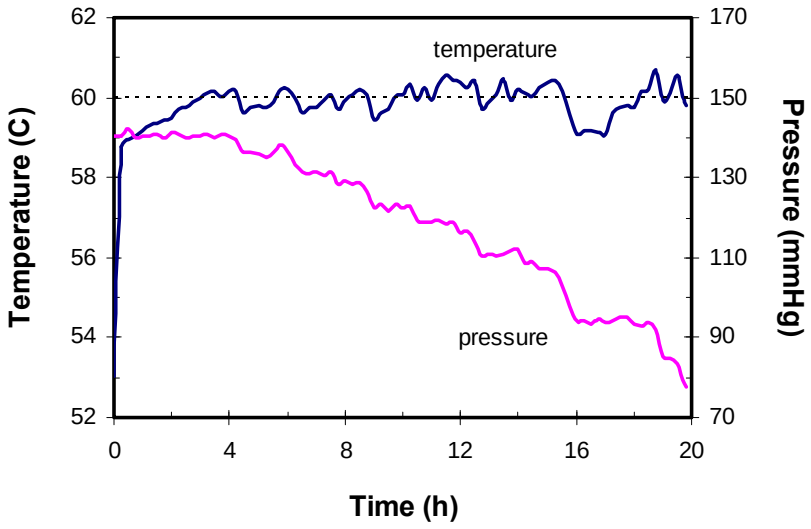

Figure 54. Temperature and pressure profiles for late feed certification Run 40
(The dotted line represents the target operating temperature of 60 °C)

3.2.2 BALANCE ON TOTAL MASS

Mass balances closures were performed as described in Chapter 2. The objectives were to (1) determine the fate of species entering the process, and (2) identify potential problems with the operating procedures. Figure 55 is a schematic diagram illustrating the results of the overall mass balance for the late feed certification Run 40. Included in the figure are definitions of quantities used in closing mass balances around each of the unit operations. The figure shows the masses of vapor generated and either recovered in the condensate receiver or the cold trap protecting the vacuum pump, crystals that accumulated on the walls of the vessel, material that adhered to the vessel and was lost in the transfer process, and the recovered slurry. The slurry recovered from the evaporative crystallization was filtered. The filtrate stream corresponds to the mass of filtrate collected inside the vacuum flask, and the funnel loss corresponds to the loss recovered after the combined filtration and crystal washing operations. The loss was determined by washing the filtration funnel with a known amount of water and using a dry paper of known mass to collect the water accumulated on the wall of the apparatus. The unwashed crystals correspond to the solids recovered at the end of the filtration and their mass was estimated by performing mass balance closure around the filtration unit. The unwashed crystals were washed with a solution saturated in the main species (sodium nitrate, sodium carbonate monohydrate, sodium sulfate, sodium hydroxide and sodium fluoride) as described in Chapter 2. The final crystals were the solid phases obtained at the end of the process and the spent wash was the filtrate of the crystal washing operation.

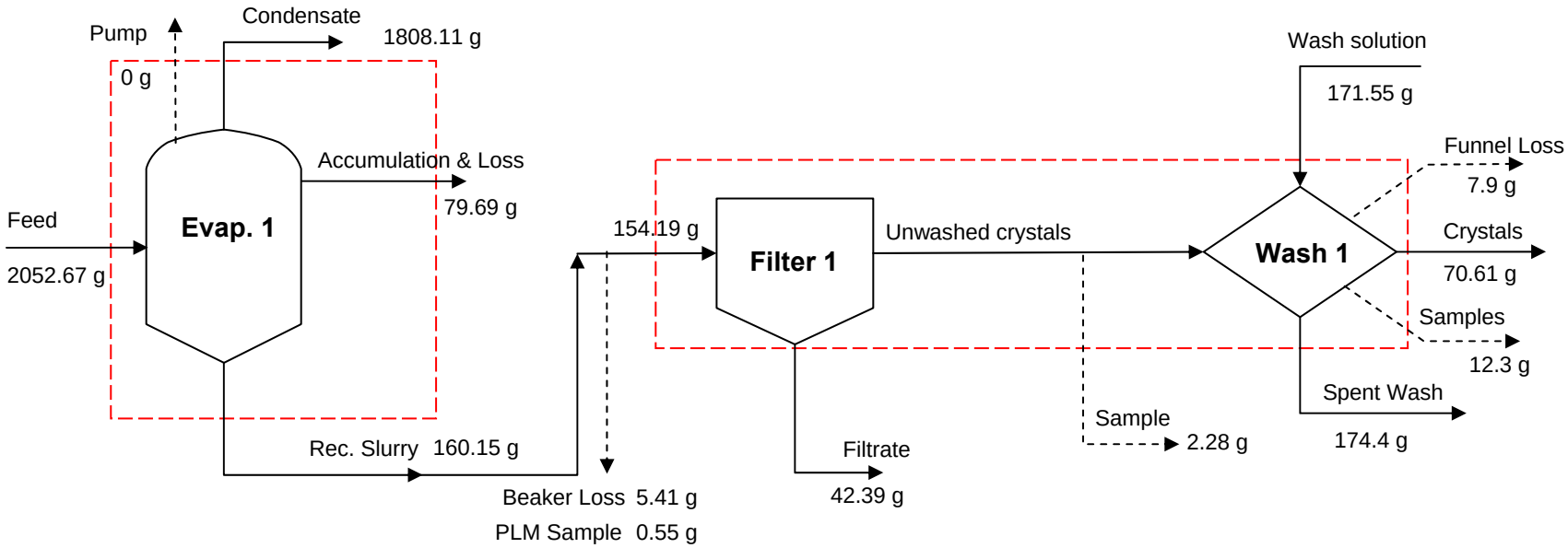

Pump	Mass of the condensate collected in the cold trap protecting the vacuum pump.
Rec. Slurry	Mass of slurry recovered from the crystallizer.
Accumulation & Loss	Mass recovered by washing the vessel with a known amount of water.
Funnel Loss	Mass recovered by washing the funnel with a known amount of water and then drying with paper of a known weight. Performed after the filtration and washing operations.
Beaker Loss	Mass of slurry lost in the beaker necessary for the transfer from the vessel to the filter.
Sample	Mass collected from the unwashed crystals or washed crystals.
PLM Sample	Mass taken from the slurry for PLM imaging.

Figure 55. Overall mass balance of late feed certification Run 40: run was performed at 60 °C and 91 g/h evaporation rate
Solid arrows are the process streams and the dotted arrows represent the quantified losses. Closure on a total mass balance was performed for each dashed box around a process unit.

Since the unwashed solids mass was not measured, a mass balance around the combined filtration-washing step was performed. The results of the mass balance closures around the combined filtration-crystal washing and evaporation unit operations are displayed in Table 21. The difference between input and output for each of the units was as follows: evaporation, 0.23%; filtration and washing, 4.87%.

Table 21. Mass balances around process units of late feed certification run (SST late feed Run 40).

Unit	Input (g)	Output (g)	Difference (g)	% Closure of Mass Balance
Evaporator	2052.67	2047.95	4.72	0.23
Filtration & Washing	325.74	309.88	15.86	4.87

3.2.3 CHARACTERIZATION OF CRYSTAL PRODUCT

Polarized Light Microscopy:

Samples of crystals removed from the slurry produced in each stage were examined using polarized light microscopy (PLM). Figure 56 displays the PLM photmicrographs obtained from the late feed certification run slurry. From Figure 56, five different crystalline species can be identified: sodium oxalate, sodium carbonate monohydrate with regular and a few "masquerade mask" habits, trisodium fluoride sulfate, sodium fluoride phosphate and sodium nitrate. Panels A, B and D display the presence of sodium nitrate, panel A the presence of sodium oxalate, panel C the presence of sodium carbonate monohydrate and panels A and B the presence of the six sided shape of trisodium fluoride sulfate and the purple cuboctahedral shape of sodium fluoride phosphate. In the slurry phase, sodium nitrate and sodium carbonate monohydrate were found in large amounts, sodium fluoride phosphate and sodium oxalate crystals were found in non negligible amounts while trisodium fluoride sulfates were found in very

small to trace amounts. Furthermore, sodium nitrate crystals were identified over a size range of 20 to 450 µm, while sodium carbonate monohydrate crystals ranged mostly between 50 and 100 µm with a maximum size of around 400 µm. Sodium fluoride phosphate crystals were observed in the 30 to 100 µm size range with an average size of 50 µm. The traces of trisodium fluoride sulfate were recovered with a 30 µm size.

The simulations (LATE_FEED_FINAL_LABORATORY_FLOWSHEET.xls) performed by the software developed by OLI System Inc predicted the formation of sodium nitrate, sodium oxalate and sodium carbonate monohydrate in large amounts, along with trisodium fluoride sulfate and burkeite in small amounts (Figure 53).

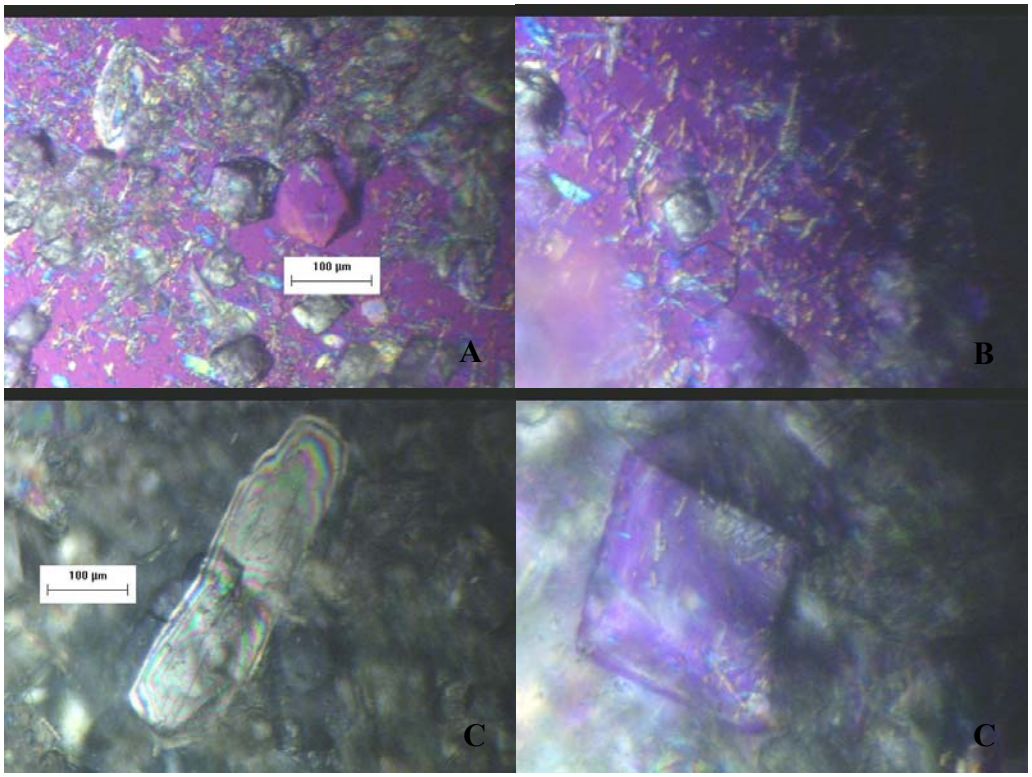

Figure 56. PLM images from the slurry of SST late feed Certification Run 40 operated at 60 °C and 91 g/h)
(Panel A, Sodium nitrate, sodium carbonate monohydrate, sodium fluoride phosphate, sodium oxalate, Panel B, trisodium fluoride sulfate, PanelC, large sodium carbonate monohydrate, Panel D, large sodium nitrate crystal)

Sieve Analyses:

A fraction of the crystals obtained at the end of the run was washed with acetone and allowed to air dry previous to sieving as outlined in Chapter 2. Figure 57 displays the mass density and cumulative distributions of the late feed certification run 40.

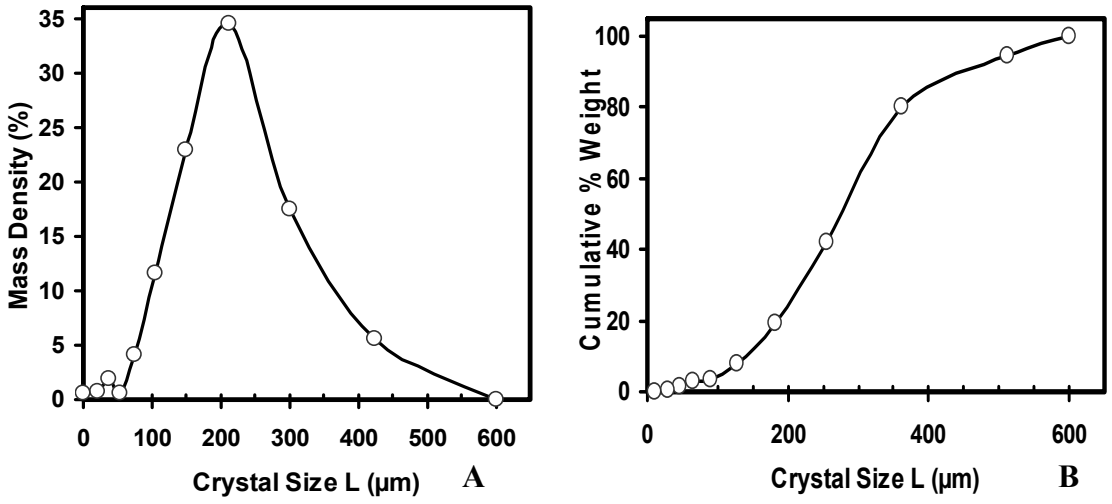

Figure 57. Mass density (Panel A) and cumulative distribution (Panel B) of crystals from SST late feed Certification Run 40

These samples displayed a bimodal curve with a major mode size around 250 µm and secondary mode around 50 µm. In addition, the curves show that less than 5% of the total crystal mass was recovered below 75 µm. This mass is expected to correspond mostly to sodium oxalate in the pan and sodium fluoride phosphate and sodium carbonate monohydrate in the first mode size with the few trisodium fluoride sulfate crystals observed in the slurry PLM images. The distribution is relatively narrow and gives a coefficient of variation of 39.1%. A corrected spread coefficient of 34 % was calculated when accounting for the agglomerates that formed in the upper sieve sizes.

Species Distribution:

Fractional crystallization generates a product that contains several solid phases. Samples from several sieves were analyzed to determine how the species formed were distributed according to size. Figure 58 shows selected PLM images of crystals from the Late Feed certification run.

Six different species were identified in the product from Late Feed crystallization. Those found on the sieve with the smallest opening are characteristic of the oblong shape of sodium carbonate (Figure 58A), small rod (or prismatic) shape of sodium oxalate (Figure 58A), and trace amounts of sodium sulfate crystals. These crystals were not broken or aggregated. Sodium carbonate monohydrate (Figure 58C) and in lesser amounts sodium fluoride phosphate crystals (Figure 58D) were observed in the vicinity of the first mode (50 μm). Non negligible amounts of trisodium fluoride sulfate crystals (Figure 58C) were observed and were exclusively collected in the 50 μm sieve size. The slight irregularity, observed in the 50-150 μm size range appeared to be due to the addition of sodium carbonate monohydrate crystals to the existing sodium nitrate population collected in this size range. Only trace amount of sodium carbonate monohydrate were observed in samples over 150 μm, displaying that the major mode size was exclusively composed of sodium nitrate crystals. Sodium nitrate crystals in the vicinity of the second mode (250 μm) are not agglomerated and not broken. The two larger sieves had particles that were agglomerated.

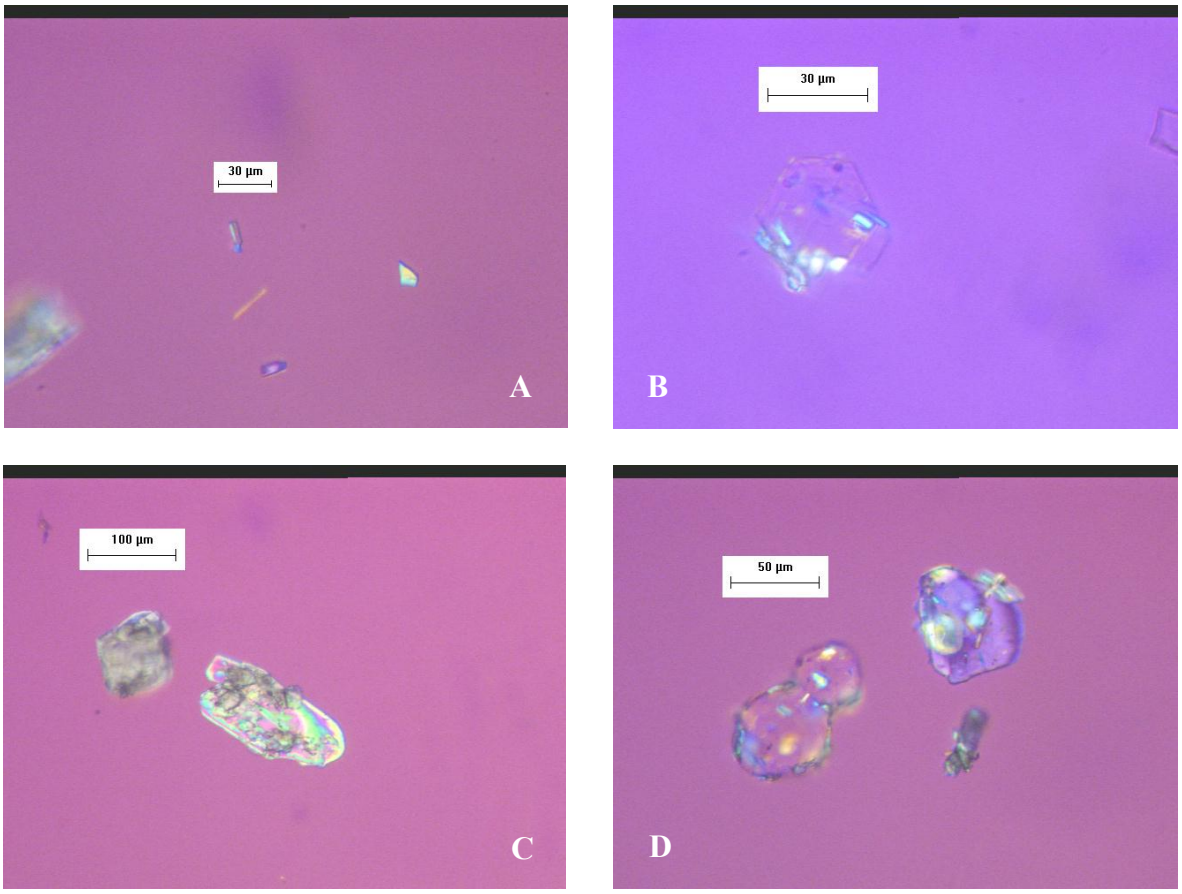

Figure 58. PLM images of sieved crystals from late feed Certification Run 40
(Panel A, sodium oxalate needle, Panel B, six-sided trisodium fluoride sulfate crystal, Panel C, sodium nitrate and sodium carbonate monohydrate crystals, Panel D, agglomerated sodium fluoride phosphate crystals)

3.2.4 SPECIES ANALYSES AND BALANCES

Figure 59 illustrates the accounting associated with the total mass entering and leaving the process. The streams label used in this figure were defined in Chapter 2. Table 22 shows the mass balances closures of the late feed certification run 40. The overall mass balance closure was calculated based on the values described in Figure 59. Chapter 2 defines the methodology used to compute the overall mass balance for each crystallization stage and the adjusted mass balance closure calculated based on the recovered mass. The results of the balances on total mass show that 49 g were lost, but that 28.44 g could be accounted for using the methods described in Chapter 2. This meant

that the unaccounted for loss was 20.58 g; another way of saying this is that the balance on total mass was closed to within 0.9%.

Table 22. Balances on total mass and mass balance closures for late feed Certification Run 40

	Input (g)		Output (g)				Accum (g)	Loss (g)
Species	**Feed**	**Wash**	**Cond**	**Washed Solids**	**Filtrate**	**Spent Wash**	**Solids**	
Feed	2052.67							
H_2O			1808.11					
Solution		171.55		70.61	42.39	174.4	79.69	
Total	2052.67	171.55	1808.11	70.61	42.39	174.4	79.69	49.02
Combined	2224.22		2175.2					49.02
								2.2%
						Corrected Loss		0.9%

Samples of each stream were obtained and sent to GTRI Laboratories for chemical analyses (appendix I). The samples were of the feed solution, filtrate, spent wash, wash solution, unwashed crystals, crystals after each wash, and accumulation. All samples were sent for analysis in liquid form in order to give a homogeneous sample. Results obtained from GTRI were tabulated in a spreadsheet and the mass of each ionic species was calculated at each sample point in the process.

Table 23 gives details of the stage-wise and stream repartition of mass balances for each species tested by GTRI. The mass balance for each of the species closed within 10%. The results of the chemical analysis showed that (1) a large fraction of the sodium was recovered in the solid phases (final crystals and accumulation), (2) the concentration of the cesium in the final crystals was two order of magnitude lower than the original concentration of the late feed, and (3) a large fraction of the original sulfate mass was recovered in the solid phases (solids and accumulation) which was recovered as trisodium fluoride sulfate.

Table 23. Species mass balances for each streams of the late feed Certification Run 40

Stage 1	Input (g)		Output (g)					|Closure|
Species	**Feed**	**Wash**	**Condensate**	**Filtrate**	**Spent Wash**	**Crystals**	**Accumulation**	**%**
Al	2.46	0	0	0.833	1.05	0.022	0.775	8.75
Cr	0.35	0	0	0.112	0.135	3.05E-03	0.099	0.12
Cs	1.12E-03	0	0	3.41E-04	3.92E-04	1.17E-05	2.96E-04	7.18
SO_4^{2-}	3.39	0	0	2.60E-03	0.155	1.80	1.55	3.52
P^-	1.54	0	0	0.031	0.16	0.782	0.577	0.67
Na	63.6	31.2	0	8.85	35.9	25.4	22.5	2.27

Table 24 shows the evolution of the species composition percent for each of the five successive washes. Results show that all 5 washes removed cesium from the filter cake but the first 4 washes led to the highest removal of cesium. This decrease is representative of the efficiency of the crystal washing. The low value of cesium in the final crystals also proves that before washing the major part of the cesium was traped in the filter cake as interstitial mother liquor, and that very few cesium were traped in the crystal matrix.

Table 24. Evolution of each species concentration with washing for the SST late feed Certification Run 40
(Composition values in percents or ppm and are of undiluted crystals)

Species	Unwashed	1 Wash	2 Washes	3 Washes	4 Washes	5 Washes
Al	0.649%	0.197%	0.085%	0.034%	0.016%	0.002%
Cr	0.085%	0.029%	0.015%	0.007%	0.005%	0.0002%
Cs	2.72	0.923	0.379	0.121	0.056	0.043
SO_4^{2-}	1.89%	2.18%	2.08%	2.10%	2.20%	2.11%
P^-	0.973%	1.11%	0.949%	0.887%	0.845%	0.916%
Na	27.99%	30.14%	30.37%	29.83%	31.00%	29.81%

3.2.5 COMPARISON TO MINIMUM AND DESIRED TARGETS

Table 25 compares the results of the late feed Certification Run 40 three process requirements. The values displayed are based on the chemical analysis performed by GTRI.

Table 25. Comparison of required and desired outcomes to experimental results obtained for the three process requirements specified for the late feed Certification Run 40
(Note that the sulfate content in the filtrate was reported as <10 ppm, so 10 ppm was used for requirement and mass balance calculations)

SST Late Feed	Required	Actual	Desired
Cs Decon Factor	-	123.3	14
Sodium Recovery	50%	75.3%	90%
Sulfate to Sodium	0.01	0.00007	0.0022

Table 25 shows that the sodium recovery was 75.3%, which exceeds the minimum target of 50% but fall short from the desired target of 90% recovery. The cesium decontamination factor was 123.3. This value was above both the minimum and desired value of 14. Finally, the sulfate-to-sodium molar ratio in the filtrate streams were calculated using the relative amounts of the two ions in the filtrate streams as determined by GTRI. The sulfate to sodium ratio was 0.00007, which exceeds the desired requirement of 0.0022 mole sulfate ion per mole sodium ion.

3.2.6 REPRODUCIBILITY STUDY

A single-stage crystallization run was performed with late feed simulated waste solution at the same conditions of Certification Run 40. The outcomes of this "reproduced run" were compared to the results obtained for Run 40. Table 26 provides a comparison of the operating conditions used for the certification and the reproduced late

feed run. This table showed that the main operating conditions were exactly identical for both runs, with a temperature of 60 °C and an evaporation rate close to 91 g/h.

Table 26. Comparison of operating conditions of certified and reproduced late feed run

Operating Condition	Certification Run	Reproduced Run
Evaporation Rate	91 g/h	95 g/h
Operating Temperature	60 °C ± 1 °C	60 °C ± 1 °C
Condensate-to-feed Ratio	0.881	0.883
Evaporation Profile	Linear	Linear

The comparison of the resulting crystal size distributions of the two runs was used as a validation of the process reproducibility. The outcome of the sieving analysis, displayed in Figure 59 shows similar bimodal distributions for both runs. The coefficient of variation for the reproduced run was slightly smaller than for the certification run with values of 39 and 34 % respectively. The XRD and PLM analyses of sieved crystals validated similar species distribution with respect to sizes for both runs.

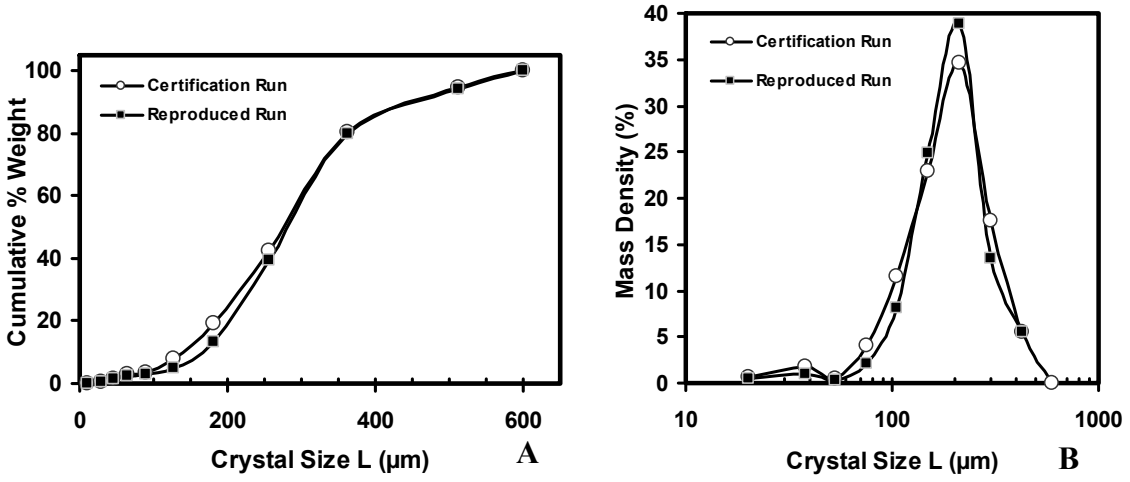

Figure 59. Histograms (Panel B) and cumulative distribution (Panel A) comparison for the late feed certification and reproduced runs

A summary of the major species nucleation points and sieving main parameters is provided in Table 27, displaying similar characteristics for the reproduced and certification run.

Table 27. Nucleation points of the main species produced during two late feed evaporative crystallizations at 60 °C and 91 g/h

Operating Condition	Certification Run	Reproduced Run
Number of Species Identified	6	6
Major Nucleation Point	0.52	0.51
Coefficient of Variation	39	34
Number of Modes	2	2

3.3 CRYSTALLIZATION OF SOLUTION PRESENTING ORGANICS

The nature of the medium-curie waste removed from the storage tanks at the Hanford site presents great variability from one tank to another. Such variability includes different compositions of the key sodium salts, differences in the effluent over the period of time a tank is being emptied (Chapter 3,sections 1 and 2) and the presence of organic constituents and solids particles. For the purposes of this study, primary emphasis was given to early-feed composition: i.e. solutions withdrawn early during the tank-emptying period. The perturbation that was examined in this section was the effects of organic constituents. A series of fourteen runs were performed in determining which organic species were detrimental to the SST Early Feed process. Runs were judged based on the following criteria: (1) ease of solid-liquid separation, particularly compared to the control run for the series of experiments; (2) formation of an organic film on the jacketed walls of the crystallizer or on the filter cake; (3) alteration of the crystal population by the addition of organics, and (4) evidence of foaming during the evaporation stage.

3.3.1 CONTROL RUN FOR SERIES OF EXPERIMENT ON ORGANICS

The simulation file EARLY_FEED_ORGANIC_LABORATORY_ FLOWSHEET3.xls was used to determine the appropriate amount of each organic species to add to the Early Feed simulant. Values for each organic compound were gathered from the simulation and these values were scaled for 600 mL of simulant. Table 28 shows the amounts of each organic species added to 600 mL of Early Feed solution. Additional details are provided in appendix J.

Table 28. Organic compounds added to prepare 600 mL of early feed solution with organics

Compound	Formula	Mass (g)
Sodium Formate	NaCOOH	6.89
Sodium Acetate	$Na(C_2H_3O_2)$	2.13
Sodium Glycolate	$Na(C_2H_3O_3)$	4.27
Trisodium Citrate Dihydrate	$Na_3[C_6H_5O_7]\cdot 2H_2O$	4.33
Tetrasodium EDTA (EDTA)	$Na_4[C_{10}H_{12}N_2O_8]$	4.16
Trisodium HEDTA (HEDTA)	$Na_3[C_{10}H_{15}N_2O_7]$	4.27
Disodium 2,2'-Iminobisacetate (IDA)	$Na_2[C_4H_5NO_4]$	2.22
Trisodium Nitriloacetate Monohydrate (NTA)	$Na_3[C_6H_6NO_6]\cdot H_2O$	0.52

An experimental run (Run 53) was performed with an early feed solution composition to which all of the organics components of Table 28 were added. This run was performed under similar operating conditions than the Early Feed certification run, meaning at 66 °C and 26 g/h. Figure 60 displays the mass of vapor generated as a function of the operating time and shows that the evaporation rate was constant. The average evaporation rates for the certification and the organics runs were 26 and 26.5 g/h, respectively. The target and actual condensate-to-feed ratios for this run were 0.456 and 0.453, respectively following the conditions stated by the simulation file EARLY_FEED_ORGANIC_ LABORATORY_FLOWSHEET.xls. The operating time for run 53 was 24.3 hours. Overall and detailed mass balances on the main organics run are provided in the appendix J.

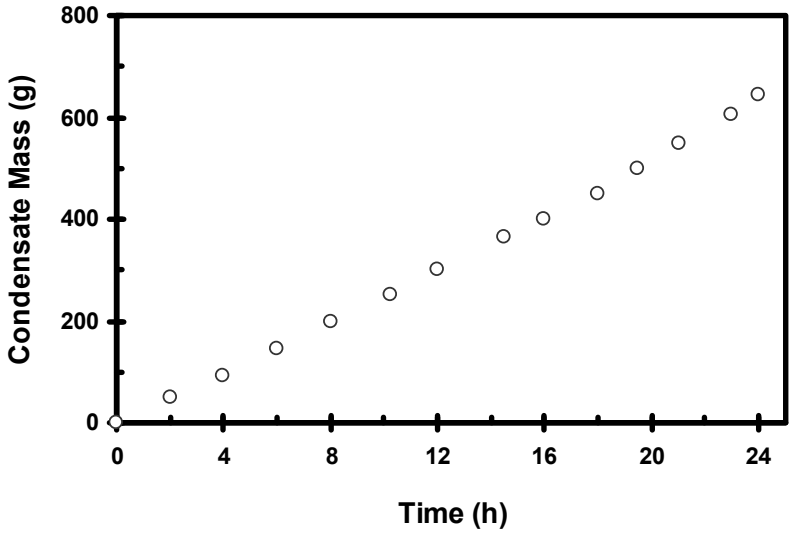

Figure 60. Mass of condensate generated as a function of operating time for early feed organics control Run 53: run was operated at 26 g/h evaporation rate and 66 °C

Figure 61 shows the temperature and pressure profiles from Run 53. The run temperature was controlled to within +/- 1 °C of the target value of 66 °C. The pressure profile reflects the step-wise changes in vacuum that are associated with manual adjustments of the regulating valve.

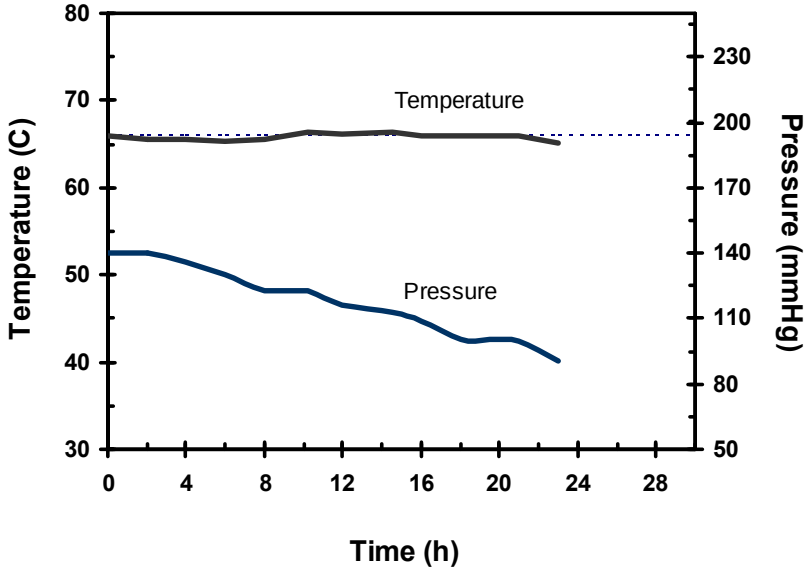

Figure 61. Temperature and pressure profilesf or early feed organics Run 53
(The dotted line represents the target operating temperature of 66 °C)

Several issues were encountered during this run that may have a great impact on the early feed process. The first issue deals with the handling of the accumulation. As displayed by the mass balance the total accumulation mass was relatively low (only 27.5 grams), but a film was created on the wall of the crystallizer. Figure 62 is a photograph of the film that remained in the crystallizer after draining the slurry. The formation of this film made it difficult to observe the contents of the crystallizer and judge the slurry density and the mass of accumulation. The accumulation was estimated by dissolving the crystals remaining inside the crystallizer with a known mass of water. However, the addition of water in this case failed to remove the film completely. In addition, the beaker used to collect the dissolved accumulation presented solids in the bottom. In conclusion, the film that formed was hydrophobic. The compound that is likely to be responsible for this phenomenon is Na_3EDTA, as this was observed to change the texture of the solution during the simulant preparation.

Figure 62. Hydrophobic film on the crystallizer wall of the early feed with organics crystallizer

Since this film is likely to form on the wall of the pilot scale crystallizer and increase in thickness during a continuous process, it represents an issue for the Early Feed processing. An attempt to eliminate the film was performed by washing the inside of the vessel with acetone and applying increased mixing. Figure 63 is a photograph of the wall of the crystallizer and displays that a great part of the film dissolved in acetone. The compound responsible for this film is hence partially soluble in acetone and acetone (or a similar solvent) might be used for apparatus cleaning in actual process.

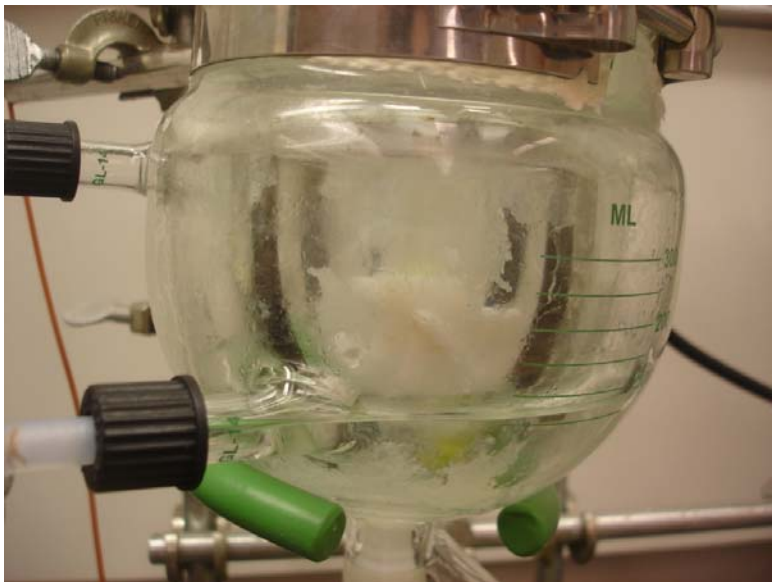

Figure 63. Partial solubility of hydrophobic film with acetone

Figure 64 displays the PLM microphotographs taken from slurry samples of Run 53. Due to the high concentration and the composition of the slurry, accurate PLM images on slurry crystals were difficult to obtain. However, images from the slurry displayed the presence of sodium nitrate crystals with sizes ranging from several micrometers to several hundreds of micrometers. These images also displayed a very high crystalline density in the recovered slurry.

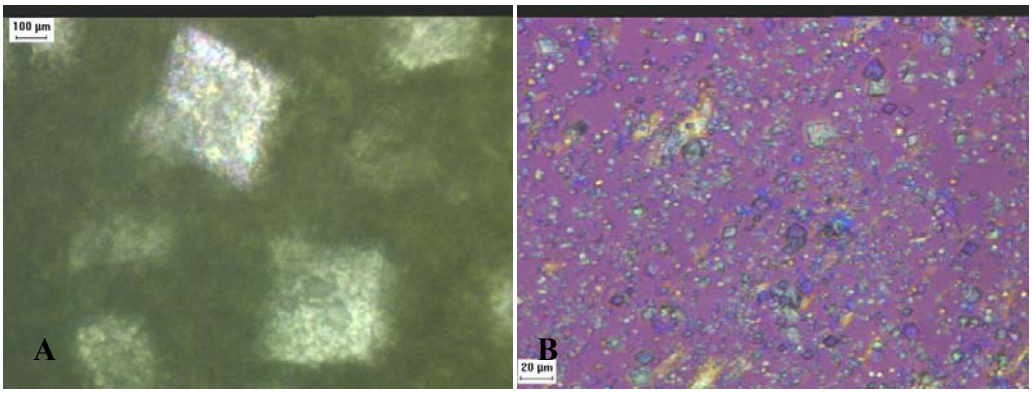

Figure 64. PLM Images from slurry Samples of the Control Organics Experiment
(Panel A, Sodium nitrate with sizes ranging between 300 and 400 µm; Panel B, High crystalline density and sodium nitrate nuclei)

Figure 65 panel A diplays a photograph of the slurry as it was recovered from the crystallizer and submitted to filtration. Panel B demonstrates that the slurry was very vicous and had the texture of the film recovered on the wall of the crystallizer. This was the main cause of the difficulties encountered during the filtration and washing operations.

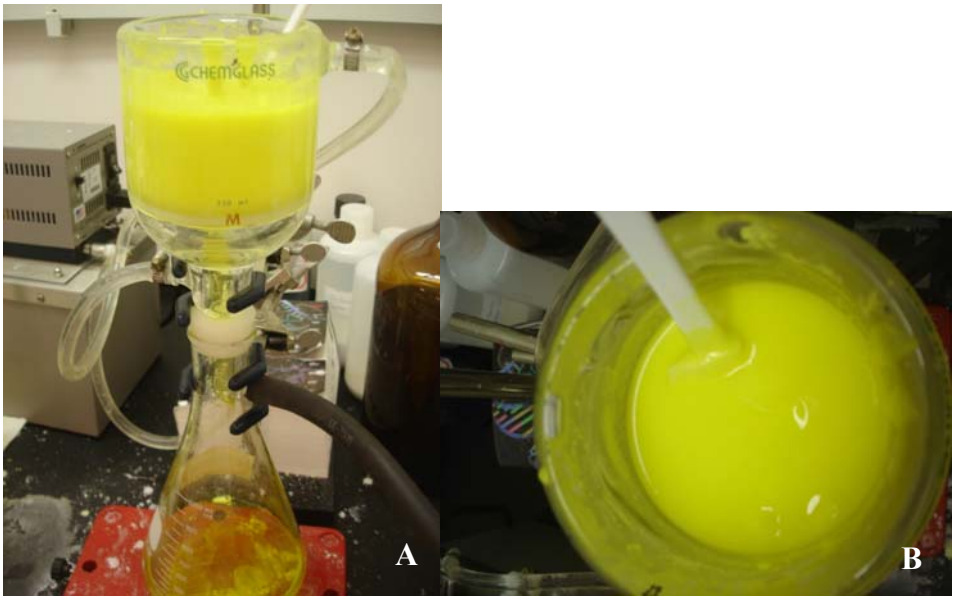

Figure 65. Recovered slurry for run 53, (Panel A) difficulty of filtration and (Panel B) zoom on slurry during solid-liquid separation

Table 29 shows the criteria that were used to evaluate the effect of organics on the solid-liquid separation steps in Run 53. A key point illustrated in Table 29 is the difference between the masses of final crystals from the two runs, Run 53 generated far more product crystals than Run 38b. It is important to notice that the mass displayed in Table 29 corresponds to the mass of final crystals added to the mass of mother liquor trapped by the final crystals. In other words, the filter cake of Run 53 was a mix of crystals and of the hydrophobic component. This component gave a "gel like" texture to the filter cake, which was then very likely to trap interstitial mother liquor. This composition also made mother liquor removal through washing more difficult, explaining why 5 washes were necessary during Run 53 and why the final crystal color failed to achieve the results observed for Run 38b. The important mass of slurry recovered (745 g) along with the apparent spread in the crystal distribution increased further the stirring difficulty and filter plugging that occured during Run 53.

Table 29. Comparisons between Runs 38b and 53 solid-liquid separations

Criteria	Early Feed 38b	Early Feed 53
Evaporation rate (g/h)	~ 26	~ 26.5
Condensate-to-Feed Ratio	0.481	0.453
Washes necessary for major mother liquor removal	3	5
Filtration & Washing Time	Typical	Greatly Increased
Slurry cake composition	Powder-like with large-medium crystals	Texture close to hydrophobic film with large crystals.
Mass of final crystals	Typical (210 g)	Increased (374g)[2]
Color of final crystals	White with slight yellow color	Pale yellow color
Ease of operation	No filter plugging, easy to stir	Very important filter plugging, difficulty to stir

In essence two main issues are likely to be encountered during the pilot scale process: (1) the organics may change the texture and composition of the slurry and

increase the solid-liquid separation time with the possibility of plugging the separation equipment and the pipes leading to the centrifuges, and (2) the wash efficiency may be considerably reduced and the amount of mother liquor trapped increased, decreasing dramatically the cesium decontamination. To illustrate the difficulties encountered during the solid-liquid separation a detailed measurement of operating time was recorded. Table 30 presents the time required for each filtration and washing operation. The total solid-liquid separation time was close to 3 hours, in comparison to about 45 minutes for run 38b.

Table 30. Time required for each separation operation for Run 53

Operation	Operating Time	Remarks
Filtration	60 minutes	Important difficulties were encountered. Filtration was performed until 378 g of filtrate was recovered. The unwashed crystals still contain important amount of solution
First Wash	30 minutes	The first wash was incomplete due to the filtration difficulty.
Second Wash	20 minutes	The second wash was incomplete and very difficult filtration
Third Wash	20 minutes	Improvements are noticed in the filter cake appearance and color is slightly changing.
Fourth Wash	20 minutes	Improvements are noticed on filter cake and color changes.
Fifth Wash	20 minutes	Improvements are noticed on filter cake and color changes.
Acetone Wash	10 minutes	Four Acetone washes were performed. Acetone efficiently separated the crystals and filtration removed the agent responsible for the filter cake texture.

[2] The final crystals recovered from run 53 trapped a significant amount of mother liquor due to its gel texture.

The acetone wash of the filter cake efficiently separated the crystals and prepared them to dry. It is likely that the chemical compound responsible for the gel like composition of the slurry is partially soluble in acetone. Hence, by submitting the filter cake to acetone washing, this component may be eliminated, leaving the crystals separated and ready to

be washed with saturated solution and dried. If organics were to be present in the solution to be submitted to the pilot scale process, their effect might be palliated by adding an acetone (or similar solvent like 85% ethanol) washing step prior to washing with saturated solution.

Figure 66 is a schematic diagram illustrating the results of the overall mass balance for the early feed with organics control Run 53. Included in the figure are definitions of quantities used in closing mass balances around each of the unit operations. The figure shows the masses of vapor generated and either recovered in the condensate receiver or the cold trap protecting the vacuum pump, crystals that accumulated on the walls of the vessel, material that adhered to the vessel and was lost in the transfer process, and the recovered slurry. The slurry recovered from the evaporative crystallization was filtered. The filtrate stream corresponds to the mass of filtrate collected inside the vacuum flask, and the funnel loss corresponds to the loss recovered after the combined filtration and crystal washing operations. The loss was determined by washing the filtration funnel with a known amount of water and using a dry paper of known mass to collect the water accumulated on the wall of the apparatus. The unwashed crystals correspond to the solids recovered at the end of the filtration and their mass was estimated by performing mass balance closure around the filtration unit. The unwashed crystals were washed with a solution saturated in the main species (sodium nitrate, sodium carbonate monohydrate, sodium sulfate, sodium hydroxide and sodium fluoride) as described in Chapter 2. The final crystals were the solid phases obtained at the end of the process and the spent wash was the filtrate of the crystal washing operation.

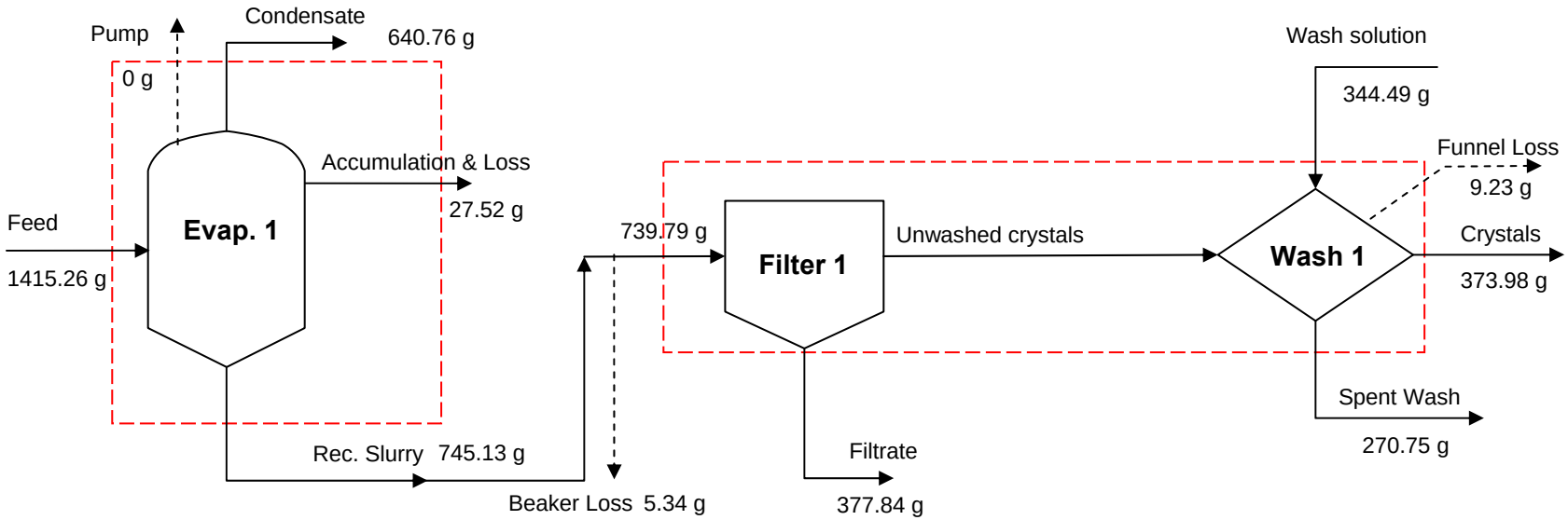

Pump	Mass of the condensate collected in the cold trap protecting the vacuum pump.
Rec. Slurry	Mass of slurry recovered from the crystallizer.
Accumulation & Loss	Mass recovered by washing the vessel with a known amount of water.
Funnel Loss	Mass recovered by washing the funnel with a known amount of water and then drying with paper of a known weight. Performed after the filtration and washing operations.
Beaker Loss	Mass of slurry lost in the beaker necessary for the transfer from the vessel to the filter.
PLM Sample	Mass taken from the slurry for PLM imaging.

Figure 66. Overall mass balance of early feed with organics control Run 53: run was performed at 66 °C and 26 g/h evaporation rate
Solid arrows are the process streams and the dotted arrows represent the quantified losses. Closure on a total mass balance was performed for each dashed box around a process unit.

The impact of the organic compounds on crystallization of the key species in early feed was evaluated by determining the crystal size distribution resulting from early feed Run 53 and by identifying the primary crystalline species recovered in each sieve used for the analysis of size distribution. Figure 67 presents the histograms resulting from the sieve analysis performed on the washed crystals from Run 53.

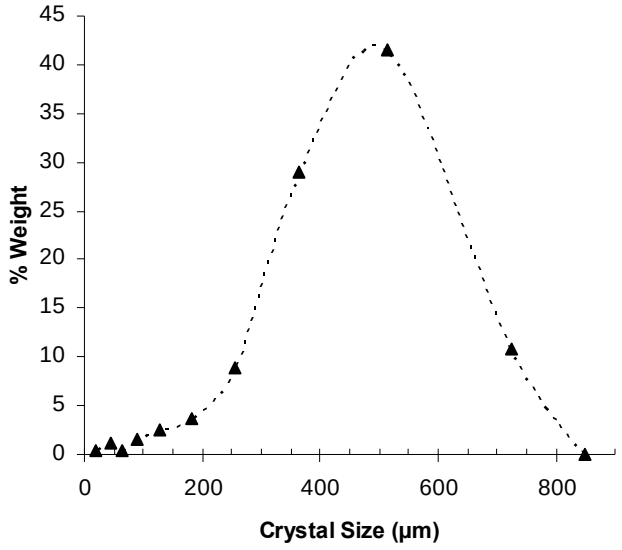

Figure 67. Histograms for the early feed with organics control Run 53

The main mode was around 500 µm and the spread in the distribution was relatively large. This mode size was expected to be composed exclusively of sodium nitrate crystals. A secondary mode was observed around the 50-µm size range. This mode was expected to correspond to burkeite crystals. Surprisingly, there was no small third mode or flattened region in the 100- to 150-µm range, which in previous runs has been populated largely by sodium carbonate monohydrate. In order to compare the CSD obtained from Run 53 to Certification Run 38b and to isolate the effect of organics on crystal population, an additional sieve analyses was performed by removing the 850-µm

sieve, which is expected to have only agglomerates of sodium nitrate that were formed due to the process complications associated with addition of the with organic species.

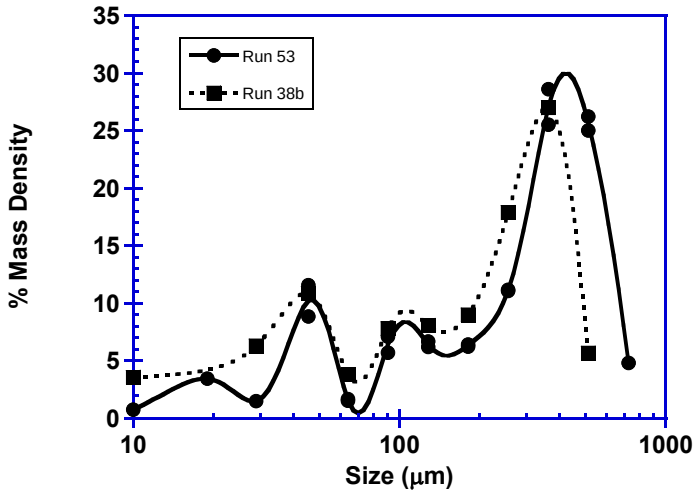

Figure 68. Comparison of mass density distributions of organics Run 53 and certification Run 38b

Figure 68 compares the mass densities of the two sieve analyses on crystals from Run 53 with that from Certification Run 38b. As with all previous data presented in this manner, the mass density plot exhibits trimodal behavior. However, the largest mode for Run 53 is significantly larger than that of Run 38b (500 μm compared to 350 μm). The larger size indicates an increased growth of sodium nitrate crystals, which is the only species observed at a size greater than 250 μm. A second difference between the two distributions is in the 50- to 200-μm size range. Run 38b had more crystal mass in this size range than did Run 53. This is early evidence of the absence of sodium carbonate monohydrate from this size range. Lastly, the mode around 30 μm in Run 38b appears to have been slightly shifted to 45 μm in run 53.

Figure 69 compares the cumulative mass distributions for early feed Run 38b and Run 53. The data for Run 53 clearly showed that larger crystals were produced than in Run 38b.

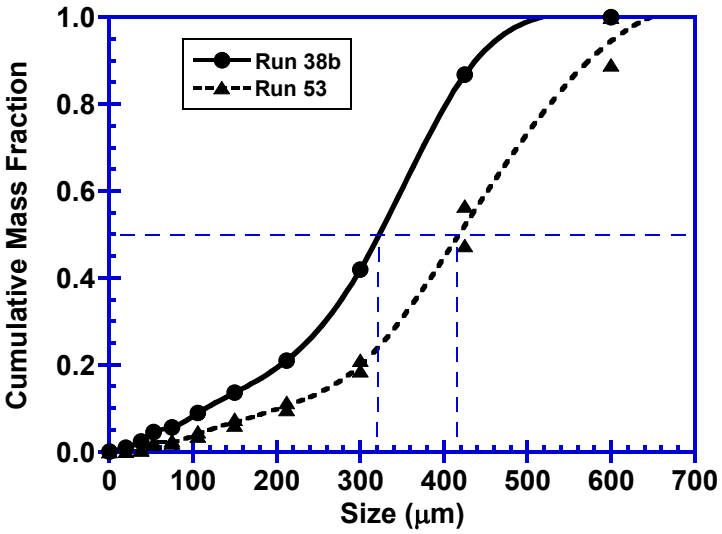

Figure 69. Comparison of cumulative distribution of organics Run 53 and Certification Run 38b

Samples of sieved crystals from the first stage ofRrun 53 were examined by polarized light microscopy (PLM). A thorough study of each sieve was performed in order to identify the sources of the inorganic species and to assist in the observations from the CSD analysis. Large quantities of sodium nitrate were expected, along with smaller quantities of sodium carbonate monohydrate and burkeite, and trace quantities of sodium oxalate. Large quantities of sodium nitrate crystals were observed along with a small amount of burkeite crystals. Trace amounts of sodium carbonate monohydrate, sodium oxalate and sodium sulfate were also observed. The main conclusion from the PLM analyses of the sieved crystals is that the presence of organics greatly affected the crystal population from the early feed run. With the exception of trace amounts of small crystals in the pan, no sodium carbonate monohydrate crystals were obtained in Run 53. This observation is in agreement with the CSDs displayed in Figure 69. This means that the organic species either hindered the nucleation of sodium carbonate monohydrate crystals or limited the growth of these crystals to 10 μm.

In addition, the sodium nitrate crystals produced in Run 53 were grown to larger sizes than in Run 38b. The spread in the sodium nitrate crystals size was also larger in Run 53. Therefore, the organic species have modified the growth and nucleation kinetics of sodium nitrate. PLM images also displayed the presence of small crystals along the edges of the sodium nitrate crystals, which are unidentified but could be either crystals of the organic species or remnants of the organic film that formed during filtration. This film led to crystal agglomeration, and was partially removed with the acetone washing of the filter cake. Some other crystals were unidentified and may either be burkeite crystals or organic crystals.

3.3.2 METHODOLOGY FOR ORGANICS EFFECT STUDY

A branched methodology was followed to identify organic species responsible for process difficulties. In this methodology, an initial run was performed with all organics and then the species were split into a carboxylate group and an amine group. A series of runs was then performed to progressively remove organics from the solution and allow identification of problem species. Figure 70 displays this experimental methodology and the runs performed during this study. Note that Run 60 did not lead to any process difficulties; therefore organics C1 and C2 were considered harmless and the individual runs labeled C1 and C2 were unnecessary

.

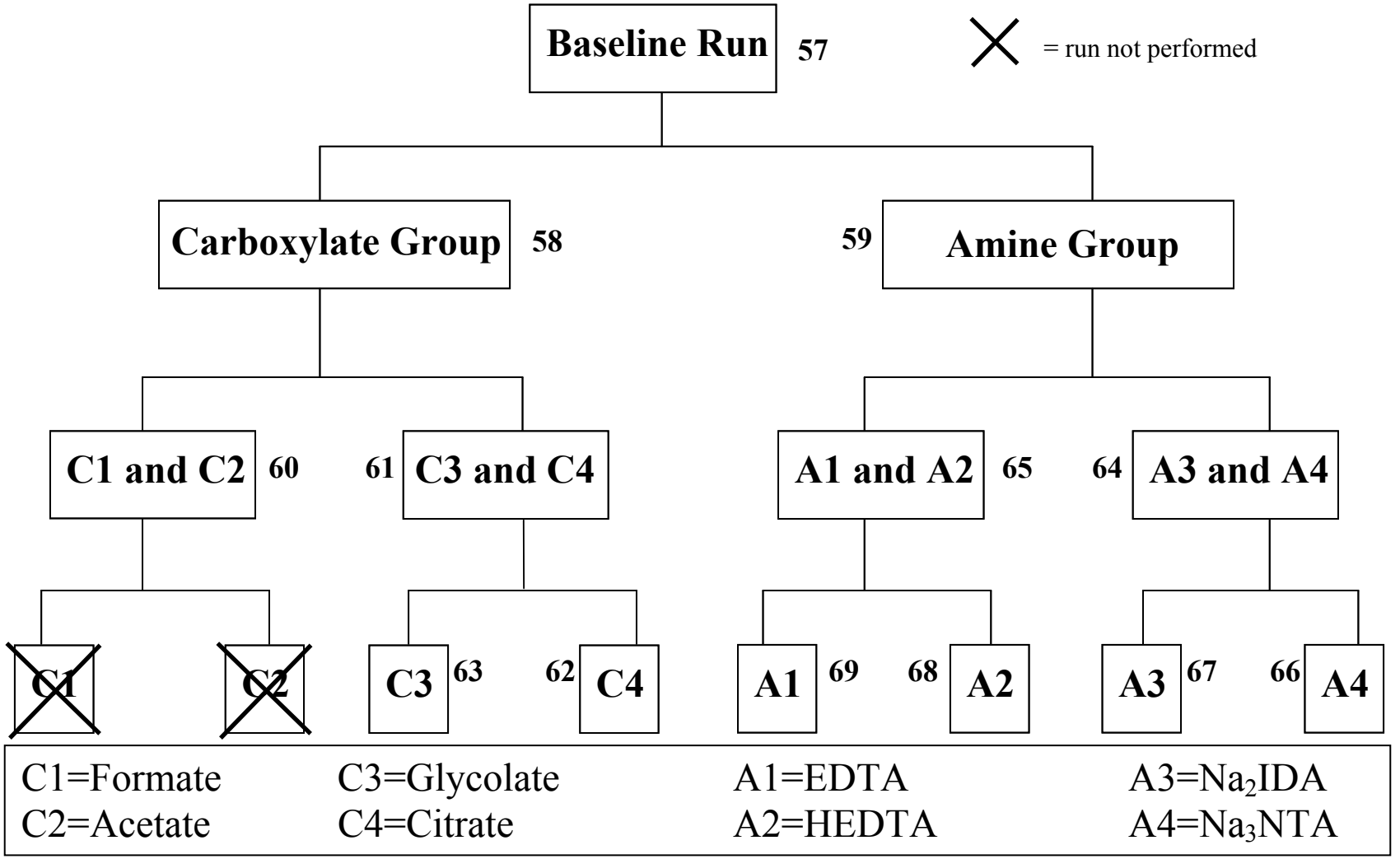

Figure 70. Organics study methodology for run completion (numbers beside each box correspond to the run number assigned to that solution)

3.3.3 SUMMARY OF RESULTS

Process Difficulties:

Each run was judged based on the following criteria: (1) ease of solid-liquid separation, particularly compared to early feed Run 56 which was a scaled down experiment performed without organics; (2) formation of an organic film on the jacketed walls of the crystallizer or on the filter cake; (3) alteration of the crystal population by the addition of organics, and (4) evidence of foaming during the evaporation stage. Table 31 shows a summary of the process difficulties encountered with each of the organics run.

Table 31. Summary of process difficulties obtainedwith all organics runs: all runs perfomed at 66 °C and 26 g/h

Run #	Organics Added	S-L Separation	Vessel Film Formation	Vessel Froth Formation	Crystal Population
56	None	Typical, 30 min	No	No	Typical
57	All	Increased, 60 min	Yes	Yes (slight)	No carbonate or burkeite, larger nitrate crystals
58	Carboxylates	Increased, 45 min	No	No	No burkeite but sodium sulfate
59	Amines	Increased, 60 min	Yes	Yes (intense)	No carbonate or burkeite, very small nitrate crystals
60	Formate & Acetate	Typical, 30 min	No	No	Typical
61	Glycolate & Citrate	Increased, 45 min	No	No	No burkeite but sodium sulfate
62	Citrate	Increased, 45 min	No	No	Typical, smaller nitrate crystals
63	Glycolate	Typical, 30 min	No	No	Typical
64	IDA & NTA	Increased, 45 min	No	No	Very small amounts of carbonate & burkeite
65	EDTA & HEDTA	Reduced, 20 min	Yes	Yes (extreme)	Very small amounts of carbonate & burkeite

66	NTA	Increased, 50 min	No	No	Trace amounts of carbonate & burkeite
67	IDA	Typical, 25 min	No	No	Typical
68	HEDTA	Reduced, 20 min	No	Yes (extreme)	Trace of burkeite, but sodium sulfate
69	EDTA	Increased, 40 min	Yes	Yes (less intense than Run 68)	Trace of large burkeite & small amount of elongated carbonate, larger nitrate

The runs with EDTA and HEDTA led to foaming during evaporation. Both compounds led to foaming, although the run with only HEDTA showed more intense foaming than the run with only EDTA. Foaming was so intense during runs 59, 65, and 68 that mother liquor bubbled up through the vessel neck and contaminated the condensate stream. This did not occur during Run 69. The table also shows that EDTA was responsible for film formation on the walls of the crystallizer. HEDTA may have added to the film thickness, but EDTA was the primary cause of the film formation. The ease and efficiency of solid-liquid separation for each run were compared to Run 56, which was the initial early feed run performed without organics. By performing the series of runs shown in Figure 70, sodium formate, sodium acetate, sodium glycolate, and IDA were proven harmless to the early feed process. Runs focusing on these species required the same time and effort for the solid-liquid separation as with Run 56.

The four species that led to solid-liquid separation difficulties were EDTA, HEDTA, NTA, and sodium citrate. EDTA, HEDTA, and NTA changed the texture of the filter cake and reduced draining efficiency of mother liquor from the cake. This led to increased filtration and washing times and also a more pronounced yellow color of the final product. Sodium citrate did not appear to alter the texture of the filter cake or the

color of the final product, but did cause longer filtration times. During this run there was some filter plugging, which led to reduced separation efficiency and difficulty stirring the filter cake.

Table 32. Details of the operating conditions and outcomes of each organics run

Run #	Evaporation Rate (g/h)	Cond:Feed Ratio	Washes for Major Mother Liquor Removal	Filtration & Washing Time	Slurry Cake Composition	Mass of Final Crystals	Color of Final Crystals	Ease of Operation
56	~ 36.4	0.497	3	Typical (30 min)	Powder-like with small crystals	Typical (135 g)	White color	No filter plugging, easy to stir
57	~ 33.4	0.472	5 (or more)	Increased (60 min)	Undetermined (gel-like filter cake)	Increased (182 g)	Yellow color	Some filter plugging, difficult to stir
58	~ 36.0	0.485	5	Increased (45 min)	Powder-like with small crystals	Increased (161 g)	Yellowish color – less pronounced than Run 57	Some filter plugging, difficult to stir
59	~ 34.9	0.498	4-5	Increased (60 min)	Very small crystals	Decreased (94 g)	White color	Increased filter plugging, difficult to stir
60	~37.6	0.490	3	Typical (30 min)	Powder-like with small crystals	Typical (140 g)	White color	No filter plugging, easy to stir
61	~ 37.8	0.481	4-5	Increased (45 min)	Slightly aggregated, lighter than Run 58	Typical (146 g)	White color	No filter plugging, slight difficulty stirring
62	~ 36.6	0.493	3-4	Increased (45 min)	Typical with smaller crystals	Typical (137 g)	White color	Some filter plugging, fairly easy to stir
63	~ 38.8	0.486	3	Typical (30 min)	Typical small crystals	Typical (124 g)	White color	No filter plugging, easy to stir
64	~ 36.4	0.500	5	Increased (45 min)	Dough-like filter cake	Increased (168 g)	White color	Minimal filter plugging, difficult to stir
65	~ 41.0	0.498	3	Reduced (20 min)	Gel-like texture	Reduced (49 g)	Yellowish color	No filter plugging, difficult to stir
66	~ 39.6	0.473	5	Increased (50 min)	Dough-like texture	Increased (150 g)	Yellowish color	Minimal filter plugging, difficult to stir
67	~ 42.3	0.493	3	Typical (25 min)	Typical small crystals	Typical (129 g)	White color	No filter plugging, difficult to stir
68	~ 37.6	0.544	3	Reduced (20 min)	Gel-like texture	Reduced (58 g)	White color	No filter plugging, fairly easy to stir
69	~ 42.7	0.487	3-4	Increased (40 min)	Mainly gel-like texture with large crystals	Typical (134 g)	White color	Some filter plugging, fairly easy to stir

Crystal Size Distributions

The fourth criteria runs were based upon was the effect of the organics on the crystal population. As shown in Table 31, crystals such as burkeite, sodium sulfate, and sodium carbonate monohydrate were observed in some runs, but were not observed in others. Figure 71, Figure 72, and Figure 73 represent the histograms obtained for the series of runs performed for the orgonics study. Figure 71 displays all histograms for runs containing carboxylates, Figure 72 displays the histograms for runs including IDA and NTA, and Figure 73 shows histograms for runs including ETDA and HEDTA.

There are three main points arising from the figures: (1) Run 62, which added only sodium citrate, had a slightly greater spread and a slightly smaller mode size than the other carboxylate runs (not including Run 57, which included all organics); (2) Runs 59, 65, and 68 display oddly-shaped distributions, which can be attributed to the fact that HEDTA caused excessive foaming during these runs and mother liquor contaminated the condensate streams, and (3) EDTA appears to have altered the nucleation and growth kinetics of sodium nitrate, as both Runs 57 and 69 led to larger sodium nitrate crystals.

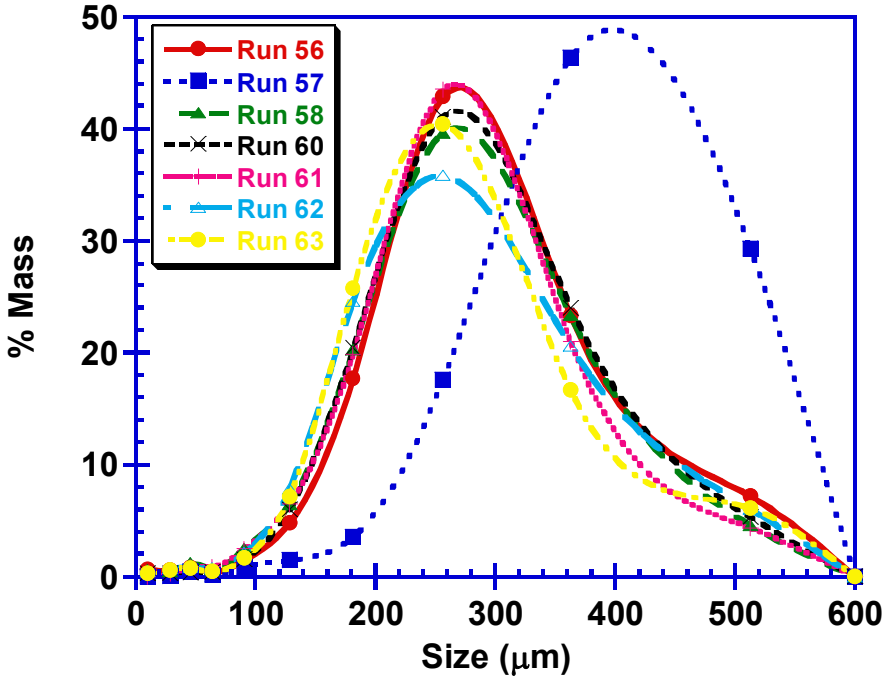

Figure 71. Mass histograms for runs containing carboxylates

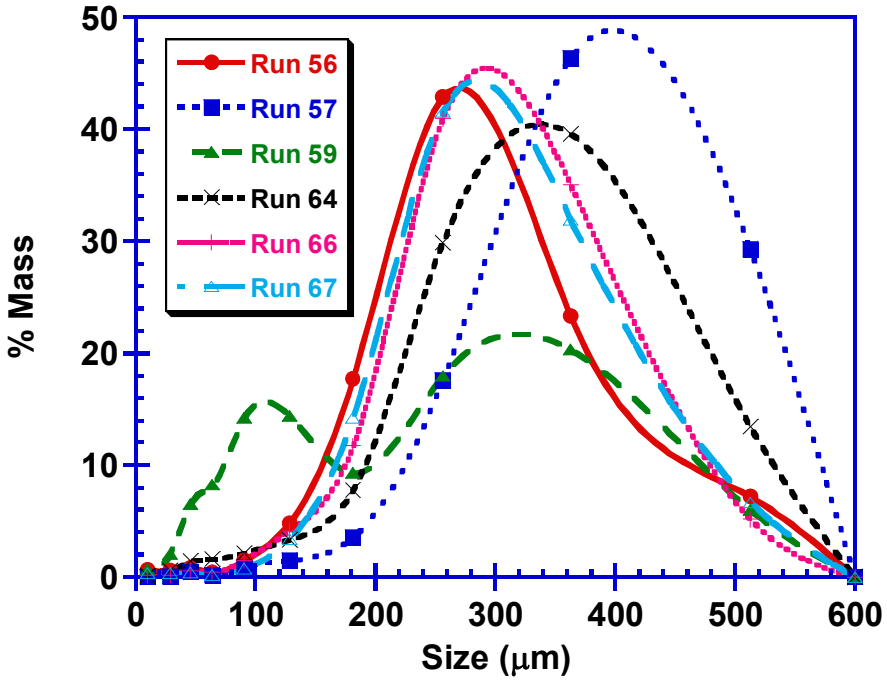

Figure 72. Mass histograms for runs containing IDA & NTA

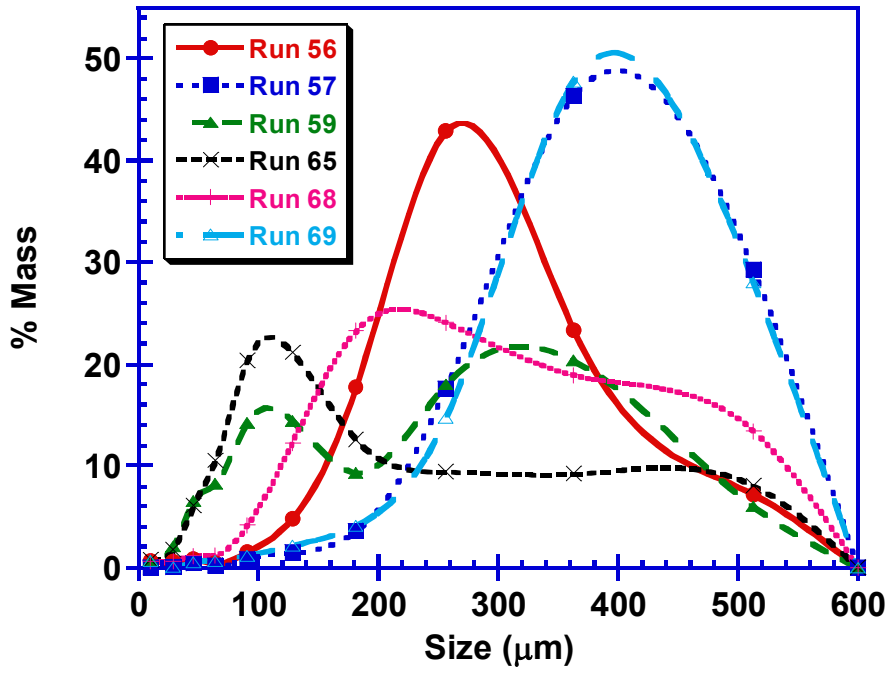

Figure 73. Mass histograms for runs containing EDTA & HEDTA

Conclusions

Analyzing both the crystal size distributions and the solid-liquid separation details leads to the conclusion that there is no consistent link between the two. Most of the difficulties observed during solid-liquid separation were related to the overall texture of the filter cake and not to any trends in crystal properties. For example, runs containing NTA led to a filter cake with a dough-like texture, whereas runs with HEDTA and EDTA led to a cake with a gel-like texture. The texture change in these runs affected the separation time and efficiency, as mother liquor was retained in the filter cake. In several of these runs this was apparent when weighing the final crystals at the end of the run; the mass of crystals was greater although run conditions were similar to Run 56. Along with the fact that the crystal product displayed a yellowish color, this proved that the texture of the filter cake was causing retention of mother liquor.

As mentioned previously, sodium citrate also led to process difficulties, but not to a change in filter cake texture. Filter plugging was the main issue with Run 62, which may be related to the slightly altered CSD for this run. Although the solid-liquid separation step required more time and effort, the final product had a similar color to that obtained during Run 62. For this reason, sodium citrate is not considered to be as troublesome to the solid-liquid separation as the other three species.

The run performed with EDTA led to film formation and foaming, although foaming was not as intense as with HEDTA. These observations prove that HEDTA is responsible for the severe foaming and that EDTA is the primary cause of the film formation. The comparison of the CSDs obtained for Run 57 and 69 and the analysis of the PLM images on sieved crystals show that EDTA is responsible for changing the crystallization kinetics of sodium nitrate.

3.4 CRYSTALLIZATION OF SOLUTION PRESENTING SOLID PARTICLES

The great variability of the medium curie waste composition within the storage tanks at Hanford site includes the presence of solids particles in some of the early feed solutions. These solids are insoluble sub-microns particles that may affect the waste processing by modifying (1) the thermodynamic equilibrium of the system(Teja A.S. et al.; 2004) - leading to the formation of different crystalline species-, and (2) the kinetics of formation of the crystals -leading to different size distributions-. Both of these phenomena may create adverse effect onto the solid-liquid separations of the recovered slurries. The investigation focused on the use of three solid reagents: gibbsite, ferric oxide, and sea sand.

Figure 74 presents micrographs of the solids reagants used to prepare the solids solution. These reagents were used with size ranging from sub-micron to around 10 μm. A two stage experimental run was performed by adding these solids to an early feed solution. The objectives of the experiment were to determine the effects of solids on the crystallization and the effects of the resulting crystal size distribution on filtration and washing of the product crystals. Results obtained from this run were compared to those from the early feed certification run.

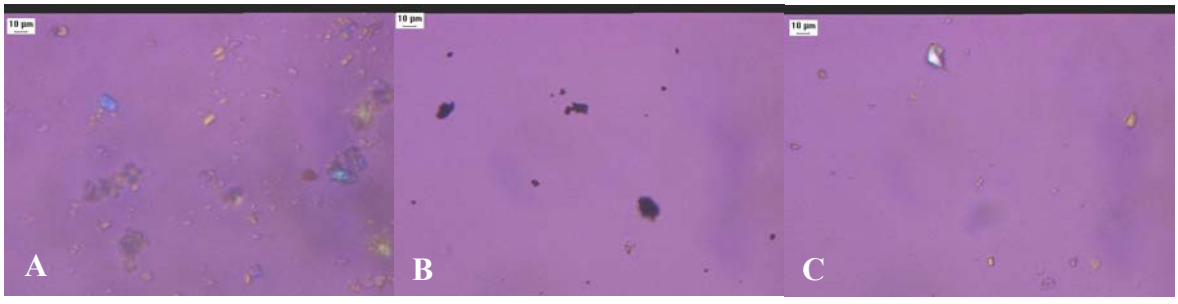

Figure 74. PLM images of the solid reagents used in feed preparation: (Panel A) gibbsite, (Panel B) ferric oxide, (Panel C) sea sand

3.4.1 OPERATING CONDITIONS

A solid solution was prepared using gibbsite, ferric oxide and sea sand and added to the early feed simulant until the feed reached a turbidity value of 5 NTU. The simulated waste solution was then submitted to a two-stage crystallization process conducted using the 300-mL and the 100-mL crystallizer for Stage 1 and Stage 2 respectively. Figure 75 displays the condensate mass evaporated as a function of the operating time for the early feed run with solids particles, showing that each stage was operated at constant evaporation rate. The evaporation rate was controlled by varying the temperature difference between the heating medium and the slurry. This was done by adjusting the temperature of the heating fluid and the pressure in the vessel. In the first stage, vapor was generated at a rate of 24 g/h by setting the temperature of the heating fluid to 77 °C and adjusting the pressure in the crystallizer during the run, so that the slurry temperature stabilized at 66 °C. Evaporation proceeded at these conditions for over 30 h, at which time the target condensate-to-feed mass ratio was achieved. The ending condensate-to-feed ratio for the first stage was 0.475, close to the target ratio of 0.474 given by the batch simulation from COGEMA, Inc. (EARLY_FEED_FINAL_LABORATORY_FLOWSHEET.xls).

The filtrate from the first stage was diluted and used as feed for the second stage. The target condensate-to-feed ratio from the above-cited simulation was adjusted to 0.55 in order to account for the dilution water added. The evaporation rate for Stage 2 followed a constant evaporation rate of 39 g/h with a slurry temperature at 40 ºC.

Evaporation proceeded at these conditions for over 10.2 h, at which time the target condensate-to-feed mass ratio of 0.56 was achieved.

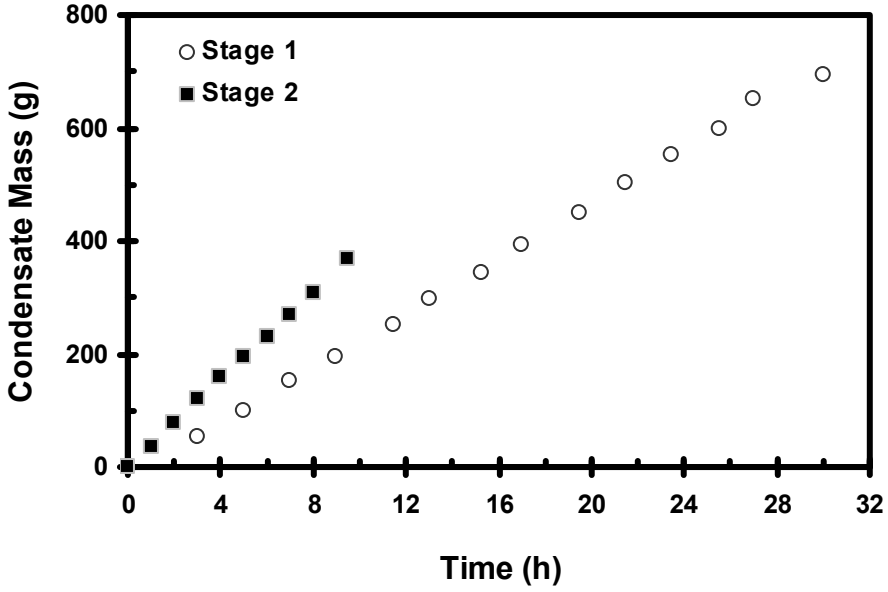

Figure 75. Mass of condensate generated as a function of operating time for early feed solids Run 54: run was operated at 24 g/h evaporation rate and 66 °C

Figure 76 displays the temperature and pressure profiles for the early feed with solids run. Throughout the first stage the temperature was controlled to within +/- 1 ^{o}C of the target value of 66 ^{o}C. Assessing Stage 2, except for an excursion at around 6 h, the temperature was controlled to within +/- 1 ^{o}C of the target value of 40 ^{o}C. For the two crystallization stages, the pressure profile reflects the step-wise changes in vacuum associated with manual adjustments of the regulating valve.

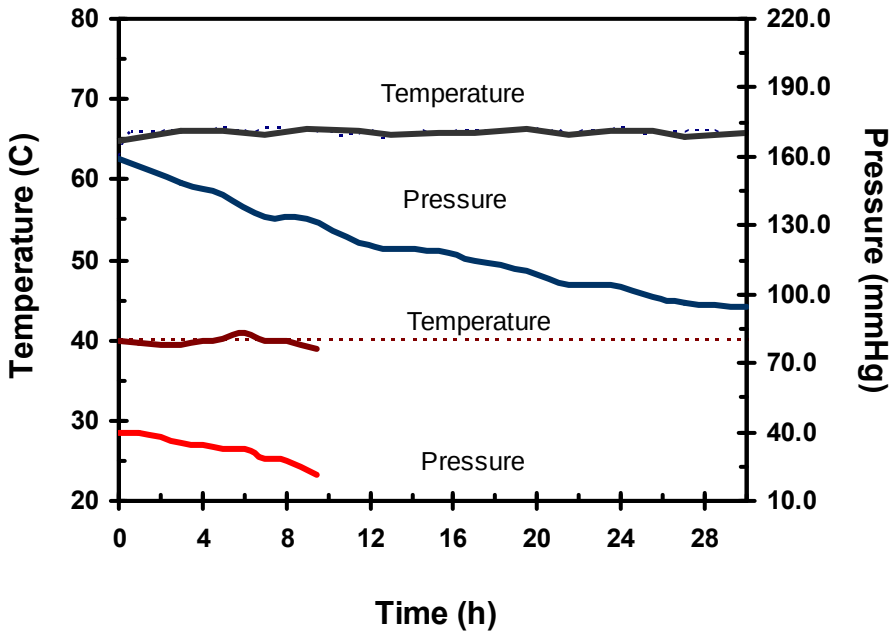

Figure 76. Temperature and pressure profiles for early feed solids Run 54
(The blue and grey lines represent the first stage temperature and pressure profiles and the red and dark red lines the second stage temperature and pressure profiles. The dotted lines represent the target operating temperatures of 66 and 40 °C for the first and second stage respectively)

3.4.2 BALANCE ON TOTAL MASS

Mass balances closures were performed as described in Chapter 2. The objectives were to (1) determine the fate of species entering the process, and (2) identify potential problems with the operating procedures. Figure 77 and Figure 78 are schematic diagrams illustrating the results of the overall mass balance around Stage 1 and Stage 2. The process units and the methods of closing total mass balances were identical for both stages. Tabe 34 presents the overall mass balance closures associated with the first and second stage of the early feed with solids crystallization Run 54. Chapter 2 defines the methodology used to compute the overall mass balance for each crystallization stage and the adjusted mass balance closure calculated based on the recovered mass. The results of the balances on total mass showed that 33.09 g were lost in Stage 1, but that 9.74 g could

be accounted for using the methods described in Chapter 2. This meant that the unaccounted for loss was 20.35 g; another way of saying this is that the balance on total mass was closed to within 1.26%. Addressing Stage 2: there was a loss of 18.47 g, of which 8.85 g were unaccounted for; in other words the total mass balance closed to within 1.01%. Furthermore, since the unwashed solids mass was not measured, a mass balance around the combined filtration-washing step was performed. Table 33 displays the results of the mass balance closures around each unit operation. The difference between input and output for each of the first stage units was as follows: evaporation, 0.35%; filtration and washing, 1.74%. Assessing the second stage, the closure around the filtration unit was 0.03% while the closure around the combined solid-liquid separations was 2.2%. Both crystallization stages display that most of the mass loss is generated during filtration.

Table 33. Mass balances around process units of early feed solids run (SST early feed Run 54)

Unit	Input (g)	Output (g)	Difference (g)	% Closure of Mass Balance
Evaporator 1	1520.82	1515.51	5.31	0.35
Filtration & Washing 1	1035.93	1017.89	18.04	1.74
Evaporator 2	727.61	727.39	0.22	0.03
Filtration & Washing 2	427.46	418.06	9.4	2.20

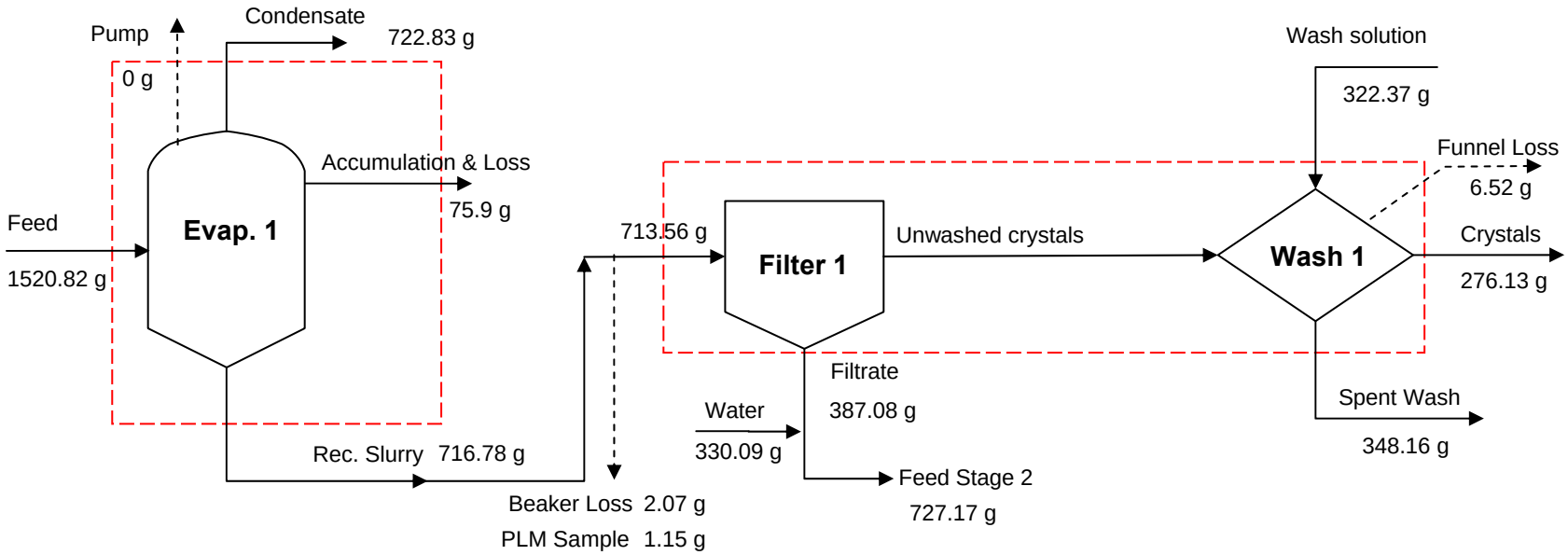

Pump	Mass of the condensate collected in the cold trap protecting the vacuum pump.
Rec. Slurry	Mass of slurry recovered from the crystallizer.
Accumulation & Loss	Mass recovered by washing the vessel with a known amount of water.
Funnel Loss	Mass recovered by washing the funnel with a known amount of water and then drying with paper of a known weight. Performed after the filtration and washing operations.
Beaker Loss	Mass of slurry lost in the beaker necessary for the transfer from the vessel to the filter.
PLM Sample	Mass taken from the slurry for PLM imaging.

Figure 77. Overall mass balance in early feed Run 54 Stage1
Solid arrows are the process streams and the dotted arrows represent the quantified losses. Closure on a total mass balance was performed for each dashed box around a process unit

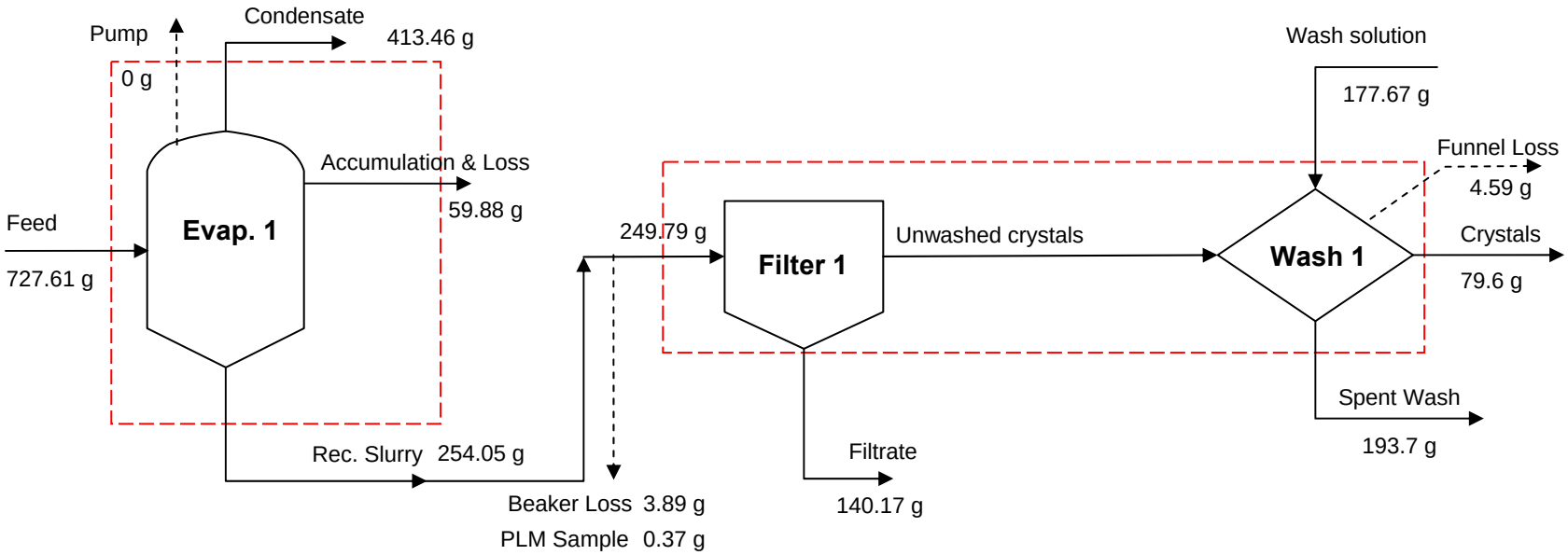

Pump	Mass of the condensate collected in the cold trap protecting the vacuum pump.
Rec. Slurry	Mass of slurry recovered from the crystallizer.
Accumulation & Loss	Mass recovered by washing the vessel with a known amount of water.
Funnel Loss	Mass recovered by washing the funnel with a known amount of water and then drying with paper of a known weight. Performed after the filtration and washing operations.
Beaker Loss	Mass of slurry lost in the beaker necessary for the transfer from the vessel to the filter.
PLM Sample	Mass taken from the slurry for PLM imaging.

Figure 78. Overall mass balance in early feed Run 54 Stage 2
Solid arrows are the process streams and the dotted arrows represent the quantified losses. Closure on a total mass balance was performed for each dashed box around a process unit

Table 34. Overall mass balance of solid run Stage 1 and Stage 2

	Input (g)		Output (g)				Accum (g)	Loss (g)
Species	**Feed**	**Wash**	**Cond**	**Washed Solids**	**Filtrate**	**Spent Wash**	**Solids**	
Feed	1520.82							
Solution		322.37		276.13	387.08	348.16	75.9	
Total	1520.82	322.37	722.83	276.13	387.08	348.16	75.9	33.09
Combined	1843.19		1810.1					33.09
								1.79%
							Corrected Loss	1.26%

9.74 grams were accounted for from this stage, leading to a corrected loss of 1.26%.

	Input (g)		Output (g)				Accum (g)	Loss (g)
Species	**Feed**	**Wash**	**Cond**	**Washed Solids**	**Filtrate**	**Spent Wash**	**Solids**	
Filtrate stage 1	727.61							
Solution		177.67		79.6	140.17	193.7	59.88	
Total	727.61	177.67	413.46	79.6	140.17	193.7	59.88	18.03
Combined	905.28		886.81					18.47
								1.99%
							Corrected Loss	1.01%

8.85 grams were accounted for from this stage, leading to a corrected loss of 1.01%.

3.4.3 SOLID-LIQUID SEPARATION

A series of process criteria were defined in order to assess the effect of solids on the solid-liquid separation. Such criteria were: (1) the number of washes necessary to remove the interstitial mother liquor from the slurry, (2) the time necessary to perform the separation by filtration, (3) the quality of the recovered filter cake (color and nature of the crystals), and (4) the crystal yield. These criteria were assessed for both the early

feed Certification Run 38b and the early feed with solids Run 54. Table 35 presents the outcomes of this study for both crystallization stages.

Table 35. Solid-liquid separation comparisons between early feed certification and solid runs

Criteria	First Stage		Second Stage	
	Certification Run	**Solids Run**	**Certification Run**	**Solids Run**
Evaporation rate (g/h)	~ 25	~24	~ 39	~ 39
Condensate-to-Feed Ratio	0.481	0.475	0.626 (target of 0.627)	0.56 (target of 0.55)
Washes necessary for major mother liquor removal	3	3	3	3
Filtration & Washing Time	Typical	Typical (Slightly Decreased)	Typical	Typical
Slurry cake composition	Powder-like with large-medium crystals	Powder-like with large-medium crystals	Powder-like with large-medium crystals	Powder-like with large-medium crystals
Mass of final crystals	Typical (210 g)[3]	Increased (276 g)	Typical (24 g)[4]	Increased (80 g)
Color of final crystals	White with slight yellow color	White with slight yellow color	White color	White color
Ease of operation	No filter plugging, easy to stir	No filter plugging, easy to stir	No filter plugging, easy to stir	No filter plugging, easy to stir

A key point is the difference between the mass of final crystals from the two runs; a far greater amount was produced during the solid run. This can be attributed to the corresponding decrease in accumulation that occurred during this run, which was 60 g less than that of the certification for both stages. Furthermore, there was a slight decrease in the condensate-to-feed ratio in the solid run during the first stage. Assessing the second stage, the mass of final crystals was also affected by the accumulation (60 g less than that in the certification run). In addition, there were 15 to 20 grams of samples taken

[3] The value of 210 g in Run 38b corresponds to the final mass of crystals collected after the washing steps. This does not account for the samples collected from the unwashed crystals or those collected after each wash step, which totaled 19 g.

[4] The value of 24 g in Run 38b corresponds to the final mass of crystals collected after the washing steps. This does not account for the samples collected from the unwashed crystals or those collected after each wash step.

from the solid streams of Certification Run 38b. The main outcome displayed by Table 35 was that the presence of solids in the feed and the filtrate recovered from the first stage did not induce any process complications.

3.4.4 CRYSTAL SPECIATION

Polarized Light Microscopy:

Figure 79 displays photomicrographs taken from the slurry of early feed run 54 Stage 1. Images from this analysis displayed the presence of sodium nitrate, sodium carbonate monohydrate, burkeite, traces of sodium sulfate, sodium oxalate, and solids. The slurry images displayed very large quantities of sodium nitrate crystals with sizes ranging from several micrometers up to 400 μm. The average size was similar to that found in the certification run. Important amounts of sodium carbonate monohydrate crystals were also observed with an average size around 50 to 75 μm. This average size for the sodium carbonate crystals is somewhat smaller than for the certification run. Sodium oxalate and sulfate crystals were observed in trace amounts, which is similar to amounts produced in certification run. Burkeite crystals were observed with an average size of 10 to 20 μm. Panel D illustrates that trace amounts of solids were also observed in the slurry images. These solid particles are expected to only correspond to the particles that were not broken to the sub-microns size during the solid feed preparation.

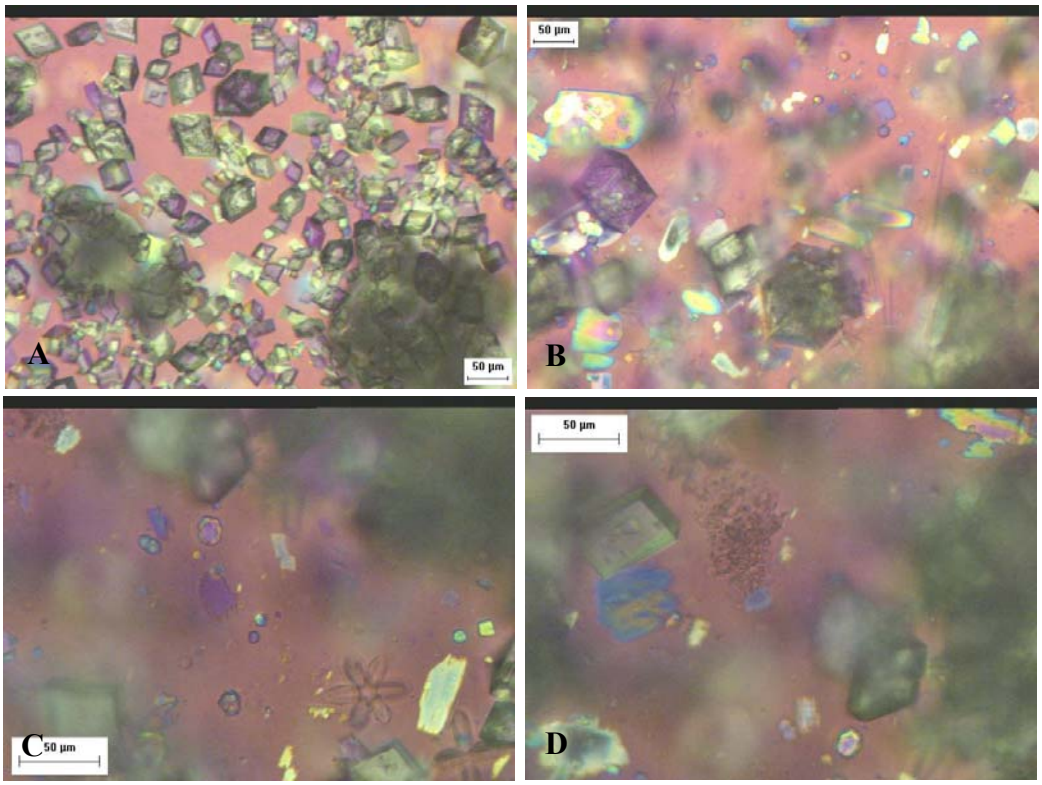

Figure 79. PLM images from the slurry sample of solid Run 54 Stage 1
(Panel A, Sodium nitrate crystals; Panel B, Sodium carbonate monohydrates with sizes ranging from 50 to 70 µm; Panel C, Burkeite crystals with sodium sulfate and solids in background; Panel D, Agglomerate of gibbsite crystals)

Assessing the second stage, Figure 80 displays PLM images from early feed Run 54 that showed the presence of large quantities of sodium nitrate and non negligible amounts of trisodium fluoride sulfate crystals was detected. The sodium nitrate crystals ranged in size from several micrometers up to 600 µm with an average size of 350 µm, which is slightly smaller than in the certification run. Their spread about the mean was also smaller. Based on microscopic observations of the slurry and sieved crystals, it would seem that a significant fraction of the small sodium nitrate crystals (below 10 µm) were either re-dissolved during the washing steps or passed through the medium-frit filter. Trisodium fluoride sulfate crystals displayed an average size around 70-100 µm. No trace amounts of solids were observed in the slurry PLM samples for the second

stage, leading to the conclusion that these solid particles were collected in the filtrate due to their small sizes.

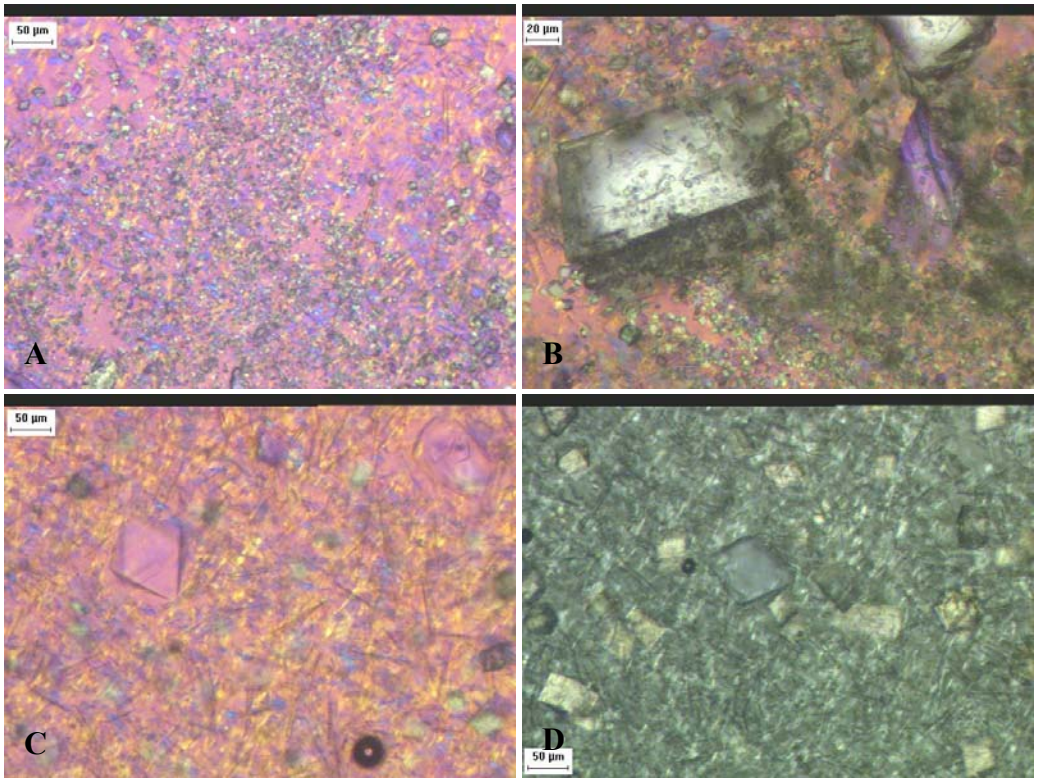

Figure 80. PLM Images from the slurry sample of solids run Stage 2
(Panel A, Sodium nitrate nuclei; Panel B, Sodium nitrate crystals; Panel C, trisodium fluoride sulfate crystals; Panel D, sodium fluoride phosphate crystals with 90 µm size)

Sieve Analysis:

A fraction of the crystals obtained at the end of Stage 1 was washed with acetone as outlined in Chapter 2 and allowed to air dry. The crystals were then subjected to sieving. Figure 81 presents histograms from the early feed Run 54. They displayed that the solids experiment produced: (1) the same major mode size around 350 µm that was produced in the certification run, but with a slightly smaller percentage of crystals at this size, (2) a similar secondary mode size around 50 µm and (3) a slightly greater spread for sodium nitrate crystals.

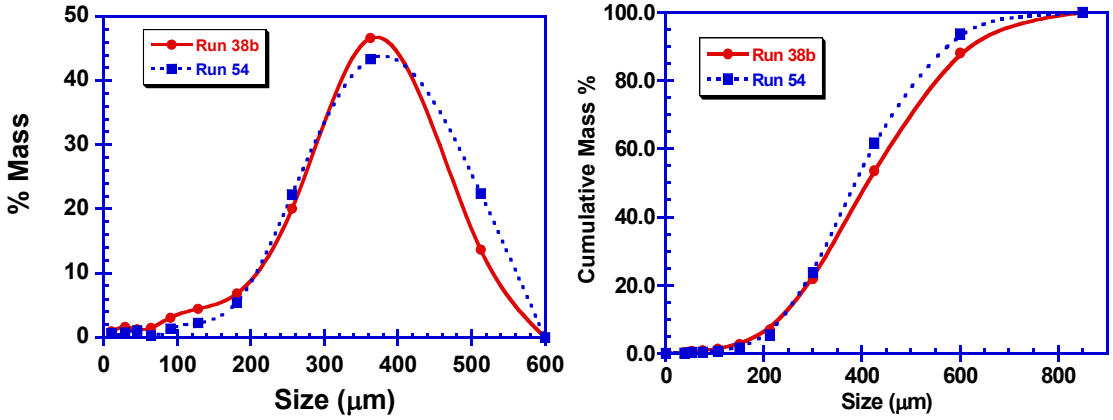

Figure 81. Mass density and cumulative distributions for the solids Run 54 Stage 1

The first section of the solids run CSD – between 0 and 200 μm - is very similar to that from certification run 38b, but the crystals obtained between 50 and 200 μm are in greater amounts for the certification run. The crystals corresponding to this size range (50–200 μm) are mainly sodium carbonate monohydrate and sodium nitrate crystals. Hence, the sodium carbonate crystals have an average size smaller than those from Run 38b which is likely to be due to the slight difference in the condensate-to-feed ratio between the two runs. In the second section of the curve -between 200 and 600 μm- the crystals obtained (mainly sodium nitrate crystals) from Run 54 have a similar size to those from Run 38b, but a larger spread. This is likely to be explained by a slightly larger amount of agglomerates in the larger sieves of Run 54. Figure 82 displays the histograms and cumulative distributions obtained for the early feed solids Run 54. The mass density and cumulative distributions display (1) very similar crystal distributions for the certification and solid runs, (2) a slightly smaller general spread for Run 54 and (3) a smaller mode size (350 μm instead of 450 μm) for sodium nitrate crystals obtained in Run 54. This difference in sodium nitrate size may be related to the difference in

condensate-to-feed ratios obtained in the first stage of these runs and the presence of increased amount of trisodium fluoride sulfate crystals.

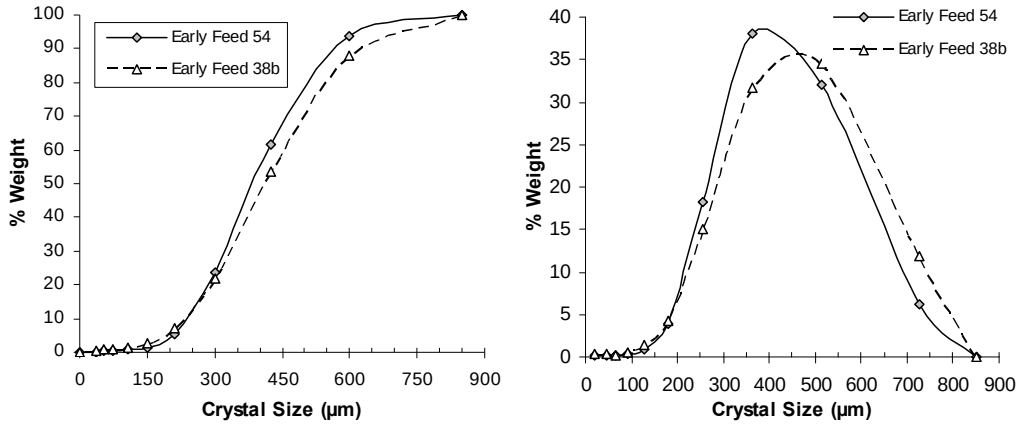

Figure 82. Histograms (Panel B) and cumulative distribution (Panel A) of solids Run 54 Stage 2

Table 36 compares the histograms distributions of the early feed certification run and the solids Run 54. The spread in distributions of the two runs are similar with similar masses recovered at mode size and fines produced.

Table 36. Comparison of histograms main criteria for early feed Runs 38b and 54

Criteria	First Stage		Second Stage	
	Certification Run	Solids Run	Certification Run	Solids Run
Coefficient of variation	34.7	34	36.6	33.7
Percent crystal mass at mode size	46.62	43.35	34.56	37.99
Percent crystal mass below 50µm	3.82	2.52	0.68	0.26

Species Distribution:

Samples from several sieves were analyzed to determine how the species formed were distributed according to size. Figure 83 and Figure 84 shows selected PLM images of crystals from Stage 1 and stage 2 respectively. Five species were identified in the product from Stage 1: sodium nitrate, sodium carbonate monohydrate, burkeite, sodium sulfate, and sodium oxalate.

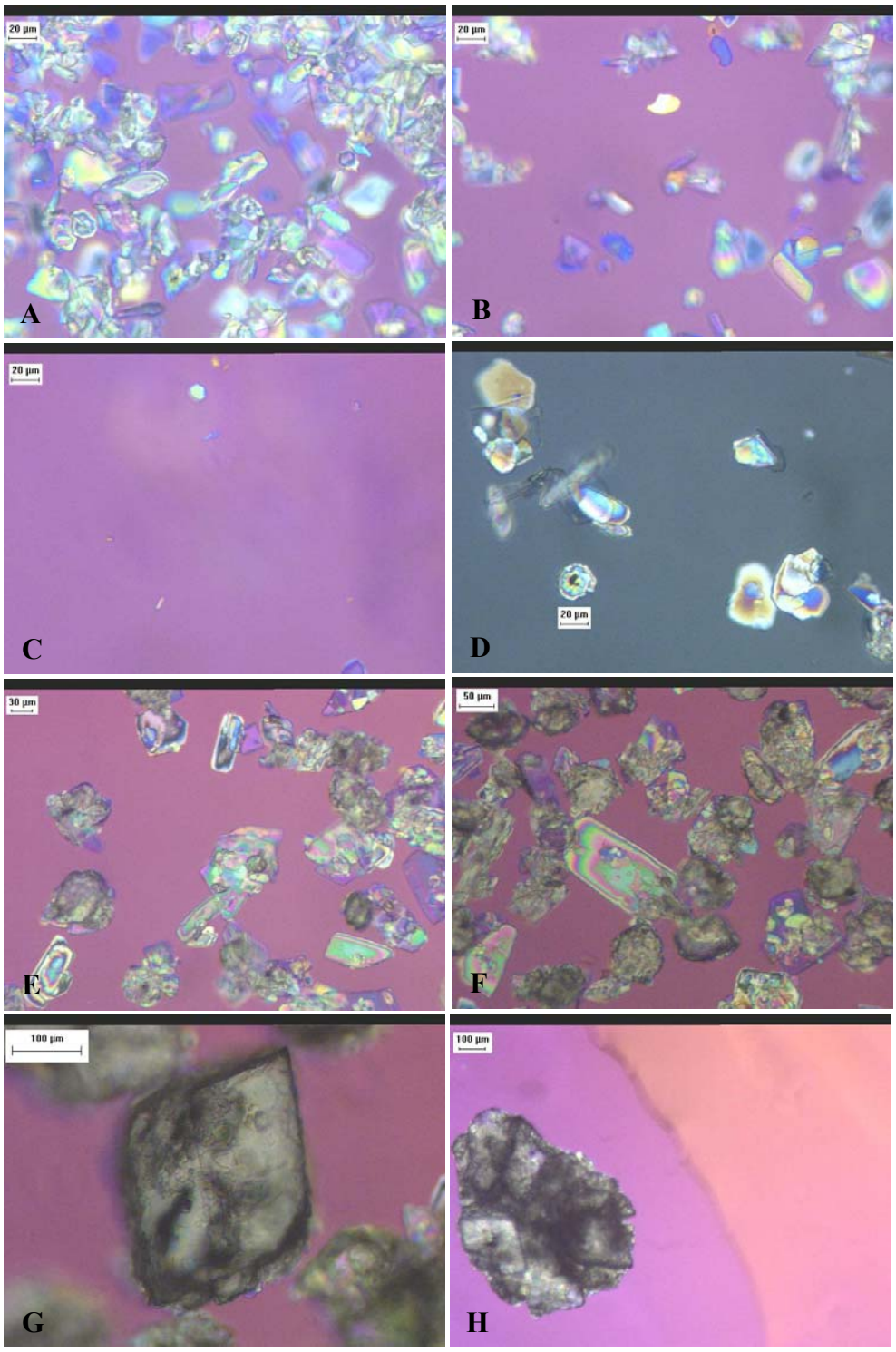

Figure 83. PLM images from the sieved samples of early feed solid run Stage 1
(Panel A, Sodium carbonate and burkeite crystals with size of 20 to 50 µm; Panel B, Sodium sulfate crystals; Panel C, Trace amounts of solids; Panel D, Heterogeneous burkeite; Panel E, Sodium carbonate monohydrate with 70 µm size; Panel F, Sodium carbonate with 100 µm size; Panel G, Single sodium nitrate crystal; Panel H, Agglomerate of sodium nitrate)

The burkeite crystal spread and size was slightly reduced compared to that from the certification run. Burkeite crystals were observed with an average size between 15 and 20 μm. The maximum burkeite crystal size observed was around 30 μm. The sodium nitrate crystals showed a similar mode size and spread to Run 38b. The main difference between the two populations is the presence of slightly more agglomerates in the 600 μm size explaining the slightly larger spread around the main mode size for the CSD of Run 54. A significant difference was noted between the sodium carbonate monohydrate crystals obtained during Run 54 and those from Run 38b. Sodium carbonate monohydrate crystals were observed with sizes ranging between 10 and 100 μm, with an average size of 50-70 μm, whereas in Run 38b the average size was between 100 and 150 μm. Very few sodium carbonate monohydrate crystals were observed at a size exceeding 100 μm. The smaller condensate-to-feed ratio for Run 54 is the best explanation for this discrepancy. Finally, only trace amount of solids were observed in the lower sieve sizes. Solids were hence either too small in size (size lesser than 10 μm) to be collected as final crystals or in too small amounts to be detected in PLM analysis. In either case, solids did not have a major impact on the crystal population and are very likely to be collected in the filtrate stream.

Figure 84 displays the PLM micrographs of the second stage samples and showed the presence of sodium nitrate and trisodium fluoride sulfate crystals. The trisodium fluoride sulfate crystal mass recovered in sieved samples was increased compared to certification run. These crystals were recovered with sizes ranging from 10 to 130 μm, with an average size of 90 μm. Furthermore, the sodium nitrate crystals were found in increasing concentration from the lowest to the highest sieve size. Crystals recovered at

sizes greater than 150 µm were exclusively sodium nitrate crystals. The sodium nitrate crystals presented a slightly smaller mode size than Run 38b but still included large crystals. The amount of agglomerates was relatively small except for the crystals recovered in the higher sieve size.

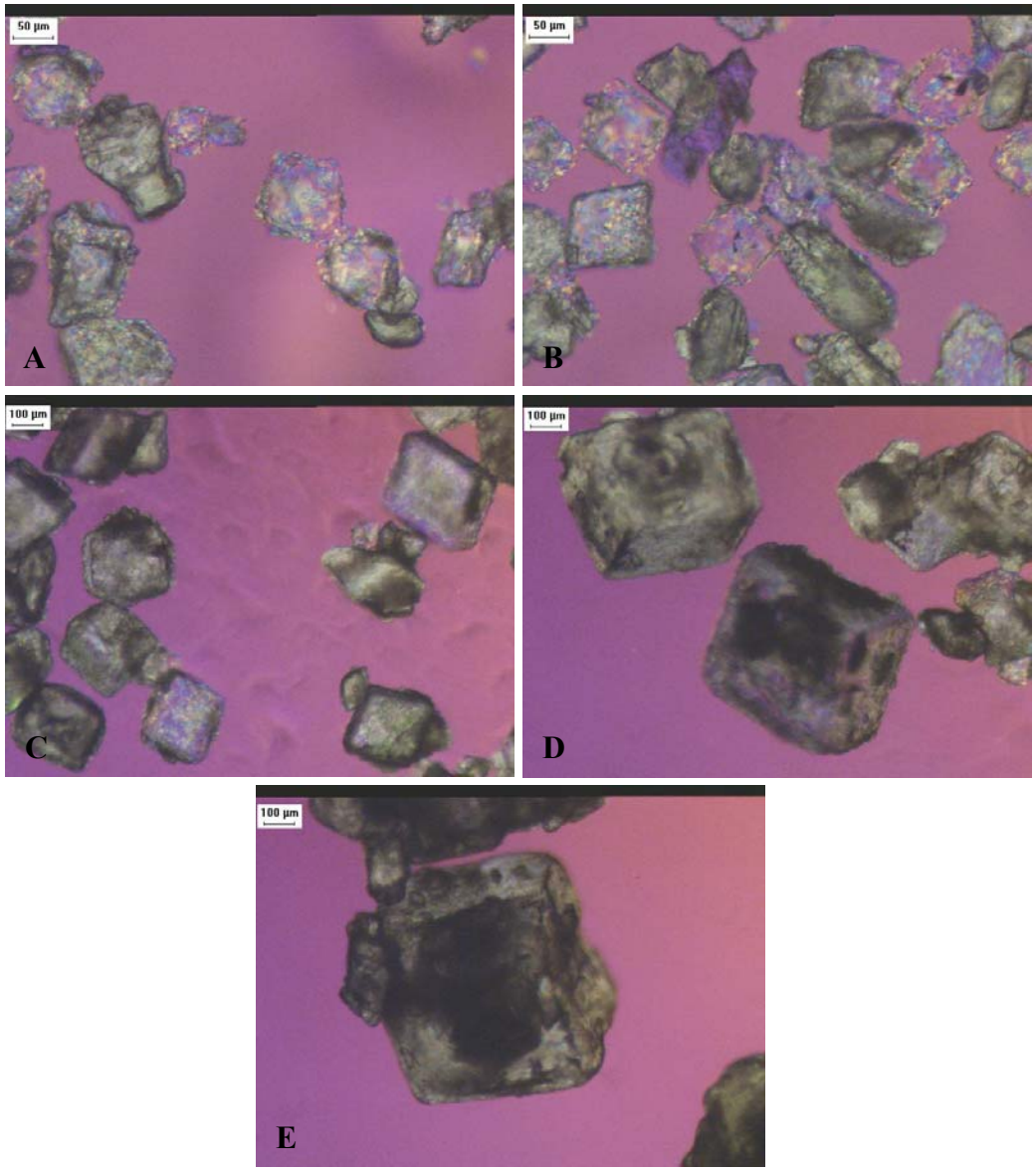

Figure 84. PLM images from the sieved sample of solid run Stage 2
(Panel A, Trisodium fluoride sulfate crystals; Panel B, High concentration of trisodium fluoride sulfate in lower pan; Panel C, High concentration of sodium nitrate crystals in medium pan; Panel D, Sodium nitrate crystals at mode size; Panel E, Large sodium nitrate crystal)

CHAPTER 4: KINETICS AND MODELING OF MULTIPLE SPECIES SIMULANT SOLUTIONS CRYSTALLIZATION

Simulated wastes are aqueous solutions containing eight main sodium salts (sodium nitrate, sodium carbonate, sodium sulfate, sodium oxalate, sodium phosphate, sodium fluoride, sodium hydroxide, and sodium aluminate). Evaporative fractional crystallization of the SST early and late feed solutions led to the formation of seven major crystalline species depending on the operating conditions: sodium nitrate, sodium carbonate monohydrate, burkeite, sodium sulfate, sodium oxalate, sodium fluoride phosphate and trisodium fluoride sulfate. Evaporative crystallization of SST early feed at the condition of Certification Run 38b produced sodium nitrate, sodium carbonate monohydrate, sodium oxalate, sodium sulfate and burkeite crystals. Assessing the case of evaporative crystallization applied to SST late feed at the condition of Certification Run 40, six species were produced: sodium nitrate, sodium carbonate monohydrate, sodium oxalate, sodium sulfate, trisodium fluoride sulfate and sodium fluoride phosphate. The population distributions from each of the certification runs described in Chapter 3 resulted from the crystallization kinetics of each of these species at the composition and operating conditions of the certification runs.

In the work to be described in this chapter, the nucleation and growth rates of each crystalline species were determined for the evaporative crystallization of early feed solutions at the conditions of Certification Run 38b. Furthermore, the crystallization kinetics (nucleation and growth rates) were evaluated as functions of operating

temperature and rate of evaporation. This was done for a series of five evaporative crystallization experiments with temperature varying by increments of 10 °C and a series of four experiments in which evaporation rate varies from 25 to 75 g/h. The results were used to (1) develop empirical kinetic expression relating nucleation and growth rates to these two process variables, and (2) define an evaporation profile to reduce heterogeneous burkeite formation and increase average burkeite crystal size.

4.1 CERTIFICATION RUN KINETICS

Chapter 4.1 is dedicated to the estimate of evaporative crystallization kinetics for early feed solutions at the conditions of Certification Run 38b. The objectives of the work described in this chapter are to (1) estimate the operating time at which each crystalline species is nucleated, (2) use the evolution of the total crystal count with operating time to estimate an average nucleation rate for each crystalline species, (3) use the measurement of the characteristic crystal size at various operating times to calculate the average growth rate, and (4) compare the experimental measured crystal size to the estimated crystal size based on the average growth rates defined in Chapter 4.3.

4.1.1 NUCLEATION POINTS

Early Feed Certification Run 38b was performed with an evaporation rate of 25 g/h at 66 °C. The details of the process conditions and outcomes were presented in Chapter 3 and the description of the different species was provided in Chapter 1. Figure 85 shows the sequence of species nucleation that was determined based on PLM analyses of slurry samples taken at regular time intervals. For example, panel A displays that sodium oxalate was the first crystalline species to be nucleated. The needle shaped crystals were first detected at the condensate-to-feed ratio (C:F)= 0.156, corresponding to an operating time of 4 hours and 49 minutes. A small amount of sodium oxalate crystals were produced during the experiment and the successive samples showed that sodium oxalates crystals had undergone breakage at higher slurry densities. Samples taken at earlier condensate-to-feed ratios (C:F)<0.156 presented clear feed and the first sodium oxalates were observed with a length size below 10 μm as shown by panel A. Panel B

shows that a few small prismatic crystals corresponding to sodium sulfate came out of solution at C:F= 0.200. Sodium sulfates were identified based on their shape and colors. Crystal size in panel B is close to 10 μm and samples with 0.200<C:F<0.247 display larger size sodium sulfate with more defined prismatic shapes and blue-yellow colors. Panel C displays that the first sodium nitrate crystals could be clearly identified at C:F= 0.247. Small amounts of sodium nitrate crystals were produced at that point with sizes below 10 μm. Panels I and J correspond to samples with C:F>0.247 and show that the few trigonal sodium nitrate crystals observed at C:F= 0.247 continued growing until sodium nitrate second nucleation was achieved as shown in panel H. Panel D shows the prismatic with rainbow colors of sodium carbonate monohydrate crystals that was the fourth species to be nucleated. Nucleation of sodium carbonate monohydrate corresponds to the change in slurry transparency in the vessel at C:F= 0.298. Only small amounts of sodium carbonate monohydrate crystals were detected at C:F= 0.298 but at C:F>0.299 the amounts of sodium carbonate monohydrate crystals was greatly increased as shown by panel G and H. Panel F displays that burkeite was nucleated at C:F= 0.299 which corresponds to an operating time of 3 hours and 40 minutes. Small amounts of small burkeite crystals were detected at C:F> 0.299 and increased in number and size in samples with C:F>.0.299. Burkeite nucleation appeared to stop or slow dramatically during the run, probably due to the difference in sulfate and burkeite saturation point described in Chapter 2. Furthermore, burkeite agglomerates were formed when the burkeite total crystal count decreased. Panels K and L show that sodium nitrate total crystal count and average crystal size increased for C:F≥0.363 and that the spike in nucleation described in Chapter 2 occurred at an operating time of 15 hours. The number

and mass of sodium nitrate crystals rapidely increased after this point and sodium nitrate became the major crystalline species in the slurry samples.

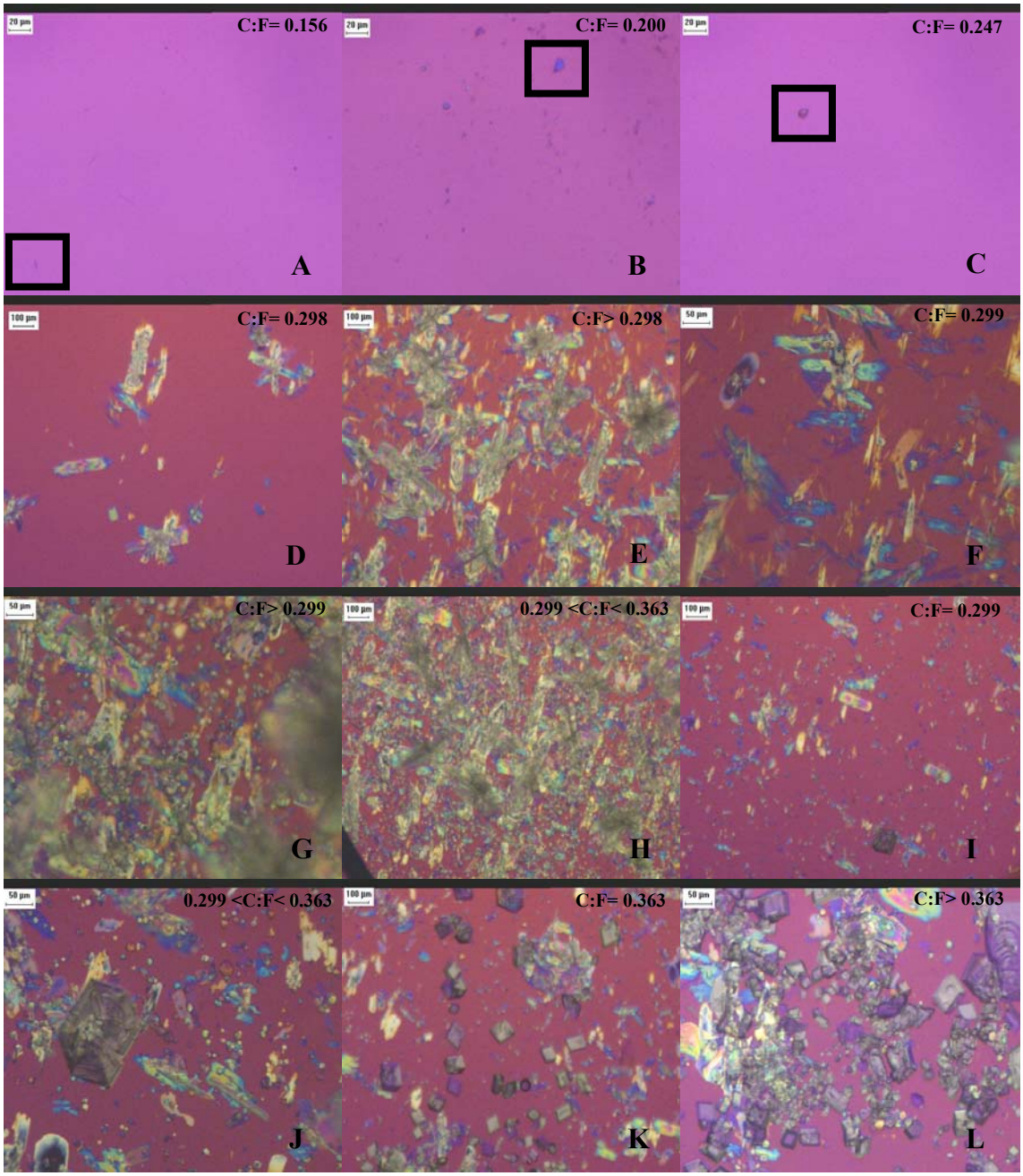

Figure 85. Crystal nucleation sequence for SST early feed Certification Run 38b
(Panel A, sodium oxalate crystal, Panel B, small sodium sulfate crystals, Panel C, small sodium nitrate crystals, Panel D, small amounts of sodium carbonate monohydrate crystals, Panel E, growth of sodium carbonate monohydrate with burkeite crystals, Panel F, burkeite crystals, Panel G, burkeite nucleation and carbonate growth, Panel H, Growth of carbonate, Panel I, large sodium nitrate, Panel J, zoom in sodium nitrate, Panel K, second nucleation of sodium nitrate, Panel L, increased sodium nitrate nucleation)

Table 37 summarizes nucleation points and corresponding operating times for each of the species crystallized during the early feed certification run.

Table 37. Specific nucleation points for the species produced during the early feed certification run at 66 °C and 25 g/h

SST Early Feed	Condensate To Feed Ratio At Nucleation	Operating Time At Nucleation (min)
Sodium Nitrate (1st Nucleation)	0.247	466
Sodium Nitrate (2nd Nucleation)	0.363	904
Sodium Carbonate Monohydrate	0.298	631
Burkeite Crystals	0.299	640
Sodium Sulfate	0.200	390
Sodium Oxalate	0.156	289

4.1.2 NUCLEATION RATE

Nucleation points of each crystalline species were determined following the methodology described in Chapter 2. Figure 86 shows the number of crystals of each species as a function of the operating time for an early feed run at 66 °C and 25 g/h. According to Figure 86, sodium nitrate has a nucleation rate close to zero until an operating time of 904 minutes. Sodium nitrate total crystal count profile follows an exponential or a power law with a relatively constant second section of the curve. The average estimated value of 3.628×10^{4} crystals/ mL·min was found for sodium nitrate using the methodology described in Chapter 2. Sodium carbonate monohydrate crystals displayed a high initial nucleation rate followed by a linear profile with a smaller constant nucleation rate. The average experimental value of the nucleation rate was 3.245×10^{3} crystals/ mL·min for sodium carbonate monohydrate. Assessing the case of the sodium sulfate crystals, a high initial nucleation rate was followed by a relatively low constant

nucleation rate with an average value of 2.724×10^3 crystals/ mL·min. Sodium oxalate presents a low initial nucleation rate followed by a nearly constant total crystal number. The average nucleation rate for the sodium oxalate is 79 crystals/ mL·min. The total burkeite profile displays a very high nucleation rate of 4.297×10^4 crystals/ mL·min followed by a decrease and a plateau. The plateau is expected to be due to two distinct phenomena: (1) the difference between sodium sulfate and burkeite saturation as shown in Chapter 2 and (2) the formation of large burkeite agglomerates and clusters.

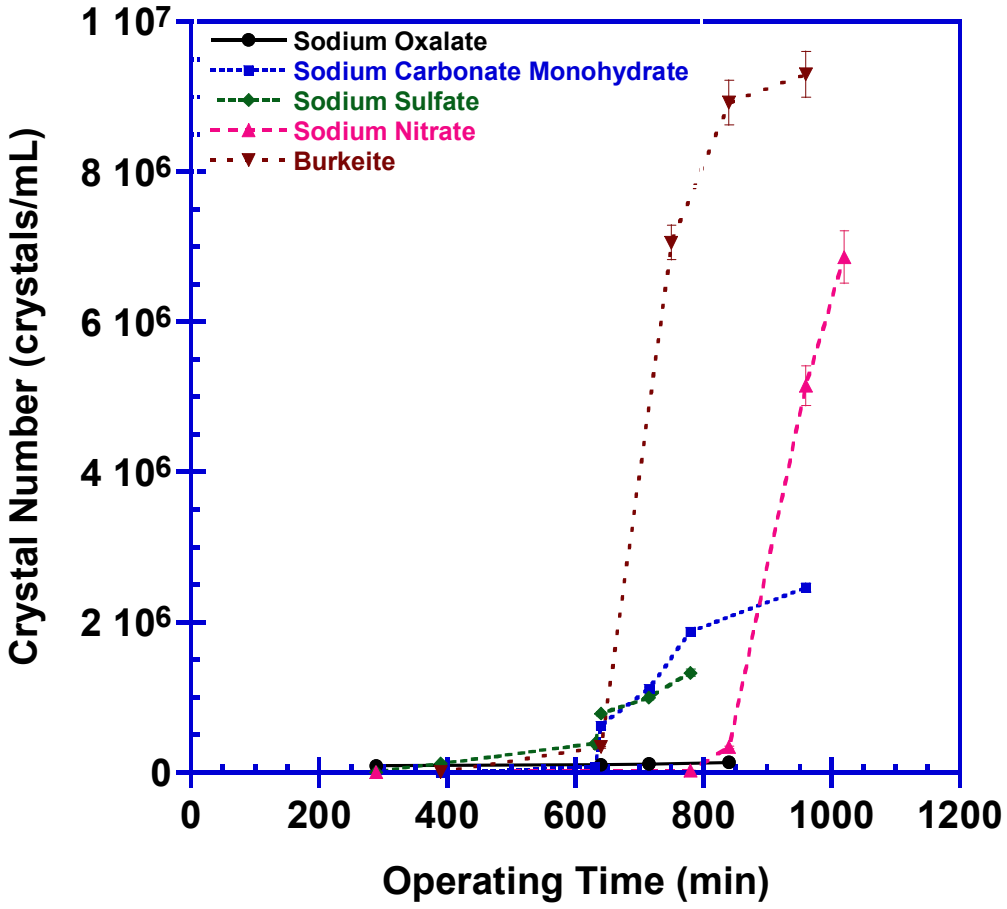

Figure 86. Evolution of total crystal count for each species formed from early feed run at 66 °C and 25 g/h

Figure 87 displays the evolution of the burkeite crystal count with operating time for which the total burkeite population was divided into two distinct categories: single burkeite crystals and burkeite agglomerates.

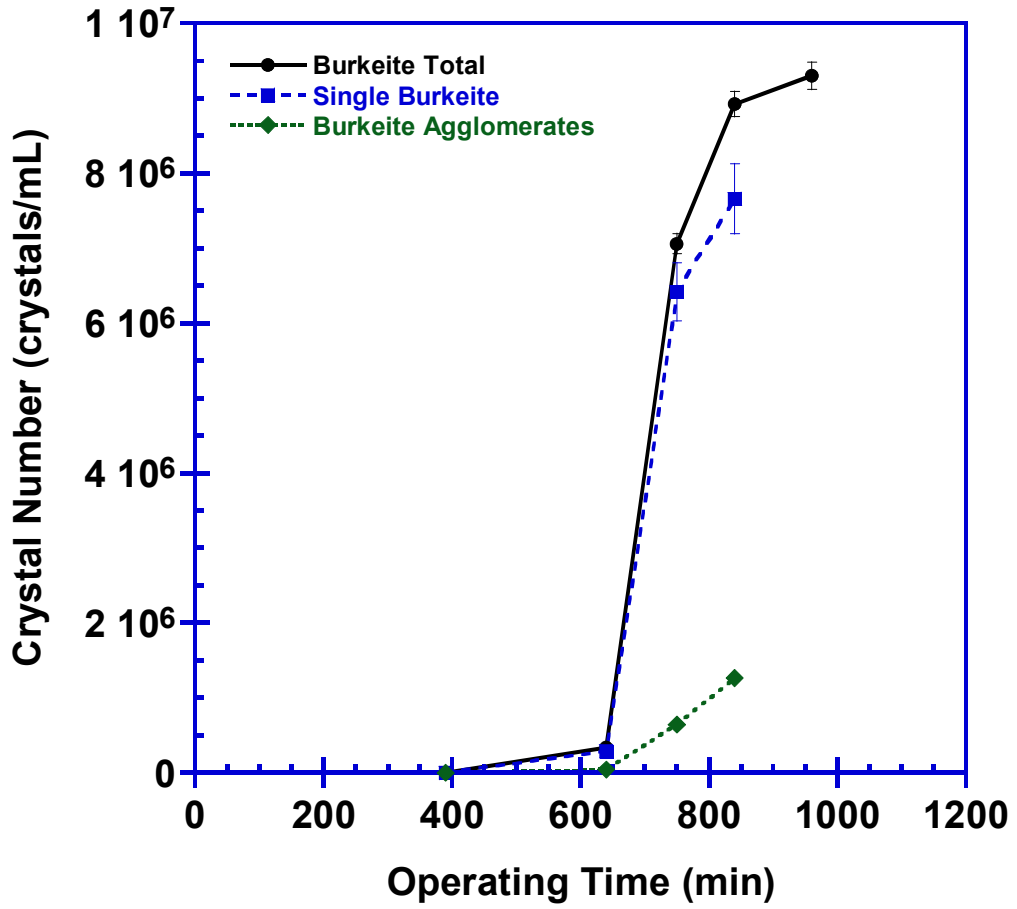

Figure 87. Evolution of total crystal count for burkeites formed from early feed run at 66 °C and 25 g/h

By considering the burkeite agglomerates as a separate entity it is possible to quantify the effect of agglomeration. The single burkeite crystals have an average nucleation rate of 3.686×10^{4} crystals/ mL·min while the agglomerate have a nucleation rate of only 6.106×10^{3} crystals/ mL·min. The agglomeration of burkeite crystals is smaller than the nucleation of single burkeite but its value remains non negligible. Moreover, in the samples of high slurry density the single burkeite crystals have been observed rearranged

into clusters. Figure 88 presents the evolution of the number of burkeite agglomerates during the experiment.

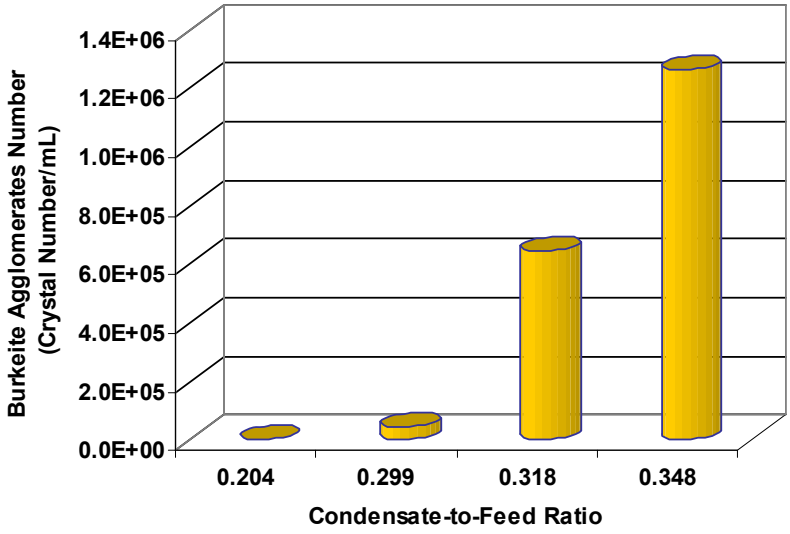

Figure 88. Evolution of total crystal count for burkeite agglomerates formed from early feed run at 66 °C and 25 g/h

4.1.3 GROWTH RATE

Crystal sizes were monitored for each sample recovered from the slurry following the protocols defined in Chapter 2. Figure 89 graphs the evolution of average length with the operating time. The methodology used to compute the specific average growth rate was outlined in Chapter 2.

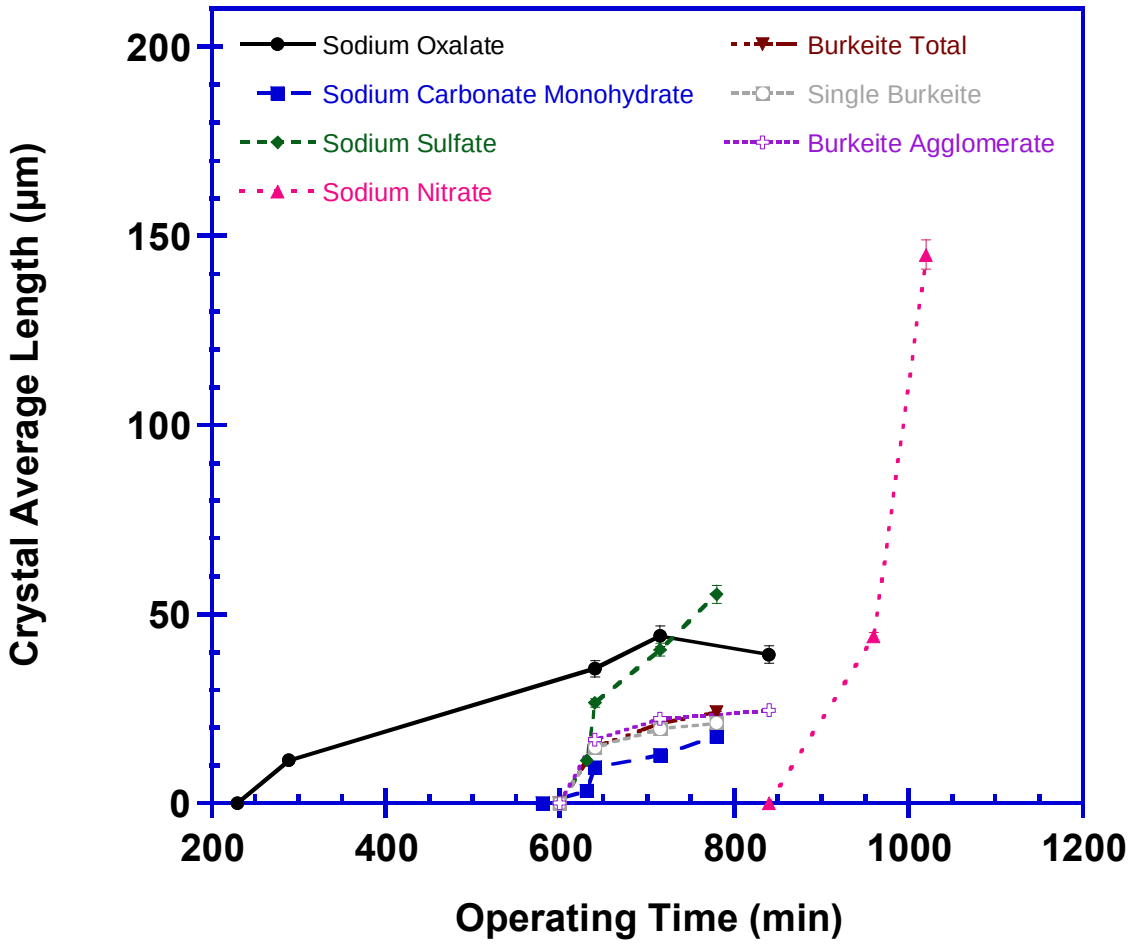

Figure 89. Evolution of crystal average length for each species formed from early feed run at 66 °C and 25 g/h

Figure 89 displays that sodium nitrate follows a nearly linear profile with an average growth rate of 1.680 µm·min^{-1}. Sodium carbonate monohydrate has a high initial growth rate followed by a constant average growth rate of 0.1580 µm·min^{-1}. Sodium sulfate and burkeite display a similar profile with an average constant value of 0.294 µm·min^{-1} and 0.170 µm·min^{-1}respectively. The sodium oxalate profile shows an increase of the length of the needles up to 50 µm and then a decrease in the average length, which likely is related to breakage of the sodium oxalate needles.

4.1.4 RELATING CRYSTALLIZATION KINETICS TO POPULATION DISTRIBUTION

Certification Run 38b crystal mass distribution histogram, which was presented in Chapter 3 Figure 51, is the result of the growth and nucleation rate of five different species: sodium nitrate, sodium carbonate monohydrate, sodium sulfate, burkeite and sodium oxalate. Figure 90 shows the crystal distribution histograms of the first stage of the early-feed Certification Run 38b.

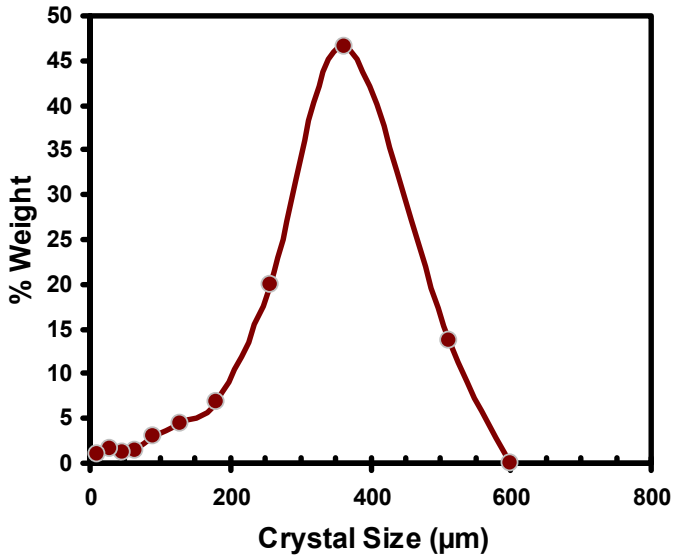

Figure 90. Mass distribution histogram for Stage 1 of Certification Run 38b

PLM analysis performed on the sieved crystals from Certification Run 38b showed that sodium nitrate was distributed over the 50 to 600 µm size range with a majority of crystal mass between 100 and 600 µm and a mode size around 360 µm. Sodium carbonate monohydrate crystals were recovered mainly in the 50 to 150 µm size range. One can estimate the average size of a crystalline species at the end of the experiment based solely on the growth rate. Table 38 displays the estimated crystal sizes

of sodium nitrate and sodium carbonate monohydrate with operating time which were calculated using $\overline{L}_i = \overline{G}_i (t - t_{n,i})$. $\overline{L}_i$ is the average crystal size for species i, $\overline{G}_i$ is the average estimated growth rate for species i, t is the operating time and $t_{n,i}$ the operating time at nucleation. Calculations were based on: (1) an average growth rate of 1.680 μm·min^{-1}for sodium nitrate and 0.158 μm·min^{-1}for sodium carbonate monohydrate, and (2) an ending of the experiment at 1324 minutes.

Table 38. Comparison of sodium nitrate and sodium carbonate monohydrate average crystal size calculated from growth rate estimate and experimental sieving results at the conditions of Early Feed Certification Run 38b

Crystalline Species	Growth Time after Nucleation (h)	Estimated Crystal Size (μm)	Measured Crystal Size (μm)
Sodium Nitrate	1	100	100
Sodium Nitrate	3.5	352	360
Sodium Nitrate	7	655	600
Sodium Carbonate Monohydrate	11.5	110	150
Sodium Carbonate Monohydrate	6	57	50

Table 38 shows that the calculated crystal sizes are in good agreement with the sizes obtained after sieving. It has to be noted that (1) an average growth rate was used, and (2) calculations were performed on the characteristic length. Dealing with sodium sulfate and burkeite crystals the sizes displayed before the plateau are in agreement with the measured crystal size after sieving. These values are close to 25 and 35 μm for the single and agglomerate burkeites diameters, and 24 μm for the sulfate second size.

4.1.5 SUMMARY

The main mode of nucleation is primary nucleation for sodium nitrate, sodium carbonate monohydrate, and sodium sulfate. The absence of significant agglomeration or breakage for these species was validated by the image analyses of the sieved crystals. Two species undergo a combination of primary and secondary nucleation:

- Sodium oxalate due to its needle shape follows a primary nucleation process until the other crystalline species are formed in the vessel. At this point significant breakage occurs modifying the number of needles in the slurry.
- Single burkeite crystals grow until they reach a certain size and then they begin to agglomerate. The agglomerates tend to become larger clusters when the growth of burkeite is stopped due to the difference in saturation between sodium sulfate and burkeite. This agglomeration is important as larger agglomerates allow reducing the loss of burkeite through filtration (pore size of 10 μm) but is likely to increase the incorporation of mother liquor and reduce the cesium decontamination.

Table 39 displays a summary of the kinetics obtained for each crystalline species under the conditions of the early feed Certification Run 38b.

Table 39. Specific kinetics for early feed Certification Run 38b at 66 °C and 25 g/h

SST Early Feed	Nucleation Rate (crystals/ mL·min)	Growth Rate (μm·min^{-1})
Sodium Nitrate	3.628×10^{4}	1.680
Sodium Carbonate Monohydrate	3.245×10^{3}	0.158
Total Burkeite Crystals	4.297×10^{4}	NA
Single Burkeite Crystals	3.686×10^{4}	0.170
Agglomerated Burkeite Crystals	6.106×10^{3}	0.039
Sodium Sulfate	2.724×10^{3}	0.294
Sodium Oxalate	79	0.193

4.2 EFFECT OF EVAPORATION RATE ON KINETICS

In order to assess the impact of evaporation rate (which is a measure of the rate at which supersaturation is generated) on crystallization kinetics, a series of experiments was performed with evaporation rates values of 25 g/h, 35 g/h, 55 g/h and 75 g/h. These values represent the largest range of evaporation rate that may be covered by the apparatus described in Chapter 2. Figure 91 shows the temperature and pressure profiles from these experiments and illustrates that the temperature was controlled to within +/- 1 ^{o}C of the target value of 66 ^{o}C. The pressure profiles reflect the step-wise changes in vacuum associated with manual adjustments of the regulating valve used to maintain a constant operating temperature. Figure 92 displays the condensate mass evaporated as a function of operating time for the series of runs.

The evaporation rate is directly linked to the supersaturation defined here as $S = C / C^*$, with the notation given in **Error! Reference source not found.**. In this section we will determine the nucleation points and kinetics associated with crystallization of early feeds at 66 °C for each of these evaporation rates.

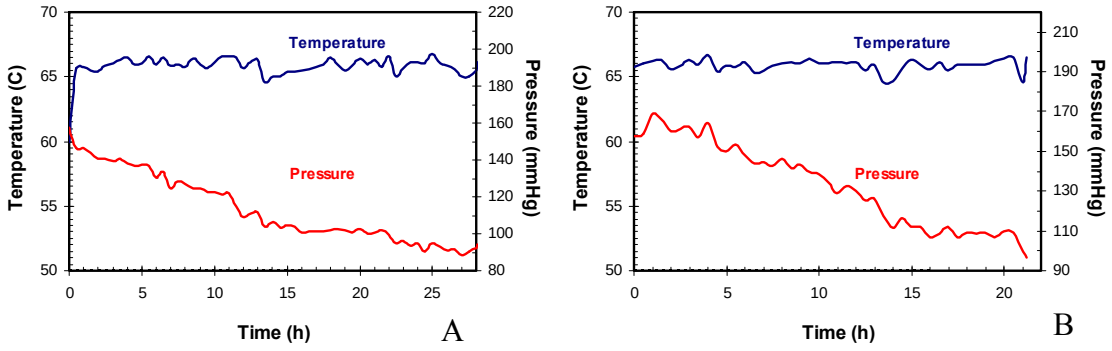

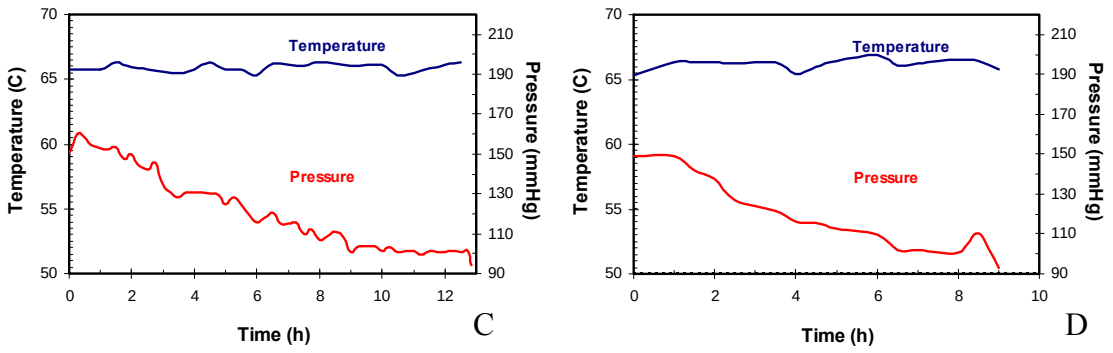

Figure 91. Temperature and pressure profiles for the series of early feed crystallization at 66 °C with varying evaporation rates
(Panel A, 25 g/h, Panel B, 35 g/h, Panel C, 55 g/h, Panel D, 75 g/h)

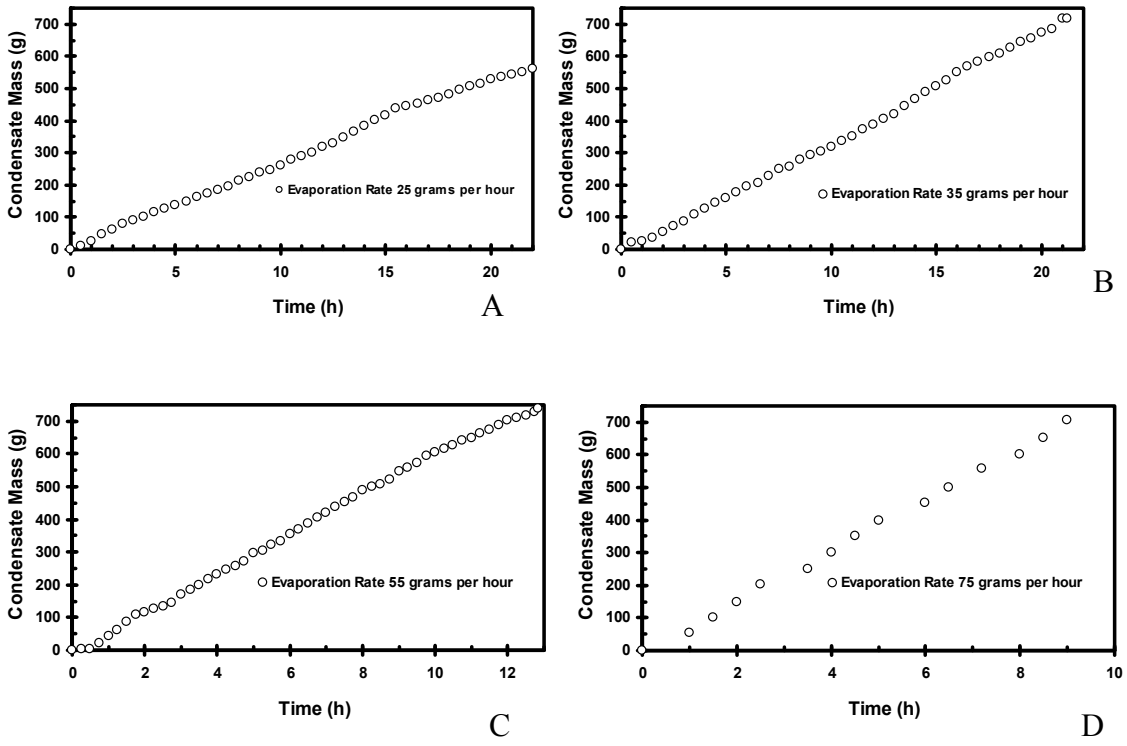

Figure 92. Mass of condensate generated as a function of operating time for early feed runs at 66 °C with varying evaporation rate
(Panel A, 25 g/h, Panel B, 35 g/h, Panel C, 55 g/h, Panel D, 75 g/h)

4.2.1 EVAPORATION RATE OF 35 GRAMS PER HOUR

Nucleation Points

The sequence of species nucleation points was determined based on PLM analyses of slurry samples taken at regular time intervals following the method described in Chapter 4.1. Sodium oxalate was the first crystalline species to be nucleated at C:F= 0.163 corresponding closely to the nucleation point of Certification Run 38b. Sodium sulfate came out of solution at C:F= 0.213, whereas the first sodium nitrate crystals could be clearly identified at C:F= 0.259. The number of sodium nitrate crystals produced at that point was very small and the few crystals that were nucleated continued growing until the second sodium nitrate nucleation was achieved at C:F= 0.387. At the end of the crystallization run the slurry was mainly composed of sodium nitrate crystals. Sodium carbonate monohydrate was the fourth species to be nucleated at C:F= 0.300 which corresponds to the nucleation point of carbonate during Certification Run 38b. Burkeite was nucleated at C:F= 0.302 corresponding to an operating time of 694 minutes. Assessing the case of burkeite crystals, their number continued increasing while their size remained small and several agglomerates were formed by association of one or several small burkeites. In samples with C:F>0.302, more agglomeration occurred until forming large clusters of burkeite.

Table 40 presents the specific nucleation points and corresponding operating times for the early feed crystallization at 35 g/h. The nucleation points remained relatively similar to these for the certification run operated at 25 g/h.

Table 40. Specific nucleation points for the species produced during the early feed run operated at 66 °C and 35 g/h

SST Early Feed	Condensate To Feed Ratio At Nucleation	Operating Time At Nucleation (min)
Sodium Nitrate (1st Nucleation)	0.259	420
Sodium Nitrate (2nd Nucleation)	0.387	930
Sodium Carbonate Monohydrate	0.300	688
Burkeite Crystals	0.302	694
Sodium Sulfate	0.213	330
Sodium Oxalate	0.163	244

Nucleation rate

Figure 93 presents the evolution of the total crystal count with the operating time for each of the crystalline species. The graph displays two types of profile similar to the base case: (1) a nearly linear profile composed of a high initial nucleation and followed by a constant rate, and (2) a profile that presents a high initial nucleation rate followed by a plateau. Sodium nitrate and sodium carbonate monohydrate present an exponential profile for which the average nucleation rates are 6.014×10^4 and 1.522×10^4 crystals/ mL·min respectively. Sodium oxalate and sodium sulfate profiles display an average nucleation rate of 5.23×10^2 and 1.362×10^4 crystals/ mL·min respectively in the ascending phase. Finally, burkeite tends to plateau with an average nucleation rate of 4.826×10^4 crystals/ mL·min.

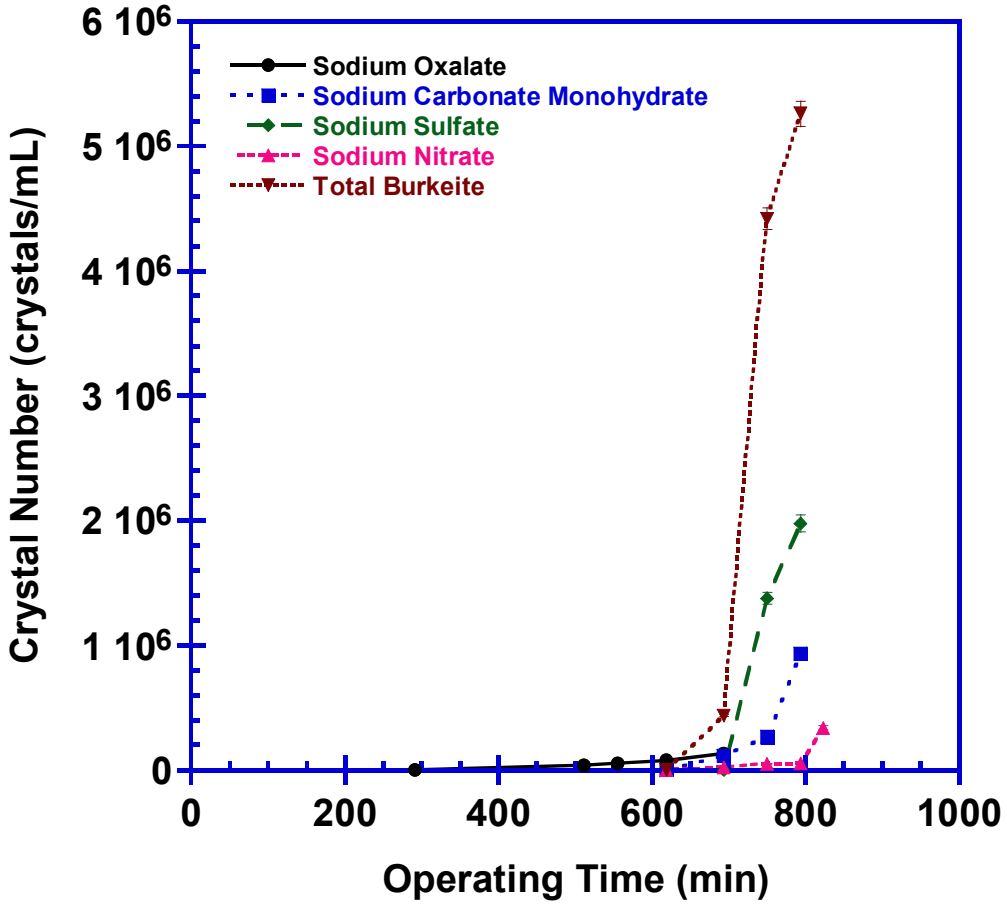

Figure 93. Evolution of total crystal count for each species formed from early feed run at 66 °C and 35 g/h

Figure 94 displays the evolution of the burkeite crystal count with operating time for which the total burkeite population was divided into two distinct categories: single burkeite crystals and burkeite agglomerates. Single burkeite crystals have an average nucleation rate of 3.767×10^{4} crystals/ mL·min while the agglomerates have a nucleation rate of only 1.058×10^{4} crystals/ mL·min. The agglomeration of burkeite crystals is greatly increased compared to the run at 25 grams per hour evaporation rate. The increase of the primary nucleation is also important but a lot less than the increase of the secondary nucleation. The graph in Figure 95 presents the evolution of the number of burkeite agglomerates during the early feed run at 66 °C and 35 g/h. The number of

agglomerates increases rapidly from C:F= 0.302 to C:F= 0.322 but the increase slows down from C:F= 0.322 to C:F= 0.332. These values validate the observation of the sample images that showed that in the first moment after nucleation a lot of agglomerates are formed with a few small burkeite crystals and then in the next samples the agglomerates number vary less but their size increases as several agglomerates join to form clusters.

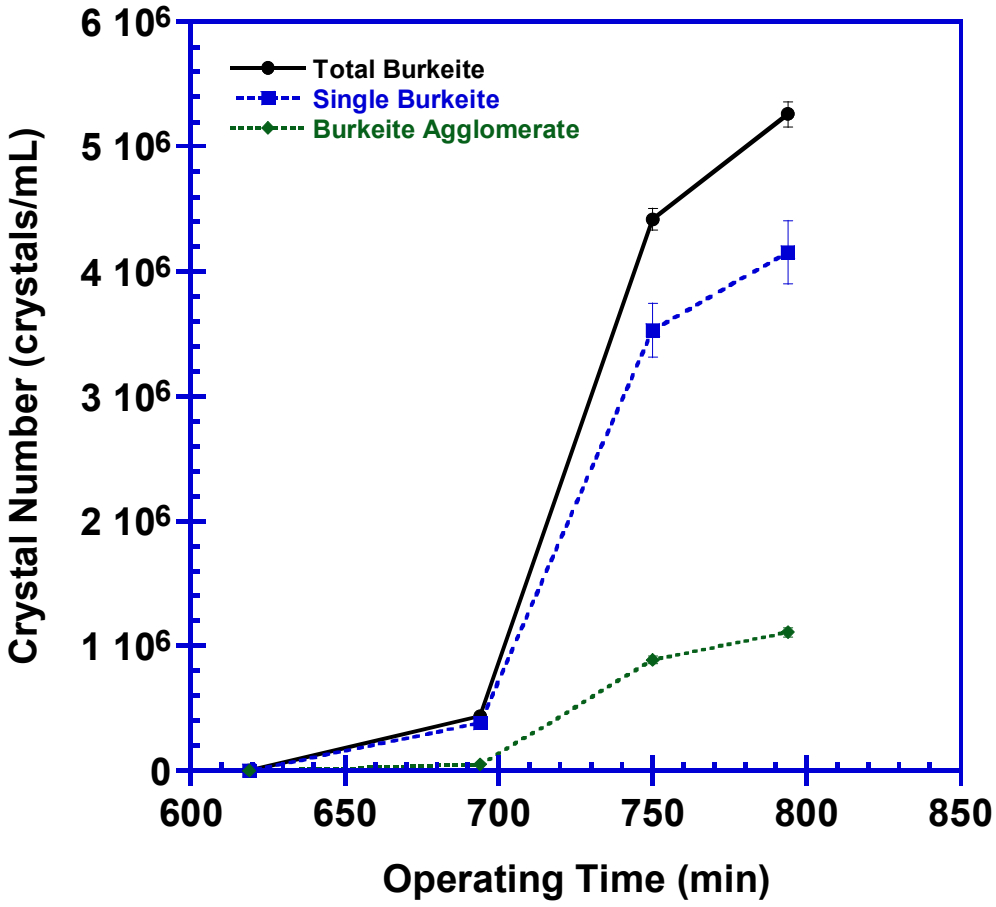

Figure 94. Evolution of total crystal count for burkeite formed from early feed run at 66 °C and 35 g/h

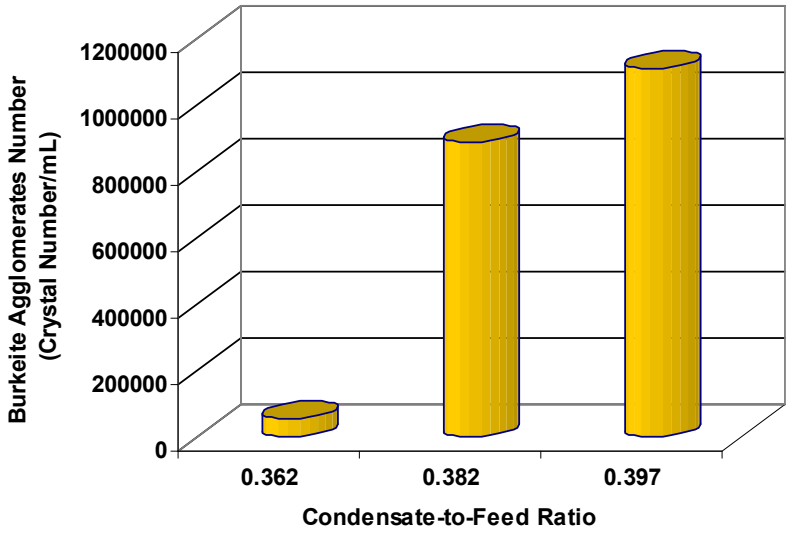

Figure 95. Evolution of total crystal count for burkeite agglomerates formed from early feed run at 66 °C and 35 g/h

Growth Rate

The crystal size was monitored for each sample recovered from the slurry following the protocols defined in Chapter 2. Figure 96 presents the graphs of the average length evolution with the operating time. The methodology used to compute the specific average growth rate was outlined in Chapter 2.

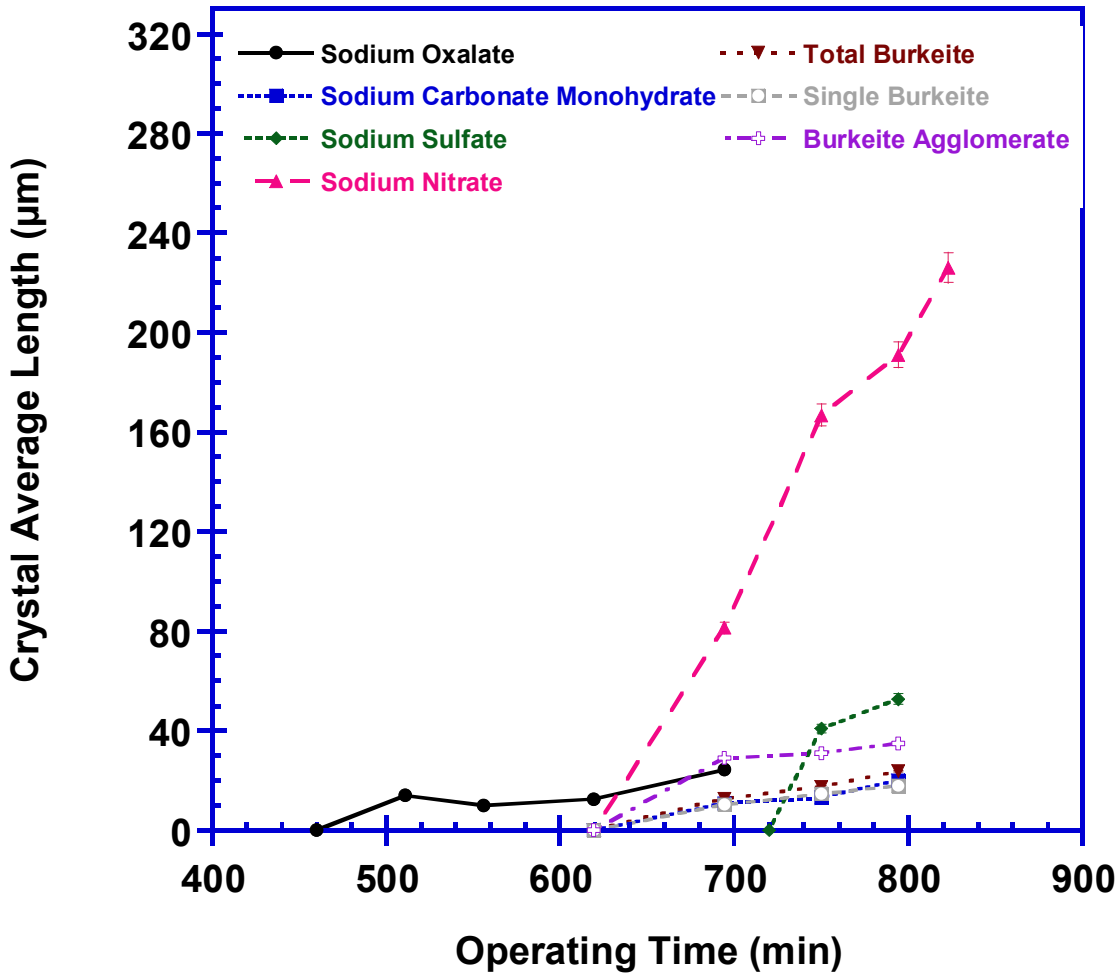

Figure 96. Evolution of crystal average length for each species formed from early feed run at 66 °C and 35 g/h

Sodium nitrate follows a linear profile with an average growth rate of 1.12 $\mu m \cdot min^{-1}$. Sodium carbonate monohydrate, burkeite and sodium sulfate have a high initial growth rate followed by a constant average growth rate of 0.091, 0.129 and 0.270 $\mu m.min^{-1}$ respectively. Finally, the sodium oxalate profile shows an increase of the length of the needles up to 20 µm and then a decrease in the average length followed by another increase, which likely is related to breakage of the sodium oxalate needles. The average growth rate in the first section of the profile is 0.158 $\mu m \cdot min^{-1}$.

Conclusion

Nucleation and growth rate profiles are very similar to these obtained for the base case of study of 25 grams per hour evaporation rate. The nucleation rate of each of the different crystalline species was increased with the increase in evaporation rate. Inversely, the growth rate was decreased with an increase in evaporation rate. The nucleation points presented values that were close to these of the base case. One of the other main discrepancies deals with the production of burkeite. Since the nucleation rate was increased a larger number of small burkeite was produced. These smaller crystals tend to form a large number of agglomerate that became large clusters during the run. In essence the agglomeration of burkeite was greatly increased in this run due to higher nucleation rate and smaller growth rate. The discrepancy in nucleation and growth rate can be inferred from Table 41, that summarize the values for the 35 grams per hour evaporation rate.

Table 41. Specific kinetics for early feed run at 66 °C and 35 g/h

SST Early Feed	Nucleation Rate (crystals/ mL·min)	Growth Rate ($\mu m \cdot min^{-1}$)
Sodium Nitrate	6.014×10^{4}	1.120
Sodium Carbonate Monohydrate	1.522×10^{4}	0.091
Total Burkeite Crystals	4.826×10^{4}	NA
Single Burkeite Crystals	3.767×10^{4}	0.129
Agglomerated Burkeite Crystals	1.058×10^{4}	0.058
Sodium Sulfate	1.362×10^{4}	0.270
Sodium Oxalate	5.23×10^{2}	0.158

4.2.2 EVAPORATION RATE OF 55 GRAMS PER HOUR

Nucleation Points

The sequence of species nucleation points was determined based on PLM analyses of slurry samples taken at regular time intervals following the method described in Chapter 4.1. Sodium oxalate was the first crystalline species to be nucleated at C:F= 0.140. This nucleation point occurred slightly later for Certification Run 38b. Sodium sulfate came out of solution at C:F= 0.140 which is significantly earlier than the certification run. These crystals were nucleated with a higher rate than the previous run. The first sodium nitrate crystals could be clearly identified at C:F= 0.257. The number of sodium nitrate crystals produced at that point was very low and the few crystals that were nucleated continued growing until the second sodium nitrate nucleation was achieved at C:F= 0.363. Sodium carbonate monohydrate was nucleated at C:F= 0.305, corresponding to the nucleation point of carbonate during the previous two runs. Burkeite was nucleated at C:F= 0.305. Assessing the case of burkeite crystals, their number continued increasing in the next samples while their size remained small. Several agglomerates formed by association of one or several small burkeite crystals in the samples right after C:F= 0.305. In the next sample more agglomeration occurred and formed large burkeite clusters. Compared to the previous run, the number of small burkeite was greatly increased and the formation of agglomerate was instantaneous

Table 42 presents the nucleation points and corresponding operating times for the early feed crystallization at 55 g/h. The nucleation points remained relatively similar to

these for the certification run operated at 25 grams per hour with the exception of sodium sulfate and sodium oxalate that was nucleated (and detected) slightly earlier.

Table 42. Specific nucleation points for the species produced during the early feed run operated at 66 °C and 55g/h

SST Early Feed	Condensate To Feed Ratio At Nucleation	Operating Time At Nucleation (min)
Sodium Nitrate (1st Nucleation)	0.257	234
Sodium Nitrate (2nd Nucleation)	0.363	374
Sodium Carbonate Monohydrate	0.305	295
Burkeite Crystals	0.305	295
Sodium Sulfate	0.140	101
Sodium Oxalate	0.140	101

Nucleation rate

Figure 97 presents the evolution of the total crystal count with the operating time for each of the crystalline species. Sodium nitrate and sodium carbonate monohydrate present a linear profile for which the average nucleation rates are 1.079×10^{5} and 1.597×10^{4} crystals/ mL·min respectively. For sodium oxalate and sodium sulfate the profiles have an average nucleation rate of 6.569×10^{3} and 1.624×10^{4} crystals/ mL·min respectively in the ascending phase. Finally burkeite tends to plateau with an average nucleation rate of 2.687×10^{5} crystals/ mL·min.

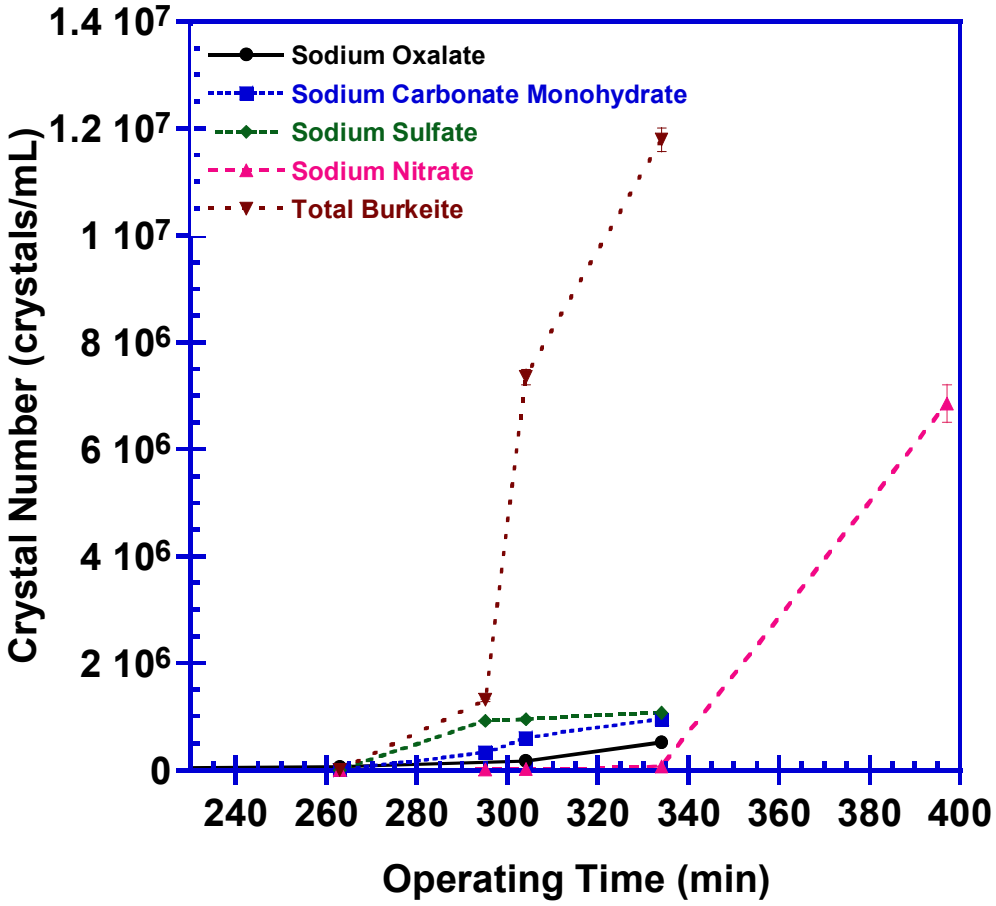

Figure 97. Evolution of total crystal count for each species formed from early feed run at 66 °C and 55 g/h

Figure 98 displays the evolution of burkeite crystal count with operating time for which the total burkeite population was divided into two distinct categories: single burkeite crystals and burkeite agglomerates. Single burkeite crystals have an average nucleation rate of 2.321×10^{5} crystals/ mL·min while the agglomerate have a nucleation rate of only 3.661×10^{5} crystals/ mL·min. The agglomeration of burkeite crystals is greatly increased compared to the run at 35 grams per hour evaporation rate (multiplied by three). The increase of the primary nucleation is however more important than the increase of the secondary nucleation (one order of magnitude).

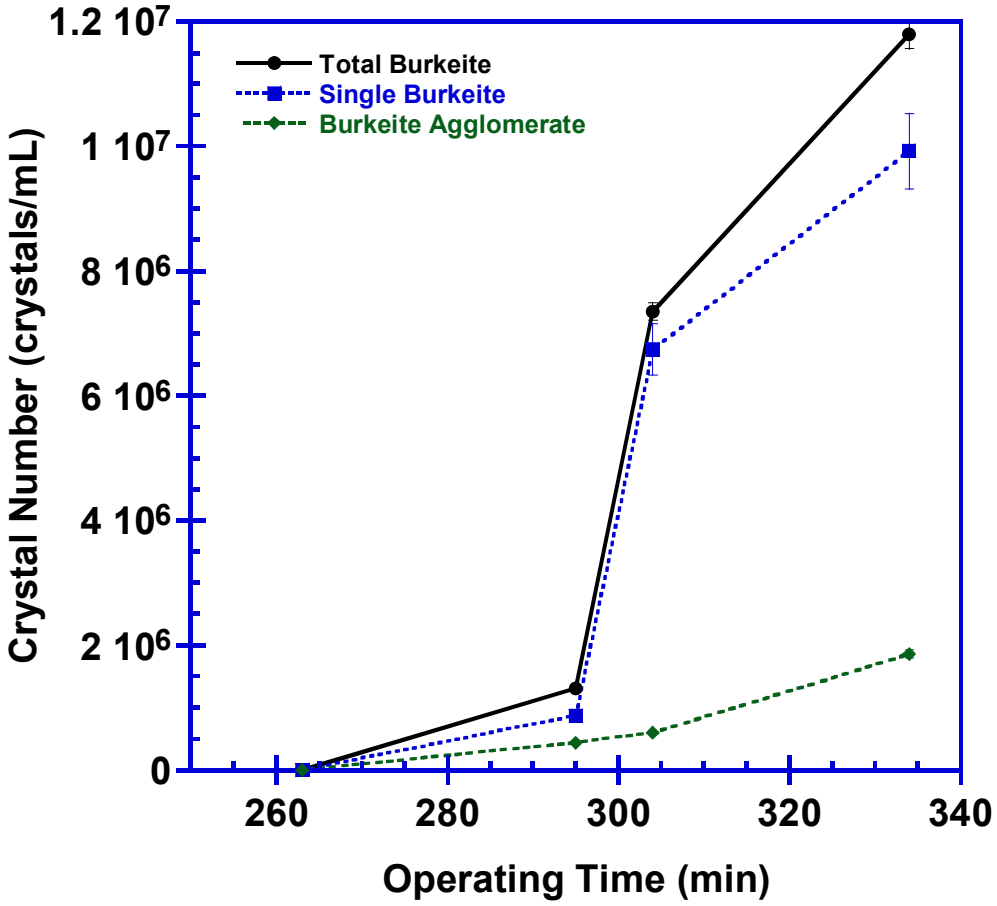

Figure 98. Evolution of total crystal count for burkeite formed from early feed run at 66 °C and 55 g/h

The graph in Figure 99 presents the evolution of the number of burkeite agglomerates during the experiment. The number of agglomerates formed initially is a lot greater with the evaporation rate of 55 grams per hour which is in agreement with PLM observations. The instantaneous formation of a large number of very small crystals creates more agglomerates with a smaller size. The agglomeration rate diminishes after the initial nucleation point as the existing agglomerates incorporates more crystals and increases in size. Finally at a condensate to feed ratio of 0.337 the proportion of agglomerates was greater for the higher evaporation rate. The formation of a large number of small crystals increases the burkeite crystal density in the vessel and the

probability of collisions between burkeite crystals leading to the formation of agglomerates.

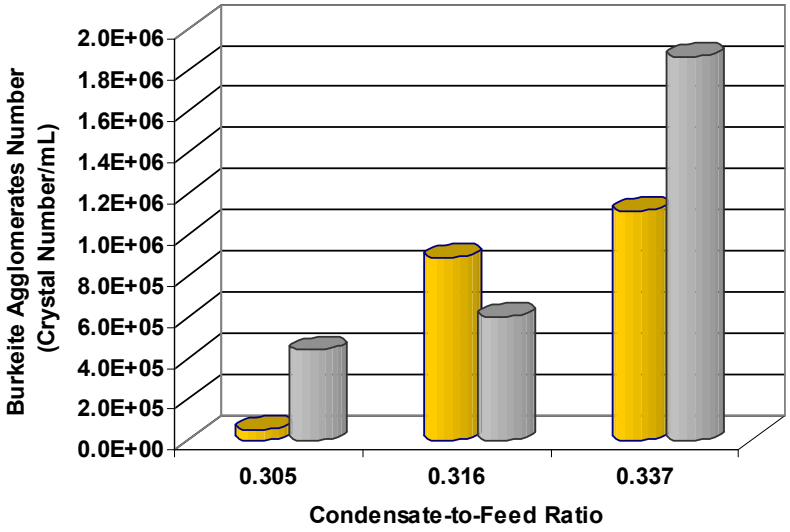

Figure 99. Evolution of total crystal count for burkeite agglomerates formed from early feed run at 66 °C and 55 g/h
(Gold column, evaporation rate of 35 grams per hour, Silver column, evaporation rate of 55 grams per hour)

Growth Rate

The crystal size was monitored for each sample recovered from the slurry following the protocols defined in Chapter 2. Figure 100 presents the graphs of the average length evolution with the operating time. The methodology used to compute the specific average growth rate was outlined in Chapter 2.

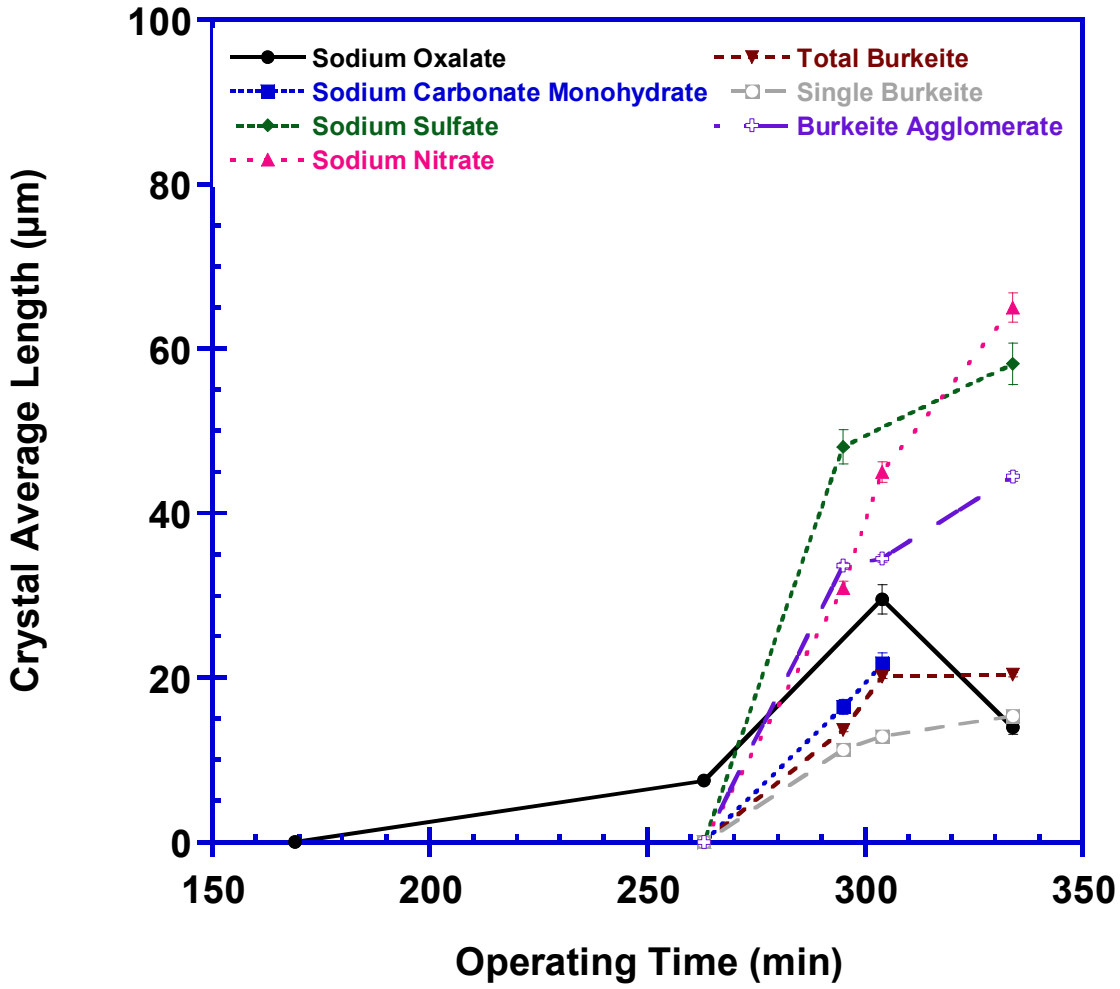

Figure 100. Evolution of crystal average length for each species formed from early feed run at 66 °C and 55 g/h

Sodium nitrate follows a linear profile with an average growth rate of 0.873 $\mu m \cdot min^{-1}$. Sodium carbonate monohydrate, burkeite and sodium sulfate have a high initial growth rate followed by a constant average growth rate of 0.052, 0.081 and 0.258 $\mu m \cdot min^{-1}$ respectively. Finally, sodium oxalate profile shows an increase of the length of the needles up to 30 µm and then a decrease in the average length, which likely is related to breakage of the sodium oxalate needles. The average growth rate in the growing phase was 0.092 $\mu m \cdot min^{-1}$.

Conclusion

The nucleation and growth profiles are very similar to these obtain for the base case of study. In this experiment, the nucleation rate of each of the different crystalline species was increased wile the growth rate was greatly decreased. This decrease led to the formation of smaller crystals especially for sodium carbonate monohydrate and sodium sulfates. Formation of large number of small burkeite crystals led to a quasi instantaneous agglomeration phenomenon. It is the increase in crystals number that is likely to have increased the probability of collisions between burkeite crystals necessary for the agglomeration phenomenon to occur. As it was observed in the previous experiments, the agglomeration followed two stages: (1) a first stage where a large amount of agglomerates is formed by a small number of crystals, and (2) a second stage where the formation of large clusters by agglomeration of single crystals to existing clusters or association of agglomerates. Another interesting discrepancy with the base case of study is the change in nucleation point for two of the crystalline species. Table 43 summarizes the values of the average growth and nucleation rate for the 55 grams per hour evaporation rate experiment.

Table 43. Specific kinetics for early feed run at 66 °C and 55 g/h

SST Early Feed	Nucleation Rate (crystals/ mL·min)	Growth Rate ($\mu m \cdot min^{-1}$)
Sodium Nitrate	1.078×10^{5}	0.873
Sodium Carbonate Monohydrate	1.597×10^{4}	0.052
Total Burkeite Crystals	2.687×10^{5}	NA
Single Burkeite Crystals	2.321×10^{5}	0.081
Agglomerated Burkeite Crystals	3.661×10^{4}	0.279
Sodium Sulfate	1.624×10^{4}	0.258
Sodium Oxalate	6.569×10^{3}	0.092

4.2.3 EVAPORATION RATE OF 75 GRAMS PER HOUR

Nucleation Points

The sequence of species nucleation points was determined based on PLM analyses of slurry samples taken at regular time intervals following the method described in Chapter 4.1. Both sodium oxalate and sodium sulfate were nucleated at C:F= 0.082. This nucleation point is different than the certification experiment where these two species were detected later in the run. Sodium sulfate total number increased in the next samples. The first sodium nitrate small crystals were identified at C:F= 0.234. The number of sodium nitrate crystals produced at that point increased rapidly in the following samples. In this experiment performed with very fast evaporation rate, sodium nitrate crystals were detected earlier and presented only one nucleation. Sodium carbonate monohydrate was nucleated at C:F= 0.290. Burkeite was nucleated at C:F= 0.306. Assessing the case of burkeite, the burkeite crystals that were nucleated were so small that they instantaneously formed large clusters. Since sodium nitrate had

undergone one early nucleation, the slurry density became very high earlier during the experiment.

Table 44 presents the specific nucleation points and corresponding operating times for the early feed crystallization at 75 g/h. Only the nucleation points of sodium carbonate monohydrate and burkeite remained relatively similar to these for the certification run operated at 25 g/h. Sodium sulfate, sodium nitrate and sodium oxalate were nucleated earlier with only one spike in nucleation observed for sodium nitrate.

Table 44. Specific nucleation points for the species produced during the early feed run operated at 66 °C and 75g/h

SST Early Feed	Condensate To Feed Ratio At Nucleation	Operating Time At Nucleation (min)
Sodium Nitrate (1st Nucleation)	0.234	159
Sodium Nitrate (2nd Nucleation)	0.234	159
Sodium Carbonate Monohydrate	0.290	224
Burkeite Crystals	0.290-0.306	224-236
Sodium Sulfate	0.082	48
Sodium Oxalate	0.082	48

Nucleation rate

Figure 101 presents the evolution of the total crystal count with the operating time for each of the crystalline species. Due to the early nucleation of sodium nitrate and the change in nucleation points for the other species, the nucleation profiles were changed compared to the previous experiments. Furthermore the slurry density became high very quickly making it difficult to observe the crystal nucleation in the samples corresponding to a condensate to feed ratio higher than 0.360. All profiles appear linear at the exception

of burkeite. Sodium nitrate and sodium carbonate monohydrate present an average nucleation rates of 6.680×10^{3} and 1.239×10^{4} crystals/ mL·min respectively. For sodium oxalate and sodium sulfate the average nucleation rates are of 4.860×10^{3} and 1.885×10^{4} crystals/ mL·min respectively. Finally burkeite shows a decrease in the nucleation profile which is explained by the important agglomeration of burkeite crystals. At such high evaporation rate (and nucleation rate) the secondary nucleation is dominant. In the first section of the profile the average nucleation rate was 2.082×10^{4} crystals/ mL·min.

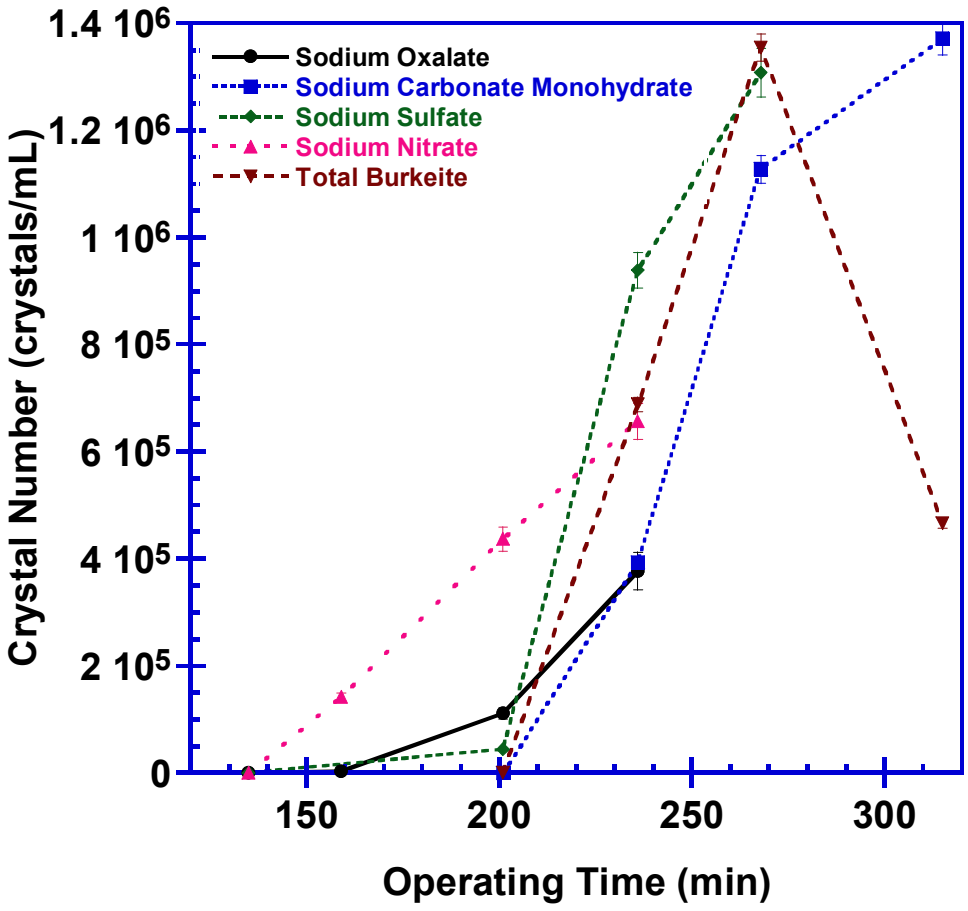

Figure 101. Evolution of total crystal count for each species formed from early feed run at 66 °C and 75 g/h

Figure 102 displays the evolution of the burkeite total crystal count with operating time for which the total burkeite population was divided into two distinct categories: single burkeite crystals and burkeite agglomerates. The increase in burkeite number is at first controlled by the increase in agglomerates and then by the nucleation of single burkeites. In the first phase (from C:F= 0.270 to C:F= 0.320), the single burkeite crystals agglomerates and the single burkeite crystals have an average nucleation rate of 1.873×10^{4} crystals/ mL·min while the agglomerate have a nucleation rate of 2.081×10^{3} crystals/ mL·min. In the second phase (from C:F= 0.320 to C:F= 0.360) the number of agglomerate and the overall burkeite nucleation decrease due to the agglomeration of the existing burkeite clusters. The agglomeration of burkeite crystals is not only greatly increased compared to the run at 55 g/h but it is also instantaneous.

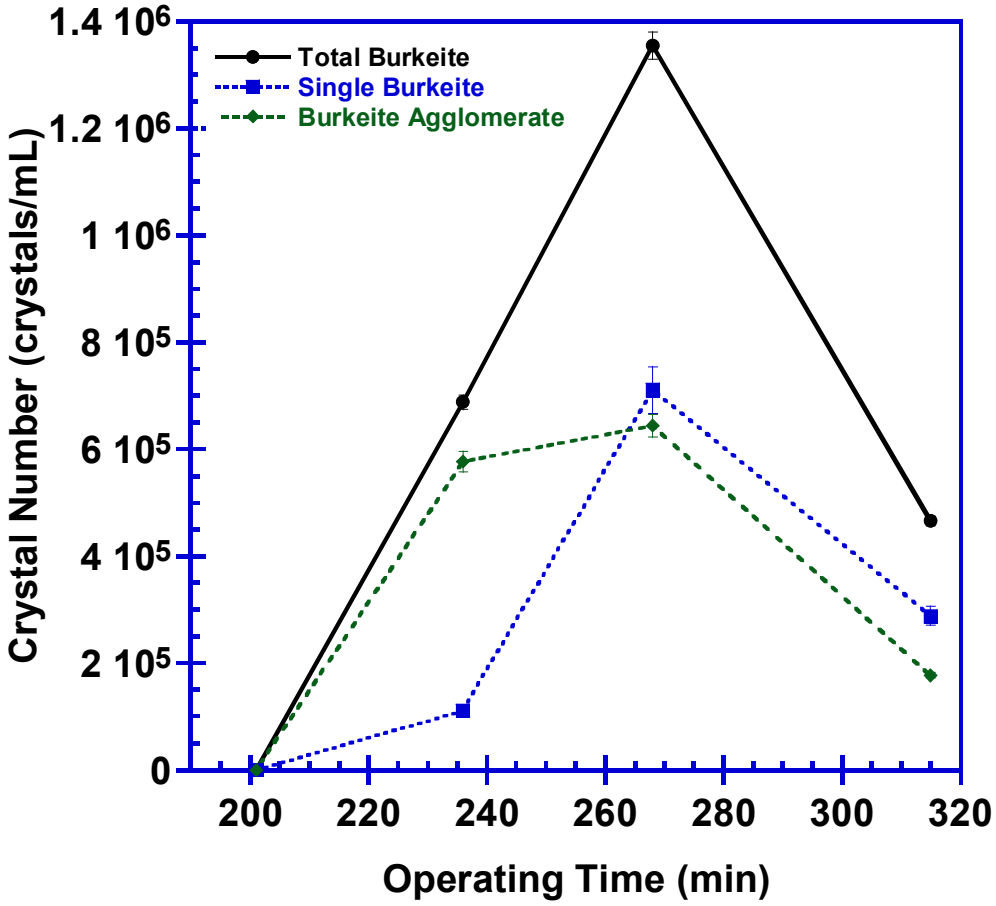

Figure 102. Evolution of total crystal count for burkeite formed from early feed run at 66 °C and 75 g/h

Figure 103 presents the evolution of the number of burkeite agglomerates during the experiment. The number of agglomerates formed initially is a lot greater with the evaporation rate of 75 grams per hour which is in agreement with the PLM observations. The agglomerates formed are large clusters. The instantaneous formation of a too large number of very small crystals creates lesser agglomerates with a greater size. The agglomeration rate is diminished compared to the two previous experiments due to the higher size of the burkeite clusters.

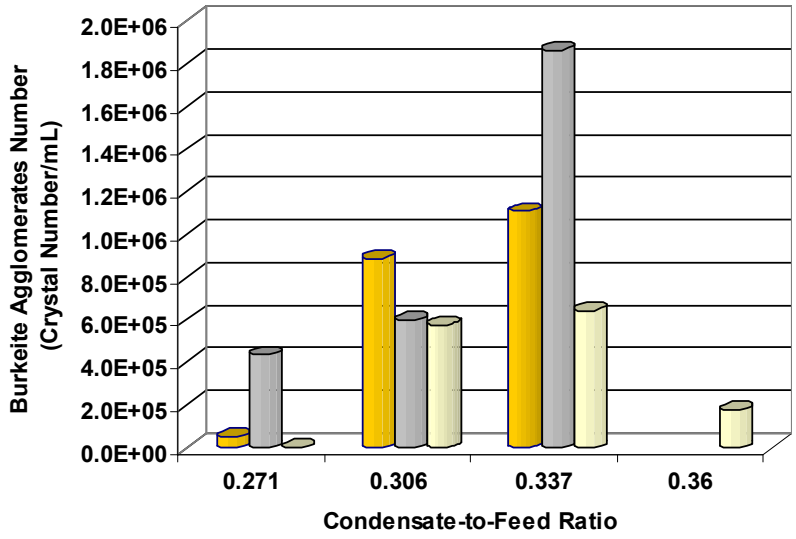

Figure 103. Evolution of total crystal count for burkeite agglomerates formed from early feed run at 66 °C and 75 g/h
(Gold column, evaporation rate of 35 grams per hour, Silver column, evaporation rate of 55 grams per hour, White column, evaporation rate of 75 grams per hour)

Growth Rate

The size of the crystals was monitored for each sample recovered from the slurry following the protocols defined in Chapter 2. Figure 104 presents the graphs of the average length evolution with the operating time. The methodology used to compute the specific average growth rate was outlined in Chapter 2. All the species presents a linear profile at the exception of burkeite that tends to plateau and sodium oxalate that undergo breakage in the last section of the profile. Sodium nitrate follows an average growth rate of 0.419 $\mu m \cdot min^{-1}$, when sodium carbonate monohydrate, burkeite and sodium sulfate have a growth rate of 0.170, 0.034 and 0.554 $\mu m \cdot min^{-1}$ respectively. Finally, the sodium oxalate profile shows an increase of the length of the needles up to 30 µm and then a decrease in the average length, which likely is related to breakage of the sodium oxalate needles. The average growth rate in the growing phase was 0.041$\mu m \cdot min^{-1}$. The single

burkeite crystals present an average growth rate of 0.034µm·min^{-1} in the ascending part of the profile when the agglomerates possess an average growth rate of 0.505µm·min^{-1}. This last growth rate is doubled compared to the previous experiment.

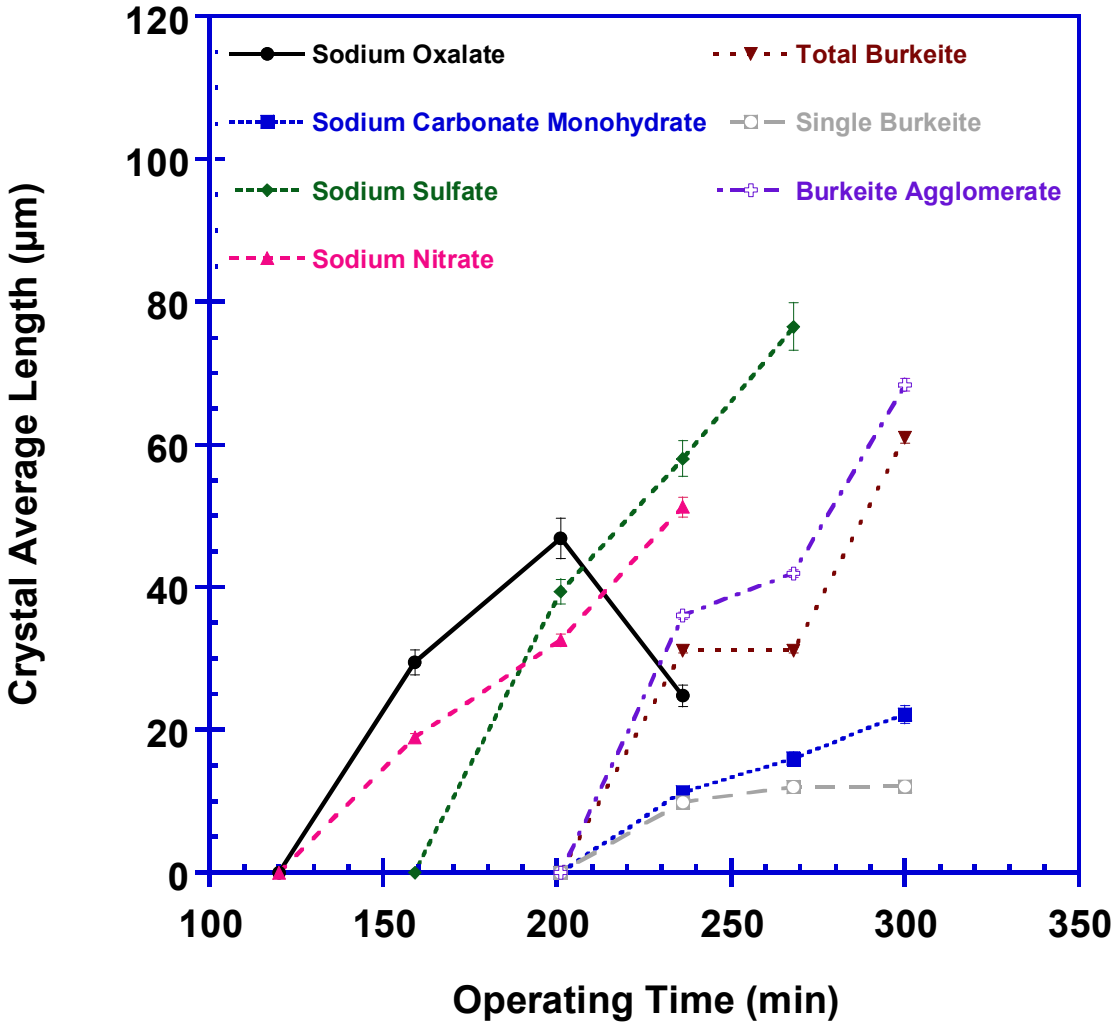

Figure 104. Evolution of crystal average length for each species formed from early feed run at 66 °C and 75 g/h

Conclusion

This experiment was performed with the maximum evaporation rate allowed by the equipment. The nucleation points of several species were change due to this increase of evaporation rate. Sodium sulfate and sodium oxalate were generated earlier.

Furthermore, sodium nitrate was nucleated earlier with only one main nucleation during the run, on contrary to the three previous experiments that presented two sodium nitrate nucleations. Because of these two elements the slurry density increased rapidly making the image analyses difficult after 320 minutes. The nucleation and crystal growth profiles appeared constant to that point whereas sodium sulfate, sodium oxalate and burkeite are expected to reach a plateau and sodium nitrate and carbonate are expected to follow an exponential curve. The values of the nucleation rate may hence not be used in the study of the effect of evaporation rate. The other main discrepancy deals with the generation of burkeite clusters which was (1) instantaneous and (2) of larger size and smaller number. The growth rate of the burkeite agglomerates was three times these of the previous crystallization run. Table 45 summarizes the values of the average growth and nucleation rate for the 55 grams per hour evaporation rate experiment.

Table 45. Specific kinetics for early feed run at 66 °C and 75 g/h

SST Early Feed	Nucleation Rate (crystals/ mL·min)	Growth Rate ($\mu m \cdot min^{-1}$)
Sodium Nitrate	6.680×10^{3}	0.419
Sodium Carbonate Monohydrate	1.239×10^{4}	0.170
Total Burkeite Crystals	2.082×10^{4}	NA
Single Burkeite Crystals	1.873×10^{4}	0.034
Agglomerated Burkeite Crystals	1.081×10^{3}	0.505
Sodium Sulfate	1.885×10^{4}	0.554
Sodium Oxalate	4.860×10^{3}	0.414

4.2.4 MODELING OF EVAPORATION RATE EFFECT ON KINETICS

Nucleation points

Figure 105 displays the main curves and zones involved in a general batch evaporative crystallization process. In panel A, solvent is removed from a system starting at an initial feed composition and temperature. The removal of the solvent occurs by fixing the evaporation rate –linked to the double jacket temperature- and since the experiment is performed isothermally, follows a vertical line. When the concentration of one of the solutes reaches saturation, the species is at thermodynamic equilibrium and nucleation and growth can occur with further evaporation. Following a stochastic approach, embryos are formed and re-dissolved until reaching critical size, at which they became stable nuclei. Therefore, in a real system, the nucleation occurs after the saturation is reached, and depending on the precision of the experimental equipment, the nucleation is detected slightly after it has occurred. In essence, a real system may be described graphically by three types of curves: (1) the saturation curve at which the system is at thermodynamic equilibrium, (2) the metastable limit at which a species is nucleated and nuclei are above the critical size, and (3) the detection curve at which the nuclei are sufficiently large to be detected.

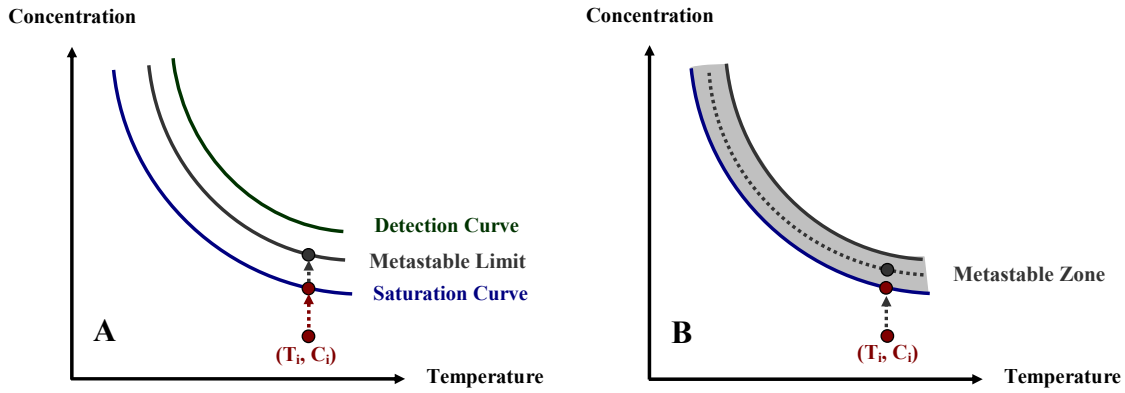

Figure 105. Sketches of the different zones and curves involved in evaporative crystallization process
(Panel A, saturation, metastable and detection curves, Panel B, metastable zone)

The influence of evaporation rate on the metastable cannot be predicted by thermodynamic simulations. However the nucleation curve in a real system may be better described by a nucleation zone for which the probability of nucleation varies as shown in Figure 105 B (Marangoni A.G. et al.; 2002). The metastable zone represents the zone within which nucleation may occur depending solely on process conditions. In essence, based on the results obtained from the study of the influence of evaporation rate on points of nucleation limit –defined as the time at which a species is nucleated–, if we cross the metastable zone slowly – i.e low evaporation rate - the nucleation will occur at a constant operating time, but if we go through the nucleation zone very fast – high evaporation rate- nucleation may be induced earlier. This phenomenon is expected to be dependant on the width of the metastable zone and is hence different for each crystalline species.

Table 46 summarizes the specific nucleation point for each early feed experiment at 66 °C and 25 g/h, 35 g/h, 55 g/h, 75 g/h. The nucleation points for burkeite and sodium carbonate monohydrate are identical for the entire range of evaporation rates. Sodium nitrate present similar values for the first and second spike in nucleations at the exception

of the highest evaporation rate of 75 g/h. For this extreme value of the evaporation, only one nucleation was observed earlier in the run. Assessing the case of sodium sulfate and sodium oxalate, a change in the nucleation rate was observed starting from an evaporation rate of 55 g/h. The nucleation point decreased from the 35 to the 55 and to the 75 g/h experiment.

Table 46. Specific nucleation points for early feed run operated at 66 °C and 25 g/h, 35 g/h, 55 g/h, and 75 g/h

Crystal Species	Condensate To Feed Ratio At Nucleation			
	25 grams / hr	35 grams / hr	55 grams / hr	75 grams / hr
Sodium Nitrate (1st Nucleation)	0.247	0.259	0.257	0.234
Sodium Nitrate (2nd Nucleation)	0.363	0.387	0.363	0.234
Sodium Carbonate Monohydrate	0.298	0.300	0.305	0.290
Burkeite Crystals	0.299	0.302	0.305	0.290-0.306
Sodium Sulfate	0.200	0.213	0.140	0.082
Sodium Oxalate	0.156	0.163	0.140	0.082

Nucleation rate

All the species presented one of the two following profiles: (1) a linear profile or (2) a logarithmic profile with an initial growth rate followed by a lower constant section and a plateau. The species following the second profile were those affected by the formation of sodium sulfate co-crystals and sodium oxalate. An average nucleation rate was calculated for each species and each evaporation rate. Figure 106 represents the evolution of the nucleation rate with respect to the evaporation rate. The graph shows that the nucleation rates of all the species (with the exception of the burkeite

agglomerates) increased with the increase of the evaporation rate. Since similar yields were achieved this means that the increase in evaporation rate led to the formation of greater number of crystals with smaller size.

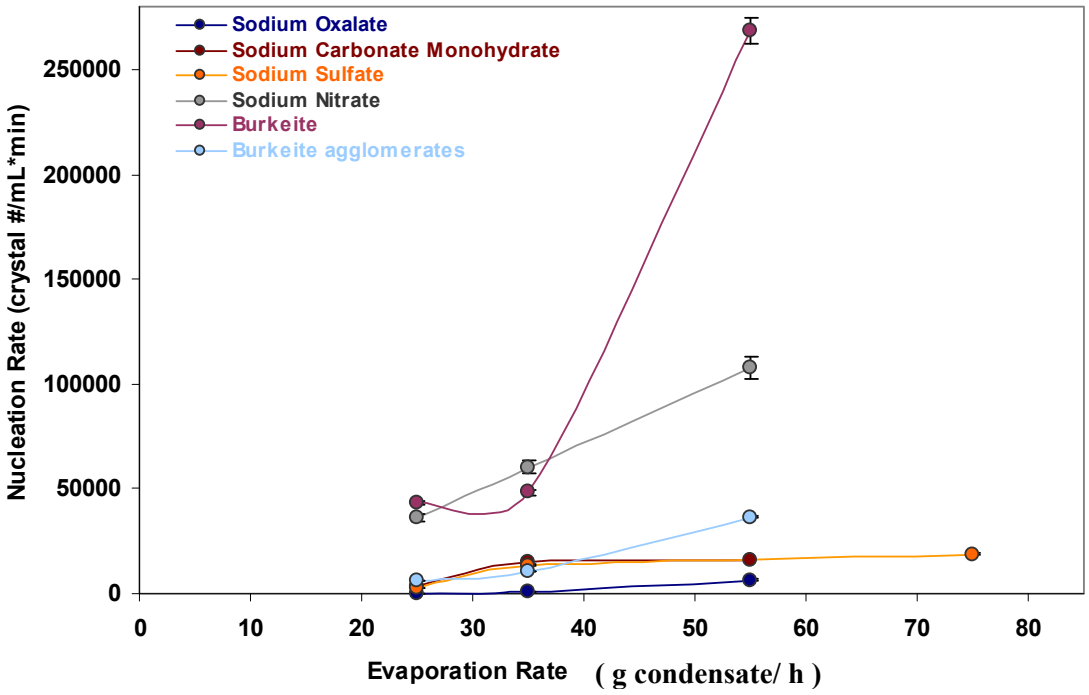

Figure 106. Evolution of the average nucleation rate with the evaporation rate for early feed experiments at 66 °C

This effect is displayed by the increase of the agglomeration rate of burkeite crystals. The higher evaporation rate increased the number of small burkeite, increasing the probability of collisions between burkeite and the number of agglomerates. Table 47 shows the system of correlation that represents the evolution of the specific nucleation rate with respect to the evaporation rate.

Table 47. Correlations describing the evolution of the average nucleation rate with the evaporation rate for early feed experiments at 66 °C

Crystal Species	Profile Type	Model Equations	Squared Correlation
Sodium Nitrate	Linear	$y = 2.386.10^{3}x - 2.337.10^{4}$	1
Sodium Carbonate Monohydrate	Binomial	$y = -38.6x^{2} + 3.517.10^{3}x - 6.052.10^{4}$	1
	Logarithmic	$y = 1.533.10^{4}Ln(x) - 4.364.10^{4}$	0.72
Burkeite Crystals	Linear	$y = 8.024.10^{3}x - 1.876.10^{5}$	0.91
Burkeite Agglomerates	Linear	$y = 1.057.10^{3}x - 2.277.10^{4}$	0.96
Sodium Sulfate	Binomial	$y = -19.1x^{2} + 2.241.10^{3}x - 4.132.10^{4}$	1
	Logarithmic	$y = 1.334.10^{4}Ln(x) - 3.761.10^{4}$	0.83
Sodium Oxalate	Linear	$y = 2.286.10^{2}x - 6.373.10^{3}$	0.93

(In the table "x" corresponds to the evaporation rate and "y" corresponds to the nucleation rate)

Growth rate

All the species presented one of the two following profiles: (1) a profile with a linear section with a constant growth rate and (2) a logarithmic profile with an initial growth rate followed by a lower constant section and a plateau. The species following the second profile were these that were affected by the formation of sodium sulfate based co-crystals and sodium oxalate. An average growth rate was calculated for each species and each evaporation rate. Figure 107 shows the evolution of the average growth rate with respect to the evaporation rate. The graph shows that all of the species growth rates (at the exception of the burkeite agglomerates) decreased with the increase of the evaporation rate.

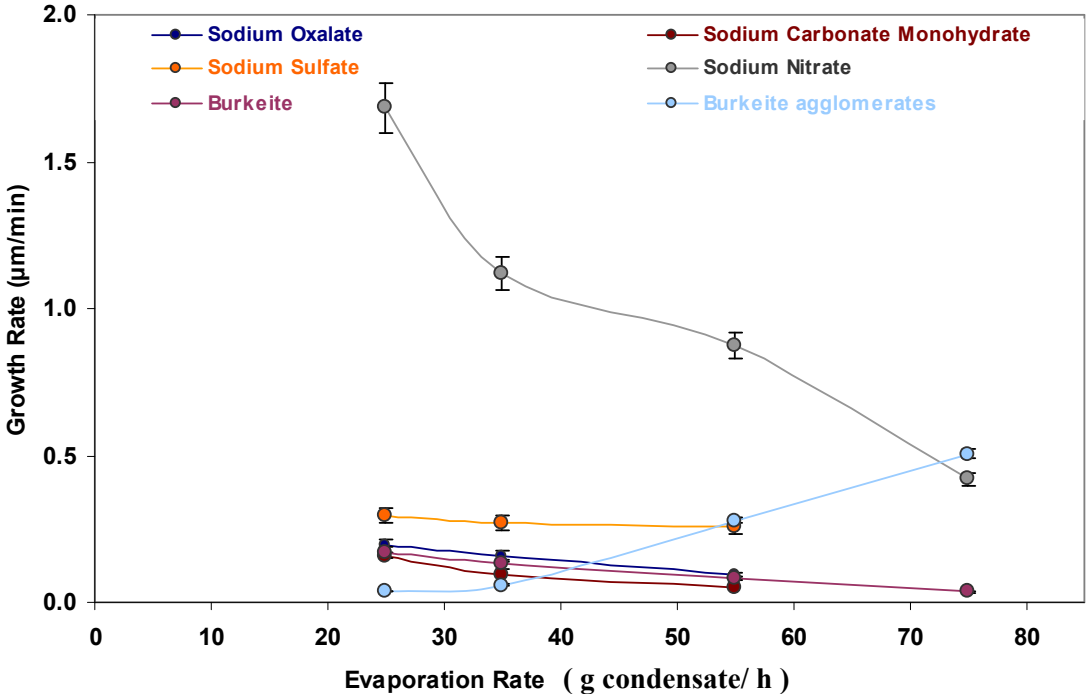

Figure 107. Evolution of the average growth rate with the evaporation rate for early feed experiments at 66 °C

All of the species presents a linear profile, with the burkeite agglomerate growth rate presenting a positive slope. Table 48 displays the correlations representing the average growth rate evolution with the evaporation rate.

Table 48. Correlations of the average growth rate with the evaporation rate for an early feed crystallization at 66 °C

Crystal Species	Profile Type	Model Equations	Squared Correlation
Sodium Nitrate	Linear	$y = -2.29.10^{-2}x + 2.1$	0.93
Sodium Carbonate Monohydrate	Linear	$y = -3.30.10^{-3}x + 0.22$	0.88
Burkeite Crystals	Linear	$y = -2.60.10^{-3}x + 0.22$	0.98
Burkeite Agglomerates	Linear	$y = 9.80.10^{-3}x - 0.24$	0.97
Sodium Sulfate	Linear	$y = -1.10.10^{-3}x + 0.31$	0.88
Sodium Oxalate	Linear	$y = -3.40.10^{-3}x + 0.27$	0.99

(In the table "x" corresponds to the evaporation rate and "y" corresponds to the growth rate)

Sieving analyses

Crystal size distribution is the outcome of the combination of the nucleation and growth rate. Figure 108 shows the mass density distributions of the four evaporation rate experiments. Table 49 presents the detailed species distribution with respect to sizes for each evaporation rate.

- The distribution of the 75 g/h evaporation rate showed that very few burkeite and sodium sulfate crystals were recovered (< 1.5 % of the total crystal mass). This is in agreement with a very small growth rate and large nucleation rate. Since the pore size of the filtration apparatus is 10µm, it is expected that a large amount of small crystals were recuperated in the filtrate. The main mode size around 360 µm is similar than the one obtained with the other evaporation rate. This is explained by the fact that even if the growth rate was smaller, the sodium nitrate nucleation occurred a lot before the nitrate nucleation in the other experiments. In the distribution, sodium carbonate was recovered in smaller sizes than the other experiments which is in agreement with the reduction of the growth rate and the increase of the nucleation rate. Finally, several burkeite agglomerates were observed in large sizes whereas very few single burkeite were recovered which validates the secondary nucleation of burkeite quantified by the kinetics study.
- The distribution of the 35 g/h evaporation rate showed a trimodal distribution. The difference with the certification run (performed at 25 g/h) deals mainly with the second mode size typically composed of sodium carbonate. The second mode size is less important than the certification run, and the third mode (originally composed of burkeite, sulfate and few carbonates) is more important. This shift

shows that sodium carbonate was produced with smaller size which is in agreement with the decrease of the growth rate. In essence sodium carbonate was recovered with smaller sizes and partially in the third mode. Furthermore, the increased agglomeration of burkeite compared to the certification run, allowed to recover more burkeite in the third mode (less were lost through filtration). Finally lesser amounts of nitrates were recovered in the main mode size which is also linked to the reduction in nitrate growth rate and increase in nitrate nucleation rate.

- The distribution of the 55 g/h evaporation rate showed a trimodal distribution. The main difference comes from the second and the third mode. The third mode is less important which is due to the reduction of the sulfate, burkeite, carbonate and oxalate growth rate. This reduction in size created more losses through solid-liquid separation apparatus. Similarly, the reduction in carbonate size is visible in the second mode which is more flat. The detailed composition displayed that parts of the second mode and the third mode were composed of sodium nitrate which were recovered in smaller size because of the growth rate reduction. Finally, since sodium nitrate was recovered in smaller sizes, the first mode is less important for this run.

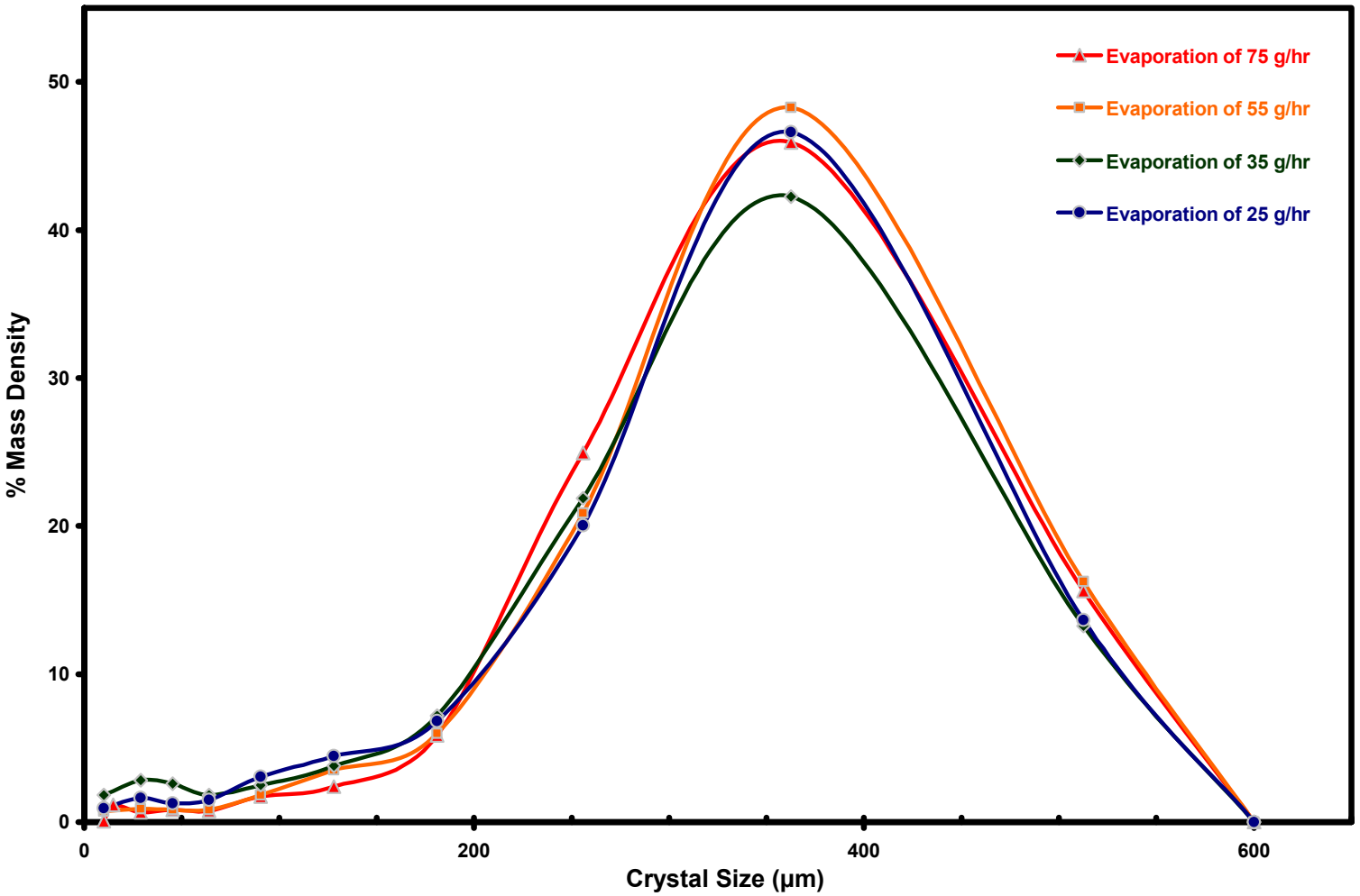

Figure 108. Mass density distributions of experiments from early feed crystallizations at 66 °C and 25, 35, 55, and 75 g/h

Table 49. Details of distribution of species with respect to size for early feed crystallizations at 66 °C and 25, 35, 55, and 75 g/h

Size Range	Evaporation 34 gr/hr	Evaporation 55 gr/hr	Evaporation 75 gr/hr
0 - 10µm	Composed mainly of sodium carbonates and homogeneous single burkeite in slightly lesser amounts. We observe very small amounts of sulfates and very small to traces amounts of nitrates, along with traces amounts of sodium oxalates.	Composed mainly of single homogenous and heterogeneous burkeites and slightly lesser amounts of sodium carbonates. Sodium sulfates and sodium nitrate are present in small amounts. Trace amounts of sodium oxalates.	Sodium carbonates and sulfates in large amounts. Very small/negligible amounts of burkeites and oxalates.
10-20 µm	----------	----------	Mainly sodium carbonates crystals with non negligible amounts of sodium sulfate crystals. Very small amounts of burkeites and traces amounts of nitrates and oxalates.
20 - 38 µm	Composed of sodium carbonates and burkeite in slightly lesser amounts. The burkeites are single crystals and have a non negligible proportion of heterogeneous crystals. We observe very small to trace amounts of sodium nitrates and traces of sulfates. No oxalates	Composed mainly of single burkeites and sodium carbonates. Presence of small amounts of sodium nitrate. Only trace amounts of sodium sulfate are observed. No oxalates.	Mainly composed of sodium carbonates with small amounts of sodium nitrate and heterogeneous agglomerated burkeites. Very few (traces) of sodium sulfate crystals are observed. No oxalates.
38 - 53 µm	Composed of sodium carbonates with small/very small amounts of burkeites and very small to trace amounts of sodium nitrates. No oxalates, sulfates, single burkeites.	Composed mainly of sodium carbonates with high concentrations of sodium nitrate and non negligible amounts of burkeite still. Burkeites are composed of some large single crystals with higher concentrations of agglomerates and heterogeneous crystals.	Mainly composed of sodium nitrate and sodium carbonate in equal proportions. Small (very small) amounts of very large burkeite agglomerates. No Sulfates or oxalates.
53 - 75 µm	Composed of sodium carbonates with small amounts of sodium nitrates.	Composed of sodium nitrates and slightly lesser amounts of sodium carbonates. Very small to trace amounts of burkeite agglomerates are detected.	Composed of sodium nitrate crystals with smaller amounts of large sodium carbonate crystals. Traces amounts of burkeite agglomerates are observed.
75 - 106 µm	Mainly composed of sodium nitrate with sodium carbonates in slightly lesser amounts.	Mainly composed of sodium nitrates with very small amounts of sodium carbonates. No burkeites are observed.	Composed of sodium nitrates with traces amounts of sodium carbonates.
106 - 150 µm	Mainly composed of sodium nitrates with very small amounts of sodium carbonates.	Composed of nitrates with traces of sodium carbonates.	Composed of nitrates with traces of sodium carbonates.
150 - 212 µm	Composed of sodium nitrates with traces amounts of very large sodium carbonates.	Composed of single sodium nitrate crystals.	Composed of single sodium nitrate crystals.
212 - 300 µm	Composed of single sodium nitrate crystals.	Composed of single sodium nitrate crystals with traces amounts of agglomerates.	Composed of single sodium nitrate crystals with small amounts of agglomerates.
300 - 425 µm	Single sodium nitrate crystals with traces of agglomerates.	Composed of single sodium nitrate crystals with small amounts of agglomerates.	Composed of single and agglomerated sodium nitrates in equal proportions.
425 - 600 µm	Single sodium nitrate crystals with non negligible amounts of agglomerates.	Sodium nitrate agglomerates with large amounts of single crystals.	Sodium nitrate agglomerates with traces amounts of single crystals.
600 - 850 µm	----------	Sodium nitrate agglomerates with traces of single sodium nitrates.	Sodium nitrate agglomerates.
850 - 1180 µm	----------	----------	----------

4.3 EFFECT OF OPERATING TEMPERATURE ON KINETICS

A series of evaporative crystallization experiments was performed at 35 °C, 45 °C, 55 °C, 66 °C and 75 °C. These values represent the largest range of operating temperatures that may be covered by the apparatus described in Chapter 2. Figure 109 shows the temperature and pressure profiles used for these experiments. These profiles displayed that the temperature was controlled to within +/- 1 ^{o}C of the target value of 35 ^{o}C, 45 ^{o}C, 55 ^{o}C, 66 ^{o}C, 75 ^{o}C. The pressure profile reflects the step-wise changes in vacuum associated with manual adjustments of the regulating valve. Figure 110 displays the condensate mass evaporated as a function of the operating time for the runs, in this study; clearly all had a constant evaporation rate of Approximatively 25 g/h. The mass balance tables associated with these experiments are displayed in appendix K.

In this section we will determine the nucleation points and kinetics associated with each of these operating temperatures, with the exception of 35 °C for which kinetics will not be presented. Empirical correlations representing the evolution of the average growth and nucleation rate with the operating temperature will be determined.

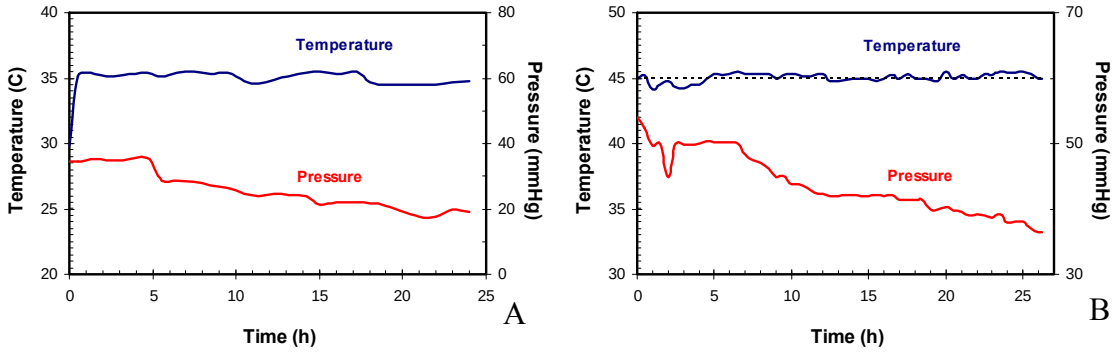

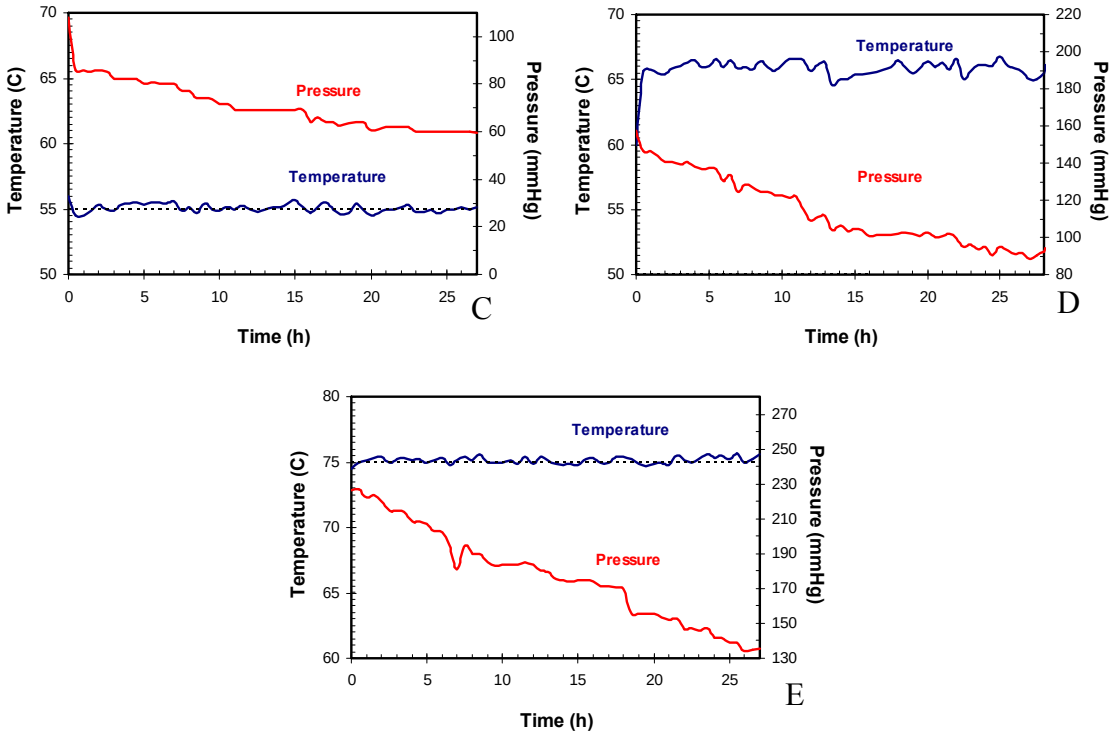

Figure 109. Temperature and pressure profiles for the series of early feed crystallization at 25 g/h with varying operating temperature
(Panel A, 35 °C, Panel B, 45 °C, Panel C, 55 °C, Panel D, 66 °C, Panel E, 75 °C)

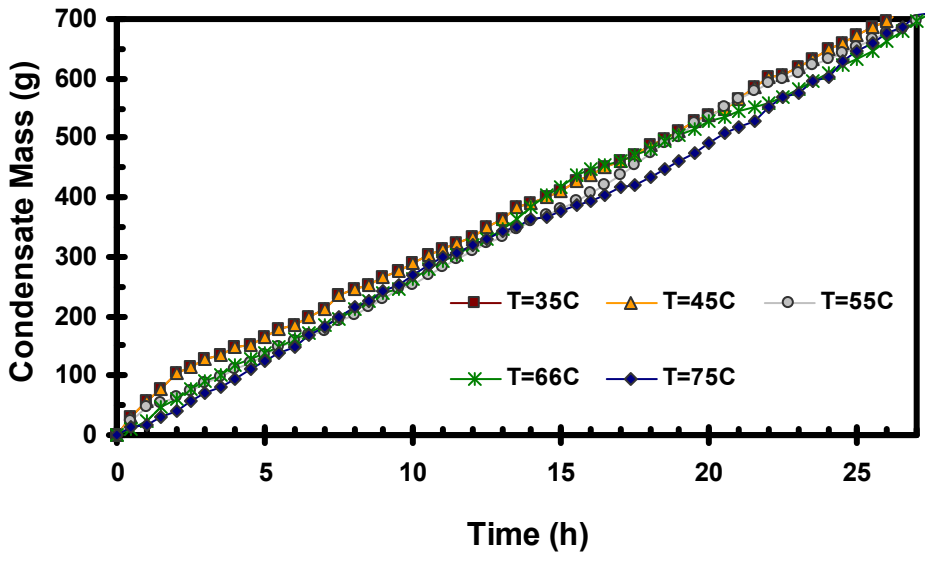

Figure 110. Mass of condensate generated as a function of operating time for early feed runs at 25 g/h with varying operating temperature

4.3.1 OPERATING TEMPERATURE OF 35 °C

Thermodynamic Simulations

Thermodynamic simulations were performed at an operating temperature of 35 °C and provided to us by AREVA NC. These simulations were performed by the software developed by OLI system Inc and assume thermodynamic equilibrium. In essence this means that to interpret the results of the simulations the crystalline species are assumed to nucleate when they reach saturation, meaning that the nucleation and saturation curves are identical. Figure 111 presents the evolution of the specific yields with respect to the percent water mass evaporated. This simulation shows that six major species are expected to reach their solubility limits during the course of the run, among which three are produced with large amounts: sodium nitrate at C:F= 0.318, sodium carbonate monohydrate at C:F= 0.302, and burkeite C:F= 0.158. Three additional species are expected to be produced in trace amounts: sodium oxalate at C:F= 0.096, trisodium fluoride sulfate at C:F= 0.154, and sodium acetate trihydrate at C:F= 0.568. Finally sodium nitrite is expected to come out of solution after the end of the crystallization at a condensate-to-feed ratio of 0.548.

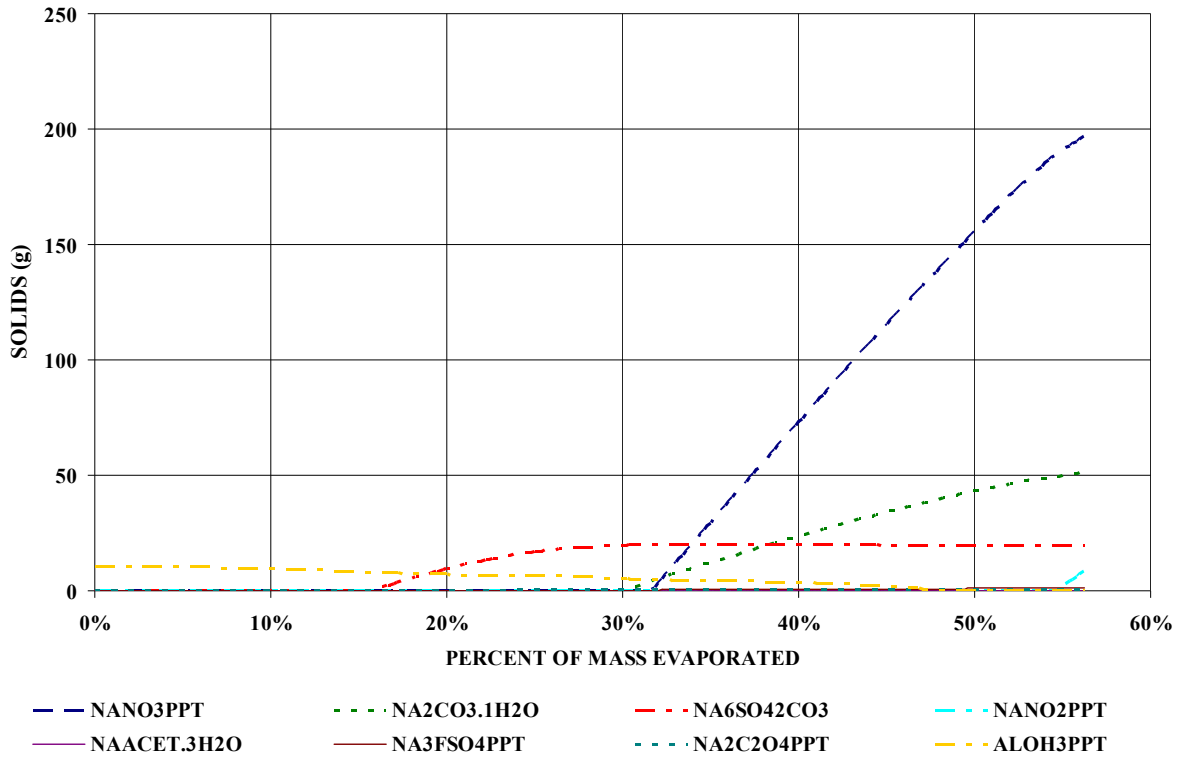

Figure 111. Thermodynamic simulation of early feed crystallization at 35 °C
(Courtesy of D. Geniesse, Areva NC)

Nucleation Points

Figure 112 shows the sequence of species nucleation that was determined based on the PLM analyses of slurry samples taken at regular time intervals. For example, panel A shows that sodium oxalate was nucleated at C:F= 0.100. Panels B and C show that sodium sulfate was nucleated slightly later at C:F= 0.125 and that the initial solution present traces of sodium aluminate crystals that precipitated at the low initial temperature of 35 °C. These crystals remained in solution until the first main nucleation. Panel D and E display that sodium nitrate and trisodium fluoride sulfate are nucleated at C:F= 0.261. These crystals continuously increase in number and size in the next samples as shown by panel F. Panel G shows that a plate like crystals is then nucleated at C:F= 0.296. According to panel H, the next species to be nucleated are sodium carbonate

monohydrate crystals at C:F= 0.309. Panels I and J shows that sodium carbonate monohydrate and mainly sodium sulfate number and size increased in the next samples until the spike in sodium nitrate nucleation at C:F= 0.339. Panels K and L display that sodium nitrate nucleation increases rapidly until a high slurry density is reached.

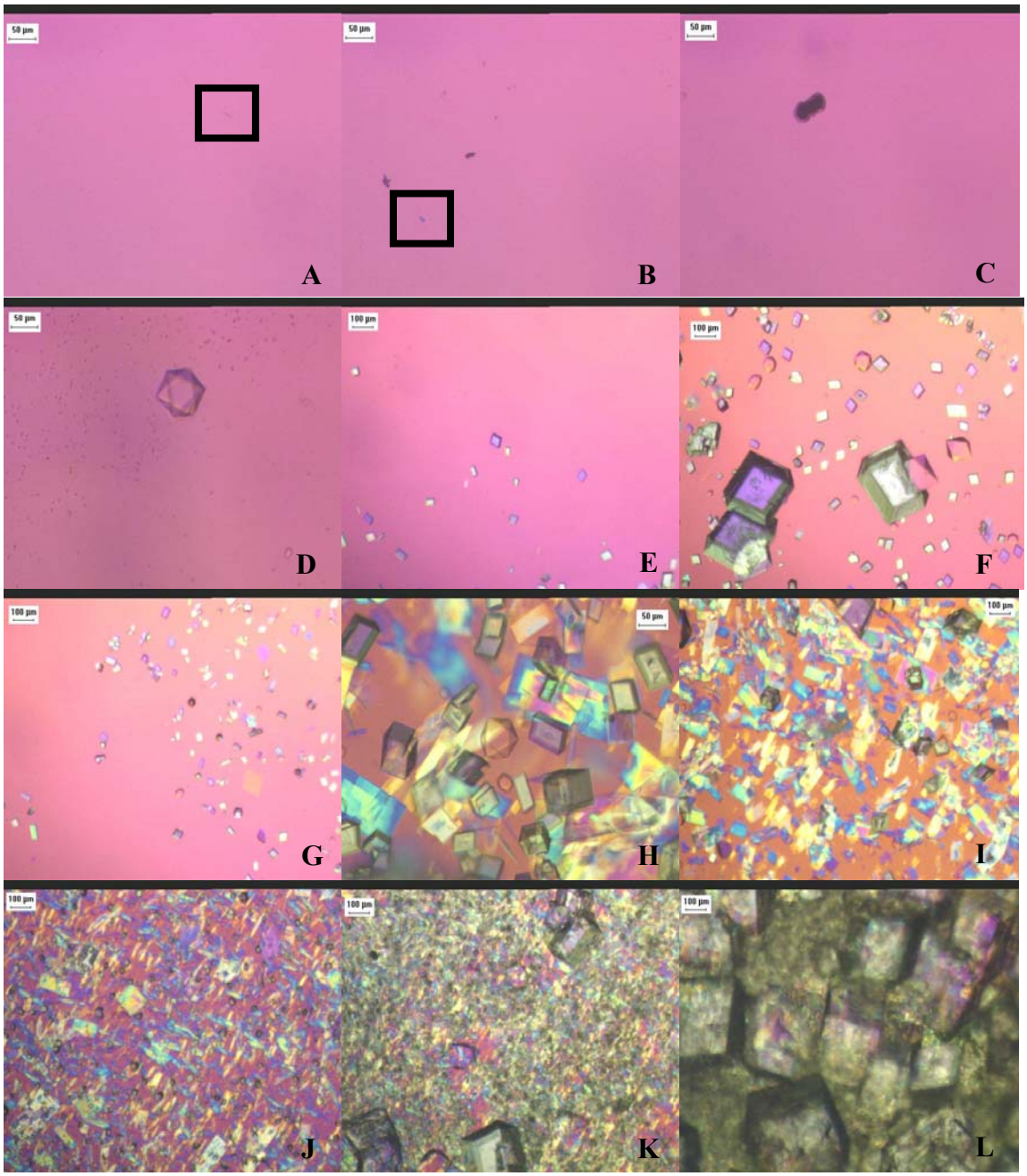

Figure 112 PLM images of samples from early feed run at 35 °C and 25 g/h evaporation rate

(Panel A, sodium oxalate, Panel B, sodium sulfate nuclei, Panel C, sodium aluminate present in solution, Panel D, trisodium fluoride sulfate, Panel E, sodium nitrate nuclei, Panel F, sodium nitrate growth and trisodium fluoride sulfate nucleation, Panel G, plate like crystals nucleation, Panel H, sodium carbonate nucleation and sodium sulfate in large amounts, Panel I, sodium sulfate and carbonate nucleation, Panel J, spike in nitrate nucleation, Panel K, sodium nitrate increase, Panel L, high slurry density)

Table 50 presents the specific nucleation points and corresponding operating times for the early feed crystallization at 35 °C. No burkeite were produced in this run on contrary to the simulations. The nucleation of sodium sulfate, sodium carbonate monoydrate and trisodium fluoride sulfate may have used up most of the sodium sulfate present in solution before the nucleation point of burkeite was reached.

Table 50. Specific nucleation points for the species produced during the early feed run operated at 35 °C and 25 g/h

SST Early Feed	Condensate To Feed Ratio At Nucleation	Operating Time At Nucleation (min)
Sodium Nitrate (1st Nucleation)	0.261	567
Sodium Nitrate (2nd Nucleation)	0.339	859
Sodium Carbonate Monohydrate	0.309	734
Burkeite Crystals	N A	NA
Sodium Sulfate	0.125	198
Sodium Oxalate	0.100	138
Trisodium Fluoride Sulfate	0.261	567
Plate Like Crystals	0.296	678

Conclusions

The run did not produce any burkeite but instead produced sodium sulfate and sodium carbonate crystals. Compared to the certification run, this experiment showed that by operating with a low temperature the production of burkeite can be stopped and some of the sulfate may be recovered as trisodium fluoride sulfate crystals. Furthermore, the nucleation points of the other species are within the range of the saturation limits estimated by thermodynamic simulation showing that (1) nucleation and saturation point are differents, but (2) a good estimate of the actual nucleation point can be obtained from the saturation limits obtained with the thermodynamic simulations.

4.3.2 OPERATING TEMPERATURE OF 45 °C

Thermodynamic Simulations

Thermodynamic simulations were performed for the early feed crystallization at 45 °C and provided to us by AREVA NC. These simulations performed by the software developed by OLI system Inc and assume thermodynamic equilibrium. Figure 113 presents the evolution of the specific yields with respect to the percent water mass evaporated. This simulation shows that five major species are expected to come out of solution during the course of the run, three of them are to be produced with large amounts: sodium nitrate at C:F= 0.350, sodium carbonate monohydrate at C:F= 0.314, and burkeite at C:F= 0.128. Two additional species are to be produced in trace amounts: sodium oxalate at C.F= 0.142, and trisodium fluoride sulfate at C:F= 0.328. Finally sodium nitrite and sodium chloride are expected to come out of solution after the end of the crystallization at a condensate-to-feed ratio of 0.556 and 0.548 respectively. Compared to the previous simulation burkeite is expected to come out of solution earlier while sodium carbonate, sodium nitrate, sodium oxalate and trisodium fluoride sulfate will be produced later.

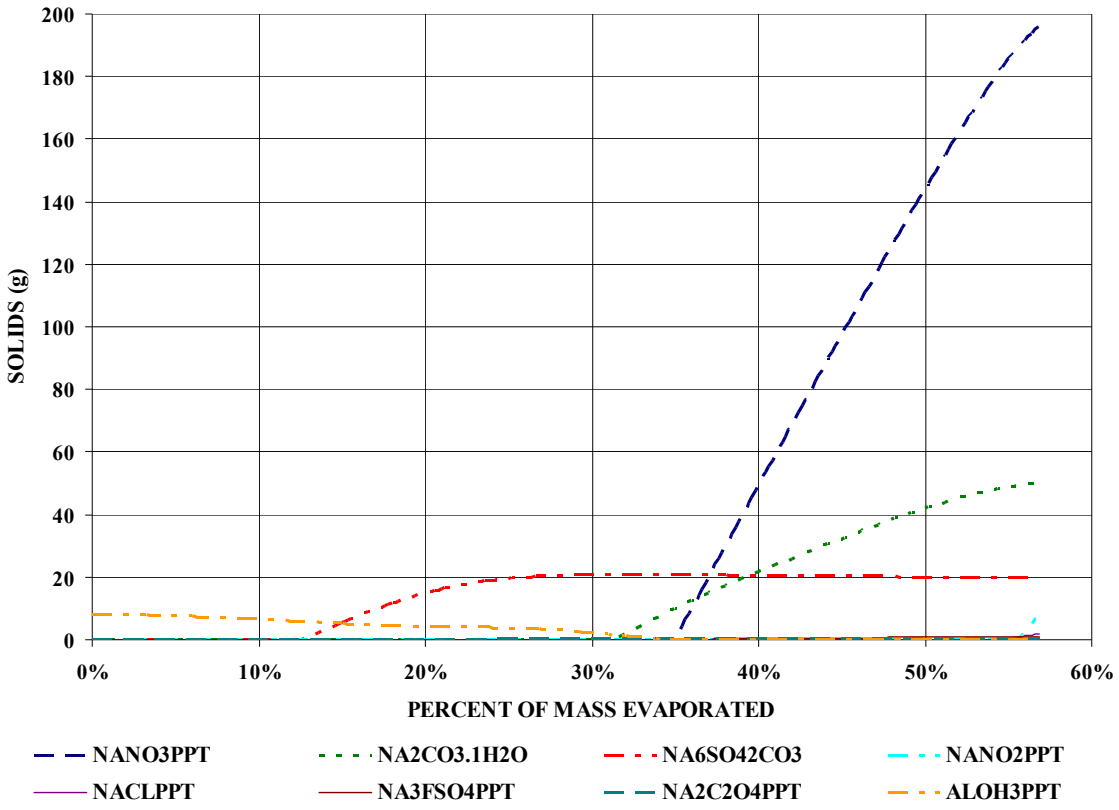

Figure 113. Thermodynamic simulation of early feed crystallization at 45 °C
(Courtesy of D. Geniesse, Areva NC)

Nucleation Points

Figure 114 shows the sequence of species nucleation that was determined based on the PLM analyses of slurry samples taken at regular time intervals. For example, panel A shows that sodium oxalate was nucleated at C:F= 0.080. Panels B and C displays that sodium oxalates increased in number and reached sizes up to 100 µm for 0.080<C:F<0.266. The oxalate size decreased after the nucleation of sodium nitrate at C:F= 0.266 most likely due to breakage, as shown by panel F. Panels E and D show that sodium sulfate was nucleated early at C:F= 0.102 and the few sulfate crystals produced were grown to larger sizes in the following samples. Sodium nitrate nucleation continued and a plate like crystals was nucleated at C:F= 0.299 as shown by panels G and H. A

zoom in the plate like crystals is presented in panel I. Panel J shows that trisodium fluoride sulfate are nucleated at C:F= 0.317. Panels L, K, and M display that these crystals increase in number and size in the next samples. The next species to be nucleated are sodium carbonate crystals at C:F= 0.317 as shown by panel N. Panel O displays that sodium carbonate monohydrate and sodium sulfate number and size increased in the next samples. Panel P and Q show that at C:F= 0.322 the first burkeite crystals are observed and their number increase slowly in the next samples. Panel R shows the spike in sodium nitrate nucleation observed at C:F= 0.299. The number of sodium nitrate crystals increased rapidly for samples with C:F>0.299 leading to high slurry density.

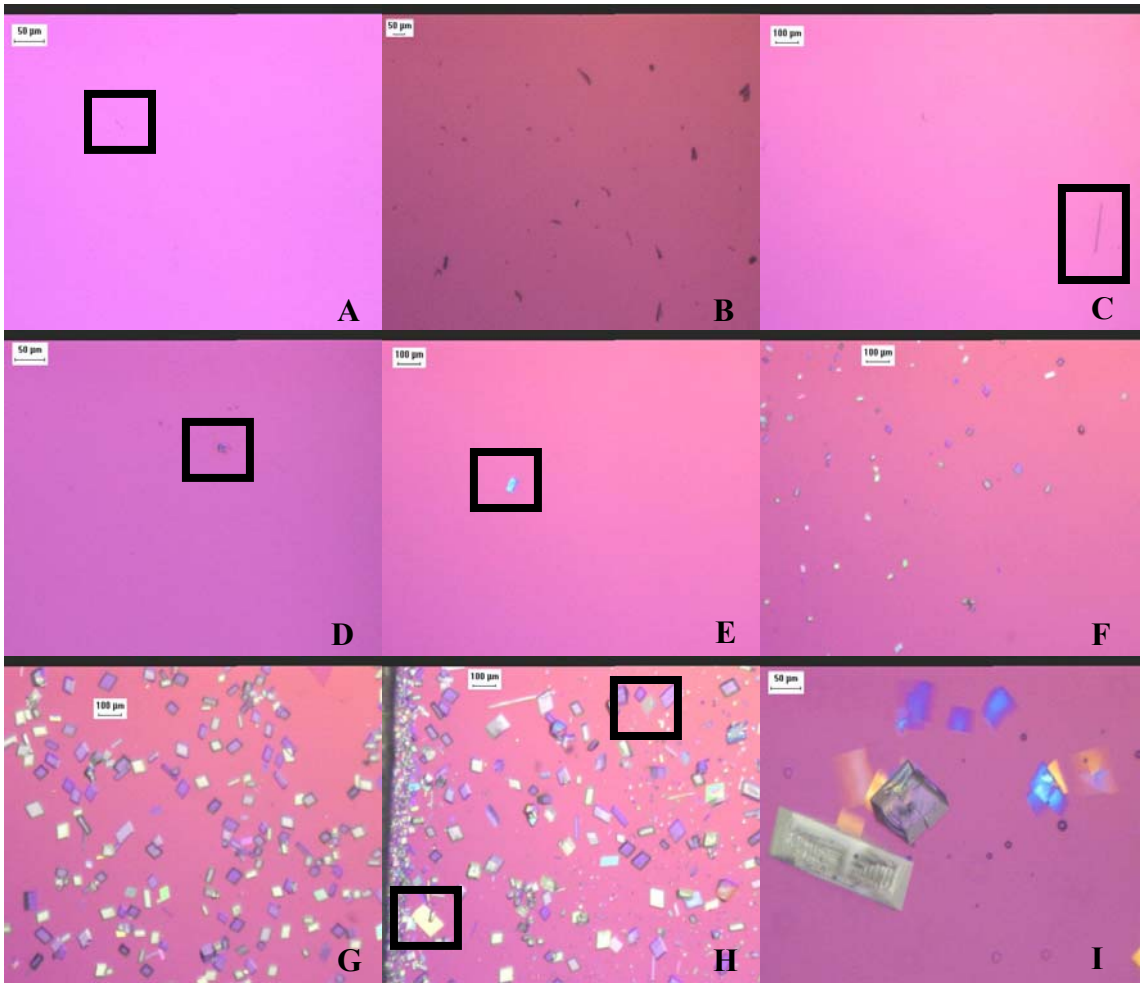

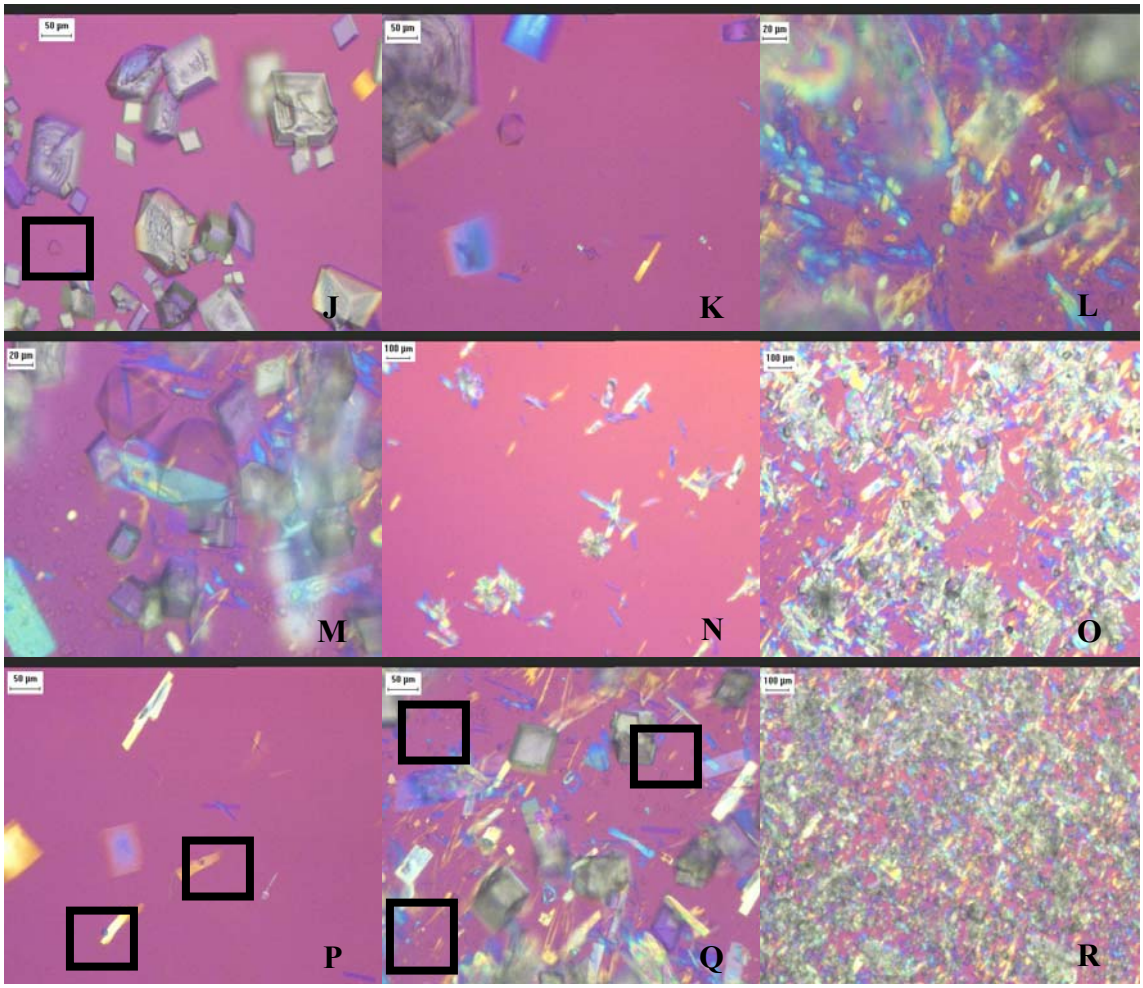

Figure 114. PLM images of samples from early feed run at 45 °C and 25 g/h evaporation rate (Panel A, sodium oxalate, Panel B, sodium oxalate nucleation, Panel C, large sodium oxalate before breakage, Panel D, sodium sulfate crystals, Panel E, sodium sulfate, Panel F, sodium nitrate nucleation, Panel G, sodium nitrates, Panel H, plate like crystals nucleation, Panel I, zoom in plate like crystals, Panel J, trisodium fluoride sulfate crystals, Panel K, trisodium fluoride sulfate crystal, Panel L, trisodium fluoride sulfate growth, Panel M, trisodium fluoride sulfate nucleation, Panel N, sodium carbonate monohydrate nucleation, Panel O, Growth of sodium carbonate monohydrate crystals, Panel P, small burkeite crystals, Panel Q, burkeite nucleation, Panel R, spike in nitrate nucleation)

Table 51 presents the specific nucleation points and corresponding operating times for the early feed crystallization at 45 °C. At a temperature of 45 °C burkeite was produced but at low nucleation and growth rates. Furthermore trisodium fluoride sulfate was produced in large quantities before the nucleation point of burkeite was reached which may have slowed down the burkeite kinetics due to the discreapancy of sodium

fluoride sulfate and burkeite saturation points. In this experiment we can not talk about a second nucleation of nitrate but more of a spike in nucleation since the first nucleation led to important number of sodium nitrate crystals. Finally both the oxalate and sulfate nucleation point appeared earlier compared to a temperature of 35 °C.

Table 51. Specific nucleation points for the species produced during the early feed run operated at 45 °C and 25 g/h

SST Early Feed	Condensate To Feed Ratio At Nucleation	Operating Time At Nucleation (min)
Sodium Nitrate (1st Nucleation)	0.266	509
Sodium Nitrate (2nd Nucleation)	0.299	631
Sodium Carbonate Monohydrate	0.317	701
Burkeite Crystals	0.322	720
Sodium Sulfate	0.102	100
Sodium Oxalate	0.080	68
Trisodium Fluoride Sulfate	0.317	701
Plate Like Crystals	0.299	631

Nucleation rate

Figure 115 presents the evolution of the total crystal count with the operating time for each of the crystalline species. As displayed by the image analysis, sodium nitrate presents a two steps profile with (1) a slight increase in nucleation from C:F= 0.266 to C:F= 0.299, and (2) a spike in nucleation at C:F= 0.299. The average nucleation rate for sodium nitrate is 9.267×10^{3} crystals/ mL·min. Sodium carbonate monohydrate profile presents an important initial increase followed by a constant nucleation rate with an average of 6.523×10^{3} crystals/ mL·min. The plate like crystals observed in the samples, have an average nucleation rate of 2.689×10^{4} crystals/ mL·min. Assessing the case of sulfate, the sulfate profile is linear and relatively flat (3.51×10^{2} crystals/ mL·min).

Trisodium fluoride sulfate present a nucleation rate of 1.262×10^{5} crystals/ mL·min. This large nucleation of trisodium fluoride sulfates used a lot of the sulfate present in solution and affected the nucleation of burkeite that presented a later saturation point. Burkeite presents a small average nucleation rate of 1.410×10^{3} crystals/ mL·min followed by a plateau. Finally sodium oxalates had an average nucleation rate of 89 crystals/ mL·min.

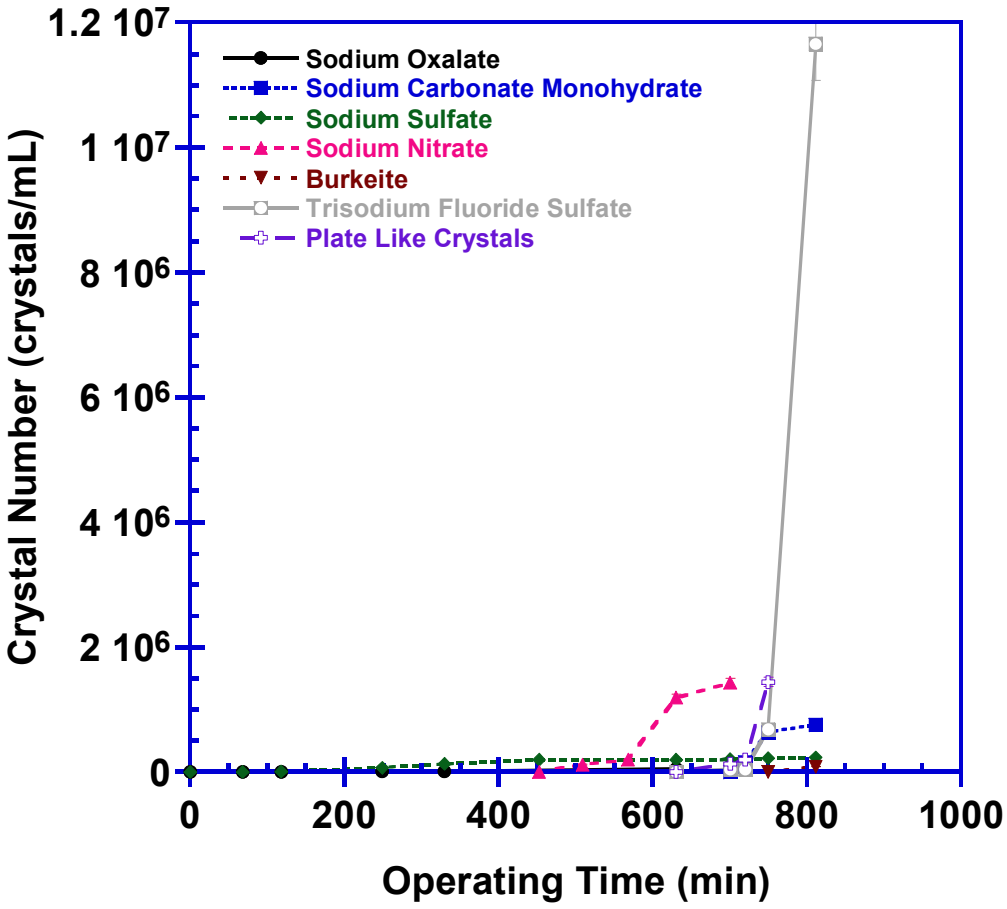

Figure 115. Evolution of total crystal count for each species formed from early feed run at 45 °C and 25 g/h

Growth Rate

The size of the crystals was monitored for each sample recovered from the slurry following the protocols defined in Chapter 2. Figure 116 presents the graphs of the average length evolution with the operating time. The methodology used to compute the

specific average growth rate was outlined in Chapter 2. All the species presents linear profiles at the exception of sodium carbonate monohydrate that tends to slow growth at higher operating time and oxalate that undergoes two series of breakage in this experiment. The first breakage is mostly due to contact with the impeller and the second to contacts with other crystals. In the first growing section, the average growth rate for sodium oxalate was 0.134 $\mu m \cdot min^{-1}$. Assessing the other crystalline species, sodium nitrate follows an average growth rate of 4.101 $\mu m \cdot min^{-1}$, when sodium carbonate monohydrate, trisodium fluoride sulfate, plate like crystals and sodium sulfate have a growth rate of 0.107, 0.371, 1.000 and 0.095 $\mu m \cdot min^{-1}$ respectively.

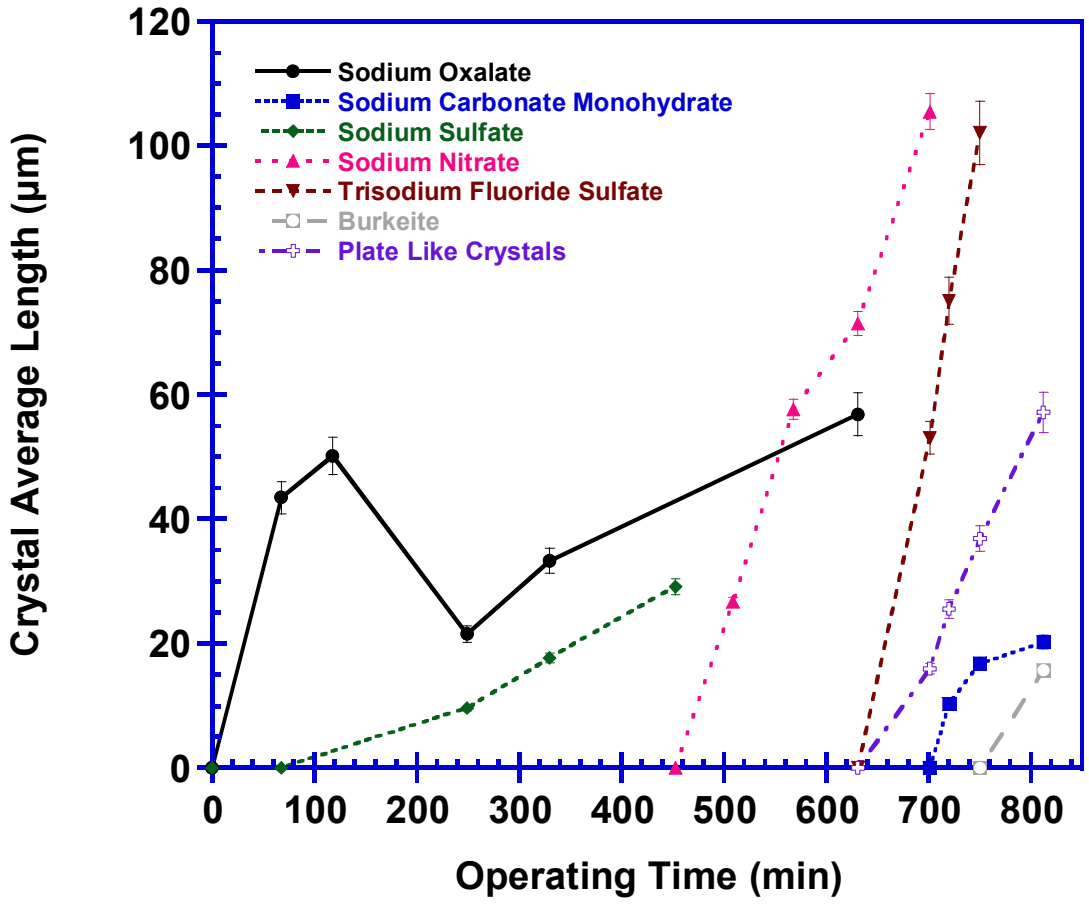

Figure 116. Evolution of crystal average length for each species formed from early feed run at 45 °C and 25 g/h

Conclusion

The run performed at 45 °C produced different crystalline species than the certification run and thermodynamic simulations. One of the major differences is the large nucleation of trisodium fluoride sulfate crystals which led to a slower burkeite nucleation rate. Sodium sulfate was nucleated, even at low nucleation rate, whereas this species was not expected. Like the previous experiment a plate like crystal was produced and sodium nitrate presented a two stage nucleation with an early nucleation point and a high growth and nucleation rate.

4.3.3 OPERATING TEMPERATURE OF 55 °C

Thermodynamic Simulations

Thermodynamic simulations were performed for the early feed crystallization at 55 °C and provided to us by AREVA NC. These simulations were performed by the software developed by OLI system Inc and assume thermodynamic equilibrium. Figure 117 presents the evolution of the specific yields with respect to the percent water mass evaporated. This simulation shows that five major species are expected to come out of solution during the course of the run, three of them in large amounts: sodium nitrate at C:F= 0.378, sodium carbonate monohydrate at C:F= 0.324, and burkeite at C:F= 0.104. Two additional species are to be produced in trace amounts: sodium oxalate at C:F= 0.196, and trisodium fluoride sulfate at C:F= 0.404. Finally sodium carbonate anhydrate and sodium chloride are expected to come out of solution after the end of the crystallization at a condensate to feed ratio of 0.552 and 0.548 respectively. Compared to the previous simulation burkeite is expected to come out of solution earlier while sodium carbonate monohydrate, sodium nitrate, sodium oxalate and trisodium fluoride sulfate will be produced later.

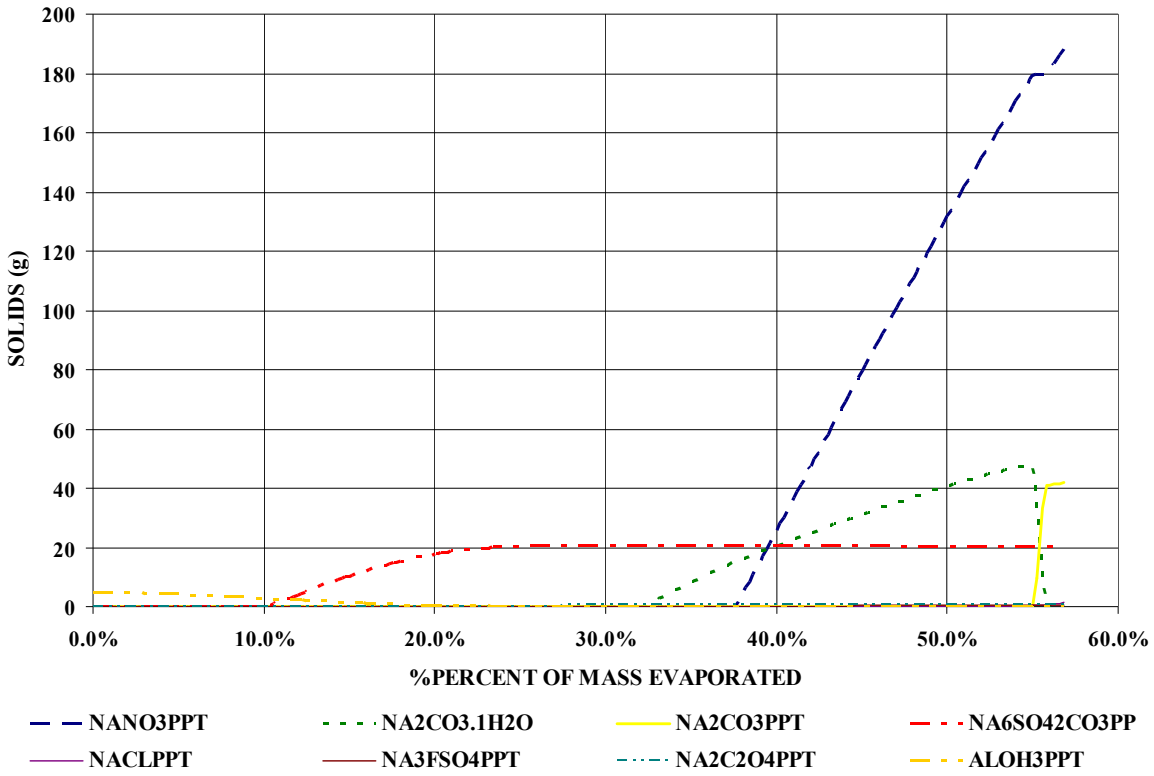

Figure 117. Thermodynamic simulation of early feed crystallization at 55 °C
(Courtesy of D. Geniesse, Areva NC)

Nucleation Points

Figure 118 shows the sequence of species nucleation that was determined based on the PLM analyses of slurry samples taken at regular time intervals. For example, panels A and B show that sodium oxalate was nucleated at C:F= 0.070 and these crystals were grown in the next sample before the nucleation of sodium nitrate. Panels C to E show that sodium sulfate was nucleated at C:F= 0.182. Panels F and L display that sodium nitrates are nucleated at C:F= 0.268 and that these crystals increase in number and size in the next samples. The next species to be nucleated are sodium carbonate monohydrate crystals at C:F= 0.300 as shown by panel G. Panel H shows that sodium carbonate monohydrate number and size increased in the next samples. Panel I displays that burkeites were nucleated at a condensate-to-feed ratio ranging between 0.303 and

0.318. The low nucleation of sulfates and the non nucleation of trisodium fluoride sulfate before burkeite led to the increased burkeite kinetics. Panels J and K show that trisodium fluoride sulfate was nucleated at C:F= 0.377.

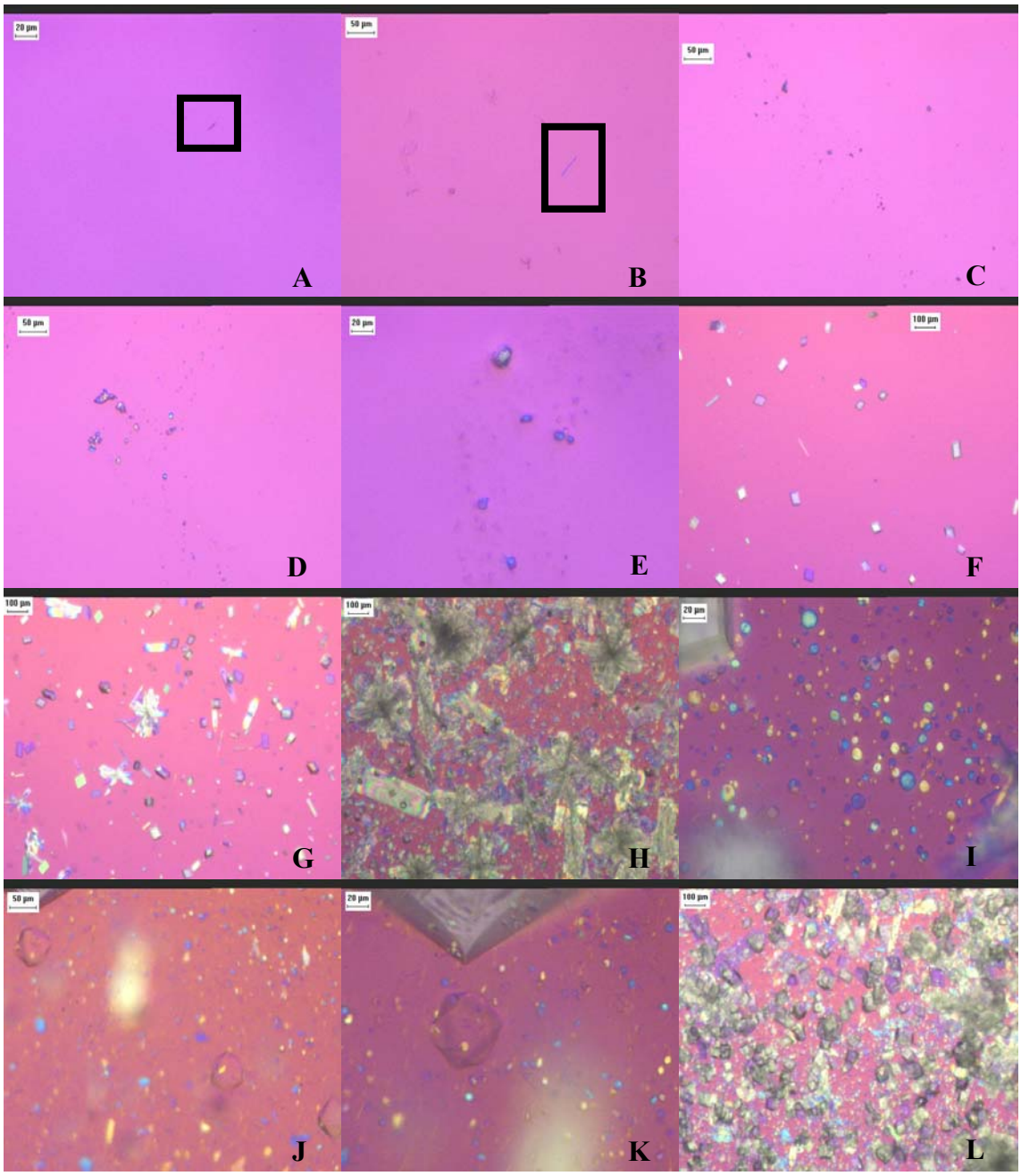

Figure 118. PLM images of samples from early feed run at 55 °C and 25 g/h evaporation rate (Panel A, sodium oxalate, Panel B, sodium oxalate, Panel C, sodium sulfate small crystals, Panel D, sodium sulfates, Panel E, zoom in sodium sulfate crystals, Panel F, sodium nitrate nucleation, Panel G, sodium carbonate nucleation, Panel H, sodium carbonate growth, Panel I, burkeite nucleation, Panel J, trisodium fluoride sulfate nucleation, Panel K, zoom in trisodium fluoride sulfate crystal, Panel L, high slurry density)

Table 52 presents the specific nucleation points and corresponding operating times for the early feed crystallization at 55 °C. At a temperature of 55 °C trisodium fluoride sulfate was produced later than the previous experiments allowing burkeite to be grown and nucleation with increased kinetics. Sodium nitrate presents one nucleation with a constant increase in total sodium nitrate number whereas at lower temperature the spike in nucleation was more important. Sodium oxalate was nucleated earlier while sodium sulfate was nucleated later than at 45 °C. Finally the discrepancy between the burkeite simulated saturation and its experimental nucleation is relatively important.

Table 52. Specific nucleation points for the species produced during the early feed run at 55 °C and 25g/h

SST Early Feed	Condensate To Feed Ratio At Nucleation	Operating Time At Nucleation (min)
Sodium Nitrate (1st Nucleation)	0.268	582
Sodium Nitrate (2nd Nucleation)	0.268	582
Sodium Carbonate Monohydrate	0.300	700
Burkeite Crystals	0.303-0.318	707-768
Sodium Sulfate	0.182	332
Sodium Oxalate	0.070	68
Trisodium Fluoride Sulfate	0.377	1047

Nucleation rate

Figure 119 presents the evolution of the total crystal count with the operating time for each of the crystalline species. Sodium nitrate has a constant linear profile with an average value of 2.329×10^4 crystals/ mL·min. Sodium carbonate monohydrate has also a linear profile with a lower averge nucleation rate value. The average sodium carbonate monohydrate nucleation rate was 4.662×10^3 crystals/ mL·min. Both sodium sulfate and

sodium oxalate have linear profiles. Their average nucleation rate were 1.484×10^{3} and 3.65×10^{2} crystals/ mL·min respectively. Burkeite crystals have a profile with a constant linear first section followed by a decrease in nucleation tending to a plateau at higher condensate to feed ratios. The average nucleation rate was 6.486×10^{4} crystals/ mL·min. The profile or average value for the trisodium fluoride sulfate crystals could not be obtained due the high slurry density at nucleation of this species.

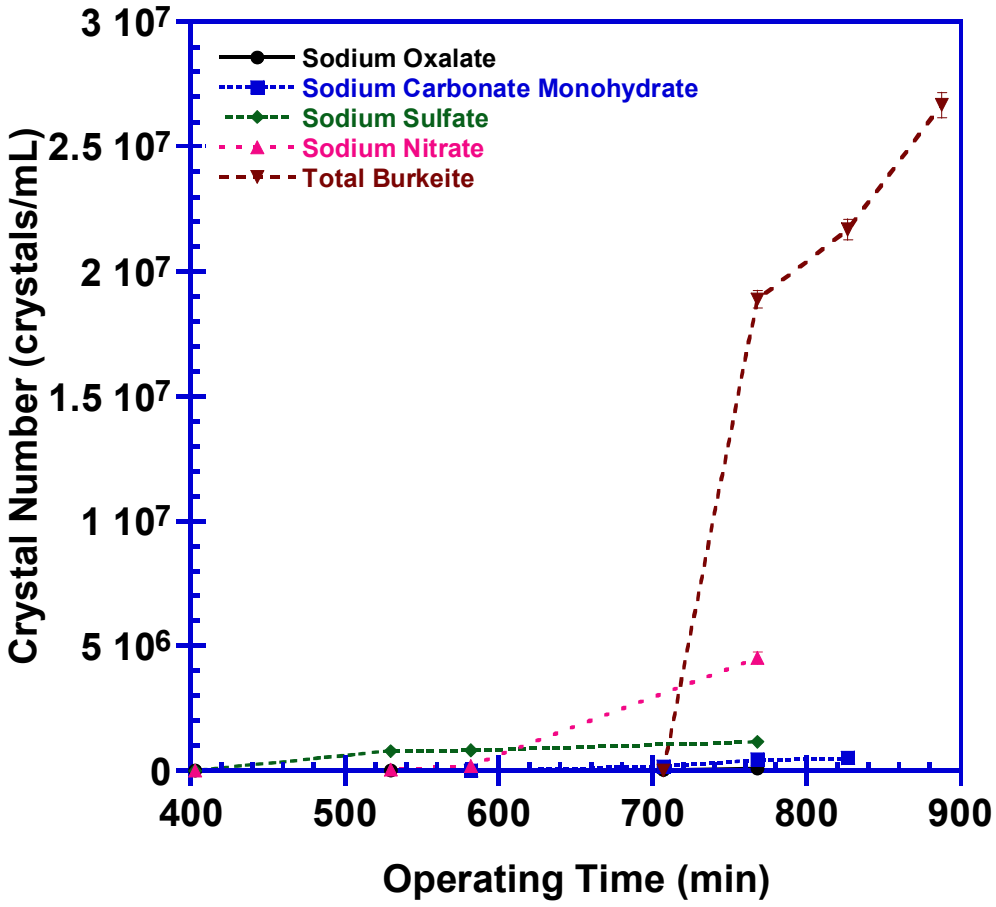

Figure 119. Evolution of total crystal count for each species formed from early feed run at 55 °C and 25 g/h

Figure 120 displays the evolution of the burkeite crystal count with operating time for which the total burkeite population was divided into two distinct categories: single burkeite crystals and burkeite agglomerates. The increase in burkeite number is at first

controlled by the increase in single crystals and then by the agglomeration of the existing burkeite crystals. The burkeite agglomerates and the single burkeite crystals have an average nucleation rate of 3.935×10^4 crystals/ mL·min and 2.550×10^4 crystals/ mL·min respectively.

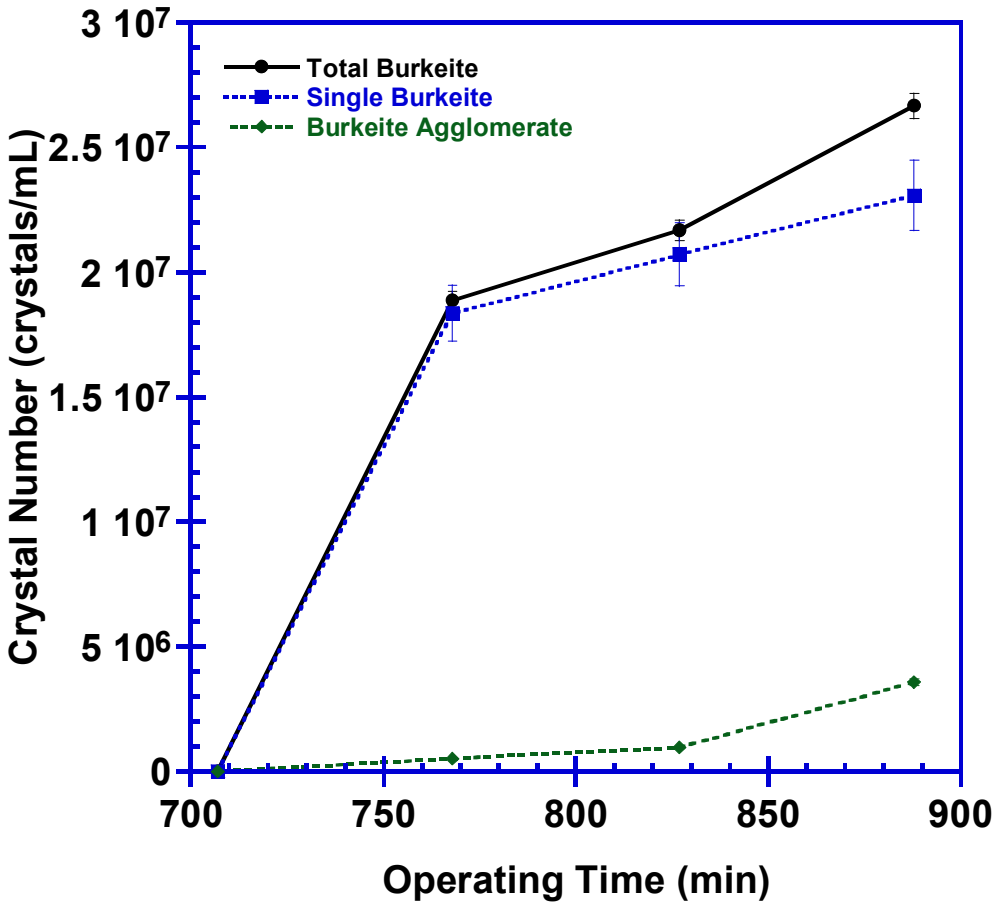

Figure 120. Evolution of total crystal count for burkeite formed from early feed run at 55 °C and 25 g/h

The graph in Figure 121 presents the evolution of the number of burkeite agglomerates during the experiment. The number of agglomerates formed initially is very small and relatively constant until a condensate-to-feed ratio of 0.347 at which point there is a spike in the agglomerate number. The agglomeration rate is in average increased by one order of magnitude compared to the certification run.

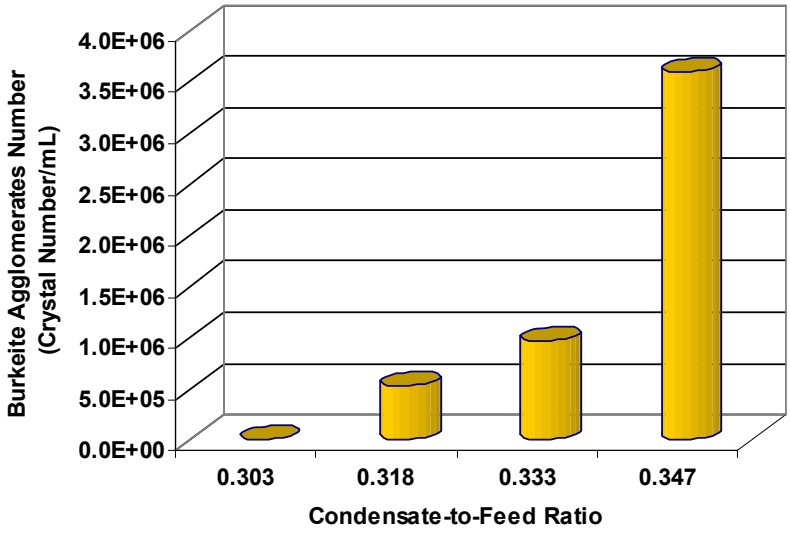

Figure 121. Evolution of total crystal count for burkeite agglomerates formed from early feed run at 55 °C and 25 g/h

Growth Rate

The size of the crystals was monitored for each sample recovered from the slurry following the protocols defined in Chapter 2. Figure 122 presents the graphs of the average length evolution with the operating time. The methodology used to compute the specific average growth rate was outlined in Chapter 2. All the species presents linear profiles at the exception of sodium oxalate that undergoes breakage in this experiment. In the first growing section, the average growth rate for sodium oxalate was 0.151 $\mu m \cdot min^{-1}$. Assessing the other crystalline species, sodium nitrate follows an average growth rate of 2.106 $\mu m \cdot min^{-1}$, when sodium carbonate monohydrates, burkeites, burkeite agglomerates and sodium sulfates have a growth rate of 0.141, 0.031, 0.024, and 0.119 $\mu m \cdot min^{-1}$ respectively.

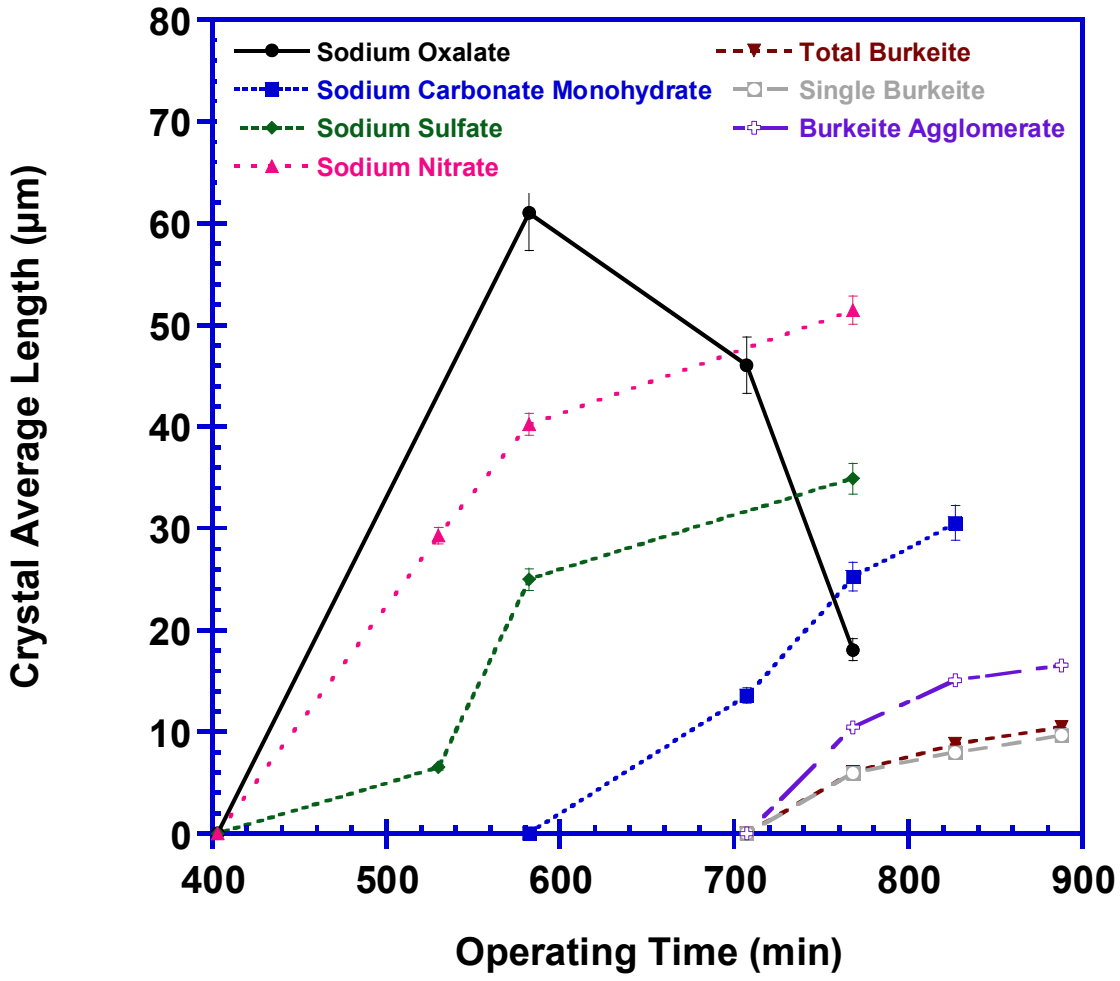

Figure 122. Evolution of crystal average length for each species formed from early feed run at 55 °C and 25 g/h

Conclusion

This experiment is closer to the certification run than to the experiment performed at 45 °C. One of the main differences is the late nucleation of trisodium fluoride sulfate which allowed the growth and nucleation of burkeite. The two species are competing for the limited amount of sulfate present in solution. The nucleation point of trisodium fluoride sulfate has been postponed by increasing operating temperature. The other main different is the linear nucleation of sodium nitrate with is not observed in the certification run. Finally, dealing with the kinetics, all of the growth rates have been decreased with

increasing temperature at the exception of sodium carbonate monohydrate. Inversely, the nucleation rates have been all increased except for the sodium carbonate monohydrate.

4.3.4 OPERATING TEMPERATURE OF 75 °C

Thermodynamic Simulations

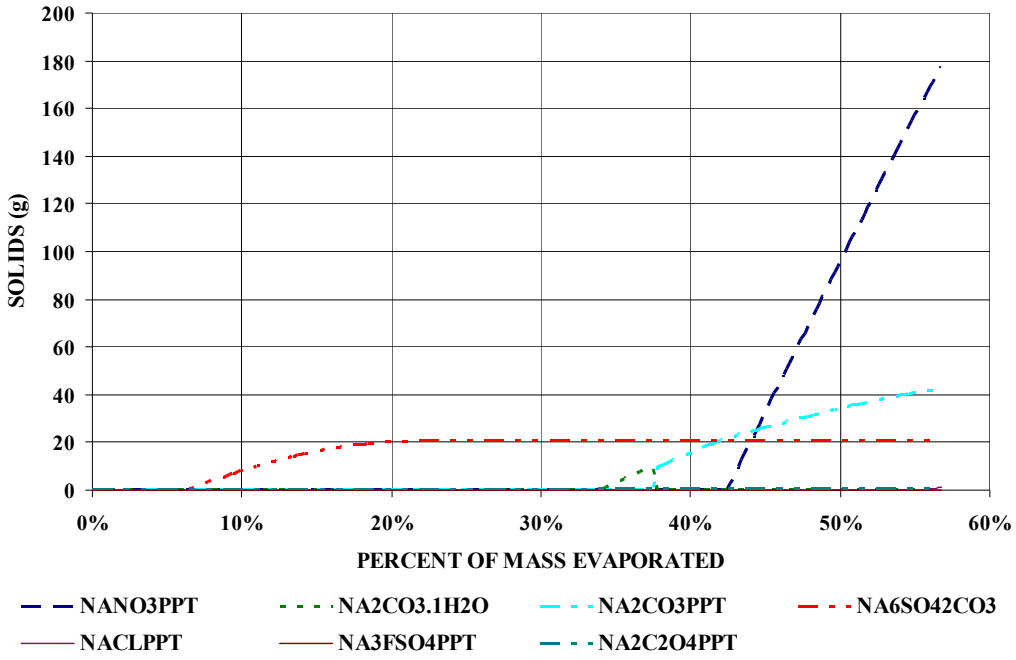

Figure 123. Thermodynamic Simulation of Crystallization at 75 °C
(Courtesy of D. Geniesse, Areva NC)

Thermodynamic simulations were performed for the early feed crystallization at 75 °C and provided to us by AREVA NC. These simulations were performed by the software developed by OLI system Inc and assume thermodynamic equilibrium. Figure 117 presents the evolution of the specific yields with respect to the percent water mass percent. This simulation shows that five major species are expected to come out of solution during the course of the run, three of them in large amounts: sodium nitrate at C:F= 0.426, sodium carbonate monohydrate at C:F= 0.342, and burkeite at C:F= 0.064.

Two additional species are expected to be produced in trace amounts: sodium oxalate at C:F= 0.248, and trisodium fluoride sulfate at C:F= 0.532. Finally sodium carbonate anhydrate and sodium chloride are expected to come out of solution after the end of the crystallization at a condensate-to-feed ratio of 0.376 and 0.558 respectively. Compared to the previous simulation burkeite is expected to come out of solution earlier while sodium carbonate monohydrate, sodium nitrate, sodium oxalate and trisodium fluoride sulfate will be produced later.

Nucleation Points

Figure 124 shows the sequence of species nucleation that was determined based on the PLM analyses of slurry samples taken at regular time intervals. For example, panel A shows that sodium oxalate was nucleated at C:F= 0.072. Panels B and C shows that sodium sulfate was nucleated at C:F= 0.097. Panels D and E display that sodium nitrates are nucleated at C:F= 0.243 and that these crystals increase in number and size in the next samples. The next species to be nucleated are sodium carbonate monohydrate crystals at C:F= 0.281 as displayed by panel F. Panels J and K show that sodium carbonate monohydrate number and especially size increased in the next samples. Panels G to I show that burkeites were nucleated at C:F= 0.281 and that several small agglomerates and large clusters were formed instantaneously. A very small amount of trisodium fluoride sulfate was detected at C:F= 0.312. The spike in sodium nitrate nucleation was observed at C:F= 0.382 as shown by panel L.

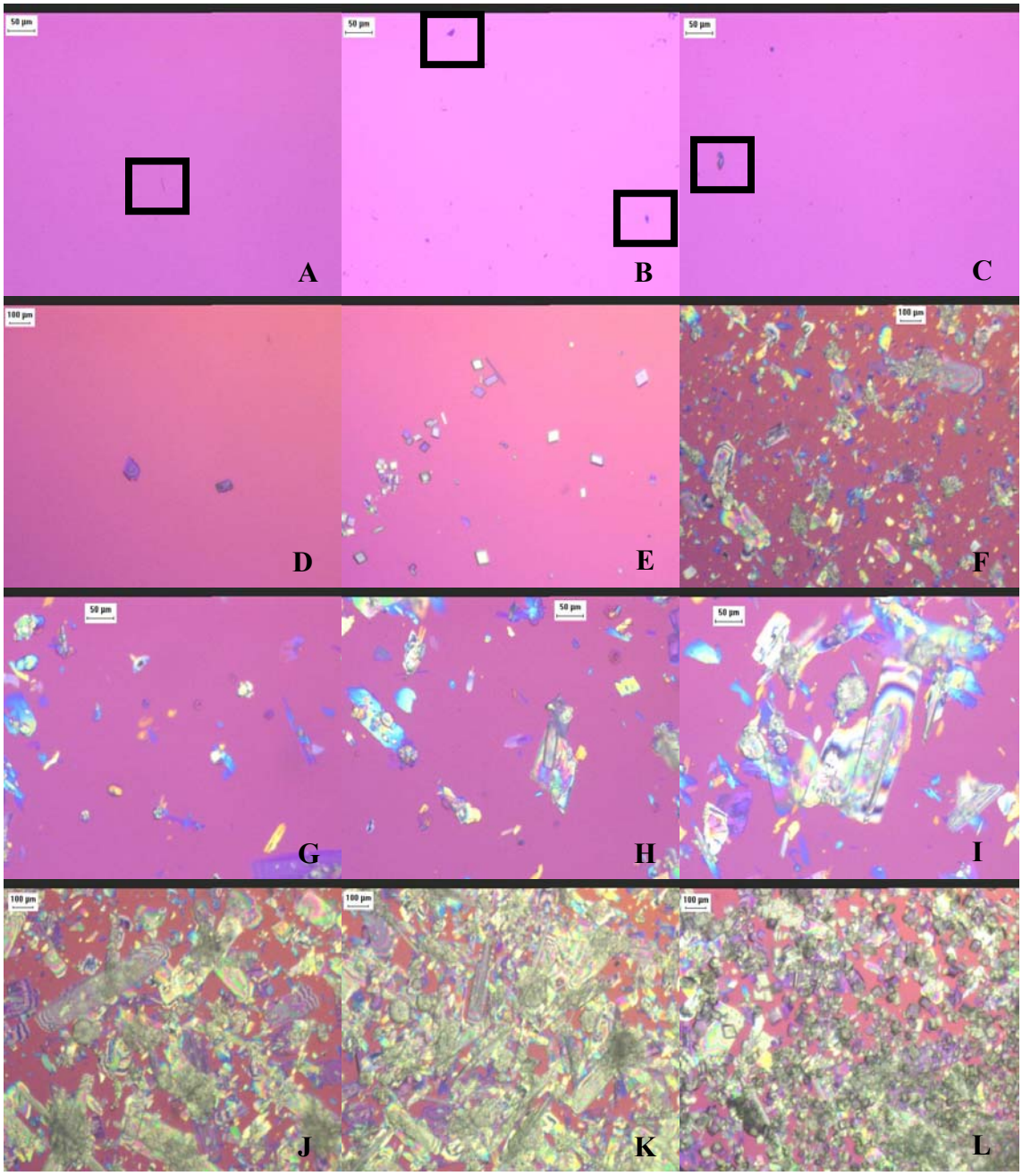

Figure 124. PLM images of samples from early feed run at 75 °C and 25 g/h evaporation rate
(Panel A, sodium oxalate crystals, Panel B, small sodium sulfate crystals, Panel C, sodium sulfate, Panel D, sodium nitrate nucleation, Panel E, sodium nitrate crystals, Panel F, sodium carbonate monohydrate nucleation, Panel G, burkeite nucleation, Panel H, burkeite agglomerates, Panel I, burkeite clusters, Panel J, sodium carbonate monohydrate growth, Panel K, high amounts of sodium carbonate monohydrate, Panel L, sodium nitrate spike in nucleation)

Table 53 presents the specific nucleation points and corresponding operating times for the early feed crystallization at 75 °C. At a temperature of 75 °C trisodium

fluoride sulfate was not produced in high amounts allowing burkeite to be grown and nucleated. Sodium nitrate was nucleated earlier than the previous experiments but with a spike in nucleation appearing only at C:F= 0.382. All other species were nucleated earlier than with the lower operating temperatures. The main discrepancy with the thermodynamic simulation deals with the burkeite nucleation which appeared a lot after the simulated saturation.

Table 53. Specific nucleation points for the species produced during the early feed run operated at 75 °C and 25 g/h

SST Early Feed	Condensate To Feed Ratio At Nucleation	Operating Time At Nucleation (min)
Sodium Nitrate (1st Nucleation)	0.243	500
Sodium Nitrate (2nd Nucleation)	0.382	1134
Sodium Carbonate Monohydrate	0.281	619
Burkeite Crystals	0.281	619
Sodium Sulfate	0.097	192
Sodium Oxalate	0.072	141
Trisodium Fluoride Sulfate	0.312	730

Nucleation rate

Figure 125 presents the evolution of the total crystal count with the operating time for each of the crystalline species. All the crystalline species have a linear nucleation rate at the exception of sodium sulfate and sodium oxalate. Sodium sulfate presents a linear profile with a high initial nucleation followed by a low average nucleation rate section. The average nucleation rate for this species is 5.159×10^3 crystals/ mL·min. Burkeite has a linear profile in the range of operating time investigated, but displays a slow down in nucleation rate and a plateau in the next samples. The average nucleation rate for this species is 7.802×10^3 crystals/ mL·min. Sodium carbonate monohydrate and trisodium fluoride sulfate have an average nucleation rate of 1.487×10^4 and 98 crystals/ mL·min

respectively. Sodium oxalate shows a profile with an initial constant linear nucleation rate followed by low average nucleation rate section. The average nucleation rate for sodium oxalate in the ascending section of the profile was 1.500×10^{2} crystals/ mL·min. Finally sodium nitrate presents a linear profile. However the slurry density was so high before the sodium nitrate spike that it was not possible to estimate the average nucleation rate of sodium nitrate.

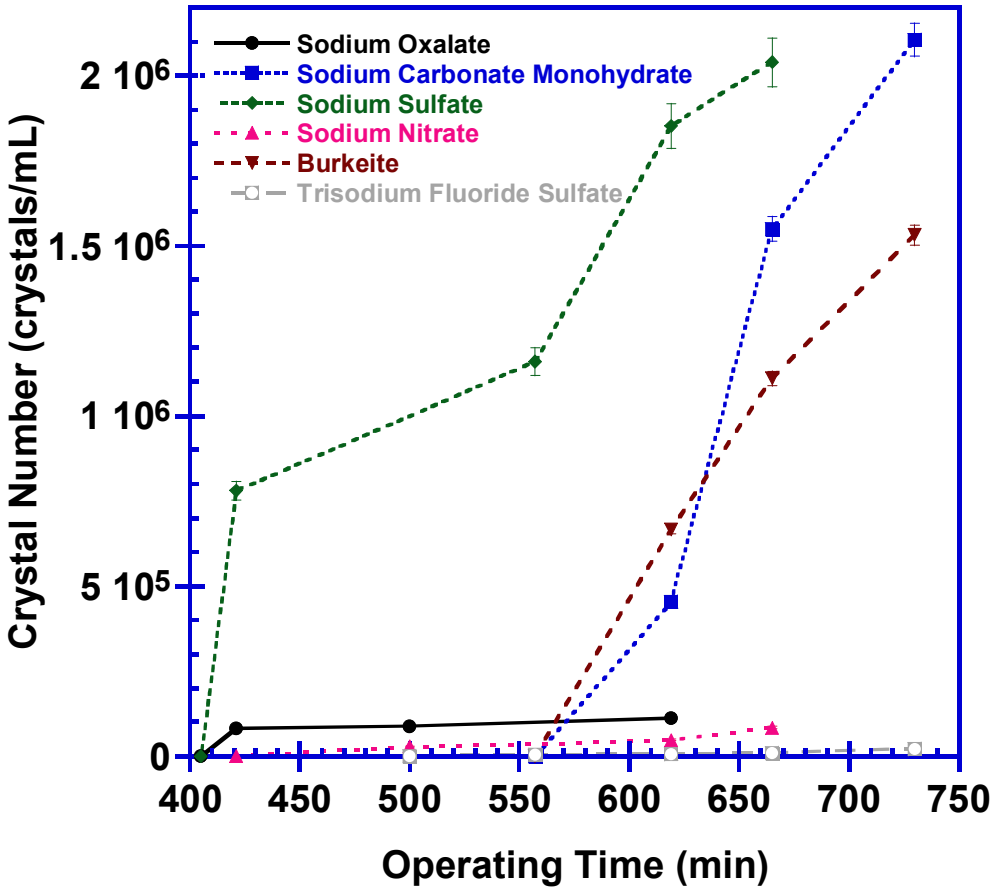

Figure 125. Evolution of total crystal count for each species formed from early feed run at 75 °C and 25 g/h

Growth Rate

The size of the crystals was monitored for each sample recovered from the slurry following the protocols defined in Chapter 2. Figure 126 presents the graphs of the

average length evolution with the operating time. The methodology used to compute the specific average growth rate was outlined in Chapter 2. All the species presents linear profiles at the exception of burkeite and trisodium fluoride sulfate which tends to plateau due to the discrepancy with the sodium sulfate saturation point. Sodium carbonate monohydrate, sodium nitrate, sodium sulfate and sodium oxalate present an average growth rate of 0.204, 1.763, 0.369 and 0.193 $\mu m \cdot min^{-1}$ respectively. Assessing the other crystalline species, burkeite and trisodium fluoride sulfate have an average growth rate of 0.057 and 0.220 $\mu m \cdot min^{-1}$.

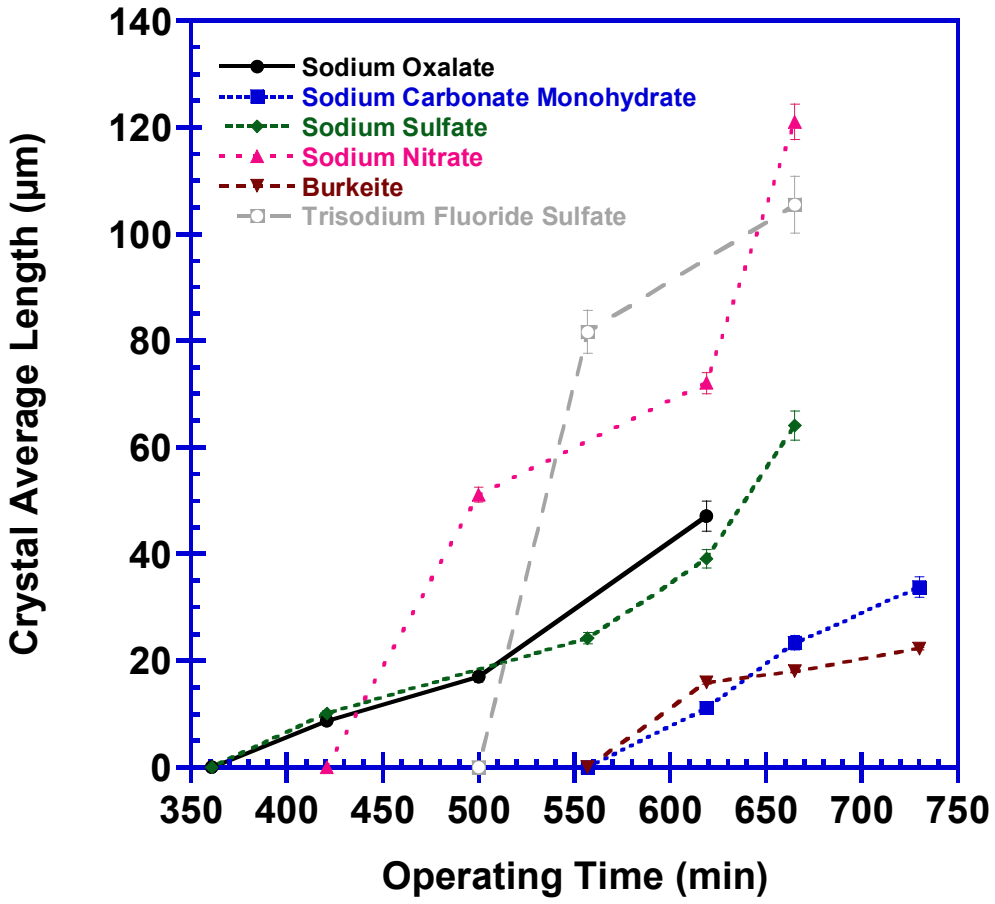

Figure 126. Evolution of crystal average length for each species formed from early feed run at 75 °C and 25 g/h

Conclusion

In this experiment, sodium nitrate was nucleated later than in the previous experiments. All other species were nucleated earlier. Trisodium fluoride sulfate presented very low kinetics, allowing burkeite and sodium sulfate to be nucleated in larger amounts. The main discrepancy with the other operating temperatures deals with sodium carbonate monohydrate crystals. Both the nucleation and growth rate of sodium carbonate monohydrate were increased leading to increased amounts with larger sizes.

4.3.5 MODELING OF OPERATING TEMPERATURE EFFECT ON KINETICS

Nucleation points

Figure 127 displays a sketch of a method used to determine the nucleation and saturation curves during a typical evaporative crystallization. This method is applied to simulated waste feed crystallizations that are initially at the early feed composition. The solvent is removed at a constant rate of 25 g/h and the crystallization is performed isothermally. By removing solvent, the concentration of each solute increases following a vertical isothermal line until saturation is reached. At saturation, it is thermodynamically possible to grow nuclei in the vessel. However, in real systems, solvent removal needs to be performed until nucleation is observed as described in Chapter 4.2. Panel A shows that the saturation and nucleation points are generally strong function of the operating temperature. In the series of experiments described in this chapter, the temperature varied from 35 °C to75 °C with increments of 10 °C with the objectives of being able to determine the experimental nucleation curve. Furthermore, thermodynamic simulations were performed by AREVA NC, providing the modeled

saturation curve for a multi salt early feed system at equilibrium for different operating temperature.

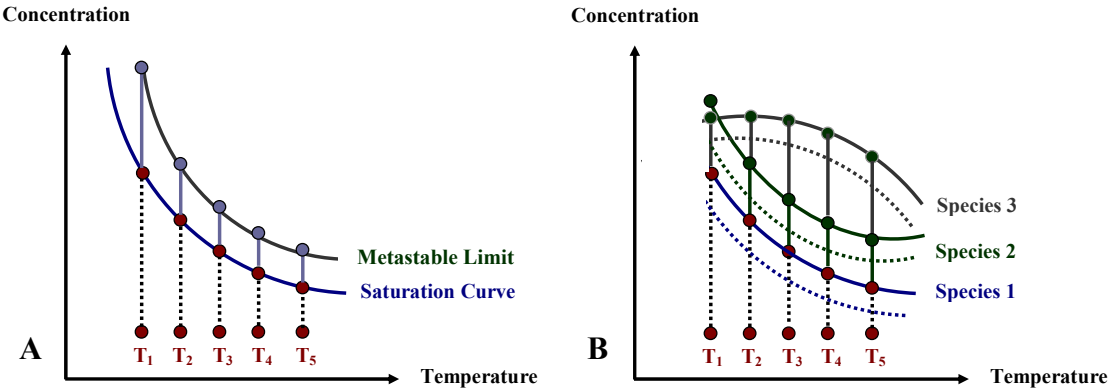

Figure 127. Metastable limit and saturation curve determination for each species in solution for a typical evaporative crystallization process
(Panel A, Metastable limit and saturation curve determination for a single species, Panel B, Metastable limit and saturation curve determination for multiple species)

Furthermore, the solution contained initially eight major sodium salts and may potentially create six different crystalline species. Panel B shows that in a general case each of these species metastable limits possess different profile that needs to be determined experimentally. Table 54 compares the points of nucleation observed for each species at the different operating temperature to the saturation points simulated by the software developed by OLI system Inc for each temperature for the early feed crystallization.

Figure 128 displays the experimental metastable limit and the simulated saturation curve of each of the crystalline species formed during the evaporative crystallization of early feed solution. Panel C shows that the gap between the saturation curve and metastable limit for burkeite is constant. This proves that (1) the model and the experiments are in good agreement on the burkeite profile, and (2) the burkeite simulated saturation underestimate the nucleation. Panel D provides the experimental metastable

limit of sodium sulfate that was not predicted by the thermodymnamic simulations. Assessing the other species the saturation model and the experiments are not agreeing. Since nucleation can not occur before saturation, the estimate of the saturation of this complex solution is at cause. One explanation for these discrepancies is that the unexpected nucleation or change in nucleation of one species (such as sulfate) may affect the entire metastable limit for the other species. The complexity of the solution and of the crystallization makes it difficult to estimate accurately saturation and nucleation through modeling. Furthermore, the thermodynamic model does not take into account the evaporation rate which may have to some extent an impact on the nucleation curve.

Table 54. Comparison of experimental nucleation and simulated saturation points for the early feed crystallization performed at 35 °C, 45 °C, 55 °C, 66 °C, 75 °C

Crystal Species	Condensate To Feed Ratio At Simulated Saturation / Experimental Nucleation									
	35 °C		45 °C		55 °C		66 °C		75 °C	
Sodium Nitrate (1st Nucleation)	0.318	0.261	0.350	0.266	0.378	0.268	0.400	0.247	0.426	0.243
Sodium Nitrate (2nd Nucleation)	0.318	0.339	0.350	0.299	0.378	0.268	0.400	0.363	0.426	0.382
Sodium Carbonate Monohydrate	0.302	0.309	0.314	0.317	0.324	0.300	0.332	0.298	0.342	0.281
Burkeite Crystals	0.158	N A	0.128	0.322	0.104	0.303-0.318	0.084	0.299	0.064	0.281
Sodium Sulfate	NA	0.125	NA	0.102	NA	0.182	NA	0.200	NA	0.097
Sodium Oxalate	0.096	0.100	0.142	0.080	0.196	0.070	0.226	0.156	0.248	0.072
Trisodium Fluoride Sulfate	0.154	0.261	0.328	0.317	0.404	0.377	0.478	NA	0.532	0.312
“Plate Like” Crystals	NA	0.296	NA	0.299	NA	NA	NA	NA	NA	NA

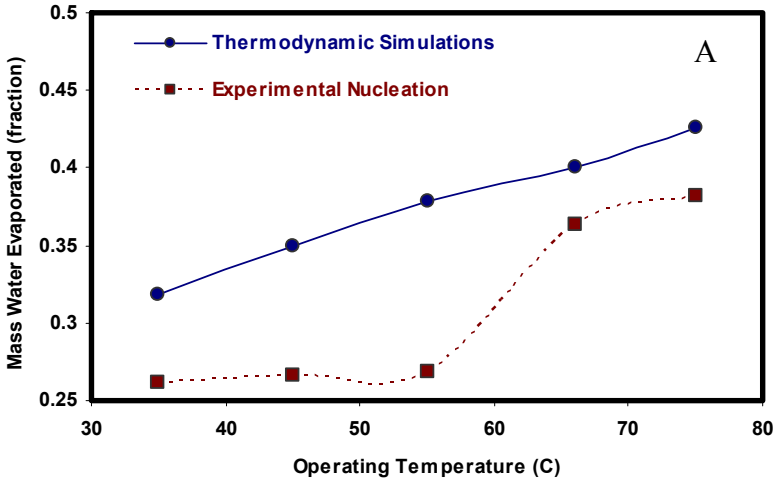
Thermodynamic Simulations
Experimental Nucleation
A
Mass Water Evaporated (fraction)
0.5
0.45
0.4
0.35
0.3
0.25
30
40
50
60
70
80
Operating Temperature (C)

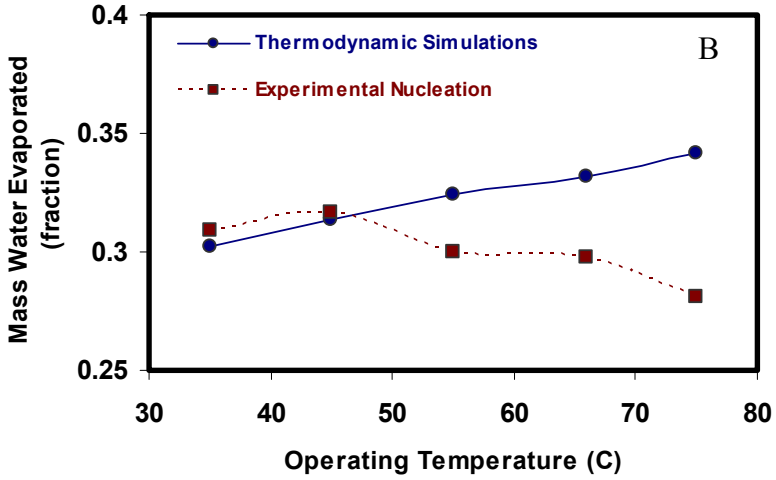
Thermodynamic Simulations
Experimental Nucleation
B
Mass Water Evaporated (fraction)
0.4
0.35
0.3
0.25
30
40
50
60
70
80
Operating Temperature (C)

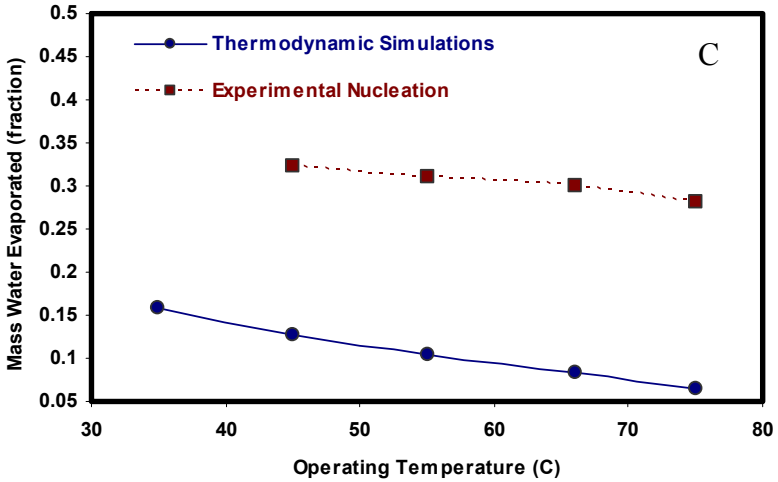
Thermodynamic Simulations
Experimental Nucleation
C
Mass Water Evaporated (fraction)
0.5
0.45
0.4
0.35
0.3
0.25
0.2
0.15
0.1
0.05
30
40
50
60
70
80
Operating Temperature (C)

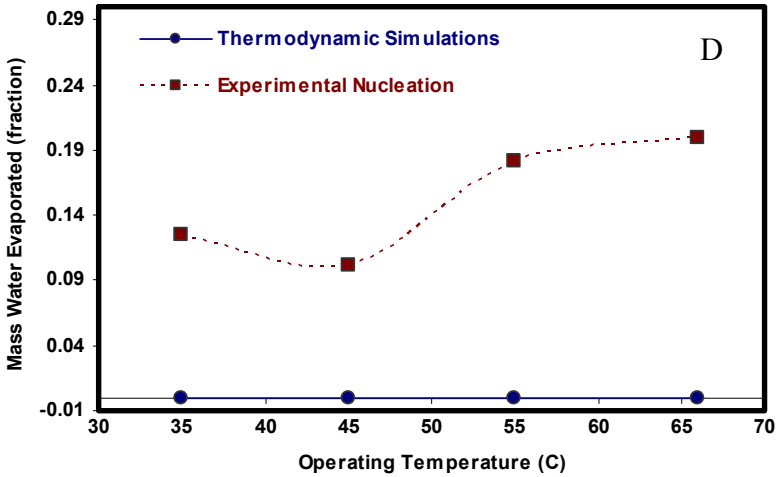
Thermodynamic Simulations
Experimental Nucleation
D
Mass Water Evaporated (fraction)
0.29
0.24
0.19
0.14
0.09
0.04
-0.01
30
35
40
45
50
55
60
65
70
Operating Temperature (C)

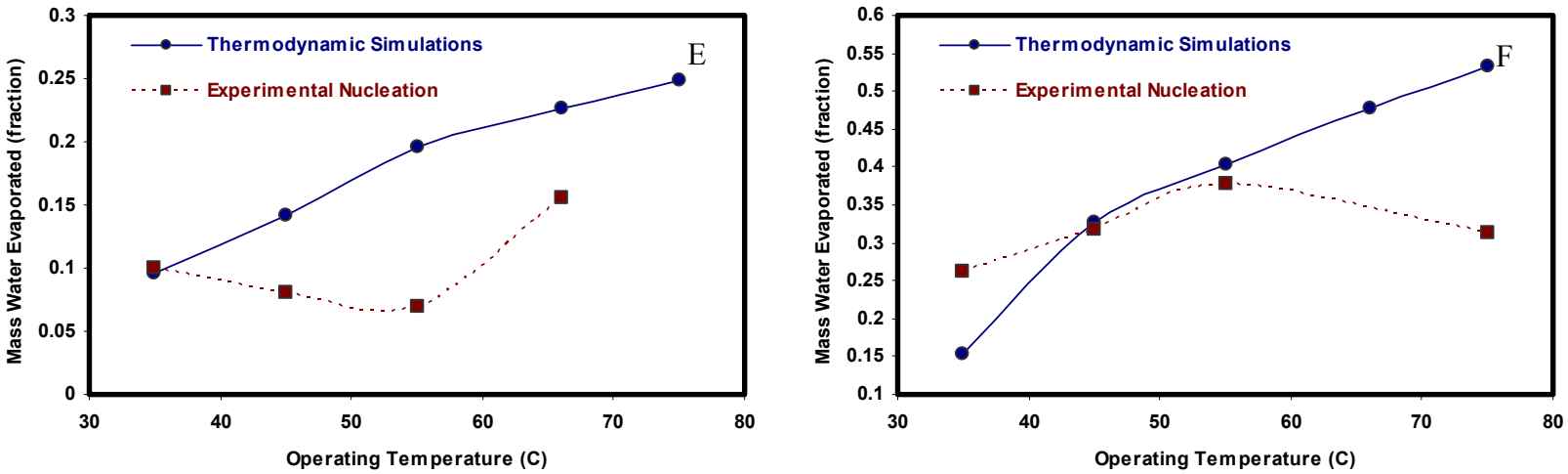

Figure 128. Experimental metastable limit and modeled saturation curve for each crystalline species produced during the early feed crystallization (Panel A, sodium nitrate, Panel B, sodium carbonate monohydrate, Panel C, burkeite, Panel D, sodium sulfate, Panel E, sodium oxalate, Panel F, trisodium fluoride sulfate)

Nucleation rate

All the species present a linear profile with the exception of sodium oxalate which presents variation due to breakage. An average nucleation rate was calculated for each species and each operating temperature following the protocols defined in Chapter 2. Figure 129 shows the semilog plot of the evolution of the average nucleation rate with the operating temperature. All of the species nucleation rates, at the exception of sodium nitrate, sodium sulfate and sodium oxalate, increased with the increase of the operating temperature.

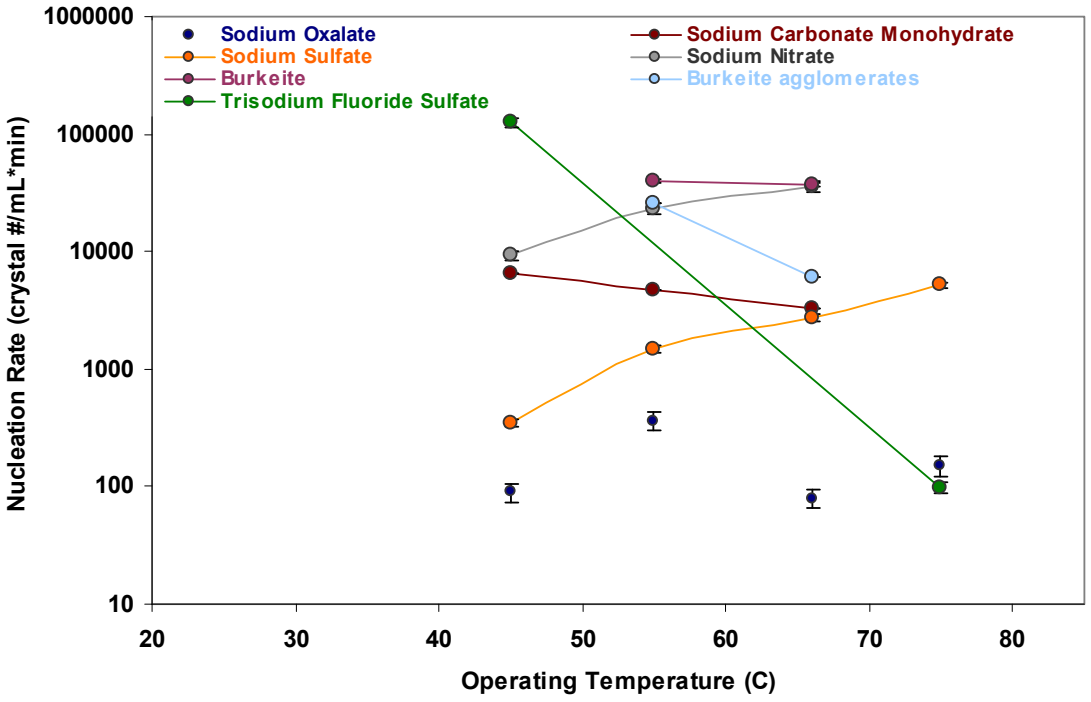

Figure 129. Evolution of the average nucleation rate of each crystalline species with the operating temperature for the early feed crystallization at 25 g/h evaporation rate

Table 55 provides the correlations representing the evolution of the specific average nucleation rate with the operating temperature.

Table 55. Correlations for the average nucleation rate evolution with the operating temperature for each species produced during the early feed crystallization at 25 g/h

Crystal Species	Profile Type	Model Equations	Squared Correlation
Sodium Nitrate	Linear	$y = 1.284.10^{3}x - 4.813.10^{4}$	0.99
Sodium Carbonate Monohydrate	Linear	$y = -1.556.10^{2}x + 1.342.10^{4}$	0.99
Burkeite Crystals	Linear	$y = -2.266.10^{2}x + 5.182.10^{4}$	1
Burkeite Agglomerates	Linear	$y = -1.763.10^{3}x + 1.225.10^{5}$	1
Sodium Sulfate	Linear	$Y = 1.539.10^{2}x - 6.843.10^{3}$	0.95
Trisodium Fluoride Sulfate	Linear	$y = -4.205.10^{3}x + 3.155.10^{5}$	1

(In the table "x" corresponds to the temperature and "y" corresponds to the nucleation rate). The polynomial correlation of sodium oxalate was not represented due to the important effect of breakage that modified the average nucleation rate)

Growth rate

An average growth rate was calculated for each species and each operating temperature following the methods described in Chapter 2. Figure 130 shows the semilog plot of the evolution of the average growth rate with the operating temperature. All of the species growth rates, at the exception of sodium nitrate and trisodium fluoride sulfate, increased with the increase of the temperature. Furthermore all the profiles are linear. Table 56 provides the correlations representing the evolution of the specific average growth rate with the operating temperature for the early feed crystallization at 25 g/h.

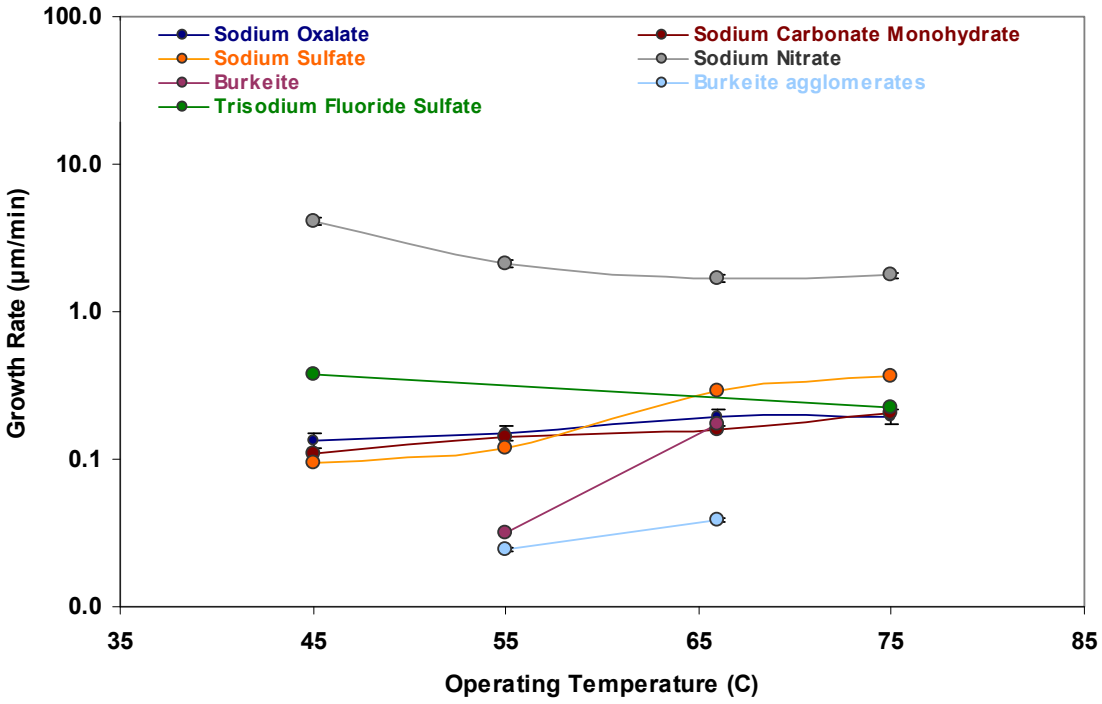

Figure 130. Evolution of the average growth rate of each crystalline species with the operating temperature for the early feed crystallization at 25 g/h evaporation rate

Table 56. Correlations for the average growth rate evolution with the operating temperature for each species produced during the early feed crystallization at 25 g/h

Crystal Species	Profile Type	Model Equations	Squared Correlation
Sodium Nitrate	Linear	$y = 2.114.10^{3}x-1.6$	0.82
Sodium Carbonate Monohydrate	Linear	$y = 3.10^{-3}x - 3.10^{-2}$	0.96
Burkeite Crystals	Linear	$Y = 1.260.10^{-2}x - 0.66$	1
Burkeite Agglomerates	Linear	$Y = 1.300.10^{-3}x - 0.05$	1
Sodium Sulfate	Linear	$y = 1.10^{-3}x - 0.37$	0.94
Sodium Oxalate	Linear	$Y = 2.200.10^{-3}x + 0.04$	0.92
Trisodium Fluoride Sulfate	Linear	$Y = -5.10^{-3}x + 0.59$	1

(In the table "x" corresponds to the temperature and "y" corresponds to the growht rate)

Sieving analyses

The crystal size distribution is the outcome of the combination of the nucleation and growth rate. Figure 131 shows the mass density distributions of the five operating temperature. Table 57 presents the detailed species distribution with respect to sizes for each operating temperature.

- The distribution of the 35 °C experiment showed that very few to no burkeite were recovered. The population was mainly composed of sodium nitrate with small amounts of trisodium fluoride sulfate crystals in the higher sizes and sodium carbonate and sulfate in the lower sizes. The continuous nucleation of sodium nitrate led to a higher spread in distribution and a higher mode size for sodium nitrate. The third mode usually composed of burkeite and sodium carbonate monohydrate was composed of sodium sulfate and sodium carbonate. The second mode generally created by sodium carbonate monohydrate was due mainly to sodium nitrate and in smaller extent to sodium carbonate and trisodium fluoride sulfate.
- The distribution of the 45 °C experiment showed a trimodal distribution. The first mode is composed of sodium nitrate crystals. The mode size is greater than for the certification run which is in agreement with the single nucleation observed, the nucleation point and above all the increased growth rate of sodium nitrate. The second mode is composed of sodium carbonate and trisodium fluoride sulfate that were produced in higher sizes. The third mode is composed of sodium carbonate and sodium sulfate. The proportion of burkeite is really low. This distribution is in agreement with observed kinetics. The sodium nitrate nucleation

rate is smaller than for the certification run but the growth rate is increased. Furthermore one nucleation is observed leading to higher nitrate size and larger mode spread. The growth rate of sodium fluoride sulfate is higher and the nucleation rate of sodium sulfate is higher. Finally, sodium carbonate has a lower growth rate and higher nucleation rate than the certification run.

- The distribution of the 55 °C experiment displayed a trimodal distribution with slightly higher sodium nitrate size than the certification run. The second mode presents less sodium carbonate which were recovered at lower sizes. Finally sodium sulfate and burkeite were collected in the lower pan. This distribution is in agreement with an increased sodium nitrate growth rate, and lower growth rate of sodium carbonate, burkeite and sodium sulfate. Furthermore, the production of burkeite agglomerates allowed collecting burkeite in the third mode size.
- The distribution of the 75 °C experiment displayed a trimodal distribution with the main mode composed of sodium nitrate and sodium carbonate monohydrate. The second mode is still composed of sodium carbonate in large amount. The third mode recovered very small crystal mass and the recovered burkeite were clusters. This is in agreement with the increased kinetics of sodium carbonate that allowed recovering more carbonates at larger sizes. Furthermore the single and agglomerated burkeite nucleation rate was decreased in this experiment explaining the low burkeite recovery.

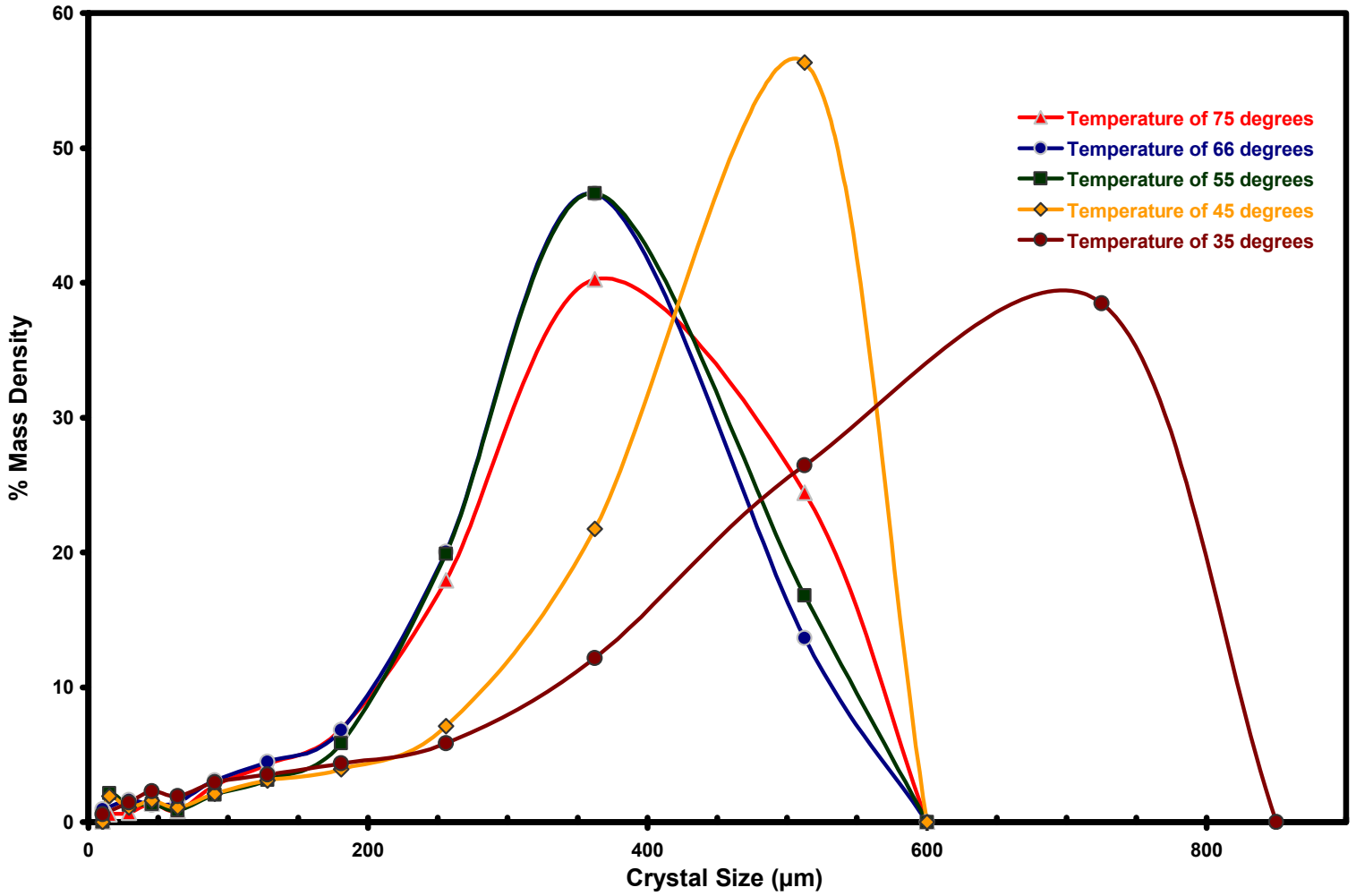

Figure 131. Mass density distributions of experiments from early feed crystallizations at 25 g/h and 35, 45, 55, 66, 75 °C

Table 57. Details of distribution of species with respect to size for early feed crystallizations at 25 g/h and 35, 45, 55, 66 and 75 °C

Size Range	Temperature 35°C	Temperature 45°C	Temperature 55°C	Temperature 75°C
0 - 10µm	Composed of sodium sulfate crystals with small (to very small) amounts of nitrates, traces of oxalates, carbonates and maybe burkeites.	Composed of sodium sulfate crystals with traces of oxalate, carbonate, burkeite and nitrate.	Composed of burkeites with small amounts of sulfates and sodium carbonates and trace amounts of oxalates and elongated nitrates. Burkeites are a mix of majority of single crystals with some flower shapes and heterogeneous.	Composed of sodium carbonates with small amounts of sodium sulfates, very small to trace amounts of burkeite and traces of oxalates.
10-20 µm	----------	Composed of sodium sulfates with non negligible amounts of sodium carbonates and small amounts of what is likely to be burkeites. Traces amounts of sodium nitrate and oxalate are observed.	Composed of sodium carbonates and burkeite with non negligible amounts of sulfates (greater than previous size). Small to very small amounts of nitrates with traces amounts of oxalates. The proportion of heterogeneous burkeite is increased.	Composed of sodium carbonates with small amounts of sodium sulfates, traces of oxalate, maybe burkeite and sodium nitrates.
20 - 38 µm	Mainly composed of sodium nitrate and sodium sulfates with non negligible amounts of sodium carbonates. No burkeites. No oxalates.	Mainly composed of sodium carbonates with (slightly) lesser amounts of sodium nitrates. Small amounts of octahedral sodium fluoride sulfate are observed and very small to trace amounts of large sulfates. Trace amounts of agglomerates or heterogeneous burkeite are observed. No oxalates.	Composed mainly of sodium carbonates and non negligible amounts of burkeites. Small amounts of sodium nitrates (increased proportions compared to previous sample) and very small amounts of sulfates. No oxalates. Burkeites are large single crystals (homogeneous and heterogeneous) and agglomerates in high proportions.	Composed of sodium carbonates with very small amounts of sodium nitrate and trace amounts of sodium sulfate. No burkeite, no oxalates.
38 - 53 µm	Composed mainly of sodium nitrates with non negligible amounts of sodium fluoride sulfate. Small amounts of sodium sulfates and very small amounts of carbonates.	Composed mainly of sodium nitrates with non negligible amounts of sodium carbonates. Small amounts/non negligible of octahedral sodium fluoride sulfate (increased amounts compared to previous sample) and an unidentified species.	Composed of sodium carbonates and slightly lesser amounts of sodium nitrates. No burkeites and sulfates.	Composed of sodium carbonates and nitrates. Presence of non negligible amounts of unidentified species and traces of maybe heterogeneous agglomerated burkeites.
53 - 75 µm	Composed mainly of sodium nitrates with non negligible amounts of sodium fluoride sulfate (slightly increased compared to previous). No carbonates or sulfates.	Composed mainly of sodium nitrates with small amounts of sodium carbonates (greatly diminished compared to previous). Small amounts/non negligible of octahedral sodium fluoride sulfate (similar amounts compared to previous sample) and traces of the unidentified species.	Composed of sodium nitrates and lesser amounts of sodium carbonates.	Composed of sodium nitrate and sodium carbonates in slightly lesser amounts. Traces of maybe burkeite clusters.
75 - 106 µm	Composed mainly of sodium nitrates with non negligible amounts of sodium fluoride sulfate (similar to previous).	Composed of sodium nitrate crystals with small/non negligible amounts of octahedral sodium fluoride sulfate (amounts slightly increased compared	Composed mainly of sodium nitrates with non negligible amounts (lesser proportions than previous sample) of large sodium carbonates.	Composed of sodium nitrate and sodium carbonates in slightly lesser amounts than previous view.

		to previous). No sodium carbonates.		
106 - 150 µm	Composed mainly of sodium nitrates with non negligible amounts of sodium fluoride sulfate (similar to previous).	Composed of sodium nitrate crystals with small/non negligible amounts of octahedral sodium fluoride sulfate (amounts identical to previous).	Composed of sodium nitrates with small amounts of sodium carbonates.	Composed of sodium nitrates and lesser amounts of sodium carbonates.
150 - 212 µm	Composed mainly of sodium nitrates with small to non negligible amounts of sodium fluoride sulfate.	Composed of sodium nitrate crystals with small amounts of octahedral sodium fluoride sulfate (amounts decreased compared to previous).	Composed of single sodium nitrate crystals and small to very small amounts of octahedral sodium fluoride sulfates. No carbonates.	Composed mainly of sodium nitrates with small to very small amounts of sodium carbonates.
212 - 300 µm	Composed mainly of single sodium nitrates with small amounts of sodium fluoride sulfate (amounts slightly decreased compared to previous).	Composed of single sodium nitrate crystals with small/non negligible amounts of octahedral sodium fluoride sulfate (amounts slightly increased compared to previous).	Composed of single sodium nitrate crystals.	Composed of sodium nitrate crystals with small amounts of agglomerates and traces of carbonates.
300 - 425 µm	Composed mainly of single sodium nitrates with very small to trace amounts of sodium fluoride sulfate (amounts slightly decreased compared to previous).	Composed of single sodium nitrate crystals with traces amounts of agglomerates and very small to trace amounts of very large sodium fluoride sulfate.	Composed of single sodium nitrate crystals with traces amounts of agglomerates.	Composed of single sodium nitrates with slightly higher proportions of agglomerates.
425 - 600 µm	Composed of single sodium nitrate crystals with traces amounts of agglomerates. No sodium fluoride sulfate.	Composed of single sodium nitrate crystals with traces amounts of agglomerates. No sodium fluoride sulfate.	Composed of agglomerates with small amounts of single nitrates.	Composed of agglomerates with traces amounts of single nitrates.
600 - 850 µm	Composed of single sodium nitrate crystals with non negligible amounts of agglomerates.	----------	----------	----------
850 - 1180 µm	----------	----------	----------	----------

4.4 APPLICATIONS OF KINETICS STUDY

4.4.1 CONTROL OF HETEROGENEOUS CRYSTAL POPULATION

Figure 132 displays PLM images of burkeite crystals produced during the early feed Certification Run 38b and shows that a portion of the burkeite crystals recovered at the end of the run was composed of heterogeneous crystals. The core of these crystals is constituted of small crystals, mainly sodium nitrate, around which burkeite had grown. By reducing the proportion of heterogeneous burkeite crystals, the crystal purity can be enhanced (heterogeneous crystals are more likely to capture mother liquor than homogenous crystals). The formation of heterogeneous burkeite crystals could be minimized by increasing burkeite nucleation and reducing the nucleation of non-burkeite species.

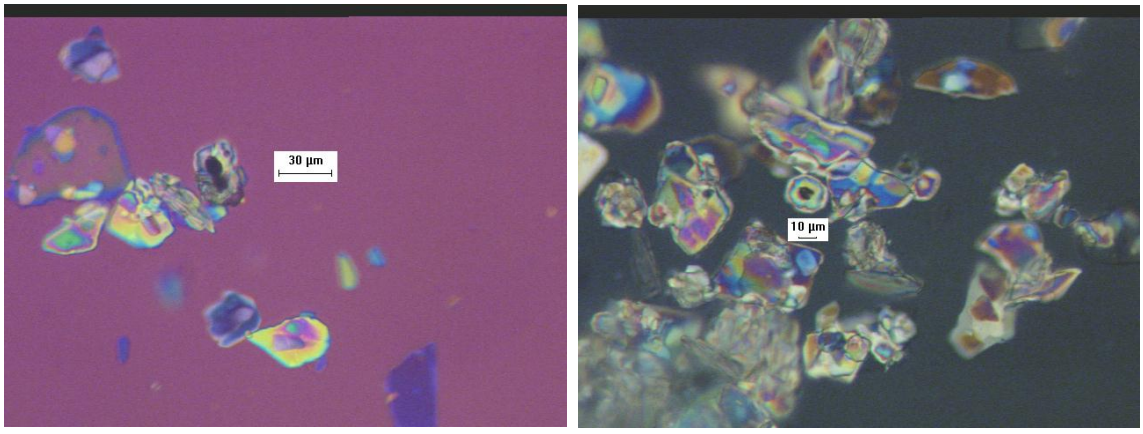

Figure 132. Micrographs of heterogeneous burkeite crystals obtained with the early feed Certification Run 38b

Based on the study performed with different evaporation rates, it was assumed that using a convex evaporation profile will allow increasing the number of burkeite crystals in the initial phase compared to the sodium carbonate and nitrate nuclei and

allow growth of larger burkeite crystals around these nuclei in a second phase. To validate this assumption a single stage crystallization run (run 50a) was performed with the simulated early feed solution with a final condensate-to-feed ratio equal to that used in Certification Run 38b.

Operating Conditions

Figure 133 displays the plots of the mass of water evaporated with the operating time and the temperature and pressure profiles for the early feed Run 50a. Specifically, Panel A shows that the variation in evaporation rate consisted of (1) a very high evaporation rate prior to saturation of the solution, (2) a high evaporation rate during the run segment in which burkeite nucleation was expected (and before sodium nitrate or carbonate nucleation), and (3) a slow evaporation rate during the segment in which nucleation and growth of sodium nitrate and sodium carbonate monohydrate were expected. Panel B shows the temperature and pressure profiles from Run 50a. The run temperature was controlled to within +/- 1 ^{o}C of the target value of 66 ^{o}C. The pressure profile reflects the step-wise changes in vacuum that are associated with manual adjustments of the regulating valve.

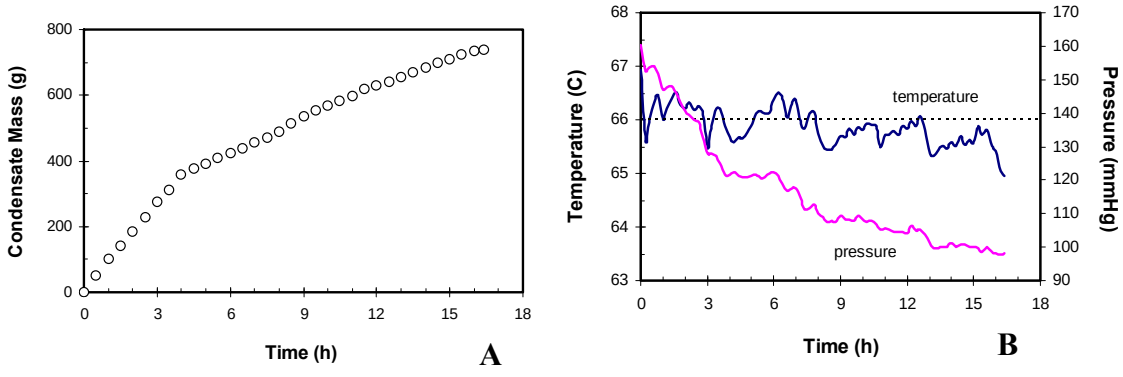

Figure 133. Condensate, temperature and pressure profiles for convex early feed crystallization Run 50a performed at 66 °C
(Panel A, Mass of water evaporated with operatig time, Panel B, Temperature and pressure profiles)

The target and actual condensate-to-feed ratios for this run were 0.474 and 0.475, respectively. The operating time for the run was 16.5 hours. Overall and detailed mass balances are provided in appendix K.

PLM Slurry Analyses

Figure 134 shows PLM images taken from the slurry of the early feed Run 50a. Images from this analysis displayed the presence of sodium nitrate, sodium carbonate monohydrate, burkeite, sodium sulfate, and sodium oxalate. Large amounts of sodium nitrate crystals were observed. Their size ranged from several microns up to sizes of 300-400 μm. There were few large (>500 μm) single sodium nitrate crystals observed. Despite a similar average size, the amount of small sodium nitrate crystals appears to be lesser than in Run 38b. The small sodium nitrate crystals, with a size of only a few microns, are expected to go through the medium-frit filter and be collected in the filtrate. Sodium carbonate monohydrate crystals were present in important amounts. Their average size was around 50-100 μm. Sodium oxalate crystals were observed in trace amounts, similar to the certification run. The burkeite crystals were observed in reasonable amounts, and their average size was smaller than in Run 38b. Burkeite crystals were present at a lower size range (20 μm or less) than in Run 38b (30-50 μm) and generally appeared as single crystals. The burkeite crystals observed in the slurry displayed a greater proportion of homogenous crystals than those seen in Run 38b. Both observations are in agreement with the expected effects of the evaporation profile.

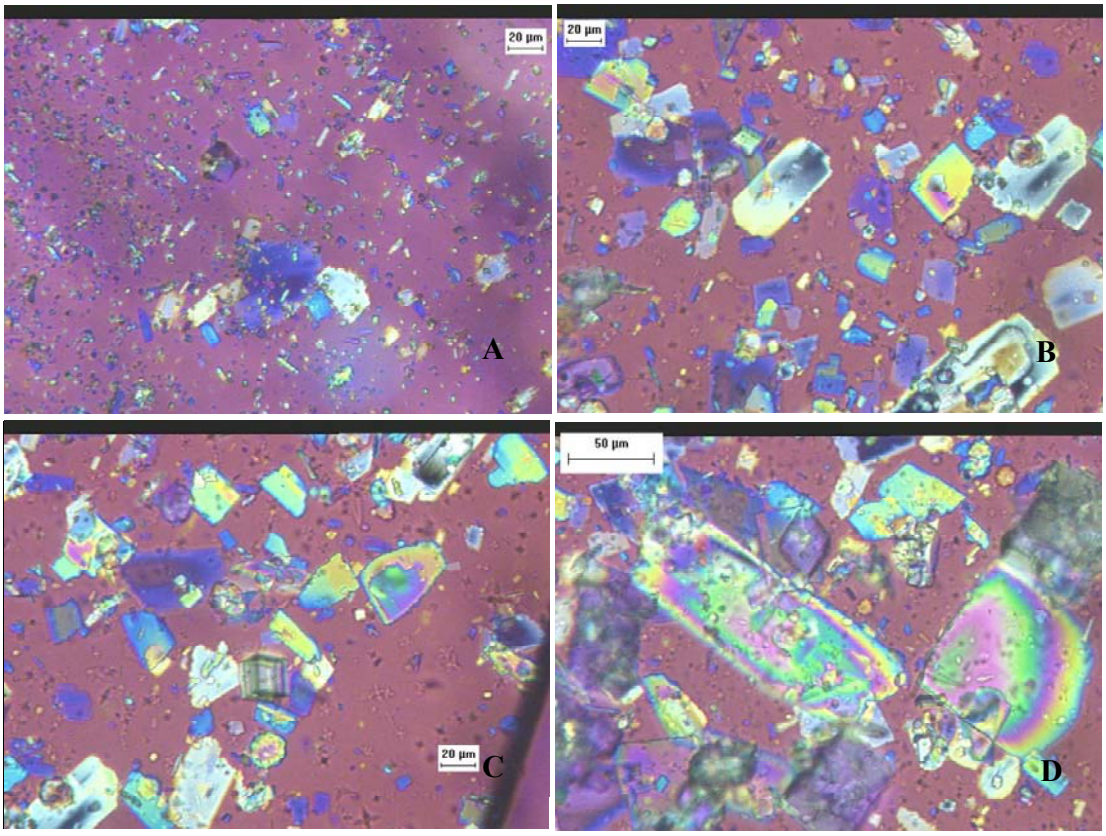

Figure 134. PLM images from the slurry of convex evaporation profile run
(Panel A, sodium nitrate, panel B and D, sodium carbonate monohydrate 50 to 100µm and sizes slightly higher than 100µm, panel C, burkeite crystals with sizes less or equal to 20µm)

The increased evaporation increased burkeite nucleation, leading to a smaller average size. On the other hand, the similar (slightly lower) evaporation rate in the region of sodium carbonate monohydrate and sodium nitrate crystal nucleation led to similar size ranges of these crystals. These effects combined to increase the proportion of burkeite nuclei with respect to nitrate nuclei during the period of burkeite growth and hence reduced the proportion of heterogeneous burkeite at the end of the run.

Sieving Analysis

Figure 135 shows the CSD histograms and cumulative distributions for the early feed Run 50a. The figure displays (1) the same mode size as the certification Run 38b, but with a smaller percentage of crystals at this size, (2) a slightly larger general spread,

(3) a slightly different first mode and (4) a slightly greater amount of large crystals (crystals over 500 µm). The first section of the CSD histogram is very close to that of certification Run 38b. However, the crystals obtained are slightly smaller than in Run 38b (a slightly higher amount between 0 and 50 µm and a slightly smaller amount between 50 and 200 µm). The crystals corresponding to this size range (0-50 µm) are mainly burkeite and sodium carbonate. Hence, the burkeite crystals have an average size smaller than those from the certification Run 38b. In the second section of the curve, between 200 and 600 µm, the crystals obtained (mainly sodium nitrate crystals) are larger for Run 50a than for Run 38b. This discrepancy may be reduced if the agglomeration analysis proves a higher percent of agglomerates in the higher sieve size for Run 50a. Table 58 compares the crystal distributions for early feed Run 38b and 50a.

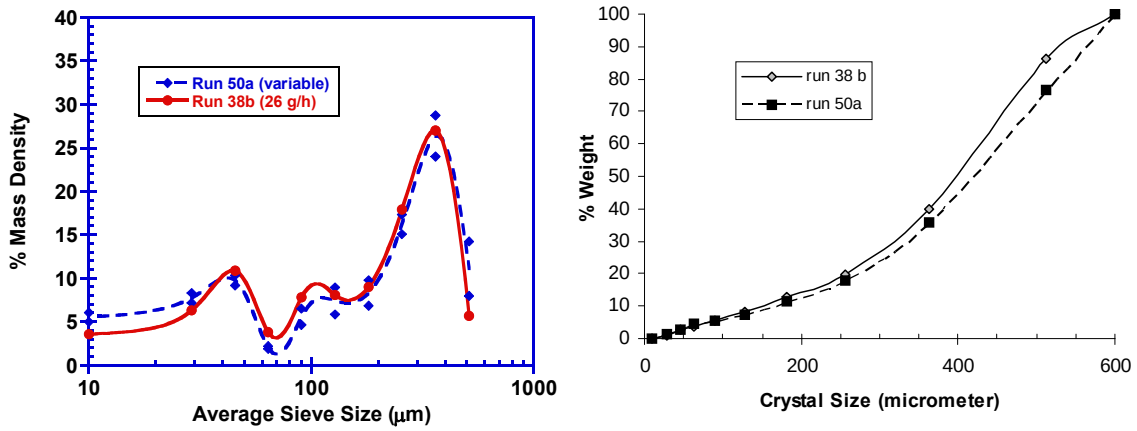

Figure 135. Crystal size histograms and cumulative distributions comparison for the convex evaporation profile early feed Run 50a and Certification Run 38b: runs performed at 66 °C
(Panel A, CSD histograms for Run 38b and 50a, Panel B, Cumulative distribution for Run 38b and 50a)

Table 58. CSD comparison for early feed Runs 38b and 50a performed at 66 °C

Criteria	Early Feed 38b	Early Feed 50a
Coefficient of variation	34.7	39.4
Percent crystal mass at mode size	46.62	39.7
Percent crystal mass below 50µm	3.82	5.2

The coefficient of variation was slightly higher for the early feed Run 50a operated with a convex profile with values of 34.7 and 39.4 % for Run 38b and Run 50a respectively. This difference in spread of the distribution is partially explained by an increase in crystals mass recovered below 50μm for Run 50a and the lower mass recovered at the main mode size composed of sodium nitrate.

Solid Liquid Separation Efficiency

Table 59 shows the criteria that were used to evaluate the effect of the convex evaporation profile on the solid-liquid separation steps in Runs 38b and 50a.

Table 59. Comparison of solid-liquid separation for early feed Run 38b and 50a

Criteria	Early Feed Certification	Convex Profile
Evaporation rate (g/h)	~ 25	~ 70 for burkeite region and ~ 25 for nitrate and carbonate region
Condensate-to-Feed Ratio	0.481	0.475
Washes necessary for major mother liquor removal	3	3-4[5]
Filtration & Washing Time	Typical	Typical
Slurry cake composition	Powder-like with large-medium crystals	Powder-like with large-medium crystals
Mass of final crystals	Typical (210 g)[6]	Increased (262 g)
Color of final crystals	White with slight yellow color	White with slight yellow color
Ease of operation	No filter plugging, easy to stir	Very slight filter plugging, still easy to stir

A key point illustrated in Table 59 is the difference between the masses of final crystals from the two runs; Run 50a generated far more product crystals. The main

[1] Three washes were necessary for major removal and no change in color was observed after the fourth wash.
[2] The value of 210 g in Run 38b corresponds to the final mass of crystals collected after the washing steps. This does not account for the samples collected from the unwashed crystals or those collected after each wash step, which totaled 19 g. The discrepancy between the two values may be explained by the difference in accumulation collected at the end of Run 38b (135 g) and Run 50a (85 g).

explanation for this is the accumulation difference between the two runs. Run 50a had 50 grams less accumulation than Run 38b, and this mass was collected as product crystals. Both runs were however very similar concerning the solid-liquid separation step.

Crystal Repartition with Sizes

Figure 136 displays PLM images taken from the sieved crystals of Run 50a. Images from the PLM analysis displayed the presence of sodium nitrate, sodium carbonate monohydrate, burkeite, sodium sulfate, and sodium oxalate.

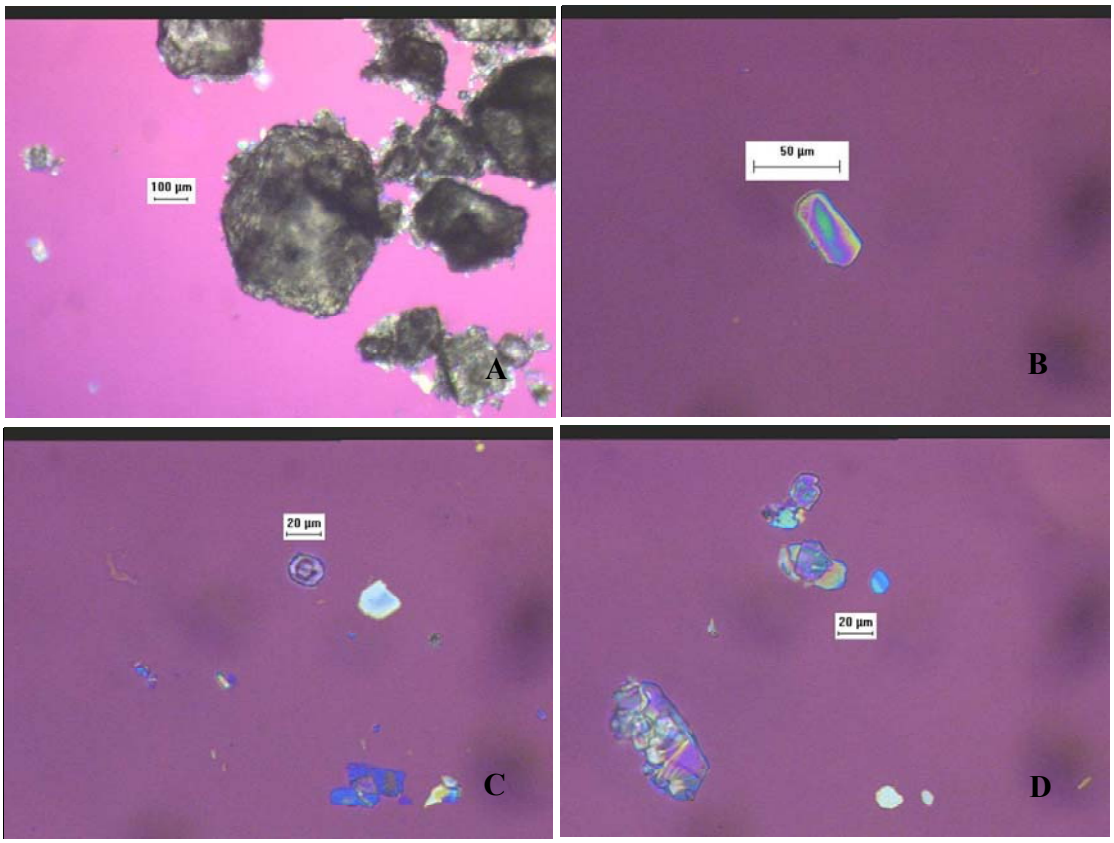

Figure 136. PLM images from sieved crystals of early feed Run 50a performed with convex evaporation profile at 66 °C
(Panel A, sodium nitrate at mode size, Panel B, sodium carbonate monohydrate with sizes ranging from 50 to 100µm, Panel C, homogenous burkeite crystals with a size equal to 20µm, Panel D, trace of sodium sulfate and sodium oxalate crystals)

Figure 137 compares the PLM images of burkeite crystals obtained from the Certification Run 38b and early feed Run 50a and shows that the fraction of heterogeneous burkeite was decreased in Run 50a. By applying a convex evaporation profile, burkeite crystals were produced at higher number but lowered size. The size range of burkeite crystals displayed in Run 50a represents the lowest obtained by crystallization with early feed. By creating a lot of burkeite nuclei, burkeite grown on the existing burkeite more in this run than on nitrate nuclei. Consequently, the proportion of heterogeneous burkeite crystals was reduced which should have an effect on decontamination. On the other hand, no real improvement or deterioration of the conditions of solid liquid separation was noticed compared to Run 38b.

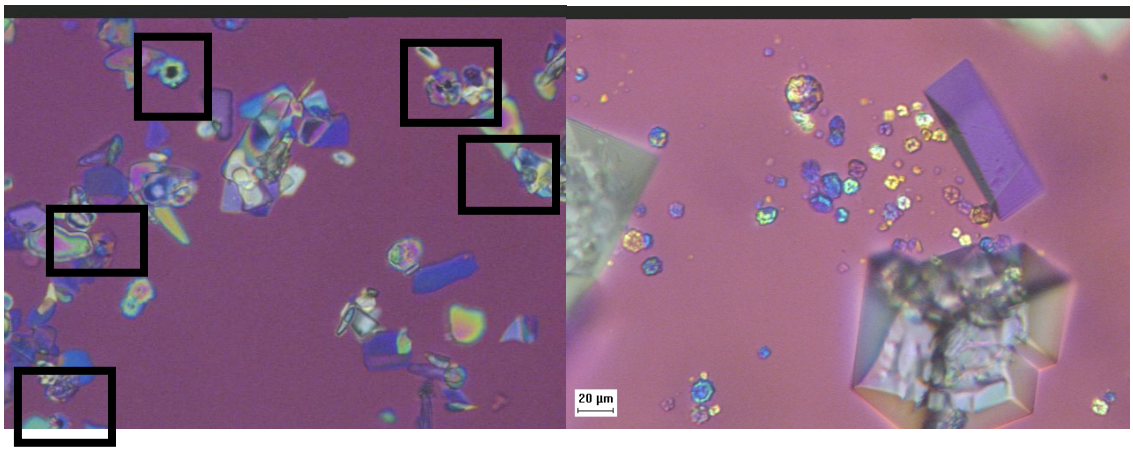

Figure 137. Comparison of burkeite crystals from certification run and convex evaporation run

4.4.2 CONTROL POPULATION DISTRIBUTION AND SOLID LIQUID SEPARATION

Based on the study of the early feed crystallization perfomed with increasing evaporation rates, a crystallization run (run 51) was performed with a concave evaporation profile in order to determine the maximum burkeite crystal size that may be obtained with an early feed solution. Furthermore, the second objective of Run 51 was to modify the crystal population in order to enhance the solid-liquid separation. Run 51 was a single stage crystallization run using a variable evaporation rate and the same condensate-to-feed ratio than the Certification Run 38b. The evaporation rate was increased slowly throughout the run. Specifically, the evaporation profile consisted of (1) a slow evaporation rate during the period of burkeite nucleation and growth, (2) the typical evaporation rate[7] at the point of sodium carbonate and nitrate nucleation and initial growth, and (3) an increased evaporation rate towards the end of the run.

The simulation graph for a typical early feed crystallization at 66 °C and the kinetics results from Chapter 4.1 and 4.2 were used as a reference to determine the evaporation profile. These were used to define four different operating regimes: (1) sodium sulfate is nucleated and most of the crystal mass of sulfate is generated in the region between 8 and 28% evaporation; (2) between 28 and 33% evaporation, sodium carbonate and burkeite are nucleated and most of the burkeite mass is generated, (3) between 33% and 35% sodium carbonate nucleation continues but there is little if any additional crystallization of burkeite; (4) between 35% evaporation and the end of a run,

[7] This was a rate of ~25 g/h, identical to that used in Certification Run 38b.

sodium carbonate and sodium nitrate crystals are nucleated and grown with important kinetics, but there is no additional burkeite crystallization. The goal of Run 51 was to produce a smaller number of burkeite crystals, but to increase their size. Accordingly, a very slow evaporation rate was used during Regime 1. The rate was increased somewhat during Regimes 2 and 3, and it was increased further during Regime 4 to reduce the total operating time of the run. Two additional effects are expected as (1) heterogeneous burkeite crystals might be produced during Regime 3 and (2) increasing the evaporation rate in Regimes 3 and 4 might influence the spread of sodium nitrate and sodium carbonate crystals, thereby affecting the solid-liquid separation .

Figure 138 displays the graph of the mass of water evaporated with the operating time. Specifically, the run was started with Regime 1 and an evaporation rate of about 10 g/h and it was slowly increased to favor burkeite growth throughout Regime 2. At the end of Regime 2, the evaporation rate reached 25 g/h, which is equal to the value used in the certification run. This evaporation rate was maintained throughout Regime 3, and it was then increased in Regime 4 (i.e., after the nucleation of sodium carbonate and sodium nitrate). Figure 138 shows the temperature and pressure histories from Run 51. The run temperature was controlled to within +/- 1 ^{o}C of the target value of 66 ^{o}C. The pressure profile reflects the step-wise changes in vacuum that are associated with manual adjustments of the regulating valve. The target and actual condensate-to-feed ratios for this run were 0.474 and 0.483, respectively. The operating time for the run was 33 hours. Overall and detailed mass balances are provided in the appendix K.

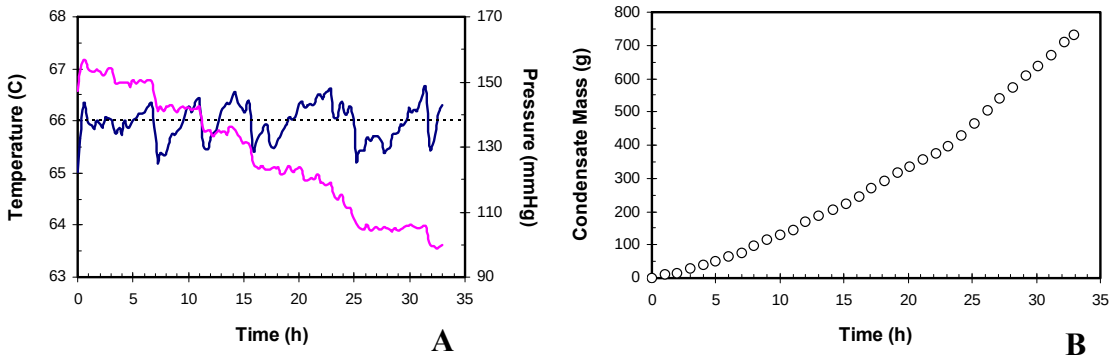

Figure 138. Condensate, temperature and pressure profiles for early feed Run 51: Run 51 was operated at 66 °C and concave evaporation profile
(Panel A, Temperature and pressure profiles for Run 51, Panel B, Mass of water evaporated with operating time for Run 51)

PLM Images of Slurry

Figure 139 shows PLM images taken from the slurry of the early feed Run 51 operated at 66 °C. The micrographs showed the presence of sodium nitrate, sodium carbonate monohydrate, burkeite, sodium sulfate, and sodium oxalate. Very large quantities of sodium nitrate crystals were observed in the samples. These crystals ranged in size from several microns up to 300 to 400 µm. The average size was similar to that found in Run 38b, but their spread about the mean was greater. Based on microscopic observations of the slurry and sieved crystals, it would seem that a significant fraction of the small sodium nitrate crystals (below a few µm) were either re-dissolved during the washing steps or passed through the medium-frit filter. Sodium carbonate monohydrate crystals were present in important amounts with an average size around 100–150 µm. Sodium oxalate crystals were observed in trace amounts, which is similar to amounts produced in Run 38b. Burkeite crystals were observed in smaller amounts but as larger crystals (single crystals with an average size from 40 to 50 µm). The burkeite crystals observed in the slurry were less numerous, had a smaller spread, and were larger than

those seen in Run 38b. These observations are in agreement with the predicted effects of the evaporation profile applied.

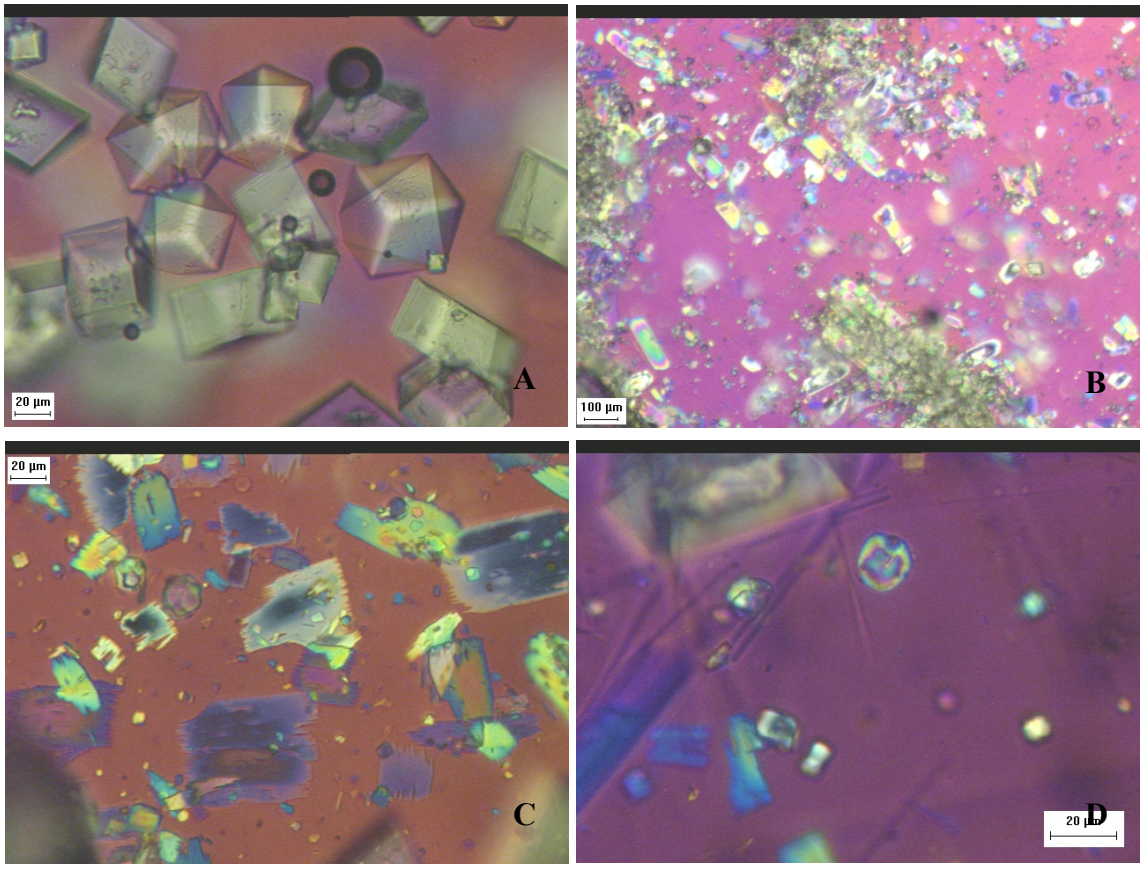

Figure 139. PLM images of Run 51 slurry
(Panel A, Sodium nitrate crystals, Panel B, Sodium carbonate with sizes ranging from 100 to 150µm, Panel C, Burkeite crystals and sodium oxalate in background, Panel D, Homogenous burkeite crystals)

The slower evaporation rate in Run 51 increased burkeite growth, leading to a higher average size and smaller number of crystals. On the other hand, the varying evaporation rate in the region of sodium carbonate monohydrate and sodium nitrate crystal nucleation led to slightly larger sizes and may have changed the spread of the size distribution of these crystals.

Sieving Analysis

Figure 140 displays the CSD histograms and cumulative distributions for the early feed Run 51 and show that (1) the same mode size that was produced in Run 38b, but with a smaller percentage of crystals at this size, (2) a slightly smaller general spread and (3) a slightly greater spread for sodium nitrate crystals. The first section of the CSD histograms from Run 51 is very close to that from certification Run 38b, but the crystals obtained are slightly smaller than in Run 38b (a slightly smaller amount between 0 and 50 μm and a smaller amount between 50 and 200 μm). The crystals corresponding to this size range (0–50 μm) are mainly burkeite and sodium carbonate monohydrate. Hence, the burkeite crystals have an average size larger than those from Run 38b and the sodium carbonate monohydrate crystals have a larger spread and a slightly higher average size. In the second section of the curve, between 200 and 600 μm, the crystals obtained (mainly sodium nitrate crystals) from Run 51 have a similar size to those from Run 38b, but a larger spread. Table 60 compares the crystal distributions for early feed Run 38b and 51.

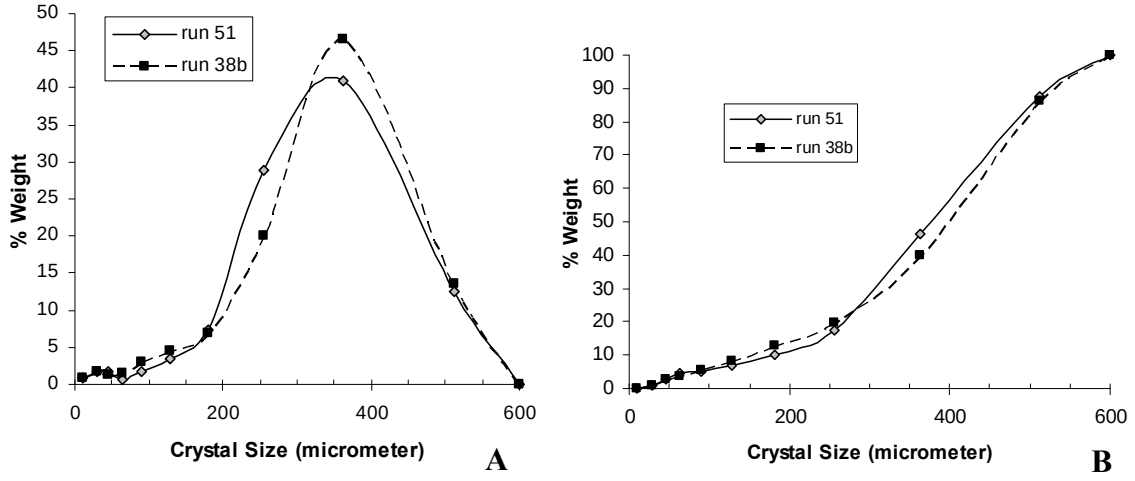

Figure 140. Crystal size histograms and cumulative distributions comparison for the concave evaporation profile early feed Run 51 and Certification 38b: runs performed at 66 °C
(Panel A, CSD histograms for Run 38b and 51, Panel B, Cumulative distribution for Run 38b and 51)

Table 60. CSD comparison for early feed Runs 38b and 51 performed at 66 °C

Criteria	Early Feed 38b	Early Feed 51
Coefficient of variation	34.7	33.1
Percent crystal mass at mode size	46.6	40.9
Percent crystal mass below 50µm	3.82	3.63

The spread in distribution for the early feed Certification Run 38b was greater than for the concave profile Run 51 with coefficients of variations of 46.6 and 40.9 %. This was however not due to the mass of crystals recovered below 50µm or the recovered mass of sodium nitrate in the main mode size that were similar for each runs. These observations show that the discrepancy is mainly due to sodium carbonate monohydrate and to some extent to burkeite crystals.

Solid Liquid Separation

Table 61 shows the criteria that were used to evaluate the effect of the concave evaporation profile on the solid-liquid separation steps in Runs 38b and 51..

Table 61. Comparison of solid-liquid separation for early feed Run 38b and 51

Criteria	Early Feed 38b	Early Feed 51
Evaporation rate (g/h)	~ 25	Variable, increased from ~10 g/h to ~40 g/h during the run
Condensate-to-Feed Ratio	0.481	0.483
Washes necessary for major mother liquor removal	3	3
Filtration & Washing Time	Typical	Decreased
Slurry cake composition	Powder-like with large-medium crystals	Powder-like with larger crystals
Mass of final crystals	Typical (210 g)[8]	Increased (275 g)
Color of final crystals	White with slight yellow color	White color
Ease of operation	No filter plugging, easy to stir	No filter plugging, easy to stir

[8] The value of 210 g in Run 38b corresponds to the final mass of crystals collected after the washing steps. This does not account for the samples collected from the unwashed crystals or those collected after each wash step, which totaled 19 g.

A key point illustrated in Table 61 is the difference between the mass of final crystals from the two runs; a far greater amount was produced in Run 51. The main explanation for this is that accumulation in Run 51 was 60 g less than that in Run 38b. Also there was a slightly increased condensate-to-feed ratio in Run 51.

Crystal Distribution with Size

Figure 141 displays PLM images taken from the sieved crystals of Run 51. Images from the PLM analysis displayed the presence of sodium nitrate, sodium carbonate monohydrate, burkeite, sodium sulfate, and sodium oxalate. Images of sieved crystals show that the burkeite crystal spread was reduced compared to that from Run 38b. For a similar crystal mass, the burkeite was produced as a smaller number of larger crystals. The mode size for the burkeite crystals is 40-50 μm. The amount of heterogeneous crystals was reduced compared to other early feed runs, however their proportion is still important. The slower evaporation rate at the start of the run reduced the nucleation rate of burkeite and favored burkeite growth. This led to fewer, but larger burkeite crystals. However, the increased evaporation rate at latter stages of the run created the heterogeneous burkeite crystals observed in PLM images. PLM images also displayed the presence of sodium nitrate crystals on the lower sieves. This was not the case in Run 38b and is a sign that the spread of the sodium nitrate crystals was increased. The sodium nitrate crystals presented a similar mode size to Run 38b and included large crystals. Once again, the small sodium nitrate crystals and the increased spread are likely due to the increased evaporation rate towards the end of the run. These assessments explain the process ease that was observed during filtration and washing. The reduced

number of small burkeite crystals avoided the potential filter plugging. Also, the slightly larger average size of the carbonate and nitrate crystals simplified the filtration and washing steps, compensating for the increased crystal mass.

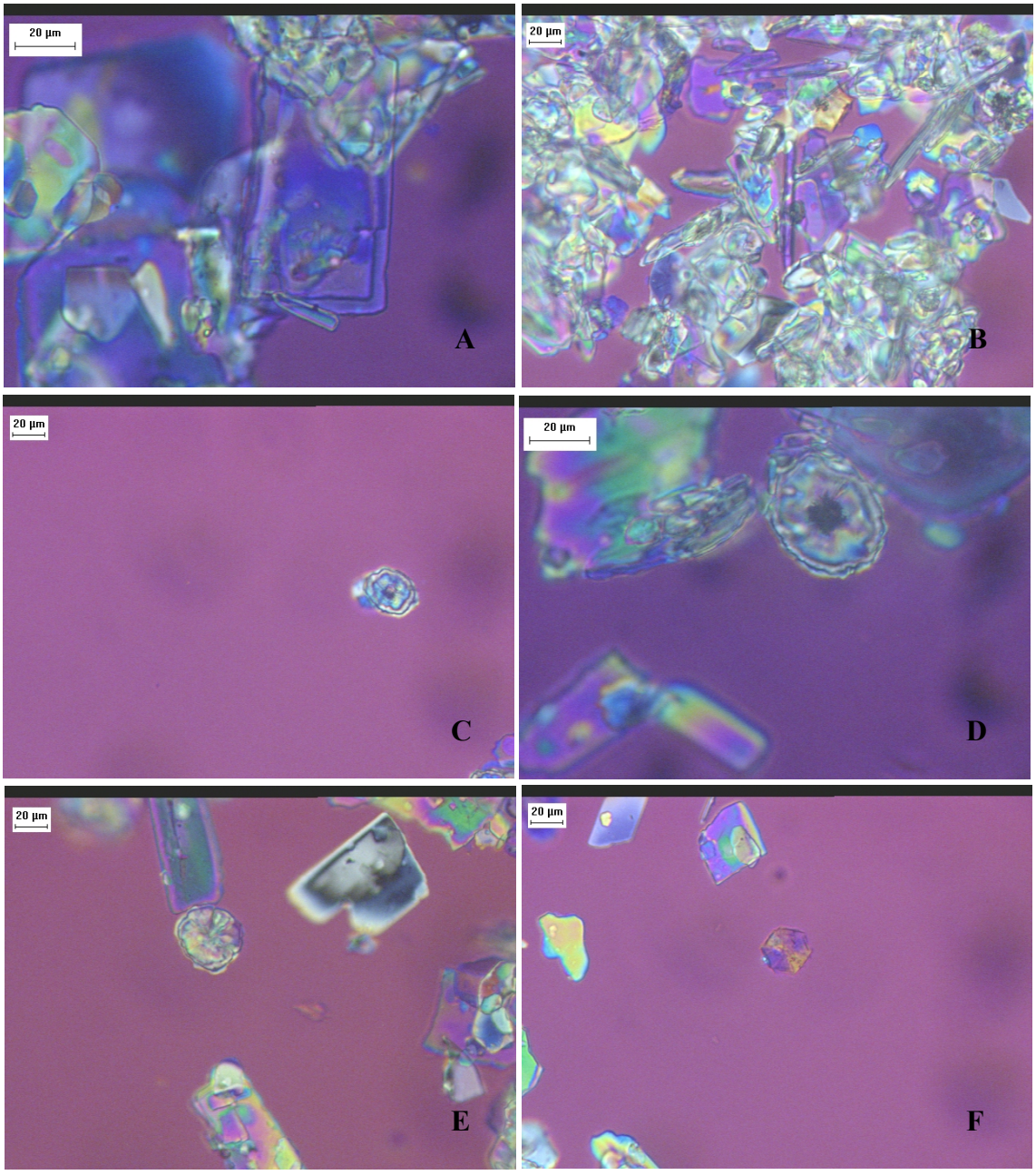

Figure 141. PLM images of sieved crystals from early feed Run 51operated at 66 °C with a concave evaporation profile
(Panels A and B, Sodium nitrate at lower size and as needle, Panels C and D, Homogenous and heterogeneous burkeite crystal, Panels E and F, zoom on flower like habit and other occurrence of burkeite)

Run 51 achieved its objectives. By applying a concave evaporation profile, burkeite crystals were produced at lower number but increased size. The size range of burkeite crystals displayed in Run 51 represents the highest obtained by crystallization with Early Feed. On the other expectation that the evaporation profile would modify the solid liquid separation revealed to be true. By increasing the size of the burkeite crystals and the spread of the sodium nitrate crystals a more homogenous crystal population was obtained which facilitated the filtration.

4.4.3 PRETREATMENT OF EARLY FEED

Link between Specific Kinetics and Requirements

The aims of the Early Feed crystallization are to be able to:

- Recover sulfate in the solid stream. This implies nucleating crystals that capture sulfate and grow them at a size higher than the pore diameter of the separation device. Burkeite crystals are the best candidates to achieve this goal as it capture close to two sulfates in their matrices for one carbonate. The nucleation of sodium sulfate (not predicted by the thermodynamic simulations) and the nucleation of trisodium fluoride sulfate (predicted to nucleate late in the run by the thermodynamic simulations) are beneficial to this goal if they do no hinder the nucleation and growth of burkeite. The agglomeration of burkeite may be beneficial in case of low growth rate at the condition that it does not exceed a critical value for which it would decrease the cesium decontamination. As mentioned by Chapter 3, this goal is quantified by the computation of the sulfate to sodium molar ratio.

- Recover sodium in the solid stream. This implies reaching a maximum yield in sodium at the end of the experiment that still allows performing separation efficiently. In the case where the final condensate to feed ratio is fixed (run time), this means controlling the crystal population. Due to kinetics consideration, sodium nitrate and sodium carbonate monohydrate are the major species that could be formed at high yield and control the sodium recovery. It is important to favor the kinetics of these two species to improve the yield. According to chapter 3, this is quantified by a sodium recovery mass percent.
- Recover most of the cesium in the liquid phase. This implies reducing the amounts of mother liquor trapped inside the crystalline matrix and in the crystal surface. The solid separation efficiency (linked to the crystal population) is determinant in achieving this goal. One need to create a crystal population that enhances the separation. This is done by reducing the discrepancies in the major crystals kinetics (to reduce the spread in distribution) and reduce the nucleation rate of some species that can create plugging. Finally as mentioned earlier, the secondary phenomena are generally detrimental to this objective. First the excessive agglomeration of burkeite may retain more mother liquor, and secondly the excessive breakage of sodium oxalate may create filter plugging. As mentioned in Chapter 3, this objective is quantified by the computation of a Decontamination Factor.

Selecting the Optimum Operating Conditions

The main operating conditions that may be modified are the operating temperature and the evaporation rate. A series of experiments with evaporation rate

ranging between 25 and 75 g/h and operating temperature ranging between 35 and 75 °C were performed. These represent the maximum ranges of conditions that can be applied to the pretreatment process. Any combination of these conditions is possible and the optimum conditions are to be determined based on the three objectives defined in the previous paragraph.

- The evaporation rates of 55 and 75 g/h are too high. The corresponding nucleation rate of each species is increased and the growth rate decreased. This decrease leads to small single burkeite crystals which are not recovered at the end of the experiments due to loss upon separation. Furthermore the burkeite agglomeration is very important leading to the formation of large clusters that are detrimental to the cesium decontamination. Finally, sodium carbonate and sodium sulfates are lost through separation due to the low growth rate and high nucleation rate leading to a decreased sodium yield. The higher proportion of small crystal, and the increased nucleation rate led to higher spread in distribution and separation difficulties. Both of these are detrimental to the mother liquor removal and cesium decontamination. A lesser evaporation rate is hence needed to obtain a trimodal population distribution.
- The two evaporation rate of 25 and 35 g/h lead to a trimodal crystal size distribution. The main difference between the two experiments deals with the repartition of sodium carbonate monohydrate and the burkeite agglomeration. With 35 grams per hour evaporation rate the sodium carbonate are recovered at lower sieve sizes and some of them are lost through filtration. Additionally, more single burkeite were lost through filtration while more burkeite agglomerates were

formed. Only a detailed requirement study may determine which process is the best, however it can be inferred from the study that the kinetics are favored by the lowest evaporation rate of 25 g/h.

- The experiments performed at 35 and 45 °C led to high sodium nitrate growth rate associated to high sodium carbonate monohydrate nucleation. Furthermore, the early nucleation of sodium nitrate contributed to high spread in crystal size distribution that is detrimental to the solid liquid separation. Furthermore, for these two low operating temperatures, no burkeite crystals were formed which is detrimental to the sulfate recovery in the solid phase. These arguments are however tampered by the formation of trisodium fluoride sulfate crystals with high nucleation rate and high growth rate.
- The experiments performed at 75 °C also failed to produce significant amounts of burkeite crystals. The small nucleation and growth rate of burkeite and trisodium fluoride sulfate led to poor sulfate recovery. Furthermore, the combination of low sodium nitrate growth rate and high sodium carbonate growth rate led to high spread in crystal distribution. Both of these elements imply that 75 °C is a too high temperature to be applied.
- Both experiments performed at 55 and 66 °C led to a trimodal crystal size distribution. The main discrepancy between the two distributions comes from the increased sodium carbonate growth rate with temperature. Three main elements may be considered in favor of the 66 °C crystallization. First, the agglomeration rate of burkeite crystals is one order of magnitude smaller while the single burkeite growth rate is one order of magnitude higher. Second, the nucleation and

growth rate of sodium sulfate are increased at 66 °C which is beneficial to the sulfate recovery. Finally, the kinetics of sodium carbonate monohydrate and sodium nitrate are close between these two temperatures ensuring close sodium recovery between the two experiments.

4.4.4 EVAPORATIVE FRACTIONAL CRYSTALLIZATION EMPIRICAL MODELING

Empirical Modeling

Table 62 provides the empirical correlations of the average crystal count and average crystal size with the operating time for the early feed evaporative crystallization at 66 °C and 25g/h.

Table 62. Correlations of the average crystal count and average crystal size with operating time for an early feed crystallization at 66 °C and 25 g/h

Crystal Species	Profile Type	Model Equations for Nucleation Rate	Squared fit Correlation
Sodium Nitrate	Linear	$y = 2.10^{8}x - 6.10^{7}$	0.99
Sodium Carbonate Monohydrate	Linear	$y = 2.10^{7}x - 7.10^{6}$	0.99
Burkeite Crystals	Logarithmic	$y = 5.10^{7}Ln(x) + 7.10^{7}$	0.83
Sodium Sulfate	Linear	$y = 2.10^{7}x - 4.10^{6}$	0.97
Sodium Oxalate	Linear	$y = 3.717.10^{5}x - 1.132.10^{3}$	0.86
Crystal Species	**Profile Type**	**Model Equations for Growth Rate**	**Squared fit Correlation**
Sodium Nitrate	Linear	$y = 0.742x - 6.352.10^{2}$	0.84
Sodium Carbonate Monohydrate	Power law	$y = 2.10^{8}x^{3.107}$	0.99
Burkeite Crystals	Linear	$y = 0.366x - 2.199.10^{2}$	1
Sodium Sulfate	Power law	$Y = 0.204x^{-104.6}$	0.99
Sodium Oxalate	Power law	$y = 2.700.10^{-3}x^{1.470}$	0.99

These equations were computed by using a fitting line of the series of data points and the corresponding squared fit correlations are displayed. Please note that in this model we considered the type of profiles that provided the best correlation of data.

Evaporation Rate Modeling

Table 63 displays the empirical correlations of the evolution of the specific kinetics with the evaporation rate for an early feed crystallization operated at 66 °C.

Table 63. Correlations of the average nucleation and growth rate with evaporation rate for an early feed crystallization at 66 °C

Crystal Species	Profile Type	Model Equations for Nucleation Rate	Squared Fit Correlation
Sodium Nitrate	Linear	$y = 2.386.10^3x - 2.337.10^4$	1
Sodium Carbonate Monohydrate	Binomial	$y = -38.60x^2 + 3.517.10^3x - 6.052.10^4$	1
Burkeite Crystals	Binomial	$y = 3.497.10^2x^2 - 2.045.10^4x + 3.357.10^5$	1
Burkeite Agglomerates	Linear	$y = 1.057.10^3x - 2.277.10^4$	0.96
Sodium Sulfate	Binomial	$y = -19.1x^2 + 2.241.10^3x - 4.132.10^4$	1
Sodium Oxalate	Linear	$y = 2.286.10^2x - 6.373.10^3$	0.93
Crystal Species	**Profile Type**	**Model Equations for Growth Rate**	**Squared Fit Correlation**
Sodium Nitrate	Linear	$y = -0.022x + 2.1$	0.93
Sodium Carbonate Monohydrate	Linear	$y = -0.003x + 0.22$	0.89
Burkeite Crystals	Linear	$y = -0.002x + 0.23$	0.99
Burkeite Agglomerates	Linear	$y = 0.009x - 0.24$	0.98
Sodium Sulfate	Linear	$y = -0.001x + 0.32$	0.88
Sodium Oxalate	Linear	$y = -0.003x + 0.28$	0.99

Temperature Modeling

Table 64 displays the empirical correlations of the evolution of the specific kinetics with the operating teperature for an early feed crystallization operated at 25 g/h evaporation rate.

Table 64. Correlations of the average nucleation and growth rate with operating temperature for an early feed crystallization at 25 g/h evaporation rate

Crystal Species	Profile Type	Model Equations for Nucleation Rate	Squared Fit Correlation
Sodium Nitrate	Linear	$Y = 1.284.10^{3}x - 4.813.10^{4}$	0.99
Sodium Carbonate Monohydrate	Linear	$Y = -1.556.10^{2}x + 1.342.10^{4}$	0.99
Burkeite Crystals	Linear	$Y = -2.266.10^{2}x + 5.182.10^{4}$	1
Burkeite Agglomerates	Linear	$Y = -1.763.10^{3}x + 1.225.10^{5}$	1
Sodium Sulfate	Linear	$Y = 1.539.10^{2}x - 6.843.10^{3}$	0.95
Trisodium Fluoride Sulfate	Linear	$Y = -4.205.10^{3}x + 3.155.10^{5}$	1
Crystal Species	**Profile Type**	**Model Equations for Growth Rate**	**Squared Fit Correlation**
Sodium Nitrate	Power Law	$y = 2.114.10^{3}x\text{-}1.67$	0.82
Sodium Carbonate Monohydrate	Power Law	$y = 1.200.10^{-3}x1.17$	0.97
Burkeite Crystals	Linear	$y = 1.200.10^{-2}x - 0.66$	1
Burkeite Agglomerates	Linear	$y = 1.300.10^{-3}x - 0.048$	1
Sodium Sulfate	Linear	$y = 9.900.10^{-3}x - 0.37$	0.94
Sodium Oxalate	Power Law	$y = 6.700.10^{-3}x0.78$	0.93
Trisodium Fluoride Sulfate	Linear	$y = -5.000.10^{-3}x + 0.59$	1

4.4.5 LINKING EXPERIMENTAL RESULTS TO CLASSICAL NUCLEATION THEORY

In this study we consider the evolution of the supersaturation with operating time for sodium nitrate and sodium carbonate monohydrate crystals produced during evaporative crystallization of early feeds. Supersaturation is here defined as the ratio of the solute concentration, *C*, to the concentration at saturation, *C**. The saturation values obtained from the thermodynamic simulations are used in the calculations. Figure 142 and Figure 143 display the evolution of sodium nitrate and sodium carbonate monohydrate supersaturations during crystallizations at 25 g/h evaporation and various operating temperatures. The classic nucleation theory is used to develop a model of the nucleation rate variation with the supersaturation, operating temperature and evaporation rate. Model parameters are determined from experimental values of the nucleation rate at different temperatures and evaporation values. The determination of the model parameters is performed by assuming that nucleation occurs at saturation.

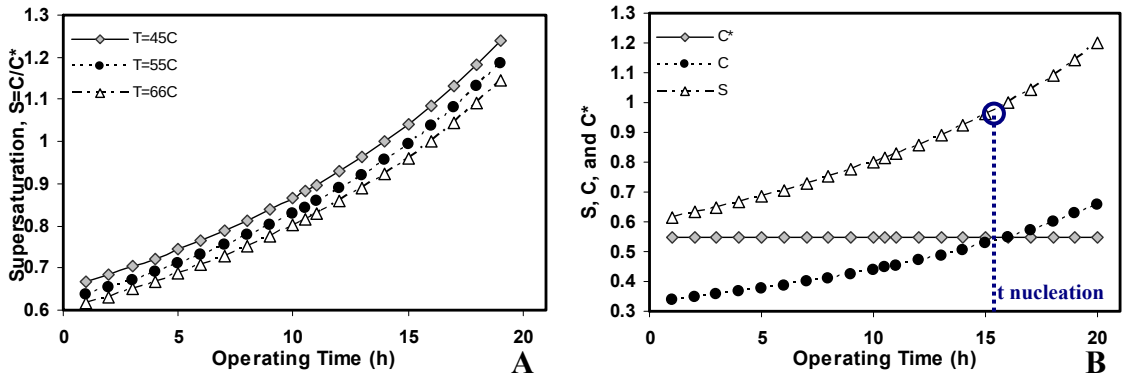

Figure 142. Evolution of sodium nitrate supersaturation at 25 g/h evaporation for various operating temperatures (Panel A) and at 66°C (Panel B)

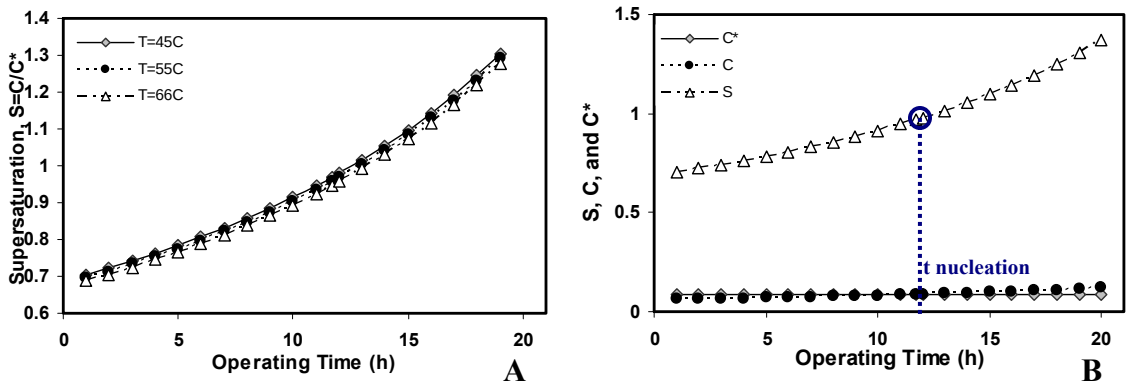

Figure 143. Evolution of sodium carbonate monohydrate supersaturation at 25 g/h evaporation for various operating temperatures (Panel A) and at 45°C (Panel B)

Classic nucleation theory

Randolph and Larson demonstrated that the free-energy change describing the homogenous nucleation of a crystal from the feed solution is given by:

$$\Delta G = \Delta G_S + \Delta G_V$$

where ΔGs is the free-energy change necessary to form the nucleus surface, and ΔGv is the bulk free-energy change per unit volume.

Assuming a spherical nucleus of radius r and specific surface energy σ, the free-energy change can written as

$$\Delta G = 4\pi \cdot r^2 \sigma + (4/3)\pi \cdot r^3 \Delta G_V$$

The nucleation rate is generally expressed as an Arrhenius-type equation

$$B^\circ = C \exp\left(\frac{-\Delta G^*}{kT}\right)$$

where k is the Boltzmann's constant, v is the molecular volume, and ΔG^* is the critical free-energy change to form a critical radius r_c defined as

$$r_c = \frac{-2\sigma}{\Delta G_V}$$

The nucleation rate $B°$ is hence given by

$$B^\circ = C\exp\left(\frac{-16\pi\sigma^3 v^2}{3k^3T^3(\ln(S))^2}\right)$$

The nucleation rate $B°$ can be empirically expressed as

$$B^\circ = J = A\dot{V}^j \exp\left(\frac{-a}{T^3(\ln(S))^2}\right)$$

And becomes in logarithmic form

$$\ln B^\circ = \ln(A) + j\ln(\dot{V}) + \left(\frac{-a}{T^3(\ln(S))^2}\right)$$

where A and a are two constants and V is the evaporation rate.

Example of calculation

Table 65 displays the values of the nucleation concentration calculated based on the evaporation rate and saturation concentration estimate for sodium nitrate and sodium carbonate monohydrate at various temperatures. The supersaturations at nucleation were all close to 1. In order to perform the calculations the supersaturations at nucleation were taken at 1.01.

Table 65. Nucleation and saturation values for sodium nitrate and sodium carbonate monohydrate at various operating temperatures

	Sodium Nitrate			Sodium Carbonate Monohydrate		
Operating Temperature	**45**	**55**	**66**	**45**	**55**	**66**
$t_{nucleation}$	631	582	904	701	700	631
C*	0.50	0.52	0.55	0.09	0.09	0.09
$C_{nucleation}$	0.45	0.44	0.55	~0.09	~0.09	~0.09
$S_{nucleation}$	0.9 (~1)	0.9 (~1)	1	~1	~1	~1

For sodium nitrate, the average nucleation rate at 45 °C and 55 °C are 9.267×10^{3} and 2.329×10^{4} crystals / mL·min respectively. Implementing these values in the nucleation model leads to the system of two equations:

$$18.86 = \ln(A) + j\ln(-4.96) + a(-0.11)$$

$$19.78 = \ln(A) + j\ln(-4.96) + a(-0.06)$$

Similarly, the average nucleation rate at 35 g/h and 55 g/h evaporation rate are 6.014×10^{4} and 1.078×10^{5} crystals / mL·min respectively. Implementing these values in the nucleation model leads to the system of two equations:

$$20.73 = \ln(A) + j\ln(-4.63) + a(-0.035)$$

$$21.31 = \ln(A) + j\ln(-4.18) + a(-0.035)$$

Substracting the first two equations provide a value for a of 18.4 °C^3. Substracting the last two equations leads to $j = 1.28$. Finally, solving the system for A, provides a value of $A = 7.11\times10^{11}$.

Nucleation rate dependence to temperature and evaporation rate

The values of parameters a, A and j are implemented to the nucleation model to determine the influence of supersaturation on nucleation rate. For sodium nitrate the resulting equation is:

$$\ln B^{\circ} = 27.27 + 1.28\ln(\dot{V}) + \left(\frac{-18.4}{T^{3}\ln(S)^{2}}\right)$$

Figure 144 displays the variation of sodium nitrate nucleation rate with supersaturation for different operating temperatures and evaporation rates. The graphs show that sodium nitrate nucleation rate increases linearly with supersaturation. The variations in temperature have a greater influence on nucleation at lower supersaturation.

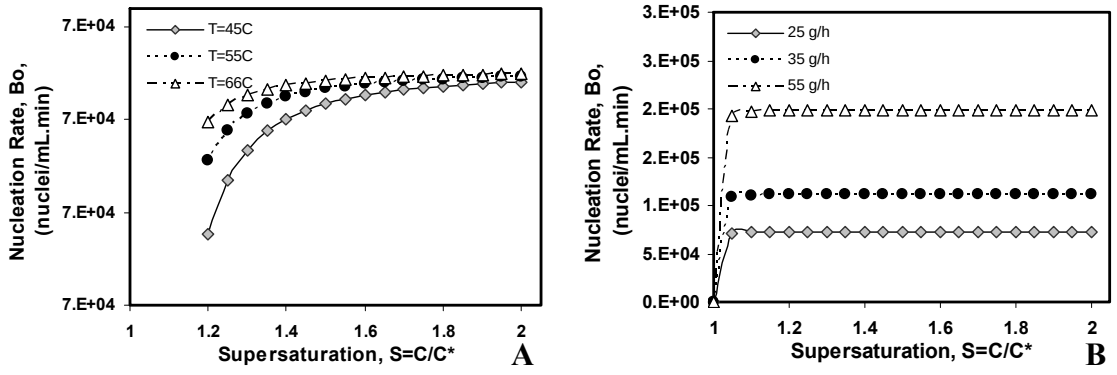

Figure 144. Variation of sodium nitrate nucleation rate with supersaturation at various operating temperatures (Panel A) and evaporation rates (Panel B)

Assessing the case of sodium carbonate monohydrate, similar methodology was applied leading to the nucleation rate model:

$$\ln B^{\circ} = 18.32 + 0.11\ln(\dot{V}) + \left(\frac{6.6}{T^3 \ln(S)^2}\right)$$

Figure 145 presents the variation of sodium carbonate monohydrate nucleation rate with supersaturation, displaying that the nucleation rate increases with supersaturation value. Panel A shows that the operating temperature has an effect of the nucleation rate variation at low supersaturation values. Panel B displays that the evaporation rate has minimal impact on nucleation rate variation with supersaturation.

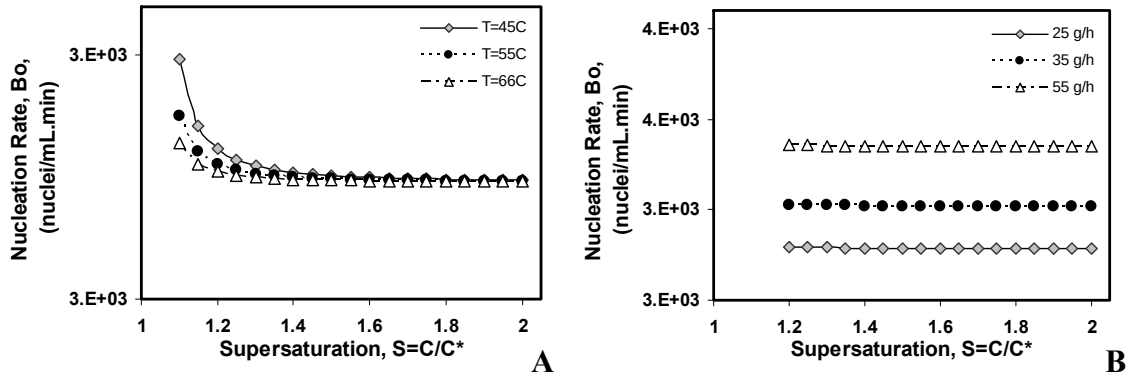

Figure 145. Variation of sodium carbonate monohydrate nucleation rate with supersaturation at various operating temperatures (Panel A) and evaporation rates (Panel B)

4.5 CRYSTALLIZATION FROM SINGLE SOLUTE FEED SOLUTION

A series of experiments were performed with single sodium nitrate and single sodium carbonate feed solutions. These evaporative crystallization experiments were performed in order to define nucleation and growth rates for single species in solutions. The single-salt kinetics are to be used as parameters for the continuous crystallizer model and to be compared to the kinetics of these species in a multi salt early feed solution. Two main variables are to be considered when performing these experiments: (1) the pH of the solution, and (2) the ionic strength of the solution. The early feed solution is very basic (pH > 14) and the basicity is maintained in the simulant feed by the high concentration in sodium hydroxide. Sodium hydroxide was hence added to the single salt solution in order to keep an identical pH for the single and multi salt feed solutions. Furthermore, the removal of the other sodium salts present in the early feed solution will reduce the ionic strength and delay the nucleation point of the single species. To assess this effect, the operating time after nucleation was recorded for the early feed certification run and a similar time was applied to the single salt experiments. This allowed: (1) recovery of crystal distribution histograms directly comparable to the multi salt distribution histograms and (2) obtaining accurate estimates of the specific kinetics in single salt solutions. Single-salt crystallizations of sodium nitrate and sodium carbonate monohydrate were performed at 66 °C and with an evaporation rate of 25 g/h. Figure 146 displays the graph of the mass of water evaporated with the operating time and the temperature and pressure profiles for the two single-solute crystallization.

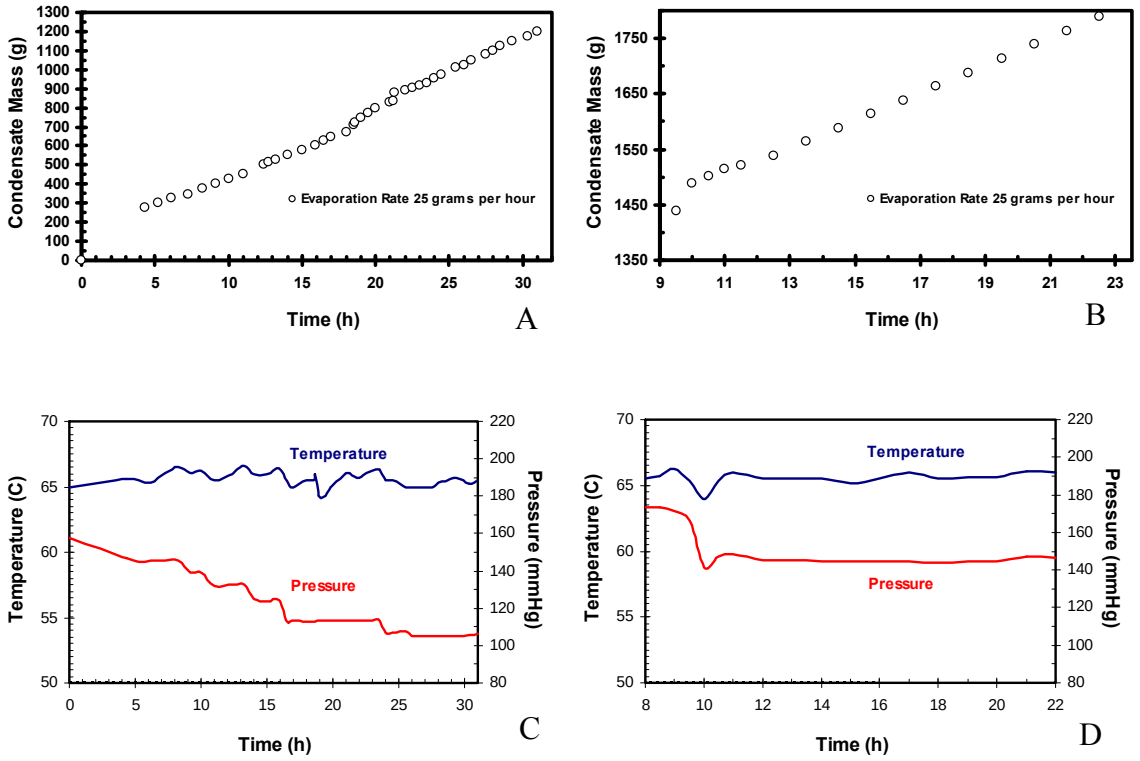

Figure 146. Evaporation, temperature and pressure profiles of single-salt sodium nitrate (A and C) and sodium carbonate (B and D) crystallization experiments performed at 66 °C 25 g/h evaporation rate

4.5.1 SODIUM NITRATE CRYSTALLIZATION

The evolution of the crystal size and number was determined based on the PLM analyses of slurry samples taken at regular time intervals, using the methodology described in Chapter 2. Figure 147 displays the PLM images taken from the slurry of the single-solute sodium nitrate run. Panels A and B shows that sodium nitrate was detected at C:F= 0.435. Panels C to F shows that the sodium nitrate crystals were nucleated and grown for the remaining of the experiment. Table 66 compares the nucleation point of sodium nitrate in the single-solute and early feed solution crystallization. The earlier detection point of sodium nitrate in the early feed crystallization is explained by the reduction in the ionic strength for a single-salt solution. Following the similar conditions

as the base case, the experiment was performed for 19.5 hours to allow similar operating time of sodium nitrate crystals after nucleation.

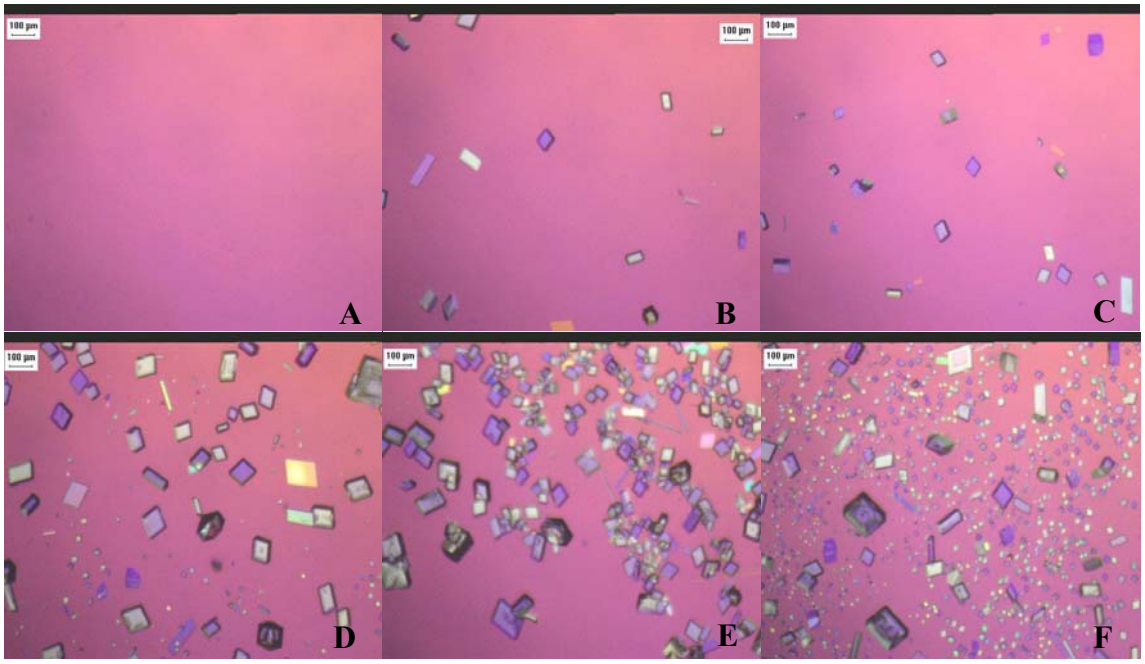

Figure 147. PLM images from sample analysis of single-salt sodium nitrate crystallization at 66 °C and 25 g/h evaporation rate
(Panel A, C:F= 0.410, Panel B, C:F=0.435, Panel C, C:F= 0.441, Panel D, C:F= 0.445, Panel E, C:F= 0.457, Panel F, C:F=0.478)

Table 66. Comparison of sodium nitrate nucleation points for single- and multi salt crystallization at 66 °C and 25 g/h evaporation rate

SST Early Feed	Condensate To Feed Ratio At Nucleation	Operating Time At Nucleation (min)
Sodium Nitrate (Multi-Salt)	0.247	466
Sodium Nitrate (Single-Salt)	0.345	744

The specific nucleations were determined following the methodology described in Chapter 2. Figure 148 presents the evolution of the crystal total count with the operating time for single-salt sodium nitrate crystallization at 66 °C. Sodium nitrate presents a low nucleation rate until reaching 200 minutes after the start of the run and then a constant nucleation rate. The profile follows a linear profile with a low initial slope. The average

estimated value of 5.066×10^{3} crystals/ mL·min was found for sodium nitrate. This nucleation rate is lower than the one found for the multi salt evaporative crystallization of 3.627×10^{4} crystals/ mL·min.

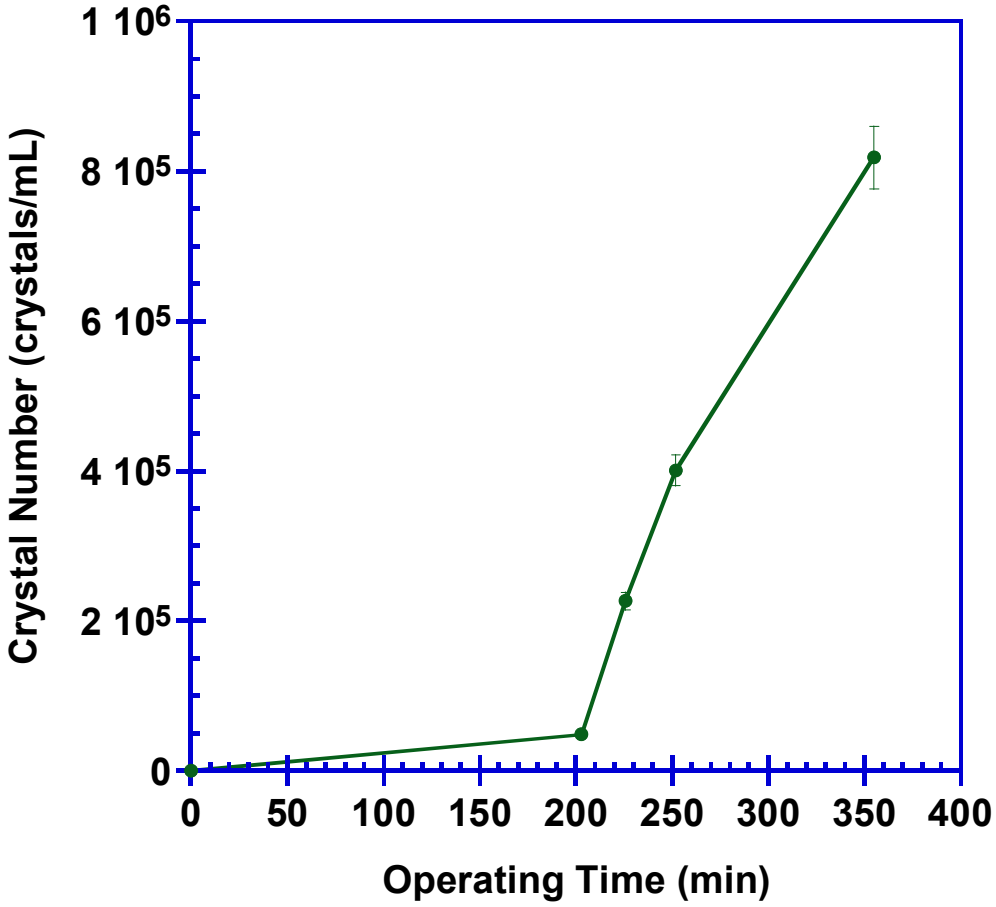

Figure 148. Sodium nitrate total crystal count evolution with operating time for single-salt sodium nitrate crystallization at 66 °C and 25 g/h evaporation rate

The size of the crystals was monitored for each sample recovered from the slurry. Figure 149 displays the evolution of the average crystal length with the operating time for single-salt sodium nitrate crystallization at 66 °C. The methodology used to compute the specific average growth rate was outlined in Chapter 2.

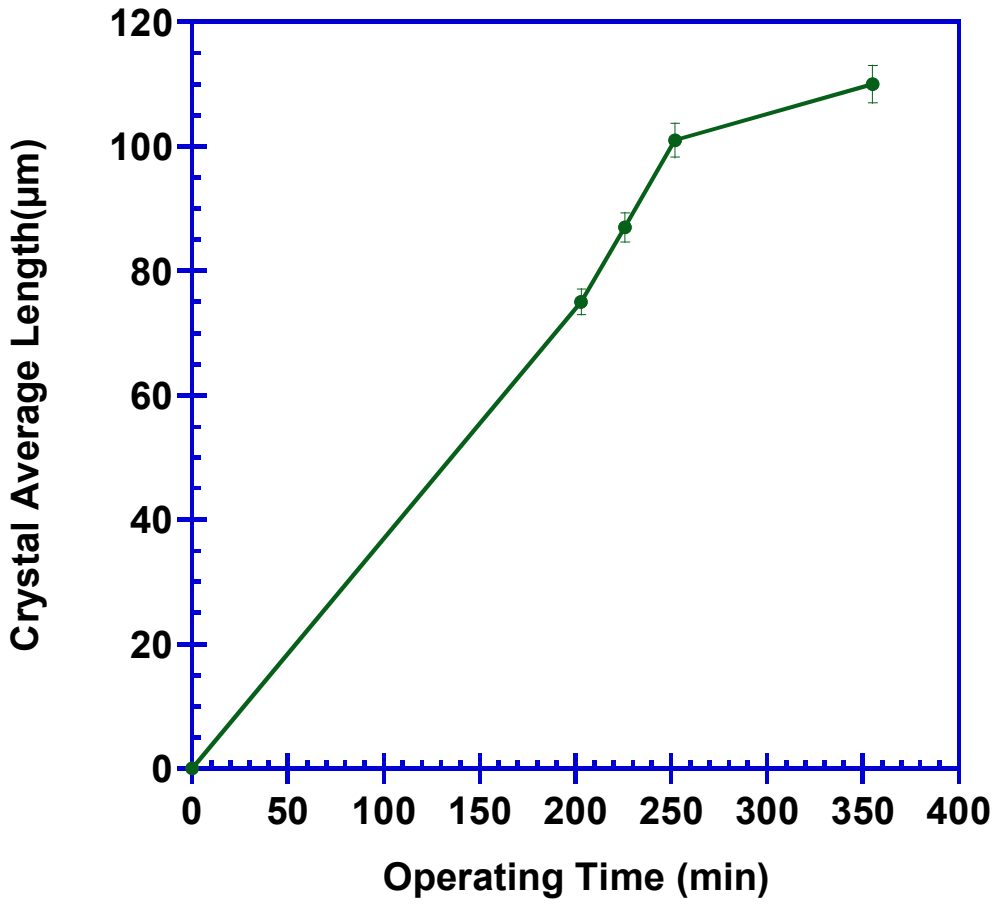

Figure 149. Evolution of sodium nitrate average length wth operating time for single-salt crystallization at 66 °C and 25 g/h evaporation rate

Sodium nitrate follows an exponential or power law profile with an average growth rate of 2.310 µm·min^{-1}. The average growth rate was hence increased compared to the multi-salt crystallization. Table 67 presents a comparison of sodium nitrate average nucleation and growth rates for the single and multi salts feed solution.

Table 67.Comparison of sodium nitrate average kinetics for single- and multi-salts crystallization at 66 °C and 25 g/h evaporation rate

SST Early Feed	Nucleation Rate (crystals/ mL·min)	Growth Rate (µm·min^{-1})
Sodium Nitrate (Single-Salt Solution)	5.066×10^{3}	2.310
Sodium Nitrate (Multi-Salt Solution)	3.628×10^{4}	1.680

A fraction of the crystals obtained at the end of the crystallization was washed with acetone as outlined in Chapter 2 and allowed to air dry. The crystals were then subjected to sieving. Figure 150 shows the resulting mass density distribution for the sodium nitrate single-salt crystallization experiment.

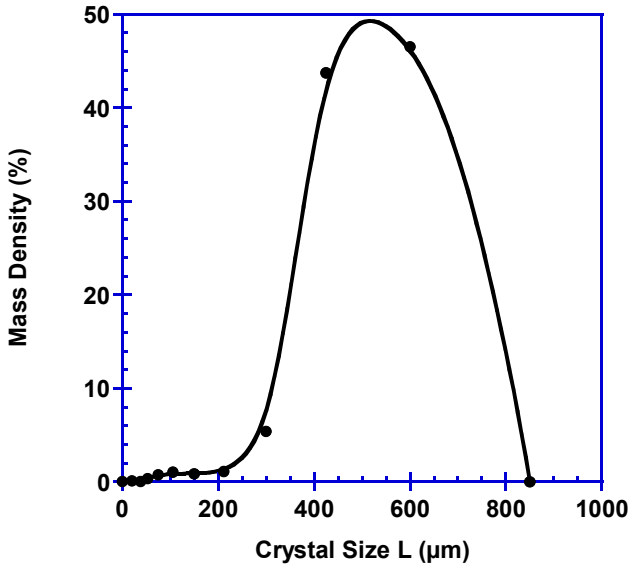

Figure 150. Mass density distribution for sodium nitrate crystallization experiment at 66 °C and 25 g/h evaporation rate

The mass density distribution displays a single mode size around 550 μm. In addition, the curves show that only 0.5% of the crystal mass is below 100 μm displaying a very low amount of fines or smaller size crystals. This resulting crystal distribution is in agreement with an increased growth rate and a lower nucleation rate. The distribution was narrow around the mode size with a coefficient of variation of 25.8%.

4.5.2 SODIUM CARBONATE MONOHYDRATE CRYSTALLIZATION

The evolution of the crystal size and number was determined based on the PLM analyses of slurry samples taken at regular time intervals, using the methodology described in Chapter 2. Figure 151 displays the PLM images taken from the slurry of the

single-solute sodium carbonate run. Panels A and B shows that sodium carbonate monohydrate was detected at a condensate-to-feed ratio of 0.728. Panels C to F shows that the sodium carbonate monohydrate crystals were nucleated and grown for the remaining of the experiment. Table 68 compares the nucleation point of sodium carbonate monohydrate in the single-solute and early feed solution crystallization. The earlier detection point of sodium carbonate monohydrate in the early feed crystallization is explained by the reduction in the ionic strength for a single-salt solution. Following the similar conditions as the base case, the experiment was performed for 11.5 hours to allow similar operating time of sodium carbonate monohydrate crystals after nucleation.

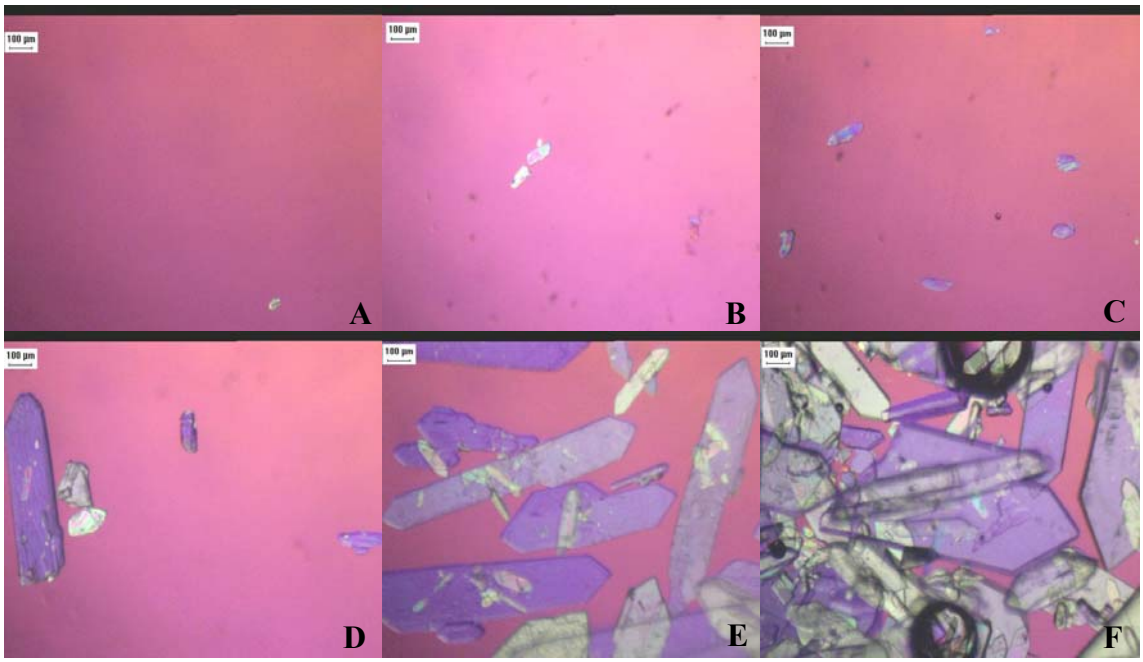

Figure 151. PLM images from sample analysis of single-salt sodium carbonate monohydrate crystallization at 66 °C and 25 g/h evaporation rate
(Panel A, C:F= 0.728, Panel B, C:F= 0.730, Panel C, C:F= 0.739, Panel D, C:F= 0.744, Panel E, C:F= 0.748, Panel F, C:F= 0.753)

Table 68. Comparison of sodium carbonate monohydrate nucleation points for single- and multi salt crystallization at 66 °C and 25 g/h evaporation rate

SST Early Feed	Condensate To Feed Ratio At Nucleation	Operating Time At Nucleation (min)
Sodium Carbonate Monohydrate (Multi-Salt)	0.298	631
Sodium Carbonate Monohydrate (Single-Salt)	0.728	636

The specific nucleations were determined following the methodology described in Chapter 2. Figure 152 presents the evolution of the crystal total count with the operating time for single-salt sodium carbonate crystallization at 66 °C. Sodium carbonate monohydrate presents a low nucleation rate until reaching 230 minutes after the start of the run and then a constant nucleation rate. The total crystal count profile follows a linear profile with a low initial slope. The average estimated value of 1688 crystals/ mL·min was found for sodium carbonate monohydrate. This nucleation rate is lower than the one found for the multi salt evaporative crystallization (3245 crystals/ mL·min).

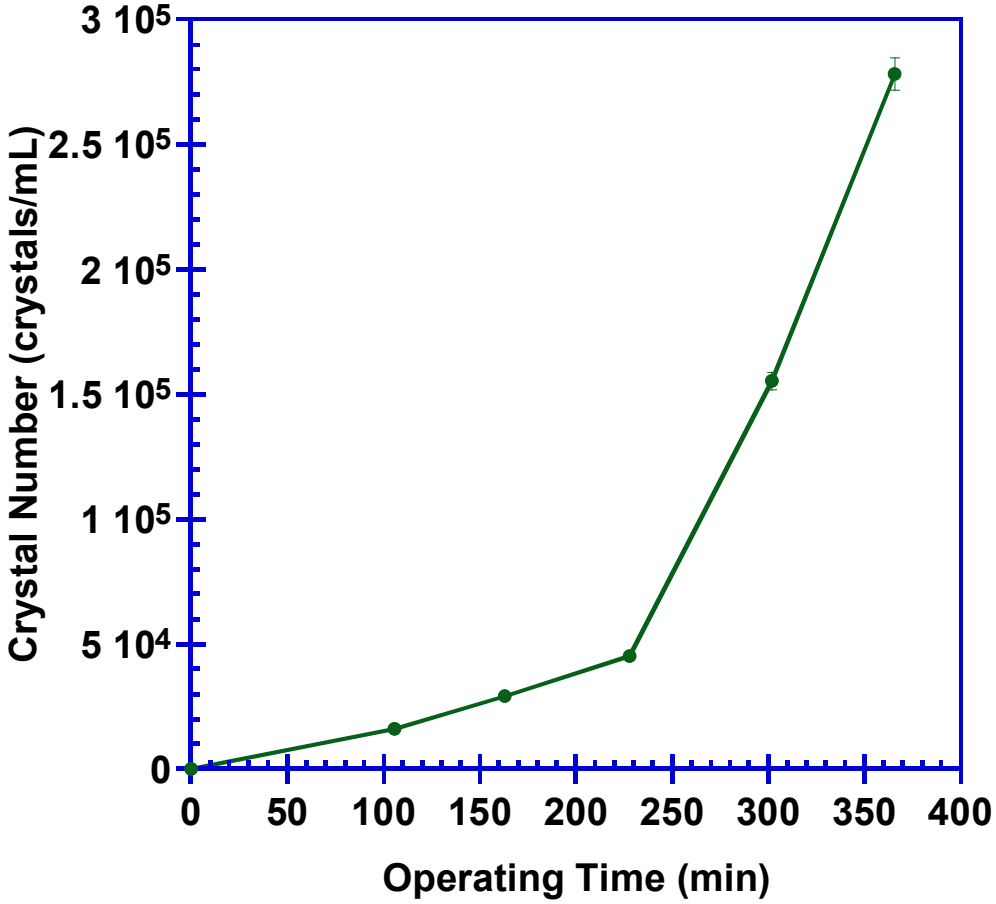

Figure 152. Sodium carbonate monohydrate total crystal count evolution with operating time for single-salt sodium nitrate crystallization at 66 °C and 25 g/h evaporation rate

The average size of the crystals was monitored for each sample recovered from the slurry. Figure 153 shows the evolution of the average crystal length evolution with the operating time obtained for single-salt sodium carbonate crystallization experiment at 66 °C. The methodology used to compute the average growth rate was outlined in Chapter 2.

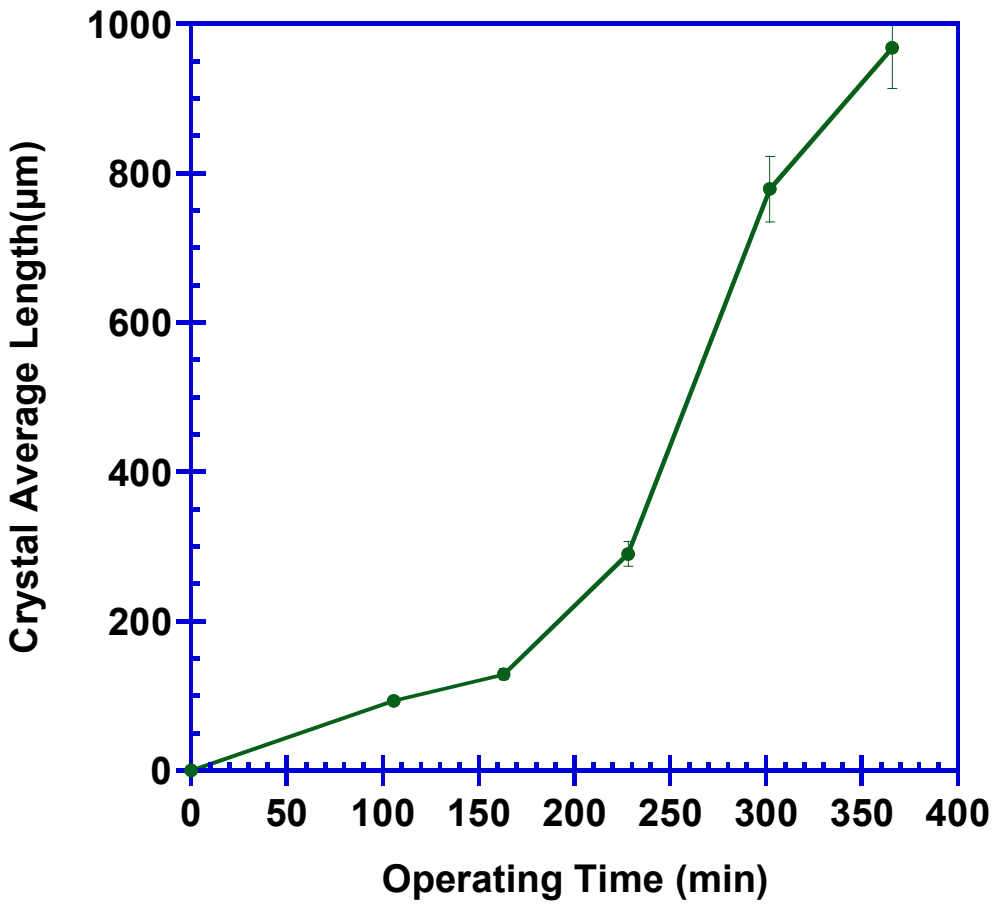

Figure 153. Evolution of sodium carbonate monohydrate average length wth operating time for single-salt crystallization at 66 °C and 25 g/h evaporation rate

Sodium carbonate monohydrate follows an exponential or power law profile with an average growth rate of 3.360 µm·min^{-1}. The average growth rate was hence increased by more than one order of magnitude compared to the multi salt crystallization. Table 69 presents a comparison of sodium nitrate average nucleation and growth rates for the single and multi salts feed solution.

Table 69. Comparison of sodium carbonate monohydrate average kinetics for single- and multi-salts crystallization at 66 °C and 25 g/h evaporation rate

SST Early Feed	Nucleation Rate (crystals/ mL·min)	Growth Rate (µm·min^{-1})
Sodium Carbonate Monohydrate (Multi-Salt)	3.245×10^{3}	0.158
Sodium Carbonate Monohydrate (Single-Salt)	1.688×10^{3}	3.360

A fraction of the crystals obtained at the end of the crystallization was washed with acetone as outlined in Chapter 2 and allowed to air dry. The crystals were then subjected to sieving. Figure 154 shows the resulting mass density distribution for the sodium carbonate single-salt crystallization experiment.

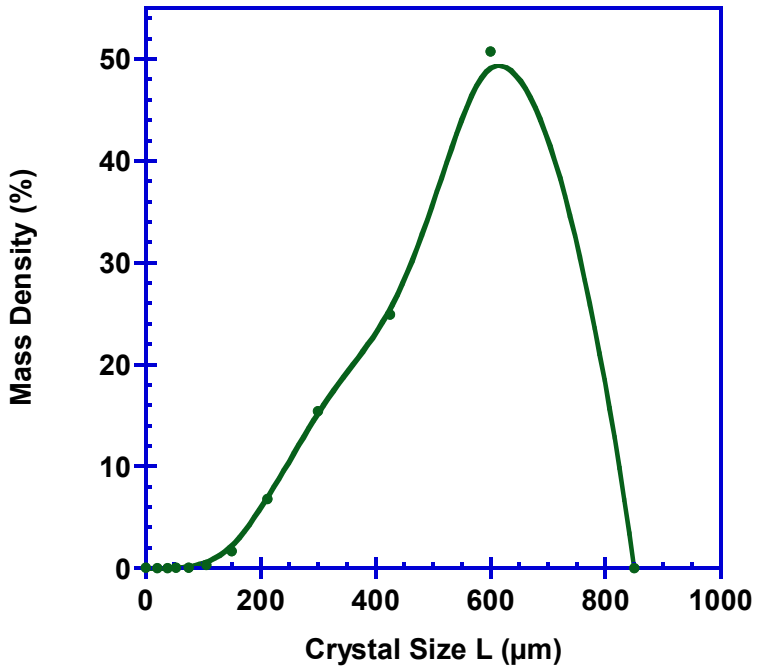

Figure 154. Mass density distribution for sodium carbonate crystallization experiment at 66 °C and 25 g/h evaporation rate

The mass density distribution displays a single mode size around 600 µm. In addition, the curves show that only 0.05% of the crystal mass is below 100 µm displaying a very low amount of fines or smaller size crystals. This resulting crystal distribution is in agreement with a large increase in growth rate and a lower nucleation rate. The distribution was narrow around the mode size with a coefficient of variation of 33.9%.

4.5.3 CRYSTAL SIZE DISTRIBUTION COMPARISON WITH MULTI-SALTS FEED SOLUTION

Figure 155 compares the crystal size distribution histograms for the single- and multi-salts feeds crystallization. In case of identical kinetics, the summation of the single profiles should overlap with the multi salts histogram. However, the growth rates of sodium nitrate and sodium carbonate were increased for the single salt solutions leading to profiles with a higher mode size than the trimodal early feed crystallization.

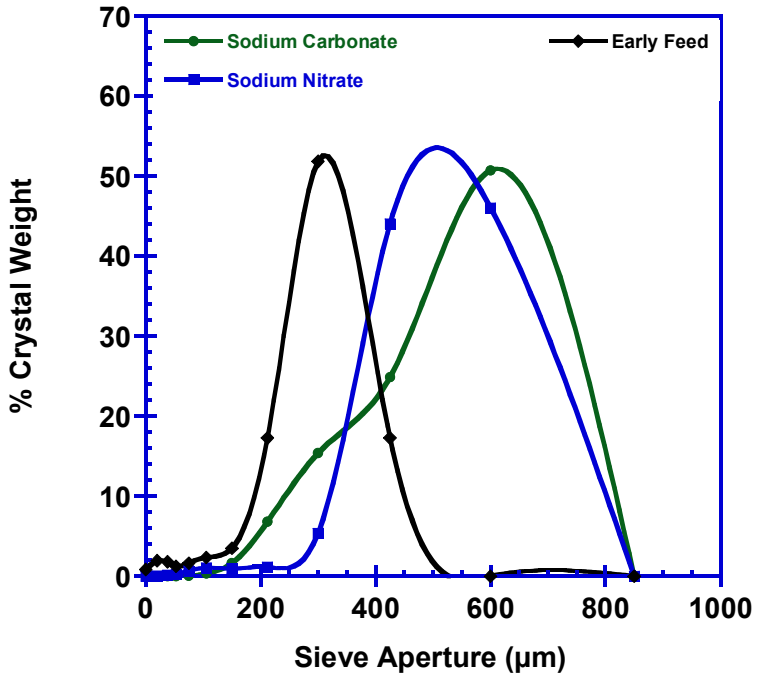

Figure 155. Comparison of the crystal size distribution histograms from the sodium nitrate, sodium carbonate single-salt feeds crystallization and early feed crystallizations: runs were performed at 66 °C and 25 g/h evaporation rate

CHAPTER 5: MODELING OF MULTIPLE SPECIES SIMULANT SOLUTIONS CRYSTALLIZATION IN CONTINUOUS CRYSTALLIZER

In the previous chapter we developed empirical correlations describing nucleation of the three main species (sodium nitrate, sodium carbonate monohydrate and burkeite crystals) at the system conditions of the Early-Feed semi-batch experiments. These correlations were developed using kinetics determined with a semi-batch process over the range of 45 to 75 °C and 25 g/h to 75 g/h. However, the pilot and large-scale pretreatment of the waste will be performed with a continuous process using a crystallizer from the group shown schematically in Figure 156.

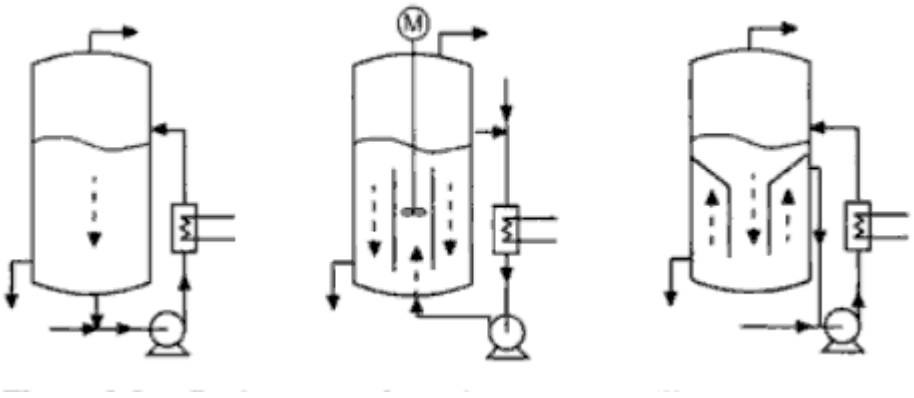

Figure 156. Basic types of continuous crystallizer used industrially
(Figure from Crystallization technology handbook, by Alfons Mersmann, ebrary, Inc, Published by CRC Press, 2001, ISBN 0824705289, 9780824705282)

It is the objective of this chapter to provide a simple model for continuous steady-state operation. The model will display the population density function of the product mixture by computing the specific population density function for each of the three main

species formed. The semi-batch specific nucleation and growth rates will be used in the model.

5.1 CONTINUOUS EVAPORATIVE CRYSTALLIZATION MODEL

5.1.1 MSMPR OPERATING CONDITIONS

During Phase III of the Hanford waste remediation project, described in Chapter 1, the radioactive wastes are to be processed in a continuously operated Mixed Suspension Mixed Product Removal crystallizer (MSMPR). Figure 157 displays the flowsheet of the Hanford waste remediation steady-state continuous process to be implemented at pilot-scale. The continuous crystallizer is to be operated following six major steps: (1) low- and medium-curie early and late feed wastes are introduced to the pretreatment feed pipe, (2) the feed is heated to the operating temperature of 66 °C for the early feed and 60 °C for the late feed crystallization and introduced to the constant volume crystallizer, (3) solvent is removed from the system by generating water vapor, (4) crystals are formed in the vessel and removed from the crystallizer at a defined volumetric flow rate and after a specific residence time, (5) the slurry is submitted to solid-liquid separation performed by centrifugation and crystals are washed, (6) the crystals are dissolved and collected as a liquid Low Activity Waste (LAW) to be treated by bulk vitrification while the liquid recovered from centrifugation and washing are collected as liquid High Level Waste (HLW) and will be disposed in the Hanford storage tank before being submitted to Vitrification in the Waste Treatment Plant (WTP).

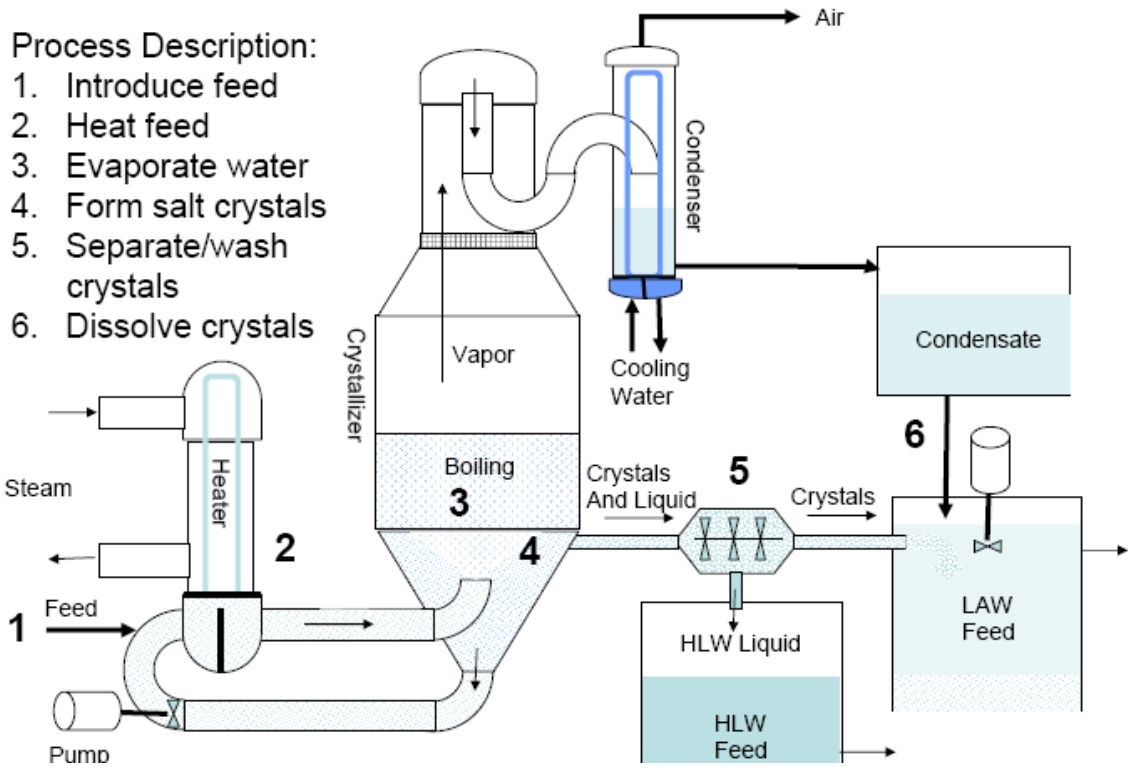

Figure 157. Schematic of the steady-state continuous crystallizer to be implemented at pilot scale at Hanford site and operated at 66 °C on early feed and 60 °C on late feed wastes
(Source: http://srnl.doe.gov/techex/PDFs/3b_2_Herting.pdf, November 2008)

In this section a set of assumptions will be made for the correlation between the operating conditions of the semi-batch process described in Chapter 2 and the continuous crystallizer to be implemented at pilot scale. These assumptions allow using average growth and specific nucleation rates developed. The following assumptions were made (Randolph and Larson; 1988):

- The semi-batch process was performed isothermally by controlling the pressure in the apparatus while the continuous crystallizer is to be operated at both constant temperature and pressure. In this study we will assume that the pressure variation does not affect the nucleation and growth kinetics.

- A constant operating volume is maintained in the crystallizer. The semi-batch process accomplished this goal by regular feed addition during the experiment. The continuous crystallizer uses a specific volumetric flow rate which is dependant on the crystallizer volume and the residence time. In this study we will assume that the residence time applied to the continuous crystallizer is 12 hours which corresponds to the exact growth time of sodium carbonate monohydrate and burkeite crystals in a semi-batch process. This residence time corresponds to the average between the growth time of sodium nitrate crystals at first and second nucleation.
- In a continuous crystallizer, the change in residence time may affect the values of the specific nucleation rate (B°) and growth rate (G). In this section, the study will be performed with a single residence time that corresponds to the growth time of crystals in the semi-batch process and for which the kinetics were experimentally determined.
- In the semi-batch crystallizer, water vapor was generated by circulating hot heating fluid in the double jacket of the crystallizer. The fixed flow rate and temperature of the heating fluid results in a constant evaporation rate. In this study we will assume that the evaporation is performed in the same manner in the semi-batch and continuous apparatus. This assumption will be used to simulate the effect of the evaporation rate on the resulting population density function.
- The mixing in the semi-batch crystallizer was provided by a mechanical stirrer associated with equally spaced baffles. In the continuous apparatus, mixing is typically provided by the pumping of the feed solution inside the crystallizer

(mixed suspension) which creates sufficient suspension to the slurry. In this study we assumed that the total contents of the crystallizer (solution and crystals) are perfectly mixed.

- Semi-batch crystallization of simulated wastes mainly displays primary nucleation mechanism with minor effects of secondary nucleation for burkeite (agglomeration) and sodium oxalate (breakage). We aknowledge that large-scale continuous crystallization processes are different in that secondary nucleation is the principal type of nucleation occurring. This discrepancy will not be taken into account in this chapter as we assume that both semi-batch and continuous processes are solely based on primary nucleation.

5.1.2 MODEL ASSUMPTIONS

We will use a set of four assumptions in the MSMPR model: (1) the process is performed at steady-state, meaning that there is no time-dependence considered in the model, (2) the growth rate is independent of size and without growth rate dispersion, meaning that all crystals of a given species grow at the same rate, (3) no agglomeration, breakage, attrition, agglomeration or classification effects are considered, and (4) crystal-free solution is added to the crystallizer and the slurry is removed isokinetically from the perfectly mixed suspension.

5.1.3 CONTINUOUS POPULATION BALANCE MODEL AT STEADY STATE

Figure 158 displays the simplified schematic notations used in this section and for the modeling of the steady-state continuous crystallizer and diagram associated with a steady state MSMPR crystallizer.

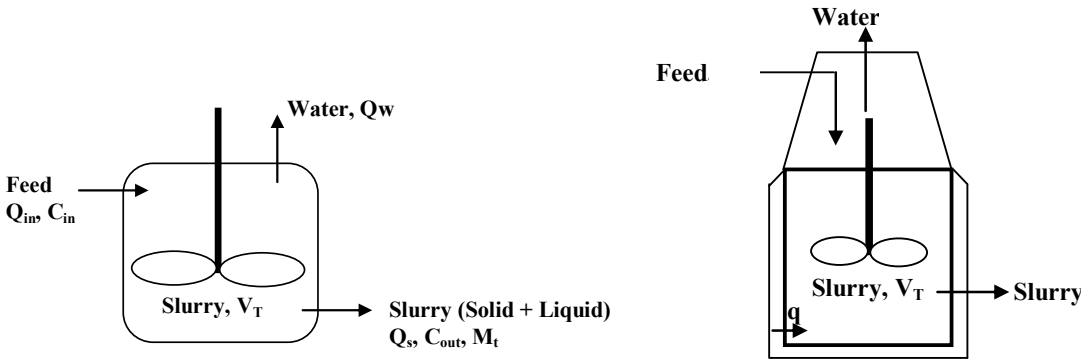

Figure 158. Simplified schematics and notations associated with a steady-state MSMPR continuous crystallizer

Population Balance equation for MSMPR

The population balance in an MSMPR crystallizer operated continuously at steady-state is written (Randolph and Larson; 1988):

$$\frac{d[n(L)]}{dL} = \frac{n \cdot Q_{\text{in}}}{V} - \frac{n \cdot Q_{\text{out}}}{V} - \frac{d[G \cdot n]}{dL} \tag{15}$$

Since there is no accumulation and n_{in} equals 0, equation 15 becomes:

$$\frac{d[G(L) \cdot n(L)]}{dL} + \frac{n(L)}{\tau} = 0 \tag{16}$$

With the given assumptions:

$$\frac{dn}{dL} = -\frac{n}{G \cdot \tau} \tag{17}$$

Where τ represents the residence time calculated as:

$$\tau = \frac{V_{\text{T}}}{Q_{\text{out}}} \tag{18}$$

Where V_T is the total active volume of the crystallizer and Q_{out} is the volumetric flow rate from the crystallizer. The residence time is set by the desired production rate typically fixed when designing a process.

The population density plot for a steady-state MSMPR crystallizer is shown in Figure 159:

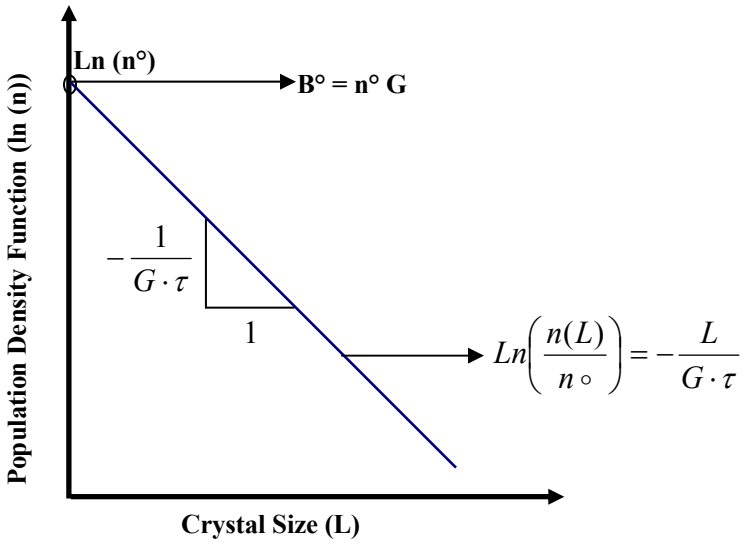

Figure 159. Semi-log representation of the population density function evolution with respect to the crystal size obtained for a steady-state MSMPR crystallizer

Using the initial condition ($n = n°$ at $L = 0$) the population balance of the steady-state MSMPR can be rewritten as:

$$n = n^{\circ}\exp(-\frac{L}{G\tau}) \tag{19}$$

Since it can be shown that B° = n° G, then

$$n = \frac{B^{\circ}}{G}\exp(-\frac{L}{G\tau}) \tag{20}$$

In equation 20, n is the population density function, $B°$ is the specific nucleation rate (in [crystal# / L^3 T]) assuming no agglomeration or breakage, G is the growth rate (in [L/T]), L is the crystal mean size, and τ is the residence time.

Equation 20 can be derived for each crystallizing species i, to give:

$$n_i = \frac{B_i^{\circ}}{G_i}\exp(-\frac{L}{G_i\tau}) \tag{21}$$

Consequently the total population density function may be expressed as the sum of the specific population density function:

$$n_{\text{T total}} = \left[\frac{B^o{}_{\text{NaNO}_3}}{G_{\text{NaNO}_3}}\exp(-\frac{L}{G_{\text{NaNO}_3}\tau}) + \frac{B^o{}_{\text{NaCO}_3}}{G_{\text{NaCO}_3}}\exp(-\frac{L}{G_{\text{NaCO}_3}\tau}) + \frac{B^o{}_{\text{burkeite}}}{G_{\text{burkeite}}}\exp(-\frac{L}{G_{\text{burkeite}}\tau})\right] \tag{22}$$

With the total population density function having the dimension of:

$$n_{\text{Total}} = \sum_i \frac{dn_i}{dL} \equiv \left[\frac{\#\text{Crystals}}{\mu\text{m}\cdot\text{mL}}\right]$$

Total Crystal Mass for Steady State MSMPR

For a steady-state MSMPR crystallizer, Randolph and Larson (1988) showed that one can find the total mass per volume of mother liquor *M*t by integration over the crystal size distribution as:

$$M_{\text{t}} = \int_0^{\infty} \rho_{\text{c}} \cdot k_v \cdot L^3 \cdot n \cdot dL = \int_0^{\infty} \rho_{\text{c}} \cdot k_v \cdot L^3 \cdot n^{\circ} \cdot e^{-\frac{L}{G\tau}} \cdot dL \tag{23}$$

Where ρ_c is the crystal density and k_v is the volume shape factor. Equation 23 can be integrated to give:

$$M_{\text{t}} = 6\rho_{\text{c}} k_v n^{\circ} (G\tau)^4 \tag{24}$$

For multiple species:

$$(M_{\text{t}})_{\text{Total}} = 6[\sum_{i=1}^{n} \rho_i k_{v_i} n_i^{\circ} G_i{}^4]\tau^4 \tag{25}$$

5.2 STEADY-STATE SIMULATIONS WITH SMALL-SCALE VESSEL

5.2.1 CONTINUOUS MODEL SIMULATIONS

In this chapter we will consider a continuous crystallizer with an operating volume of 300 mL at 25 g/h evaporation rate and 66°C. The semi-batch kinetics of sodium nitrate, sodium carbonate monohydrate and burkeite obtained with multi-salts solution crystallization were implemented in equation 22. This model incorporates the effect of the species interactions and their effect on their respective kinetics. To illustrate the effects of variations in the kinetics, which are caused by having multiple solutes, the results are compared to those obtained using the single-salt kinetics.

Table 70 summarizes the nucleation and growth rates values of sodium nitrate, sodium carbonate monohydrate and burkeite obtained based on Early-Feed semi-batch crystallization.

Table 70. Kinetics parameters obtained from the semi-batch crystallization of early feed solution at 66 °C and 25 g/h evaporation rate

SST Early Feed	Nucleation Rate (crystals/ mL·min)	Growth Rate (μm·min^{-1})
Sodium Nitrate	3.628×10^{4}	1.680
Sodium Carbonate Monohydrate	3.245×10^{3}	0.158
Single Burkeite Crystals	3.686×10^{4}	0.170

These values were implemented in equation 22 to obtain the total population density function model provided in equation 26.

$$n_{total}=\left[\frac{3.628\cdot10^{4}}{1.680}\exp(-\frac{L}{1.680\tau})+\frac{3.245\cdot10^{3}}{0.158}\exp(-\frac{L}{0.158\tau})+\frac{3.686\cdot10^{4}}{0.170}\exp(-\frac{L}{0.170\tau})\right] \quad (26)$$

Figure 160 shows the semi-logarithmic plots of specific and total population density as functions of crystal size for a continuous crystallizer operated at steady-state with a temperature of 66 °C and an evaporation rate of 25 g/h, using a typical residence time of 12 hours and the kinetics given in Table 70. The total population density plot shows that the lower crystal size is dominated by sodium carbonate monohydrate while the larger sizes are dominated by sodium nitrate.

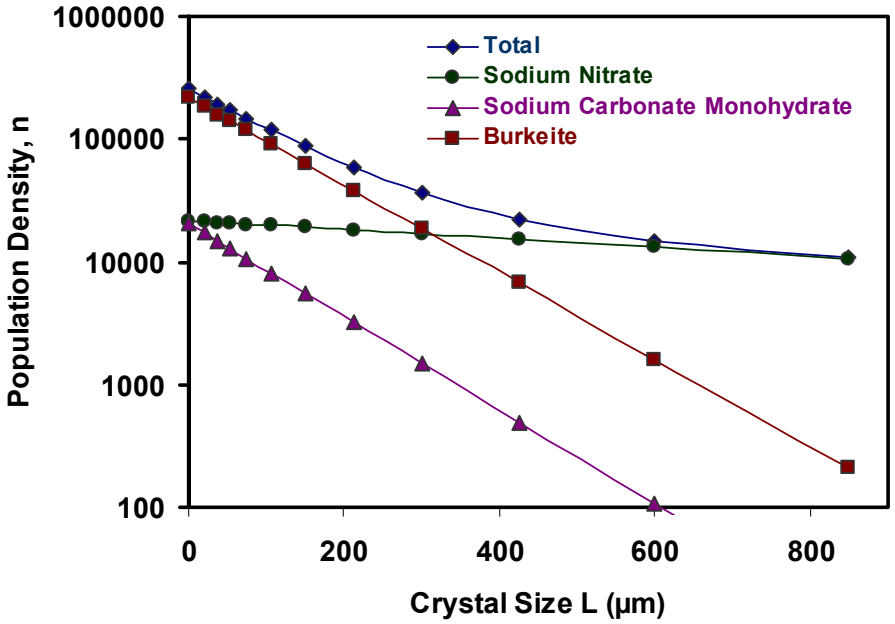

Figure 160. Variation of total and specific population density functions with crystal size in steady-state continuous crystallizer using multi-species kinetics and residence time of 12 hours

Table 71 gives the values of the nucleation and growth rates of sodium nitrate, sodium carbonate monohydrate and burkeite measured in single-solute experiments.

Table 71. Kinetics obtained from the semi-batch crystallization of single-salt sodium nitrate and sodium carbonate solutions at 66 °C and 25 g/h evaporation rate

SST Early Feed	Nucleation Rate (crystals/ mL·min)	Growth Rate (μm·min^{-1})
Sodium Nitrate	5.066×10^{3}	2.310
Sodium Carbonate Monohydrate	1.688×10^{3}	3.360
Single Burkeite Crystals	3.686×10^{4}	0.170

Substituing these values into equation 22 gives

$$n_{total} = \left[\frac{5.066\cdot10^{3}}{2.310}\exp(-\frac{L}{2.310\tau}) + \frac{1.688\cdot10^{3}}{3.360}\exp(-\frac{L}{3.360\tau}) + \frac{3.686\cdot10^{4}}{0.170}\exp(-\frac{L}{0.170\tau})\right] \quad (27)$$

Figure 161 shows the population density plots resulting from equation 27 with a value of $\tau = 12$ h.

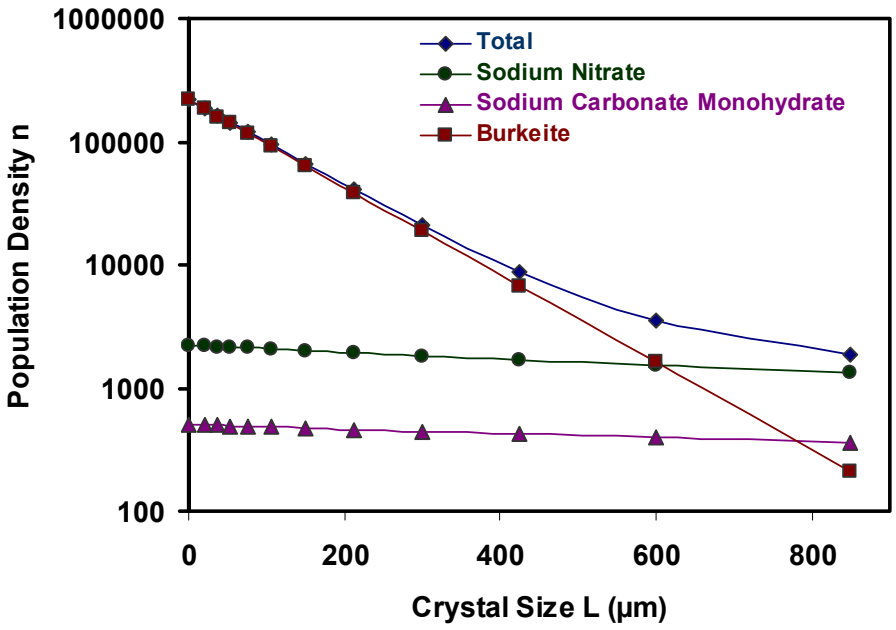

Figure 161. Variation of total and specific population density functions with crystal size in steady-state continuous crystallizer using single-species kinetics and residence time of 12 hours

Due to the higher growth rates of sodium nitrate and sodium carbonate monohydrate in a single-salt solution compared to the multi-salts early feed solution, the

two correlations display very different population density functions. The distributions of sodium nitrate and sodium carbonate monohydrate obtained for a residence time of 12 hours and using the single-salt kinetics model presents linear profiles with low values of the slope of the profiles. In essence the distribution of sodium carbonate monohydrate and sodium nitrate is homogeneous. The discrepancy between the population density functions presented in Figure 160 and Figure 161 is more important for sodium carbonate monohydrate for which the difference in kinetics is of one order of magnitude. Consequently, the total distribution in the lower particle size is guided by the distribution of sodium carbonate monohydrate and burkeite with equation 26 (smaller growth rate and larger nucleation rate), while for higher crystal sizes sodium nitrate is dominating the total population density profile. With equation 27, sodium carbonate monohydrates are collected mainly at higher crystal sizes than at smaller sizes. The use of single-salts kinetics is hence leading to important error when performing continuous crystallization simulations, revealing the importance of multi-salt crystallization experiments.

5.2.2 CUMULATIVE AND DIFFERENTIAL DISTRIBUTIONS FROM CONTINUOUS SIMULATIONS

Cumulative and Differential Crystal Count Distributions

The number of crystals per unit volume *N(L)* of size lower or equal to *L* is given by:

$$\frac{N(L)}{V_{ML}} = \int_0^L n \cdot dL \tag{28}$$

Where V_{ML} is the total volume of suspension or mother liquor (magma). When *L* tends to infinity, *N(L)* becomes the total crystal population N_{Total}:

$$\frac{N_{\text{Total}}}{V_{\text{ML}}} = \int_0^{\infty} n \cdot dL \tag{29}$$

Subsituing equation 20 into equation 28 and 29, the cumulative fractional number distribution is:

$$\frac{N_{\text{L}}}{N_{\text{Total}}} = \frac{\int_0^{L} n \cdot dL}{\int_0^{\infty} n \cdot dL} = \frac{\int_0^{L} n \circ \cdot e^{\frac{-L}{G \cdot \tau}} \cdot dL}{\int_0^{\infty} n \circ \cdot e^{\frac{-L}{G \cdot \tau}} \cdot dL} = 1 - e^{-\frac{L}{G \cdot \tau}} = 1 - e^{-Z} \tag{30}$$

where $Z = L/(G\tau)$

The population cumulative undersize distribution is hence defined by equation 31 in integrated from, and equations 32 in differential form.

$$x_n = 1 - e^{-z} \tag{31}$$

$$\frac{dx_n}{dz} = e^{-z} \tag{32}$$

Figure 162 displays the cumulative and differential distributions of the crystal count for sodium nitrate, sodium carbonate monohydrate and burkeite crystals, obtained with a steady-state continuous crystallizer at 66 °C, 25 g/h evaporation rate and a residence time of 12 hours. Figure 162 displays very different distributions for sodium carbonate monohydrate and burkeite compared to sodium nitrate. Close to 50 % of the total count of sodium carbonate monohydrate and burkeite crystals are recovered in sizes greater than 15 μm. These results show that with a residence time of 12 hours, the crystals obtained are small which do not facilitate the solid-liquid separation and crystal washing. Assessing the case of sodium nitrate, the cumulative distribution of crystal

count is in higher size ranges. Close to 50 % of the sodium nitrate crystal count is recovered at sizes greater than 90 µm. Panel B illustrates better this effect. This difference in distribution is the direct result of the large sodium nitrate growth rate that leads in average to larger crystals. The high nucleation rate of sodium nitrate is however detrimental to the distribution that will present a larger spread at a high value of the residence time such as τ =12 hours.

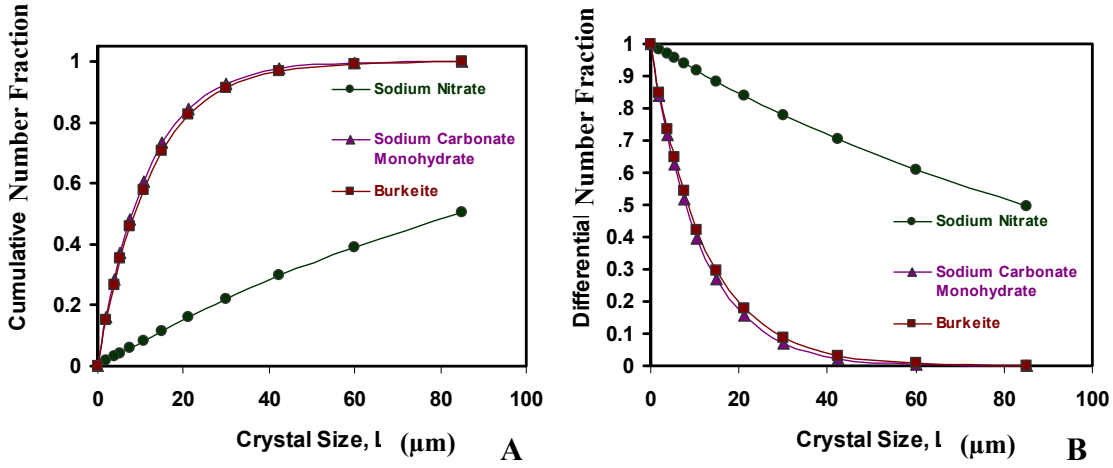

Figure 162. Crystal count cumulative (panel A) and differential (panel B) number fractions for sodium nitrate, sodium carbonate monohydrate and burkeite produced with a steady-state continuous crystallizer at 66 °C, 25 g/h evaporation rate and 12 h residence time

Mass Distribution

The mass cumulative undersize distributions are defined by equations 34 and 35 in integrated and differential forms respectively.

$$x_m = 1-(1+z+\frac{z^2}{2}+\frac{z^3}{6})e^{-z} \tag{34}$$

$$\frac{dx_m}{dz} = \frac{z^3}{6}\cdot e^{-z} \tag{35}$$

Figure 163 displays the cumulative and differential mass distributions for sodium nitrate, sodium carbonate monohydrate and burkeite crystals, obtained with a steady-state continuous crystallizer at 66 °C, 25 g/h evaporation rate and a residence time of 12 hours. 50 % of the sodium carbonate monohydrate and burkeite crystal mass were recovered at sizes greater than 45 μm. Assessing the case of sodium nitrate, 50 % of the crystal mass was recovered at sizes greater than 0.5 mm. The discrepancies between the cumulative distributions of nitrate and sodium carbonate monohydrate or burkeite are explained by the higher growth rate of sodium nitrate compared to the value for the other two species. Assessing the distributions, panels B and D show that sodium nitrate present a higher spread in distribution than burkeite and sodium carbonate monohydrate which is resulting from the higher nucleation rate of sodium nitrate. Panels C and D display the comparison between the crystal count, length and mass distributions for the case of sodium nitrate, showing that mass, size and number of crystals are not distributed identically with respect to crystal size. This was anticipated as the larger crystals present a greater mass than the smaller crystals, and since the growth rate is high and the residence time is long, more of the larger crystals are produced leading to a shift of the mass distribution toward the higher sizes. Similarly, a high nucleation rate lead to the production of large number of smaller size crystal, for which the total cumulative mass is low but the total crystal count is high, leading to a shift in crystal count toward the lower crystal sizes.

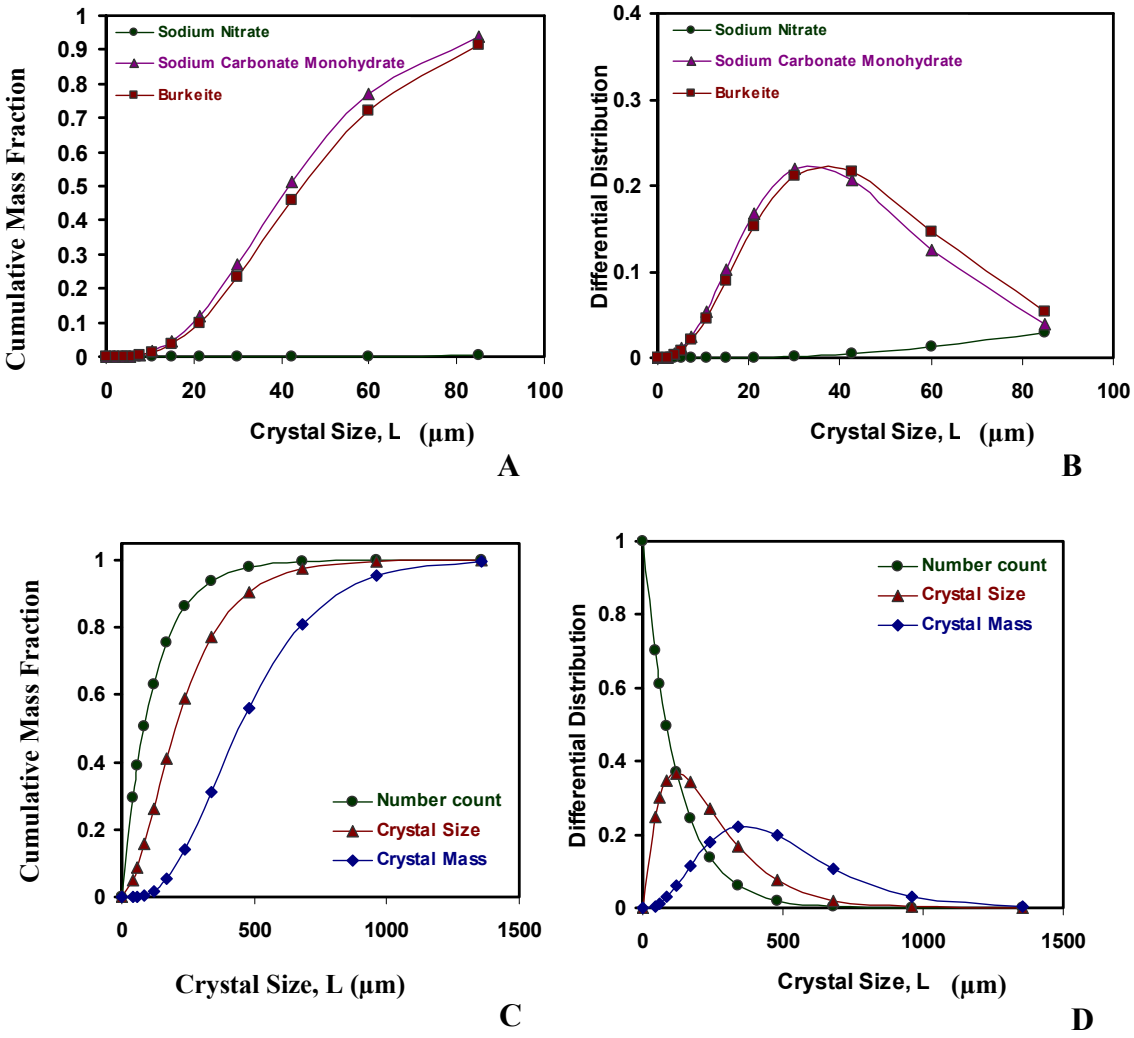

Figure 163. Cumulative and differential mass fraction distributions for sodium nitrate, sodium carbonate monohydrate and burkeite produced with a steady-state continuous crystallizer at 66 °C, 25 g/h and 12 hours residence time
(Panel A, Crystal mass cumulative distribution, Panel B, Crystal mass differential distribution, Panel C, Sodium nitrate length, count, and mass cumulative distribution, Panel D, Sodium nitrate length, count, and mass differential distribution)

Mass Density Distribution Comparison between Semi-Batch and Continuous Crystallizers

Equation 23 was used to plot the mass density distributions for an MSMPR crystallizer operated with a residence time of 12 hours. Figure 164 displays a comparison of mass density histograms obtained (1) experimentally with an early feed solution at 66

°C and 25 g/h evaporation rate in a semi-batch crystallizer, and (2) by simulation of the crystallization of sodium nitrate, sodium carbonate monohydrate and burkeite in a steady-state continuous crystallizer operated at 66 °C and with a residence time of 12 hours. Figure 164 displays important discrepancies between the semi-batch and the continuous processes. Panel A shows that crystals obtained with a MSMPR process have greater sizes than the semi-batch process and a higher spread in distribution. Panel B demonstrates that this discrepancy is mainly due to sodium nitrate as the total crystal distribution is dominated by sodium nitrate in a continuous crystallizer. The mode size for sodium nitrate in the continuous model is close to 250 μm with a large fraction of the crystal mass recovered at 650 μm. This large size compared to the semi-batch experiments is due to the fact that a residence time of 12 hours represent the average growth time of sodium nitrate between the first nucleation and the point at which the average kinetics are established. In essence, in semi-batch crystallizer sodium nitrate kinetics were valid only for an operating time of 7 hours. It is hence expected that in a large-scale continuous crystallizer the residence time will be lower than 12 hours and closer to 7 hours. Furthermore, the MSMPR model do not account for the agglomeration and breakage mechanisms which are predominant in large-scale continuous processes as mentioned at the beginning of this chapter. Assessing the case of sodium carbonate monohydrate, Panel B shows that the mode size is close to 50 μm in the MSMPR model which is slightly higher than the semi-batch experimental data but still very close to the mode size value of 100 μm. For burkeite crystals, Panel B displays an average mode size of 50 μm for the MSMPR model. This small discrepancy with the outcomes of the semi-batch experiments for which the average burkeite mode size was closer to 25-30 μm, is

explained by the formation of sulfate co-crystal and theire effect on burkeite kinetics as shown in Chapter 2.

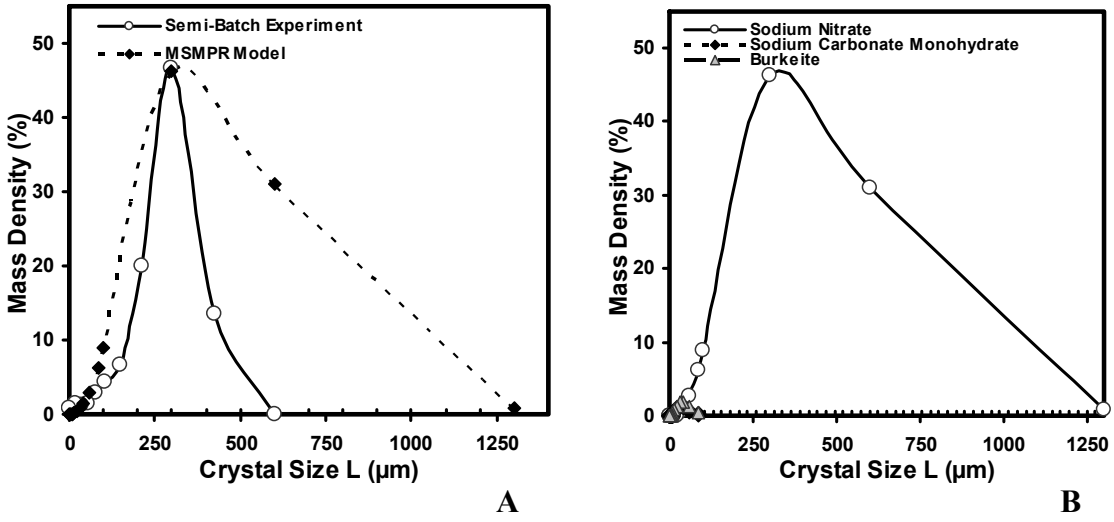

Figure 164. Comparison of mass denstity histograms from semi-batch experiments and MSMPR model operated at 66 °C, 25 g/h evaporation rate and a residence time of 12 hours
(Panel A, Mass density hitograms comparison between semi-batch and continuous process, Panel B, Sodium nitrate, Sodiu carbonate monohydrate and burkeite density histograms form MSMPR model)

Cumulative Mass Distribution Comparison between Semi-Batch and Continuous Crystallizers

Figure 165 displays a comparison of the total cumulative mass distributions obtained (1) experimentally with an early feed solution at 66 °C and 25 g/h evaporation rate in a semi-batch crystallizer, and (2) by simulation of the crystallization of sodium nitrate, sodium carbonate monohydrate and burkeite in a steady-state continuous crystallizer operated at 66 °C and with a residence time of 12 hours. Figure 165 displays important discrepancies between the semi-batch and the continuous processes. The mass cumulative distribution for the continuous crystallizer produced larger crystals with a larger spread in distribution than the semi-batch. This difference is due to the fact that (1) in a semi-batch crystallizer, nucleation of burkeite and carbonate monohydrate do not

occur at the same time as sodium nitrate nucleation, leading to a growth time lesser than 12 hours for sodium nitrate crystals, (2) the effect of sulfate co-crystals formation that reduces the growth and nucleation rate of some species such as burkeite in the semi-batch process, which does not occur in the continuous crystallizer, (3) some agglomeration of burkeite crystals occurs in the semi batch-crystallizer which were not taken into account in the MSMPR model. In essence, the comparison of the cumulative and mass density distributions demonstrate the differences between semi-batch and continuous process operations and the need of smaller residence time for a continuous crystallizer operation.

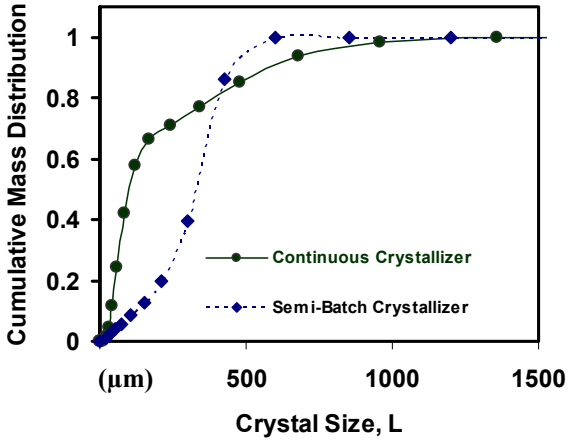

Figure 165. Total cumulative mass distribution comparison between a semi-batch and a continuous crystallizer operated at 66 °C with an early feed solution and a growth or residence time of 12 hours

5.2.3 OPERATING TEMPERATURE EFFECT ON CONTINUOUS SIMULATIONS

Results were given in Chapter 4 of series of crystallization experiments with operating temperatures at 45, 55 and 66 °C performed in a semi-batch apparatus at an evaporation rate of 25 g/h, using the early-feed solution. The values of the kinetics of

sodium nitrate, sodium carbonate monohydrate and burkeite were used in the population balance model defined by equation 22. The series of equation for parameters at 45, 55 and 66 °C are shown by equations 36, 37 and 38 respectively.

$$n_{total} = \left[\frac{9.267 \cdot 10^3}{4.101} \exp(-\frac{L}{4.101\tau}) + \frac{6.523 \cdot 10^3}{0.107} \exp(-\frac{L}{0.107\tau}) + \frac{1.410 \cdot 10^3}{0.010} \exp(-\frac{L}{0.010\tau}) \right] (36)$$

$$n_{total} = \left[\frac{2.329 \cdot 10^4}{2.106} \exp(-\frac{L}{2.106\tau}) + \frac{4.662 \cdot 10^3}{0.141} \exp(-\frac{L}{0.141\tau}) + \frac{3.935 \cdot 10^4}{0.031} \exp(-\frac{L}{0.031\tau}) \right] (37)$$

$$n_{total} = \left[\frac{3.627 \cdot 10^4}{1.680} \exp(-\frac{L}{1.680\tau}) + \frac{3.245 \cdot 10^3}{0.158} \exp(-\frac{L}{0.158\tau}) + \frac{3.686 \cdot 10^4}{0.170} \exp(-\frac{L}{0.170\tau}) \right] (38)$$

Figure 166 shows the variation of the specific and total population density functions with the crystal size and operating temperature for a continuous crystallizer operated at steady-state with an evaporation rate of 25 g/h, using a residence time of 12 hours. The operating temperature has important effect on the population density function of sodium nitrate, carbonate monohydrate and burkeite. For sodium nitrate, the profile are similar but present a lower value of the intercept in the Y axis (B°=n° G) and the value of the population density within the 0 to 600 μm size range. For sodium carbonate monohydrate crystals, the semi-logarithmic population density functions crosses at 200μm for the 45 °C and 55 °C curves, and at 400 μm for the 55 °C and 66 °C curves. Assessing the case of burkeite population density function, the 55 °C and 66 °C curves cross at 100 μm. The resulting total population density functions are very different for the three temperature investigated. The distribution with respect to crystal size is more uniform for the 66 °C than for the 45 and 55 °C curves.

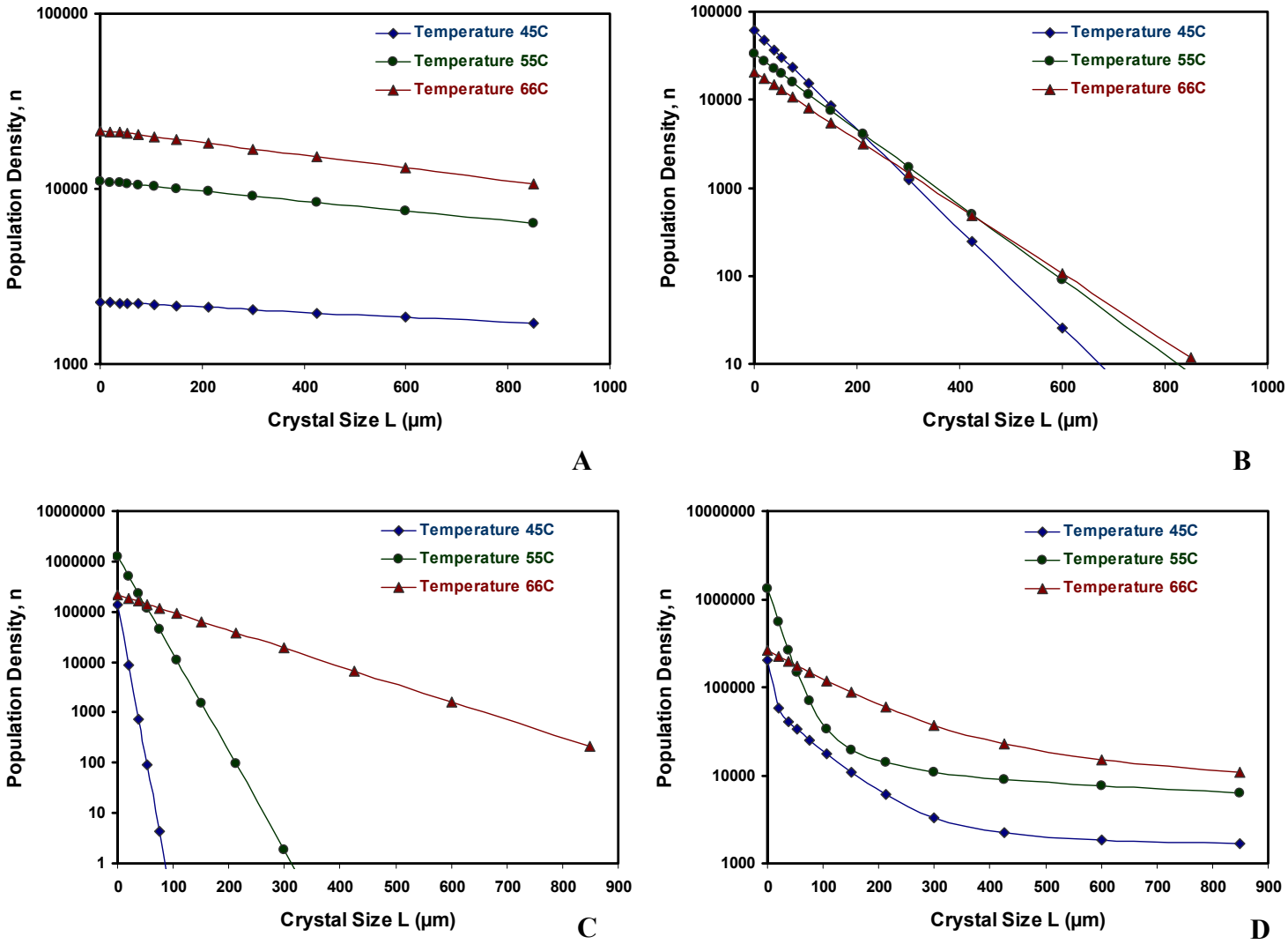

Figure 166. Variation of specific and total population density function with temperature for steady-state continuous crystallizer operated at 25 g/h evaporation rate with an early feed solution.
(Panel A, sodium nitrate, Panel B, sodium carbonate monohydrate, Panel C, burkeite, Panel D, total)

5.2.4 EVAPORATION RATE EFFECT ON CONTINUOUS SIMULATIONS

The crystallization kinetics of the main crystalline species produced in the steady-state continuous crystallizer will vary with the value of the evaporation rate. A series of crystallization experiment with evaporation rate of 25, 35 and 55 g/h were performed in a semi-batch apparatus at an operating temperature of 66 °C using the early feed solution as displayed in Chapter 4. The values of the kinetics of sodium nitrate, sodium carbonate monohydrate and burkeite were used in the population balance model defined by equation 22. The series of equation for parameters at 25, 35 and 55 g/h are shown by equations 39, 40 and 41 respectively. Note that in this study we make the assumption that the evaporation is performed in a similar fashion between the semi-batch and the continuous crystallizer. This assumption is supported by the similar operating volumes.

$$n_{total} = \frac{3.627 \cdot 10^4}{1.680} \exp(-\frac{L}{1.680\tau}) + \frac{3.245 \cdot 10^3}{0.158} \exp(-\frac{L}{0.158\tau}) + \frac{3.686 \cdot 10^4}{0.170} \exp(-\frac{L}{0.170\tau}) \quad (39)$$

$$n_{total} = \frac{6.014 \cdot 10^4}{1.122} \exp(-\frac{L}{1.122\tau}) + \frac{1.522 \cdot 10^4}{0.091} \exp(-\frac{L}{0.091\tau}) + \frac{4.826 \cdot 10^4}{0.129} \exp(-\frac{L}{0.129\tau}) \quad (40)$$

$$n_{total} = \frac{1.078 \cdot 10^5}{0.873} \exp(-\frac{L}{0.873\tau}) + \frac{1.597 \cdot 10^4}{0.052} \exp(-\frac{L}{0.052\tau}) + \frac{2.687 \cdot 10^5}{0.081} \exp(-\frac{L}{0.081\tau}) \quad (41)$$

Figure 167 shows the variation of the specific and total population density functions as a function of crystal size and evaporation rate value for a continuous crystallizer operated at steady-state with an operating temperature of 66 °C, using a residence time of 12 hours.

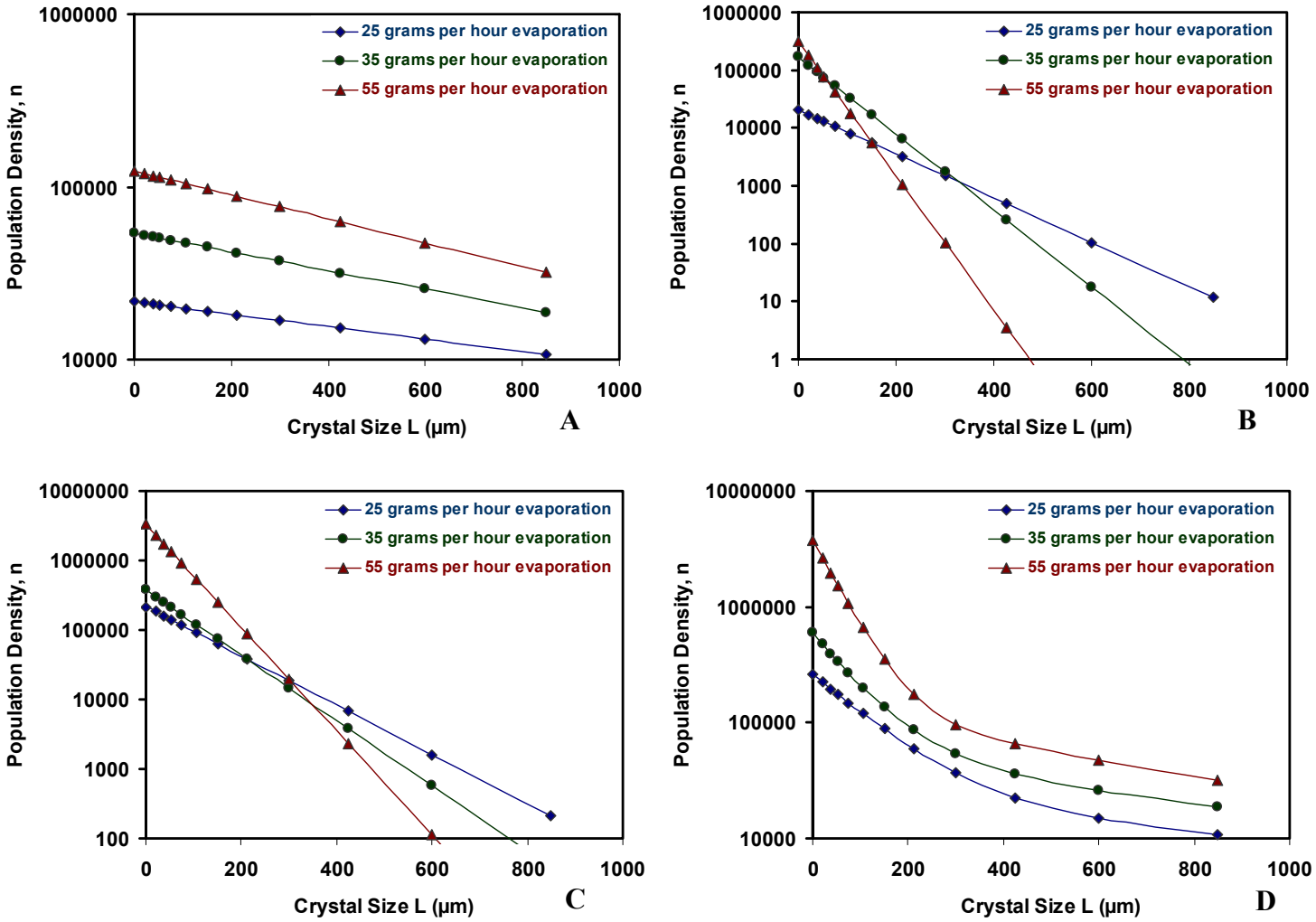

Figure 167. Variation of specific and total population density function with evaporation rate for steady-state continuous crystallizer operated at 66 °C with an early feed solution
(Panel A, sodium nitrate, Panel B, sodium carbonate monohydrate, Panel C, burkeite, Panel D, total)

The evaporation rate has important effect on the population density function of sodium nitrate, carbonate monohydrate and burkeite. For sodium nitrate, the profile are similar but present a lower value of the intercept in the Y axis (B°=n° G) and the value of the population density within the 0 to 600 μm size range. For sodium carbonate monohydrate crystals, the semi-logarithmic population density functions crosses at 150μm for the 55 and 35 grams per hour curves, 200 μm for the 25 and 55 grams per hour curves and at 400 μm for the 25 and 35 grams per hour curves. Assessing the case of burkeite population density function, the three curves cross at 300 μm. The resulting total population density functions are very different for the three evaporation rates investigated: the lower the value of the evaporation rate, the more uniform the population density distribution with respect to crystal size are.

5.3 STEADY STATE SIMULATIONS WITH PILOT-SCALE VESSEL

5.3.1 CONTINUOUS MODEL FOR PILOT-SCALE VESSEL

The pilot-scale continuous process is to be operated with a crystallizer having an operating volume ranging from 1100 and 1300 gallons and with a residence time ranging from 6 to 10 hours. In this section we will consider a continuous crystallizer with an operating volume of 1300 gallons and operated with a retention time of 10 hours. In the base case, the crystallization is operated at 66°C and with an evaporation rate of 410 kg/h, obtained by multiplying the small-scale vessel evaporation rate value (25 g/h) by the ratio of active volumes (1300 gallons / 300 mL) of the large-scale and small-scale crystallizers. In this chapter we will investigate the effect of residence time on the specific growth rate and provide estimates of the population density plot for the large scale crystallizer to be implemented at Hanford.

Model Assumptions:

We will use a set of four major assumptions in the MSMPR model developed in this chapter:

- The saturation concentrations of each of the species crystallizing in the continuous process will be derived from the thermodynamic simulations performed at equilibrium conditions by AREVA NC.
- The feed concentrations of sodium nitrate and sodium carbonate monohydrate were taken from the feed compositions and the feed concentration of burkeite was calculated from the mass of burkeite crystals produced according to thermodynamic simulations.
- The average nucleation rate will be assumed to be constant in order to estimate the effect of the residence time on the average growth rate. The values of the average nucleation rate will correspond to the values obtained with the semi-batch process at similar temperatures.
- The product slurry inside the crystallizer will be fixed at 30 % solids, i.e the ratio of the mass of crystals and the mass of slurry is set at 0.3.
- The pilot-scale continuous process is a class II system (Fast Growth) for which the exit concentrations approach the equilibrium concentrations.

Steady State Mass Balance:

The rate at which the mass is gained by the solid phase is equal to the rate at which the solute is lost from the mother liquor (Randolph and Larson; 1988):

$$Q_{\text{in}} C_{\text{F}} - Q_{\text{out}} C_{\text{out}} = Q_{\text{out}} M_{\text{t}} \tag{42}$$

For which Q_{out} represent the sum of the flow rates exiting the process and for which the exit concentration is the saturation concentration (Class II system). M_{t} can hence be calculated as

$$M_{t_i} = \frac{C_{\text{Fi}} Q_{\text{in}}}{Q_{\text{out}}} - C_i^* \tag{43}$$

Growth Rate Correlation:

Beginning with equation 24 for a given B_i° and substituting $n_i^\circ = \frac{B_i^\circ}{G_i}$, allow G_i to be estimated as

$$G_i^3 = \frac{M_{t_i}}{6\rho_i k_{v_i} B^\circ \tau^4} \tag{44}$$

Population Balance:

Using the growth rate from equation 44, one can compute the population density using a simple population balance model:

$$n_i = \frac{B_i^\circ}{G_i} \exp\left(-\frac{L}{G_i \tau}\right)$$

Example Calculations:

In the base case study the crystallization is to be performed at 66 °C with a residence time of 12 h. The evaporation rate is estimated as:

$$Q_{\text{W}} = 25\frac{\text{g}}{\text{h}} \times \frac{1300\text{gal} \times 3785.4\frac{\text{mL}}{\text{gal}}}{300\text{mL}} = 410\frac{\text{kg}}{\text{h}}$$

Corresponding to a mass of vapor after 12 h of:

$$m_{\text{V}} = 410\frac{\text{kg}}{\text{h}} \times 12\text{h} = 4920\text{kg}$$

The slurry mass flow rate was estimated using the slurry density value of 1.2 g/mL as:

$$Q_{\mathrm{S}} = \frac{1300\mathrm{gal} \times 3785.4 \dfrac{\mathrm{mL}}{\mathrm{gal}}}{12\mathrm{h}} \times 1.2 \frac{\mathrm{g}}{\mathrm{mL}} = 492 \frac{\mathrm{kg}}{\mathrm{h}}$$

The mass ratio of solids in the slurry was used to compute the mass flow rate of solids (Q_{ss}) and mother liquor (Q_{ls}) in slurry:

$$Q_{\mathrm{SS}} = 492 \frac{\mathrm{kg_{slurry}}}{\mathrm{h}} \times 0.3 \frac{\mathrm{kg_{solids}}}{\mathrm{kg_{slurry}}} = 148 \frac{\mathrm{kg}}{\mathrm{h}}$$

$$Q_{\mathrm{ls}} = 492 \frac{\mathrm{kg_{slurry}}}{\mathrm{h}} \times 0.7 \frac{\mathrm{kg_{motherliquor}}}{\mathrm{kg_{slurry}}} = 344 \frac{\mathrm{kg}}{\mathrm{h}}$$

Meaning that the mass of solids and mother liquor in the slurry after 12 h are:

$$m_{\mathrm{SS}} = 148 \frac{\mathrm{kg}}{\mathrm{h}} \times 12\mathrm{h} = 1776\mathrm{kg}$$

$$m_{\mathrm{ls}} = 344 \frac{\mathrm{kg}}{\mathrm{h}} \times 12\mathrm{h} = 4128\mathrm{kg}$$

The mass and mass flow rate of the feed solution can be derived from a total mass balance around the process using:

$$m_{\mathrm{f}} = m_{SS} + m_{lS} + m_{V}$$

$$m_{\mathrm{f}} = 1776 + 4128 + 4920 = 10824\mathrm{kg}$$

And $Q_F = \dfrac{10824\mathrm{kg}}{12\mathrm{h}} = 902 \dfrac{\mathrm{kg}}{\mathrm{h}}$

The feed and equilibrium concentrations for each crystalline species (sodium nitrate, sodium carbonate and burkeite) were provided by the thermodynamic simulations. These values are summarized in Table 72.

Table 72. Feed and saturation concentration for sodium nitrate, sodium carbonate monohydrate and burkeite at 66 °C

Crystalline Species	Feed Concentration $C_{F,i}$ (kg/L)	Saturation Concentration C_i^* (kg/L)
Sodium Nitrate	0.329	0.548
Sodium Carbonate Monohydrate	0.061	0.091
Single Burkeite Crystals	0.021	0.022

M_t can hence be calculated for sodium nitrate as:

$$M_t = \frac{0.329 \times 902}{344} - 0.548 = 0.31 \frac{\text{kg}}{\text{L}}$$

Allowing G to be estimated as:

$$G^3 = \frac{0.31 \frac{\text{kg}}{\text{dm}^3}}{6 \times 1.20 \frac{\text{kg}}{\text{dm}^3} \times 1 \times 36279 \frac{(-)}{\text{min} \times \text{cm}^3} \times (12 \times 60\,\text{min})^4}$$

$$G = 1.87 \frac{\mu\text{m}}{\text{min}}$$

The population density function plot can hence be calculated by varying the value of the average crystal size (L). For a residence time of 12 h, an average crystal size of 100 μm, the population density function of sodium nitrate is:

$n = \frac{36279}{1.87} \exp - \left(\frac{100}{1.87 \times 12 \times 60} \right)$, and Ln ($n$) = 9.79.

In this chapter, the effect of the residence time was measured by using τ = 6 h, 8 h, 10 h, and 12 h in the calculations. The population density functions for sodium carbonate monohydrate and burkeite were computed by using the feed and saturation values in Table 72, the nucleation rate

values in Table 70, values of k_v of 5 and 0.52 for sodium carbonate and burkeite respectively, and values of the crystal density at 66 °C of 1.1 and 1.2 kg/m^3.

One can quantify the effect of the operating temperature on the population density function by changing: (1) the values of the nucleation rate to these described in Chapter 4 for different operating temperature, (2) the saturation concentrations with these given by thermodynamic simulations at 45 °C, 55 °C, 66 °C and 75 °C. Variation in the crystal density for this temperature range was negligible. Assessing the effect of the evaporation rate on the population density function, only the flow rates values and nucleation rates values were adjusted compared to the base case study of 66 °C.

5.3.2 CONTINUOUS SIMULATION FOR PILOT-SCALE VESSEL

Base Case Study:

The pilot-scale continuous process is to be operated at 66°C with a scaled evaporation rate of 410 kg/h. In this section we will investigate the effect of residence time on the specific growth rate and provide estimates of the population density function for the large scale crystallizer to be implemented at Hanford under these conditions. Figure 168 displays the variation of the specific growth rate with the residence time for a 1300 gallons continuous crystallizer at 66°C and 410 kg/h evaporation rate. Graphs show that for sodium nitrate, sodium carbonate monohydrate and burkeite crystals, an increase in the residence time lead to a decrease in the growth rate. Furthermore, the values of the growth rate for a residence time of 12 hours exceed the semi-batch values with one order of magnitude for sodium carbonate monohydrate and burkeite.

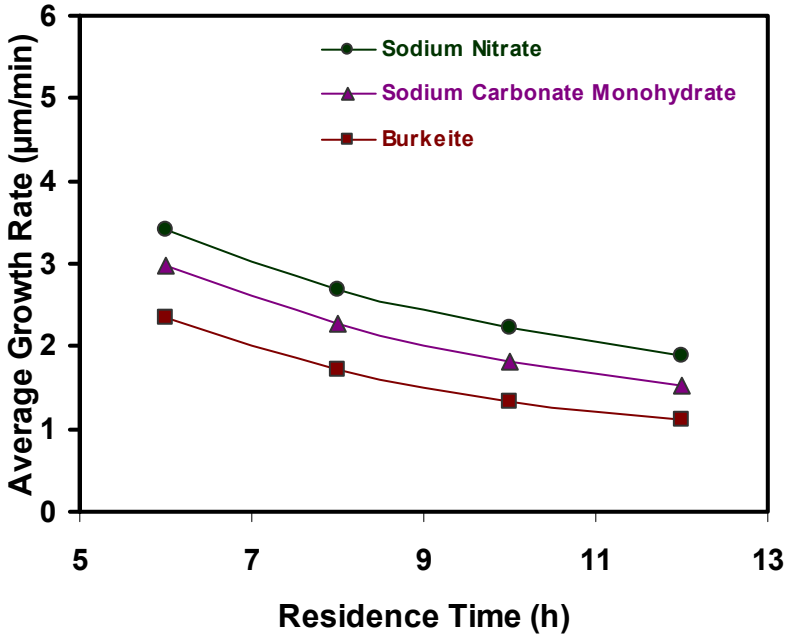

Figure 168. Variation of the specific growth rate with the residence time at 66°C and 410 kg/h evaporation rate for a 1300 gallons continuous crystallizer

Figure 169 shows the population density functions with the residence time for a 1300 gallons continuous crystallizer at 66 °C and 410 kg/h evaporation rate. Plots show that the population density function for each species is strongly dependant to the residence time, and increases with increasing residence time. Furthermore, the discrepancy between the population density function profiles increases with decreasing residence time.

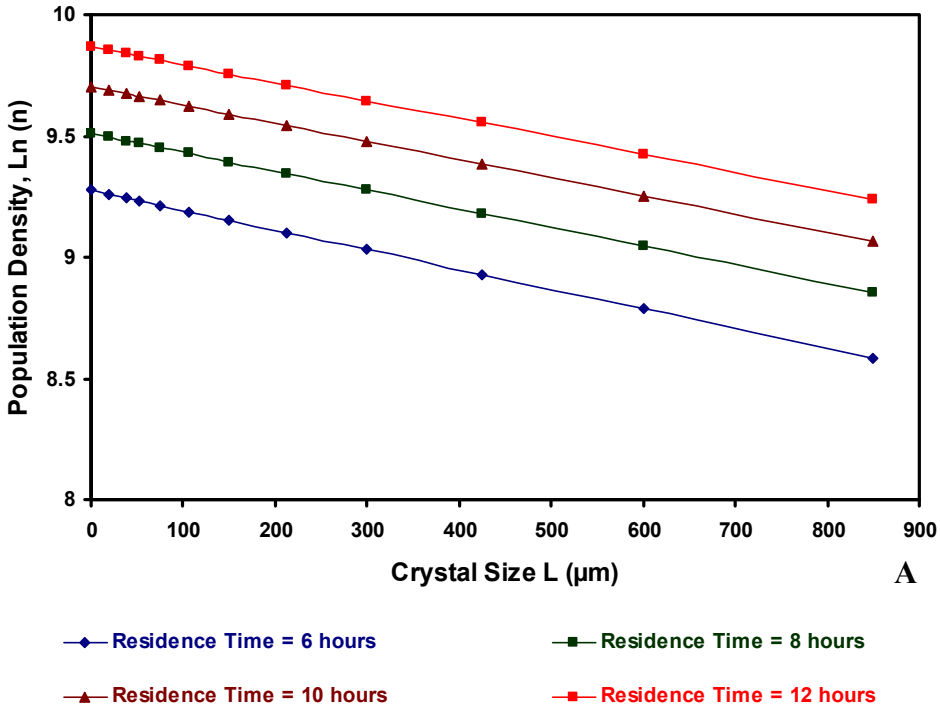
Population Density, Ln (n)
10
9.5
9
8.5
8
0
100
200
300
400
500
600
700
800
900
Crystal Size L (μm)
A
Residence Time = 6 hours
Residence Time = 8 hours
Residence Time = 10 hours
Residence Time = 12 hours

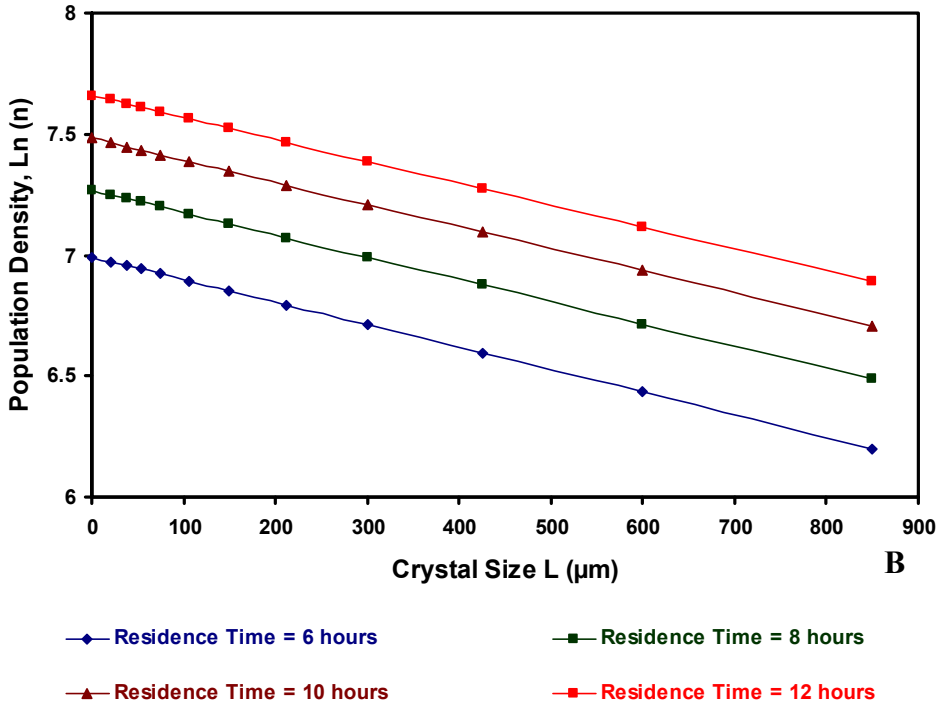
Population Density, Ln (n)
8
7.5
7
6.5
6
0
100
200
300
400
500
600
700
800
900
Crystal Size L (μm)
B
Residence Time = 6 hours
Residence Time = 8 hours
Residence Time = 10 hours
Residence Time = 12 hours

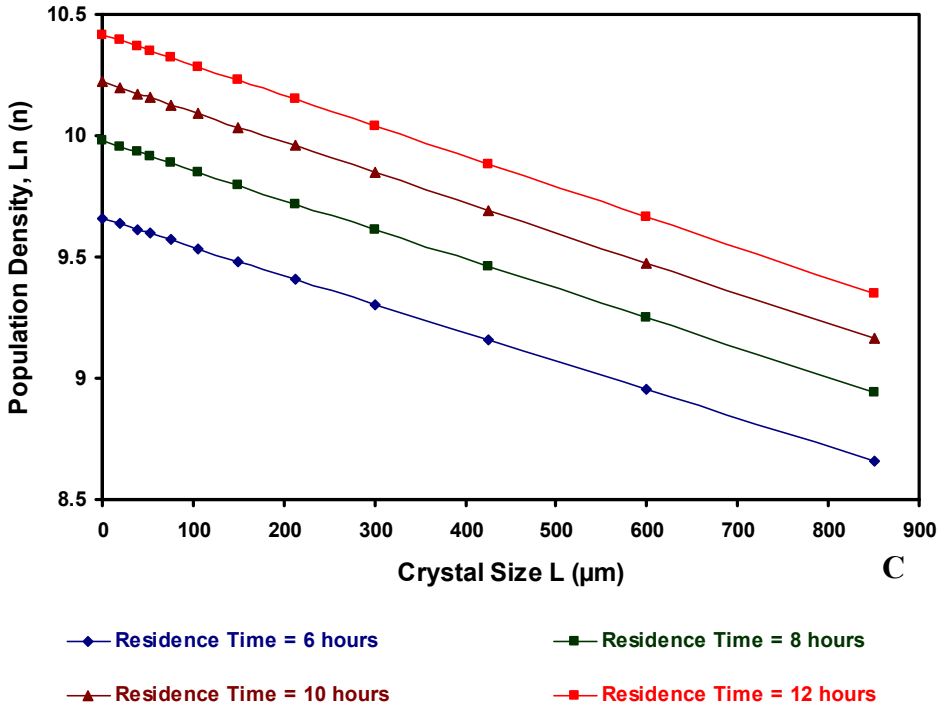

Figure 169. Evolution of population density function for sodium nitrate (Panel A), sodium carbonate monohydrate (Panel B) and burkeite (Panel C) for 1300 gallons continuous crystallizer at 66 °C and 410 kg/h evaporation rate

Combined Effect of Residence Time with Operating Temperature and Evaporation Rate:

A set of simulations was performed with temperatures of 45 °C, 55 °C, 66 °C and evaporation rate of 410 kg/h, 574 kg/h and 902 kg/h. In this section we will investigate the effect of residence time, operating temperature and evaporation rate on the specific growth rate and provide estimates of the population density function for a 1300 gallons continuous crystallizer. Figure 170 displays the variation of the specific growth rate with the residence time, operating temperature and evaporation rate for a 1300 gallons continuous crystallizer. Graphs show that for sodium nitrate, sodium carbonate monohydrate and burkeite crystals, a decrease in temperature lead to a decrease in the growth rate and a decrease in the evaporation rate lead to an increase of the growth rate. Figure 171 displays the values of the population density functions corresponding to each variation in temperature and evaporation rate.

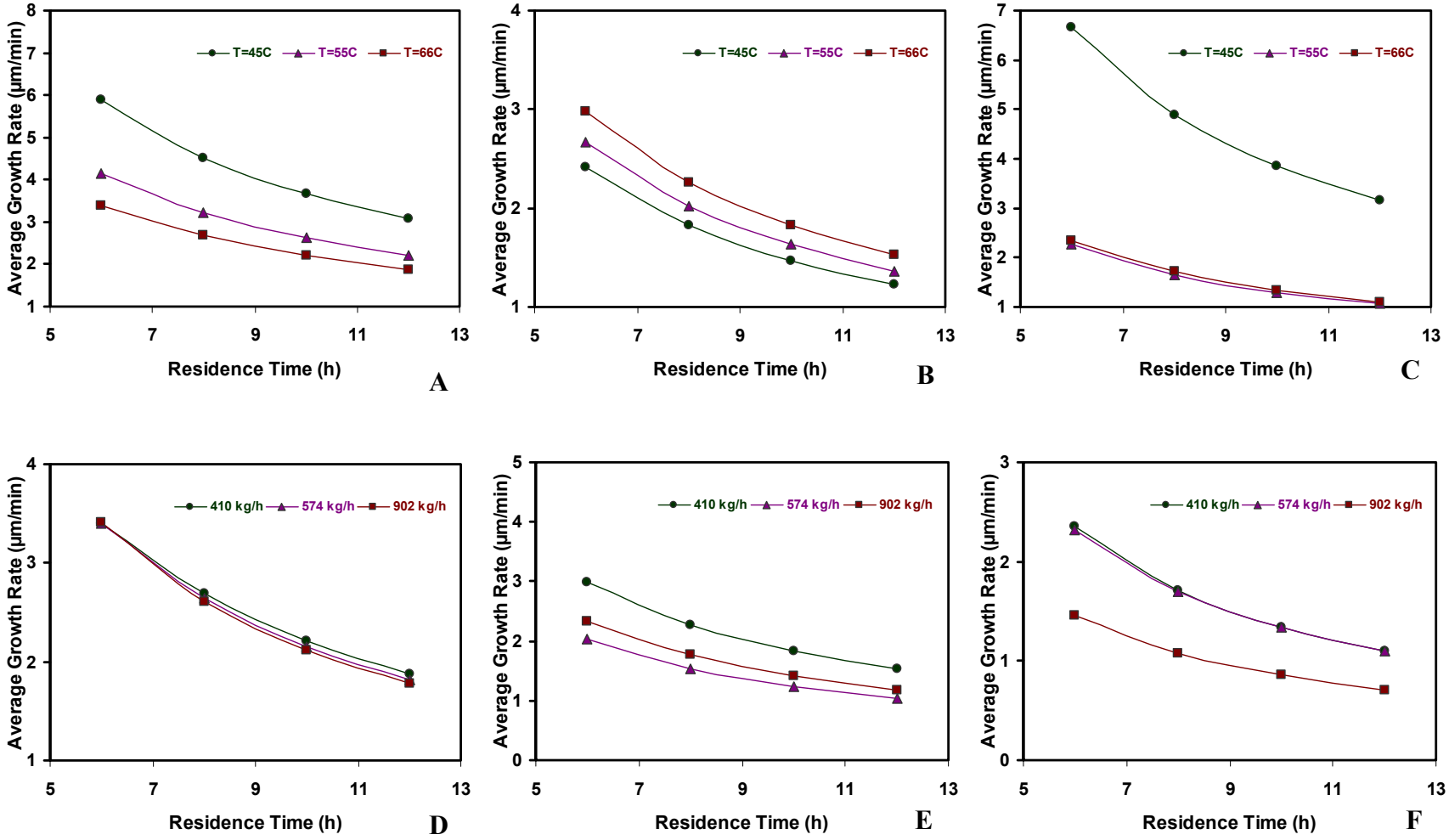

Figure 170. Growth rate variation for sodium nitrate (Panels A and D), sodium carbonate monohydrate (Panels B and E) and burkeite (Panels C and F) with residence time for varying temperature and evaporation rate

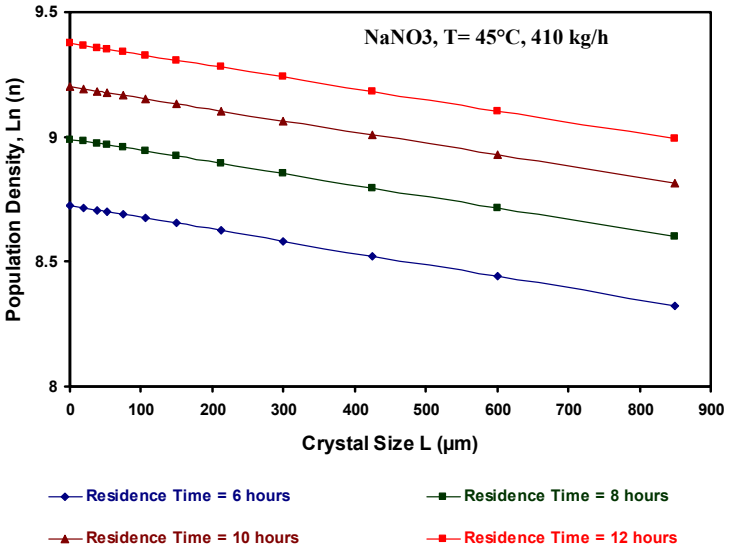
NaNO3, T= 45°C, 410 kg/h
Population Density, Ln (n)
Crystal Size L (µm)
Residence Time = 6 hours
Residence Time = 8 hours
Residence Time = 10 hours
Residence Time = 12 hours

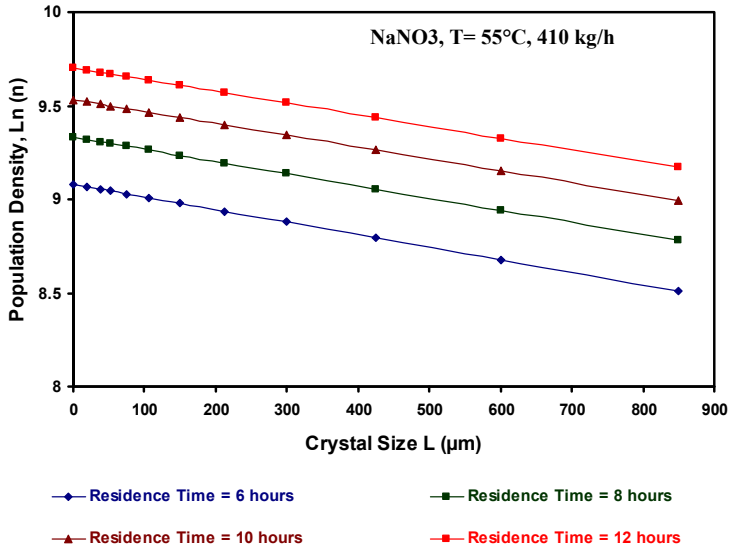
NaNO3, T= 55°C, 410 kg/h
Population Density, Ln (n)
Crystal Size L (µm)
Residence Time = 6 hours
Residence Time = 8 hours
Residence Time = 10 hours
Residence Time = 12 hours

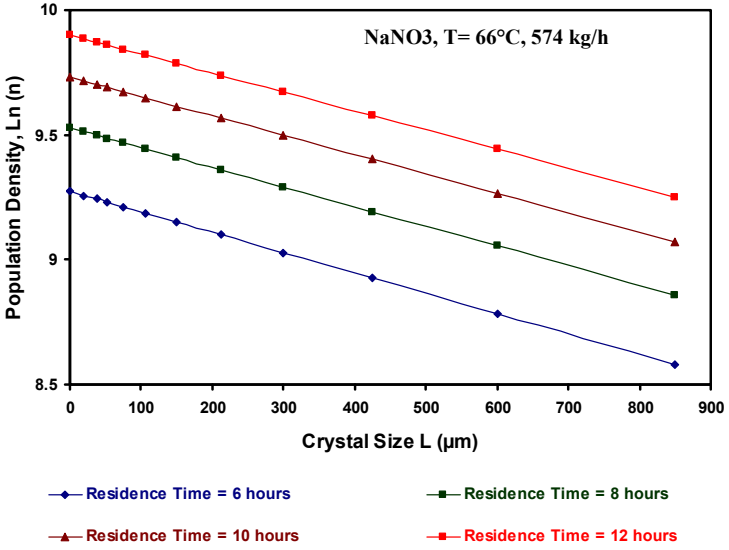
NaNO3, T= 66°C, 574 kg/h
Population Density, Ln (n)
Crystal Size L (µm)
Residence Time = 6 hours
Residence Time = 8 hours
Residence Time = 10 hours
Residence Time = 12 hours

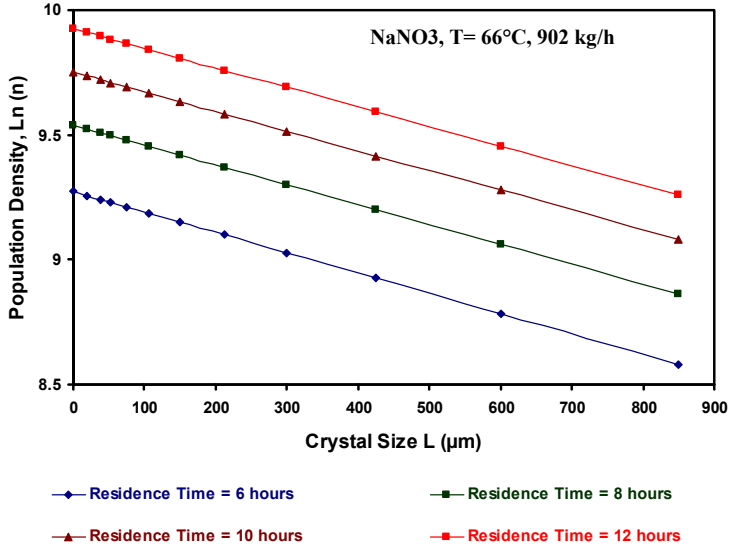
NaNO3, T= 66°C, 902 kg/h
Population Density, Ln (n)
Crystal Size L (µm)
Residence Time = 6 hours
Residence Time = 8 hours
Residence Time = 10 hours
Residence Time = 12 hours

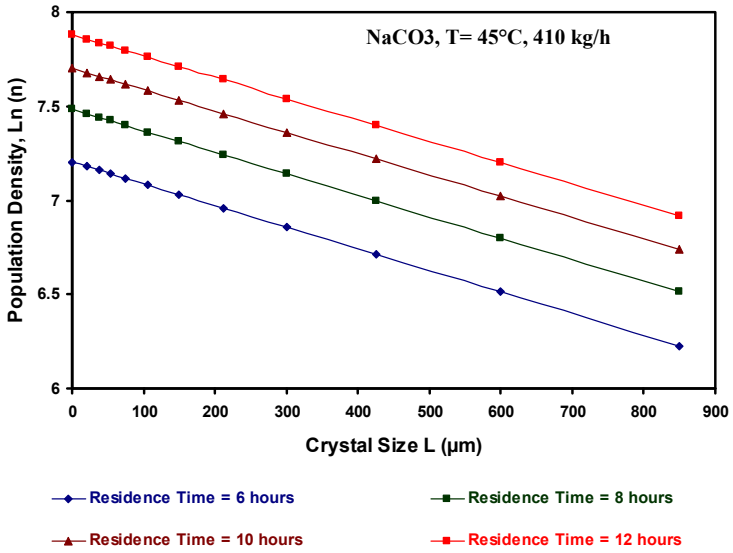
NaCO3, T= 45°C, 410 kg/h
Population Density, Ln (n)
Crystal Size L (µm)
Residence Time = 6 hours
Residence Time = 8 hours
Residence Time = 10 hours
Residence Time = 12 hours

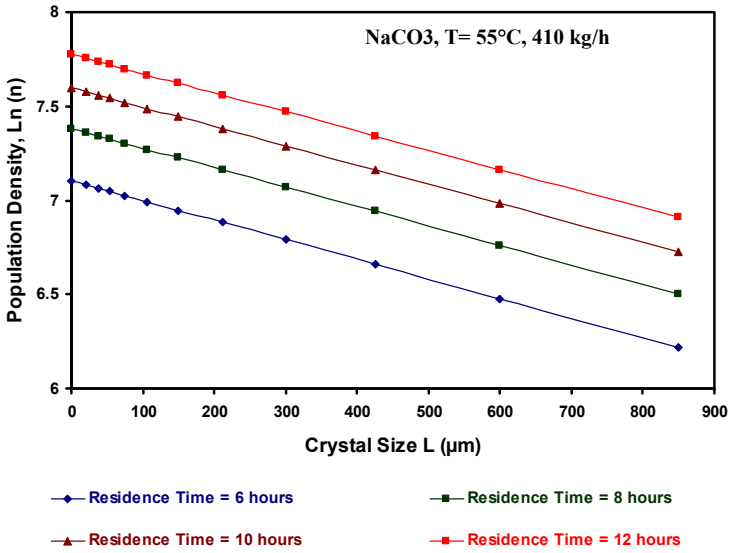
NaCO3, T= 55°C, 410 kg/h
Population Density, Ln (n)
Crystal Size L (µm)
Residence Time = 6 hours
Residence Time = 8 hours
Residence Time = 10 hours
Residence Time = 12 hours

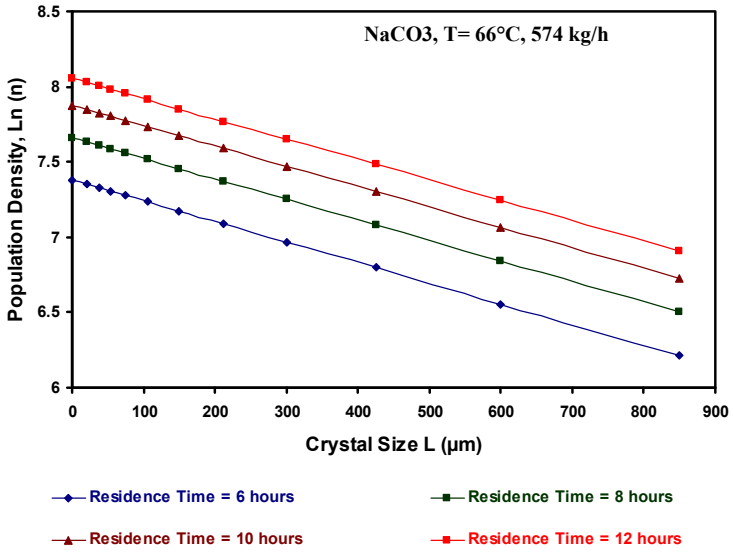
NaCO3, T= 66°C, 574 kg/h
Population Density, Ln (n)
Crystal Size L (µm)
Residence Time = 6 hours
Residence Time = 8 hours
Residence Time = 10 hours
Residence Time = 12 hours

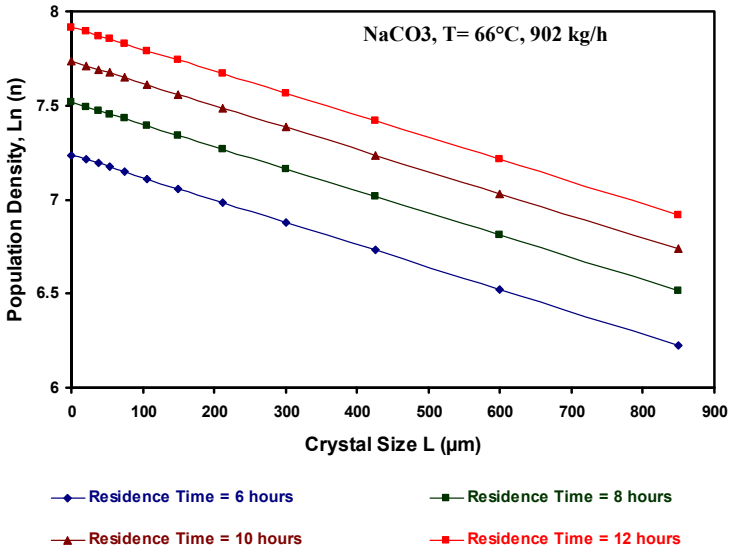
NaCO3, T= 66°C, 902 kg/h
Population Density, Ln (n)
Crystal Size L (µm)
Residence Time = 6 hours
Residence Time = 8 hours
Residence Time = 10 hours
Residence Time = 12 hours

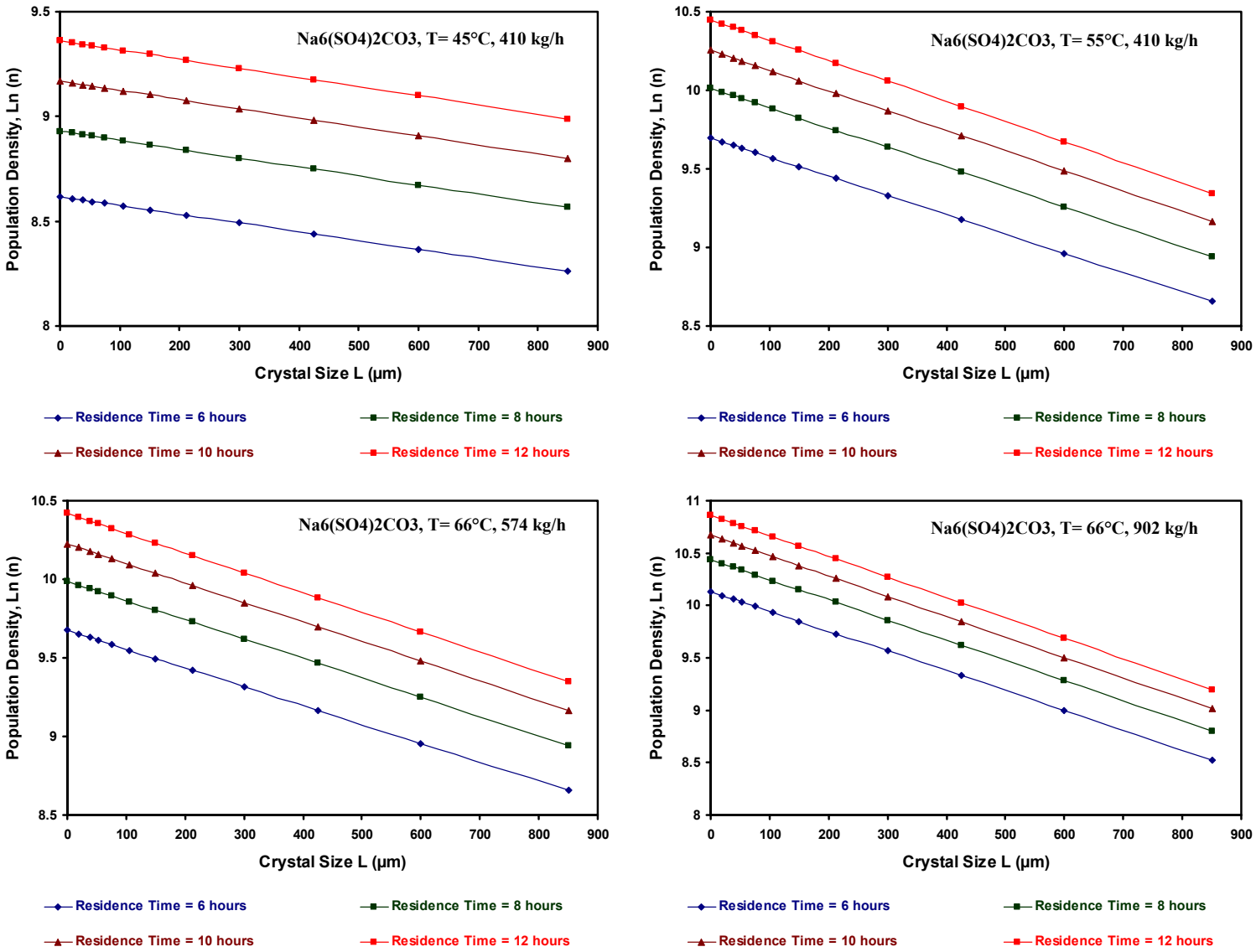

Figure 171. Variation of the population density function for sodium nitrate (Panels A-D), sodium carbonate monohydrate (Panels E-H) and burlkeite (Panels I-L) with varying residence times, operating temperature and evaporation rates

CONCLUSIONS

The purpose of this Section is to review the key findings from the study and to put them in context relative to the work still to be performed.

In the research conducted, the operating conditions were controlled so as to balance four objectives: (1) to control the resulting population distribution and assess its impact on solid-liquid separation and meeting process requirements, (2) to assess the impact of operating conditions on specific kinetics and develop the appropriate empirical correlations, (3) to simplify operations under hot-cell environment and (4) to prepare operation with continuous crystallizer by developing an appropriate and simplified model of the total population density.

As shown in Chapter 3, two certification runs were performed on SST early and SST late feed simulated waste solutions. These solutions represent variability in waste composition during the emptying of the Hanford waste storage tanks. For the early feed certification run, a two stage isothermal evaporative crystallization process was applied following a semi-batch approach. The first and second stages were performed with an evaporation rate of 25 g/h, with temperatures of 66 °C and 40 °C respectively. Assessing the case of the late feed certification run, the experiment used a single crystallization stage performed with an evaporation rate of 91 g/h and at an operating temperature of 60 °C. The design of each of the certification runs was based on an operating temperature for each stage in the run and a final solids fraction in the slurry from each stage. The solubility of key salts was a major factor in selecting the operating

temperature; on the other hand, selection of a target for solids fraction was based on maintaining good mixing and flow characteristics of the slurry. The mass of crystals produced in each stage of a given run, as well as the composition of that mass, was estimated from modeling based on the ESP (Environmental Simulation Program) software with the MSE (Mixed Solvent Electrolyte) supplement, obtained from OLI Systems, Inc (OLI Systems, Morristown, NJ, http://www.olisystems.com/, November 2008), and implemented by COGEMA. With this model, the amount of water that had to be evaporated in order to obtain that crystal mass was determined and used as a guide in operating a run.

In case it is not apparent, it should be pointed out that the mass produced from the batch crystallizer should correspond to what could be expected from a continuous unit. In other words, if the total mass fed to the batch crystallizer were fed to a continuous unit at a specific rate, then the production rate of condensate divided by the feed rate should be the same as the condensate-to-feed ratio from the batch operation. The solids fraction of the product (or, in case selective removal has been implemented, the value resulting if all product streams are combined) would correspond to that in the batch unit. Irrespective of the rate of evaporation, the compositions and amounts of the resulting phases are fixed if the solid-liquid slurry is allowed to reach equilibrium. However, as already pointed out, the nucleation and growth kinetics of each species formed determine the respective crystal size distributions and therefore the handling characteristics of the product. Hence the last three steps (separation, washing, and drying) are greatly influenced by the kinetics.

How each certification run was conducted and the details of the outcomes of each were provided in Chapter 3. Table 73 summarizes comparisons of the process criteria with experimentally determined (actual) values for the three SST Feed certification runs performed.

Table 73. Comparison of required and desired outcomes to experimental results for Hanford waste pretreatment technology

SST Late Feed	Stage	Requirement Value		
Requirement		**Minimum**	**Actual**	**Desired**
Cs Decontamination Factor	Total	-	123.3	14
Sodium Recovery	Total	50%	75.3%	90%
Sulfate to Sodium	Total	0.01	0.00007	0.0022
SST Early Feed	**Stage**	**Requirement Value**		
Requirement		**Minimum**	**Actual**	**Desired**
Cs Decontamination Factor	1	1.15	210	48
	2	1.15	66	48
	Total	1.15	162	48
Sodium Recovery	Total	50%	63.4%	90%
Sulfate-to-Sodium	1	0.01	0.0032	0.0022
	2	0.01	0.0052	0.0022
	Total	0.01	0.0037	0.0022

There are two types of criteria to be met by the process: one type has to do with the exclusion of species (i.e., Cs) from the crystals produced while the other is related to the fractions of sodium and sulfate in the feed solutions that are removed in the crystalline product. Table 73 shows that: (1) all of the actual values exceed those required, (2) the cesium decontamination for both runs and the sulfate to sodium molar ratio for the late feed run meet the desired value.

The mechanisms by which Cs could become part of the crystalline product include the formation of inclusions through overgrowth of mother liquor by the crystal surface, entrapment of mother liquor in either the irregularities of individual crystals or in the crystal cake, in lattice substitution or in interface between two different matrices in the case of heterogeneous crystal formation. Because cesium has such a high solubility in the feed solutions, it is unlikely that it would be

captured by lattice substitution, which leaves the possibility of inclusions, heterogeneous crystallization effect and entrapment. Inclusions typically are formed when crystal growth occurs at high super-saturations. In the certification runs, attempts were made to control the supersaturation at which nucleation and growth occurred, but it is highly likely that some inclusions were formed for the homogeneous crystals obtained. This is obvious in some of the PLM images taken of product crystals and displayed in Chapter 3. Moreover, it is important to add that the operation of a continuous crystallizer would undoubtedly maintain a significantly lower system supersaturation, and there should be less possibility of forming inclusions in homogenous crystals.

Inclusions in heterogeneous crystals are however more important. In heterogeneous crystallization, a crystal is formed following a specific matrix until the system conditions are changed and growth of a different species, following a different matrix, occurs on the first crystal. The interface between the two matrices is a location where inclusions (in particular cesium inclusions) occur. PLM images displayed in Chapter 3 attest of the presence of this type of inclusions and crystal identification performed on early feed certification run shows that this phenomenon is not negligible.

Entrapment of mother liquor in the irregularities of individual crystals or in the void spaces of multi-crystal agglomerates or cakes formed during filtration present problems quite different from inclusions. In principle, mother liquor can be flushed from crystal surfaces provided wash liquid flows through all void spaces. An excellent example of the effect of washing was provided in the experiments described in appendix H. In that work, crystals produced from SST early feed solution were subjected to a series of washing steps and the color of the crystals was used as a measure of how well the washing had been performed. The yellowish color of the

freshly produced crystals, which was attributed to the presence of chromium, was gradually eliminated each successive wash until after four washing stages the crystals were white. The washing done in this experiment involved mixing the crystals in a saturated wash liquid, so that there was no issue of flow through a filter cake, and filtering the resulting slurry. Table 74 displays the evolution of the decontamination factor for both stages of the early feed certification run with respect to the successive wash performed.

Table 74. Decontamination factor evolution for the early feed Certification Run 38b

Sample	DF Value Stage 1	DF Value Stage 2
Feed	N/A	N/A
Unwashed	2.8	1.2
1 Wash	6.3	3.1
2 Washes	21.7	10.8
3 Washes	69.3	24.2
4 Washes	76.7	46.2
Final Crystals	210	66.2

Additional variations to the simulated waste solutions were tested by investigating the effect of solids particles and organics compounds on the crystallization of early feed solutions. A series of fourteen runs were performed to determine which organic species were detrimental to the SST early feed process. Runs were judged based on the following criteria: (1) ease of solid-liquid separation, particularly compared to the control run for the series of experiments; (2) formation of an organic film on the jacketed walls of the crystallizer or on the filter cake; (3) alteration of the crystal population by the addition of organics, and (4) evidence of foaming during the evaporation stage. Analyzing both the crystal size distributions and the solid-liquid separation details leads to the conclusion that there is no consistent link between the two. Most of the difficulties observed during solid-liquid separation were related to the overall texture of

the filter cake and not to any trends in crystal properties. After analyzing the results from these runs it appears that there were four harmless organic species and four troublesome species. For example, runs containing NTA led to a filter cake with a dough-like texture, whereas runs with HEDTA and EDTA led to a cake with a gel-like texture. The texture change in these runs affected the separation time and efficiency, as mother liquor was retained in the filter cake. In several of these runs this was apparent when weighing the final crystals at the end of the run; the mass of crystals was greater although run conditions were similar to the control run for the series of experiments. Along with the fact that the crystal product displayed a yellowish color, this proved that the texture of the filter cake was causing retention of mother liquor. As mentioned in section 3, sodium citrate also led to process difficulties, but not to a change in filter cake texture. Filter plugging was the main issue with sodium citrate, which may be related to the slightly altered CSD for this run. Although the solid-liquid separation step required more time and effort, the final product had a similar color to that obtained during the control run. For this reason, sodium citrate is not considered to be as troublesome to the solid-liquid separation as the other three species. The run performed with EDTA led to film formation and foaming, although foaming was not as intense as with HEDTA. These observations prove that HEDTA is responsible for the severe foaming and that EDTA is the primary cause of the film formation. The comparison of the CSDs and the analysis of the PLM images on sieved crystals show that EDTA is responsible for changing the crystallization kinetics of sodium nitrate.

Assessing the effect of solids particles, a solid solution was prepared using gibbsite, ferric oxide and sea sand and added to the early feed simulant until the feed reached a turbidity value of 5 NTU. The simulated waste solution was then submitted to a two-stage crystallization process operated at 66 °C and 40 °C respectively with an evaporation rate of 25 g/h. The crystal size

distribution, PLM analysis and solid-liquid separation assessment displayed no major discrepancies due to the presence of solid particles in the feed solution. This implies that at pilot scale, using a continuous crystallizer the only necessary modification will be the implementation of a purge in the process to avoid excessive accumulation of solid particles in the pipes and equipments.

It is unlikely that an operation like that performed on the early feed certification run would be possible in a full-scale unit, and that is why so much effort went into studying the influence of process variables on the specific kinetics and resulting crystal size distributions. A series of experiments with evaporation rate ranging between 25 and 75 g/h and operating temperature ranging between 35 and 75 °C were performed. These represent the maximum ranges of conditions that can be applied to the pretreatment process with the equipment described in Chapter 2. Any combination of these temperature and evaporation rate is possible and the optimum conditions are to be determined based on the three process objectives -cesium decontamination, sodium recovery and sulfate to sodium molar ratio- defined in Chapter 1.

Table 75 shows that for this series of experiments on the evaporation rate, the nucleation rate increases with the increase of evaporation while the growth rate decreases. This rule is valid for each species and in the range of evaporation of 25 to 55 g/h. For the experiment performed at 75 g/h, the evaporation rate was too high and the nucleation points, slurry density evolution, crystallization kinetics were affected.

Table 75. Average nucleation and growth rates values for series of experiment on varying evaporation rate

	Nucleation Rate (crystals/ mL·min)				Growth Rate ($\mu m \cdot min^{-1}$)			
Evaporation rate (g/h)	**25**	**35**	**55**	**75**	**25**	**35**	**55**	**75**
Sodium Nitrate	$\mathbf{3.628\times10^{4}}$	$\mathbf{6.014\times10^{4}}$	$\mathbf{1.078\times10^{5}}$	6.680×10^{3}	**1.683**	**1.122**	**0.873**	0.419
Sodium Carbonate Monohydrate	$\mathbf{3.245\times10^{3}}$	$\mathbf{1.522\times10^{4}}$	$\mathbf{1.597\times10^{4}}$	1.239×10^{4}	**0.158**	**0.091**	**0.052**	0.170
Burkeite Crystals	$\mathbf{4.297\times10^{4}}$	$\mathbf{4.826\times10^{4}}$	$\mathbf{2.687\times10^{5}}$	2.081×10^{4}	**0.170**	**0.129**	**0.081**	0.034
Burkeite Agglomerate	$\mathbf{6.106\times10^{3}}$	$\mathbf{3.767\times10^{4}}$	$\mathbf{3.661\times10^{4}}$	2.081×10^{3}	**0.038**	**0.058**	**0.279**	0.505
Sodium Sulfate	$\mathbf{2.724\times10^{3}}$	$\mathbf{1.362\times10^{4}}$	$\mathbf{1.624\times10^{4}}$	1.885×10^{4}	**0.294**	**0.270**	**0.258**	0.554
Sodium Oxalate	**79**	$\mathbf{5.23\times10^{2}}$	$\mathbf{6.569\times10^{3}}$	4.860×10^{3}	**0.193**	**0.158**	**0.092**	0.414

Results showed that values of 55 and 75 g/h were too high leading to an increase in specific nucleation rate and decease in specific growth rate. The decrease in burkeite growth led to smaller single burkeite crystals which were not recovered at the end of the experiments due to loss upon filtration. Furthermore the burkeite agglomeration rate was increased leading to the formation of large clusters that are detrimental to the cesium decontamination. Finally, large fractions of sodium carbonate monohydrate and sodium sulfates were lost through separation due to the low growth rate and high nucleation rate leading to a decreased sodium yield. The higher proportion of fines, and the increased nucleation rate led to higher spread in distribution and separation difficulties. The two evaporation rates of 25 and 35 g/h lead to a trimodal crystal size distribution. The main difference between the two experiments dealt with the repartition of sodium carbonate monohydrate and the burkeite agglomeration. With 35 g/h evaporation rate the sodium carbonate are recovered at lower sieve sizes and some of them are lost through

filtration. Additionally, more single burkeite were lost through filtration while more burkeite agglomerates were formed.

Table 76 shows the average nucleation and growth rates obtained with early feed crystallization at 25 g/h and varying operating temperature. Results showed that: (1) the nucleation rate of all species increased with temperature at the exception of sodium carbonate monohydrate and burkeite crystals, (2) the growth rate of all species increased with temperature at the exception of sodium nitrate, (3) trisodium fluoride sulfate crystals were formed only at extreme temperatures of 45 °C and 75 °C , and (4) nucleation and growth rate at 75 °C were not following the trends defined for a range in temperature from 45 °C to 66 °C.

Table 76. Average nucleation and growth rates for early feed experiments at 25 g/h and varying operating temperature

	Nucleation Rate (crystals/ mL·min)				**Growth Rate ($\mu m \cdot min^{-1}$)**			
Operating Temperature	**45 °C**	**55 °C**	**66 °C**	**75 °C**	**45 °C**	**55 °C**	**66 °C**	**75 °C**
Sodium Nitrate	**9.267×10^{3}**	**2.329×10^{4}**	**3.627×10^{4}**		**4.101**	**2.106**	**1.683**	1.763
Sodium Carbonate Monohydrate	**6.523×10^{3}**	**4.662×10^{3}**	**3.245×10^{3}**	1.487×10^{4}	**0.107**	**0.141**	**0.158**	0.204
Burkeite Crystals	**1.410×10^{3}**	**3.935×10^{4}**	**3.686×10^{4}**	7.802×10^{3}	**0.010**	**0.031**	**0.170**	--------
Burkeite Agglomerate	**---------**	**2.550×10^{4}**	**6.106×10^{3}**	----------	**---------**	**0.024**	**0.038**	----------
Sodium Sulfate	**3.51×10^{2}**	**1.484×10^{3}**	**2.724×10^{3}**	5.159×10^{3}	**0.095**	**0.119**	**0.294**	0.369
Sodium Oxalate	**89**	**3.65×10^{2}**	**79**	1.50×10^{2}	**0.134**	**0.151**	**0.193**	0.193
Trisodium Fluoride Sulfate	1.262×10^{5}	---------	---------	98	0.371	--------	-------	0.220

Assessing the optimum operating temperature, experiments at 35 and 45 °C led to high sodium nitrate growth rate associated to high sodium carbonate monohydrate nucleation. These are detrimental to the requirements mentioned in Chapter 2 given that: (1) the early nucleation of sodium nitrate contributed to high spread in crystal size distribution that is detrimental to the

solid liquid separation, and (2) no burkeite crystals were formed which is detrimental to the sulfate recovery in the solid phase even if trisodium fluoride sulfate crystals were formed with high nucleation and growth rates. The crystallization performed at 75 °C also failed to produce significant amounts of sulfate based crystals due to the low nucleation and growth rate of burkeite and trisodium fluoride sulfate. Furthermore, the combination of low sodium nitrate growth rate and high sodium carbonate growth rate led to high spread in crystal distribution. Only the experiments performed at 55 and 66 °C led to a trimodal crystal size distribution. The main discrepancy between the two distributions came from the increased sodium carbonate monohydrate growth rate with temperature. Three main elements may be considered in favor of the 66 °C crystallization: (1) the agglomeration rate of burkeite crystals is one order of magnitude smaller while the single burkeite growth rate is one order of magnitude higher, (2) the nucleation and growth rate of sodium sulfate are increased at 66 °C which is beneficial to the sulfate recovery, (3) the kinetics of sodium carbonate monohydrate and sodium nitrate are close between these two temperatures ensuring sufficient sodium recovery for both experiments.

A series of empirical correlations were defined to describe the evolution of the crystal number and crystal size with respect to the operating time at the operating conditions of the early feed certification run. This represent a good model of the specific crystal nucleation and growth with a semi-batch process under these conditions that can be used to describe the results obtained during Phase I and Phase II of the project. However, at Phase III, the process has to be implemented at pilot scale using a continuous approach. A population balance based model was hence developed to describe the population density of the three major species crystallizing in a steady-state continuous process. This model used the specific nucleation and growth rate values determined by the semi-batch experiments on single and multi salts feed solutions at 66 °C and

25 g/h evaporation rate. The model of the total population density function is provided in equations 22 and 26:

$$n_{T_{otal}} = \left[\frac{B^{o}_{nano_3}}{G_{nano_3}} \exp(-\frac{L}{G_{nano_3}\tau}) + \frac{B^{o}_{naco_3}}{G_{naco_3}} \exp(-\frac{L}{G_{naco_3}\tau}) + \frac{B^{o}_{burkeite}}{G_{burkeite}} \exp(-\frac{L}{G_{burkeite}\tau}) \right] \quad (22)$$

$$n_{total} = \left[\frac{3.627 \cdot 10^4}{1.680} \exp(-\frac{L}{1.680\tau}) + \frac{3.245 \cdot 10^3}{0.158} \exp(-\frac{L}{0.158\tau}) + \frac{3.686 \cdot 10^4}{0.170} \exp(-\frac{L}{0.170\tau}) \right] \quad (26)$$

A series of simulations were performed using this model allow to obtain for a steady-state continuous crystallizer operating on early feed solution at 66 °C and 25 g/h evaporation with a residence time of 12 hours: (1) the semi-logarithmic plot of the population density function with respect to the crystal size, and (2) the recovered total count, length and mass cumulative distributions. Since the chosen residence time of 12 hours corresponds to the growth time of the first species to be nucleated in the semi-batch crystallizer, the experimental cumulative mass distribution obtained with the semi-batch apparatus and the simulated cumulative mass distribution of the steady state continuous crystallizer could be compared in the same graph as displayed in Figure 172.

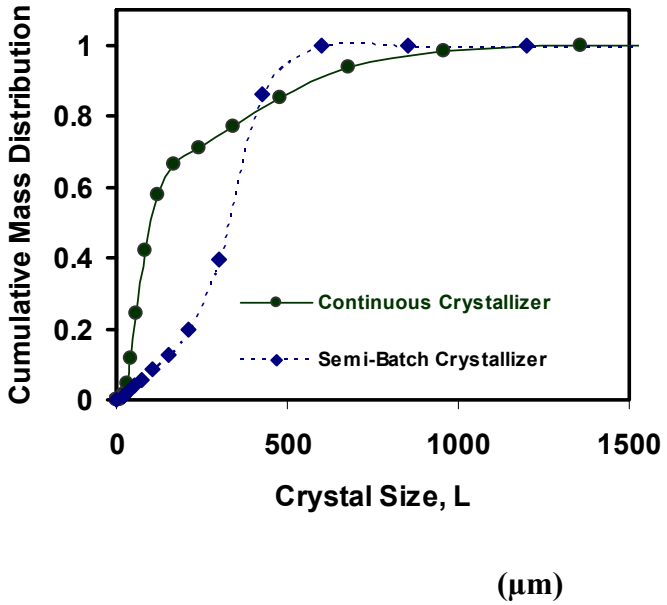

Figure 172. Total cumulative mass distribution comparison between a semi-batch and a continuous crystallizer operated at 66 °C with an early feed solution and a growth or residence time of 12 hours.

Figure 172 displays that the crystals produced in the continuous crystallizer are larger in size than these produced with a semi batch process which is due to:

- The different mode of functioning of the two apparatus. Since the continuous crystallizer is supposed to be performed at steady-state we are neglecting the transitory initial phase of the process during which water is removed by evaporation until the content of the crystallizer (slurry density, crystal mass) reaches the desired value for the steady state. On contrary a semi-batch process require a certain time to achieve nucleation of the different species and the proper slurry density in the crystallizer. Some additional phenomenon occurs in the batch crystallizer for which different mixing conditions, operating conditions (pressure variation) and method of generation of supersaturation (heating of the slurry) are used.

- (2) The non equivalency of residence time and growth time for all of the species. In a continuous crystallizer, the residence time as a fixed and constant value for each of the crystalline species present in solution. However, the semi batch operation displayed a sequence in nucleation leading to different growth times for sodium nitrate, sodium carbonate monohydrate and burkeite.
- (3) The apparent depletion of burkeite crystals due to the formation of sulfate co-crystals in a semi-batch process is not present in a continuous crystallizer model. Additional effect of agglomeration, attrition and breakage may occur during the semi-crystallization that were not simulated by the steady-state continuous crystallizer.

Furthermore, the model developed in equation 27 was used with the kinetics parameters obtained with a semi-batch process operated at 45 °C, 55 °C, 66 °C and 25, 35 and 55 grams per hour evaporation to simulate the evolution of the population density with the operating temperature and evaporation rate. The semi-logarithmic plot of the population density function obtained with a steady-state continuous crystallizer under different temperatures and evaporations with a residence time of 12 hours are displayed in Figure 173.

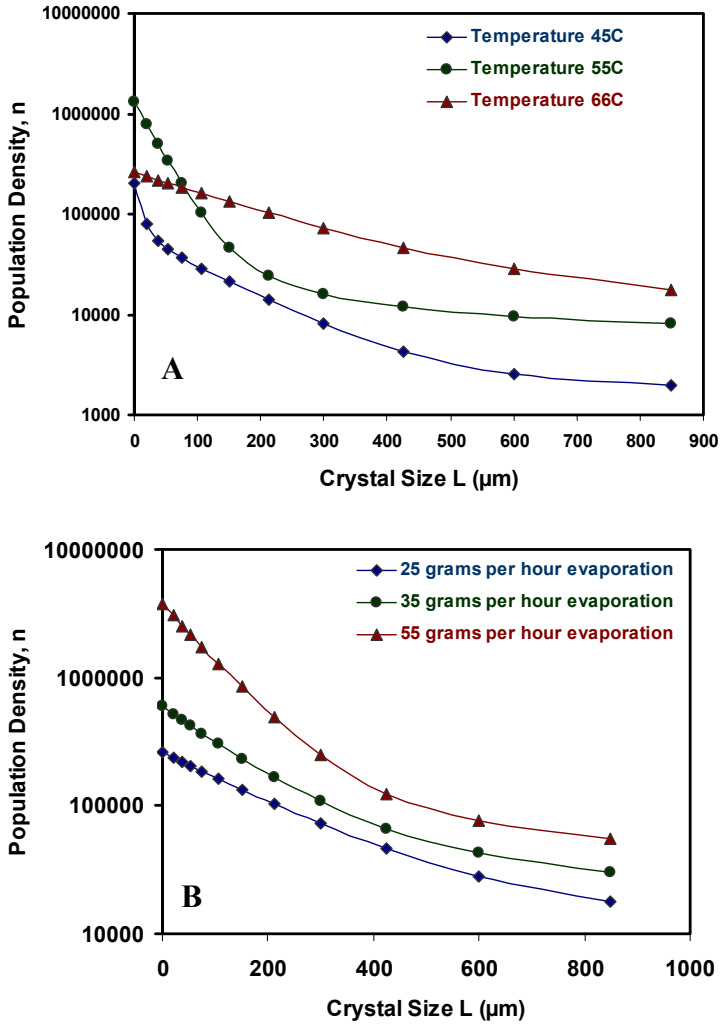

Figure 173. Evolution of the total population density function with operating temperature and evaporation rate for steady-state continuous crystallizer operated with an early feed solution
(Panel A, Operating temperature variation performed with an evaporation rate of 25 g/h, Panel B, Evaporation rate variation performed at 66 °C)

Figure 173 displays a strong dependency of the spread in distribution with the operating temperature and evaporation rate. In essence, (1) the lower the evaporation rate the more uniform the distribution is, and (2) operation at 66 °C provides more uniform distribution than at 55 °C and 45 °C. These results may help deciding the appropriate operating temperature for the continuous crystallizer assuming a certain residence time and evaporation. Note that in this thesis we assumed that the kinetics were influenced by the evaporation rate in a similar manner

in a semi-batch and continuous crystallizer while the heating of the slurry is not performed identically.

The work described in this thesis emphasizes four major accomplishments dealing with evaporative crystallization of multi-component systems.

The first achievement is development of an apparatus and procedures leading to successful fractional crystallization of simulated radioactive waste. The equipment and procedures were duplicated and tested in a hot-cell on actual wastes at the Hanford site. Results obtained with the original and reproduced systems were similar (crystal yield, crystal distribution, crystal speciation, pretreatment requirements) and were used as a basis for a pilot-scale crystallization plant, which is under construction. This thesis describes a novel application of fractional crystallization to the field of radioactive waste pre-treatment, and could be extended to the multi-salt systems present in other waste storage facilities such as Savannah River Site (SC) and Rocky Flats Environmental Technology Site (CO). Future work may focus on (1) ensuring the good functioning of the pilot-scale Hanford pre-treatment facility, (2) extending the technology to different systems present at Hanford, such as Double Shell Tank solutions, and (3) establishing the potential application of the evaporative crystallization technology to systems presents in other waste storage sites.

A second accomplishment is development of a technique to estimate conditions at nucleation, average nucleation rate, average growth rate, and width of metastable zone for a multi-component system. Literature on this topic describes the use of multiple techniques (FBRM, PIV, method of moments applied to resulting crystal distribution) to estimate the kinetics of single component system, or simple shape bi-component systems. However, none of these techniques were successfully applied to multi-component system leading to several

crystalline species with different morphologies, or processes operated under vacuum. This thesis describes how PLM image analysis applied to samples extracted from the active volume of simulant feed solutions crystallizations was used to estimate average kinetics. The novelty of the technique described in this thesis is not the concept (use of PLM image analysis) but the successful application of this method to complex multi-component system and the extent of the analyses performed with this method. One of the main limitations of this technique, other than the important analytical work required to perform the image analysis, is the fact that it depends on sampling and is hence not considered as "on-line" equipment. Future work would require improving the current apparatus by implementing:

- An adiabatic box with circulating heating fluid surrounding the microscope in order to control more accurately the temperature of the microscope slide and the cooling conditions of the sample that could affect the accuracy of the analysis
- A pumping system that could allow the sample to be automatically taken from the operating volume and reintroduced after sample analysis
- An image analysis software using a crystal morphology database with information such as crystal shape, average size, and color to allow an automated and accurate analysis of PLM images.

Such a device would present a successful alternative to current methods, a consequent progress toward the quantitative analysis of multi-component systems, and could find applications in chemical production, pharmaceutics and pulp and paper industries. Figure 174 displays the schematic of the proposed equipment.

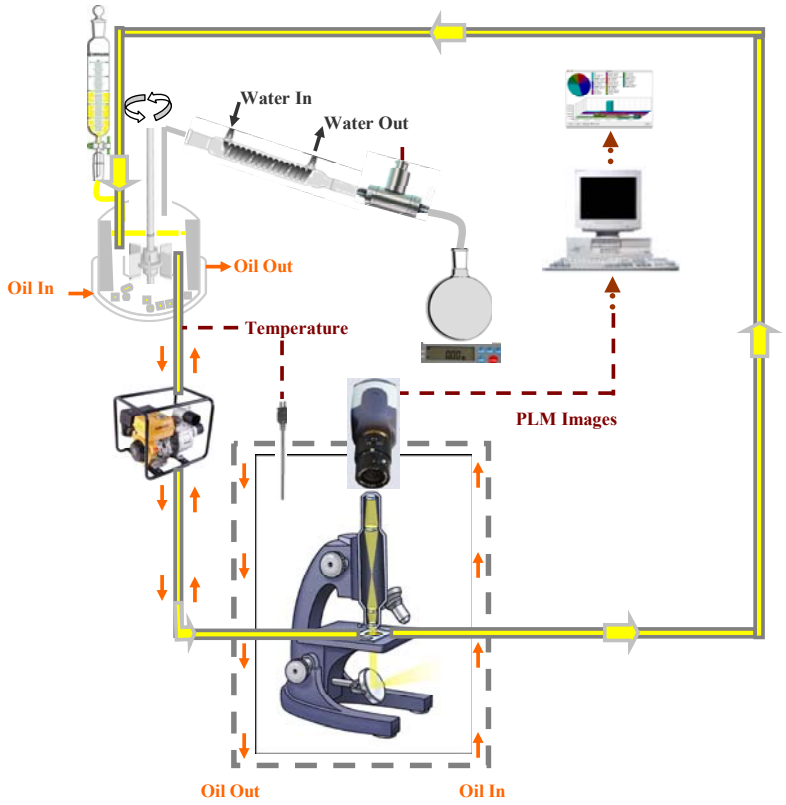

Figure 174. Proposed equipment to perform crystallization kinetics estimates based on sampling and PLM analysis

A third achievement is description of the crystallization of multiple crystalline species with various morphologies, kinetics and thermodynamics properties based on the evaporative crystallization of multi-component systems with the composition of the early feed solution and at the operating conditions of Hanford waste pretreatment. This thesis studied the effect of operating conditions (temperature and evaporation rate) on kinetics, metastable zone, crystal distribution and supersaturation. The sodium salts presents in these solutions (sodium carbonate, sodium nitrate, sodium sulfate, sodium oxalate and burkeite) are very common sodium salts in systems studied in the pulp and paper (burkeite) and the chemical production fields (carbonate salts). The work described in this thesis could hence be extended to multi-salts systems with different compositions using the results, apparatii and methodologies developed in this work.

The fourth accomplishment is study of the link between semi-batch and scaled-up continuous processes. In chapter 5, two simple steady-state MSMPR models were developed. The first model is based on the population balance for a small-scale steady-state MSMPR operated continuously and uses kinetics determined experimentally with a small-scale semi-batch apparatus. This simple model simulates the performance of a small-scale continuous crystallizer and do not necessitate the implementation or operation of a continuous crystallizer. The advantage of this method is that small-scale batch apparatii are easier to built and operate than continuous processes. The application of this model is not limited to tri-salt systems at the conditions of the early feed pretreatment and could be extended to any multi-component system operated with various operating temperature and evaporation values.

The second model uses both population balance and mass balance of steady-state large-scale continuous crystallizers to investigate the effect of operating conditions (such as residence time) on crystallization kinetics (growth rate) and on population density function. In the thesis, this model presents two strong limitations:

- The values of the concentration at saturation are needed and were obtained by thermodynamic simulations due to the complex nature of the early feed system (more than three major crystalline species with unconventional compositions and high pH). The concentrations at saturation would most likely be available in the literature or easily obtained experimentally with a less complex multi-component system.
- The value of the nucleation rate was assumed to be constant and equal to the one obtained with batch experiments. Even if this represents a strong assumption, the model would still be

useful for scaling up continuous system providing that a small scale continuous apparatus was built and operated.

This work could be extended to different systems by developing a computer program using the population balance and the mass balance of continuous steady-state MSMPR to calculate the population density function for a specific species for various residence time values based on semi-batch and continuous small-scale experimental kinetics values.

APPENDICES

WASHING-FILTRATION APPARATUS DESIGN

Figure A1. Illustration of the custom designed washing-filtration apparatus as per chemglass drawing.

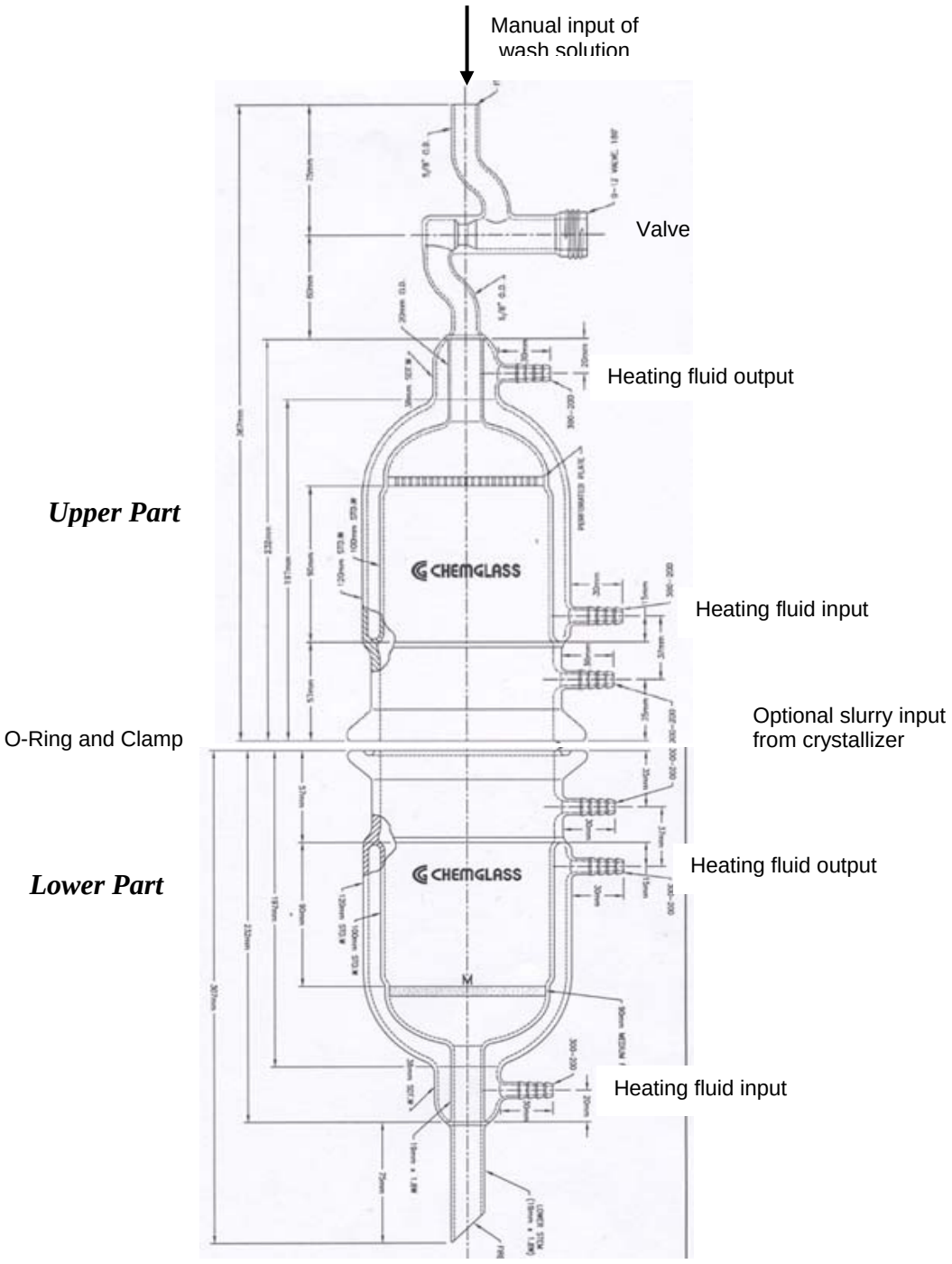

Figure A2. Detailed components of the filtration and washing apparatus.

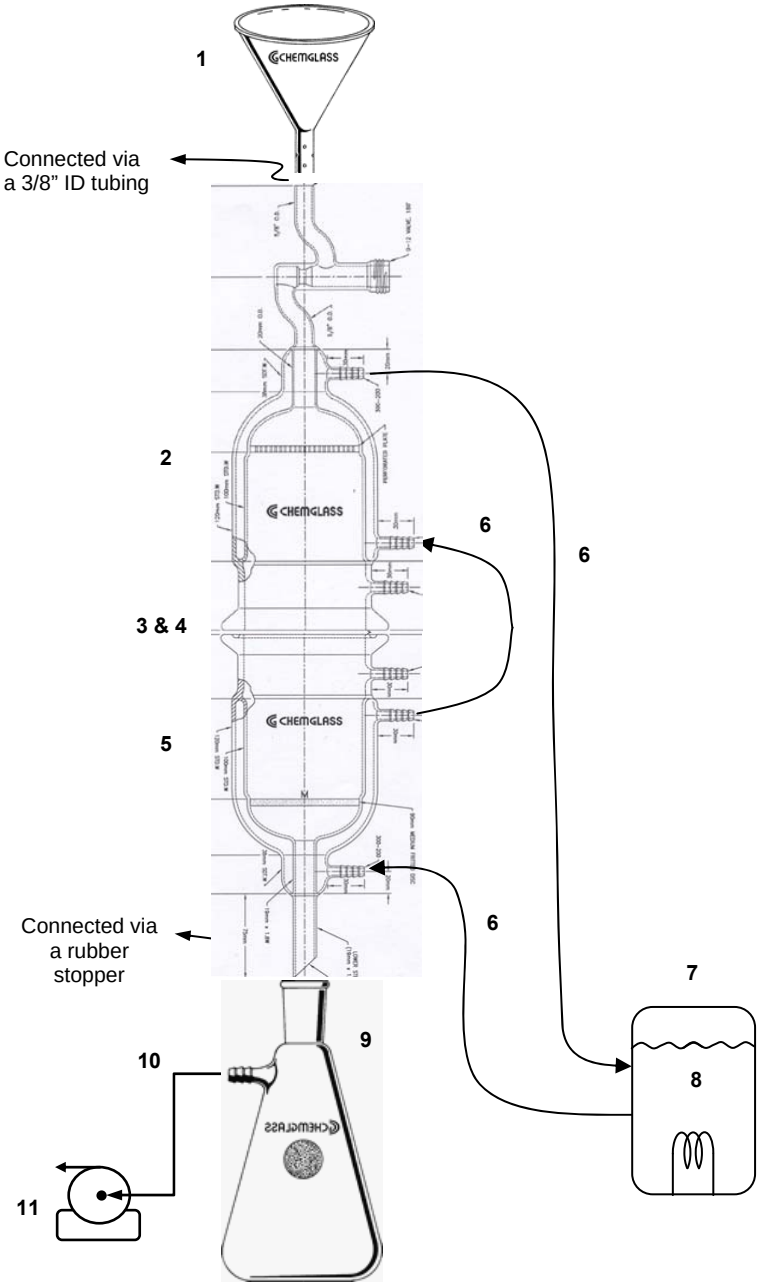

Table A3. Itemized list of filtration/washing on apparatus components according to figure A2.

Item	Description	Provider	Catalog No.	Notes
1	Funnel	GA Tech		
2	Jacketed Buchner Funnel, 90mm Diameter Perforated Plate, 0-12mm Chem-Vac Valve on top, 100mm ID Schott Flat Flange on the bottom, 10mm OD Hose Connection@90° located between the Jacket and Flange per Chemglass Drawing	Chemglass	Special/GT-0507-011JS	Special design
3	Clamp for Duran® reaction PER Quote# JS-16810	Chemglass	CG-141-02	
4	O-ring, Viton®, 100mm Flange	Chemglass	CG-147-21	
5	Jacketed Buchner Funnel, 90mm Diameter Medium Frit, 100mm ID Schott Flat O-ring Flange on the top, 10mm OD Hose Connection@90° located between the Jacket and Flange, 3/4" OD Lower Drain, per Chemglass Drawing	Chemglass	Special/GT-0507-012JS	Special design
6	Tygon Tubing, 1/2” OD x 3/8 ID, 10ft	GA Tech		
7	VWR Heating bath 13l programmable 1157P	VWR	13271-106	
8	Heating fluid DC 200 5 cs	Ashland, GA	3311089 600	
9	Vacuum Filtration flask, 1000 mL	GA Tech		
10	Vacuum tubing, 5/16" ID	Fisher	14-175D	
11	Dry pressure/vacuum pump, Welch	Fisher	01-051-1C	

Figure A4. Detailed crystallizer components.

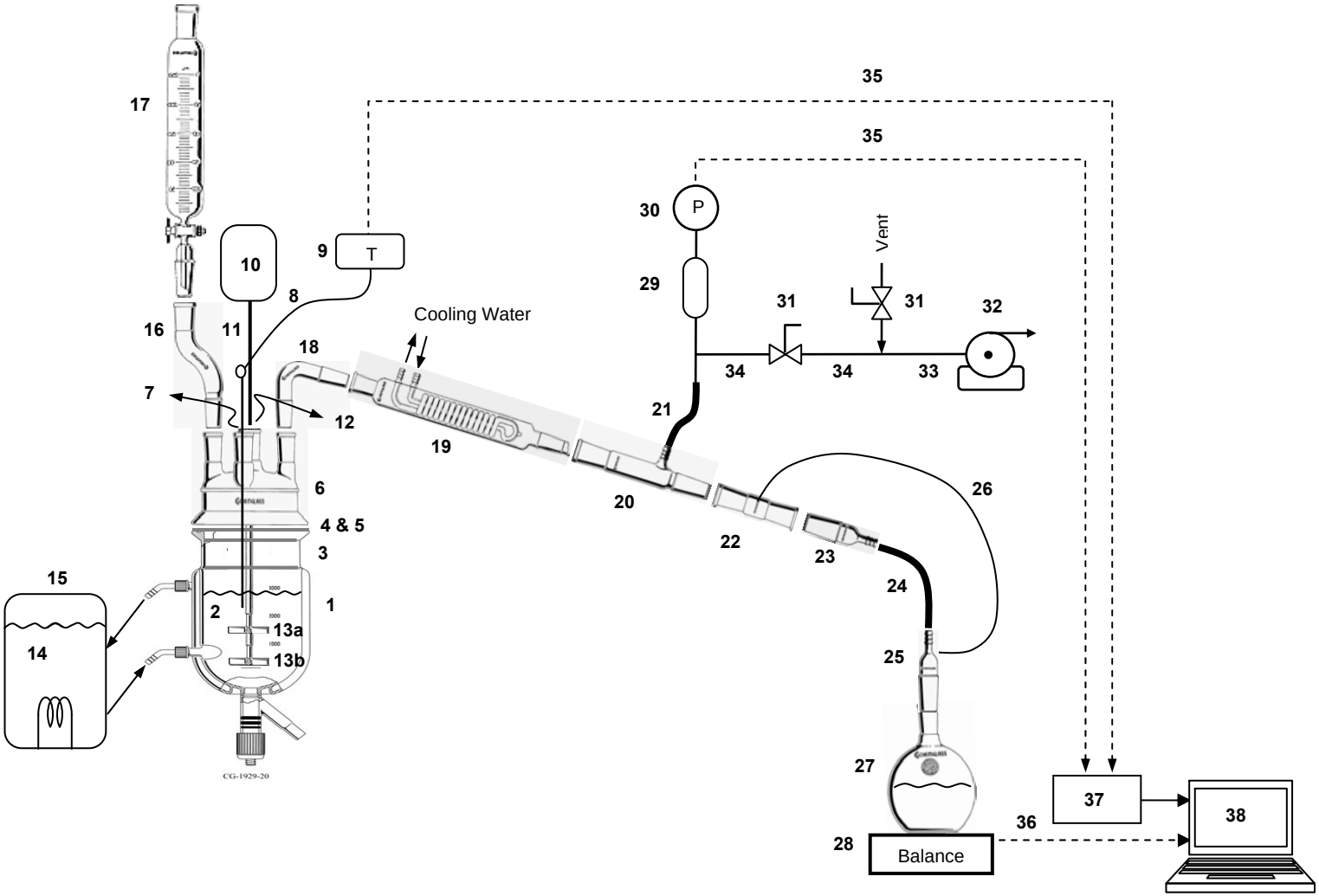

Table A5. Itemized list of crystallizer components according to figure A4

Item	Description	Provider	Catalog No.	Notes
1	Jacketed Reaction Vessel, 1-Liter	Chemglass	CG-1929-14	
	Jacketed Reaction Vessel, 300 mL	Chemglass	CG-1929-10	
2	Baffles	GA Tech		Home made
3	Clamp, 100mm	Chemglass	CG-141-02	
4	Viton O-Ring, 100mm	Chemglass	CG-147-21	
5	Support clamp, 100 mm	Chemglass	CG-1947-01	
6	Reaction Vessel Lid, 4-necks, all 24/40 joints	Chemglass	CG-1941-01	
7	Thermocouple, Hastalloy C-276, Type “T”, 1/8”, 12” long	Chemglass	CG-3498-302	
8	Thermocouple Adapter, 24/40, 1/8"	Chemglass	CG-1042-E-01	
9	Analog Temperature Controller/Display	Omega	CNi3253	
10	Stirrer motor, IKA Model RW 16	Fisher	14-260-31	
11	Stirrer Shaft, 555 mm	Chemglass	CG-2075-B-03	
12	Stirrer Bearing, Chemvac™, Teflon®, 24/40, 10mm	Chemglass	CG-2077-G-01	
13a	Agitator, TFE, 10 mm Stir Shaft, 4 Blades, 45°, 75 mm Diameter	Chemglass	CG-2091-02	
13b	Agitator, TFE, 10 mm Stir Shaft, 4 Blades, 45°, 50 mm Diameter	Chemglass	CG-2091-01	
14	Heating fluid DC 200 5 cs	Ashland, GA	3311089 600	
15	VWR Heating bath 13l programmable 1157P	VWR	13271-106	
16	Offset Adapter, 24/40 joint size	Chemglass	CG-1033-01	
17	250 mL Graduated separatory funnel, 2mm Teflon stopcock, 24/40 joint size	Chemglass	CG-1734-03	
18	Adapter, Distillation, 75°, 24/40	Chemglass	CG-1010-01	
19	Reflux Condenser, 175mm Coil Length, 24/40	Chemglass	CG-1213-L-21	
20	Inlet adapter, straight, 24/20 joint, hose connection	Chemglass	CG-1062-01	
21	TYGON Vacuum Tubing, 3/8"ID x 7/8"OD	Cole-Parmer	EW-06413-30	
22	Adapter, 24/40 Outer Jt. to 24/40 Outer Jt. with a ¼”-28 Thread sealed in between the Jts., supplied complete with ¼”-28 Tefzel Union	Chemglass	GT-0505-061JS	Custom designed
23	Inner adapter, 24/40 Inner Joint, 86mm Height	Chemglass	CG-1012-01	
24	Nalgen 980 Braided Clear PVC Tubing, 1/4" ID	Fisher	14-169-10A	
25	Inlet Adapter, Top Hose Connection, Lower 24/40 Inner Jt. with a ¼”-28 Thread sealed in between the Jts., supplied complete with ¼”-28 Tefzel Union	Chemglass	GT-0505-062JS	Custom designed
26	Teflon Tubing, .062” ID x .125” OD, 10 ft.	Chemglass	CG-1164-02	
27	Flat Bottom Flask, 24/40, 1000 mL	Chemglass	CG-1500-07	

Item	Description	Provider	Catalog No.	Notes
28	Balance PB1502-S, Mettler Toledo	VWR	11274-918	
29a	Pressure Transducer, 0-50 psia, Current Output)	Omega	PX305-050AI	
29b	Snubber	Swagelok	SS-4-SA-EA	
30	Process Meter and Controller	Omega	DP25B-E	
31	Stainless 1-Piece Ball Valve, 1/4 in. Tube Fitting	Swagelok	SS-42S4	
32a	Two-stage Welch Vacuum Pump	Fisher	01-129-4	
32b	Regulating Valve for Welch Pump	Fisher	NC9186594	
33	PTFE Tubing,1/8" ID x 1/4" OD	Cole-Parmer	EW-06605-13	
34	316/316L Seamless Stainless Steel Tubing	Swagelok	SS-T4-S-035	
35	Teflon Coated Cable, 10 ft	Omega	TECT10-11	
36	RS-232 Serial Port	Measurement Computing	PCI-COM232/4-9	
37	USB Based Data Acquisition Module	Measurement Computing	PMD-1208FS	
38	LabView software on a PC			

OPTICAL SETUP AND ILLUMINATION ADJUSTMENT FOR THE PLM

B1.0. OPTICAL SETUP AND ILLUMINATION ADJUSTMENT FOR THE PLM

This procedure is supplementary to the description of the use of the PLM given in chapter 2.

1. Turn on the illuminator and place the slide on the microscope stage (11) and fix it with the clamp. Slide out the analyzer (16) and compensator (21 placed in 14) plates from the light path then rotate the 10X objectives into position for focus.
2. Move the substage condenser up to its top position using the substage focusing control (7). Check to make sure that both the field iris (3a) and the aperture iris (3b) are fully open.
3. Focus down on the specimen slide (9) without bombing the objective into the slide until details can be seen in the eyepiece (18). Adjust the light brightness using the intensity control knob (6).
4. Adjust the distance between the two binocular eyepieces (18a and 18b) to fit the observer's eyes.
5. Fine focus (9b) to get a sharp image in the right eyepiece (18b) using your right eye.
6. Using your left eye, adjust the diopter adjustment collar on the left eyepiece (18a) (not the fine focus) to get the sharpest image.
7. Now turn the field iris adjustment ring (3a) until the field iris is seen.
8. Raise or lower the substage condenser (7) to focus the field iris sharp in the plane of the specimen. Then open out the field iris until it is just outside the field of view.
9. Remove one of the eyepieces (18) and reduce the intensity of the disc of light coming from the back of objective to about 75% using the aperture iris (3b).
10. Similar adjustments should be repeated for each objective.

[*] All numbers in parenthesis correspond to element numbers appearing in Figure 14.

B2.0 PLM OBJECTIVE CENTERING PROCEDURE

This procedure is supplementary to the description of the use of the PLM given in chapter 2.

The objectives should be precisely seated in the optical axis. If it is even lightly off the axis the specimen image will stray from the center of view upon rotation of the stage. If this happens then the objective needs centering using two hexagon keys supplied with microscope as follows:

1. Remove the analyzer and compensator plates from the light path and swing in the 10X objective which is mounted in the non-centerable opening. All other objectives are mounted in floating centerable nosepiece holes.
2. Focus down on the specimen and memorize the pinpoint appearing on the eyepiece cross-line center (18b).
3. Turn the nosepiece (13) and bring the higher power objective to position and focus then see if the memorized specimen pinpoint is located at the cross mark. If not, insert the two centering screws into the key holes on the nosepiece ring above the objective and turn to move the pinpoint to the cross point.
4. Repeat the same procedure for the remaining objectives.

All numbers in parenthesis correspond to element numbers appearing in Figure 14.

B3.0 OBJECTIVE SCALE CALIBRATION

This procedure is supplementary to the description of the use of the PLM given in chapter 2.

1. Turn on the illuminator and place the standard micrometer slide on the stage (11). Slide out the analyzer (16) and rotate desired objective, e.g., 10X, into position for focus. Turn on the Digital camera and start the Image-Pro Plus software and the live preview.
2. Focus down on the micrometer slide (9) and adjust the light intensity (6) until the graduated micro-ruler appears clearly on the live preview. Record the image of the micro-ruler by pressing "Snap."
3. On the Image-Pro Plus main menu, select *Measure* → *Calibration* → *Spatial* sequence where the Spatial Calibration window is displays. This window is linked to the active image of interest. Press "New" to create a new set of calibration value or to edit current ones. Edit the name to desired Objective power value, e.g., 10X, and then select the desired unit from the *Unit* list, preferably microns. This will be the unit of measurement that will appear on the graphs. On the "Pixels/Unit" group box press the "Image" button, where a scaling dialog box opens, and draw a straight horizontal line on the recorded micro-slide reference image between two grids of known length, e.g., 25 μm. Then write this value in the scaling dialog box and press OK to close the box and return the Spatial Calibration menu. Keep other values un-changed and press OK.
4. Repeat steps 1-3 for all other objectives to calibrate them.

All numbers in parenthesis correspond to element numbers appearing in Figure 14.

SIEVE TEST PROCEDURE

C.1 Sieve Test Simplified Procedure

Sample Preparation

1- Dispose the final dried crystals into a cookie dish and spread them evenly

2- Separate the weak aggregates with a Teflon spatula.

3- Choose the eleven sieves[1] to be used for the sieving analysis (refer to the last paragraph for more precision on this topic).

4- With a large spatula collect the crystals and sieve them manually through the sieve presenting the highest size among the selected sieves.

5- Collect these crystals on a weighing paper until reaching 35 g of crystals.

6- Separate the 35 g of crystals into three samples of 15 g each. Place them on a weighing paper. Label them by writing the sample number on the paper[2].

Sieving Preparation

7- Wash the sieves to be used with hot water and allow them to dry for 30 minutes to one hour in an oven.

8- Place the sieves to be used in "sieve number" increasing order when going from top to the bottom of the sieve column[3].

9- Measure the weigh of the empty sieves and record this number. At the end of the sieving, the difference in mass will determine how many crystals were collected.

10- Insert the crystals evenly on the top sieve and place the cover on the sieve column.

Sieving Performing

11- Place the column in the Rotap apparatus. Place the Rotap cover and position the agitated arm above the cover[4].

12- Set the sieving time to 30 minutes[5]. Press the "power "button.

13- Close the sieving doors (keep the noise from spreading in the sieving machine surroundings) and let the sieving being performed during the 30 minutes.

Results Collection and Analysis

14- At the end of the sieving, collect the weight of each of the sieves with the crystals recuperated inside. Determine the mass of crystals in each sieve by making difference with the weigh recorded in step 9.

15- Plot on Excel or any appropriate software the "cumulative mass"[6] and CSD graphs.

16- Perform three times the procedure (steps 7 to 14) for the three samples prepared in 6.

Compare each of the three graphs obtained and conclude on crystal size distribution of the studied sample.

Validation with PLM Imaging and XRD

17- Weight and label eleven plastic cups. Labels have to present the type of feed (i.e. Early, Late, DST), the Stage (i.e. 1 or 2) and the crystal size range for each sieve

18- Collect the crystals contained in each sieve inside the properly labeled plastic container. Record the final weigh.

19- Determine the sample mass of crystals by subtracting the weight recorded in 19 to the one recorded in 18.

20- Prepare at least 3 slides for each crystal size. Preparation consists in disposing a sample of crystal in one slide, adding some silicone oil, and placing a round shape slide to cover the sample.

21- Take pictures of each sample for each size range and conclude on the content of each sieve in terms of crystals species collected and potential agglomeration or breakage.

22- Collect at least 0.7 g of crystals for each sieve to prepare the sample to be used for XRD analysis.

23- Perform XRD on each sample and conclude on crystals species identification and CSD.

C.2.0 Sieve Size Selection

The sieves may be selected by (1) performing the sieving of one of the three samples selected in 6, (2) performing the sieving of an additional sample, or (3) by following the tables presented in appendix A and B.

[1] Eleven represents the maximum number of sieves that can be used with the Rotap Apparatus.

[2] Refer to figure 1.

[3] refer to figures 2 and 3.

[4] refer to figure 3.

[5] The sieving time is important when operating sieving analysis. A fairly large sieving time would eventually lead to crystals breakage inside the sieving due to chocks with the sieves walls or between crystals. On the other hand a small sieving time would lead to poor segregation between the crystal sizes and hence would bias the sieving experiment. 30 minutes sieving time associated with a sample size of 15 g have been determined as appropriate sieving conditions.

[6] An example calculation of cumulative mass is presented in appendix C.

Figure C1. Random samples selection

Figure C2. Sieves available for sieving

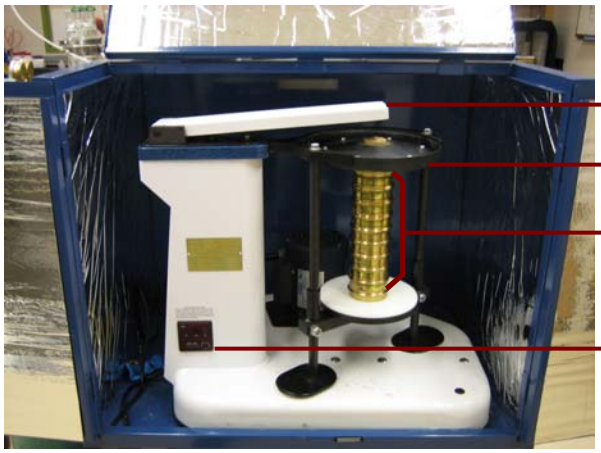

Figure C3. Sieving apparatus

Table C4. Sieves used for the first stage of early feed run

No.	ASTM Sieve No.	Nominal Sieve Opening (μm)
1	16	1180
2	20	850
3	30	600
4	40	425
5	50	300
6	70	212
7	100	150
8	140	106
9	200	75
10	270	53
11	Pan	0

Table C5. Sieves used for the second stage of early feed run

No.	ASTM Sieve No.	Nominal Sieve Opening (μm)
1	20	850
2	30	600
3	40	425
4	50	300
5	70	212
6	100	150
7	140	106
8	200	75
9	270	53
10	400	38
11	Pan	0

Table C6. Sieves used for the first stage of late feed run.

No.	ASTM Sieve No.	Nominal Sieve Opening (μm)
1	20	850
2	30	600
3	40	425
4	50	300
5	70	212
6	100	150
7	140	106
8	200	75
9	270	53
10	400	38
11	635	20
12	850	10
13	Pan	0

For the first stage a first sieving was performed with the sieves numbered from 1 to 11. A second sieving was then performed on the crystals collected in the sieve 11 by replacing sieves 1 and 2 by sieves 11 and 12.

Table C7. Sieves used for the second stage of late feed run

No.	ASTM Sieve No.	Nominal Sieve Opening (μm)
1	20	850
2	30	600
3	40	425
4	50	300
5	70	212
6	100	150
7	140	106
8	200	75
9	270	53
10	400	38
11	Pan	0

C3.0 Sample calculation for CSD and cumulative mass distribution

Sample Name	Late feed stage 1
Sample weight (g)	14.06
Sieving time (min)	30

Sieve no.	Mesh opening	Range	Ave. Size (micron)	Before sieving (g)	After sieving (g)	Crystal weight (g)	Collected %	Cumulative %
20	850	>850	850	126.74	126.74	0.00	0.00	100.00
30	600	600-850	725	125.02	125.16	0.14	1.00	100.00
40	425	425-600	512.5	115.98	116.44	0.46	3.27	99.00
50	300	300-425	362.5	110.7	111.99	1.29	9.17	95.73
70	212	212-300	256	112.5	116.85	4.35	30.94	86.56
100	150	150-212	181	106.69	110.07	3.38	24.04	55.62
140	106	106-150	128	105.23	106.53	1.30	9.25	31.58
200	75	75-106	90.5	105.1	105.93	0.83	5.90	22.33
270	53	53-75	64	103.93	104.52	0.59	4.20	16.43
400	38	38-53	45.5	102.78	103.3	0.52	3.70	12.23
635	20	20-38	29	104.56	105.1456	0.59	4.17	8.53
850	10	10-20	15	107.7	108.3144	0.61	4.37	4.37
Pan	0	0-10	5	82.9	82.9	0.00	0.00	0.00
					TOTAL	14.06	100.00	100

The “crystal weight” column corresponds to the mass of crystals collected on each pan. This mass is obtained by subtracting the “before sieving” and “after sieving” recorded mass.
This mass is converted in percent (collected percent column) by using the total crystal weigh (total mass of the sample). The crystal size distribution presented in figure C1 corresponds to the plot of the “crystal weight” column with respect to the “average crystals size”.
The “cumulative percent” is obtained by adding the collected percent of each preceding crystal size. The cumulative mass distribution presented in figure C2 corresponds to the plot of the “cumulative percent” column with respect to the “average crystal size” column.

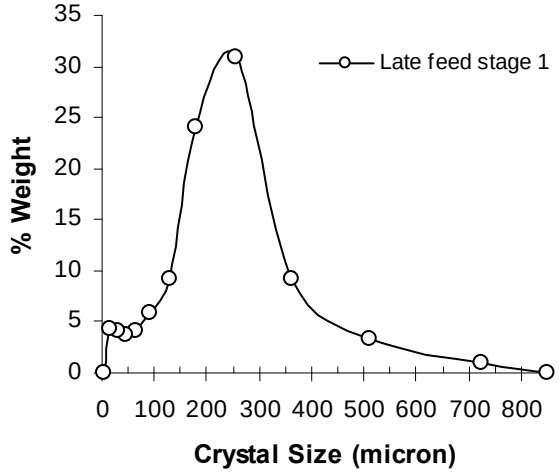

Figure C4. Crystal size distribution

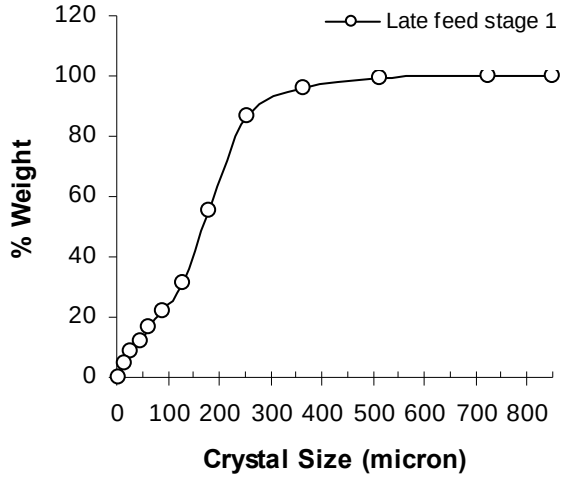

Figure C5. Cumulative mass distribution

SEEDING AND PRELIMINARY CERTIFICATION RUNS

D1.0 SEEDING OF BATCH RUNS

The addition of seed crystals is a well-accepted procedure for controlling nucleation and the resulting crystal size distribution produced in batch crystallization; on the other hand, seeding is unnecessary, except in special circumstances, when the operation is of a continuous nature. It is thought that burkeite is the most suitable candidate for seeding for the following reasons: (1) it is one of the major species and it grows relatively slowly, and (2) crystals larger than 20 μm may facilitate solids separation.

Seeding was examined in experiments involving a 3-salt solution of sodium nitrate, sodium carbonate and sodium sulfate. The main purposes of these experiments were to study the effect of seeding on product properties and to investigate potential modifications in procedures that would reduce the amount of crystal accumulation on the walls of the crystallizer. Seeded 3-salt experiments (Runs 17 and 18) used sodium sulfate and sodium carbonate crystals as seed crystals.

The objective of using burkeite seed crystals in the 3-salt crystallization experiments was to obtain larger burkeite product crystals. The seed crystals were obtained from an earlier burkeite run performed according to the simulation Lab1B.xls. The product from that run was sieved, and the crystals retained on the smallest sieve (35 to 58 μm) were used as seeds in Run 18. Unfortunately, after performing Run 18, some question as to the actual composition of the seed crystals arose and they may have instead been a physical mixture of sodium sulfate and sodium carbonate.

The amount of seed crystals added in Run 18 was 10% of the expected mass of burkeite crystal yield as predicted by the simulation. The majority of the seed crystals appeared to be agglomerates comprised of constituent fine crystals whose shapes were similar to that of sodium sulfate. These agglomerates were close to 35 μm in size. The addition of seed crystals was expected to lead to larger product crystals. Since it was thought originally that the seed crystals were burkeite, larger crystals of this species were expected. PLM observations of the product from this run showed larger sodium carbonate and sodium sulfate crystals than in previous non-seeded 3-salt crystallization runs. There appeared to be little effect of the seed crystals on the size of the burkeite crystals in the product, and it was this observation that threw the composition of the seed crystals into question.

The product from Run 18 was washed with acetone, dried, and sieved to give the results shown in the following figure. The distribution is quite uniform and exhibits no significant post-washing agglomeration.

Figure D1. Size distribution of the seeded 3-salt experiment (Run 18).

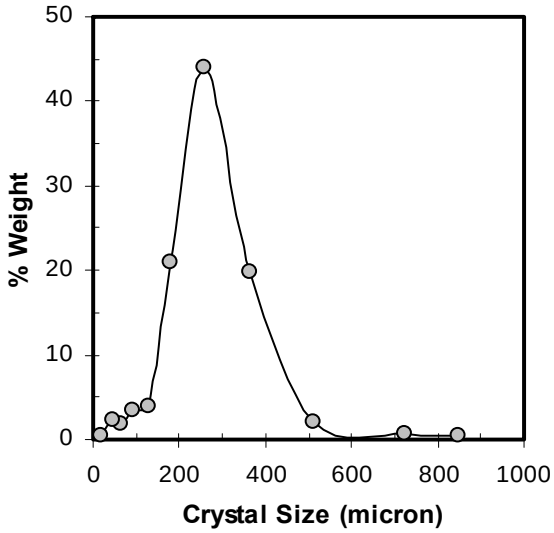

D2.0 TEMPERATURE AND PRESSURE PROFILES FOR THE CERTIFICATION RUNS 26 and 27 (preliminary early and late feed certification runs)

Figure D2. Temperature and pressure profiles for the SST early feed solution certification run. dotted lines represent target temperatures.

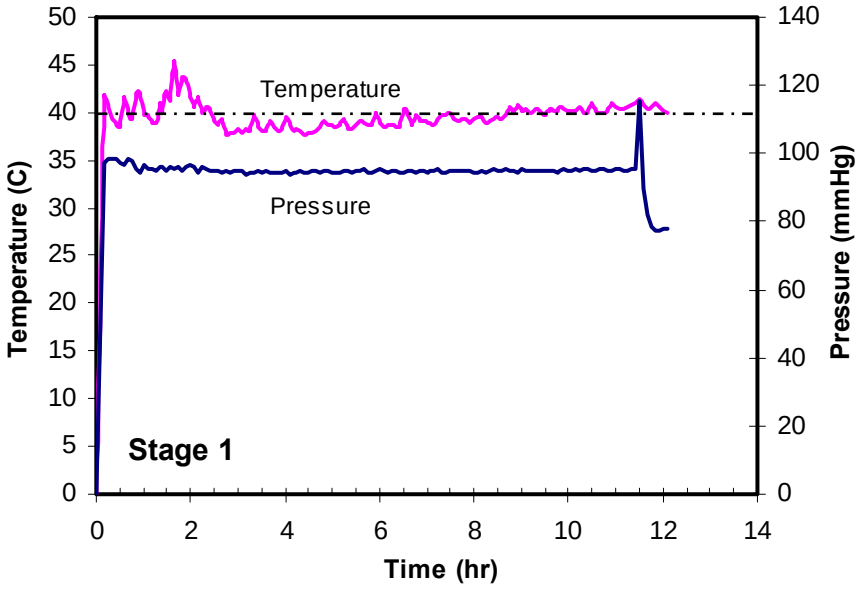

Figure D3. Temperature and pressure profiles for the SST late feed solution certification run. dotted lines represent target temperatures.

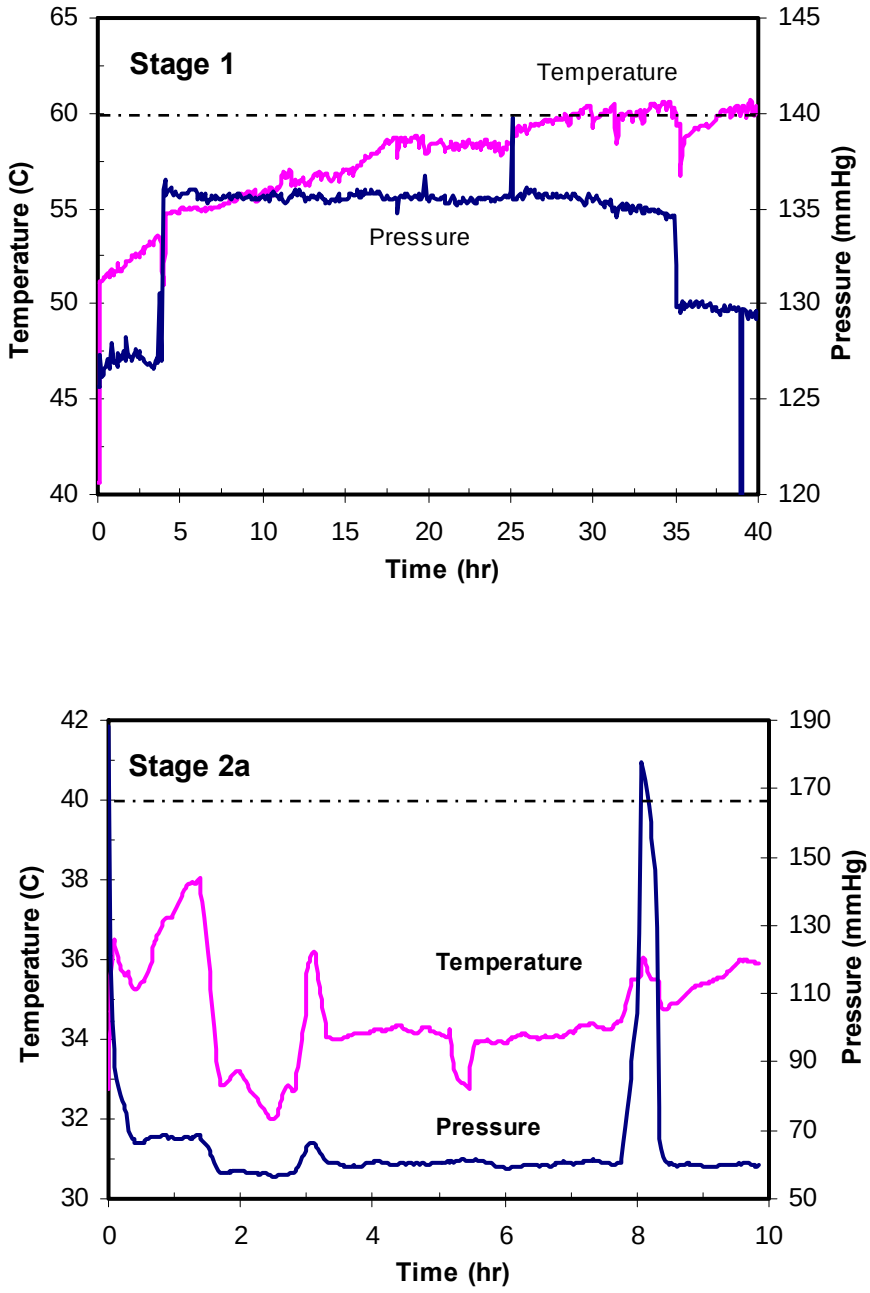

D3.0 RESULTS FOR THE PRELIMINARY EARLY FEED CERTIFICATION RUN 26

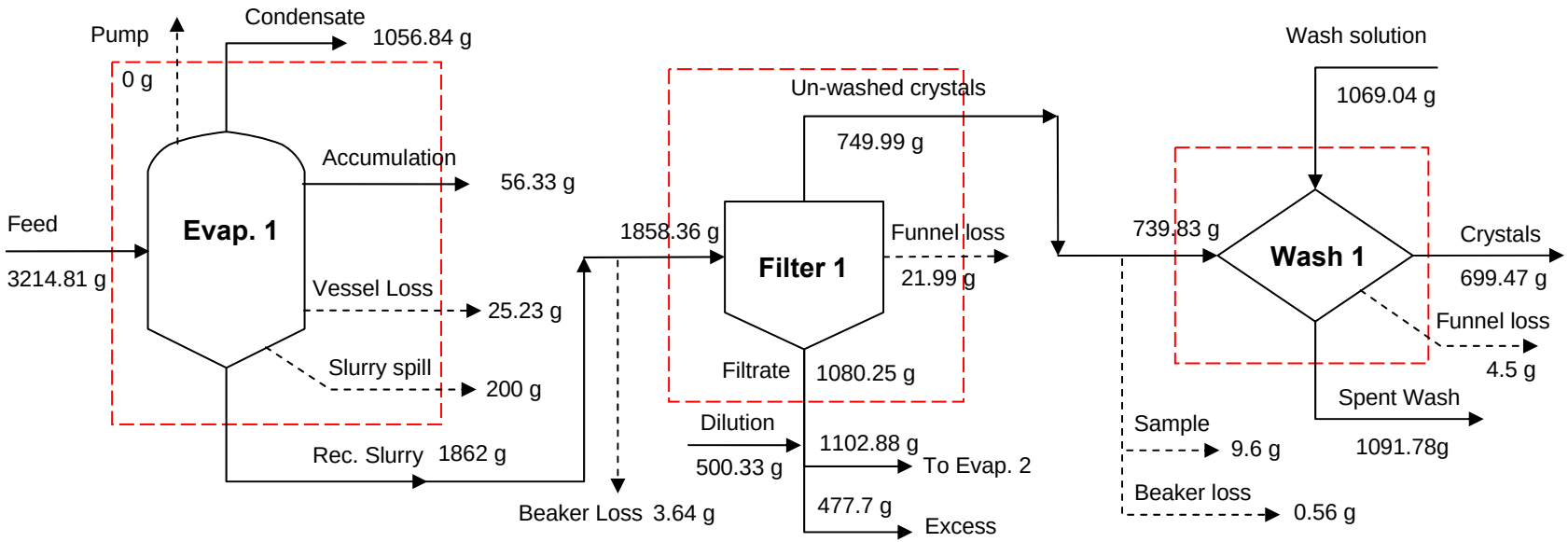

Pump	Mass of the condensate collected in the cold trap protecting the vacuum pump.
Slurry Spill	A spill that took place during transfer of the slurry between units. This was estimated at 200 g.
Rec. Slurry	Mass of slurry recovered from the crystallizer. Due to the slurry spill that occurred during Stage 1, this is an estimated value.
Vessel Loss	Mass recovered by washing the vessel with a known amount of water.
Dilution	Water added to the filtrate to dissolve any precipitated crystals.
Funnel Loss	Mass recovered by washing the funnel with a known amount of water and then drying with paper of a known weight. Performed after the filtration and washing operations.
Beaker Loss	Mass of slurry lost in the several beakers necessary for the transfer from the vessel to the filter.
Sample	Mass collected from the un-washed crystals for chemical analysis.

Solid arrows are the process streams and the dotted arrows represent quantified losses. Closure on a total mass balance was performed for each dashed box around a process unit.

Figure D4. Overall mass balance in Stage 1 of SST early feed solution run 26.

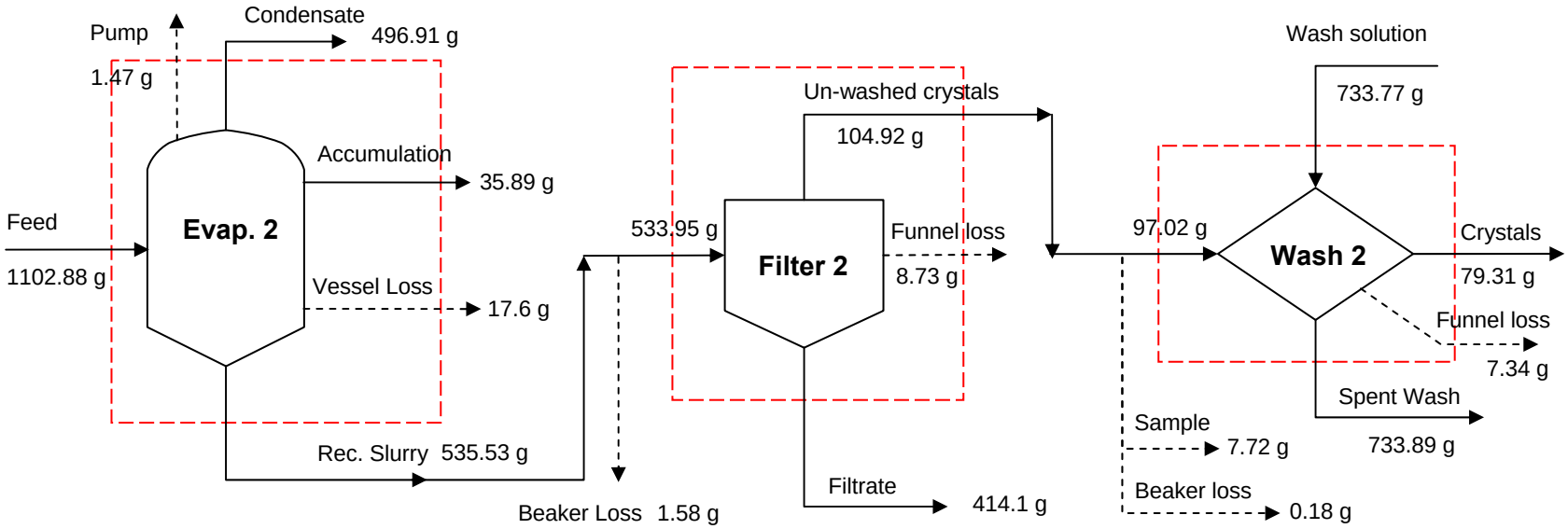

Pump	Mass of the condensate collected in the cold trap protecting the vacuum pump.
Rec. Slurry	Mass of slurry recovered from the crystallizer.
Vessel Loss	Mass recovered by washing the vessel with a known amount of water.
Funnel Loss	Mass recovered by washing the funnel with a known amount of water and then drying with paper of a known weight. Performed after the filtration and washing operations.
Beaker Loss	Mass of slurry lost in the several beakers necessary for the transfer from the vessel to the filter.
Sample	Mass collected from the un-washed crystals for chemical analysis.

Solid arrows are the process streams and the dotted arrows represent the losses. Closure on a total mass balance was performed for each dashed box around a process unit.

Figure D5. Overall mass balance in Stage 2 of SST early feed solution run 26.

Table D6. Mass balances around process units of run 26 (SST early feed solution).

Unit	Input (g)	Output (g)	Difference (g)	% Closure of Mass Balance
Evaporator 1	3214.81	3200.40	14.41	0.45
Filtration 1	1858.36	1852.23	6.13	0.33
Washing 1	1808.87	1795.75	13.12	0.73
Evaporator 2	1102.88	1087.40	15.48	1.40
Filtration 2	533.95	527.75	6.20	1.16
Washing 2	830.79	820.54	10.25	1.23

Table D7. Balances on total mass around each unit in run 26 (SST early feed solution).

Stage 1	**Input (g)**		**Output (g)**					**Loss (g)**
Species	**Feed**	**Wash**	**Cond**	**Washed Solids**	**Filtrate**	**Spent Wash**	**Accum**	
Early feed	3214.8							
H_2O		634.1	1056.8					
Na_2CO_3		98.9						
$NaNO_3$		336.0						
Solution				699.5	1080.3	1091.8	56.3	
Total	3214.8	1069.0	1056.8	699.5	1080.3	1091.8	56.3	299.1
Combined	4283.8		3984.7					299.1
						% Loss		7.0%
						Accounted loss (g)		265.5
						% Corrected Loss		0.8%

Stage 2	**Input (g)**		**Output (g)**					**Loss (g)**
Species	**Feed**	**Wash**	**Cond**	**Washed Solids**	**Filtrate**	**Spent Wash**	**Accum**	
Stage 1 Filtrate	753.8							
H_2O	349.1	413.2	496.9					
Na_2CO_3		75.8						
$NaNO_3$		244.8						
Solution				79.3	414.1	733.9	35.9	
Total	1102.9	733.8	496.9	79.3	414.1	733.9	35.9	76.6
Combined	1836.7		1760.1					76.6
						% Loss		4.2%
						Accounted loss (g)		44.6
						% Corrected Loss		1.7%

D4.0 RESULTS FOR THE PRELIMINARY LATE FEED CERTIFICATION RUN 27

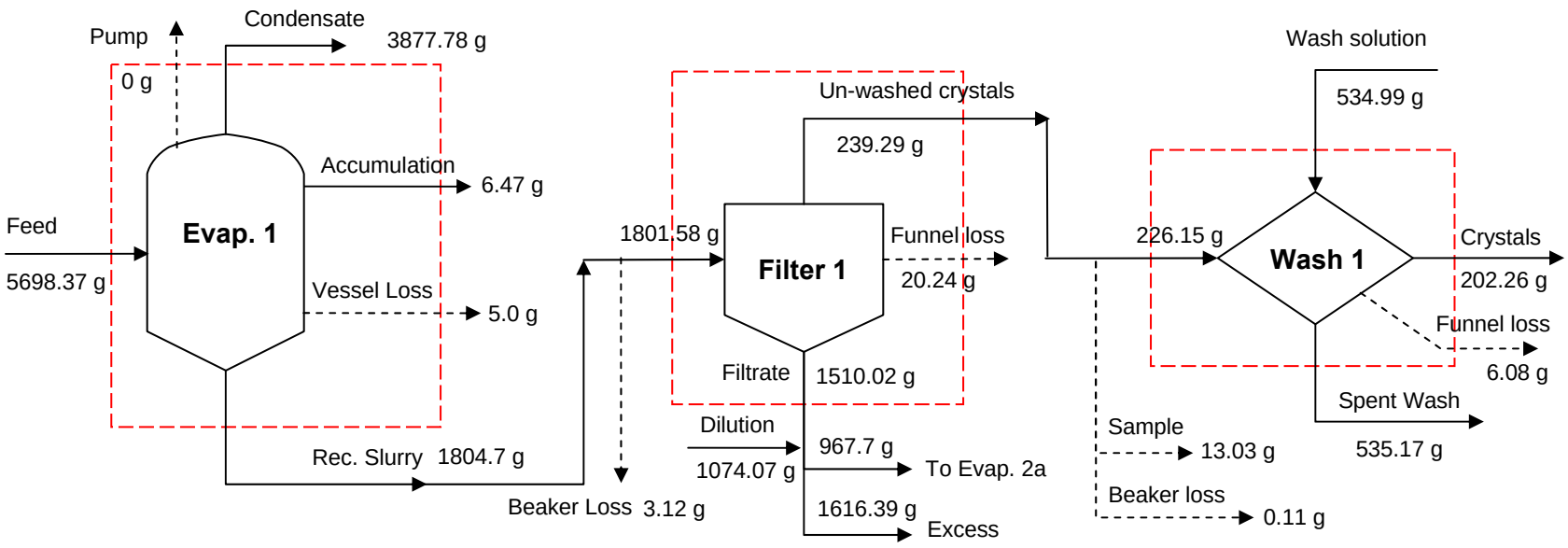

Pump	Mass of the condensate collected in the cold trap protecting the vacuum pump.
Rec. Slurry	Mass of slurry recovered from the crystallizer.
Vessel Loss	Mass recovered by washing the vessel with a known amount of water.
Dilution	Water added to the filtrate to dissolve any precipitated crystals.
Funnel Loss	Mass recovered by washing the funnel with a known amount of water and then drying with paper of a known weight. Performed after the filtration and washing operations.
Beaker Loss	Mass of slurry lost in the several beakers necessary for the transfer from the vessel to the filter.
Sample	Mass collected from the un-washed crystals for chemical analysis.

Solid arrows are process streams and dotted arrows represent quantified losses. Closure on a total mass balance was performed for each dashed box around a process unit.

Figure D8. Overall mass balance on Stage 1 of run 27 (SST late feed solution).

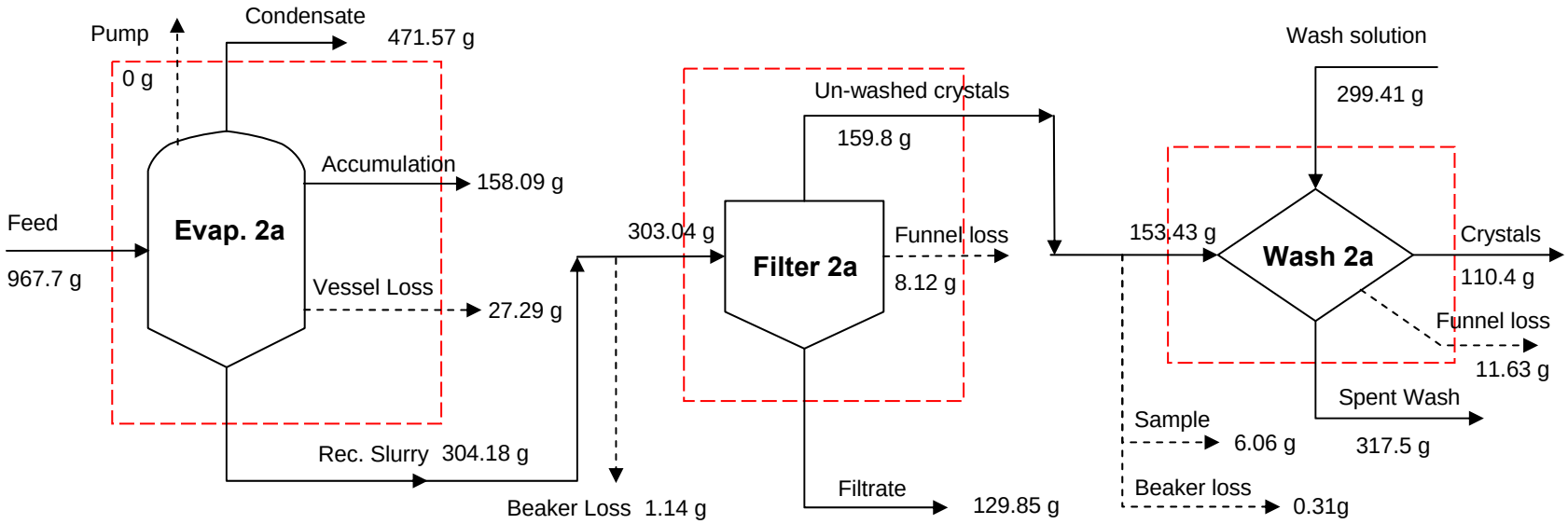

Pump	Mass of the condensate collected in the cold trap protecting the vacuum pump.
Rec. Slurry	Mass of slurry recovered from the crystallizer.
Vessel Loss	Mass recovered by washing the vessel with a known amount of water.
Funnel Loss	Mass recovered by washing the funnel with a known amount of water and then drying with paper of a known weight. Performed after the filtration and washing operations.
Beaker Loss	Mass of slurry lost in the several beakers necessary for the transfer from the vessel to the filter.
Sample	Mass collected from the un-washed crystals for chemical analysis.

Solid arrows are process streams and dotted arrows represent losses. Closure on a total mass balance was performed for each dashed box around a process unit.

Figure D9. Overall mass balance on Stage 2 of run 27 (SST late feed solution).

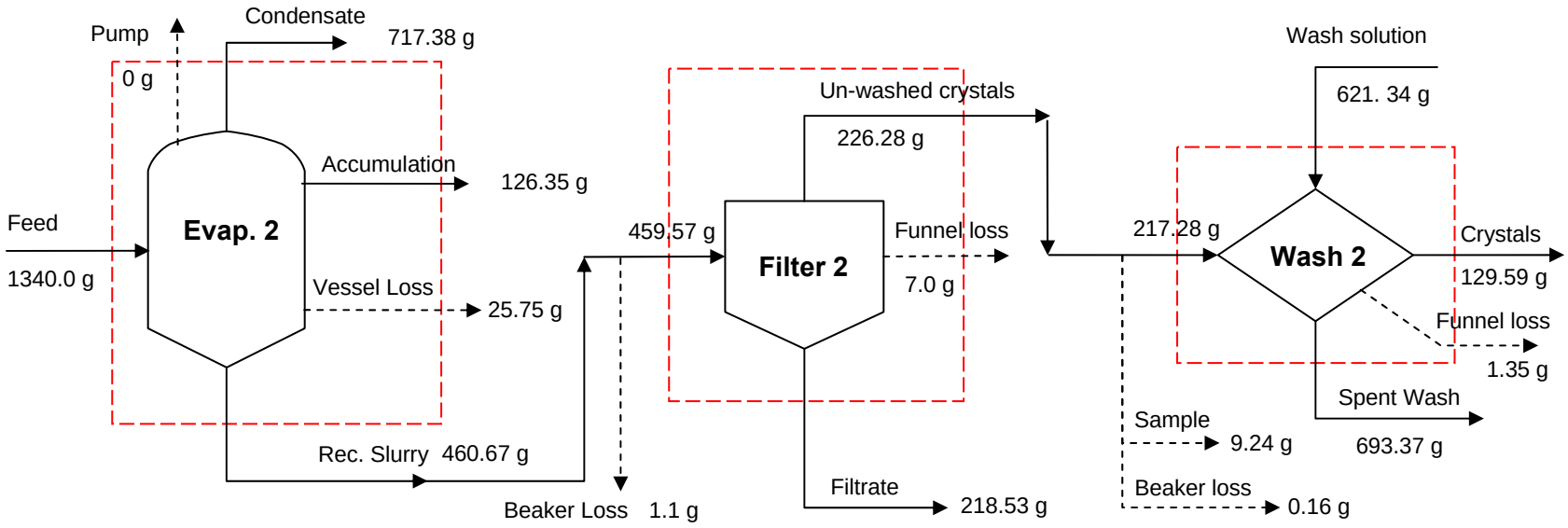

Pump	Mass of the condensate collected in the cold trap protecting the vacuum pump.
Rec. Slurry	Mass of slurry recovered from the crystallizer.
Vessel Loss	Mass recovered by washing the vessel with a known amount of water.
Funnel Loss	Mass recovered by washing the funnel with a known amount of water and then drying with paper of a known weight. Performed after the filtration and washing operations.
Beaker Loss	Mass of slurry lost in the several beakers necessary for the transfer from the vessel to the filter.
Sample	Mass collected from the un-washed crystals for chemical analysis.

Solid arrows are process streams and dotted arrows represent losses. Closure on a total mass balance was performed for each dotted box around a process unit.

Figure D10. Overall mass balance on Stage 2, trial 2 of run 27 (SST late feed solution).

Table D11. Mass balances around process units of run 27 (SST late feed solution).

Unit	Input (g)	Output (g)	Difference (g)	% Closure of Mass Balance
Evaporator 1	5698.37	5693.95	4.42	0.08
Filtration 1	1801.58	1769.55	32.03	1.78
Washing 1	761.14	743.51	17.63	2.32
Evaporator 2a	967.70	961.13	6.57	0.68
Filtration 2a	303.04	297.77	5.27	1.74
Washing 2a	452.84	439.53	13.31	2.94
Evaporator 2	1340.00	1330.15	9.85	0.74
Filtration 2	459.57	451.81	7.76	1.69
Washing 2	838.62	824.31	14.31	1.71

Table D12. Balances on total mass for each unit in run 27 (SST late feed solution).

Stage 1	Input (g)		Output (g)					Loss (g)
Species	**Feed**	**Wash**	**Cond**	**Washed Solids**	**Filtrate**	**Spent Wash**	**Accum.**	
Late Feed	5698.4							
H_2O		283.1	3877.8					
Na_2CO_3		49.1						
$NaNO_3$		202.8						
Solution				202.3	1510.0	535.2	6.5	
Total	5698.4	535.0	3877.8	202.3	1510.0	535.2	6.5	101.6
Combined	6233.4		6131.8					101.6
						% Loss		1.6%
						Accounted loss (g)		47.6
						% Corrected Loss		0.9%

Stage 2a (trial 2)	Input (g)		Output (g)					Loss (g)
Species	**Feed**	**Wash**	**Cond**	**Washed Solids**	**Filtrate**	**Spent Wash**	**Accum.**	
Filtrate stage 1	565.5							
H_2O	402.2	162.6	471.6					
Na_2CO_3		36.7						
$NaNO_3$		100.1						
Solution				110.4	129.9	317.5	157.8	
Total	967.7	299.4	471.6	110.4	129.9	317.5	157.8	80.0
Combined	1267.1		1187.1					80.0
						% Loss		6.3%
						Accounted loss (g)		54.6
						%Corrected Loss		2.0%

Stage 2(trial 1)	Input (g)		Output (g)					Loss (g)
Species	**Feed**	**Wash**	**Cond**	**Washed Solids**	**Filtrate**	**Spent Wash**	**Accum**	
Filtrate stage 1	783.0							
H_2O	557.0	347.6	717.4					
Na_2CO_3		73.3						
$NaNO_3$		200.4						
Solution				129.6	218.5	693.4	126.4	
Total	1340.0	621.3	717.4	129.6	218.5	693.4	126.4	76.0
Combined	1961.3		1885.3					76.0
						% Loss		3.9%
						Accounted loss (g)		44.6
						%Corrected Loss		1.6%

D5.0 PROCESS REQUIREMENTS RESULTS FOR THE PRELIMINARY EARLY AND LATE FEED CERTIFICATION RUN 26 AND 27

Table D13: Comparison of required and desired outcomes to experimental results

SST Early Feed FY05	Stage	Required	Actual	Desired
Cs Decon Factor	1	1.15	5.9	48
	2	1.15	6.7	48
	Total	1.15	6.0	48
Sodium Recovery	Total	50%	58.1%	90%
Sulfate to Sodium	1	0.01	0.0027	0.0022
	2	0.01	0.0017	0.0022
	Total	0.01	0.0023	0.0022
SST Late Feed				
Cs Decon Factor	1	-	24.5	14
	2	-	11.2	14
	Total	-	14.8	14
Sodium Recovery	Total	50%	74.7%	90%
Sulfate to Sodium	1	0.01	0.008	0.0022
	2	0.01	0.0191	0.0022
	Total	0.01	0.01	0.0022

CRYSTALLIZATION RUNS

Table E1. List of crystallization runs performed

61Run #	Stage	Crys Nom. Vol. (mL)	Date	Feed Solution	Comments
1	1	1000	3/24/2005	NaNO3	
2	1	1000	3/30/2005	burkeite	
3	1	1000	4/5/2005	NaNO3	
4	1	1000	4/7/2005	NaNO3	
5	1	1000	4/12/2005	burkeite	
6	1	1000	4/15/2005	NaNO3	
7	1	1000	4/22/2005	NaNO3	
8	1	1000	4/28/2005	3-salt	
9	1	1000	5/2/2005	3-salt	
10	1	1000	5/6/2005	NaNO3	
11	1	1000	5/11/2005	NaNO3, CsNO3, NaOH	Cesium used as a tracer
12	1	1000	5/12/2005	3-salt	tested two-stage experiment
	2	600	5/13/2005	3-salt	
13	1	1000	5/17/2005	Early Feed	initial examination of simulant
	2	600	5/19/2005	Early Feed	sent samples for analysis
14	1	1000	5/24/2005	3-salt	
	2	600	5/26/2005		
15	1	1000	6/2/2005	3-salt	
16	1	1000	6/6/2005	DST Feed	DST practice run
	2	600	6/7/2005	DST Feed	initial examination of simulant
17	1	1000	6/14/2005	3-salt	used seed crystals from earlier burkeite run
18	1	1000	6/15/2005	3-salt	used seed crystals from earlier burkeite run
19	1	1000	6/16/2005	burkeite	grow new burkeite seed crystals
20	1	600	6/21/2005	3-salt	test spray nozzle for washing crystallizer walls during run
21	1	600	6/22/2005	3-salt	initial test of semi-batch operation
22	1	1000	6/27/2005	Late Feed	test operations with late feed simulant
	2	600	6/28/2005	Late Feed	
23	1	600	7/1/2005	3-salt	operate at a constant level with a semi-continuous feed
24	1	600	7/8/2005	burkeite	attempt to grow burkeite seed crystals
25	1	1000	7/21/2005	Late Feed #2	test operation at constant level in preparation for a certification run

	2	300	7/23/05	Late Feed	
26	1	1000	7/26/05	Early Feed	Certification Run
	2	300	7/28/05	Early Feed	
27	1	1000	8/1/2005	Late Feed #3	Certification Run
	2	300	8/4/2005	Late Feed	Reduced evaporation rate for both stages
	2a	300	8/11/2005	Late Feed	
28	1	1000	8/7/2005	DST	carbonation on first stage, batch experiment
	2	600	8/15/05		
29	1	1000	8/17/2005	DST	carbonation on both stages, batch experiment
	2	600	8/17/05		
30	1	1000	8/23/05	DST	test operation for certification run
	2	300	8/25/05		identified gelling problems
31	1	1000	8/28/05	DST	Certification Run
	2	300	8/31/05		
32	1	300	11/20/05	Early Feed	tested small-scale apparatus with constant-level procedure
	2	100	11/29/05		
33	1	300	1/16/06	Early Feed	small scale/variable level => high accumulation
	2	100	1/18/06		Stage 2 aborted
34	1	300	2/8/06	Early Feed	compare results from small-scale apparatus to Run 32
	2	100	2/12/06		
35	1	100	2/22/06	Late Feed	demonstration run for CH2M Hill representatives; inadequate filtrate for operation of second stage, test FY 2006 simulant
36	1	300	4/10/06	Early Feed	Test water as heating medium, temperature control, new saturated solution composition and acetone alternative, test FY 2006 simulant
37	1	300	4/23/06	Early Feed	New Procedure Testing On Laboratory feed
	2	100	4/26/06		
38	1	300	4/30/06	Early Feed	Certification Run On Hanford Feed
	2	100	5/3/06		
38a	1	300	5/22/06	Early Feed	Certification Run, evaporation rate issues
38b	1	300	5/25/06	Early Feed	Final Certification Run
	2	100	5/29/06		
39	1	100	6/1/06	Late Feed	Procedure testing Run on Laboratory Feed

40	1	100	6/7/06	Late Feed	Certification Run on Hanford Feed
41	1/2	300/100	5/26/06	Early Feed	222-SA using GT crystallizer
42	1/2	300/100	6/6/06	Early Feed	222-SA using Hanford Boil-down rig
43	1	100	8/00/06	Early Feed	Practice Run in 222-S Hot Cell (simulant)
44	1	100	8/23/06	Early Feed	222-S Hot Cell using actual waste
45	1	100*	8/22/06	Late Feed	222-SA Practice Run using boil-down apparatus (*175 mL)
46	1	100	8/31/06	Late Feed	222-S Hot Cell using actual waste
47					
48	1	300	7/18/06	Early Feed	Fast evaporation rate, ~58 g/h (originally Run 41)
49	1	300	7/25/06	Early Feed	Temperature target of 55^{o}C
50a	1	300	8/30/06	Early Feed	Concave-down evaporation rate
50b	1	300	8/23/06	Early Feed	Concave-down evaporation rate, increased C:F ratio
51	1	300	9/13/06	Early Feed	Concave-up evaporation rate
52	1	300	9/28/06	Early Feed	Took several samples throughout the run to study nucleation points and burkeite growth
53	1	300	11/26/06	Early Feed w/organics	Separation issues due to organics
54	1	300	12/11/06	Early Feed w/solids	
54	2	100	12/15/06		
55	1	100	1/12/07	Early Feed	Test in small vessel to prepare for organics runs
56	1	100	1/18/07	Early Feed	Repeated test with shorter run time(new test plan)
57	1	100	2007	Early Feed	Organics Baseline (RPP-Plan-32605)
58	1	100	2007	Early Feed	Carboxylate Group
59	1	100	2007	Early Feed	Amine Group
60	1	100	2007	Early Feed	Sodium Formate/Acetate
61	1	100	2007	Early Feed	Glycolate and citrate
62	1	100	2007	Early Feed	Citrate
63	1	100	2007	Early Feed	Glycolate
64	1	100	2007	Early Feed	IDA and NTA
65	1	100	2007	Early Feed	EDTA and HEDTA
66	1	100	2007	Early Feed	NTA
67	1	100	2007	Early Feed	IDA
68	1	100	2007	Early Feed	HEDTA
69	1	100	2007	Early Feed	EDTA
70	1	300	2008	Early Feed	Reproduced 38b

71	1	300	2008	Early Feed	Reproduced 38b stoped at C:F=0.4
72	1	300	2008	Early Feed	Evaporation rate = 35 g/h
73	1	300	2008	Early Feed	Evaporation rate = 55 g/h
74	1	300	2008	Early Feed	Evaporation rate = 75 g/h
75	1	300	2008	Early Feed	Operating Temperature = 35 °C
76	1	300	2008	Early Feed	Operating Temperature = 45 °C
77	1	300	2008	Early Feed	Operating Temperature = 55 °C
78	1	300	2008	Early Feed	Operating Temperature = 75 °C
79	1	300	2008	Early Feed	Triple Salts+ NAOH+NaAL
80	1	300	2008	Early Feed	Triple Salts+ NAOH
81	1	300	2008	Early Feed	Triple Salts
82	1	300	2008	Early Feed	Double Salts (nitrate-carbonate)
83	1	300	2008	Early Feed	Double Salts (nitrate-sulfate)
84	1	300	2008	Early Feed	Double Salts (sulfate-carbonate)
85	1	300	2008	Early Feed	Reproduced Double Salts (sulfate-carbonate)
86	1	300	2008	Early Feed	Sodium nitrate
87	1	300	2008	Early Feed	Sodium carbonate
88	1	1000	2008	DST	DST + LiNO3 precipitation 1
89	1	1000	2008	DST	DST + LiNO3 precipitation 1
90	1	1000	2008	DST	DST + LiNO3 precipitation 1

CONDENSATE-TO-FEED RATIO

F1.0 CONDENSATE-TO-FEED RATIO

Each certification run followed the corresponding simulation file provided by COGEMA (shown in parenthesis in the table) and the endpoint for the operation of each stage was determined by the amount of condensate collected. The Table F1 gives the target condensate-to-feed ratios along with the actual experimental results. Since the laboratory experiments involved adding dilution water to the filtrate from the first stage, the target ratios had to be adjusted for the second stage of each run. The feed to the second stage of each run was a portion of the diluted filtrate from the first stage. An example of the adjusted target ratio calculations is given for the SST Early Feed Solution Run 26.

Example calculation of the revised condensate-to-feed ratio for the SST Early Feed Solution certification run:

$$AdjustedRatio = \frac{(Filtrate \times OldRatio + DilutionWater)}{(Filtrate + DilutionWater)} \tag{1}$$

$$AdjustedRatio = \frac{(1080.25 \times 0.189 + 500.33)}{(1080.25 + 500.33)} = 0.446 \tag{2}$$

Table F1. Determination of condensate-to-feed ratio from simulations

Experimental Stage	Experimental Value	Early Feed (SST1SIM.xls)		Late Feed (SST2SIM1.xls)	
		Simulation	**Experimental**	**Simulation**	**Experimental**
Stage 1	Feed (g)	1000.1	3214.81	1000	5698.37
	Condensate (g)	332.4	1056.84	681	3877.78
	Condensate-to-Feed Ratio	**0.329**	**0.332**	**0.681**	**0.681**
	Filtrate from Stage 1 (g)	333.4	1080.25	282.3	1510.02
	Dilution water to filtrate (g)		500.33		1074.07
Stage 2	Feed (g)	333.4	1102.88	282.3	967.7
	Condensate (g)	63.1	496.91	58.7	471.57
	Adjusted Target Ratio		**0.446**		**0.537**
	Condensate-to-Feed Ratio	0.189	**0.451**	0.208	**0.487**

COEFFICIENT OF VARIATION CALCULATION

G1.0 COEFFICIENT OF VARIATION

Table G1. Sieve test results for certification run 38b Stage 1

Sample Name	Early Feed 38b_Stage 1
Sample weight (g)	15.96
Sieving time (min)	30

Sieve no.	Mesh opening	Range	Ave. Size (micron)	Before sieving (g)	After sieving (g)	Crystal weight (g)	Fractional Mass %	Cumulative oversize %	Cumulative undersize %
30	600	600-850	600	125.06	125.06	0	0.00	0.00	100.00
40	425	425-600	512.5	115.9	118.08	2.18	13.66	13.66	86.34
50	300	300-425	362.5	110.71	118.15	7.44	46.62	60.28	39.72
70	212	212-300	256	112.52	115.72	3.2	20.05	80.33	19.67
100	150	150-212	181	106.69	107.78	1.09	6.83	87.16	12.84
140	106	106-150	128	105.25	105.96	0.71	4.45	91.60	8.40
200	75	75-106	90.5	105.13	105.62	0.49	3.07	94.67	5.33
270	53	53-75	64	103.95	104.19	0.24	1.50	96.18	3.82
400	38	38-53	45.5	102.81	103.01	0.2	1.25	97.43	2.57
635	20	20-38	29	104.58	104.84	0.26	1.63	99.06	0.94
Pan	0	0-20	10	82.89	83.04	0.15	0.94	100.00	0.00

The coefficient of variation is calculated based on the cumulative undersize percent data. Cumulative undersize values are plotted in graph displaying in the Y axis the cumulative undersize and in the X axis the mesh opening (Figure G2). The coefficient of variation is calculated based on the relation: $CV = \frac{100(d_{84\%} - d_{16\%})}{2d_{50\%}}$, where the values $d_{84\%}$, $d_{16\%}$ and $d_{50\%}$ corresponds to the sizes (X axis) for 84%, 16% and 50% cumulative undersize weight percent respectively. Figure G2 led to the values 415 µm, 187.5 µm and 327.5µm for $d_{84\%}$, $d_{16\%}$ and $d_{50\%}$ respectively leading to a coefficient variation of 34.7%

Figure G2. Run 38b Stage 1 coefficient of variation graph

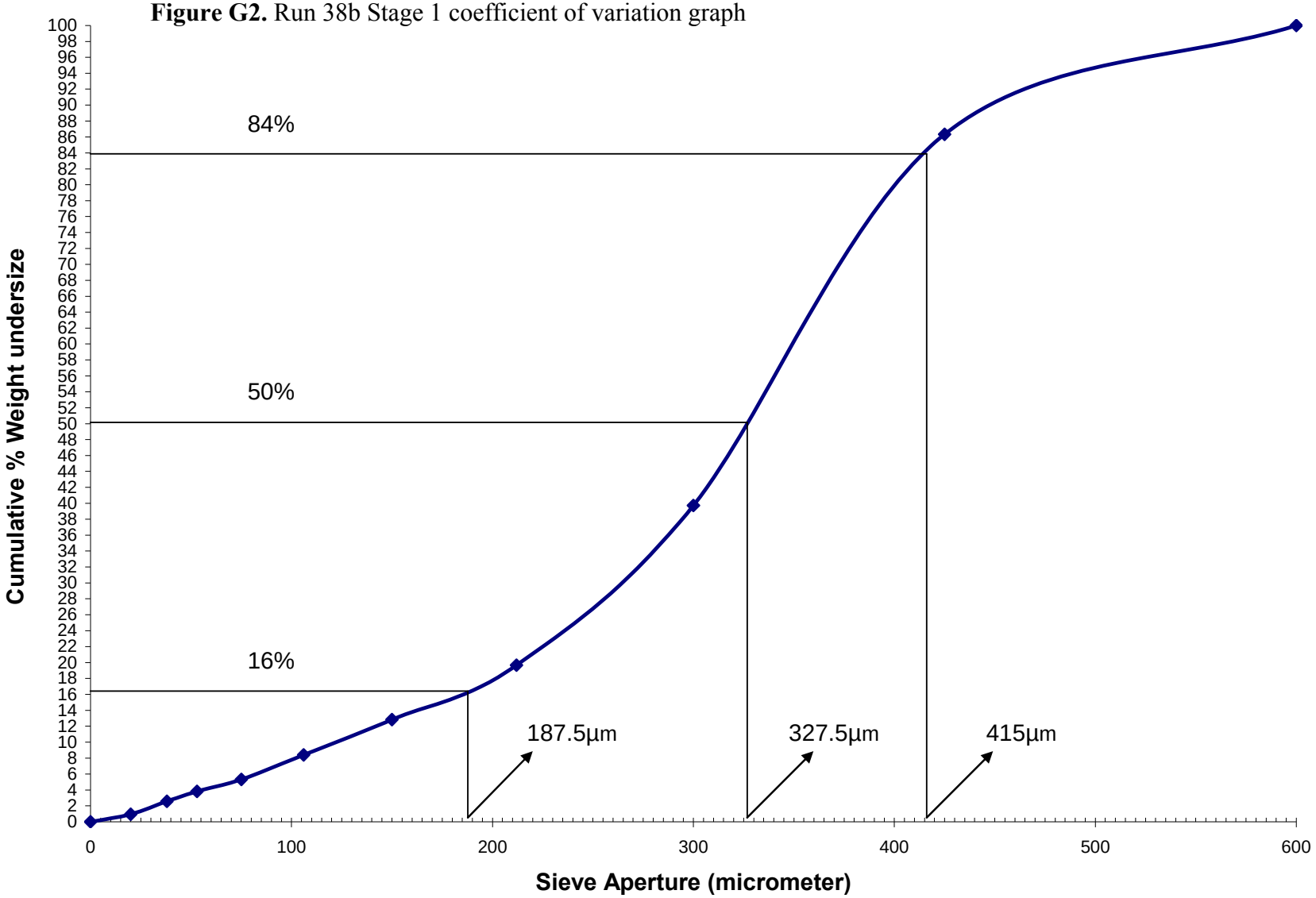

SAMPLE PREPARATION

H1.0 SAMPLE IDENTIFICATION FOR THE CERTIFICATION RUNS

The following tables give the sampling information necessary to accurately calculate the species balances. Each table identifies the samples taken and gives the amounts of pure sample and water added to each sample container. As shown in the tables, the only samples sent in solid form were the final crystals from each stage.

Late Feed Stage 1

Code	Name	Pure sample	Water added	Total mass	State
LF3-ST1-1	filtrate	60.07	42.73	102.8	L
LF3-ST1-2	Spent wash	92.70	61.32	154.01	L
LF3-ST1-3	final crystals	7.83	0	7.83	S
LF3-ST1-4	accumulation	6.33	128.03	134.36	L
LF3-ST1-5	unwashed solids	13.03	125.04	138.07	L
LF3-ST1-6	feed (CH2M HILL)	30.78	0	30.78	L
LF3-ST1-7	Feed (lab)	39.53	0	39.53	Ll

Early Feed 38b Stage 1

Code	Name	Pure sample	Water added	Total mass	State
EF38b-ST1-1	Feed hanford	129.92	0	128.92	L
EF38b-ST1-2	feed mixed	114.39	0	114.39	L
EF38b-ST1-3	accumulation	136.9	880.74	1017.64	L
EF38b-ST1-4	filtrate	385.86	498.06	883.92	L
EF38b-ST1-5	wash solution	36.80	74.32	111.12	L
EF38b-ST1-6	spent wash	51.09	69.01	120.1	L
EF38b-ST1-7	unwashed solids	3.20	85.36	88.56	L
EF38b-ST1-8	first wash	1.99	102.09	104.08	L
EF38b-ST1-9	second wash	2.03	95.73	97.77	L
EF38b-ST1-10	third wash	2.13	100.31	102.45	L
EF38b-ST1-11	fourth wash	2.58	107.08	109.66	L
EF38b-ST1-12	fifth wash	6.99	111.22	118.22	L

Early Feed 38b Stage 2

Code	Name	Pure sample	Water added	Total mass	State
EF38b -ST2-1	accumulation	100.73	619.54	120.27	L
EF38b -ST2-2	filtrate	126.33	374.4	500.73	L
EF38b -ST2-3	wash solution	19.97	86.03	106.01	L
EF38b -ST2-4	spent wash	56.98	80.16	137.15	L
EF38b -ST2-5	unwashed solids	1.91	111.37	113.29	L
EF38b-ST2-6	first wash	2.04	121.81	123.85	L
EF38b-ST2-7	second wash	1.53	112.12	113.66	L
EF38b-ST2-8	third wash	1.00	122.97	123.97	L
EF38b-ST2-9	fourth wash	1.76	114.46	116.22	L
EF38b-ST2-10	fifth wash	2.54	113.71	116.25	L

GTRI LABORATORIES SAMPLE ANALYTICAL RESULTS

I1.0 CHEMICAL ANALYSES FROM GTRI LABORATORIES

Identification of Samples from Crystallization from SST Early Feed Solution Certification run 38b sent to GTRI Laboratories for Analysis

			Concentration (% or ppm)					
GTRI ID #	Sample ID	Sample Name	Al	Cr	Cs	SO4	P	Na
52418	EF38B-ST1-01	Hanford Feed	0.75%	810	3.300	<10.0	0.150%	15.0%
52419	EF38B-ST1-02	Mixed Feed	0.76%	0.15%	3.150	1.19%	0.160%	15.0%
52420	EF38B-ST1-03	Accumulation	0.11%	260	0.391	0.443%	230	4.10%
52421	EF38B-ST1-04	Filtrate	1.10%	0.22%	3.340	0.125%	0.180%	9.50%
52422	EF38B-ST1-05	Wash Solution	20.0	<0.10	<0.002	<100	2.20	6.50%
52423	EF38B-ST1-06	Spent Wash	0.21%	440	0.568	0.120%	430	8.80%
52424	EF38B-ST1-07	Unwashed Crystals	230	50.0	0.082	0.111%	45.0	1.10%
52425	EF38B-ST1-08	1 Wash	63.0	13.0	0.019	560	13.0	0.57%
52426	EF38B-ST1-09	2 Washes	16.0	3.80	0.006	661	3.60	0.62%
52427	EF38B-ST1-10	3 Washes	6.30	1.60	<0.002	635	<2.00	0.66%
52428	EF38B-ST1-11	4 Washes	3.70	1.30	<0.002	702	<2.00	0.73%
52429	EF38B-ST1-12	Final Crystals	5.10	2.40	<0.002	0.166%	2.20	2.00%
52430	EF38B-ST2-01	Accumulation	0.16%	350	0.511	195	480	2.50%
52431	EF38B-ST2-02	Filtrate	0.93%	0.19%	3.020	0.119%	0.110%	5.50%
52432	EF38B-ST2-03	Wash Solution	2.40	<0.10	<0.002	<100	<2.00	3.50%
52433	EF38B-ST2-04	Spent Wash	0.22%	460	0.813	350	370	8.40%
52434	EF38B-ST2-05	Unwashed Crystals	260	53.0	0.073	29.0	41.0	0.43%
52435	EF38B-ST2-06	1 Wash	82.0	17.0	0.029	<10.0	21.0	0.43%
52436	EF38B-ST2-07	2 Washes	20.0	4.00	0.007	<10.0	11.0	0.36%
52437	EF38B-ST2-08	3 Washes	2.80	0.550	<0.002	<10.0	3.90	0.23%
52438	EF38B-ST2-09	4 Washes	3.20	0.620	<0.002	<10.0	5.00	0.44%
52439	EF38B-ST2-10	Final Crystals	3.60	0.710	<0.002	<10.0	4.90	0.63%
52440	LF40-ST1-01	Hanford Feed	0.12%	170	0.546	0.165%	750	3.10%
52441	LF40-ST1-02	Accumulation	860	110	0.328	0.172%	640	2.50%
52442	LF40-ST1-03	Filtrate	0.32%	430	1.310	<10.0	120	3.40%
52443	LF40-ST1-04	Wash Solution	2.10	<0.10	<0.002	<100	<2.00	4.20%
52444	LF40-ST1-05	Spent Wash	0.38%	490	1.420	562	580	13.0%
52445	LF40-ST1-06	Unwashed Crystals	160	21.0	0.067	465	240	0.69%
52446	LF40-ST1-07	1 Wash	32.0	4.70	0.015	354	180	0.49%
52447	LF40-ST1-08	2 Washes	18.0	3.10	0.008	438	200	0.64%

52448	LF40-ST1-09	3 Washes	8.40	1.80	0.003	522	220	0.74%
52449	LF40-ST1-10	4 Washes	5.60	1.80	0.002	781	300	1.10%
52450	LF40-ST1-11	Final Crystals	<1.00	<0.10	<0.002	993	430	1.40%
52451	LF40-ST1-12	GT Feed	0.13%	340	0.713	0.159%	870	3.30%

I2.0 WASHING EFFICIENCY

To determine qualitatively the effect of multiple wash steps on product purity, crystals recovered from run using an SST Early Feed simulant were washed and filtered four times in series. The following figure displays the change in color of crystals at the bottom of the sample bottles (from left to right) as the product crystals were washed. The sample labeled –1 corresponds to the filtered slurry obtained from the crystallization and bottle 0 is a sample of the washed crystals produced in the experiment. Bottles 1 through 4 are samples taken after each of four additional wash steps. Each wash was performed by slurrying the crystals in a saturated solution of sodium nitrate. The experiment was stopped when the color between two successive samples remained unchanged. At this point the amount of adhering mother liquor and its associated impurities can be assumed negligible and the remaining color is a result of the crystal inclusions. The progression of the color to a virtually white sample after three additional washings leads to the conclusion that the majority of the remaining liquid (mother liquor remaining after the filtration operation) is present in a form other than inclusions.

Effects of Washing on Crystal Color

The graph presented in the figure to the right shows the chromium analyses of the washed crystals. Clearly, the expected coloration of the crystals due to the presence of chromium corresponds to the visual observations described above and the quantitative analysis shown on the graph.

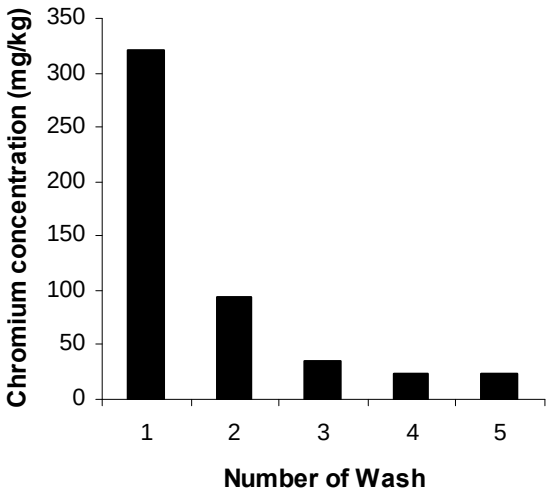

Figure I3. Chromium evolution with washing

EARLY FEED WITH ORGANICS

J1.0 SIMULATION FILES FOR ORGANICS RUN

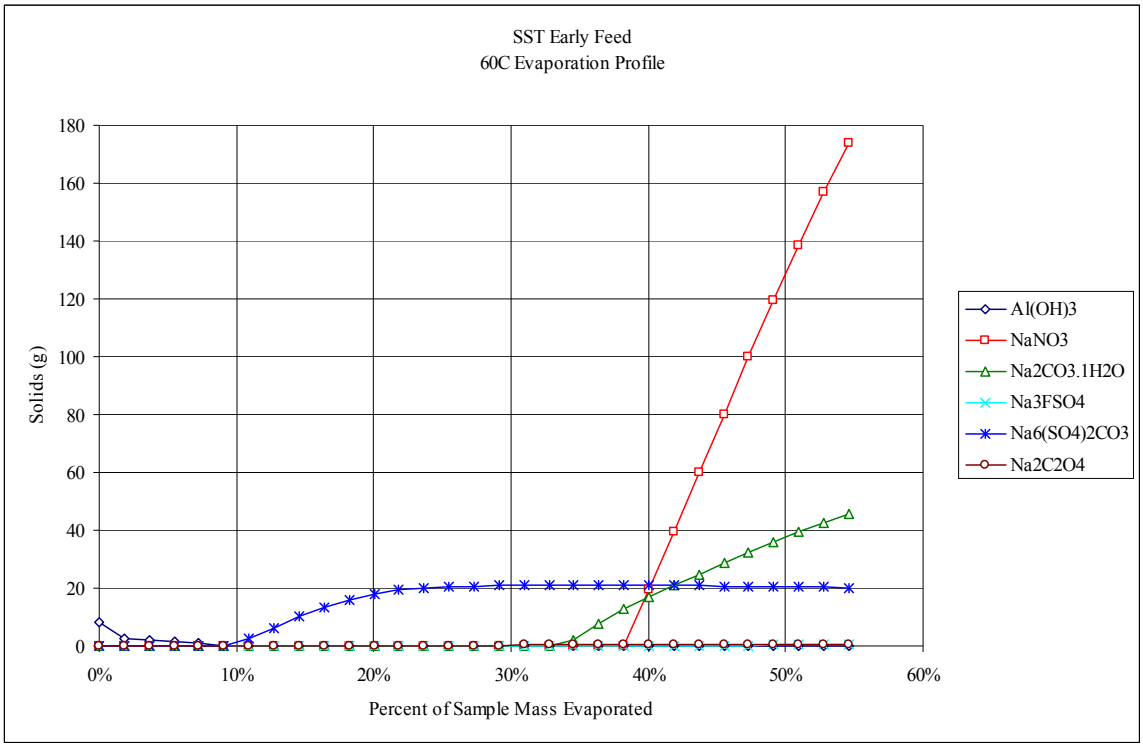

Figure J1. Thermodynamic simulation of runs performed with organics compounds

J2.0 OVERALL MASS BALANCE ON MAIN ORGANICS RUN

Table J2. Mass balance closure for early feed run with the 8 organics compounds

	Input (g)		Output (g)				Accum (g)	Loss (g)
Species	**Feed**	**Wash**	**Cond**	**Washed Solids**	**Filtrate**	**Spent Wash**	**Solids**	
Feed	631.51							
Solution		198.20	298.34	181.70	127.65	178.59	10.72	
Total	631.51	198.20	298.34	181.70	127.65	178.59	10.72	32.71
Combined	829.71		797.00					32.71
								3.94%
							Corrected Loss	2.73%

10.06 grams were accounted for from this stage, leading to a corrected loss of 2.73%.

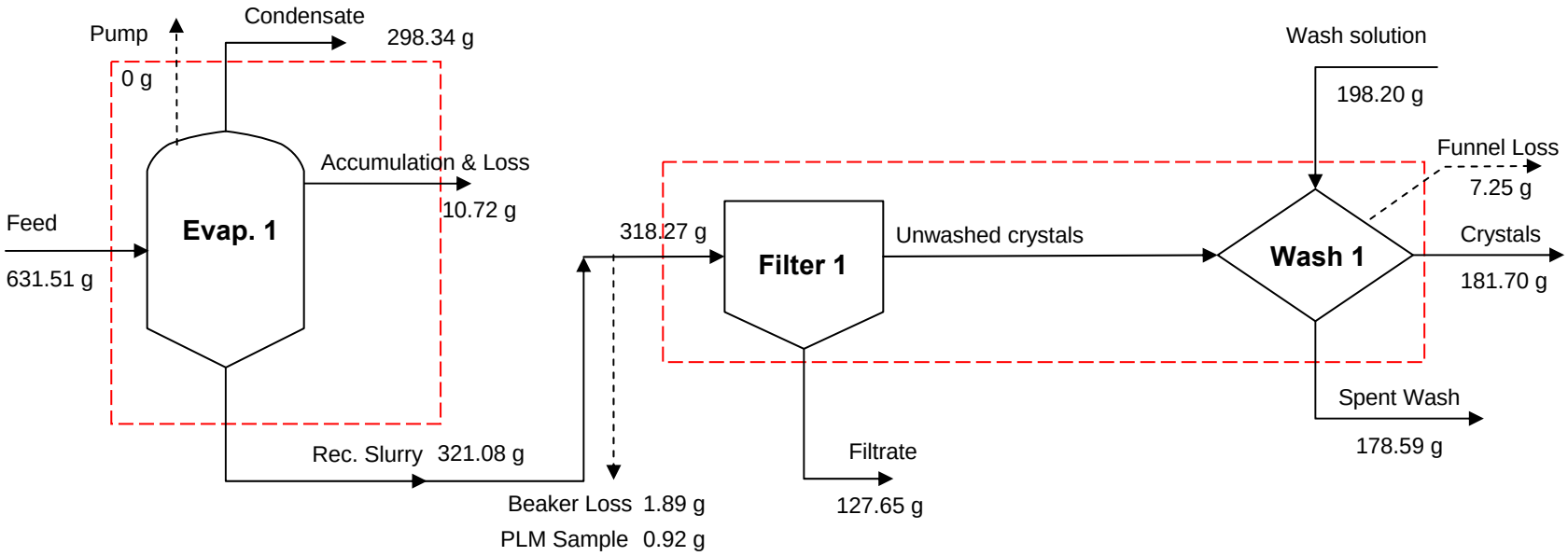

Pump	Mass of the condensate collected in the cold trap protecting the vacuum pump.
Rec. Slurry	Mass of slurry recovered from the crystallizer.
Accumulation & Loss	Mass recovered by washing the vessel with a known amount of water.
Funnel Loss	Mass recovered by washing the funnel with a known amount of water and then drying with paper of a known weight. Performed after the filtration and washing operations.
Beaker Loss	Mass of slurry lost in the beaker necessary for the transfer from the vessel to the filter.
PLM Sample	Mass taken from the slurry for PLM imaging.

Figure J3. Overall mass balance in early feed run with 8 organics. Solid arrows are the process streams and the dotted arrows represent the quantified losses. Closure on a total mass balance was performed for each dashed box around a process unit.

J3.0 PREPARATION OF ORGANICS AND SOLIDS SOLUTIONS

Sample Calculations for Organic Additives

The following section gives a walkthrough of the procedure used to determine the amount of each organic compound to add to the Early Feed simulant. As mentioned in the body, simulation file EARLY_FEED_ORGANIC_LABORATORY_ FLOWSHEET3.xls was used as the basis for the calculations. Specifically, the feed stream was used as a basis, which had a volume of 194.241 mL. The masses for all organic compounds in this solution are shown below in Table J4.

Table J4. Compound masses given in simulation file.

Compound	Formula	MW	Mass (g)	Moles
Formic Acid	CH_2O_2	46.03	1.509	0.0328
Sodium Acetate	$Na(C_2H_3O_2)$	82.03	0.691	0.0084
Sodium Glycolate	$Na(C_2H_3O_3)$	98.03	1.384	0.0141
Citric Acid	$C_6H_8O_7$	192.13	0.917	0.0048
EDTA	$H_4[C_{10}H_{12}N_2O_8]$	292.25	0.942	0.0032
HEDTA	$H_3[C_{10}H_{15}N_2O_7]$	278.26	0.992	0.0036
2,2'-Iminobisacetic Acid (H_2IDA)	$H_2[C_4H_5NO_4]$	133.10	0.377	0.0028
Nitriloacetic Acid (H_3NTA)	$H_3[C_6H_6NO_6]\cdot H_2O$	191.94	0.116	0.0006

To ensure that all organic compounds would readily dissolve when preparing the Early Feed simulant, the organic acids were replaced by their sodium counterparts. For example, citric acid was replaced by trisodium citrate dihydrate. Equation 1 shows that the compounds were scaled by their molecular weights and Table J5 displays the corresponding organic masses with the replacement compounds included.

$$x(g) = 0.917g \times \frac{294.10}{192.13} = 1.403g \quad (1)$$

Table J4. Organics compounds masses

Compound	Formula	MW	Moles	Mass (g)
Sodium Formate	NaCOOH	68.01	0.0328	2.230
Sodium Acetate	$Na(C_2H_3O_2)$	82.03	0.0084	0.691
Sodium Glycolate	$Na(C_2H_3O_3)$	98.03	0.0141	1.384
Trisodium Citrate Dihydrate	$Na_3[C_6H_5O_7]\cdot 2H_2O$	294.10	0.0048	1.403
Na_4EDTA	$Na_4[C_{10}H_{12}N_2O_8]$	380.16	0.0032	1.225
Na_3HEDTA	$Na_3[C_{10}H_{15}N_2O_7]$	344.20	0.0036	1.228
Na_2IDA	$Na_2[C_4H_5NO_4]$	177.07	0.0028	0.501
$Na_3NTA\cdot H_2O$	$Na_3[C_6H_6NO_6]\cdot H_2O$	275.10	0.0006	0.167

The next step in the process was to simply scale each compound for the amount of solution needed to perform a given run. 600 mL was chosen as the necessary value. A sample calculation is given below for trisodium citrate dihydrate and all scaled values are given in Table J5.

$$x(g) = 1.403g \times \frac{600}{194.24} = 4.334g \qquad (2)$$

Table J5. Organic compound masses, scaled to 600 mL.

Compound	Formula	MW	Mass (g)
Sodium Formate	NaCOOH	68.01	6.888
Sodium Acetate	$Na(C_2H_3O_2)$	82.03	2.134
Sodium Glycolate	$Na(C_2H_3O_3)$	98.03	4.274
Trisodium Citrate Dihydrate	$Na_3[C_6H_5O_7]\cdot 2H_2O$	294.10	4.334
Na_4EDTA (EDTA)	$Na_4[C_{10}H_{12}N_2O_8]$	380.16	3.786
Na_3HEDTA (HEDTA)	$Na_3[C_{10}H_{15}N_2O_7]$	344.20	3.792
Na_2IDA (IDA)	$Na_2[C_4H_5NO_4]$	177.07	1.548
$Na_3NTA\cdot H_2O$ (NTA)	$Na_3[C_6H_6NO_6]\cdot H_2O$	275.10	0.517

The final step in the scaling process was to account for moisture in three of the compounds. EDTA, HEDTA, and IDA were labeled as unspecified hydrates, so this information had to be gathered and accounted for so that the appropriate amount of the actual organic compound could be added. For example, the container of IDA that was purchased had a moisture content of 30.1%. Equation 3 shows the method used to determine the necessary amount of mass to add in order to obtain the correct mass of IDA. Table J6 gives the scaled results for all three of these compounds.

$$x(g) = \frac{1.548g}{(1-0.301)} = 2.215g \quad (3)$$

Table J6. Organic compounds listed as an unknown hydrate.

Compound	Formula	Mass (g)	Moisture Content (%)	Corrected Mass (g)
Tetrasodium EDTA Dihydrate	$Na_4[C_{10}H_{12}N_2O_8]\cdot 2H_2O$	3.785	9.0	4.159
Trisodium HEDTA Dihydrate	$Na_3[C_{10}H_{15}N_2O_7]\cdot 2H_2O$	3.792	11.3	4.275
Disodium 2,2'-Iminobisacetate (Na_2IDA)	$Na_2[C_4H_5NO_4]$	1.548	30.1	2.215

OVERALL AND DETAILLED MASS BALANCE OF RUNS IN CHAPTER 4

K1.0 OVERALL MASS BALANCE ON RUNS DESCRIBED IN CHAPTER 4

Table K1. Mass balance run 50a Stage 1

	Input (g)		Output (g)				Accum (g)	Loss (g)
Species	**Feed**	**Wash**	**Cond**	**Washed Solids**	**Filtrate**	**Spent Wash**	**Solids**	
Total	1547.16	289.57	736.17	262.29	414.98	299.82	85.45	
Combined	1836.73		1798.71					38.02
								2.1%
						Corrected Loss		1.2%

15.93 grams were accounted for from this stage, leading to a corrected loss of 1.2%.

Table K2. Mass balance run 51 Stage 1

	Input (g)		Output (g)				Accum (g)	Loss (g)
Species	**Feed**	**Wash**	**Cond**	**Washed Solids**	**Filtrate**	**Spent Wash**	**Solids**	
Total	1545.72	347.60	746.64	274.52	390.94	372.46	70.88	37.88
Combined	1893.32		1855.44					37.88
								2.0%
						Corrected Loss		1.1%

16.14 grams were accounted for from this stage, leading to a corrected loss of 1.1%.

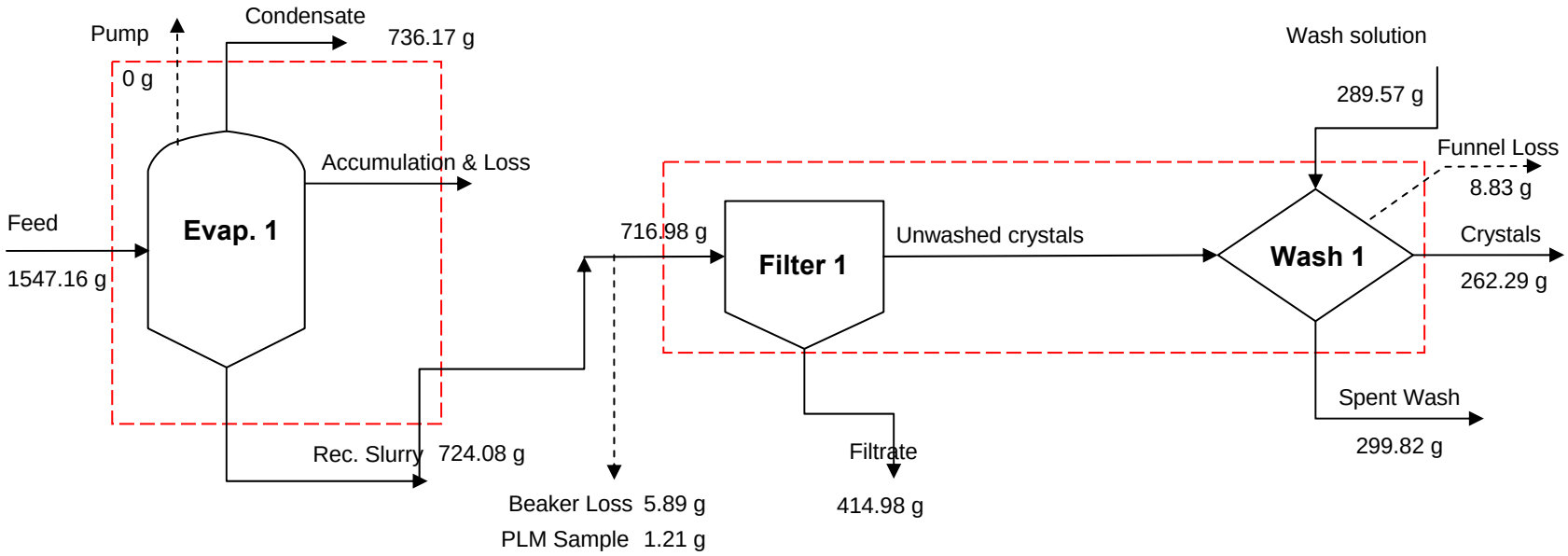

Pump	Mass of the condensate collected in the cold trap protecting the vacuum pump.
Rec. Slurry	Mass of slurry recovered from the crystallizer.
Accumulation & Loss	Mass recovered by washing the vessel with a known amount of water.
Funnel Loss	Mass recovered by washing the funnel with a known amount of water and then drying with paper of a known weight. Performed after the filtration and washing operations.
Beaker Loss	Mass of slurry lost in the beaker necessary for the transfer from the vessel to the filter.
PLM Sample	Mass taken from the slurry for PLM imaging.

Figure K3. Overall mass balance in early feed run 50a. Solid arrows are the process streams and the dotted arrows represent the quantified losses. Closure on a total mass balance was performed for each dashed box around a process unit.

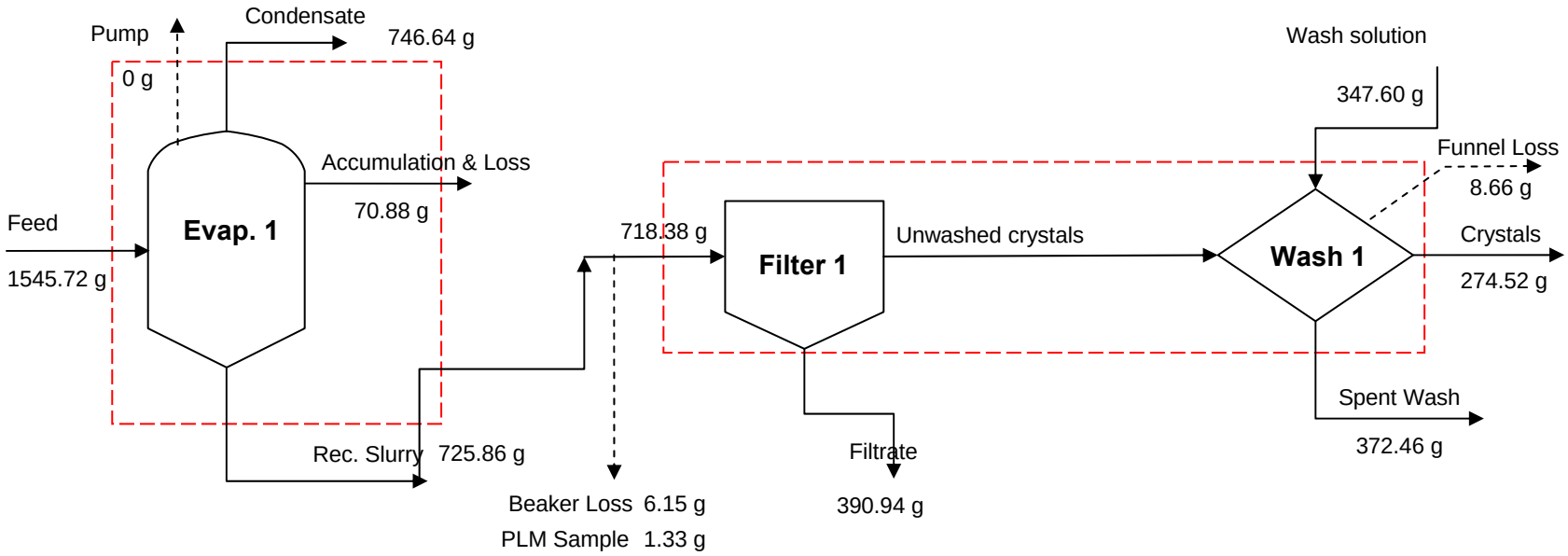

Pump	Mass of the condensate collected in the cold trap protecting the vacuum pump.
Rec. Slurry	Mass of slurry recovered from the crystallizer.
Accumulation & Loss	Mass recovered by washing the vessel with a known amount of water.
Funnel Loss	Mass recovered by washing the funnel with a known amount of water and then drying with paper of a known weight. Performed after the filtration and washing operations.
Beaker Loss	Mass of slurry lost in the beaker necessary for the transfer from the vessel to the filter.
PLM Sample	Mass taken from the slurry for PLM imaging.

Figure K4. Overall mass balance in early feed run 51. Solid arrows are the process streams and the dotted arrows represent the quantified losses. Closure on a total mass balance was performed for each dashed box around a process unit.

REFERENCES

The research team drew on several references during the course of this project, and these are catalogued in the following list. Those cited in the thesis are shown as footnotes on the page of the citation.

Al Nasser W.N., A. Shaikh, C. Morriss, M.J. Hounslow, A.D. Salman. (2007). "Determining kinetics of calcium carbonate precipitation by inline technique" Chemical Engineering Science 63 (2008) 1381 – 1389

Aloise, Gene. United States Government Accountability Office April 6 (2006). "Hanford Waste Treatment Plant". GAO-06-602T.

Barrett P. and B. Glennon. (2002). "Characterizing the metastable zone width and solubility curve using lasentec FBRM and PVM" Chemical Engineering Research & Design 80 (2002), pp. 799–805

Barthe, Stephanie, Rousseau, Ronald W. (2006). "Utilization of focused beam reflectance measurement in the control of crystal size distribution in a batch cooled crystallizer" Chemical Engineering and Technology, v 29, n 2, February, 2006, p 206-211

Bryan, Sam.. June 12-14 (2003). "Flammable gas issue in stored Hanford Waste". American Chemical Society, Bozeman, MT. Pacific Northwest National Laboratory, Richland, WA.

Carreon, Rudy; Mauss, Billie M.; Johnson, Mike E.; Holton, Langdon K.; Wright, Todd G.; Peterson, Reid A.; Rueter, Ken J. (2002)."Selection of Pretreatment Processes for Removal of Radionuclides from Hanford Tank Waste". WM'02 Conference, February 24-28, 2002, Tucson, A.

Chapman, C.C.; Buelt, J.L.; Slate, S.C.; Katayama, Y.B.; Bunnell, L.R.. (1979). " Vitrification of Hanford wastes in a joule-heated ceramic melter and evaluation of resultant canisterized product". Abstract, Energy Res. Battelle Pac. Northwest Lab., Richland, WA, USA.

Chitry, Frederic; Pellet-Rostaing, Stephanie; Nicod, Laurence; Gass, Jean-Louis; Foos, Jacques; Guy, Alain; Lemaire, Marc. Cesium/Sodium Separation by Nanofiltration-Complexation in Aqueous Medium. Separation Science and Technology, 2001.

P. Colombo ; G. Brustatin; E. Bernardo; G. Scarinci. (2003). “Inertization and reuse of waste materials by Vitrification and fabrication of glass-based products.” Solid State and Materials Science, August 2003.

Cowley, W.L.; Vail, T.S.; Reynolds, D.A.; Herting, D.L. April 19-23 (1998). “Technical basis for selecting radionuclide concentrations for use in Hanford tank basis for interim operation source term”. Technologies for the New Century topical conference, Nashville. American Nuclear Society, La grange Park, III.

DOE/EM-0319. January (1997). “Connecting the Cold War Nuclear Weapons Production Processes To Their Environmental Consequences”. Linking Legacies, US Department of Energy DOE/EM-0319, United States Department of Energy, Washington, DC 20585 .

DOE/EM-0266. (1996). “Closing the Circle on the Splitting of the Atom: The Environmental Legacy of Nuclear Weapons Production and What the Department is Doing About It”.

DOE/EM-0232 and DOE/EM-0290. (1995-1996). “Estimating the Cold War Mortgage: The 1995 Baseline Environmental Management report”.

DOE. (1996). “Risks and the Risk Debate: Searching for Common Ground”.

Faria, N., Pons, M.N., Feyo de Azevedo, S., Rocha, F.A. and Vivier, H. (2003). “Quantification of the morphology of sucrose crystals by image analysis” Powder Technol, 133(1–3): 54–67.

Felder R. M. and Rousseau R. W., *Elementary Principles of Chemical Processes*, 3rd ed., John Wiley & Sons, Inc., New York, 2000.

Fullam, H.T.(1976). “Solubility and dissolution behavior of strontium-90 difluoride in aqueous media”. ERDA Energy Res. Abstract. Battelle Pac. Northwest Lab., Richland, WA, USA.

Garside J., Alfons Mersmann, Jaroslav Nývlt. (2002). “Measurement of Crystal Growth and Nucleation Rates”
Institution of Chemical Engineers, European Federation of Chemical Engineering Working Party on Crystallization
Published by Institution of Chemical Engineers (IChemE), 2002
ISBN 0852954492, 9780852954492

Geniesse, Donald James; (2004). “Volume reduction of Aqueous Waste by Evaporative Crystallization of Burkeite and Sodium Salts”. US Patent. Cogema Engineering Corporation, Richland, WA, USA.

Hamilton, D.W. (2006). ."HanfordMedium/LowCurie Waste Pretreatment Project - Pretreatment Process Plan", RPP-PLAN-27238 Rev 0,January 2006

Hammitt, A.P.; Schulz, W.W.. (1979). "Hot Cell Facility and Equipment for Tests of the Hanford Radionuclide Removal Process". Proceedings of the Conference on Remote Systems Technology, Volume No. 26 413-29. Rockwell Hanford Oper., Richland, WA, USA.

Hassan, N.M.; McCabe, D.J.; King, W.D.; Hamm, L.L.; Johnson, M.E.. Ion exchange removal of cesium from Hanford tank waste supernates with SuperLig® 644 resin. Journal of Radioanalytical and Nuclear Chemistry. Vol. 254, No. 1 (2002), pp. 33-40.

Herting, D.L. (1992). "Identification of crystals in Hanford nuclear waste using polarized light microscopy". Energy Res. Abstract, 17(08), Abstract No. 22486. Westinghouse Hanford Co., Richland, WA, USA.

Herting, Daniel L. September 7-11 (1997). "Clean salt process for Hanford nuclear waste treatment". Book of Abstracts, 214th ACS National Meeting, Las Vegas, NV. American Chemical Society, Washington, D.C.

Herting D. L., G. A. Cooke, R. W. Warrant, *Identification of Solid Phases in Saltcake from Hanford Site Waste Tanks,* CD of typical product characterization, Fluor Hanford, Richland, 2002.

Herting, Dan. June 12-14 (2003). "Inorganic tank waste speciation". Abstracts, 58th Northwest Regional Meeting of the American Chemical Society.

Herting D. L., Fractional Crystallization of Waste from Tank 241-S-112, Technical Report, 2005.

Hrma P., Crum J.V., Bates D.J., Bredt P.R., Greenwood L.R., Smith H.D. (2005). "Vitrification and testing of a Hanford high-level waste sample. Part 1: Glass fabrication, and chemical and radiochemical analysis."Journal of Nuclear Materials 345 (2005) 19-30

Hrma P., Crum J.V., Bredt P.R., Greenwood L.R., Arey B.W., Smith H.D. (2005). "Vitrification and testing of a Hanford high-level waste sample. Part 2: Phase identification and waste form leachability."Journal of Nuclear Materials 345 (2005) 31-40

Huang, Frank H.; Mitchell, Dolores E.; Conner, John M.. (1994). "Low-Level Radioactive Hanford Wastes Immobilized by Cement-Based Grouts". Nuclear Technology. Westinghouse Hanford Company, Richland, WA,USA.

Jones A. G. (2002). “Crystallization Process Systems”
Published by Butterworth-Heinemann, 2002
ISBN 0750655208, 9780750655200

Kaldor, R.A.; McDaniel, E.W.; Treat, R.L.. September 7-11 (1985). “Immobilization of Selected Low-Level Hanford Wastes in Grout”. Waste Management (Tucson, Arizona). Pacific Northwest Lab., Richland, WA, USA.

Kaminski, Michael D.; Nunez, Luis. Cesium Extraction from a Novel Chemical Decontamination Process Solvent Using Magnetic Microparticles. Separation Science and Technology Vol. 37, No. 16 2002.

Kougoulos E., A.G. Jones, K.H. Jennings and M.W. Wood-Kaczmar, (2005). “Use of focused beam reflectance measurement (FBRM) and process video imaging (PVI) in a modified mixed suspension mixed product removal (MSMPR) cooling crystallizer”.
Journal of Crystal Growth 273 (2005), pp. 529–534.

Krumme A. et al. (2003). “Measuring crystallization kinetics of high density polyethylene by improved hot-stage polarized light microscopy”
Department of Polymer Materials, Tallinn Technical University, Ehitajate tee 5 19086 Tallinn, Estonia
Polymer Testing 23 (2004) 29–34

Larsen P.A, , J.B. Rawlings and N.J. Ferrier. (2006). “An algorithm for analyzing noisy, in situ images of high-aspect-ratio crystals to monitor particle size distribution”
Chemical Engineering Science 61 (2006), pp. 5236–5248.

Lewis, R E.; Butler, T.A.; Lamb, E. (1965). “Recovery of 137Cs from fission-product wastes and transport by an aluminosilicate ion exchanger”. U.S. At. Comm. Oak Ridge Natl. Lab., Oak Ridge, TN, USA.

McCabe, W.L., Smith, J.C., and Harriott. (2005). “Unit Operations of Chemical Engineering”, 7th Ed., McGraw-Hill, New York, 2005, ch. 27

Manara, D.; Grandjean, A.; Pinet, O.; Dussossoy, J. L.; Neuville,D. R. ”Factors Influencing the Sulphate Incorportion in Radioactive Waste Glasses”.
Mater. Res. Soc. Symp. Proc. 2006, 932

Marangoni, A.G; Narine, S. (2002). “Physical Properties of Lipids“
Published by CRC Press, 2002
ISBN 0824700058, 978082470005. Page 15.

Mersmann Alfons, (2001). “Crystallization technology handbook”
Published by CRC Press, 2001
ISBN 0824705289, 9780824705282

Mika. M; Patek. M; Maixner.J; Randakova.S; Hrma.P;. (2001).“The effect of temperature and composition on spinel concentration and crystal size in high-level radioactive waste vitrification.” Proceedings of the International Conference on radioactive Waste Management and Environmental Remediation, 2001.

Moyers C. G. and Rousseau R. W., “Crystallization Operations,” in *Handbook of Separation Process Technology*, Chapter 11, pp. 578–643, John Wiley and Sons, Inc., 1987.

Mullin John W., *Crystallization*, 4th ed., Butterworth-Heinemann, Oxford, 2001.

Myerson A. S., ed., *Handbook of Industrial Crystallization*, Butterworth-Heinemann, Boston, 1993.

Nassif, L. “Use of Evaporative Fractional Crystallization in the Pretreatment Process of Multi-Salts Single Shell Tank Hanford Nuclear Wastes”
M.S. Thesis, Georgia Institute of Technology,2007.

Nassif L., Dumont G., Geniesse D., Alsyouri H., Rousseau R. (2008). “Pretreatment of Hanford Medium-Curie Wastes by Fractional Crystallization”
Environ. Sci. Technol.April 4, 2008.

O'Grady, Des ; Glennon, Brian. (2005). “Use of in-situ instrumentation to characterize anti-solvent addition crystallization”
AIChE Annual Meeting, Conference Proceedings, 05AIChE: 2005 AIChE Annual Meeting and Fall Showcase, Conference Proceedings, 2005, p 2412-2416

Öhman G., H. Saxén ”Transportprocesser”
Åbo Akademi
Värmeteknik (1997) 3rd ed., chapter 4

Oncul A. A. et al. (2006). “Numerical and analytical investigation of barium sulphate crystallization”
Chemical engineering science ISSN 0009-2509 CODEN CESCAC
2006, vol. 61, n°2, pp. 652-664 [13 page(s) (article)] (35 ref.)

Polannen K, A.W. Hakkinen, S.P. Reinikainen, A. Louhi-Kultanen and L. Nystrom. (2006). “A study on batch cooling crystallization of sulphathiazole—process monitoring using ATR-FTIR and product characterization by automated image analysis”
Chemical Engineering Research

Ponder, Sherman M.; Helkowski, Robert; Mallouk, Thomas E. Continuous-Flow Process for the Separation of Cesium from Complex Waste Mixtures. Ind. Eng. Chem. Res. Vol. 40, No. 15 2001.

Pons, M., Vivier, H., Belaroui, K., Bernard-Michel, B., Cordier, F., Oulhana, D., Dodds, J. (1999). "Particle morphology: from visualization to measurement"
1999. Powder Technology 103, 44–57.

Puel, F., Marchal, P., Klein, J. (1997). "Habit transient analysis in industrial crystallization using two dimensional crystal sizing technique"
Chemical Engineering Research and Design 75 (A2), 193–205.

Puel F, G. Fevotte and J.P. Klein. (2003). "Simulation and analysis of industrial crystallization processes through multidimensional population balance equations. Part 1: a resolution algorithm based on the method of classes"
"Simulation and analysis of industrial crystallization processes through multidimensional population balance equations. Part 2: a study of semi-batch crystallization, Chemical Engineering"
Chemical Engineering Science 58 (2003), pp. 3715–3727.

Rabiger K. ; Keldenich K. ; Scheffer J.. Glastech Ber. (1995). "Experience in operation of a pilot plant melting residual substances."
Glass Sci technol, Vol. 68, 84-90, 1995.

Randolph A. D. and Larson M. A., Theory of Particulate Processes: Analysis and Techniques of Continuous Crystallization, 2nd ed., Academic Press, San Diego, 1988.

Reynolds, D.A.; Herting, D.L. (1985). "Solubilities of Sodium Nitrate, Sodium Nitrate, Sodium Nitrite, and Sodium Aluminate in simulated nuclear waste ". Energy Res. Abstr.. Rockwell Hanford Oper., Rockwell Int. Corp., Richland, WA, USA.

Robert A. Smith ; David H. Nyman; B. Nick Anderson. (1990) "Getting ready to build the Hanford Waste Vitrification Plant." Nuclear Engineering International, Vol. 35, No 428, 40-43, March 1990.

Rousseau R. W., "Crystallization," in *Kirk-Othmer Encyclopedia of Chemical Technology*, Volume 7, 4th ed., John Wiley & Sons, Inc., pp. 683–730, 1993.

Rousseau R. W., "Crystallization," in *Encyclopedia of Separation Technology*, Douglas M. Ruthven, Ed., Volume 1, Wiley Interscience, pp. 393–439, 1997.

Rousseau R. W., "Crystallization Processes," in *Encyclopedia of Physical Science and Technology*, 3rd ed., Academic Press, Volume 4, pp. 91–119, 2002.

Rousseau, R. W. Alsyouri, H. Dumont, G. and Nassif, L. RPPRPT-27239 Rev 0 Phase I Laboratory Report, Jan 2006

Salmeron Sanchez M., Vincent B. F. Mathot, Geert Vanden Poel, and Jose´ Luis Go´mez Ribelles. (2007). "Effect of the Cooling Rate on the Nucleation Kinetics of Poly(L-LacticAcid) and Its Influence on Morphology. " Macromolecules 2007, 40, 7989-7997

Seader J.D., E.J Henley "Separation process principles" John Wiley, 2nd edition (2006) chapter 17

Sohnel O. and Garside J., *Precipitation*, Butterworth-Heinemann, Oxford, 1992.

Teja A. S. and Rousseau R. W., "Thermodynamics of Crystallization," Chapter 20 in *Chemical Thermodynamics for Industry*, T. Letcher, editor, Royal Society of Chemistry, Cambridge, UK, pp. 230–242. 2004.

Thompson, LE.; Lowery, P.S. (2003). "Development of the bulk vitrification treatment process for the low activity fraction of Hanford single shell tank waste" Conference, February 23-27,2003 Tucson, AZ

Toghiani, Rebecca K.; Lindner, Jeff S.; Herting, D.L. March 11-14 (2002). "Modeling of Hanford saltcake dissolution". American Institute of Chemical Engineers, Spring National Meeting, New Orleans, LA, USA.

Trifkovic M., M. Sheikhzadeh, and S. Rohani. (2008). "Kinetics Estimation and Single and Multi-Objective Optimization of a Seeded, anti-Solvent, Isothermal Batch Crystallizer" Ind. Eng. Chem. Res. 2008, 47, 1586-1595

Tyree Geoff.."First glass made at Hanford via bulk vitrification." CH2M Hill Hanford group Publication

Vance, E.R.; Hart, K.P.; Carter, M.L.; Hambley, M.J.; Day, R.A.; Begg, B.D.(1998). "Further studies of Synroc immobilization of HLW sludges and Tc for Hanford tank waste remediation". Materials Research Society. Materials Division, ANSTO, Menai, Australia.

Wang, X.Z., Calderon De Anda, J., Roberts, K.J. (2007). "Real-time measurement of the growth rates of individual crystal facets using imaging and image analysis: a feasibility study on needle-shaped crystals of L-glutamic acid" Chemical Engineering Research & Design 85A, 921–927

Wilson.B.K; Hrma.P; Alton.J; Plaisted.T.J; Vienna.J.D . (2002). “The effect of composition on spinel equilibrium and crystal size in high-level waste glass.” Journal of Materials Science, Vol 37 (24), 5327-5331, 2002.

Internet References:

http://web.abo.fi/~rzevenho/MOFST08-OH17.pdf , November 2008

http://www.uolab.lsu.edu/documents/crystalOPS.pdf, November 2008

http://www.emse.fr/pratsolis/list/animp2002barresi.pdf, November 2008

http://srnl.doe.gov/techex/PDFs/3b_2_Herting.pdf, November 2008